GEOLOGY AND GEOCHEMISTRY OF LINARES-LA CAROLINA Pb-ORE FIELD (SOUTHEASTERN BORDER OF THE HESPERIAN MASSIF).

BY

FRANCISCO JAVIER LILLO RAMOS

Submitted in accordance with the requirements for the degree of doctor of philosophy.

Department of Earth Sciences,

The University of Leeds.

October, 1992.

To my parents

To Maribel

Acknowledgements

I would like to express my gratitude to the following people for their contributions towards this thesis:

My supervisors, Bruce Yardley, Simon Bottrell and Mike Leeder deserve my immense thanks for giving me their best advise. Harry Clemmey, my former supervisor, contributed with fruitful comments 'on the ground'.

Joe Cann gave me encouragement to finish when hard times became. Eric Condliffe and Geoff Lloyd, provided microprobe and SEM tuition and I benefitted greatly from their advice on many occasions. The fluid inclusion work was notably improved from the invaluable assistance of David Banks and Lorena Ortega (University of Madrid). The EDX work on fluid inclusions was performed by Javier García Vargas (University of Barcelona). Alan Gray provided expert assistance with XRF analyses. Dave Hatfield gave me priceless help in the sulphur lab, respectively. Tom Oddy, Keith Reid, Keith Cowling and Mary Riley provided suitable (powder and thin sections) samples to study.

The former suggestion to do this thesis became from Roberto Oyarzun, who has been 'heavily' supporting until its completion. Roberto and Charo Lunar suggested to me to come to Leeds four years ago.

In addition I would like to thanks all my friends at Leeds: Deborita, Carmen, Polito, Sunil, Ricardo, David, Elias, Poppy, Manolo, Samaira, University for all their help, frienship and encouragement over the past four years.

Finally, my immense thanks to my family, specially my parents, who gave me the education required to get this work, even with large effort from them during hard times.

Last, but not least, Maribel deserves all my gratitude. Without her love, and great efforts, the thesis never could be finished.

PAGE MISSING IN ORIGINAL

GEOLOGY AND GEOCHEMISTRY OF LINARES-LA CAROLINA Pb-ORE FIELD (SOUTHEASTERN BORDER OF THE HESPERIAN MASSIF).

ABSTRACT

Base-metal late Hercynian vein and stratabound-type deposits occur in the Linares-La Carolina mining district (Sierra Morena, Spain).

No other ore deposits than iron beds and a supergene iron-manganese karst-related deposit were found in the studied area. However, Upper Ordovician-Lower Silurian rocks show Ni, Zn, Pb content above the average values of sandstones.Upper Ordovician-Lower Silurian country rocks are grouped into two stratigraphical sequences that reflect sea-level rise-fall cycles in a basin developed in a passive margin. The duration of these cycles indicates that they were caused by a combination of eustatic processes and intraplate extensional tectonics.

The Late Hercynian hydrothermal deposits hosted by metasediments and granitoids, comprise (Ba)-(Pb-Zn-Cu-[Ag]) vein and stratabound type deposits that were emplaced before the Ladinian, during an extensional stage starting in the Upper Permian.Three stages of ore deposition have been recognised, the first stage is characterised by the formation of pyrrhotite, arsenopyrite, Ag sulphosalts and minor arsenopyrite and Bi sulphides. In the second stage, pyrite, Cu sulphides, barite and Ni-Co minerals precipitated. Main deposition of galena and sphalerite took place at the end of the first stage and the beginning of the second stage. There is no evidence of selective Ag enrichment.

Hydrothermal alteration of granitic host rocks is characterised by argillic-phyllic, argillic-propylitic assemblages overprinted by a late alkali metasomatism. There is a strong relation between composition of secondary minerals, mineralogy of the alteration zone and

whole-rock composition. Mass transfers of alumina appear to be important. There is a significant introduction of Si, Al, K, Na, Rb and Pb, together with a depletion in Ca and Sr. Chlorite and illite geothermometers indicate temperatures of 276.7-321.5 °C.

Three events of fluid entrapment at hydrostatic pressures have been recognised, with fluids evolved from low to moderate, locally carbonaceous hot fluids to high-moderately polysaline cooler fluids.

Ore-lead was derived from Palaeozoic U-'enriched' country rocks, although some participation from the Hercynian granitoids can not be ruled out.

The distribution of sulphur isotopes is not homogeneous in the scale of the district. Differences exist between those deposits at the El Centenillo-Santa Elena sector (where the dominant process was the mixing of 'magmatic'-derived sulphur and sulphur derived from the metasediments) and those occurrences at the Linares-La Carolina sector (where the dominant sulphur was 'magmatic'-derived).

TABLE OF CONTENTS

LIST OF TABLES

Fig.2.1.(Pag.5). a) Zonation of the Hesperian Massif proposed by Julivert et al. (1972). A: Cantabrian Zone; B: Precambrian core in the Narcea antiform; C: West-Asturian Leonese Zone (a= Precambrian core in the Mondoñedo fold); D: 'Ollo de Sapo' antiform; E: Central Iberian Zone (a= polymetamorphic complexes of Galicia and Portugal: 1.Cabo Ortegal, 2.Ordenes, 3.Lalín, 4.Bragança, 5.Morais, 6.Malpica-Tuy; b= porphyroblastic gneisses); F: Pedroches batholith; G: Ossa-Morena Zone (a= Precambrian outcrops); H: South Portuguese Zone (a= Pyrite Belt). b) Original zonation proposed by Lotze (1945).

Fig.2.2.(Pag.11). Ordovician palaeogeographical domains in the Hesperian Massif. a) Scheme from Julivert and Truyols (1983), A: domain with an Ordovician succession of moderate thickness; B: West-Asturian furrow; C: domain with the 'Armorican' quartzite facies unconformably overlaying the Precambrian-Cambrian basement, D: domain without 'Armorican' quartzite facies. b) Scheme proposed by Hamman et al. (1982), A: Northeast Iberian region (1: Cantabro-Ebro rise; 2: Navia-Alto Sil domain; 3: Mondoñedo-Peñalba domain); B: West-Iberian region, (4: Truchas-Central System domain; 5 and 6: Central Iberian domain; 7,8 and 9: Ossa-Morena domain).

Fig.2.3.(Pag.18). Almadén district. a) Outcrop map of the Criadero quartzite and location of mercury mines in the Chillón syncline. 1: faults, 2: Devonian, 3: Criadero quartzite, 4: active mine, 5: abandoned mine; 6: prospect or showing. b) Vertical cross section trough the Almadén mine (From Saupé, 1990).

faults, defining the so-called 'Celtiberian corridor' or 'Celtiberian rift' (based on data from Alvaro et al., 1979; Capote, 1983c; Muñoz et al., 1983; Sopeña et al., 1983). A, B, C are the plutonic domains in the Hesperian Massif.

Fig.2.8.(Pag.34). Late-Hercynian evolution of central Iberia. a) Deformational events, A: extensional episode, B: ductile-transcurrent episode C: brittle-transcurrent episode. b) Schematic cross-sections showing the kinematic evolution during the extensional episode. 1: Migmatites and orthogneisses. 2: Precambrian to Ordovician metasediments, 3: 'pre- to syn-extensional' granitoids, 4:Permian sediments and volcanics (from Doblas, 1991).

Fig.2.9.(Pag.37). Ba-(F)-(base metal sulphides) mineralisations in the Spanish Central System. a) Geological sketch of the central sector. b) Schematic diagram depicting the relationships between alteration zones and mineral assemblages. 1: adamellitic host rock, 2: quartz-argillic alteration, 3: quartz-sericitic alteration, 4: chloritisation, 5: adularia zone, 6: veins (after Lillo et al., 1992).

Fig.2.10.(Pag.42). Simplified geological map of the Hiendelaencina-Atienza area. 1: Cenozoic sediments; 2: Mesozoic sediments; 3: Permian sediments and andesitic volcanics; 4: low-grade Ordovician metasediments; 5: Precambrian-Cambrian metamorphic core-complexes (a: augengneisses, b: orthogneisses and metasediments); 6: brittle faults; 8: transcurrent shear zones; 9: traces of upward arched crustal domains; 10: pitches of Variscan minor fold axes; 11: ore deposits. Localities: AN: Angon, AT: Atienza; CO: Congostrina; HI: Hiendelaencina; LB: La Bodera;

ABBREVIATIONS USED IN THIS THESIS

M	Mudstone facies
Hw	Heterolithic facies
Sb	Evenly Laminated Sandstone facies (Sedimentology)
Hs	Hummocky Cross-bedding Sandstone facies
St	Large/Medium Scale Cross-bedding Sandstone facies
Sa	Low angle Cross-bedding Sandstone facies
Mh	Mudstone and Heterolithic facies
Lc	Medium and Small Scale Cross-bedding Limestone f.
Lb	Evenly Laminated Limestone facies
La	Large Scale Cross-bedding Limestone facies
R_d	Rate of deposition
R_a	Rate of accommodation
RPS	Retrogradational parasequence set
PPS	Progradational parasequence set
APS	Aggradational parasequence set
ppm	part per million
wt%	weight per cent
L.o.I.	Loss on ignition
ECQ	El Caño Quartzite Fm.
BQ	Botella Quartzite Fm.
MB	Mixed Beds Fm.
COS	Correderas Shales Fm.

CAS	Cantera Shales Fm.
CHS	Chavera Shales Fm.
UL	Urbana Limestone Fm.
HM	Hydrolysate modulus
PTM	Potassium modulus
SM	Sodium modulus
IM	Iron modulus
TM	Titanium modulus
OIA	Oceanic Island Arc
ARC	Oceanic Island Arc
CIA	Continental Island Arc
ACM	Active Continental Margin
PM	Passive Margin
BSE	Backscattered electron image
COM	Conventional optical microscopy
EDX	Energy dispersive X-ray microanalysis
EMP	Electron microprobe analysis
p.f.u.	per formulae unit
X_i	molar fraction of compound i
Ill	Illite
wm	White mica
Mus	Muscovite
Par	Paragonite

Ca-Par	Ca-paragonite
Fe-Cel	Fe-celadonite
Mg-Cel	Mg-celadonite
Pyr	Pyrophyllite
Chl	Chlorite
Kspar	K-feldspar
Ab	Albite
Or	Orthoclase
An	Anorthite
Bt	Barite
Q	Quartz
Te	Temperature (°C) of first melting of ice
Tmi	Temperature (°C) of final melting of ice
Tm_{CO2}	Temperature (°C) of melting of CO_2
Tms	Temperature (°C) of melting of sylvite
Tmh	Temperature (°C) of melting of halite
Tmhy	Temperature (°C) of melting of clathatre
Th_V	Temperature (°C) of homogenization to vapour
Th_L	Temperature (°C) of homogenization to liquid
Th_{CO2}	Temperature (°C) of homogenization to CO_2
TP_{CO2}	Temperature (°C) of homogenization of CO_2
Tt	Temperature of trapping
Pt	Pressure of trapping

1.Introduction.

The Linares-La Carolina Pb-ore field (Sierra Morena, Spain) was a world-class mining district during the 1875-1920 period, with an average lead production of 65,000 tn/yr. Silver obtained as by-product reached 500 g/tn. The mineralisation occurs almost exclusively as hydrothermal veins, where the mining works (over 800 Km. of galleries) were concentrated. Actually, the economic interest is limited to one lode (El Cobre) and small scale works of stratabound hydrothermal mineralisations in the basal beds of the post-Hercynian succession (Las Torrecillas).

Despite the large number of studies that have been carried out on the mineralisations, very little is now about the processes involved in the ore genesis.

In the earlier 70s, Tamain (1972) established a hypothetical model where the Pb-Zn mineralisation is related to a regional 'metallogenic' envelope surrounding the granitic bodies.

Studies undertaken by Enadimsa (1971) yielded the first relevant geochemical data on isotope geochemistry and mineral chemistry of the ores.

Charpentier (1976) continued in the area of La Carolina-Santa Elena the work started by Tamain (1971) in El Centenillo, covering structural, stratigraphical and ore geology aspects.

Rios (1977) presented additional data about the stratigraphical and structural controls of the mineralisation hosted by Ordovician-Silurian rocks.

Further work by Enadimsa (1981) produced detailed geological maps of the district.

In all these works the origin of the mineralisation has been related to the late Hercynian magmatism that developed in the area. However, Jacquin and Pineda (1980) considered the possible remobilisation of metals from the Palaezoic host rocks on the

basis of some minor stratabound/stratiform occurrences in the Ordovician-Silurian succession (Rios, 1977; Rios and Claverias, 1979).

Another question arises when taking into account the ore deposits in the basal beds of the sedimentary late- to post-Hercynian cover, which traditionally have been considered as related to eo-Alpine mineralisation stages (Enadimsa, 1971), likely involving remobilisation of metals from the late-Hercynian veins (Pineda et al., 1981).

The main aim of this thesis is to improve our knowledge of the genesis of the different mineralisations (Palaeozoic stratabound/stratiform, late Hercynian veins and the late Hercynian stratabound ore deposits) in the area. A secondary aim derived from the first one is to asses the relationship between the different types of ore deposits as the hydrothermal vein type mineralisation and the reported stratabound/stratiform occurrences in the Upper Ordovician-Silurian rocks seem to reflect the two main events of mineralisation that evolved in the Hesperian Massif. To get the proposed goals, a methodology with diverse approaches involving geological and geochemical studies is required: from sedimentological work (to define the sedimentary environment where the reported stratiform mineralisation took place) to isotopic studies (to infer the source of ore-forming elements).

To provide better understanding of the specific geological information related to Linares-La Carolina that is presented in this work, additional information about the regional geology of the Hesperian Massif during the considered periods is given in Chapter 2.

Sedimentological, whole-rock and sulphur isotope geochemistry studies were conducted on those metasedimentary formations related to eh Palaeozoic mineral deposits to constrain the geological settings where they were formed, and their potential participation as source of metals for the vein-type mineralisations (Chapter 3).

Detailed description of the geological setting and the ore geology of the hydrothermal mineralisation is presented in Chapter 4. Analysis of the structural pattern of the lodes in the whole district, together with whole-rock geochemical analyses and cross-cutting relationship between ores and stratigraphy have been used to constrain the timing of the ore emplacement. The information about ore petrography and mineral assemblages is completed with mineral compositional data in last section of Chapter 4.

A detailed mineralogical description, compositional data from electron probe microanalyses and whole rock XRF analyses have been used to asses the effects of hydrothermal fluids on the host granitic rocks (Chapter 5). Mineral compositions have been used as indicators of temperature of mineralisation.

Fluid inclusions studies have been carried out to get information about the generations of fluids involved in the ore forming processes and further data about conditions of pressure and temperature of mineral deposition (Chapter 6).

Lead isotope data from Enadimsa (1971) have been reexamined. These, together with data of sulphur isotope geochemistry have been used to investigate the source of ore forming components.

In essence, this study gives information on geological, structural, and geochemical constrains for the formation of the mineralisation in the Linares-La Carolina district.

Chapter 2. The Hesperian Massif: Upper Ordovician-Early Silurian events. Late Variscan (Upper Stephanian-Permian) events.

2.1.Introduction.

The Upper Ordovician-Early Silurian and Late Variscan (Upper Stephanian-Permian) time spans deserve special consideration as they are the two periods of greatest development of mineralisation in the Hesperian Massif. The aim of this chapter is to give additional information to better understanding of the following chapters. For obvious reasons, it was not intended to offer an exhaustive review and only relevant aspects are covered.

2.2.The Hesperian Massif.

The term "Hesperian Massif" (or its synonym "Iberian Massif") is commonly used to identify those Precambrian and Palaeozoic terrains in the Iberian Peninsula which are not incorporated in the Alpine Chains (i.e. Pyrenees, Betics) but also includes those pre-Mesozoic rocks located in the Alpine Celtiberian Range as they display similar features to those rocks in the Hesperian Massif (s.s.) and their "Hercynian" features have not been overprinted by Alpine tectonometamorphic processes.

The Hesperian Massif occupies almost the whole western half of the Peninsula and represents the southernmost part of the West European Variscan orogenic belt. It is limited by the Basque-Cantabrian Chain (the western end of the Pyrenees) on the north, by the Celtiberian Range and the Tertiary basins of Duero and Tajo on the east, by the Portuguese Mesozoic Coastal Range and the Sado Basin on the West, and by the Tertiary basin of Guadalquivir and the Betics on the south.

The oldest rocks in the Hesperian Massif are late Precambrian in age. They comprises two geologic units separated by an unconformity (see Capote, 1983a and references therein). The lower group is a polymetamorphic basement deformed in the Precambrian.

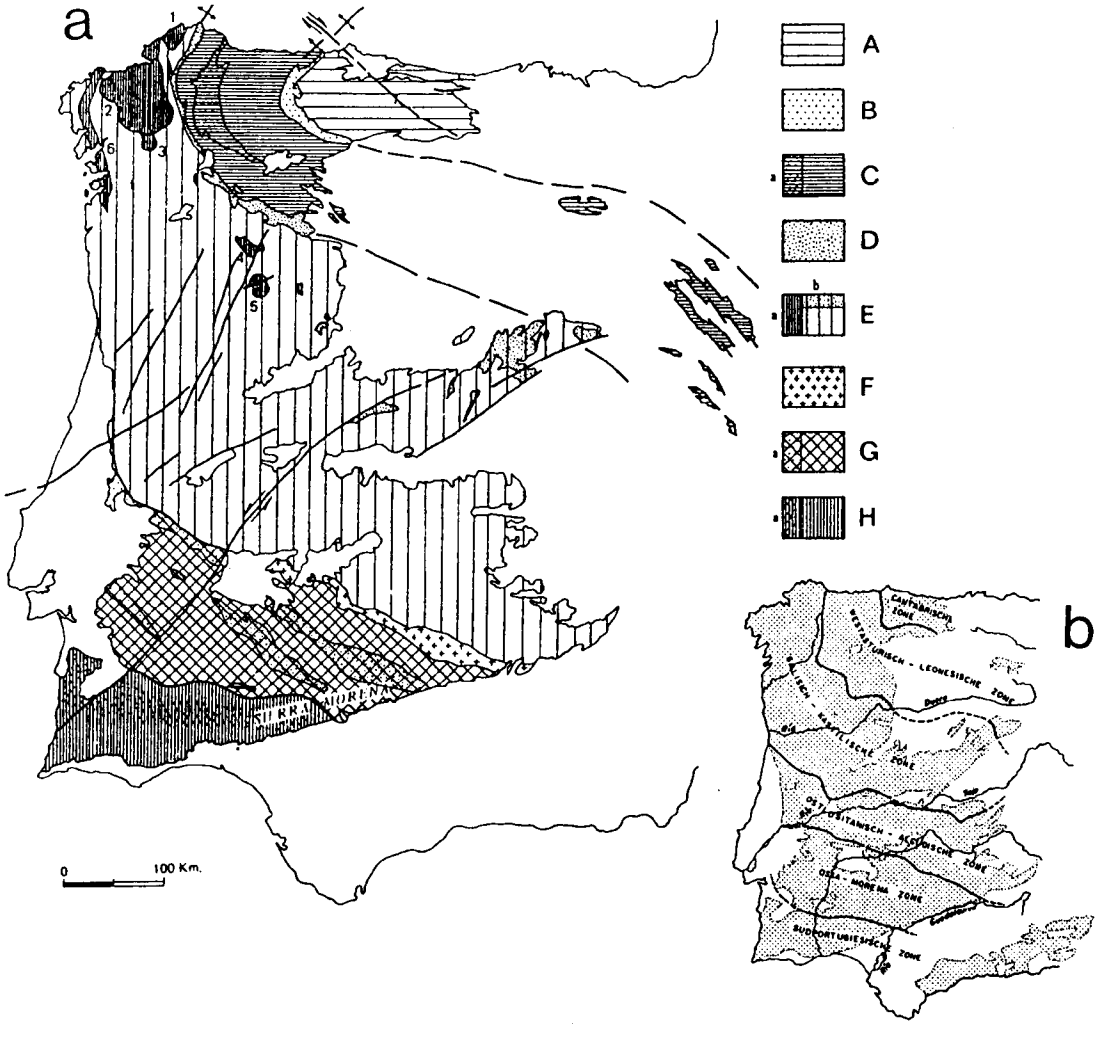

Fig.2.1. a) Zonation of the Hesperian Massif proposed by Julivert et al. (1972). A: Cantabrian Zone; B: Precambrian core in the Narcea antiform; C: West-Asturian Leonese Zone (a= Precambrian core in the Mondoñedo fold); D: 'Ollo de Sapo' antiform; E: Central Iberian Zone (a= polymetamorphic complexes of Galicia and Portugal: 1.Cabo Ortegal, 2.Ordenes, 3.Lalín, 4.Bragança, 5.Morais, 6.Malpica-Tuy; b= porphyroblastic gneisses); F: Pedroches batholith; G: Ossa-Morena Zone (a= Precambrian outcrops); H: South Portuguese Zone (a= Pyrite Belt). b) Original zonation proposed by Lotze (1945).

It consists of a schist-greywacke succession ("Serie Negra") and the "Ollo de Sapo" porphyroblastic gneisses and equivalents.

The upper group comprises most of the so-called "Schist-greywacke Complex "(*s.s.*).

The Precambrian rocks display Hercynian deformation and metamorphic features and only rarely is there evidence of Precambrian deformation and metamorphism (Capote 1983a).

Most of the Hesperian Massif is made up of Palaeozoic metasediments and metavolcanics. They display varying degrees of metamorphism, mainly in the greenschist facies. Shales, schists, quartzites, and volcanic rocks ranging from basalts to rhyolites in composition are the most common lithologies. The whole succession was intruded by large volumes of granitoids during the Hercynian orogeny.

Only an angular unconformity related to the Caledonian orogeny has been recognised in the Iberian Massif (see Julivert, 1983d and references therein). This unconformity is located at the bottom of the Ordovician succession except in the Cantabrian Zone and the West Asturian-Leonese Zone, where there is no evidence for pre-Hercynian folding phases during the Palaeozoic.

During the Stephanian and the Permian a fracture network formed. It is defined by long strike-slip faults trending dominantly NE, NW and E-W (Arthaud and Matte, 1975). Most of these fractures were reactivated (some of them with associated magmatism) during the Alpine orogeny giving as a result "block tectonics" with important rotational and vertical displacements.

Lotze (1945) established a zonation in the Hesperian Massif on the basis of stratigraphic, magmatic and structural criteria (Fig 2.1.b). A redefinition of Lotze's zonation has been presented by Julivert et al.(1972a), which will be considered in the present work although it is being revised nowadays (Quesada and Ribeiro, 1989). This zonation comprises five zones (Fig.2.1.a), briefly described as follows:

a.Cantabrian zone. It occupies the inner part of the so-called "Iberoarmorican Arc" ("Asturian Knee"). It is characterised by pre-Carboniferous metasediments with shallow-depth marine facies and several stratigraphic hiatuses. The overlying Carboniferous sequence is several hundreds of meter thick and comprises syn- and post-orogenic sediments with a wide range of facies: condensed, turbiditic, paralic, and fluvial facies. As a generalisation, it was an offshore area which progressively became an external zone adjacent to the orogen as the orogenic building developed (Julivert, 1983a)

This succession was deformed in three main phases. The first phase took place during the Westphalian A-D and produced overthrusts and folds. The second phase generated upright folds during the Late Westphalian D-Stephanian A. The third phase formed isoclinal folds and normal and strike-slip faults during the Stephanian B-C. (Julivert, 1983b)

Low-grade regional metamorphism is restricted to areas next to the Narcea anticline.

b.West Asturian-Leonese Zone. This zone is bounded by two antiforms which correspond to the Narcea and "Ollo de Sapo" anticlines. It consists of a Cambrian to Silurian succession of quartzites, schists and occasional limestones which overlay Precambrian metasediments. The regional metamorphism is of greenschists facies but amphibolitic facies rocks are found on the west. Granitoids are not very important in volume except in the western portion between the Mondoñedo fold and the "Ollo de Sapo" antiform.

The structural pattern is the result of three phases of deformation. The first phase developed overturned and recumbent folds, such as Modoñedo and Caurel. The second phase gave place to overthrusting and minor folds. The third phase generated upright folds. The three phases took place during the (?)late Devonian-Stephanian A (Julivert, 1983c).

c.Central Iberian Zone: This zone is the largest geotectonic unit in the Iberian Massif.

Two tectonosedimentary units separated by an angular unconformity have been recognised in this area. The oldest unit consists of pre-Ordovician rocks (Precambrian and Cambrian). The younger formation consists essentially of Cambrian to Devonian slates, conglomerates, basic and acid volcanic rocks, and occasionally limestones. Metamorphism is plurifacial defining "metamorphic bands" of high grade, spatially related with plutonic rocks (essentially aluminous, alkaline and calc-alkaline granitoids). As some of these granitoids have been affected by the last main Variscan tectonic phases, there are syn- to late-kinematic and post-kinematic plutons, the so-called 'younger' and 'older' granites.

An important feature of this zone is the occurrence of several polymetamorphic massifs in Galicia and Portugal (Ortegal, Ordenes, Lalín, Bragança, Morais, Forcarey, Fig.2.1) as well as the 'Blastomylonitic Graben' (Malpica-Tuy unit) consisting of ultramafic, mafic rocks, greywackes and pelites which show mineralogical assemblages of the amphibolite, granulite and eclogite facies. They have been occasionally retrograded by Hercynian regional metamorphism of lower grade (Martinez and Ibarguchi, 1983).

Three main Hercynian tectonic phases have been recognised which took place before the Autunian (Capote,1983b, Macaya et al., 1991) although the ages remain unknown.

d.Ossa-Morena Zone: This zone is located between the limits defined by the Pedroches batholith and system of faults on the north (e.g Hornachos-Villarta fault) and south (e.g Ficalho fault), but these limits are being redefined (Quesada and Ribeiro, 1989). It consists of a succession of rocks ranging in age from Precambrian to Carboniferous although the main feature is the large development of the Precambrian, more of 5.000 m. thick, which includes slates, greywackes , schists, quartzites,

metaconglomerates, amphibolites, and gneisses. The Cambrian, up to 800 m., consists of slates, carbonates, metaconglomerates, greywackes with interbedded volcanites (acid and intermediate-type). The regional metamorphism is limited to two bands: the blastomylonitic band of Abrantes-Elvas-Badajoz-Córdoba with metamorphism of intermediate pressure Barrowian-type and a later retrogradation to greenschist facies, and a southern band with high T-low P metamorphism (Martinez and Gil Ibarguchi,1983).

There are three facts to point out regarding the Hercynian magmatism in the Ossa-Morena zone: the common association of basic and acid rocks, the abundance of basic massifs and the occurrence of hyperalkalic granites (Corretge, 1983).

Two main Variscan phases of deformation have been recognised: the first phase yielded shear zones associated with large folds during the Givetian. The second phase generated folds before the Westphalian D (Chacon et al., 1983).

f.South Portuguese Zone. This zone lies almost entirely in Portugal. It consists almost exclusively of Upper Devonian and Carboniferous rocks. A generalised stratigraphic sequence of this zone shows from bottom to top (Julivert et al., 1983): a) siliceous and pelitic schists of unknown thickness containing some fossiliferous limestones of Famenian age near the top; b) a volcanic-sedimentary complex up to 750 m in thickness defined by a sequence of shales, schists, quartzites, greywackes and tuffs, basic volcanites (mainly spilites) and pyroclastic rocks. This volcanic-sedimentary formation defines the so-called 'Iberian Pyrite Belt', which extends from the north of Sevilla in Spain to Lousal in Portugal. Large stratiform sulphide deposits are found associated with the felsic volcanites; and c) a 'flysch' sequence, consisting of shales, greywackes and interbedded conglomerates up to 3000 m thick, Upper Visean to Lower Westphalian.

There is a regional metamorphism in greenschist facies and prehnite-pumpellyite, pumpellyite-actinolite facies but the rocks

are anchimetamorphic on the southwest of the Pyrite Belt (Martinez and Gil Ibarguchi,1983).

The syn- to late-orogenic plutonism is characterised by a 'basic band' from the Beja Massif (Portugal) to the Sevilla province with rocks ranging from olivine gabbros to quartzdiorites. In the Beja Massif a 'gabbro-dioritic' complex is associated with tonalites, granites and granodiorites (Corretge, 1983).

Isoclinal, recumbent folds overturned towards the SW and tectonic imbrications, developed in this area during the Middle Westphalian.

2.3.Upper Ordovician - Lower Silurian events.

2.3.1.Sedimentation.

On the basis of structural, lithological and palaeontological data several palaeogeographic units may be distinguished during the Ordovician in the Iberian Massif (Hamman et al., 1982; Julivert and Truyols, 1983; Figs 2.2.a and b).

The palaeogeographical zonation presented in this thesis is mostly based on that suggested by Hamman et al., (1982), but further modifications are introduced in considering the southern part of Ossa Morena as a separated zone. This modification is based on the supposed coincidence of the Porto-Badajoz-Cordoba shear band with a suture between two different plates (Robardet, 1976) or a synsedimentary fault belt separating basins with different sedimentary and structural features (Herranz, 1984) or a transform fault (Lefort and Ribeiro, 1980).

a. <u>The Northeast Iberian Region</u>. This comprises the Cantabro-Ebro rise and the West Asturian-Celtiberian trough with the Navia-Alto Sil and the Mondoñedo-Peñalba Domains. As the present work mainly deals with the sedimentation and palaeogeography during the Upper Ordovician-Lower Silurian, the Truchas domain (initially included by Hamman et al.,1982 in the West Iberian region) has

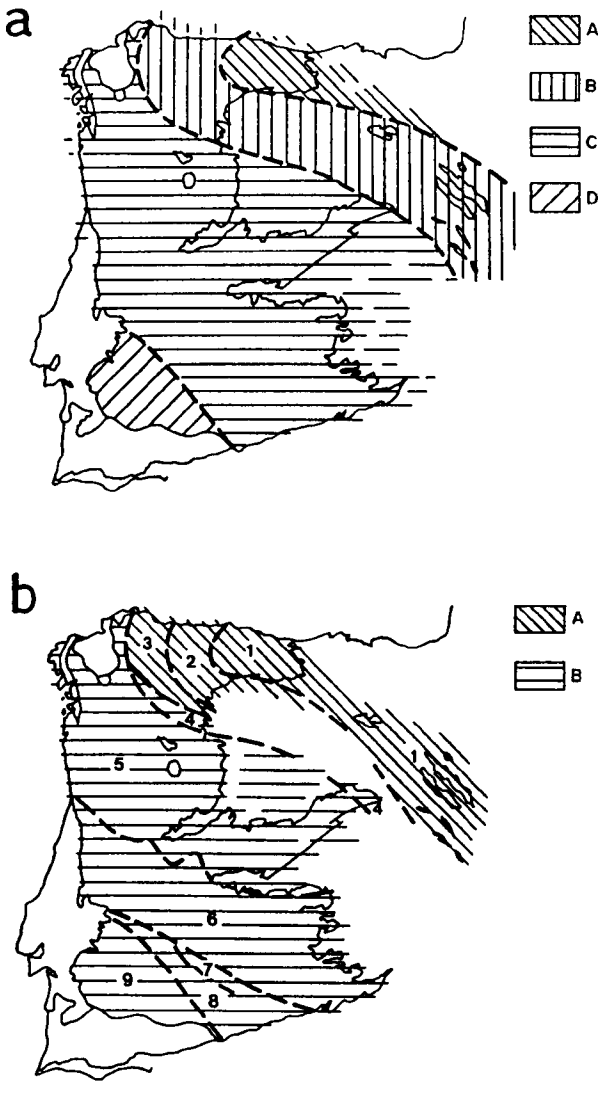

Fig.2.2. Ordovician palaeogeographical domains in the Hesperian Massif. a) Scheme from Julivert and Truyols (1983), A: domain with an Ordovician succession of moderate thickness; B: West-Asturian furrow; C: domain with the 'Armorican' quartzite facies unconformably overlaying the Precambrian-Cambrian basement, D: domain without 'Armorican' quartzite facies. b) Scheme proposed by Hamman et al. (1982), A: Northeast Iberian region (1: Cantabro-Ebro rise; 2: Navia-Alto Sil domain; 3: Mondoñedo-Peñalba domain); B: West-Iberian region, (4: Truchas-Central System domain; 5 and 6: Central Iberian domain; 7,8 and 9: Ossa-Morena domain).

been included in the Northeast Region. This region is characterised by Lower Ordovician rocks conformably overlying a Precambrian-Cambrian substratum and a thick succession of turbidites deposited during the Caradoc, the latter is not found in the other two regions of the Iberian Massif.

a.1.The Cantabro-Ebro Rise. This is exposed in the Cantabrian Zone. Upper Ordovician volcano-sedimentary rocks (Castro Formation) at the western border of the Cantabrian rise and the approximately coeval sedimentation of turbidites (Agüeira Formation) in the West Asturian trough may indicate that uplift and (?)erosion started during the Caradocian (Julivert et al. 1972b, Hamman et al. 1982). No unconformity is found between the Ordovician succession and the transgressive Silurian deposits.

a.2.The Navia-Alto Sil Domain. This corresponds to the main 'furrow' of the West Asturian trough. During Caradocian to Ashgillian times water depths reached a maximum relative to that during the Lower-Middle Ordovician. A turbidite succession (Agüeira Formation) was deposited in the basin by relative uplift of the adjacent Cantabrian rise and probably the Mondoñedo-Peñalba rise.

At the end of the Ashgillian-early Silurian shallow-water conditions were established with deposition of sandstones (Vega de Espinareda Quartzite Formation) without any discernible stratigraphical gap.

a.3.The Mondoñedo-Peñalba Domain. Different sequences and stratigraphical gaps exist showing different uplift and erosional episodes during late Ordovician when this domain temporarily became an emerged ridge. In some areas (e.g. Sil syncline) a brief transgression is represented by shallow water sediments (Guiana Limestone Formation) deposited during the Ashgillian. Others areas may have remained emergent till the beginning of the Silurian but there is little evidence for this since a second erosional period took place prior to the late Ashgillian-Silurian transgression (Irüela Formation) and the deposits could have been eroded.

a.4. The Truchas Domain: This area seems to belong to the Northeast Iberia Region during the Upper Ordovician even if most of the succession is lacking. The presence of Caradocian turbidites (Agüeira Formation) suggests similar conditions to those in the Navia-Alto Sil Domain but Llandoverian shales overly the Agüeira Formation with erosional unconformity.

b.The West Iberian Region. This is characterised by the existence of an angular unconformity between the Lower Ordovician and its substratum. Considering the Upper Ordovician succession, this region comprises the eastern Central System in the West Asturian-Leonese Zone, the Central Iberian Zone and the northern part of the Ossa-Morena Zone (the Portalegre-Montoro area).

b.1. The Central System. The Upper Ordovician succession comprises shelf deposits. An erosional unconformity is suspected at the Ordovician-Silurian boundary.

b.2. The Central Iberian Zone. This zone corresponds to a wide shelf with different types of shallow water sediments (e.g. Botella Quartzite Formation, Bancos Mixtos or Mixed Beds Formation) with some brief transgressive episodes (e.g. Cantera Shales). Emersion of the basin took place during the Late Ashgillian after the deposition of shallow water limestones (Urbana Limestones Formation). Upon the erosional surface a succession of black shales and siltstones with slumps (Chavera Shales Formation) and sandstones (Castellar Quartzites Formation) represent the beginning of the Silurian transgression.

b.3. The Northeastern Ossa Morena Region. The upper portion of the Ordovician succession can be lithologically compared with the Upper Ordovician sequence of the eastern Sierra Morena (described in b.2.). This succession is (?)unconformably overlain by a late Ashgillian-early Silurian quartzite (Hamman et al., 1982, Julivert and Truyols, 1983, Herranz, 1984).

c.The Southwestern Ossa Morena Region. This is separated from the Portalegre-Montoro area by the Porto-Badajoz-Cordoba Shear

Band. The Upper Ordovician succession in this region consists of a heterolithic sequence ("Greywackes and sandstones") which is overlain by limestones ("Pelmatozoan Limestone"). The whole succession is lithologically compared with that in the eastern Sierra Morena but palaeontological data support the palaeogeographical singularity of this region (Gutierrez-Marco et al., 1984). The Ordovician-Silurian boundary is thought to be located in a sequence of shales (Valle Shales Formation) resting (?)unconformably upon the limestones.

2.3.2.Magmatism.

The occurrence of Upper Ordovician-Lower Silurian volcanic rocks is ubiquitous in the whole Hesperian Massif. The metavolcanites are lavas, ignimbrites and tuffs interbedded in the metasedimentary succession. Pre-Hercynian plutonic rocks occur mainly in the northwestern portion of the Central Iberian Zone and it is associated to the Badajoz-Cordoba Band in the Ossa Morena Zone. Being metamorphosed in the Hercynian events, they appear as orthogneisses of variable composition (basic, intermediate, acid, hyperalkaline) (Corretgé, 1983).

a.Cantabrian Zone. Interbedded basic lavas and tuffs are found in the Castro Formation (Succession vulcanodétritique, Julivert and Truyols, 1972).

b.West Asturian-Leonese Zone. Rhyolites and albitophyres occur at the top of the Agüeira Formation outcropping in the Truchas syncline (Matte, 1964).

c.Central Iberian Zone.

c.1. Volcanic rocks. Transitional to alkaline basalts (protoliths of eclogites and orthoamphibolites), outcropping in some catazonal complexes in northwestern Iberia (e.g. the Blastomylonitic Graben), could be emplaced during the Upper Ordovician-Lower Silurian time span. Peralkaline rhyolites and

tholeiitic MORB-type basalts are adjacent to some of these complexes (Ribeiro, 1987).

Volcanic formations are found at the bottom of the Silurian succession in the Cabo Ortegal and Alcañices synclines. They consist of dacites and rhyolites (Ancoechea et al., 1988) with compositions plotting close to the volcanic arc/intraplate granites boundary in the Rb versus Y+Nb diagram of Pearce et al. (1984).

Dolerites and tuffs have been described in the Upper Ordovician succession (Porto do Santa Ana Formation) outcropping in the Buçaco syncline in Portugal (Mitchell, 1974).

Dolerites and alkaline basalts occur at the base of the Silurian succession upon the Criadero Quartzite Formation (the host rock of the Almadén Hg deposit, Saupé, 1990).

Rhyolitic tuffs are found interbedded in the Caradocian-Ashgillian succession in eastern Sierra Morena (Charpentier, 1976).

c.2. Plutonic rocks. Radiometric data for orthogneisses from the polymetamorphic massifs in Galicia and Portugal suggest emplacement of alkaline and calc-alkaline granitoids and granodiorites with some minor amounts of peralkaline rocks during the Upper Ordovician-Lower Silurian (Priem et al., 1970, Kuijper et al, 1982 among others) as part of a major event of peralkaline to calc-alkaline plutonism that took place between 500 and 400 Ma (Van Calsteren et al., 1979; Van der Meer Mohr et al., 1981). Hybridization with gabbros and diorites is also associated with this magmatic pulse.

d.Ossa Morena Zone. Upper Ordovician-Lower Silurian peralkaline and calc-alkaline granites are spatially related to the Badajoz-Cordoba Blastomylonitic Band (Bellon et al., 1979; Dupont et al., 1981; Pinto, 1984; Pinto and Andrade, 1987).

f.South Portuguese Zone. There are no outcrops of magmatic rocks older than the Upper Devonian-Carboniferous volcanic series which are ascribed to the Hercynian magmatism (*s.s.*).

2.3.3.Metamorphism.

Evidence of Palaeozoic pre-Hercynian stages of metamorphism are mostly found in the polymetamorphic massifs of northwestern Iberia. Formation of B-type eclogite facies (600 °C, 10-11 kb, M_O phase; Kuijper, 1979) took place 1000-600 Ma ago, apparently with no relation with Palaeozoic orogenic events. A long period of infracrustal metamorphism (from 500 to *ca.* 290 Ma ago) giving as result high-P granulite facies (M1 phase, starting about 500 Ma ago, ending about 400 Ma ago), hornblende-granulite facies (M2 phase: 400 to 350 Ma ago), amphibolite facies (M3 phase, *ca.* 310 Ma ago) and greenschist facies (M4 phase: *ca.* 290 Ma ago) has been suggested by several authors (e.g. Van Calsteren et al., 1979, Van Der Meer Mohr et al., 1981, Kuijper and Arps, 1983). This tectonometamorphic evolution together with the magmatic history are interpreted (e.g. Van Der Meer Mohr et al., 1981; Kuijper and Arps, 1983) as being caused by the emplacement of a 2^{nd} order diapir from a mantle plume about 500 Ma ago. Alternatively, the high-P metamorphism has been related to an early, pre-collisional, subduction event (Gil Ibarguchi and Ortega Girones, 1985; Vielzeuf and Pin, 1989; Peucat et al., 1990; Arenas, 1991 among others).

2.3.4.Mineral Deposits.

Several strata-bound mineral deposits are located in the Upper Ordovician-Lower Silurian sequence, most of them close to the Ashgillian erosional unconformity. They are spatially related with volcanics but the genetical relationship remains unknown. Only one of them (Almadén) has been the subject of intensive study. The rest, even if frequently cited, appear in the literature almost as curiosities. Analytical data are very scarce and hypotheses about genesis are highly speculative.

a.The Almadén Mercury Deposit (Saupe, 1990). Almadén is the largest known mercury deposit in the world having produced more than 250,000 metric tons. It is located in the Central Iberian Zone, between the Montes de Toledo and Sierra Morena. The ore basically consists in three strata-bound impregnations in the Criadero Quartzite Formation (Llandovery in age) which is adjacent to a lens (up to 60 m. thick and about 300 m. diameter) of phreatomagmatic breccia, the so-called 'Frailesca', roughly conformable with the stratigraphic sequence (Fig.2.3). Cinnabar is by far the major sulphide constituent with some native mercury, pyrite and subordinate metacinnabar. Alkaline dolerites and basalts overlying the ore show strong carbonatisation and sericitic alteration whereas the overlain, the intercalated and the overlying shales are not hydrothermally altered. Stable isotope geochemistry is not conclusive. The carbon and oxygen isotope data from carbonates yield an average of $\delta^{13}C_{PDB} = -6.1 \pm 1.3$ $^{o}/_{oo}$ and $\delta^{18}O_{SMOW} = +15.6 \pm 15$ $^{o}/_{oo}$ (Eichmann et al., 1977) and do not indicate whether the CO_2 was derived from the mantle or from hydrolysis of organic matter. The measured $\delta^{34}S$ values for cinnabar are in a range of +4.5 - +9.0 $^{o}/_{oo}$ which has been considered by Saupe (1990) as undiscriminating among 'juvenile' or 'sedimentary' sources. The ore-forming processes seem to be related to Hg remobilisation from Ordovician black shales, likely enhanced by phreatomagmatic explosions. Calvo and Guilemany (1975) showed an alternative interpretation involving participation of 'magmatic' sulphur and molten-phase transport of mercury.

b.Antimony deposits. Villarbacú (Caurel Domain, West Astur-Leonese Zone) is the most important antimony occurrence. The mineralisation is located at the top of the La Aquiana Limestone Formation of Ashgillian age (Gillou, 1969). The paragenesis is very simple: stibnite, berthierite, pyrite. Stibnite is commonly found associated with quartz segregations. Berthierite is subordinate. The origin of this mineralisation has been interpreted as synsedimentary and related to acid volcanism (Gumiel, 1982) and probably took place during the Caradocian-

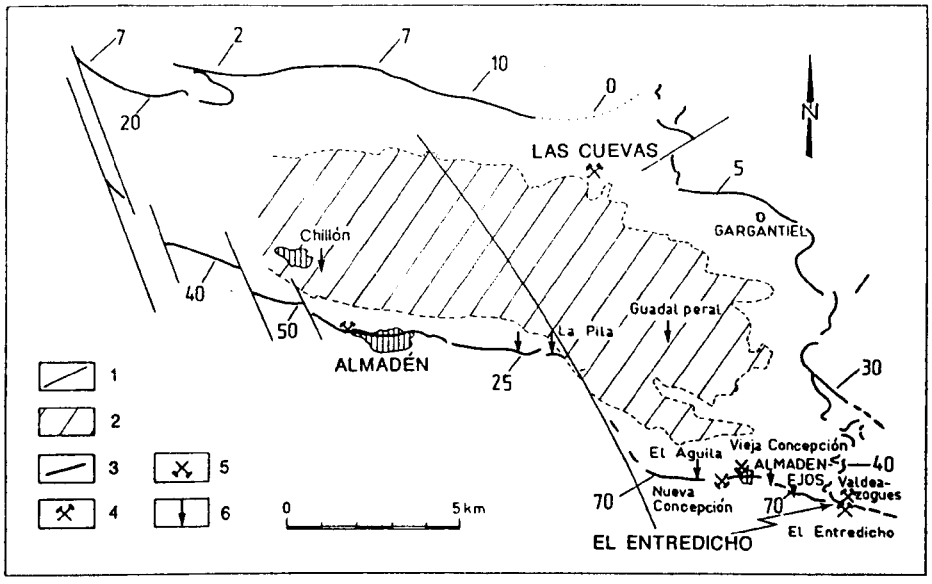

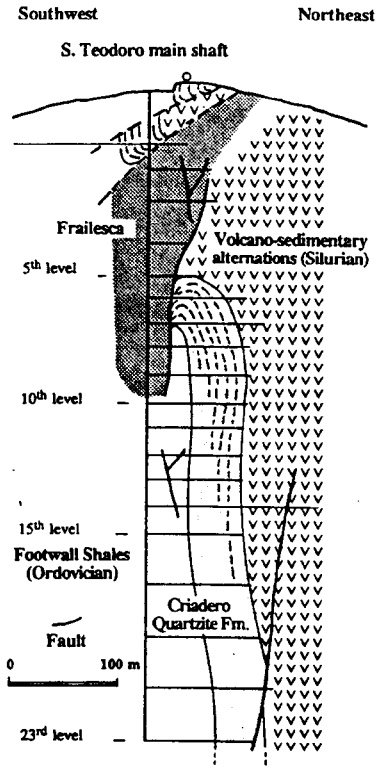

Fig.2.3. Almadén district. a) Outcrop map of the Criadero quartzite and location of mercury mines in the Chillón syncline. 1: faults, 2: Devonian, 3: Criadero quartzite, 4: active mine, 5: abandoned mine; 6: prospect or showing. b) Vertical cross section trough the Almadén mine (From Saupé, 1990).

Ashgill as there are some Sb occurrences in the interbedded rhyolites (Guillou, 1971).

Antimony, absent from the Almadén ore (*s.s.*), is found in two localities near the mercury deposit. In the Balanzona Mine (Cordoba), the mineral association is limited to quartz, stibnite and its oxidation products filling small fractures (Gumiel, 1982; Gumiel and Arribas, 1987). The paragenesis in Los Accesos Mine (Cordoba) consists of arsenopyrite, chalcopyrite, famatinite and dominant stibnite. Berthierite is scarce. Cinnabar is absent in both deposits. The host rock in the Balanzona Mine is the Criadero Quartzite Formation (Llandoverian age), the ore in Los Accesos is hosted by the Estratos Mixtos Formation which is Caradocian-early Ashgillian in age. The genesis of both deposits is related to submarine hydrothermal activity associated with mafic volcanism (Gumiel and Arribas, 1987).

c.Base-metal deposits. Gillou (1971) reported the occurrence of galena in La Aquiana Formation in El Caurel where there is a spatial relationship between ore and dolomitisation. There is no apparent relation with the antimony deposit.

Zn-Pb stratabound mineralisations are also found in the Urbana Limestone Formation in the southern part of the Central Iberian Zone (Puertollano syncline and El Centenillo-Santa Elena area). The mineral paragenesis consists of dominant sphalerite, galena, chalcopyrite and pyrite with dolomite and quartz. A syn-diagenetic origin has been proposed (Rios, 1977, Palero and Martin-Izard, 1988) likely related to the interbedded acid volcanic rocks. Jacquin and Pineda (1980) and Pineda (1987) pointed out the occurrence of barite-sphalerite-galena-pyrite parageneses which are locally related to intraformational breccias. A similar sphalerite-galena-pyrite association has been reported in the Castellar Quartzite Formation (= Criadero Quartzite) (Rios and Claverias, 1979). Zn-Pb deposits are also found in the Upper Ordovician-Lower Silurian successions in the Celtiberian range.

d.Iron (Manganese). The Ashgillian erosional unconformity commonly shows supergene Fe-(Mn) ores deposited in palaeokarsts developed on the Urbana Formation or the La Aquiana Formation (Gillou, 1971, Tamain, 1972). The mineral paragenesis basically comprises Fe oxides and hydroxides and Mn minerals. Siderite, ankerite, dolomite and calcite may be present. The ore appears as massive irregular bodies, irregular masses with breccias (fragments of quartzite, limestone, shales) and karstic fillings. Mineralisation may be associated with dolomitisation of the host limestone. Time of deposition is controversial. An early karstification and concentration could have taken place during the basin emersion in the Ashgillian times. Alternatively, iron supergene concentration could have taken place in the post-Variscan erosional periods prior to Lower Triassic terrigenous deposition. This later hypothesis is supported by the occurrence of similar deposits in Upper Palaeozoic limestones. For example, in the Sierra Menera (Celtiberian range, Astur-Occidental Leonese Zone, Zitmann and Newmann-Redlin, 1976) occurs an economically important ore in Ashgillian dolostones. As Upper Carboniferous dolostones are also ore-bearing, the time of mineralisation can be confined to Upper Carboniferous-Permian.

Other minor non-supergenic iron occurrences have been found (disseminated pyrite is common elsewhere). Pyrite-magnetite rich thin beds in Linares-La Carolina will be described in detail in the following chapter.

2.3.5.Synthesis. Geodynamic setting.

After a period of relative tectonic inactivity from Early Ordovician to Middle Ordovician, a time of crustal instability began. Tectonic units with different rates of uplift and subsidence and with associated bimodal volcanism (alkaline to calc-alkaline) developed in the upper continental crust.

During Caradocian and part of Ashgillian times, the Hesperian Massif was an extensional marine basin with three individualised domains: 1) The West Asturian trough and marginal areas (the

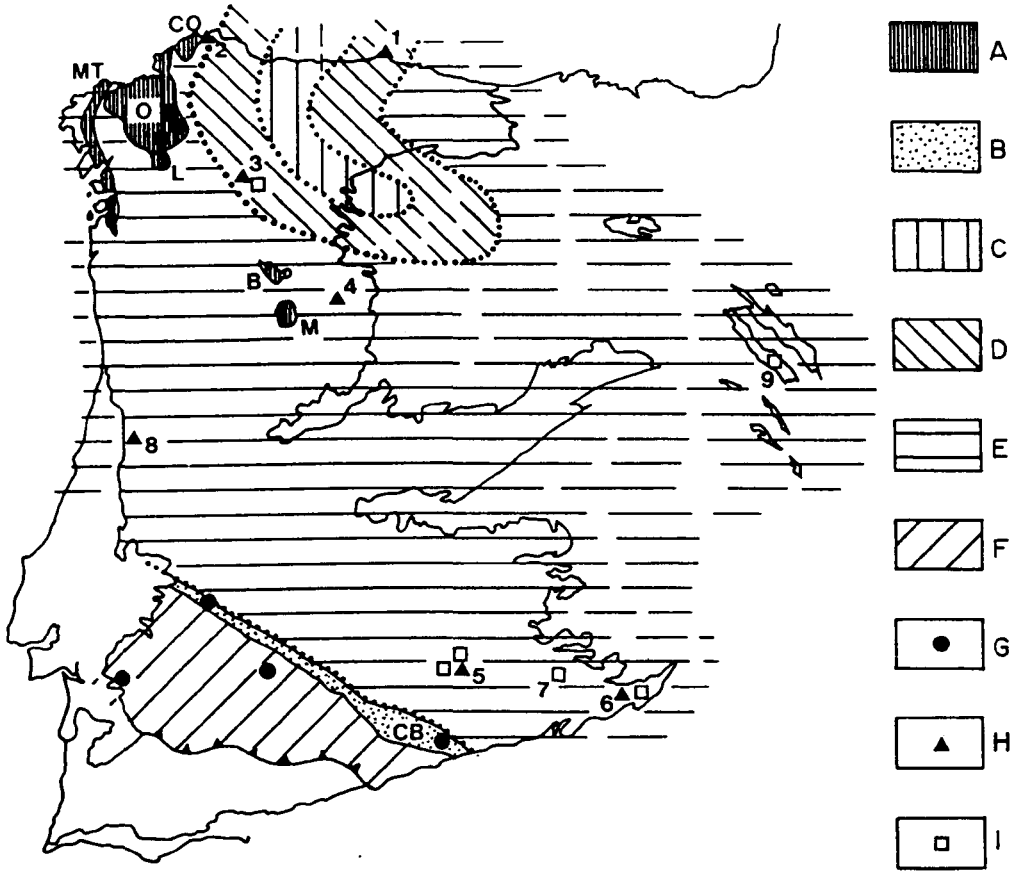

Fig.2.4. Upper Ordovician-Lower Silurian palaeo-geographical domains of the Hesperian Massif. A: allochthonous polymetamorphic complexes (CO: Cabo Ortegal, O: Ordénes, L: Lalín, B: Bragança, M: Morais, MT: Malpica-Tuy); B: Córdoba-Badajoz shear zone (CB); C: West-Asturian trough (WAT); D: marginal areas of the trough (MPT); E: West-Central Iberian shelf (WCIS); F: South Iberian shelf (SIS); G: granitoids, H: volcanic rocks; I: stratabound ore deposits. Localities: 1.Cabo de Peñas, 2.Ortegal, 3.El Caurel, 4.Alcañices, 5.Almadén, 6.El Centenillo-Santa Elena, 7.Puertollano, 8.Buçaco.

Northeast-Iberian Region), 2) The West-Central Iberian Shelf and 3) The South Iberian Shelf. (Fig. 2.4.)

The West Asturian trough started to subside in the Cambrian (Julivert and Truyols, 1983). It was during the Caradocian-Ashgillian interval when subsidence rates were highest, that the basin evolved to a turbiditic basin without continuity to the southeast (in terms of present configuration of the massif). Facies variations and palaeocurrent data indicate increasing depth to the north and they reflect the local extension of the furrow which would be bounded by the uplifted Cantabrian rise, and Mondoñedo-Peñalba and Truchas Domains. In these marginal areas there is evidence of emersion during the Caradocian-early Ashgillian (Hamman et al., 1982, Julivert and Truyols, 1983 and references therein).

The West-Central Iberian Shelf, surrounding the West-Asturian trough on the west, south and likely the east, was a wide epicontinental basin that recorded some sea-level changes although the depth remained within those ranges considered typical of epicontinental seas. Relatively stable shelf conditions, with remarkable lateral continuity of formations and facies, developed from the Lower Ordovician to the Upper Ordovician (Brenchley et al., 1986, Portero and Dabrio, 1988).

The South Iberian Shelf was a basin with similar sedimentary conditions but with diferent fauna to those encountered in the West Central Iberian Shelf (Gutierrez-Marco et al., 1984) and likely to have been located far away from the West-Central Iberian Shelf (Paris and Robardet, 1990).

Emersion during the late Ashgillian was general throughout the basin. Shales overlying the unconformity reflect uniform depth conditions in a still tectonically unstable basin. The Ashgillian emersion has been related to glacioeustatic sea-level changes during a period of intensive faulting in an extensional regime (Julivert, 1983d, Portero and Dabrio, 1988).

There is no evidence for compressional tectonics in the upper crustal evolution of the basins. An extensional supracrustal regime is generally acknowledged (Julivert and Truyols, 1983; Van Der Meer Mohr et al., 1981 among others).

During the time span considered, high-P granulite facies and B-type eclogite facies metamorphism took place in the lower part of the crust associated with migmatisation and hybridation of magmas producing alkaline and calc-alkaline granitoids which intruded higher levels of the crust.

There is some evidence for oceanic crust created during Upper Ordovician-Lower Silurian times. Ophiolitic complexes with oceanic affinity are found in the allochthonous polymetamorphic units in northwestern Galicia and Portugal. They are thought to represent remains of an ocean located on the west of the actual Hesperian Massif (Iglesias et al., 1983).

Several geotectonic settings can be proposed:

a.Continental rifts not associated with destructive plate margins (plume-rift system model, Fig.2.5.a). This model has been developed by the Leiden Group (Van der Meer Mohr et al., 1981, Kuijper et al, 1982, Arbs and Kuijper, 1983). These workers explain both supracrustal and infracrustal histories as a consequence of a mantle plume which reached the base of the lithosphere. Heat and volatiles derived from second-order diapirs emplaced in the lower continental crust gave as a result high-P granulite metamorphism, migmatisation and magmatic hybridation (calc-alkaline to peralkaline granitoids and gabbroids lherzolite-derived). Local uplift and subsidence with formation of furrows and generation of a limited amount of oceanic crust could be due to crustal arching upon the emplacement of the second-order diapirs.

The Hercynian crustal shortening induced the progressive emplacement of the metamorphosed infracrustal rocks in upper levels by inyective folds (Weber, 1984) (Fig. 2.5.a).

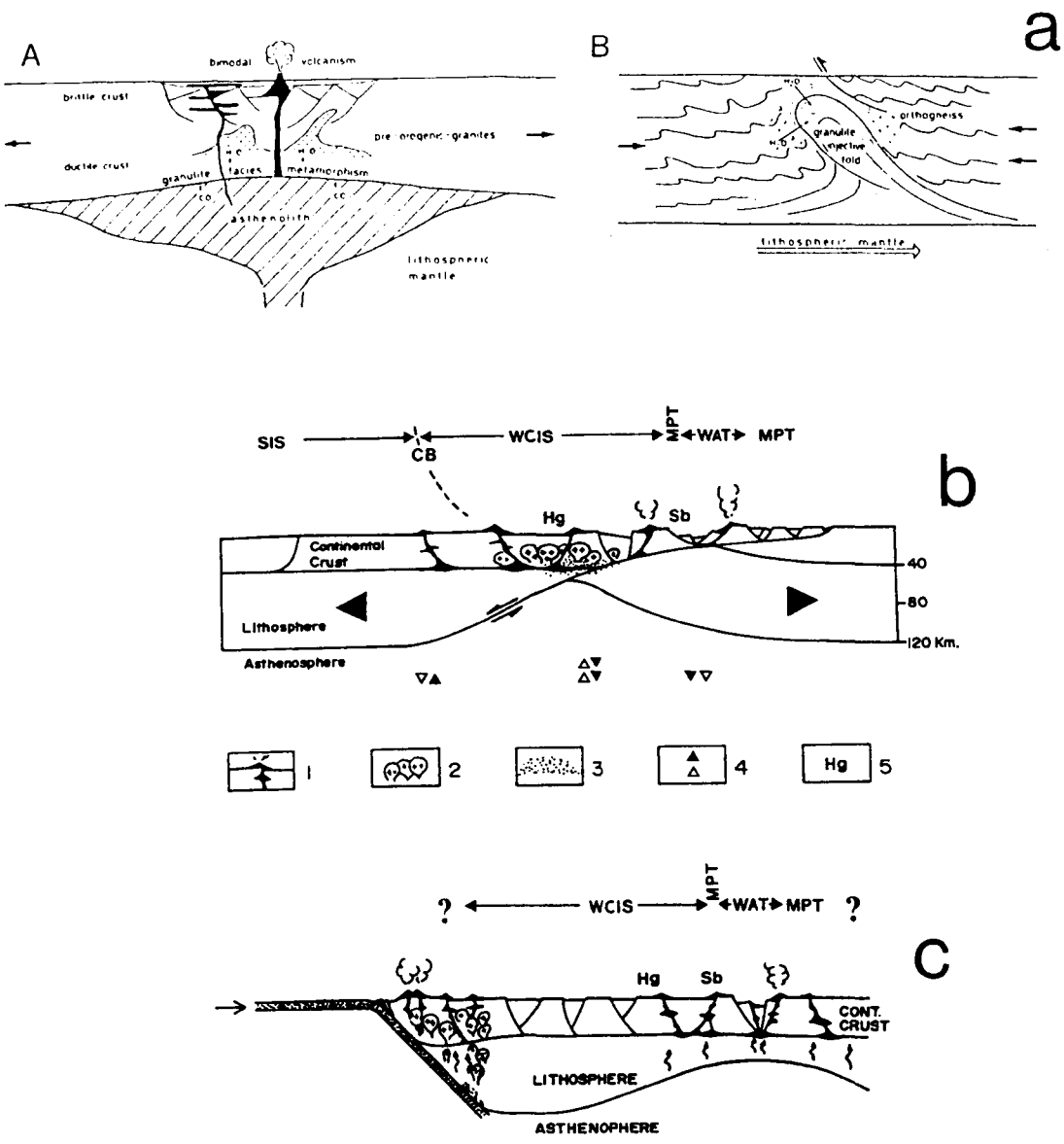

Fig.2.5. Proposed geotectonic settings of the Hesperian Massif during the Upper Ordovician-Lower Silurian. a) Plume-rift system model and emplacement of granulites by Variscan injective folds (from Weber, 1984). b) large-scale detachment model (partly based on Wernicke, 1985). c) Active continental margin/marginal basin model. 1: volcanoes, 2: granites, 3: high-grade metamorphism, 4: tectonic subsidence (solid triangles) and thermal subsidence (outlined triangles), 4: ore deposits. CB: Córdoba-Badajoz shear zone; WAT: West-Asturian trough; MPT: marginal areas of the trough; WCIS: West-Central Iberian shelf (WCIS); SIS: South Iberian shelf (SIS).

This model accounts for the lack of well developed ophiolites; continental volcanic-arc and slope prisms, and rare occurrence of high-P/low-T facies metamorphism in the Hesperian Massif. But it fails to account for the Variscan deformation style and the emplacement of the high-P rocks as unroofed allochtonous units in the upper crustal levels even if high-P granulites (formed at 7-11 kb and 700-850^{o}C conditions) could be produced under stretching conditions at the base of an approximately 30-40 Km thick continental crust.

b.Extensional basins on simple shear systems involving lithosphere (Fig.2.5.b). This case can be considered as a variation of the ensialic model discussed above as subduction processes are not involved. It is based on the simple shear model of Wernicke (1985) where extensional detachments can affect the entire lithosphere. This setting has been outlined by Doblas and Oyarzun (1990) as a part of a major extensional province developed further east from the Caledonian foldbelt in continental Europe.

An extensive low-angle detachment, beneath normal fault systems, has affected the crust and lithosphere. The sedimentary basin so formed is segmented into several zones with different subsidence/uplift evolution as thinning of crust, thinning of mantle lithosphere or both may occur. In that zone where only the mantle lithosphere is thinned, uplift and doming of the surface occur and the asthenosphere may reach the base of the crust. The heat anomaly under the crust would induce high-P granulite metamorphism and anatexis (calc-alkaline to peralkaline granitoids and grabboic partial melt-products) by raising the temperature in the surroundings. In late stages high-P granulites and B-eclogites would be emplaced in the upper crust as allochtonous imbrications by inverse reactivation of the detachment during the folding Variscan stages.

This model accounts for some of the points unsolved by the plume-rift system model, like longitudinal features of the basin (e.g.furrows), evolution and supracrustal emplacement of the polymetamorphic massifs, style of deformation and occurrence of

blastomylonitic bands (e.g. Badajoz-Cordoba Band) spatially related to granitoids. The main criticism is the weak justification for the high-P metamorphism.

c.Marginal basins in destructive continental margins (Fig. 2.5.c). This model explains the crustal evolution as a consequence of subduction processes acting in a continental margin. Dominant supracrustal extension in destructive margins can be attained when the subduction angle is steep (Megard and Philip, 1976). This geometry may result in intense volcanism and formation of marginal basins subparallel to the margin as proposed by Åberg et al., (1984) for Central Chile. In this scenario, high-P granulite and eclogite facies metamorphism are induced by the subducted slab and alkaline to calc-alkaline magmatism takes place in the continental plate. The marginal basin evolves to an aborted marginal basin, with moderate thinning of the continental crust without (or very little) generation of oceanic crust.

In the late stages (Silurian-Devonian) decoupling of the oceanic plate would result in an early Variscan compressional stage with obduction of the oceanic crust.

The model accounts well for the high-P metamorphism, alkaline to calc-alkaline plutonism, volcanics with intermediate compositions between those considered as typical of intraplate and those typical of island-arc, and ophiolitic complexes with MORB signatures.

This geotectonic setting was established by Cadomian times (Pinto and Andrade, 1987). The commonly acknowledged collisional model for the Variscan orogen (Dewey and Burke, 1973, Riding, 1974, Bard et al., 1980, Matte, 1986 among others) is based on the assumption of the existence of oceanic crust, destructive margins and continental plates. But some problems remain to be explained if these models are considered: the lack of well developed ophiolitic complexes , volcanic arc terrains and slope prisms.

The geodynamic settings presented here are not conclusive as they do not still offer explanation for the whole of magmatic, tectonometamorphic and sedimentological features. In addition, palaeomagnetic data from this Massif relative to the Palaeozoic times are rare and the reconstructions differ between them (*c.f.* Morel and Irving, 1978, Scotese et al., 1979, Smith, 1981; Van der Voo, 1982, Zonenshain et al, 1985).

2.4.Late Hercynian events.

Those sedimentary, magmatic and tectonic events, which took place after the last Hercynian main folding phase (late Westphalian D-Stephanian A) and before the start of the Alpine cycle (represented by the Buntsandstein sedimentation), are relevant for the purpose of this thesis. As the base of the Buntsandstein succession is diachronous (late Permian to Ladinian), only those events during the late Stephanian-Permian will be considered as "late Hercynian" in *sensu stricto*. But it must be noted that some of the events could start during the early Stephanian in some areas of the Massif.

2.4.1.Sedimentation.

Early Permian continental sediments rest unconformably on the Carboniferous with the exception of some areas where Autunian rocks conformably overlay Stephanian formations (Fig.2.6). This feature is in relation to the development of local transtensional basins as semigrabens with different subsidence. Virgili et al., (1983) and Sopeña et al., (1988) summarised the basin evolution during the Permian in Iberia. Three zones relative to the Hesperian Massif (i.e. excluding Pyrenees) have been distinguished:

a.Cantabrian zone. Upper Stephanian molassic sediments (Cordel Formation) exist adjacent to strike-slip faults. They are unconformably overlain by an early Permian succession which consists of two units separated by an unconformity (Martinez

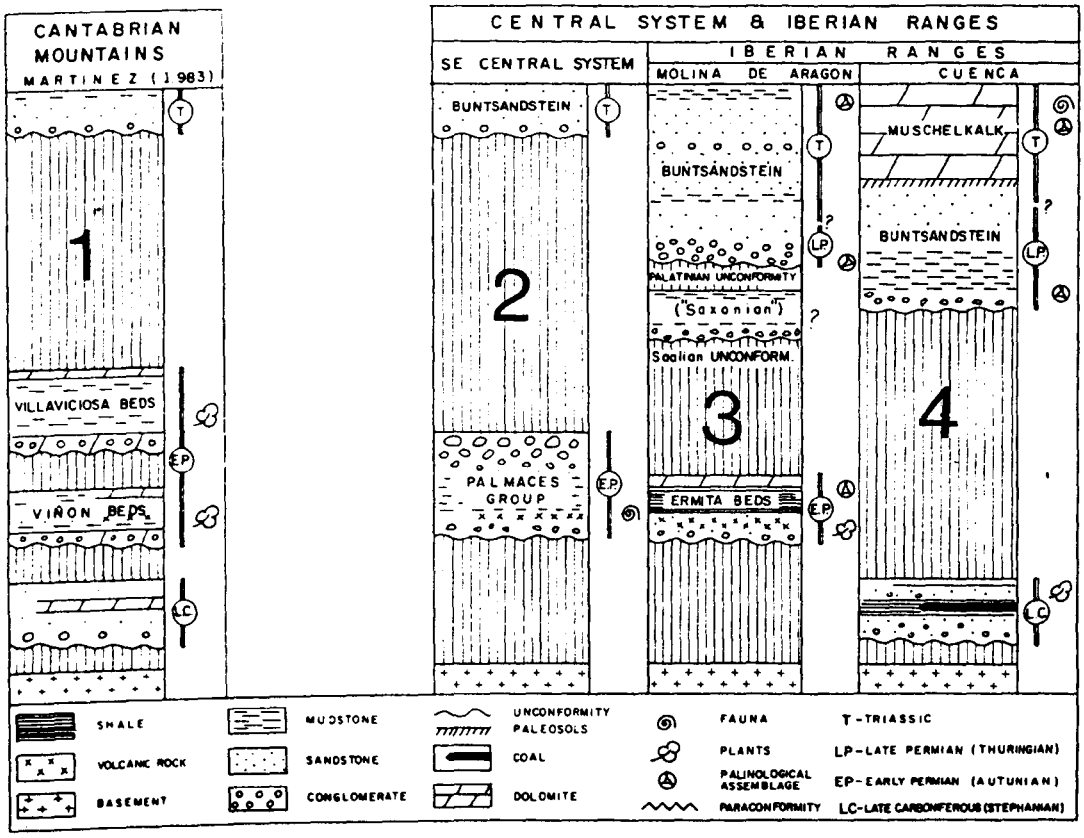

Fig.2.6. Early and Late Permian sediments of selected areas in the Hesperian Massif and their mutual relationships (From Sopeña et al., 1988). Striped areas indicate hiatus.

García, 1983a). The lower unit (Capas de Viñón Formation) up to 500 m. in thickness, contains limestones, conglomerates, sandstones, mudstones and grey and black marls with some interbedded volcanites. The upper unit (Capas de Villaviciosa Formation) exhibits variable thickness, from a few m. to 600-700 m. This formation consists of feldspathic quartz conglomerates, sandstones, "caliche" limestones, red shales and limestone conglomerates. Both units contain Autunian floras. The whole succession displays alluvial fan, fluvial and lacustrine facies related to fault-bounded basins.

b.Central System margins and the Celtiberian range. The Permian succession of the northeast margin of the Central System contains more than 2000 m. of sediments including volcanites at the bottom (Hernando, 1977). A coarsening-upward megasequence of mudstones, sandstones and conglomerates is interpreted as alluvial fans and fault-bounded basin fillings. The semigraben of Pálmaces at the southeast margin of the Central System, displays a 700 m. thick coarsening-upward sequence of mudstones, sandstones and conglomerates with several prograding alluvial fan cycles (Palmaces Group, Sopeña, 1979) where macro and microflora yielded an Autunian age. A minor basin (Valdesotos-Tamajon) is located at the southeast margin of the Central System consisting of 400 m. thick succession of alluvial fan deposits and lacustrine beds.

The Autunian succession of the Celtiberian range differs from those commented on above. The Molina de Aragon basin consists of up to 300 m. of sediments (Capas de la Ermita Formation; Ramos, 1979) which have been grouped into three units, from bottom to top: 1) Volcaniclastics with conglomerates and mudstones, 2) lacustrine deposits, dark mudstones and fine volcaniclastics and 3) dolomites, sandstones and mudstones evolving to dolomites with siliceous concretions. This succession is interpreted as deposited in an arid lake. Palynofloras indicate Autunian age. The Capas de la Ermita Fm. is unconformably overlaid by a 'Saxonian' succession (Capas de Montesoro Fm.; Ramos, 1979) of several tens of meter in thickness. It consists of breccias at the basal beds and mudstones

with interbedded sandstones and conglomerates. The Capas de Montesoro Fm. is unconformably overlain by the Bundsandstein succession. The basal beds of this succession are diachronous and consist of conglomerates and sandstones deposited in alluvial fans and low-sinuosity fluvial systems. Palynofloras indicate Thuringian age for the lowermost Bundsandstein beds in some sectors of the Celtiberian Range (Virgili et al., 1983, and references therein).

c.Southern margin of the Hesperian Massif. Several small basins occur at the north of the province of Sevilla. One of them, the Rio Viar basin, is a semi-graben caused by a NNW-SSE-oriented dextral transcurrent fault system. The succession consists of basal basic volcanic beds overlain by red conglomerates, sandstones and mudstones with interbedded volcanites. Macro and microflora indicate Autunian age (Broutin, 1981).

The succession in other basins of this area consists up to 100 m. of sandstones, conglomerates, mudstones and coal seams of fluviolacustrine origin.

2.4.2.Magmatism.

2.4.2.1.Plutonism.

On the basis of lithological, geochemical, structural and geochronological features relative to Hercynian plutonic rocks, the Hesperian Massif may be divided into three regions or domains: Northern Domain, Central Domain and Southern Domain (fig 2.7). Late-Hercynian plutonism in these domains is summarised as follows (see Corretge, 1983 and Bea et al., 1987 for an extensive treatment of the plutonism in the Hesperian Massif):

a.Northern Domain. This region comprises the Cantabrian Zone, West Asturian Leonese Zone and the Galician-Castillian zone (*sensu* Lotze, 1945). In the northwest region of Spain some two-mica alkaline granitoids may have been emplaced during the Upper Stephanian-Lower Permian time span, but the late-Hercynian plutonism (*s.s.*) is mainly represented by calc-alkaline granitoids

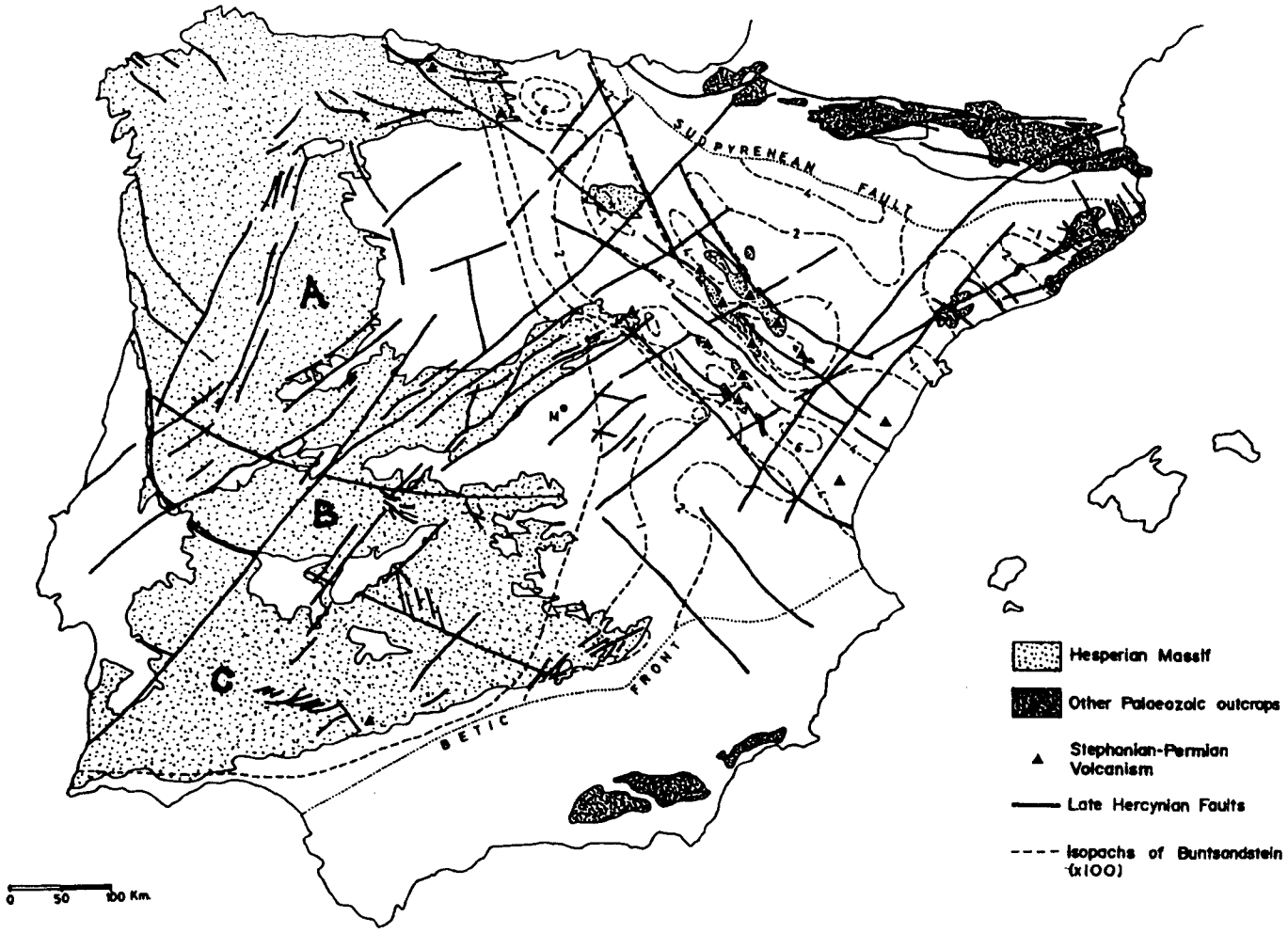

Fig.2.7. Late-Hercynian fault systems and location of Stephanian-Permian volcanic rocks. Isopachs of the Buntsandstein show the structural control of the basin by the Late-Hercynian faults, defining the so-called 'Celtiberian corridor' or 'Celtiberian rift' (based on data from Alvaro et al., 1979; Capote, 1983c; Muñoz et al., 1983; Sopeña et al., 1983). A, B, C are the plutonic domains in the Hesperian Massif.

with dominant biotite. The late-plutonism in this area is quantitatively less important than that in the north of Portugal, where the so-called 'younger' granites occur. This group comprises basically two-mica calc-alkaline to alkaline and biotite granites with basic and intermediate precursors (gabbros and diorites).

b.Central Domain. This region corresponds to the East Luso-Alcudian Zone (Lotze, 1945). Late-Hercynian plutonism consisting mainly of calc-alkaline granitoids with dominant biotite is similar to that in the Galician-Castillian sector.

c.Southern Domain. This region is characterised by the common association of basic and acid plutonic rocks, the abundance of basic complexes and the occurrence of hyperalkaline granitoids, some of them emplaced during the Lower-Middle Permian (e.g. the Sierra Vieja Massif, Dupont et al., 1981)

2.4.2.2.Volcanism.

Most of the late-Hercynian volcanism is associated with large faults. Volcanic rocks are interbedded in the Autunian sediments outcropping in the Cantabrian Zone, Celtiberian range and Ossa Morena Zone (Fig.2.7). Muñoz et al., (1983) and Navidad (1983) have summarised some features of this volcanism:

a.Cantabrian Range. Olivine basalts, and other basic lavas and intermediate to acid rocks of alkaline character (rhyodacites, quartz-trachytes, quartz latiandesites, mugearites and hawaiites) are found interbedded in the Autunian succession (Martinez García, 1983b).

b.Margins of the Central System and Celtiberian Range. Stephanian-Autunian volcanic rocks consist of rhyolites, dacites, andesites, basaltic andesites and basalts. They occur as pyroclastics, lavas, dykes and domes. The climax of the volcanic activity took place by the Stephanian-Autunian boundary with residual activity during the Autunian (Muñoz et al., 1983).

c.Ossa-Morena Zone. Basic lavas are found at the bottom of the Autunian sedimentary sequence in the Rio Viar Basin (Broutin, 1983).

2.4.3.Tectonics.

The late-Hercynian tectonism is characterised by a variety of compressional, extensional and transcurrent features. Extensional features include dyke swarms and shear zones. Compressional structures are folds, kink-bands, crenulations and flat-lying foliation within granitoids. Transcurrent features consists of brittle faults trending NE-SW/NNE-SSW; NW-SE/NNW-SSE and E-W/ENE-WSW (Arthaud and Matte, 1975; Capote, 1983c; Doblas, 1991 among others) (Figs. 2.7)

The compressional and transcurrent deformations are interpreted as taking place during early Stephanian to Lower Permian as a result of a continental-scale shear zone (Arthaud and Matte, 1975) or a Himalayan-type collision (Lefort and Van Der Voo, 1981).

The extensional features are mostly ascribed to a distensive stage starting in the Upper Permian as the Bundtsandstein facies were deposited in extensional basins (e.g. Alvaro et al., 1979, Sopeña et al., 1988). However, extensional features like dyke swarms have been related to an early extensional stage by Doblas (1991). That author has suggested a model for late-Hercynian evolution of Central Iberia during the considered time span. This model is based on an early extensional event involving lithosphere-scale low-angle detachment systems which is postdated by a ductile-transcurrent episode with E-W-oriented compressional stresses. Finally, a brittle-transcurrent event with a N-S-oriented compression associated to a continental shear zone took place (Fig. 2.8).

2.4.4.Synthesis.

After the main Hercynian folding phases, the Iberian Variscan building underwent a stage of fracturing and breakup during the

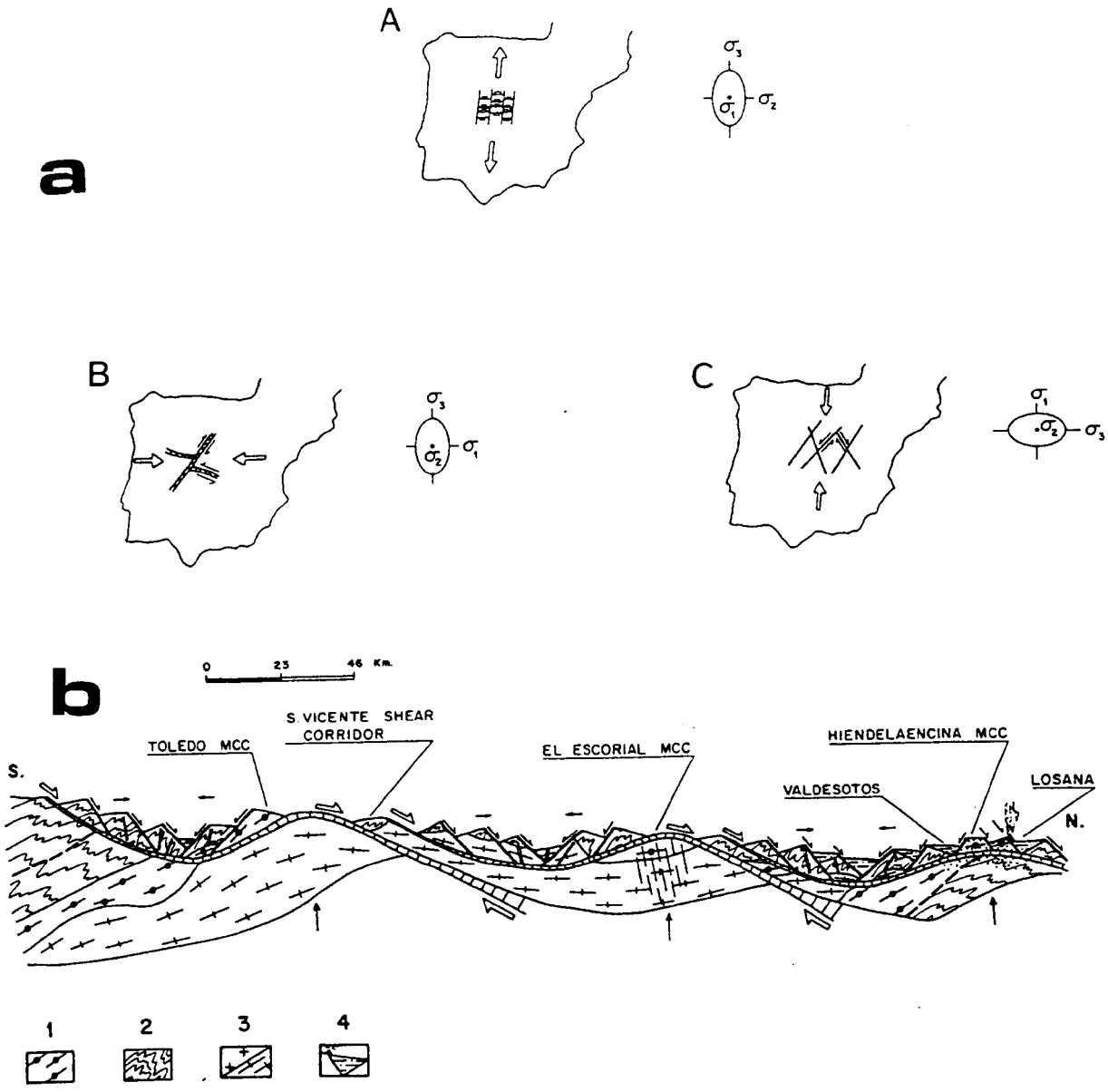

Fig.2.8. Late-Hercynian evolution of central Iberia. a) Deformational events, A: extensional episode, B: ductile-transcurrent episode C: brittle-transcurrent episode. b) Schematic cross-sections showing the kinematic evolution during the extensional episode. 1: Migmatites and orthogneisses. 2: Precambrian to Ordovician metasediments, 3: 'pre- to syn-extensional' granitoids, 4:Permian sediments and volcanics (from Doblas, 1991).

late Stephanian-Lower Permian time span (Fig.2.7). Residual compressional stresses resulted in the formation of a network of transcurrent faults already initiated during the early Stephanian. These strike-slip systems produced transtensional troughs and releasing bends with formation of intermontane semigraben basins of limited extent. They were infilled by alluvial fans and lacustrine sediments (Sopeña et al., 1988). A early extensional stage could result from the gravitational collapse of the building involving lithosphere-scale low-angle detachment systems (Doblas, 1991).

Alkaline to calc-alkaline and minor volumes of hyperalkaline granitoids were emplaced during that period (Corretge, 1983). Alkaline with calc-alkaline volcanism took place mainly associated with large faults in the Celtiberian 'corridor' (Muñoz et al., 1983; Navidad, 1983; Fig.2.7).

The transtensional/extensional episode was postdated by the early Alpine rifting stages starting in the Upper Permian time.

As a consequence of the fracturing of the crust, thinning of lithosphere and associated magmatism, hydrothermal convecting systems developed at supracrustal levels, involving variable inputs of meteoric waters, magmatic-derived fluids and brines from the Permian basins in marginal areas.

The geodynamic models proposed for this scenario were already commented on the above paragraphs. Arthaud & Matte, (1975) proposed a mega-scale shear zone with development of compressional and tensional structures. Lefort and Van Der Voo, (1981) invoked a Himalayan-type collision based model *sensu* Molnar and Tapponier, (1977). An extensional model Basin and Range-type was suggested by Lorenz and Nicholls (1976) who considered faulting and volcanism as due to an ascending mantle diapir causing generalised doming of the crust. None of these models offers a satisfactory explanation for all magmatic, tectonic and sedimentary features. The model proposed by Doblas (1991) for Central Iberia, based on an early extensional stage by gravitational collapse with two subsequent

transcurrent episodes, fails to account for compressional deformation and E-W transcurrent movements prior to extensional movements in other areas of the Hesperian Massif (e.g. Cantabrian Zone).

2.5.Late-Hercynian Pb-Zn vein-type ore deposits: the Spanish Central System.

A large number of Pb-Zn vein-type mineralisations are found in the Central System, Montes de Toledo, Alcudia Valley, Pedroches Batholith and Ossa-Morena. Conversely, Pb-Zn mineralisations are lacking in the northwestern region.

On the basis of availability of data and occurrence in different geological settings, the Pb-Zn deposits in the Central System (central and northeastern sectors) and the Alcudia Valley may serve to outline the features and ore forming processes relative to these mineralisations in the Hesperian Massif.

a.Central sector of the Spanish Central System: Ba-(F)-(Base metal sulphides) mineralisations are generally hosted by peraluminous porphyritic adamellites and peraluminous leucogranites (347 to 310 Ma and 291 to 288 Ma in age, Ibarrola et al., 1988) (Fig.2.9.a). Some occurrences cut across high-grade metamorphic rocks. The veins are subvertical, up to 1 m. thick, with a strike between N10° and N130° and up to several hundred meters in length.

The great number of veins prevents a precise definition of a standard paragenesis for all the deposits (*cf.* Vindel, 1980; Locutura and Tornos, 1987; Mayor et al., 1988; Ortega et al., 1988). Lillo et al., (1992) have recognised two main hydrothermal mineralising episodes followed by a third involving supergene mineral formation. The first one (ore stage I) involved the deposition of quartz (I), barite (I), fluorite (not always present), galena and minor chalcopyrite, sphalerite, pyrite, freibergite, pearcite, and complex Bi-Ag-sulphosalts. The ore stage II was characterised by the deposition of a second

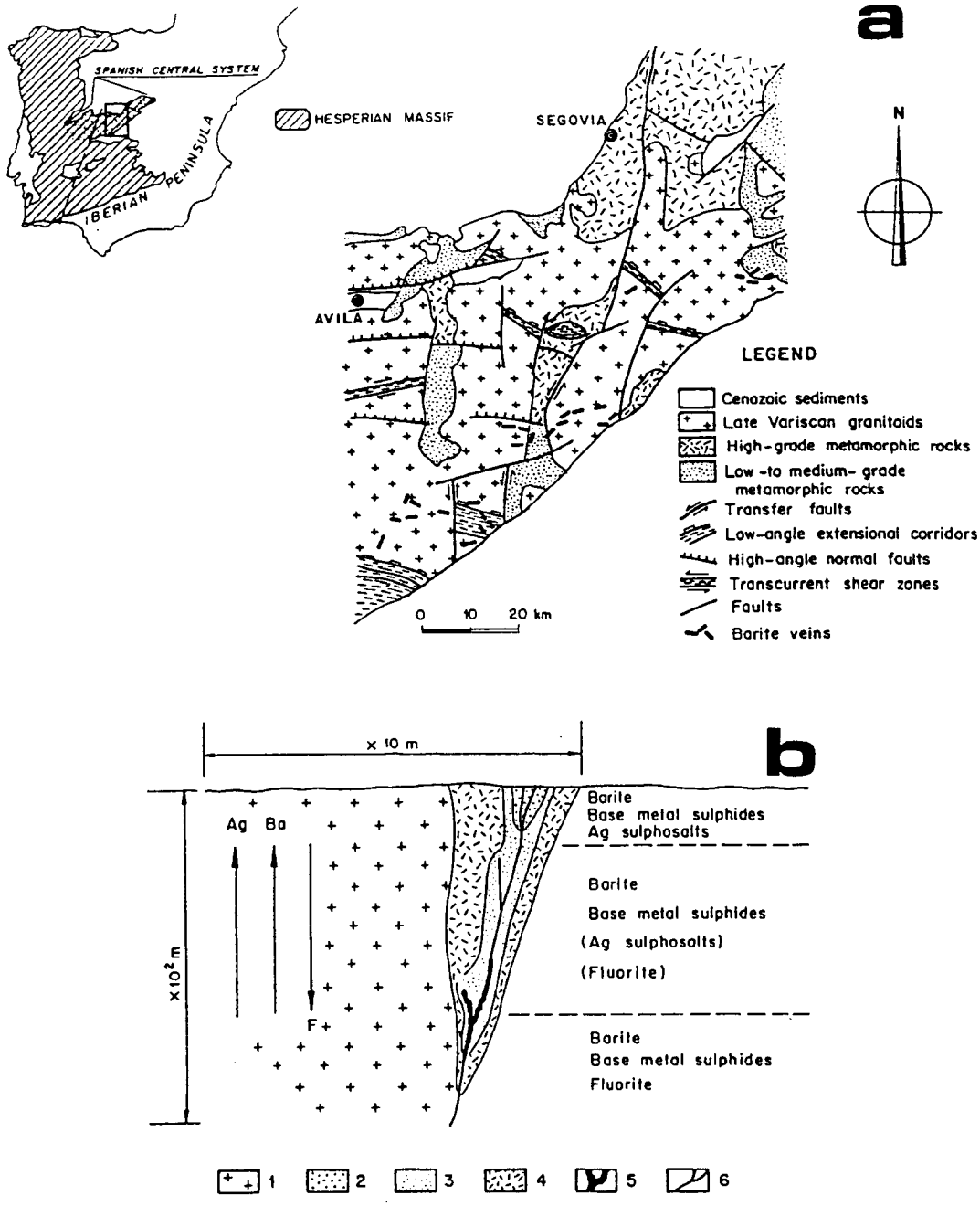

Fig.2.9. Ba-(F)-(base metal sulphides) mineralisations in the Spanish Central System. a) Geological sketch of the central sector. b) Schematic diagram depicting the relationships between alteration zones and mineral assemblages. 1: adamellitic host rock, 2: quartz-argillic alteration, 3: quartz-sericitic alteration, 4: chloritisation, 5: adularia zone, 6: veins (after Lillo et al., 1992).

generation of quartz (II) and barite (II). The final ore (ore stage III) was characterised by supergene mineral formation; cerussite, anglesite, covellite, chalcocite, azurite, malachite and goethite.

Hydrothermal alteration is defined by (from the vein to fresh rock, Fig. 2.9.b): a) Zone of silicification of some centimeters wide. b) Argillic alteration in some tens of centimeters. c) Quartz-sericite alteration. d) A wider zone of chloritisation of biotite which completes the 10-50 m. wide alteration envelope. As depth increases, the alteration envelope narrows and adularia becomes more important. Tornos et al., (1991) distinguished four zones in terms of age and depth. The deeper and earlier zone (Acidic Zone) is characterised by the alteration of micas and feldspars to sericite, quartz and chlorite. Intermediate zones are defined by the presence of fluorite and fluorite + barite. The shallower and younger zone is the Barite Zone.

Fluid inclusion studies have been carried out by Locutura and Tornos (1987); Tornos et al., (1991) and Lillo et al. (1992). Data are summarised in the table 2.1. Interpretation of leachates and microthermometric data in terms of equilibrium/disequilibrium of the fluid with the Q-muscovite-feldspar buffer suggests disequilibrium with the enclosing rocks ($Na/K_{rock} > Na/K_{fluid}$ or $Na/K_{rock} < Na/K_{fluid}$) (Table 2.2, Tornos et al. 1991).

Barites from the study area exhibit a range of $\delta^{34}S$ of +12.2 to +16.5 $^{o}/_{oo}$ (mean = +14.8; n = 16). Galena exhibits a range of $\delta^{34}S$ = -4.4 to +0.4 $^{o}/_{oo}$ (mean = -2.4, n = 6). Two samples of sphalerite yielded $\delta^{34}S$ values of -1.6 and -1.9 $^{o}/_{oo}$. Two samples of chalcopyrite yielded $\delta^{34}S$ values of -1.1 and +3.2 (Table 2.3.a, Lillo et al., 1992). Isotopic geothermometry (based on the equilibrium factors presented by Kajiwara and Krouse, 1971; and Sakai and Dickson, 1978) reflects an equilibrium exchange temperature in the range of 355 to 324°C suggesting coeval precipitation in equilibrium (or near equilibrium) for barite, galena and sphalerite, but a second generation of galena can be involved (Table 2.3.b). Lillo et al., (1992) interpret these data

Mineral	Stage	System	T_h °C	%NaCl eq.	Source
Quartz	I	H_2O-NaCl-CO_2?	200-320	3-6 *	(b)
Quartz	II	H_2O-NaCl-CO_2?	170-380	4-6 *	
Quartz	Pre-ore?	H_2O-NaCl ◇	260-300	0-3.4	(a)
Fluorite	?	H_2O-NaCl ◇	150-270	0-10.5	
Barite	?	H_2O-NaCl-KCl-$CaCl_2$-$MgCl_2$ ◇	120-200	3.4-14	

(*) Not corrected for CO_2.

(◇) From leachates.

Sources:

(a) Tornos et al. (1991).

(b) Lillo et al. (1992)

Table 2.1. Fluid inclusions data from Ba-(F)-(base metal) veins in the central sector of the Central System.

Sample	Mineral	Na	K	Ca	Mg	Fe	m_{total}
Q-2	Quartz	1.14	1.42	---	0.12	0.40	0.23
Q-3		1.02	1.70	---	0.15	0.52	0.23
F-1	Fluorite	15.74	1.02	3.64	0.06	0.27	0.23
F-2		15.00	0.93	2.15	0.04	0.22	0.23
F-3		27.58	1.03	3.91	0.05	0.14	0.23
B-1	Barite	14.50	10.69	13.78	5.38	0.11	2.01
B-2		10.22	1.70	1.54	0.90	0.11	0.60
B-3		8.27	2.31	2.13	2.20	0.36	0.60
B-4		4.28	4.14	2.78	2.91	---	2.01
B-5		6.96	14.97	2.78	3.58	---	2.01
B-6		6.86	1.54	7.26	0.23	---	2.01

Table 2.2. Analyses of leachates of the Acidic Zone (Quartz), Fluorite Zone (Fluorite) and Fluorite and Barite + Fluorite Zones in ppm. Analised values for Fe are close to the detection limit. Sample B-6 is quartz in the Barite Zone. m_{total} is assumed to be *m*NaCl eq. From Tornos et al., 1991).

		$\delta^{34}S$ (‰)$_{CDT}$			
Sample	Location	Barite	Galena	Sphalerite	Pyrite
SCS-11	Sotillo	+16.5			
SCS-12	Colmenar Arroyo	+15.6	-3.6	-1.6*	-1.1
SCS-13	San Martín	+15.9	+0.4		
SCS-16	Almorox	+14.3			
SCS-17	Colmenar Viejo	+13.6*			
SCS-18	Colmenar Arroyo	+15.1	-1.8*	-1.9	
SCS-19	Lamprophyre				+3.2*
SCS-21	Almorox	+16.3			
SCS-22	Colmenar Viejo	+13.1			
SCS-25	Cadalso	+12.2			
SCS-26	Sotillo	+15.3			
SCS-28	Colmenar Arroyo	+15.5	-4.4		
SCS-29	Colmenar Arroyo	+16.5	-3.4		
SCS-32	Navalagamella	+13.6			
SCS-33	Navalagamella	+13.6			
SCS-35	Almorox	+14.2			
SCS-36	Fresnedillas	+14.9*	-1.7		

(*) Sample duplicated, mean value.

Table 2.3.a. Sulphur isotopes data. From Lillo et al., (1992).

Sample	Δ	Sp-Gn T°C	Δ	Cp-Gn T°C
SCS-12	2.03	355±68	+2.5	236±45
SCS-18	-0.12	–		

Sample	Δ	Ba-Gn T°C	Δ	Ba-Sp T°C
SCS-12	20.26	324±35	17.30	337±4
SCS-13	17.47	412±46		
SCS-18	16.93	381±42	17.05	341±4
SCS-28	20.00	328±36		
SCS-29	20.03	328±36		
SCS-36	16.90	381±42		

Table 2.3.b. Sulphur isotopes geothermometry (Lillo et al., 1992)

as representative of magmatic-derived sulphur occurring as aqueous species isotopically equilibrated prior the mineral deposition.

The origin of these deposits remains controversial. Vindel (1980) linked these F-Ba-(Base metal sulphides) with the outermost envelope of a periplutonic hydrothermal zonation in relation to "La Cabrera" granite which is 40 km. to the east. Martinez et al. (1988) and Ortega et al., (1988) reinterpreted the lodes as formed by a hydrothermal system with mixing of magmatic fluids and oxidizing or meteoric waters. Alternatively, Locutura and Tornos (1985, 1987) and Tornos et al., (1991) proposed an origin by mixing of ascending deep waters (meteoric in origin) with shallower brines derived from the Permian-Triassic sedimentary basins. Lillo et al. (1992) support the model involving mixing of magmatic-derived fluids with meteoric waters in a hydrothermal convecting system triggered by extensional detachment tectonics at lithosphere scale.

b.Northeastern sector of the Spanish Central System: The Hiendelaencina silver-base metal district was extensively mined during the period 1844-1925. At present there are no underground mining operations. Three main zones of veins can be distinguished: Hiendelaencina, La Bodera and Congostrina (Fig. 2.10). The first two areas were silver-rich while the third one was base metal-rich. These are hosted by a pre-Ordovician complex of metamorphic rocks (micaschists, quartzites, gneisses and marbles). Veins with barite, quartz, calcite and traces of sulphides hosted by Stephanian-Permian andesites occur in the nearby locality of Atienza (Martinez Frias, 1987).

The veins (up to 1 m thick and up to 5 Km of strike length) follow three main trends: N-S, E-W and NE-SW. A vertical zoning is present (Martinez Frias, 1987): a) 0-100 m.(shallow oxidation zone) with silver chlorides and bromides b) 100-200 m. with barite-quartz e) 200-400 m. displaying barite, quartz, complex silver sulphosalts, sphalerite and galena; and d) a quartz-rich, barite-poor zone containing ruby silvers, sphalerite, galena,

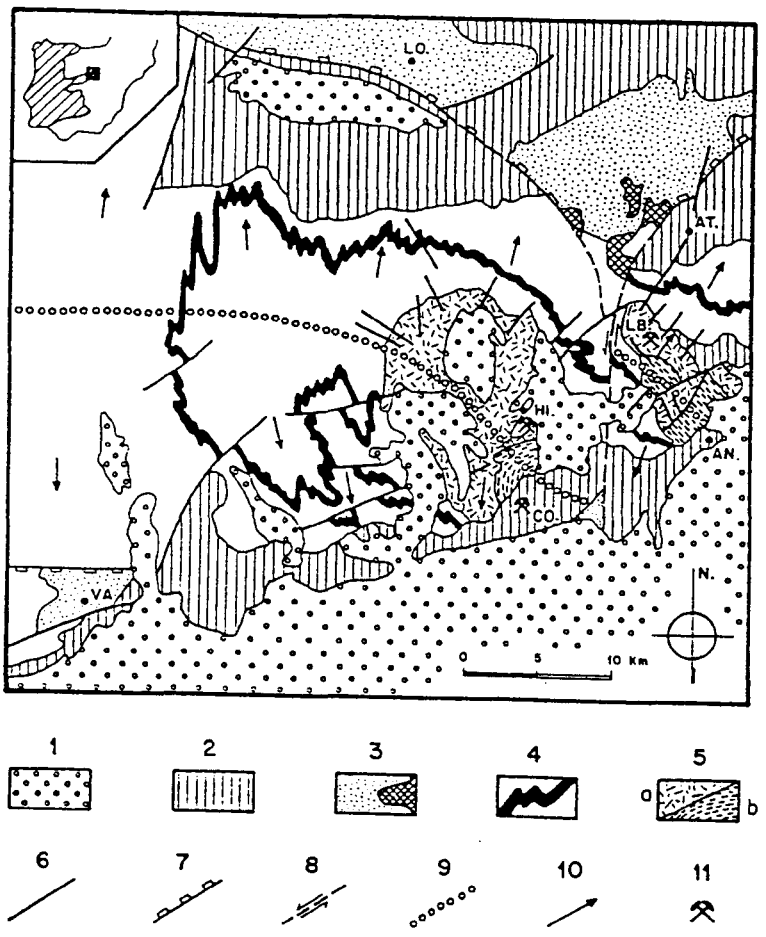

Fig.2.10. Simplified geological map of the Hiendelaencina-Atienza area. 1: Cenozoic sediments; 2: Mesozoic sediments; 3: Permian sediments and andesitic volcanics; 4: low-grade Ordovician metasediments; 5: Precambrian-Cambrian metamorphic core-complexes (a: augengneisses, b: orthogneisses and metasediments); 6: brittle faults; 8: transcurrent shear zones; 9: traces of upward arched crustal domains; 10: pitches of Variscan minor fold axes; 11: ore deposits. Localities: AN: Angon, AT: Atienza; CO: Congostrina; HI: Hiendelaencina; LB: La Bodera; LO: Losana; VA: Valdesotos (from Concha et al., 1991).

STAGE	I			II			III			IV
Ore Deposit	H	LB	C	H	LB	C	H	LB	C	H
Arsenopyrite	♦		♦							
Pyrite	♦						(♦)	♦	♦	
Chalcopyrite				♦	♦	♦				
Sphalerite				♦	♦	♦				
Freibergite				(♦)	(♦)	(♦)	♦	♦	♦	
Pyrrhotite				♦						
Barite				♦				♦	♦	♦
Fluorite								♦		
Quartz	♦		♦	♦	♦	(♦)		♦	♦	♦
Galena							♦	♦	♦	
Pyrargirite							♦	♦		
Polybasite							♦	♦		
Stephanite							♦			
Bournonite				(♦)			♦			
Freislebenite							♦	♦		
Aramayoite									♦	
Sakharovaite									♦	
Marcasite							♦	♦		
	Fe-As			Cu-Zn-Ba-(F)			Ag-Pb-(Ba)			Ba

Table 2.4. Mineral assemblages and deposition stages in the Hiendelaencina district. H: Hiendelaencina; LB: La Bodera; C: Congostrina (from Concha et al., 1992).

Mineral	Stage	System	T_h °C	%NaCl eq.	Source
Quartz	I	H_2O-NaCl-CO_2-CH_4	275-350	?	
Quartz	II	-	275-315	8-11	
Quartz	II	H_2O-NaCl-KCl-$CaCl_2$-$MgCl_2$	90-340	3-15	
Barite	II	-	220-310	11-15	
Quartz	III	-	90-190	5-22	H
Quartz	IV	-	90-140	9-13	
Barite	IV	-	100-250	5-24	
Quartz	III?	H_2O-NaCl-KCl-$CaCl_2$-$MgCl_2$	80-120	18-27	B
Fluorite	III?	-	90-150	3-24	
Barite	-	H_2O-NaCl-KCl-$CaCl_2$-$MgCl_2$	250-310	21 to 24 10 to 13	A

Sources:

(H) Hiendelancina area, Concha et al, (1992)

(B) Bodera area, Sierra et al, (1988)

(A) Atienza area, Concha et al. (1992)

Table 2.5. Fluid inclusions data from the silver-base metal veins in the northeastern sector of the Central System.

		$\delta^{34}S$ (‰)$_{CDT}$		
Sample	Location	Barite	Sphalerite	Pyrite
SCS-41	Hiendelaencina	+25.67*		
SCS-42		+26.14		
SCS-46				+2.91
SCS-47	La Bodera	+18.21		
SCS-48		+18.04	+6.74*	
SCS-49			+6.37	
SCS-20	Atienza	+6.24		
SCS-51A		+6.19		
SCS-51B		+6.68*		

(*) Sample duplicated, mean value.

Table 2.6. Sulphur isotopes data. From Concha et al, (1992).

chalcopyrite and pyrite. Mineral paragenesis and stages are presented in table 2.4.

Hydrothermal alteration is restricted to the vein walls and includes quartz-sericite, propylitic (chlorite + epidote) assemblages and adularisation. The andesitic rocks of Atienza exhibit a pervasive and strong propylitic (chlorite + calcite) alteration (Concha et al., 1992).

Three main types of inclusions were recognised in the Hiendelaencina area (Table 2.5., Concha et al., 1992 b): 1) complex aqueous-saline inclusions; 2) aqueous-carbonic (CO_2-poor) two-phase inclusions and 3) complex-carbonic (CO_2-CH_4) monophase inclusions. Fluorite and quartz samples from La Bodera sector shown complex aqueous-saline inclusions (Sierra et al., 1988, table 2.5). The microthermometric data have been interpreted by Concha et al., (1991) as relative to four mineralising episodes: Ore stage I was characterised by aqueous-carbonic fluids from which pyrite and arsenopyrite were precipitated (salinity data are not available) around a temperature of 275-350°C. Mixing of likely magmatic-derived fluids and meteoric waters caused a drop in temperature and salinity thus probably inducing precipitation of barite, chalcopyrite and sphalerite (Ore Stage II). Ore Stage III was characterised by fluids of low temperature and contrasting salinities (Th= 100-150°C; 3 to 18-22 wt % equivalent NaCl). A late stage involving aqueous saline fluids led to the deposition of barite.

Mixing of fluids is also supported by sulphur data (table 2.6., Concha et al., 1992). The wide range of $\delta^{34}S$ values in barites (which are internally consistent in each deposit) has been interpreted as due to variable mixing of magmatic-derived sulphur and sulphur derived from the metasediments.

The mineralisations in the whole sector have been related to remobilisation of older ores by processes not linked to the late-Hercynian magmatism (Locutura and Tornos, 1985). An alternative interpretation was presented by Martinez Frias (1987) who

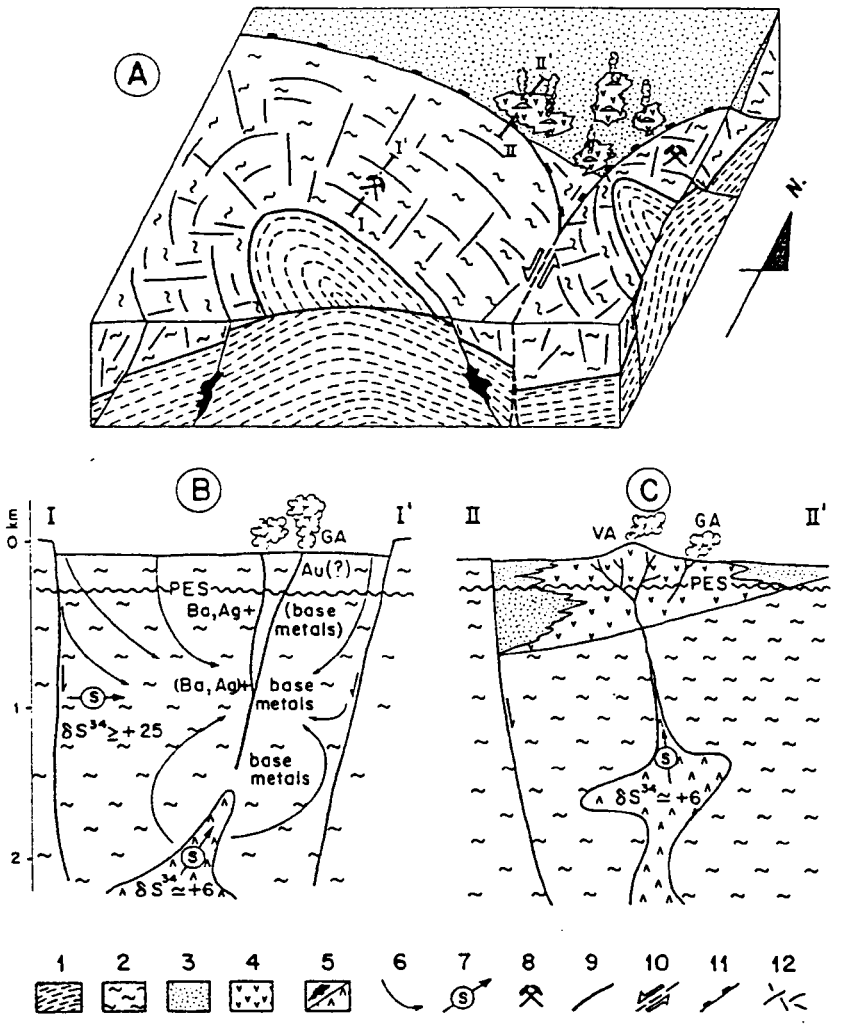

Fig.2.11. A) Idealised block section showing the final structural development of the Hiendelaencina district. B) and C) speculative cross sections depicting the metallogenic and magmatic processes at Hiendelaencina (B) and Atienza(C), 1: orthogneisses and metasediments, 2: augengneisses, 3: Permian sediments, 4: andesitic volcanic edifice, 5: andesitic magma chambers, 6: hydrothermal circulation patterns, 7: sources of sulphur, 8: ore bodies, 9: veins, 10: transfer fault, 11: major bounding faults, 12: fracture pattern, GA: geothermal activity, PTS: present erosion surface, VA: volcanic activity (from Concha et al., 1992).

considers ore genesis in relation to the magmatism. The model was redefined as an epithermal system with mixing of meteoric water and magmatic-derived fluids (Martinez Frias et al, 1988). The epithermal-type system and andesitic volcanism were induced by extensional collapse of the crust by lithosphere-scale, low-angle detachment faulting (Doblas et al., 1988). This epithermal model is supported by Concha et al., (1991, 1992) who point out a complex history of fluid mixing in the hydrothermal convecting system (Fig.2.11).

c.Alcudia Valley. It is located adjacent to the northern border of the Pedroches Batholith (Sierra Morena range), as a prolongation to the west of the Linares-La Carolina district. The Alcudia Valley district comprises four types or modes of occurrence of hydrothermal Zn-Pb deposits, but only one type is undoubtedly late-Hercynian. Therefore, only that type (that named as type IV by Palero et al., 1992) is considered in this thesis.

The late-Hercynian base-metal hydrothermal deposits at the Alcudia valley occur as veins and lodes. Banded textures and hydrothermal breccias are commonly found in these bodies that fill extensional faults developed on Precambrian and Palaeozic successions.

Ore mineral parageneses comprise galena, sphalerite, chalcopyrite, pyrite, pyrrhotite, marcasite, boulangerite, jamesonite, bournonite, arsenopyrite, 'red sylver', tetrahedrite, freibergite, linneite, millerite, stannite, cubanite, cobaltite, ullmanite, vaesite, gerdosffite, stibnite. Gangue minerals: ankerite, quartz, barite, calcite, siderite and chlorite.

Hydrothermal alteration is weak and restricted to the ore body. It consists of chloritisation, carbonatisation, silicification and sericitisation.

Five stages of mineral deposition have been recognised for the whole district: i) the first or 'early' stage is related to the deposition of arsenopyrite and pyrrhotite, ii) the second

stage is characterised by the deposition of sulphosalts, iii) the third stage is the main stage of sulphide deposition, iv) the fourth stage is associated with the deposition of sphalerite and glassy quartz, and v) the last stage which is related to the deposition of barite, pyrite and calcite.

Only complex aqueous-saline inclusions have been observed in ankerite and barite samples. They show either two phases (liquid and gas) or one phase (liquid) at room temperature. Two-phase inclusions in ankerite samples (precipitated during the main deposition stage) have Th temperatures ranging from 89° to 122°C. Tmi temperatures indicate salinities varying from 12 to 14 wt % equivalent NaCl. One-phase inclusions in barite samples (deposited during the third stage of mineralisation) have Th temperatures within the 60-70°C range and Tmi varying from -19°C to 0°C.

Galena exhibits a range of $\delta^{34}S$ = -2.7 to -9.8 $^{o}/_{oo}$ (mean = -7.2, n = 8). Four sphalerite samples display $\delta^{34}S$ values ranging from -4.6 to -5.9 $^{o}/_{oo}$. Isotopic geothermometry (based on the fractionation factors proposed by Ohmoto and Rye, 1979) suggests precipitation in isotopic non-equilibrium, as expected since the deposition of both sulphides was in different stages (Palero et al., 1992).

The above data have been interpreted by Palero et al. (1992), who suggest that the late-Hercynian base-metal veins at the Alcudia valley are related to a major hydrothermal event triggered by the residual heat of late-Hercynian granitoids. The fluids involved in the mineralisation were brines, with no large variations in salinity throughout the different stages. Most of the sulphur was magmatic-derived but there was some participation of bacteriogenic sulphur derived from the host metasediments.

Chapter 3. The Upper Ordovician-Lower Silurian succession in Linares-La Carolina district.

3.1.Introduction.

Some stratabound ore occurrences in the Upper Ordovician-Lower Silurian succession in Linares-La Carolina district and adjacent areas have been reported previously (Rios, 1977; Rios and Claverías, 1979; Jacquin and Pineda, 1980; Pineda, 1987; Palero and Martín-Izard, 1988). Among the initial aims of this thesis, was an investigation of this mineralisation whose origin has been only speculated upon as syn-diagenetic and possibly related to volcanic activity. Unfortunately, only minor syn-diagenetic occurrences of Fe were detected during the surveys in the area; some alluded occurrences are clearly related to the Late-Hercynian vein-type mineralisations (e.g. veinlets in Renegadero River) and other probable occurrences could not be observed as they have been cited from drill-core data (e.g. El Centenillo). However, basic sedimentological and geochemical studies were carried out, the results of which are presented in this chapter.

3.2.Stratigraphy.

The Upper Ordovician-Lower Silurian sediments in Linares-La Carolina district crop out in a narrow E-W-oriented band located in the northern part (El Centenillo-Sta. Elena) of the district (fig.3.1). The succession is made up of three sandstone formations separated by two units of marine shales. Several names for these formations have been proposed (fig.3.2). Those names suggested by Tamain (1972) will be used in this thesis, the only exception being the term of 'Quartzites Superieurs' where the alternative 'Castellar Quarzit' (Henke, 1926) is preferred. Most of the fauna listed in this work corresponds to that summarised in the synthesis of Hamman et al., 1982. The succession consists, from bottom to top, of:

-Botella Quartzites Formation (Guindo Quarzit, Richter, 1967; Argilites intermédières, Saupé, 1971; Quartzites Botella, Tamain,

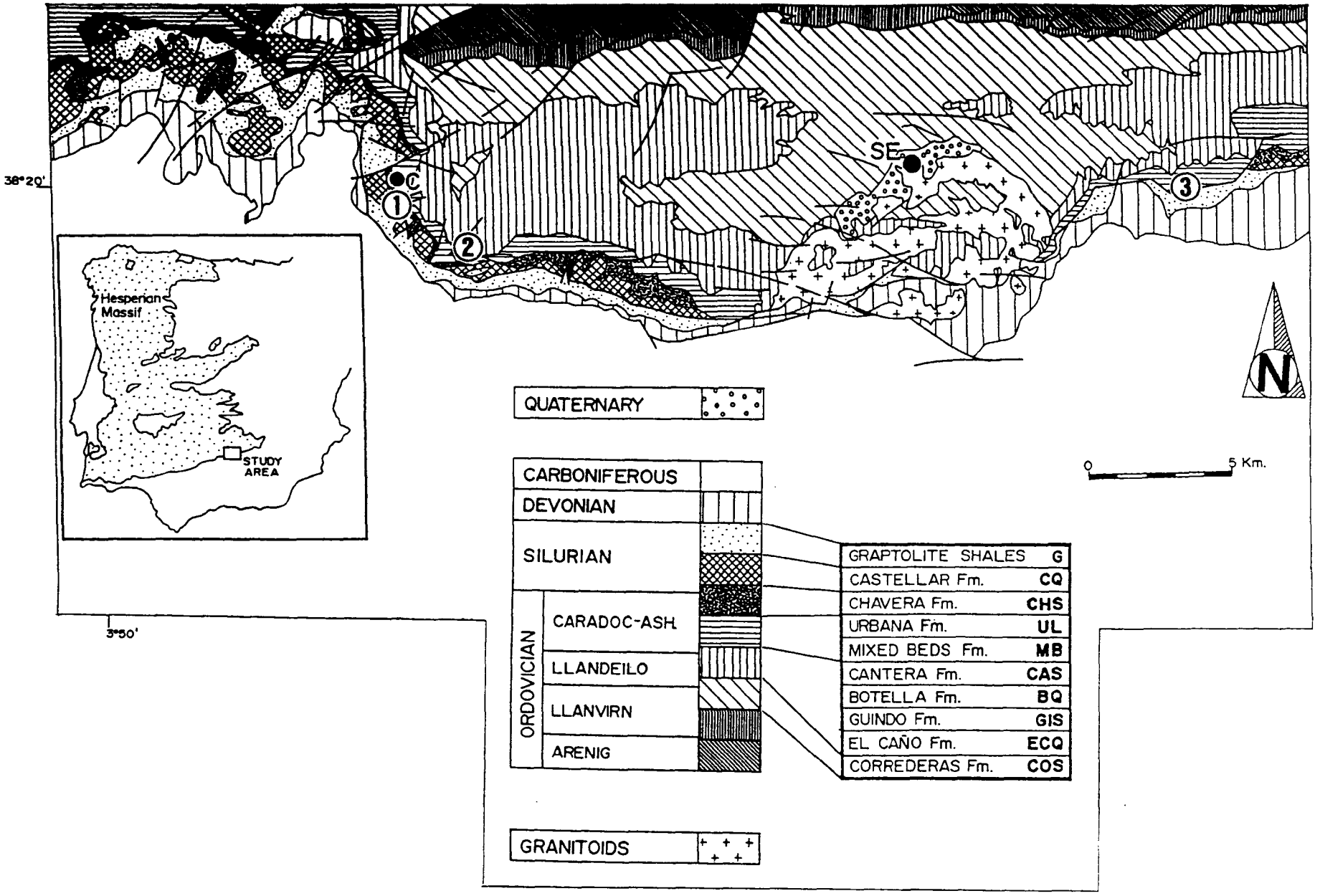

Fig.3.1. Geological skecth of El Centenillo (C)-Santa Elena (SE) area at Linares-La Carolina district and locations of the studied sections. 1: El Centenillo-La Carolina road; 2: Rio Grande valley; 3: La Despreciada quarry.

1972). Thickness: up to 150 m.. This formation is made up of quartzite beds with interbedded siltstones and some intercalations of shales, mainly in the lower portion. The upper portion is characterised by two sets of quartzite beds up to 4 m. in thickness, separated by a 10-12 m. thick unit of siltstones. The Botella Quartzites formation displays a fauna of brachiopods (*Heterorthina morgatensis*) and trilobites (*Eohomalonotus sdzuyi, E. brongniarti, E. vicaryi, Kerfornella brevicaudata, Iberocoryphe verneuili, I. bonissenti, Plaesiacomia oehlerti, Crozonaspis incerta*). The Llandeilo-Caradoc boundary is supposed to be close to or at the top of the formation. the type section is in the pit of Botella mine near el Centenillo, while the studied section is in the Rio Grande valley (location 2, fig.3.1).

-Cantera Shales Formation (Orthis-Schiefer, Richter, 1967, Schistes Cantera, Tamain, 1972). Thickness: about 25 m. It consists of alternating mudstones, greenish siltstones and micaceous thin bedded sandstones. A thin sedimentary iron ore bed may be present at the top. Fauna of brachiopods (*Aegiromena*), cephalopods, trilobites (*Onnia* cf. *seunesi, Colpocoryphe grandis*) and chitinozoans indicate Caradocian age. The type section is located in a small quarry at the southern entrance of El Centenillo (location 1, fig.3.1)

-Mixed Beds Formation (Orthis-Wechsellagerung, Richter, 1967; Alternances Supérieures, Saupé, 1971; Bancs Mixtes, Tamain, 1972). Thickness: 150-250 m. It is made up of alternating siltstones, sandstones and quartzites. Locally volcanic tuffs and coquinas occur ('Lumachelles terminales', Tamain, 1972). In the lower portion there are trilobites (*Onnia*, cf. *seunesi, Dalmanitina* cf. *acuta, Calymenella* cf. *boisseli, Crozonaspis dujardini*), brachiopods and molluscs indicating a Caradocian age. The upper portion yielded trilobites (*Onnia* n. sp. aff. *grenieri, Cekovia munieri, Zetillaenus ibericus, Calymenella boisseli, Prionocheilus costai, Dalmanitina acuta, Chattiaspis almadenensis, Dreyfussina exophtalma castiliana, Eudolatites* sp., *Eccoptochile ? impedita, Actinopeltis spjeldnaesi, Diacanthaspis morenaica*), brachiopods

Saupé (1973) (Area of Almadén)	Henke (1926)¤ Richter (1967)*	Tamain (1972)
Alt. Vulcanodétritiques	Graptolithenshiefer	Schistes à Monograptidés
Quartzite Criadero	Castellar Quarzit¤	Quartzites Superieurs
Argillites du Mur	Castellar Schiefer*	Schistes Chavera
Alternances Supérieures	A: Urbana Kalk¤ B:Orthis Wechsellagerung*	A: Calcaire Urbana B: Bancs Mixtes
Argillites Intermédières	Orthis Schiefer*	Schistes Cantera
Quartzites Canteras	Guindo Quarzit*	Quartzites Botella
Argillites Inférieures	Guindo Schiefer¤	Schistes Botella

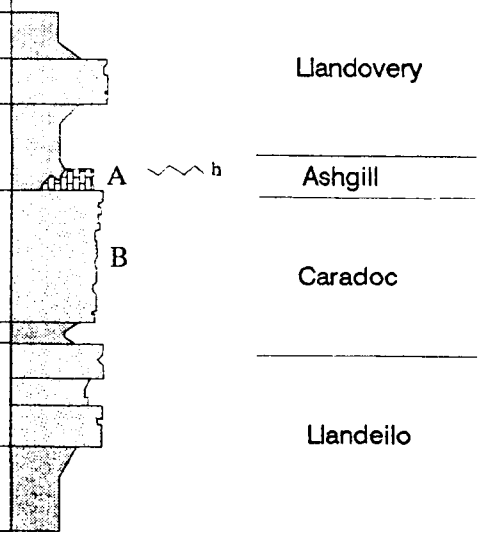

(h): erosional unconformity

Fig.3.2. Stratigraphic nomenclature proposed by different authors for the Upper Ordovician-Lower Silurian formations in eastern Sierra Morena.

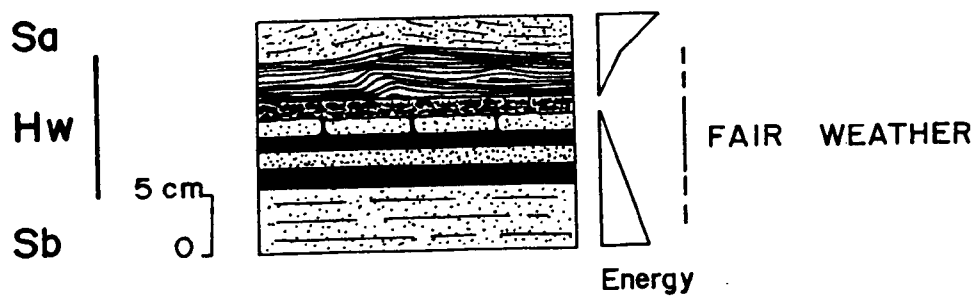

Fig.3.3. Storm heterolithic facies consisting of microalternations of silts-mudstones. Note the presence of climbing and wave ripples at top, which may represent the beginning of a new storm event. Abbreviations allude to facies abbreviations used in the text.

(*Svobodaina cf. armoricana*), bryozoans, molluscs, echinoderms chitinozoans and graptolites (*Orthograptus sp.*) indicate a late Caradocian to early Ashgillian age. A good section is exposed in El Centenillo ,on the road from La Carolina to El Centenillo (location 1, fig.3.1) but better sections are found out of the study area (Hamman, 1976).

-Urbana Limestone Formation (Urbana-Kalk, Henke, 1926). Up to 80 m. in thickness of pure limestone mostly bioclastic. Very variable thickness due to several factors: a) existence of an erosional unconformity on top (the whole formation may be missing), and b) confused location of the lower boundary. Volcanic tuffs are frequent in the lower portion (Charpentier, 1976; Pineda, 1987). The fauna consists of bryozoans, debris of echinoderms, trilobites, brachiopods and conodonts of the *Amorphognathus Ordovicica Zone*. Age: early Ashgillian. A section is exposed in La Despreciada quarry near to the east of Santa Elena (location 3, fig.3.1, plate 4.2.A).

-Chavera Shales Formation (Castellar Schiefer, Richter, 1967; Schistes Chavera, Tamain, 1972). It is a 100-150 m. thick unit of black unfossiliferous mudstones and siltstones with some intercalated sandstones beds in the upper portion. Locally, slumps and fragments of the unconformably underlying Urbana Limestone are found. The upper part contains Lower Silurian acritarchs (*Dictyotidium stenodyctium, D. dictyotum, Estiastra magna, Eupoikilofusa striatifera, Goniosphaeridium uncinatum, Leiofusa bernesgae, Lophosphaeridium citrinum, Multiplicisphasphaeridium arbusculiferum, Diexallophasis denticulatum, Neoveryhachium carminae*). The basal portion may represent the latest Ashgill (Hafenrichter, 1980). Sections are exposed in Renegadero Valley, and La Carolina-El Centenillo road (about 1 km from this village; location 1, fig. 3.1).

-Castellar Quartzite Formation (Castellar-Quarzit, Henke, 1926; Criadero Quartzites, Saupé, 1973; Quartzites Supérièurs, Tamain, 1972). Thickness: up to 70 m but may be very variable due to tectonic stacking caused by thrusting subparallel to the

Plate 3.1. Sedimentary structures in Upper Ordovician formations. A) Amalgamated hummocky cross-bedding (HS facies). Mixed Beds Fm. B) Accretionary planar cross-bedding (LC facies). Urbana Fm. C) Amalgamated hummocky cross-bedding (HS facies). Mixed Beds Fm. D) Evenly laminated sandstone facies (Sb facies). Mixed Beds Fm.

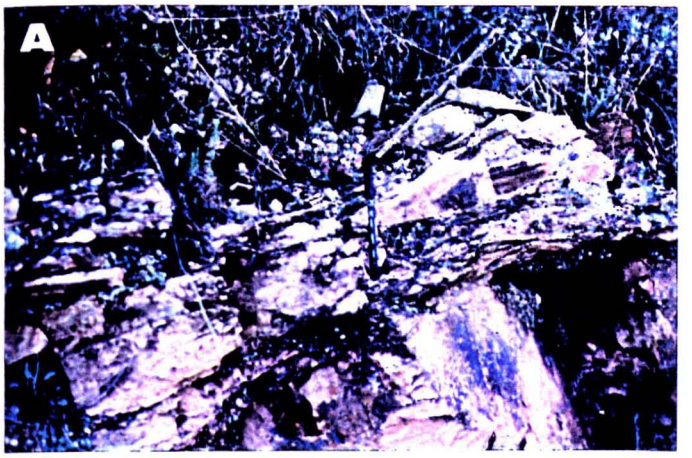
A

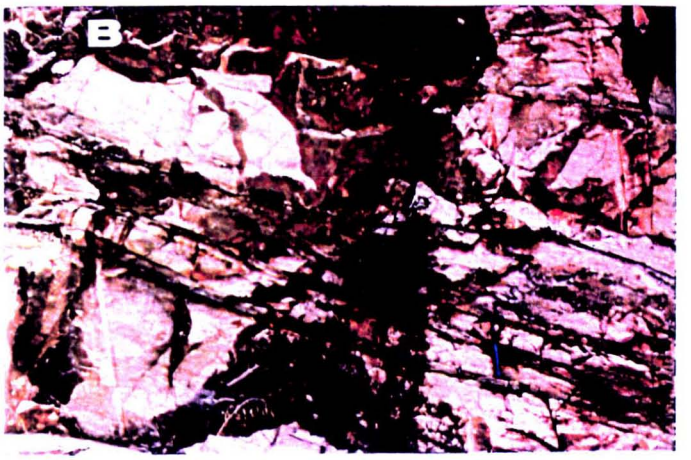
B


C

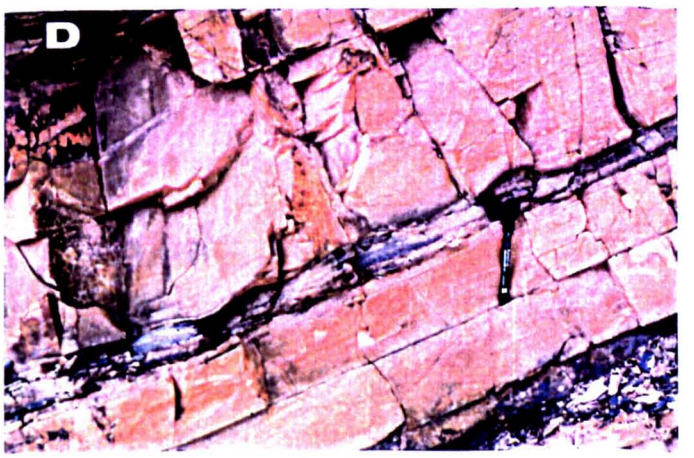
D

bedding. It is comprised of quartzite beds in massive sets. Very thin intercalations of siltstones and mudstones contain fauna of graptolites (*Magnus Zone*, early Middle Llandovery, Gutierrez-Marco and Pineda, 1988). This unit is conformably overlain by the 'Graptolite Shales' (Schistes à Monograptidés Llandovériens, Tamain, 1972) of Llandovery age (location 1, fig.3.1).

3.3.Sedimentology.

3.3.1.Facies.

The facies recognised may be divided into two groups: a) those relative to the formations made up by sandstones, siltstones and mudstones (i.e. Botella Quartzites Fm., Cantera Shales Fm., Mixed Beds Fm., Chavera Shales Fm. and Castellar Quartzites Fm.); and b) those relative to the Urbana Limestone Fm.

a.Mudstone, siltstone and sandstone facies.

a.1.Mudstone facies (M): Medium to dark grey and greenish mudstones, fissile and variably weathered to pale grey, pale green or orange-pink. This facies may occur as subordinate facies in centimetric (or exceptionally decimetric) beds interbedded with siltstones and sandstones (e.g. Mixed Beds) or as dominant facies (e.g. Chavera Shales).

a.2. Heterolithic facies (Hw): Beds of siltstone 1 to 50 mm. thick interbedded with bioturbated siltstone and mudstone of similar thickness in finely laminated alternations which are typically parallel but may show symmetrical wave ripples, climbing ripples and hummocky laminae. The siltstone beds display occasional scape burrows. The alternations define units of centimetric (or sporadically decimetric) order either finning or coarsening upwards. The base and top of the units are planar or undulatory. Undulations at the top display some periodicity with exagerated wave amplitude perhaps due to loading effects. Coquinas and shell detritus are ubiquitious (plate 3.1.D.).

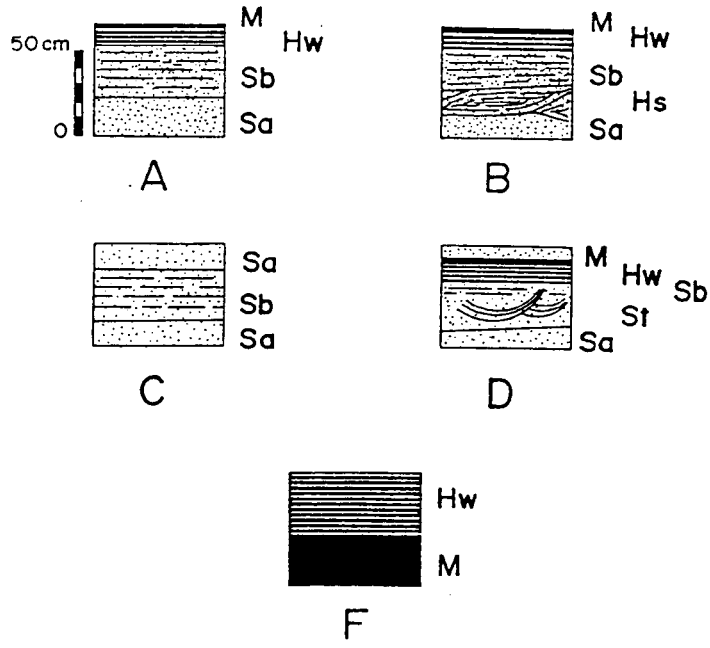

Fig.3.4. Idealised facies sequences in sandstone formations. Abbreviations refer to facies and parasequence abbreviations in the text.

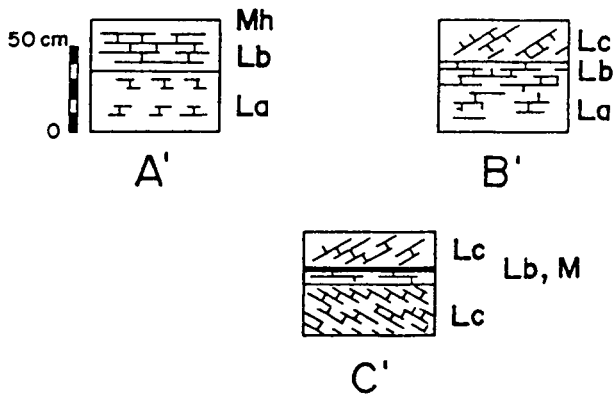

Fig.3.5. Idealised facies sequences in the Urbana Limestone Fm. Abbreviations refer to facies abbreviations used in the text.

This facies is interpreted as having been formed by a decrease in flow energy which gave as result the deposition of silt from suspension to form thin parallel-laminated beds (Fig.3.3).

a.3.Evenly Laminated Sandstone Facies (Sb): sandstones and siltstones ranging from 3 to 100 cm. in thickness with parallel laminae. Interpretation of this facies is not clear. Apparent horizontal or low-angle lamination could be, if observed in three dimensions, hummocky type cross-stratification. Alternatively, it may be a true planar lamination of low angle.

a.4.Hummocky Cross-bedding Sandstone Facies (Hs): Sandstones and coarse siltstones 3 to 100 cm. thick with hummocky cross-bedding. Hummocks are mostly of erosional type (*sensu* Harms et al., 1975) but also examples of accretionary type (*cf.* Brenchley and Newall, 1982) are found. Wave length ranges from a few centimetres to 1-2 meters (plates 3.1.A and C).

This facies is equivalent to the division H of the ideal hummocky cross-bedding (HCS) sequence of Walker et al. (1983).

a.5.Large and Medium Scale Cross-bedding Sandstone Facies (St): Sandstones in beds of centimetric to decimetric (exceptionally metric) thickness with planar and trough cross-bedding. Tabular beds usually display planar cross-laminae with accretionary pattern.

a.6.Large Scale (Low Angle) Cross-bedding Sandstone Facies (Sa). Massive sandstones in beds of decimetric to centimetric (exceptionally metric) thickness with tabular cross-bedding (angle < 5°) where no others structures have been identified.

b.Limestone facies. The Urbana Limestone Formation is characterised by its occurrence in discontinuous lenses as it is affected by the Ashgillian erosional unconformity. In addition, the scarce remains appear with a large variation of facies, locally associated with volcanic tuffs (Tamain, 1972, Charpentier,

1976, Pineda, 1987). On this basis, the sedimentological interpretation here presented is just one possibility.

b.1. Mudstone and Heterolithic Facies (Mh): greenish mudstones, siltstones and (?) volcanic tuffs in beds with very variable thickness from some milimeters to 10 cm.

b.2.Medium and Small Scale Cross-Bedding Limestone Facies (Lc): Edge-shaped decimetric beds of white and grey clastic limestones with cross-laminae, locally bimodal (i.e. with opposite dip)(plate 3.1.B).

b.3.Evenly laminated Limestone Facies (Lb): Decimetric and centimetric beds of white and grey clastic limestones with parallel or very low-angle cross-laminae.

b.4. Large scale Cross-bedding Limestone Facies (La): Decimetric and metric beds of white and grey clastic limestones with tabular cross-bedding where no other structures have been recognised.

3.3.2. Vertical facies changes.

3.3.2.1.Facies sequences: parasequences.

-Facies Sequence A: It is a centimetric to decimetric sequence of Sa, Sb, Hw, and M facies, typically fining and thinning upwards. Basal beds are formed by massive Sa facies passing upwards into Sb facies (fig. 3.4) Bases are sharp, either planar or undulatory. Dominant facies are Sa and Sb. Hw and M facies may be reduced to only very thin beds. When adjacent to hummocky cross-bedding sequences, this sequence is interpreted as having originated during a storm/waning-storm/fair-weather cycle in the inner shelf-near shore close to the storm-wave base, where bottom unidirectional currents (either as a result of storm-surge ebb flows, Allen, 1982; wind-forced current or by downwelling coastal jets, Swift et al., 1983) were important relative to the oscillatory flows giving as a result a strong combined flow. There is no sign of waning oscillatory flow (i.e. hummocky cross-

bedding, Duke et al. 1991) except in the Hw facies where hummocky cross-laminae and wave ripples may be present.

-Facies Sequence B: It comprises Sa, Hs, Sb, Hw and M facies in a decimetric (rarely metric) finning upwards sequence. The whole sequence is assimilated to the ideal HCS sequence of Walker et al. (1983) (fig.3.4) The facies may be variably developed. If amalgamation takes place, Hw and M facies only remain at the top of the erosional hummocks. Basal contacts are sharp, erosional, either planar or undulatory, but hummocks, swales and ripples may be preserved at the top of the underlying parasequence. This facies sequence is interpreted as having been formed by storm-generated bottom flows with a strong oscillatory component (e.g. Harms et al., 1982; Walter et al., 1983; Duke at al., 1991). Structures indicating unequivocal action of unidirectional flows (e.g. basal sole marks, gutter casts) have not been seen, but Sa and Sb facies in the basal portion could be formed by a strong combined (oscillatory plus unidirectional) flow. The most stable conditions of low energy (fair-weather) are represented by the preserved Hw and M facies. Occurrence of coarsening upward Hw alternances with ripples and hummocky laminae at the top of the sequence could reflect the start of a new storm event (fig.3.3).

-Facies Sequence C: It is of decimetric to metric order comprising Sa (dominant) and Sb facies (fig.3.4). Grain size decreases upwards from medium size sandstone to silt. Bases are sharp, either planar or ondulatory. This facies sequence with absent M and Hw facies, represents a variation by amalgamation of the parasequence A, either related to storm-derived deposits or offshore deposits generated by dominant unidirectional currents.

-Facies sequence D: This comprises Sa, St, Sb, Hw and M facies (fig. 3.4). Bases are sharp, planar or partially ondulatory. Hw and M facies are subordinate, with thicknesses of few centimeters or even reduced to thin partings. This parasequence may be interpreted as generated by unidirectional offshore currents. Alternatively, trough cross-bedding adjacent to

HCS has been ascribed to conditions of combined flow (Nøttvedt and Kreisa, 1987).

-Facies sequence F: It is a parasequence where the sandstone units are almost lacking, being reduced to beds of few centimeters interbedded with mudstones and siltstones (fig.3.4). Despite their thinness, they display a well developed lateral continuity. The ubiquitious presence of hummocky cross-laminae and the small scale (mm. to cm) alternations adjacent to mudstone beds may be related to a distal environment (middle shelf) close/below the storm wave base where the supply of sands was very restricted (*cf.* Aigner and Reineck, 1982; Brenchley et al., 1986).

-Facies Sequence A': It is formed by La (dominant), Lb and thin partings of Mh facies (fig. 3.5). Bases are planar or undulatory (metric wave lentgh). Amalgamation is common.

-Facies Sequence B': This can be considered as a variation of the parasequence A' as Lc facies is present, showing an accretionary planar cross-bedding laminae up to 20° dip (fig.3.5). Both parasequences are interpreted as having been formed by unidirectional currents.

-Facies Sequence C': This parasequence is characterised by the association Lc, Lb, and Mh facies (fig.3.5). The remarkable feature is the presence of reverse lamination upon thin mud drapes (Mh) associated to reactivation surfaces. The whole sequence is interpreted in terms of ebb-flood tidal currents of asymmetrical velocities (*cf.* Allen, 1980)

3.3.2.2.Parasequence sets: sedimentary environments.

-Botella Quartzite Formation (fig. 3.6).

The basal portion comprises parasequences A,B,C,D, and F type. The lowermost part is characterised by parasequences of F type succeeded by a set about 30 m. thick of amalgamated parasequences A and C type where only few intercalations of mudstone appear. Sa and Sb facies are dominant.

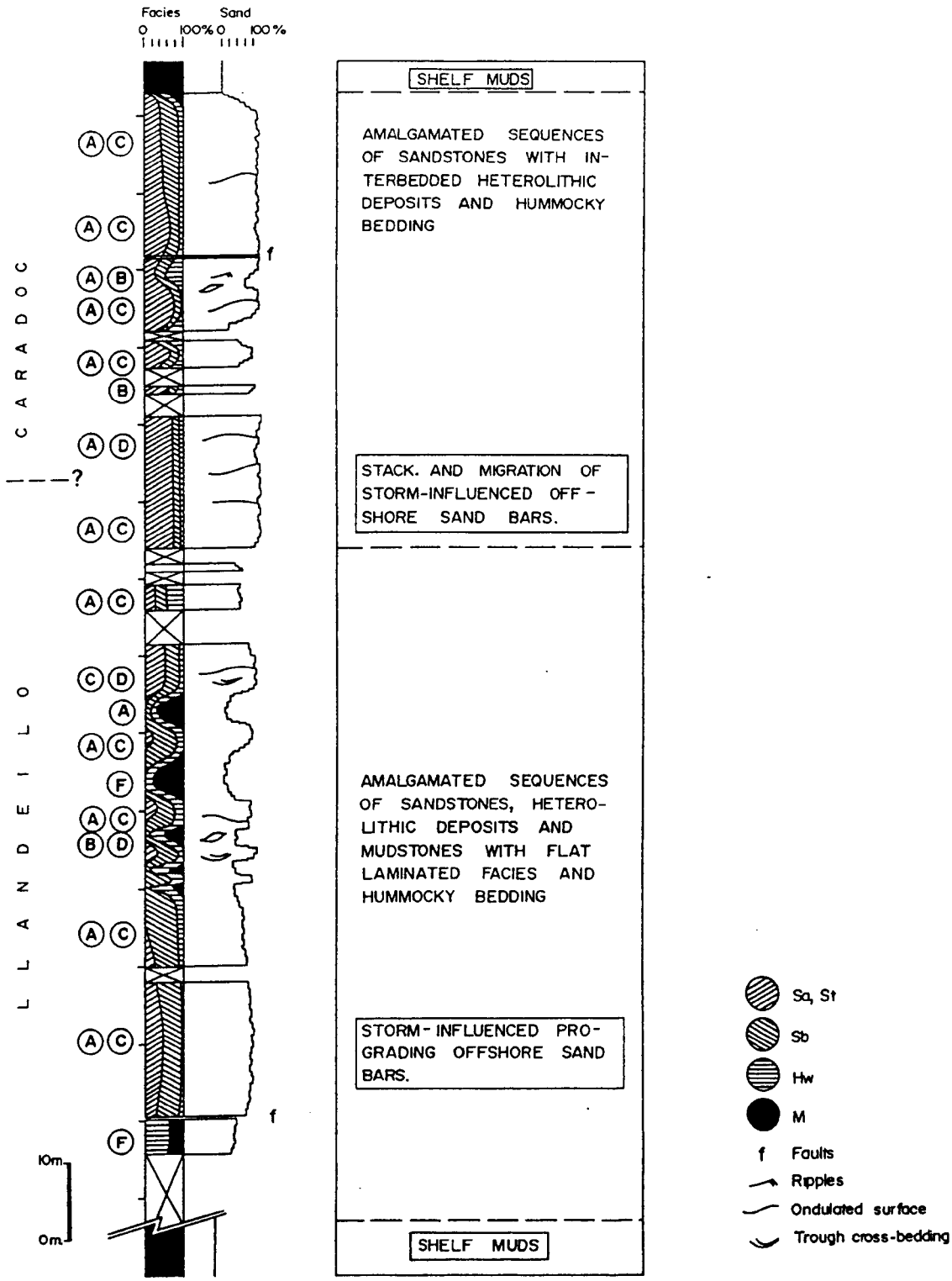

Fig.3.6. Sedimentological log of the Botella Quartzites Fm. at Rio Grande valley (location 2, fig.3.1.). A,B and C are facies sequences described in the text.

The middle-upper part of the basal portion (about 45 m. thick) consists of a set of A, B, C, D and F types where storm-related parasequences (i.e. C and F type) are well developed adjacent to sandstones with trough cross-bedding.

The whole set of the basal portion is interpreted as storm-influenced prograding sand bar deposits. The gradual (although relatively rapid) change from muds/siltstones to sands/siltstones at the bottom reflects the progradation of a sandy (inner) shelf environment over a muddy (outer) shelf. The amalgamated parasequences of sandstones with no clear evidences of oscillatory flow can be related to unidirectional currents, either storm-related (storm-surge, wind-forced or downwelling coastal jets), or non-storm-related currents (oceanic or tidal). With the limited amount of data is not possible to establish if the currents were storm-induced, oceanic or tidal dominated. There is no evidence (e.g. in the form of transverse bedforms or bimodal laminae) of tidal currents, but the preservation of these structures is rare in offshore tidal deposits (Johnson and Baldwin, 1986). Alternatively, amalgamation involving B and F parasequences may be produced by erosion due to strong oscillatory flows in distal environments (middle shelf) close to the storm-wave base with very restricted sand supply and strong reworking in the early stages of the storm (Brenchley et al, 1986).

The upper portion of this formation is made up of A, B, C, and D parasequence types, but B parasequences are only present in the middle part. Dominant facies is Sa.

This portion is interpreted as an agradational set defined by stacking and migration of offshore sand bars with some deposits related to the predominance of oscillatory flows over unidirectional currents. Hummocky beds adjacent to amalgamated sandstone A and C type parasequences with very little development of M facies were thus formed in a middle-inner shelf environment close-below the storm wave base.

The change to the overlaying Cantera Shales Formation is sharp.

-Cantera Shales Formation.

It consists of greenish mudstones reflecting an environment relatively starved of siliciclastic influx. This facies thus is interpreted as an outer shelf deposit. The green colour may be related to relatively oxiding conditions at the sediment-water interface, but this is not unequivocal indicator of shallow waters (Drever, 1982).

-Mixed Beds Formation (fig. 3.7).

The lower portion (about 50 m. thick) displays a rapid and gradual change from the overlain Cantera Shales Formation. This set is made up of A and B amalgamated parasequences. M and Hw facies are well preserved at top of the erosional hummocks. Swales may locally have a dip angle larger than 25°. Dominant facies are Hs and Sb.

The whole set is interpreted as a rapid progradation of inner shelf-near shore storm deposits produced by strong combined and waning oscillatory flows.

The upper portion constitutes a set of amalgamated parasequences A and in less proportion, B type. Dominant facies are Sa, Sb and Hw but some deposits already interpreted as Sb may be Hs. They constitute an aggradational set of storm deposits where wave scours associated to Sa facies are frequent. That is interpreted as the result of storm wave erosion followed by deposition from a turbulent suspension under conditions of high shear stress (Middleton, 1967). The scarcity of Hs facies could be explained by the persistent strong combined flow (unidirectional plus oscilatory) succeded by a rapid waning of the flow (*cf.* Duke et al. 1991). Those flow conditions (oscillatory by storm waves and unidirectional by storm-related currents) are expected to be found close-above the storm wave base in the inner (nearshore) shelf (*cf.* Brenchley et al., 1986).

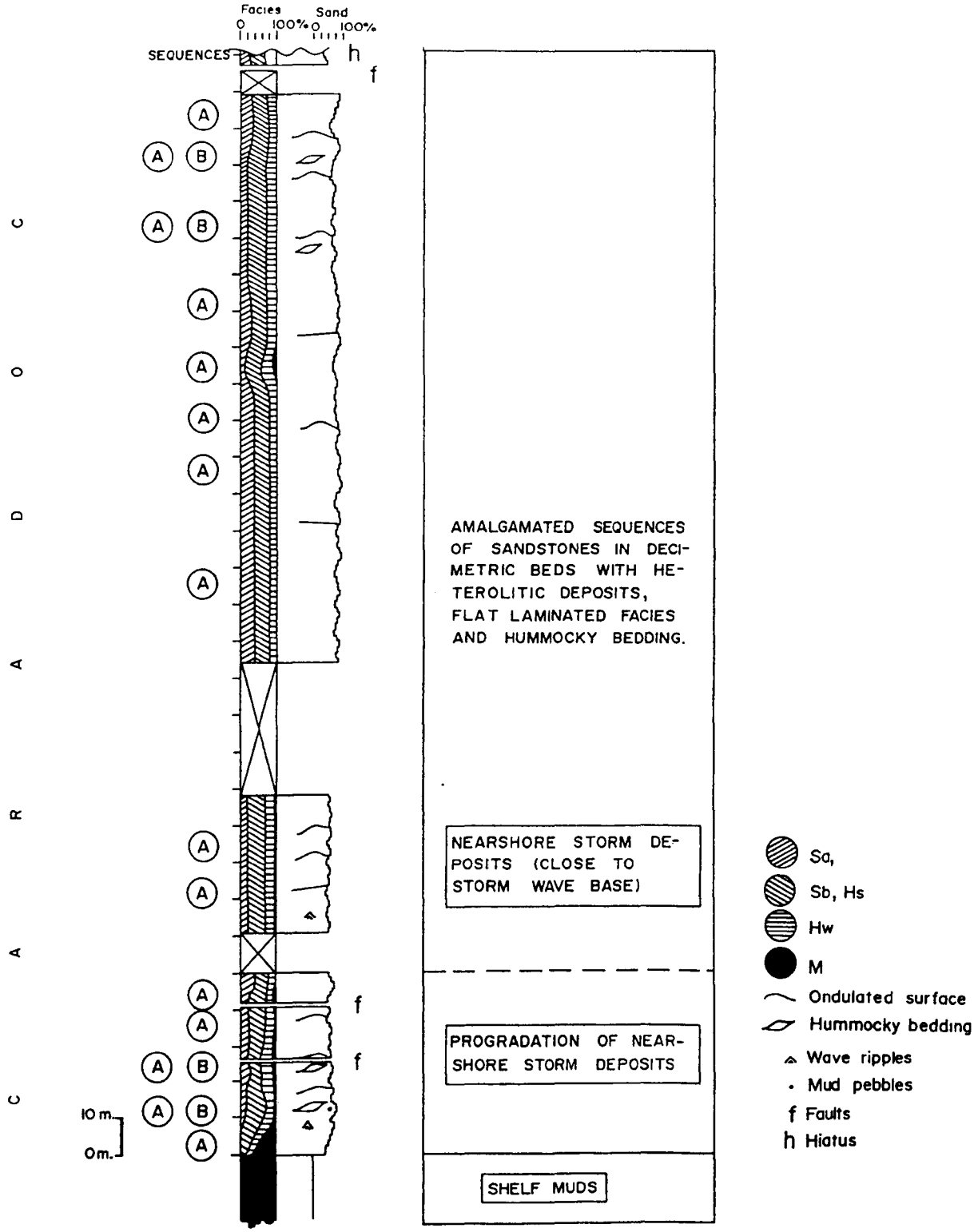

Fig.3.7. Sedimentological log of the Mixed Beds Fm. at El Centenillo (location 1, fig.3.1.). A and B refer to facies sequences described in the text.

-Urbana Limestone (Fig. 3.8.)

It is made up by amalgamated A' and B' type parasequences separated by three hierarchical levels of surfaces (types E1, E2 and E3 of Allen, 1980). Large-scale tabular sets are separated by E1 surfaces that are either planar or slightly undulatory. They are truncated by planar or curved E2-type pause planes or reactivation planes (fig. 3.9). Formation of pause planes is related to reworking of bedforms by reversed subordinated currents (Klein, 1970), or migration of superimposed bedforms (McCave and Jones, 1977), or to unsteady flow (Boersma and Terwindt, 1981). Internal stratification consists of accretional laminations that increase in dip in the direction of transport which may indicate progressively increasing current velocities. Locally developed bimodal lamination is interpreted in terms of subordinated reversed flow.

The whole set is interpreted as nearshore tide-influenced clastic carbonate deposits (sand waves(?)).

-Chavera Shales

Most of this formation consists of azoic dark grey mudstones (facies M) reflecting a environment starved of siliciclastic influx. Lack of fauna is associated with cold waters during the late Ashgill-early Llandovery (*cf.* Brenchley and Storch, 1989).

-Castellar Quartzites (Fig. 3.10)

The lower portion is constituted by A, C, D parasequences with dominant Sa, Sb and Hw facies in low-angle tabular beds. Internal cross-bedding is restricted to parallel, low-angle, and locally, trough lamination. Basal vertical change from mudstones of the overlain Chavera Shales to sandstones is progressive but in few meters (~ 3 m.).

Cross-strata pattern indicates that these deposits were generated by unidirectional currents (oceanic (?), tidal (?), storm induced (?)) in distal environments of the inner shelf as no

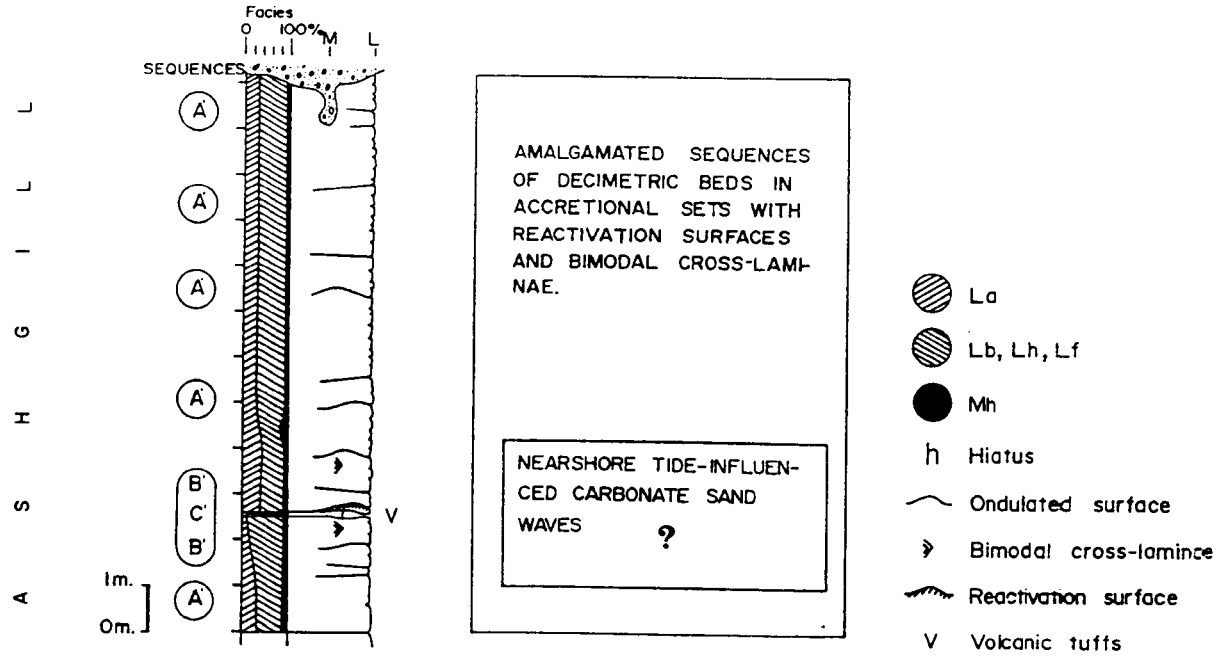

Fig.3.8. Sedimentological log of the Urbana Limestone Fm. at La Despreciada quarry (location 3, fig.3.1.). A', B' and C' are facies sequences described in the text.

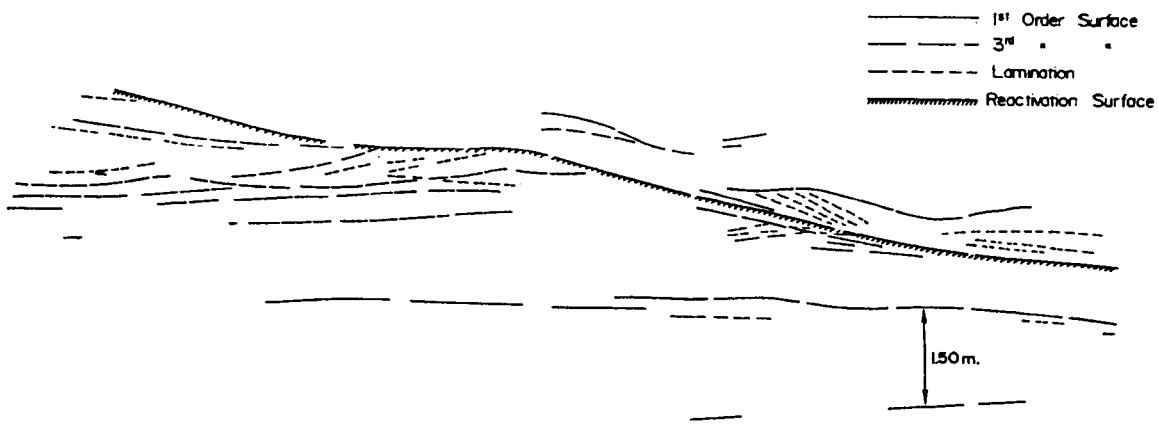

Fig.3.9. Bedding in the Urbana Limestone Fm. 1st order, 3rd order and reactivation surfaces allude to E1, E3 and E2 surfaces of Allen (1980), respectively.

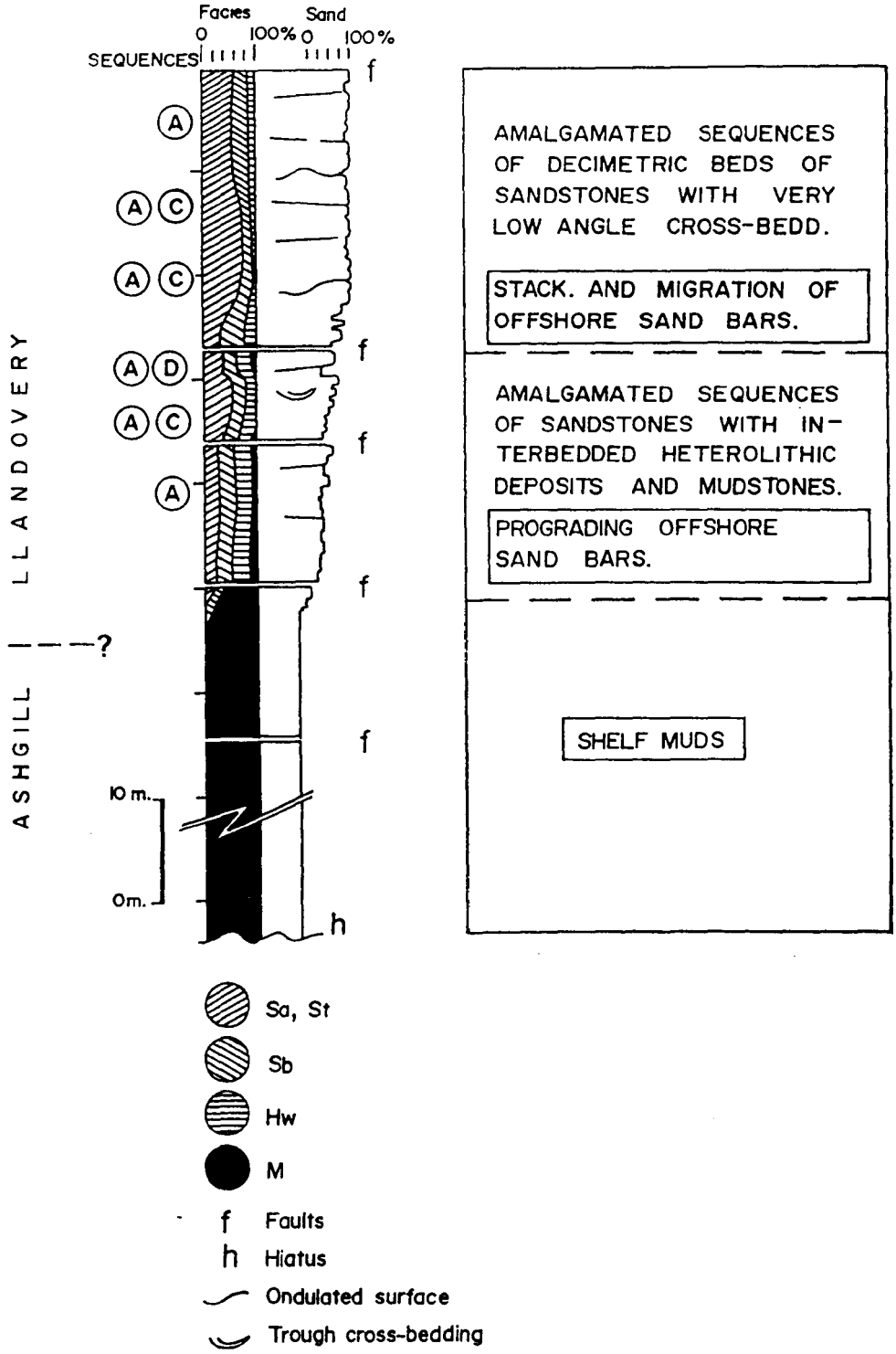

Fig.3.10. Sedimentological log of the Castellar Quartzites Fm. at El Centenillo (location 1, fig.3.1.). A, B and C are facies sequences described in the text.

wave related structures have been found. The lack of visible sedimentary structures due to metamorphism does not allow other more precise analysis. The whole lower portion may represent the progradation of sand bars over self muds in the outer shelf.

The upper portion is made up of A, B, and C parasequences with dominant Sa facies. Abundance of this massive facies likely is due the overprinting recrystallisation during the Variscan metamorphism. If they represent original massive sands, their interpretation is enigmatic. A pausible explanation is that some of these beds represent turbulent suspension deposits (*cf.* Kumar and Sanders, 1976). In that case, scours are expected to be present in the base of the parasequences. But the bedding surfaces in this formation are commonly planar or slightly undulatory.

The whole set may be interpreted in terms of stacking and migration of offshore sand bars.

3.3.2.3.Sequences. Sea-level changes.

Principles of sequence stratigraphy (Vail et al., 1977; Vail et al., 1984, Vail, 1987; Van Wagoner et al., 1988; Posamentier et al., 1988; Posamentier and Vail, 1988) are based largely on subsurface data but they are now being applied to outcrops (e.g. Christie-Blick et al., 1988; Jackson et al, 1990; Harris and Eriksson, 1990; Simpson and Eriksson, 1990). In contrast to most surface studies, three-dimensional analysis is hardly available from outcrop; and sequence boundaries (specially type-2 boundary of Van Wagoner et al., 1988) may lack appreciable relief, being difficult to recognise in the field; their positions must be inferred from changes of the stacking patterns of parasequences (Jackson et al., 1990). Despite these limitations, an approach based on principles of sequence stratigraphy may be worthwhile in reconstructing the stratigraphic evolution of the basin, as a result of the application of the concept of 'sequence' as a time-bounded record of sea-levels oscillations.

Patterns of stacking of parasequences are controlled by the ratio between rate of deposition and rate of accommodation or space creation in the basin (R_d/R_a; Van Wagoner et al., 1988). Parasequence sets may be progradational ($R_d>R_a$), retrogradational ($R_d<R_a$) or aggradational ($R_d=R_a$). Thus, the parasequence sets described above are interpreted in terms of R_d/R_a ratios in fig. 3.11, where the idealised curve of relative sea-level changes reflects the variation of space due to a combination of eustacy and subsidence. Mudstone formations are assimilated to retrogradational parasequences ($R_d<R_a$).

A remarkable feature is the aggradational set formed by the Mixed Beds and the Urbana Limestone, which is thicker than the progradational set at bottom of the Mixed Beds. If the maximum rate of sedimentation is assumed to occur during the progradation (*s.s.*), then most of the Mixed Beds and the Urbana Limestone would have been deposited in a 'steady' basin (in terms of R_d/R_a ratios) during a relatively long period.

Parasequences sets are grouped in sequences (note that in stratigraphic sequence analysis, sequences are made up of systems tracts which group different depositional systems on the basis of parasequences sets, *cf.* Posamentier and Vail, 1988). Systems tracts involve a palaeogeographical component that can not be evaluated here as no lateral variation of depositional environments is observed in the area.

Sequences are bounded by unconformities or their correlative conformities (Vail et al., 1977). The boundaries may be type 1 (when fluvial systems become incised across the former shelf) or type 2 (when shoreline advances to a mid-shelf position with no significant entrechment of shelf strata, Vail et al., 1984). A subaerial erosional unconformity occurs at top of the aggradational set of the Urbana Limestone Fm. but no fluvial or coastal deposits are found. Therefore, the sequence is not 'complete' and the type-1 sequence boundary may coincide with a marine ravinement diastem (*cf.* Demarest and Kraft, 1987; Nummedal and Swift, 1987). The lowermost portion of the Urbana Limestone

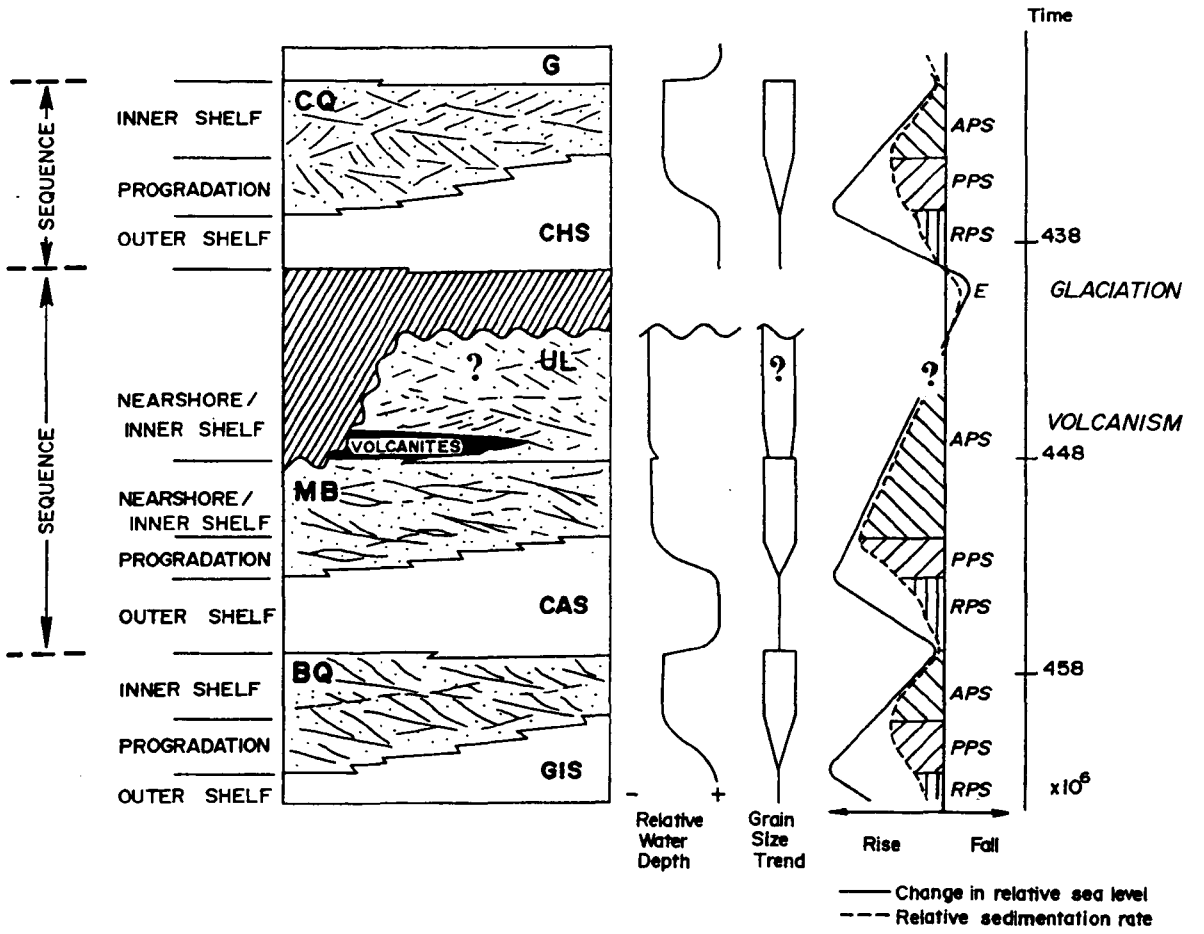

Fig.3.11. Synthetic stratigraphy of the Upper Ordovician-Lower Silurian formations in El Centenillo-Santa Elena area. Formation abbreviations as in fig.3.1. *RPS:* retrogradational parasequence set, *PPS:* progradational parasequence set; *APS:* aggradational parasequence set, *E:* erosional unconformity. Lowermost portion of the Urbana Limestone is based on Pineda (1987).

Fm., locally consisting of bryozoan greenish marls and volcanoclastics (Pineda, 1987), is assumed to represent no significative changes in depth.

Since the changes from the aggradational sets of the Botella Fm. and the Castellar Fm. to the overlaying mudstone formations are very rapid, the sequence boundaries are supposed to be at the top of the aggradational set (type-2 boundary of Van Wagoner et al., 1988) and below the diastem defined by the lack of gradual transition (*cf.* Nummedal and Swift, 1987). The flooding maximum is assumed to be at top of the retrogradational parasequence set since there is no additional data to infer the position of the condensed parasequences *sensu stricto*.The validity of the inferred sequence boundaries is supported by their large regional extension (*cf.* Portero and Dabrio, 1988).

Two sequences, comprising retrogradational, progadational and aggradational sets, have been recognised. The lower sequence includes the Cantera Fm., the Mixed Beds Fm. and the Urbana Limestone Fm. It reveals a sea-level rise-fall cycle with a duration between 20 Ma and 10 Ma. That cycle ceased with an event of subaerial erosion related to a glaciation in the late Ashgillian (see chapter 2).

On the basis of its duration, the cycle is compared to the second order cycles of Vail et al., 1977 and Haq et al, 1987. Eustatic changes due to glaciation have been related to fourth order cycles (0.3-1 Ma) whereas second order cycles (10-30 Ma) are interpreted as having been caused by a combination of eustatic processes and regional geologic processes like thermal subsidence and intraplate stresses (Fulthorpe, 1991). The study area was part of the West-central Iberian shelf, an area relatively stable during the Caradocian-Ashgillian span, although evidence of tectonic instability are found in adjacent palaeogeographical domains (West-Asturian trough and marginal areas, where a high rate of subsidence took place, see chapter 2). Furthermore, interbedded volcanics occur frequently in the Urbana Limestone or its equivalents (Matte, 1964, Tamain, 1972; Charpentier, 1976;

Rios, 1977; Pineda, 1987). In that scenario, relative sea-level fluctuations were controlled by factors other than those merely eustatic, and likely related to extensional tectonics (Portero and Dabrio, 1988).

The other recognised sequence includes the Chavera Fm. and the Castellar Fm. It defines a cycle starting with a deglaciation in the latest Ashgillian, and concluding in the early Middle Llandoverian. Cycles of 5 Ma duration can be ascribed to the third order cycles (1-5 Ma) of Vail et al. (1977) which are caused by a combination of eustatic factors and regional factors such as intraplate stresses, current activity and slope failure (Fulthorpe, 1991). Evidence of local tectonic instability have been found in areas adjacent to the study area by Portero and Dabrio (1988). Volcanic events took place during the Lower-Middle Llandoverian (e.g. Almadén; Saupé, 1990). Therefore, the sedimentary cycle could be controlled by a combination of global and regional factors: deglaciation and intraplate stresses. A similar explanation has been presented for Early Proterozoic marine sequences reflecting long-term, high-magnitude sea-level oscillations (10^5-10^7 Ma) which are interpreted as produced by the combination of eustatic oscillations and tectonic events (Harris and Eriksson, 1990). Thermal subsidence seems a relatively important factor in both cycles, as a combination of rapid thermal subsidence and a sinusoidal eustatic curve may produce a relative sea-level curve consisting of only slight falls (in this case, represented by the aggradational inner shelf/near shore parasequence sets) separated by periods of rapid rise (in this case, denoted by the diastems at the bottom of the sequences, *cf.* Nummedal and Swift, 1987).

3.4. Geochemistry.

3.4.1. Sampling.

Samples for XRF and sulphur isotope analysis were collected from selected outcrops of metasediments of well known stratigraphical position. Only one sample (LC90164-8) of limestone

Sample	LC149-1	LC59-12	LC9088-2	LC9088-3	LC9098-7	LC308-7	LC308-6	LC153-1
Formation	ECQ	ECQ	ECQ	ECQ	BQ	MB	MB	MB
SiO_2	83.92	80.01	79.43	83.53	97.61	72.36	75.41	63.10
TiO_2	0.65	0.46	0.57	0.65	.09	0.91	1.16	0.82
Al_2O_3	7.02	7.47	8.22	6.61	1.38	16.53	15.00	20.76
Fe_2O_3*	2.99	2.44	3.05	3.79	.93	1.49	1.70	3.32
MnO	0.11	0.06	0.05	0.01	0.03	0.00	0.00	0.01
MgO	0.90	0.63	0.64	0.62	0.09	0.31	0.28	1.01
CaO	1.00	2.92	1.54	0.17	0.06	0.04	0.04	0.11
Na_2O	1.11	1.61	1.73	0.69	0.07	0.29	0.23	0.43
K_2O	1.46	2.10	2.61	1.06	0.44	2.87	2.40	6.99
P_2O_5	0.08	0.05	0.12	0.11	0.07	0.11	0.15	0.08
L.o.I.	1.20	3.21	1.97	1.78	0.29	4.77	3.58	4.00
Total	100.42	100.96	99.93	99.02	101.05	99.69	99.94	100.62
Al_2O_3/SiO_2	0.08	0.09	0.10	0.08	0.01	0.23	0.20	0.33
K_2O/Na_2O	1.32	1.30	1.51	1.54	6.29	9.90	10.43	16.26
Ni	13	9	5	21	3	16	5	17
Cu	26	5	6	7	0	16	16	18
Zn	42	27	25	100	53	68	61	29
Rb	49	63	67	38	16	116	87	231
Sr	108	161	128	30	7	77	40	72
Y	41	20	25	27	8	61	33	22
Zr	750	354	463	555	43	344	326	258
Nb	13	9	10	11	1	18	29	16
Ba	268	485	791	233	51	695	899	1406
Pb	40	8	21	15	11	45	93	48
Th	19	12	18	18	5	16	14	15
U	4	3	4	4	2	5	5	3
Zr/Nb	57.69	39.33	46.30	50.45	43.00	19.11	11.24	16.38
Zr/Th	39.47	29.50	25.72	30.83	8.60	21.50	23.29	17.20
Nb/Y	0.32	0.45	0.40	0.41	0.13	0.30	0.88	0.73
Ti/Y	95.04	137.89	136.69	144.33	67.44	89.43	210.74	223.45
K/Rb	247.35	276.72	323.39	231.57	228.29	205.39	229.01	251.0
Rb/Sr	0.45	0.39	0.52	1.27	2.29	1.51	2.18	3.21
Ba/Sr	2.48	3.01	6.18	7.77	7.29	9.03	22.48	19.53
Th/U	4.75	4.00	4.50	4.50	2.50	3.20	2.80	5.00

Table 3.1.a. Chemical XRF analyses of and ratios sandstones. Major element oxides are in wt%. Fe_2O_3* is total iron. L.o.I. is loss on ignition. Trace elements in ppm. ECQ: El Caño Quartzite Fm., BQ: Botella Quartzites Fm., MB: Mixed Beds Fm.

Sample	LC153-2	LC143-1	LC93-5	LC9031-13	LC9031-2	LC9078-1	LC9078-2	LC9078--3
Formation	MB	MB	MB	MB	MB	CQ	CQ	CQ
SiO_2	80.75	77.68	70.68	84.09	72.64	83.70	87.26	92.41
TiO_2	0.43	0.78	0.87	0.68	0.75	0.49	0.51	0.23
Al_2O_3	10.43	13.98	17.84	9.54	15.23	10.06	7.85	4.74
$Fe_2O_3^*$	1.98	0.91	1.14	0.88	2.55	1.12	0.39	0.42
MnO	0.01	0.00	0.01	0.01	0.01	0.01	0.01	0.01
MgO	0.37	0.36	0.41	0.26	0.75	0.13	0.16	0.07
CaO	0.14	0.02	0.06	0.03	0.20	0.03	0.02	0.02
Na_2O	2.90	0.20	0.88	0.10	0.51	0.13	0.07	0.08
K_2O	1.82	3.74	4.47	2.93	3.36	2.81	2.12	1.28
P_2O_5	0.06	0.04	0.06	0.04	0.10	0.13	0.05	0.05
L.o.I.	1.66	2.80	3.67	1.40	4.30	2.23	1.50	0.77
Total	100.54	100.51	100.38	99.97	100.41	100.82	99.93	100.07
Al_2O_3/SiO_2	0.13	0.18	0.25	0.11	0.21	0.12	0.09	0.05
K_2O/Na_2O	0.63	18.70	5.08	29.30	6.59	21.62	30.29	16.00
Ni	5	4	10	2	12	4	5	2
Cu	4	7	5	1	20	11	2	0
Zn	21	13	88	16	177	41	21	24
Rb	60	99	116	92	121	75	55	31
Sr	97	35	42	13	40	30	19	12
Y	17	22	40	26	42	17	18	8
Zr	283	380	329	571	304	367	502	193
Nb	8	15	19	13	16	10	10	4
Ba	478	608	627	284	663	279	236	114
Pb	21	96	54	12	74	665	737	419
Th	10	13	15	14	15	5	5	3
U	3	4	7	5	5	2	2	1
Zr/Nb	35.38	25.33	17.32	43.92	19.00	36.70	50.20	48.25
Zr/Th	28.30	29.23	21.93	40.79	20.27	73.40	100.40	64.33
Nb/Y	0.47	0.68	0.48	0.50	0.38	0.59	0.56	0.50
Ti/Y	151.64	212.55	130.39	156.79	107.06	172.80	169.86	172.36
K/Rb	251.81	313.61	319.89	264.38	230.52	311.03	319.98	342.77
Rb/Sr	0.62	2.83	2.76	7.08	3.03	2.50	2.89	2.58
Ba/Sr	4.93	17.37	14.93	21.85	16.58	9.30	12.42	9.50
Th/U	3.33	3.25	2.14	2.80	3.00	2.50	2.50	3.00

Table 3.1.b. Chemical XRF analyses and ratios of sandstones. Major element oxides are in wt%. $Fe_2O_3^*$ is total iron. L.o.I. is loss on ignition. Trace elements are in ppm. MB: Mixed Beds Fm.; CQ: Castellar Quartzites Fm.

Sample	LC59-13	LC90138-4	LC9098-8	LC90148-1	LC308-8	LC9031-4
Formation	COS	BQ	CAS	CHS	CHS	CHS
SiO_2	64.30	54.10	64.54	73.74	50.24	57.48
TiO_2	0.99	1.30	0.90	0.53	1.17	1.11
Al_2O_3	19.26	25.42	17.88	8.65	25.47	20.40
$Fe_2O_3^*$	5.22	5.83	4.93	9.13	8.39	7.14
MnO	0.02	0.03	0.02	0.14	0.06	0.05
MgO	1.41	1.33	1.23	1.72	2.58	1.88
CaO	0.09	0.23	0.11	0.04	0.15	0.21
Na_2O	0.87	0.34	0.75	0.16	0.49	0.72
K_2O	4.51	6.72	5.22	2.26	5.20	6.62
P_2O_5	0.12	0.13	0.06	0.08	0.21	0.12
L.o.I.	3.51	4.72	3.29	3.29	5.51	3.60
Total	100.31	100.15	98.94	99.74	99.47	99.32
Al_2O_3/SiO_2	0.30	0.47	0.28	0.12	0.51	0.35
K_2O/Na_2O	5.18	19.76	6.96	14.13	10.61	9.19
Ni	15	48	32	44	58	30
Cu	18	10	17	18	38	22
Zn	86	66	50	4301	235	574
Rb	161	216	209	114	233	232
Sr	38	65	45	10	139	25
Y	37	35	23	21	52	38
Zr	293	234	232	347	145	180
Nb	20	24	18	10	25	22
Ba	886	1135	786	212	1224	1226
Pb	23	11	12	389	25	18
Th	16	22	18	7	28	21
U	6	4	4	2	7	5
Zr/Nb	14.65	9.75	12.89	34.70	5.80	8.18
Zr/Th	18.31	10.64	12.89	49.57	5.18	8.57
Nb/Y	0.54	0.69	0.78	0.48	0.48	0.58
Ti/Y	160.41	222.67	234.59	151.30	134.89	175.12
K/Rb	1186.84	1033.85	1160.00	2260.00	374.10	2648.10
Rb/Sr	4.24	3.32	4.64	11.40	1.68	9.28
Ba/Sr	23.32	17.46	17.47	21.20	8.81	49.04
Th/U	2.67	5.50	4.50	3.50	4.00	4.20

Table 3.2. Chemical XRF analyses and ratios of mudstones. Major element oxides are in wt%. $Fe_2O_3^*$ is total iron. L.o.I. is loss on ignition. Trace elements are in ppm. COS: Correderas Shales Fm.; BQ: Botella Quartzites Fm.; CAS: Cantera Shales Fm.; CHS: Chavera Shales Fm.

Sample	LC71-1	LC73-2	LC73-4	LC73-5
Formation	UL	UL	UL	UL
SiO_2	7.65	7.85	5.65	1.85
TiO_2	0.04	0.25	0.23	0.10
Al_2O_3	0.30	1.88	0.88	0.53
Fe_2O_3*	0.25	0.95	1.01	0.57
MnO	0.09	0.04	0.18	0.04
MgO	0.52	0.69	0.51	0.66
CaO	49.71	47.79	50.05	53.03
Na_2O	0.02	0.05	0.04	0.03
K_2O	0.08	0.52	0.26	0.13
P_2O_5	0.02	0.05	0.03	0.03
L.o.I.	40.27	39.06	40.50	42.37
Total	98.93	99.15	99.34	99.38
MgO/CaO	0.01	0.01	0.01	0.01
Ni	5	7	6	2
Cu	6	5	11	6
Zn	12	12	18	362
Rb	1	16	8	3
Sr	216	198	253	183
Y	5	5	9	4
Zr	3	43	20	11
Nb	1	4	2	3
Ba	25	126	41	26
Pb	1	2	9	101
Th	7	7	6	7
U	1	1	2	1
Zr/Nb	3	10.75	10	3.67
Zr/Th	0.43	6.14	3.33	1.57
Nb/Y	0.20	0.80	0.22	0.75
Rb/Sr	0.00	0.08	0.03	0.02
Ba/Sr	0.12	0.64	0.16	0.14
Th/U	7	7	3	7

Table 3.3. Chemical XRF analyses and ratios of limestones. Major element oxides are in wt%. Fe_2O_3* is total iron. L.o.I. is loss on ignition. Trace elements are in ppm. UL: Urbana Limestone Fm

for sulphur isotope analysis was collected from a mine dump. This sample was assigned to the Urbana Limestone as it is the only formation consisting of limestones in the area. Caution was taken in collecting the samples sufficiently far away from veins to avoid hydrothermal metasomatism effects. Sample preparation and analytical procedures are described in Appendix I.

Special emphasis was placed on sampling the Mixed Beds formation as some stratabound occurrences have been reported (Jacquin and Pineda, 1980). Furthermore, volcanic tuffs of rhyolitic composition occur locally at the top of this formation (Charpentier, 1926).

Some samples from the underlying Correderas Shales Formation (denominated 'Schistes du Rio' by Tamain, 1972, age: Llanvirnian) and El Caño Quartzites Formation (denominated 'Quartzites inferieurs' by Tamain, 1972, age: Late Llanvirnian-Llandeilan) have been included to comparison.

3.4.2.Geochemical evidence of tectonic setting and volcanism.

Sandstones (tables 3.1.a and b) have an SiO_2 range of 63.10-97.61 %. Al_2O_3/SiO_2 ratios are variable and reflect grain-size and/or compositional variations from heterolithic siltstones to quartz-arenites, these ones having the lowest ratios. Large-ion-lithophile (LIL) elements such as K, Rb, Sr, Th and U display a wide range of abundances. Specific element ratios (e.g. K/Rb and Th/U) are relatively consistent within some formations (El Caño Formation and Castellar Formation) but they show large variations in the Mixed Beds Formation due to the 'mixed' lithology (mud+sandstone) of the samples.

The high field strength elements, Ti, Zr, Y, Nb exhibit internally consistent ratios (Ti/Y, Nb/Y) except in the Mixed Beds due to the reasons noted on above. Pairs involving Zr show variable values as its distribution is largely governed by the sedimentary concentration of zircons.

Petrochemical classification of sandstones based on the scheme proposed by Crook (1974) and Blatt et al. (1980) indicates that they are mostly quartz-rich arkoses with K_2O/Na_2O ratios between 1.30 and 30.29 (fig.3.12). One sample from the Mixed Beds may be considered a quartz-intermediate greywacke. There is a trend across the stratigraphic succession showing a greywacke/lithic affinity (increases in Na_2O and Fe_2O_3*(1) versus K_2O) for the older rocks and a quartz-rich arkosic affinity for the younger sediments (i.e. maturity increases towards the top of the succession).

Mudstones (table 3.2) yielded a SiO_2 range of 50.24-73.74% . Al_2O_3/SiO_2 ratios range from 0.12 to 0.51. LIL elements display variable inter-element ratios. Similarly, Ti, Zr, Y and Nb exhibit a wide range of abundances without consistent inter-relationships.

Limestones (table 3.3) exhibit a low content in SiO_2 (1.87-7.85%) and variable Al_2O_3/SiO_2 ratios due to the existence of thin mudstone partings. MgO/CaO ratio is very low (0.01). LIL and high field strength elements show low abundances with the exception of Sr (183-253 ppm).

Factors affecting the sediment chemistry are source rocks (including weathering products), grain sorting, diagenesis, relative proportion of detrital versus biogenic/chemical inputs and metamorphism (metasomatism) (Sawyer, 1986; Wronkiewicz and Condie, 1987, Floyd et al., 1991). Source rocks and sedimentary processes are intimately linked to the tectonic setting of the basin. Diagenesis also controls the bulk composition of sediments but the nature of diagenesis is itself dependent on the tectonic setting (Siever, 1979). Except for the loss of volatiles and certain trace elements, the regional metamorphism of metapelites is generally regarded as an isochemical process (e.g. Shaw, 1956; Yardley, 1977, 1986; Wood and Walther, 1986). In a recent study, Ague (1991) has demonstrated that there may exist some mobility of silica, Ca, Na and K during medium- and high-grade metamorphism

---

(1) Fe_2O_3* = total iron

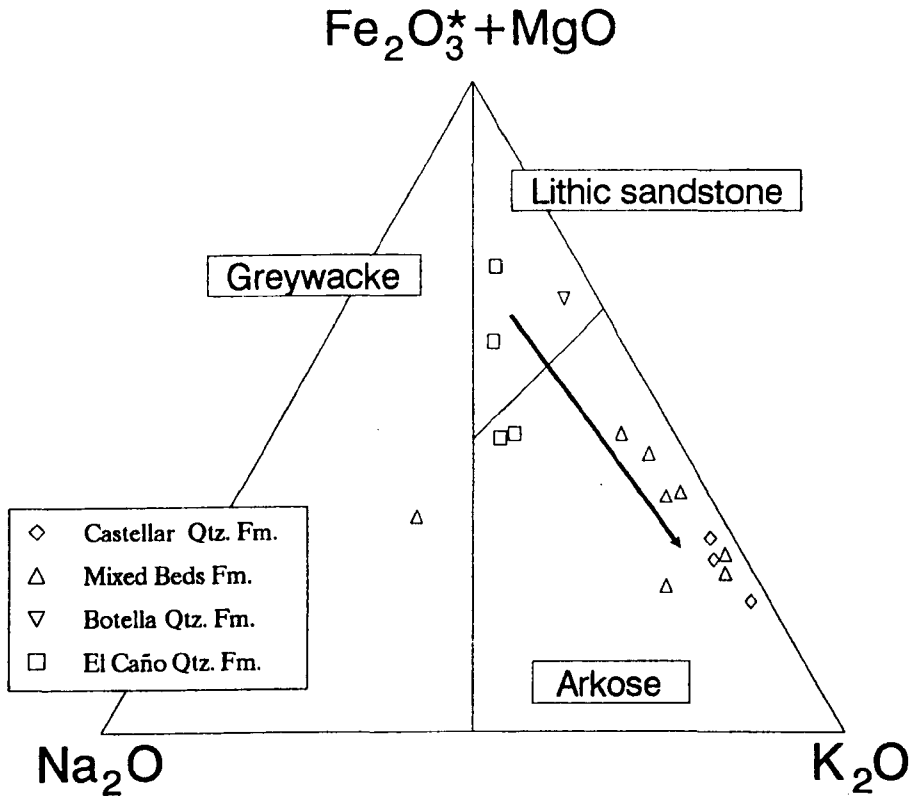

Fig.3.12. Petrochemical classification of sandstones from Upper Ordovician-Lower Silurian formations in estern Sierra Morena (based on Blatt et al., 1980).

but those changes can be similar to or smaller than the original compositional variations of the protoliths. Additionally, metasomatism may be significant in carbonates or shear zones (Yardley, 1989).

Since the bulk chemistry of the terrigenous sediments is eminently constrained by the basin environment and source rocks, whole-rock geochemical analyses of sediments may be used to infer the plate tectonic setting of the basin (Crook, 1974; Maynard et al., 1982; Bhatia, 1983, 1985; Roser and Korsch, 1986; Floyd and Leveridge, 1987 among others). Thus, Bhatia (1983) considered four tectonic provenances:

a)Oceanic Island Arc (OIA). Sediments are mainly derived from the calc-alkaline or tholeiitic arc.

b)Continental Island Arc (CIA). Sediments are mainly derived from felsic volcanic rocks.

c)Active Continental Margins (ACM). Sediments are dominantly derived from granite-gneisses of older fold belts and siliceous volcanic rocks of the uplifted basement.

d)Passive Margins (PM). Sediments are derived by the recycling of older sedimentary and metamorphic rocks of platforms or rejuvened orogens.

Roser and Korsch (1986) proposed a similar classification but they considered the continental island arc as a subtype of the active continental margin setting.

Bhatia (1983) found that the most affective discriminating geochemical parameters relative to tectonic settings are TiO_2 wt%, Al_2O_3/SiO_2, K_2O/Na_2O and $Al_2O_3/(CaO + Na_2O)$ ratios all plotted against $Fe_2O_3^*$+ MgO wt%. In this study a modified version of the Bhatia fields was used, which includes the majority of the original data. To enable direct comparison, all oxides have been recalculated to 100% volatile free. In the TiO_2 wt% plot (fig.3.13), most of the points fall outside the fields, three

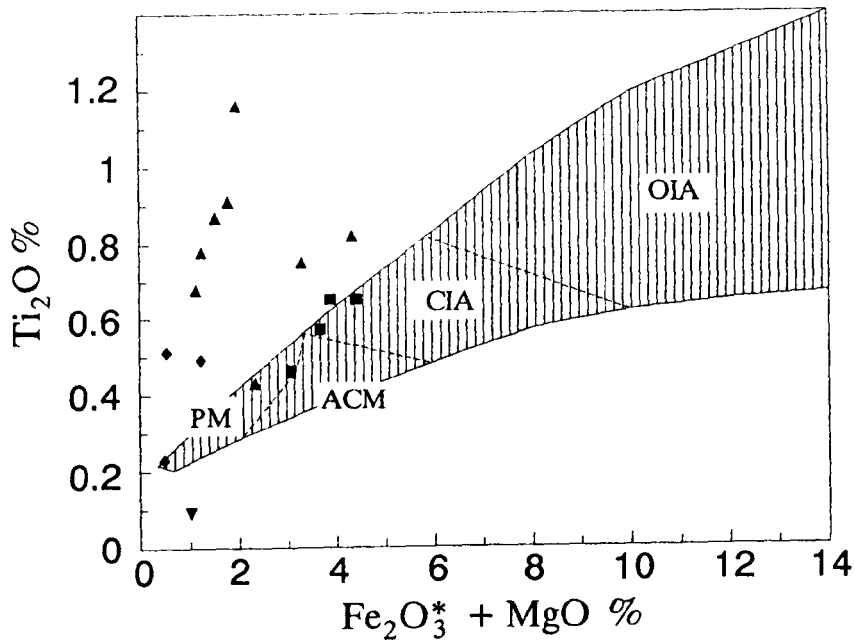

Fig.3.13. TiO_2 versus Fe_2O_3*+MgO plot for discrimination of plate tectonic setting of sandstones from eastern Sierra Morena. PM: passive margin, ACM: active continental margin; CIA: continental island arc; OIA: oceanic island arc (fields based on Bathia, 1983). Simbols as for fig. 3.16.

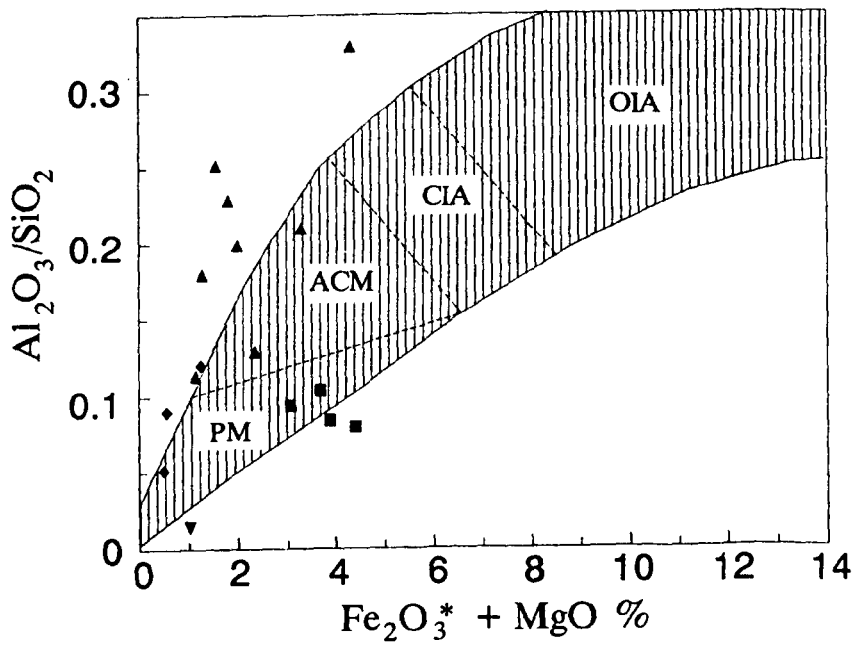

Fig.3.14. Al_2O_3/SiO_2 versus Fe_2O_3*+MgO plot for discrimination of plate tectonic setting of sandstones from eastern Sierra Morena (fields based on Bathia, 1983). Simbols as for fig. 3.16. Abbreviations as for fig. 3.16.

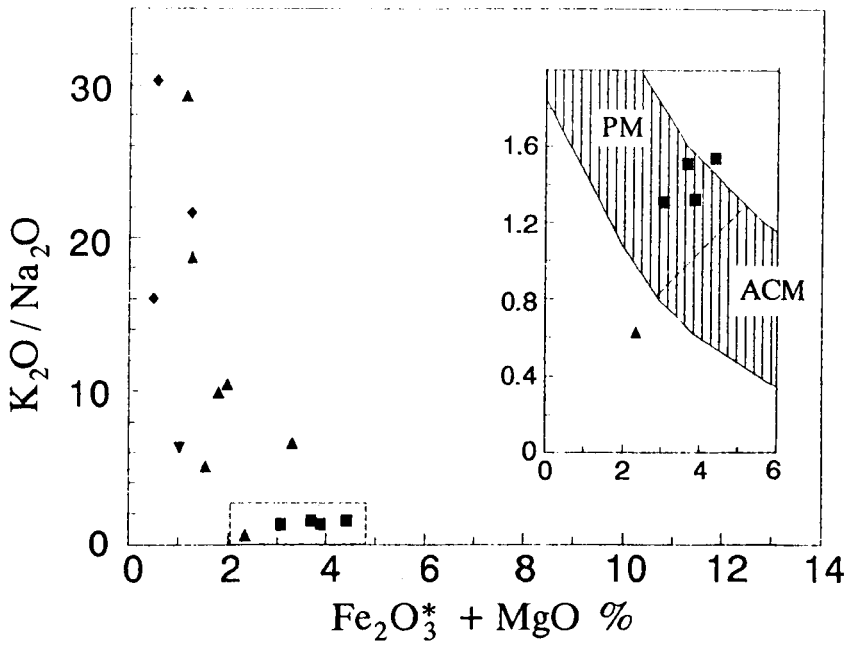

Fig.3.15. K_2O/Na_2O versus $Fe_2O_3^*$+MgO plot for discrimination of plate tectonic setting of sandstones from eastern Sierra Morena (fields based on Bathia, 1983). Simbols as for fig. 3.16. Abbreviations as for fig. 3.13.

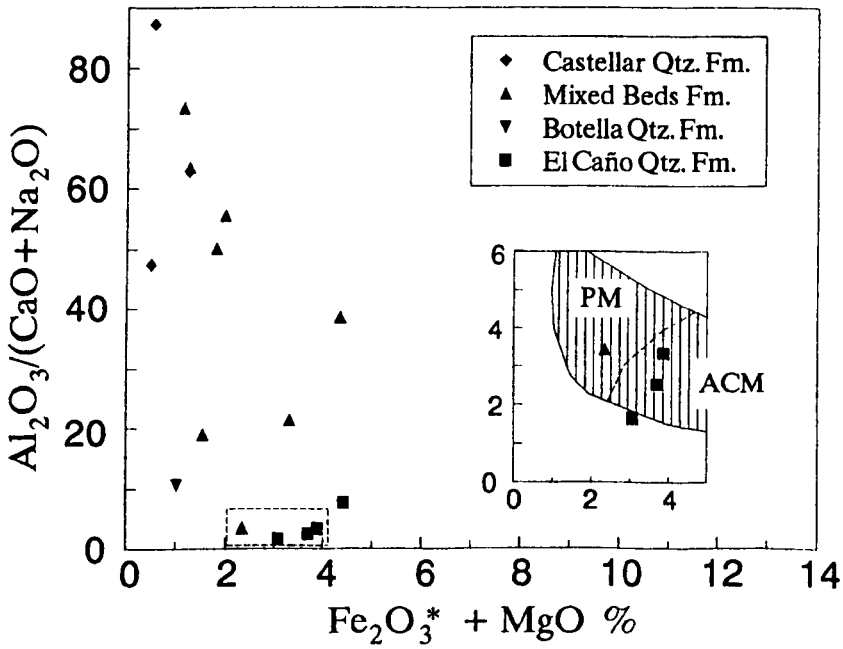

Fig.3.16. $Al_2O_3/(CaO+Na_2O)$ versus $Fe_2O_3^*$+MgO plot for discrimination of plate tectonic setting of sandstones from eastern Sierra Morena (fields based on Bathia, 1983). Abbreviations as for fig. 3.13.

samples show compositions assigned to continental island arc and another three plot within the passive margin field. Plotting the ratio Al_2O_3/SiO_2 (fig.3.14) produces a distribution where most of the samples fall within or very close to the PM and ACM fields, as may be expected for arkosic sediments. Most of the observed vertical variation in both plots is interpreted as due to varying concentrations of detrital phyllosilicates, which is specially evident in the Mixed Bed Formation.

There is a large vertical variation of the data in the K_2O/Na_2O plot (fig.3.15). Four samples from El Caño formation plot within the Passive Margin field. Vertical displacement is related to the degree of maturity of sediments, maturity being directly reflected in the relative feldspar ratios (K_2O/Na_2O increases with maturity, fig.3.12). Similar causes can be envisaged to explain the vertical variation in the $Al_2O3/(CaO + Na_2O)$ plot (fig.3.16) although Al_2O_3 may be also related to the variable participation of phyllosilicates in the sediments. In this plot, three samples (from El Caño formation) plot within or close to the ACM field and one from the Mixed Beds lies in the PM field.

Discriminant function analysis of sandstones was done using the function coefficients proposed by Bhatia (1983) to calculate discriminant scores following the expression;

$$D_i = a_i a_s + b_i b_s + c_i c_s + \ldots\ldots\ldots + p_i p_s + C_i$$

Where $a_i \ldots . p_i$ represent the values of unstandarised discriminating coefficients, $a_s \ldots\ldots p_s$ represent the abundance (in %) of the element oxides in the sample, C_i is a constant and D_i is the discriminant score. Values obtained by this procedure are listed in table 3.4 and plotted in fig.3.17 where also the fields established by Bhatia (1983) have been drawn. Distribution of discriminant scores either reflects a PM or an ACM setting. Samples from the same formation may be in both fields but points lying in the PM are relatively close to the PM/ACM boundary.

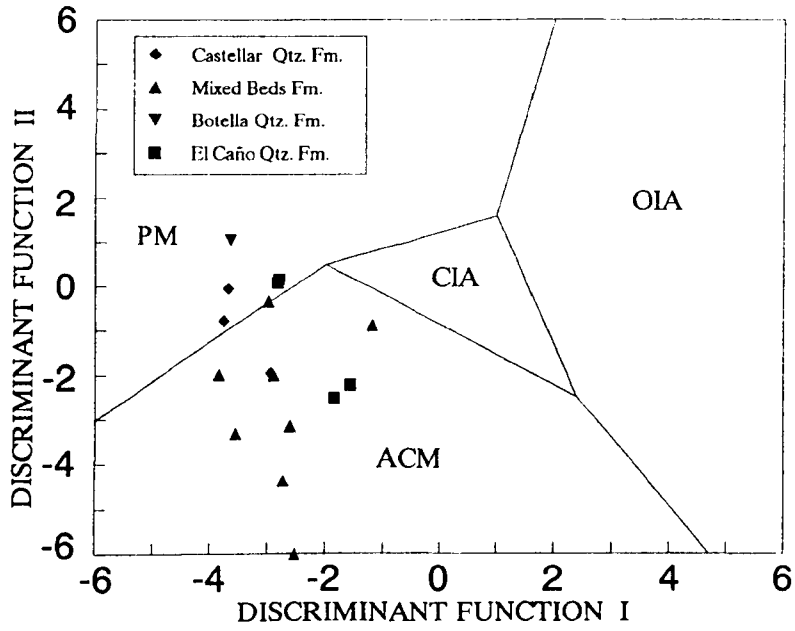

Fig.3.17. Plot of discriminant scores along functions I and II for sandstones for eastern Sierra Morena. Abbreviations as for fig. 3.13. Simbols as for fig. 3.16.

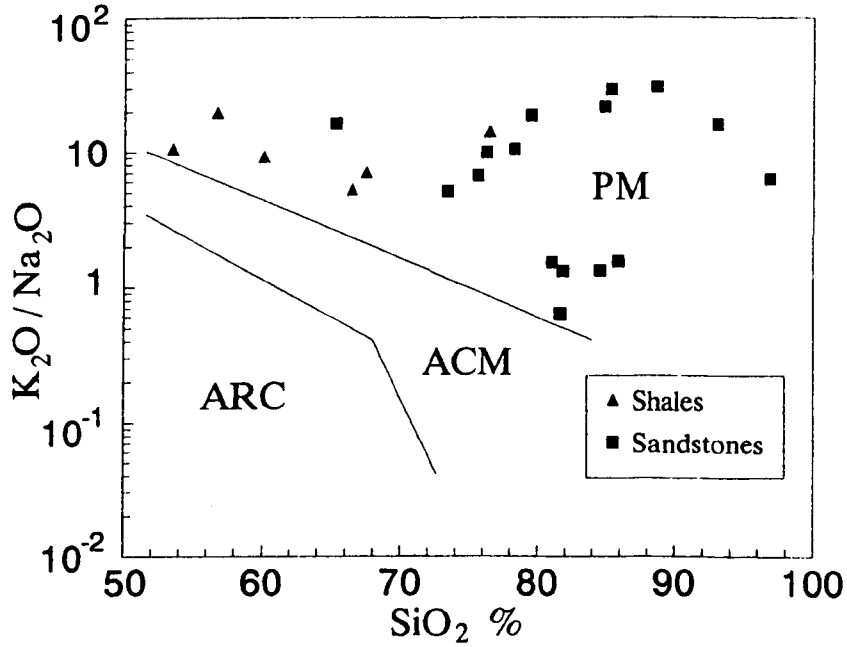

Fig.3.18. K_2O/Na_2O versus SiO_2 plot for discrimination of plate tectonic setting of sandstones from eastern Sierra Morena. PM: passive margin, ACM: active continental margin, ARC: oceanic island arc (fields after Roser and Korsch, 1986).

On the basis of SiO_2 content and K_2O/NaO ratios (table 3.1) the sandstones from the Middle-Upper Ordovician-Lower Silurian in La Carolina-Sta. Elena may be considered as having been deposited at a passive continental margin (Crook, 1974; Maynard et al., 1982). Roser and Korsch (1986) have presented a refinement of the SiO_2 versus K_2O/NaO discrimination in considering that there is a systematic variation in both parameters with change in grain size. Therefore, such discrimination can be applied either to sandstones or finer-grained members (mudstones) of sedimentary sequences. Fig.3.18 shows the distribution of samples from metasediments of La Carolina-Sta. Elena (oxides were recalculated to 100% volatile-free for direct comparison). This distribution is consistent with a origin related to a passive margin setting for all the samples. A singular group with the lowest K_2O/Na_2O ratios includes the four samples from El Caño formation and one from the Mixed Beds.

Floyd and Leveridge (1987) have applied K versus Rb contents to discriminate between acidic-intermediate and basic provenance of sandstones (fig.3.19). All the sandstones have a K/Rb ratio above a typical differentiated magmatic suite (K/Rb = 230; Shaw, 1968). Only one sample (LC9098-7) yielded anomalously low K and Rb, but the high SiO_2 content (97.61%) precludes its interpretation as basic rock.

Yudovich et al., (1985) have proposed the use of modular diagrams comparing chemical parameters such as TiO_2 / Al_2O_3 (the titanium modulus, TM), (Al_2O_3 + TiO_2 + Fe_2O_3*) / SiO_2 (the hydrolysate modulus, HM), (Fe_2O_3* + MnO) / Al_2O_3 (the iron modulus, IM), Na_2O / Al_2O_3 (the sodium modulus, SM), K_2O / Al_2O_3 (the potassium modulus, PTM) and the over-all normalised alkalinity (SM+PTM) to diagnose the occurrence of small amounts of volcanogenic material in sediments. Thus, it is assumed that high contents in Fe and Mn may be related to exhalations, and high values in SM and PTM moduli reflect the presence of feldspars which together with elevated Ti abundances may be caused by the incorporation of basic-intermediate volcanoclastic material. The HM modulus serves to test the variations in these moduli (e.g. low

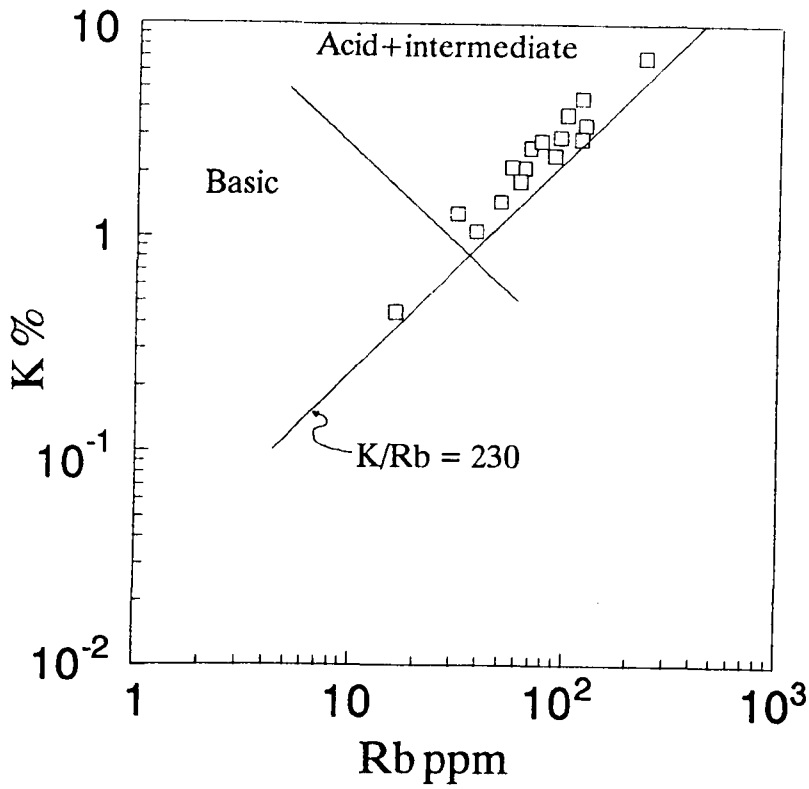

Fig.3.19. Distribution of K (wt%) versus Rb (ppm) of sandstones from eastern Sierra morena. K/Rb curve corresponds to the Main Trend of Shaw (1968). Boundary line between acid/intermediate and basic compositions after Floyd and Leveridge (1987).

Sample	LC149-1	LC59-12	LC9088-2	LC9088-3	LC9098-7	LC308-7	LC308-6	LC153-1
Formation	RQ	RQ	RQ	RQ	BQ	MB	MB	MB
HM	0.13	0.13	0.15	0.13	0.02	0.26	0.24	0.39
PTM	0.21	0.28	0.32	0.16	0.32	0.17	0.16	0.34
SM	0.16	0.22	0.21	0.10	0.05	0.02	0.02	0.02
IM	0.40	0.32	0.35	0.52	0.65	0.09	0.11	0.15
TM	0.09	0.06	0.07	0.10	0.07	0.06	0.08	0.04
FUNCTION I	-2.80	-1.84	-1.57	-2.83	-3.64	-2.90	-2.98	-2.52
FUNCTION II	0.16	-2.52	-2.23	-0.07	1.04	-2.01	-0.35	-9.19

Sample	LC153-2	LC143-1	LC93-5	LC9031-13	LC9031-2	LC9078-1	LC9078-2	LC9078-3
Formation	MB	MB	MB	MB	MB	CQ	CQ	CQ
HM	0.16	0.20	0.28	0.13	0.26	0.14	0.10	0.06
PTM	0.17	0.27	0.25	0.31	0.22	0.28	0.27	0.27
SM	0.28	0.01	0.05	0.01	0.03	0.01	0.01	0.02
IM	0.18	0.06	0.06	0.09	0.16	0.11	0.05	0.09
TM	0.04	0.06	0.05	0.07	0.05	0.05	0.06	0.05
FUNCTION I	-1.19	-3.55	-2.73	-3.84	-2.62	-2.94	-3.75	-3.68
FUNCTION II	-0.89	-3.32	-4.38	-2.00	-3.15	-1.97	-0.80	-0.06

Sample	LC59-13	LC90138-4	LC9098-8	LC90148-8	LC308-8	LC9031-4
Formation	COS	BQ	CAS	CHS	CHS	CHS
HM	0.40	0.60	0.37	0.25	0.70	0.50
PTM	0.23	0.26	0.29	0.26	0.20	0.32
SM	0.05	0.01	0.04	0.02	0.02	0.04
IM	0.26	0.22	0.26	1.01	0.32	0.33
TM	0.05	0.05	0.05	0.06	0.05	0.05

Sample	LC73-1	LC73-2	LC73-4	LC73-5
Formation	UL	UL	UL	UL
HM	0.80	0.39	0.38	0.64
PTM	0.27	0.28	0.30	0.25
SM	0.07	0.30	0.05	0.06
IM	1.00	0.46	1.07	0.97
TM	0.13	0.13	0.26	0.19

Table 3.4. Chemical moduli of sandstones, mudstones and limestones (HM: hydrolysate modulus; PTM: potassium modulus; SM: sodium modulus; IM; iron modulus; TM: titanium modulus. See explanation in the text). Scores of discriminant functions I and II of sandstones are calculated using the unstandarised discriminating coefficients proposed by Bhatia (1983). Formation abbreviations as in Tables 3.1, 3.2 and 3.3.

HM values associated with high TM and low PTM and SM moduli is interpreted as due to sorting in a mature sediment. Note that K and Na may be mobile during metasomatism and conclusions based only on PTM and SM may lead to misinterpretation).

The TM modulus has been plotted against the PTM modulus in fig. 3.20, the IM modulus against SM+PTM in fig. 3.21 and the HM modulus against SM+PTM in fig. 3.22. Values are listed in table 3.4.

The high content of Ti (TM > 0.1,) in Urbana limestones probably is due to biogenic concentration (Yudovich et al., 1985) as the potassium modulus (PTM) lies in a range of 0.25-0.30 representative of a hydromica plus chlorite mixture. PTM+SM values close to those PTM levels and petrographical evidence exclude the presence of feldspars, and therefore the probable occurrence of volcanic material. High-elevated values of iron (IM=1) are congruent with the existence of local concentrations of pyrite and magnetite. Exhalative origin of the iron is questionable because the 'heavy' $\delta^{34}S$ values (+16.52, +39.7 and +45.4 $^{o}/_{oo}$) obtained from three samples are difficult to explain if a magmatic source of sulphur is assumed (see 3.5. in this chapter and chapter 8). Such $\delta^{34}S$ values in pyrite coexisting with magnetite reflect a environment where the bacteriogenic H_2S production was faster than the sulphate supply ($\delta^{34}S$ of Ordovician marine sulphate is around +27 $^{o}/_{oo}$, after Claypool et al., 1980) but not enough to precipitate all the reactive iron as sulphide (Ohmoto and Rye, 1979). A sedimentary source of the sulphur does not exclude a volcanogenic origin of the iron as oxihydroxides may be transportated as supensates or colloids in opposition to the 'igneous' aqueous sulphate, that is rapidly mixed with the sea water sulphate. High HM values in the limestones are due to thin mudstone partings.

Sandstones from the El Caño Fm. display an elevated TM modulus, some of the highest SM+SP values and intermediate IM levels. HM values are in the clay-siliceous range (0.1-0.2). The TM and SM+SP moduli indicate the presence of small amounts of

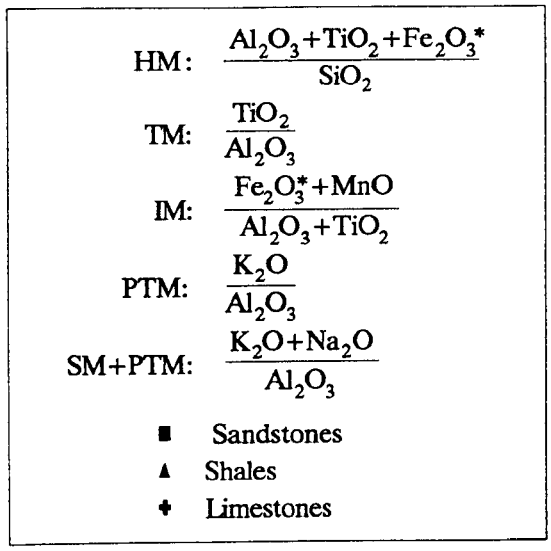

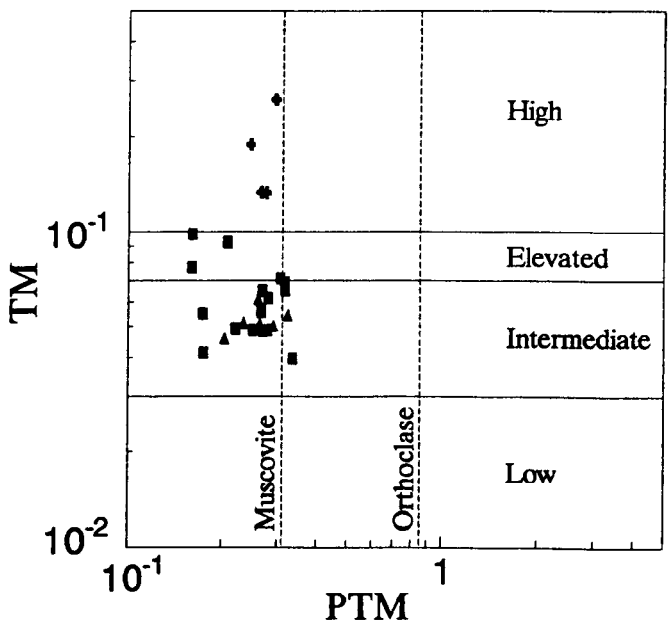

Fig.3.20. Titanium modulus (TM) versus potassium modulus (PTM) plot. Fields from Yudovich et al (1985). Normative muscovite and orthoclase are also shown to compare.

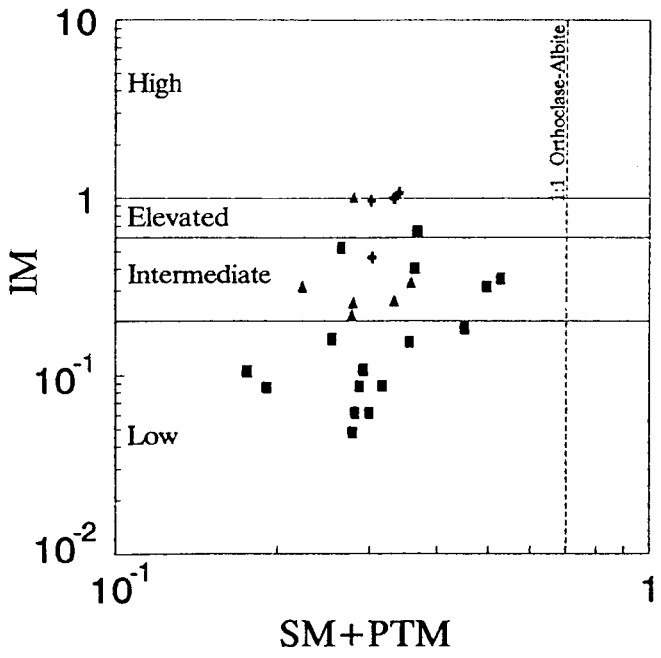

Fig.3.21. Iron modulus (IM) versus the over-all normalised alkalinity (SM+PTM). Fields from Yudovich et al (1985). Orthoclase-albite line corresponds to the normative composition for a 1:1 mixture of orthoclase and albite. Calculation of modulus is explained in fig. 3.20.

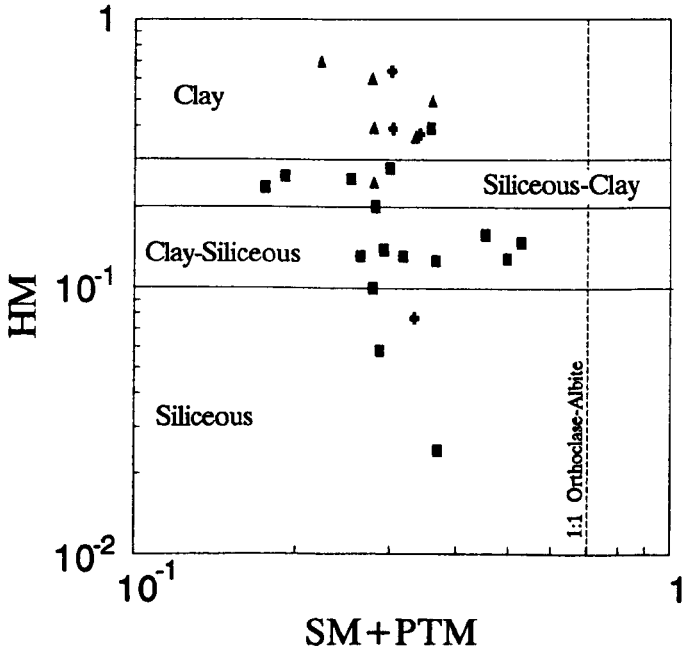

Fig.3.22. Hydrolysate modulus (HM) versus the over-all normalised alkalinity (SM+PTM). Fields from Yudovich et al (1985). Orthoclase-albite line corresponds to the normative composition for a 1:1 mixture of orthoclase and albite. Calculation of modulus is explained in fig. 3.20.

basic (?) volcanogenic material. Similar TM modulus is found in sample LC9098-7 (Botella Quartzites Fm.) although it presents a SM modulus smaller (0.05) than those in samples from the El Caño Fm. As HM modulus is also very low (0.02) due to the high silica content, the elevated levels of IM (0.65) and TM (0.07) are not interpreted as volcanic-derived, and they are likely due to sedimentary dilution in a well-sorted mature sediment.

Most of the sandstones and siltstones from the Mixed Beds Fm. exhibit low levels of iron (IM < 0.2) and 'normal' levels of Ti (0.03 < TM < 0.07), the only exceptions being sample LC308-6 (TM = 0.8, SM+PTM = 0.18) and sample LC9031-13 (TM = 0.07, SM+PTM = 0.32). This last sample was collected from the beds considered by Charpentier (1976) as volcanic tuffites of rhyolitic affinity on the basis of petrographical evidences (minor occurrences of potassium feldspars and 'recrystallised bubbles'(?)). At least in this sample, volcanogenic material seems to be absent. The rock is not considered a volcanic tuff as the PTM modulus is similar to the normative muscovite limit (PTM = 0.31) and unequivocal petrographic evidence has not been found. A sample from the Mixed Beds Fm. yielded $\delta^{34}S_{py}$ = +8.21 $^{o}/_{oo}$. Given the inner shelf/near shore environment of sedimentation, such a value is consistent with bacterial reduction of seawater sulphate in a system close to SO_4^{2-}. That process produces isotopic displacements up to -25 $^{o}/_{oo}$ from the original values of sea water (Ohmoto and Rye, 1979; Goldhaber and Kaplan, 1980, see fig. 3.26). Further discusion will be presented in chapter 7.

Samples from the Castellar Formation yielded 'normal' levels of Ti (TM = 0.05-0.06), low levels of iron (IM = 0.16-0.05) and PTM levels within the chlorite plus hydromica range (PTM = 0.20-0.31, Yudovich et al., 1985). Therefore, there is no evidence of volcanogenic material incorporated in these mature sediments.

The shales from the Correderas Shales Fm., Botella Quartzites Fm., and Chavera Shales Fm. display 'normal' levels of Ti (TM = 0.05-0.06, fig.3.20) and 'normal' levels of iron (IM = 0.22-0.33, fig.3.21) except in sample LC90148-1 (Chavera Fm., IM = 1.01,

close to the elevated-high boundary) which yielded the lowest HM observed in shales (0.25, siliceous-clay). As it will be noted below, this sample is characterised by high contents of Zn (4,301 ppm) and Pb (389 ppm) and apparent depletion of Th, U, Ba and Sr compared to the average shales of Turekian and Wedepohl (1961). That pattern differs from that expected if participation of volcanic materials occurred. In fact, a normalisation to the average Al_2O_3 in shales is required for a correct comparison because the ratio Al_2O_3/SiO_2 in the sample is too low. After that normalisation, Th and U (12.18 and 3.4 ppm respectively) are close to the average values but depletion of Ba and Sr still remains. Such depletions and dilution of immobile elements by incorporation of SiO_2 are better explained in terms of hydrothermal metasomatism (see chapter 5) rather than by volcanogenic participation. Therefore, the shales can be considered as 'normal' sediments (*sensu* Yudovich et al., 1985) with no significative participation of volcanogenic materials. If that premise is assumed, then the $\delta^{34}S_{py} = -13.65\,^{o}/_{oo}$ yielded by a sample from the Chavera shales is consistent with pyrite formation from a bacteriogenic H_2S source in a relatively anoxic environment. Slow rate of sulphate reduction produces large kinetic isotopic effects, giving as result displacements in the $\delta^{34}S$ values between $-40\,^{o}/_{oo}$ and $-60\,^{o}/_{oo}$ (Ohmoto and Rye, 1979, Goldhaber and Kaplan, 1980; see chapter 7).

Bhatia (1985) used trace elements to determine the tectonic setting of mudstones. The discrimination is based in concentrations and inter-element ratios of Nb, Y, Rb, Sr, Th, Ba, and Ni. The results obtained from the samples (sample LC90148-1 was excluded) are relatively consistent and reveal a passive margin setting (PM, table 3.5). Incongruous Zr/Th ratio is due to a high abundances of Zr whereas high abundances in Nb give a Zr/Nb ratio close to that assumed for passive margins.

	Sandstone	Mudstone	Limestone
Ni	2	68	20
Cu	25*	45	4
Zn	16	95	20
Rb	60	140	3
Sr	20	300	610
Y	40	26	30
Zr	220	160	19
Nb	26*	11	0.30
Ba	550*	580	10
Pb	7	20	9
Th	1.70	12	1.7
U	0.45	3.70	2.20

Table 3.5 Trace element averages (After Turekian and Wedepohl, 1961; except Cu, Ba and Nd in sandstone (*) which are averages in the upper crust, from Taylor and McLennan, 1985).

	Mean (n=5)	OIA	CIA	ACM	PM
Ni	36.60	15.00	18.00	26.00	36.00
Nb	21.80	3.70	9.00	16.50	15.80
Th	21.00	5.50	16.20	28.00	22.00
Zr/Nb	10.25	38.00	21.00	11.00	10.00
Zr/Th	11.12	28.00	12.00	7.00	7.00
Nb/Y	0.61	0.17	0.35	0.50	0.54
Rb/Sr	4.63	0.29	1.31	2.90	5.80
Ba/Sr	23.22	2.50	6.30	8.70	17.60

Table 3.6. Discrimination of tectonic setting by trace elements in mudstones. Values for the tectonics settings OIA (oceanic island arc), CIA (continental island arc), ACM (active continental margin) and PM (passive margin) after Bhatia (1985). Sample LC90148-1 is excluded from the mean.

3.4.3.Trace elements. Distribution of ore-forming elements (Ba, Cu, Pb and Zn).

Multi-element diagrams may be used to examine the distribution of trace elements in metasediments. To facilitate the comparison, the elements presented in table 3.6 are normalised against the averages of sandstones, shales and carbonates presented by Turekian and Wedepohl (1961) and Taylor and McLennan, (1985). Anomalous compositions in ore forming elements have been tested by observation of the 'behaviour' of high field strengh elements (Y and Nb) and LIL elements such Th and U. These elements can provide invaluable information, even if they are strongly influenced by sedimentary factors (e.g. grain size), because they exhibit distinctive ranges in some formations.

A significant feature of the trace elements in sandstones is their variable distribution in relation to the average (fig.3.23.). Thus, most of the samples are depleted in Cu, Y, Nb and enriched in Ni, Zn, Zr, Pb, Th, and U. Another singular feature is that the highest values are generally found in samples from El Caño Fm. (arkoses and lithic sandstones with graywackic affinity) whereas the lowest ones are found in the more siliceous (i.e. more mature) sediments (Botella Fm. and Castellar Fm.). There are exceptions to this trend as Zn exhibits an erratic distribution and Pb abundance increases toward the top of the stratigraphical succession (Castellar Fm., *cf*. Rios and Claverias, 1979). These 'lithological' trend of Th, Sr, Zr, Y, etc. and 'stratigraphical' trend of Pb rule out a Pb enrichment due to metasomatism by Late-Variscan hydrothermal fluids. Causes of the Zn distribution are not clear albeit relative enrichment due to Late-Variscan fluids seems unlikely as no hydrothermal dilution of immobile elements is observed.

Shales exhibit a variable distribution relative to the average of Turekian and Wedepohl (1961). The most remarkable feature is the generalised depletion of Sr. U, Th, Rb, Y, Nb, and Ba are internally consistent, displaying no large variations among different formations (fig. 3.24). One sample from Chavera Fm.

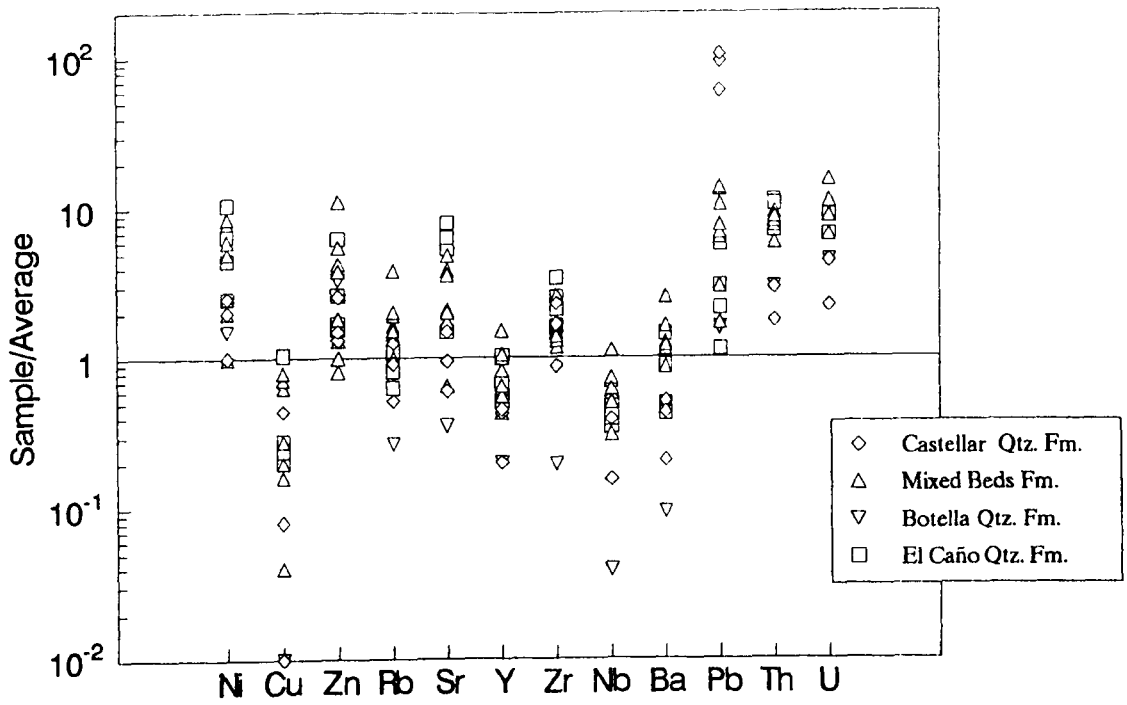

Fig.3.23. Normalised trace element diagram of sandstones from eastern Sierra Morena. Average values used for normalisation are listed in table 3.5.

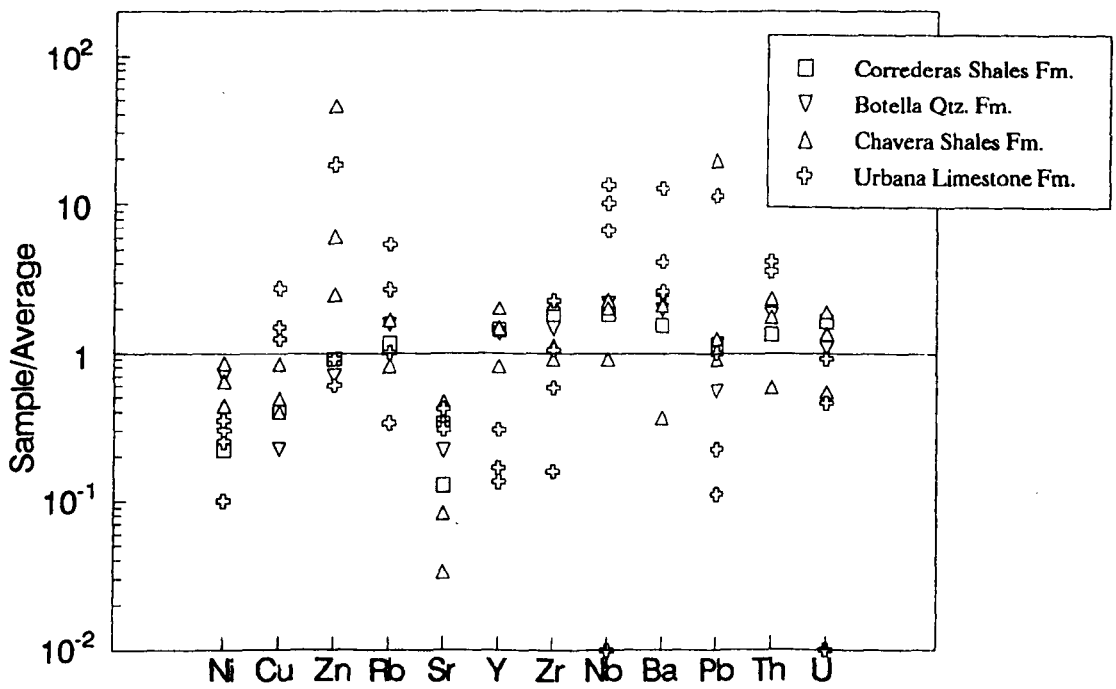

Fig.3.24. Normalised trace element diagram of mudstones and limestones from eastern Sierra Morena. Average values used for normalisation are listed in table 3.5.

(LC90148-1) shows apparent depletion in Th, U, Ba, Nb, Y and high abundance of Zn and Pb. As was commented on above, compositional variations of this singular sample are produced by hydrothermal metasomatism with incorporation of silica and ore-forming elements (Pb and Zn) likely related to the proximity of a concealed vein. Two samples (LC308-8 and LC9031-4) from the same formation are enriched in Zn with no special variations in the inmobile elements.

Distribution in limestones is erratic (fig.3.24), provide that all samples were collected from the same outcrop (La Despreciada quarry). Absolute abundances in ore-forming elements are very low with exception of sample 73-5 that exhibits 362 ppm of Zn and 101 ppm of Pb. The arbitrary distribution of Y, Zr, and Rb may be related to the clastic origin of this formation.

3.5. Ore deposits. Iron occurrences.

Several stratabound Pb-Zn-Ba occurrences in the Urbana Limestone Fm. and the Castellar Quartzite Fm. have been briefly cited in the literature. Thus, Rios (1977) has reported the existence of disseminated galena in the Urbana Limestone at the environs of La Despreciada quarry (fig. 3.1, location 3). Jacquin and Pineda (1980) and Pineda (1987) have described disseminations, vugs and veinlets of barite, sphalerite, galena and siderite in drill cores of that formation at El Centenillo. Palero and Martín-Izard (1988) have documented some occurrences in exposures of the same formation at the Puertollano syncline (located on the northwest from Linares-La Carolina district). The mineral paragenesis is simple, mainly consisting of sphalerite and minor amounts of galena and chalcopyrite. Gangue minerals are carbonates and quartz. The mineralisation occurs at the top of the formation, spatially related to dolomitised limestones.

Rios (1977) and Rios and Pineda (1979) have reported several occurrences in the Castellar Quartzite Fm. cropping out in the study area (e.g. Renegadero valley) and adjacent sectors (e.g. La

Alamedilla). The mineralisation consists of interbedded nodules of galena and sphalerite and disseminations of sphalerite and pyrite.

During the survey carried out as part of this thesis, the reported occurrences in outcrops in the study area were either not found, or when found they were clearly related to the Late-Hercynian mineralising events. Thus, veinlets with quartz, sphalerite, galena and pyrite in the Castellar Fm. at Renegadero valley that were reported as probable syn-diagenetic ores (Rios, 1977), are spatially restricted to the neighbourhood of the Federico lode and no occurrences are present in other large outcrops of that quartzitic formation (e.g. Rio Grande valley or El Centenillo sector).

Similarly, neither galena, sphalerite or barite were found in the Urbana Limestone at La Despreciada quarry and its environs.

A thin (5 cm-8 cm thick) garnetiferous bed with sphalerite, pyrite and minor galena was observed in the Mixed Beds cropping out behind the forge of El Guindo mine. There is textural evidence to rule out a syn-diagenetic origin: a) ore and gangue (mainly 'chlorite') are filling microcracks subparallel to the bedding plane. b) the veinlets are not deformed, ore and phyllosilicates are subhedral and crystallographically arranged in a random fabric. Therefore, ore deposition postdated the Variscan deformation. A sphalerite sample (LC93-3) was analysed for sulphur isotopes, yielding a $\delta^{34}S$ value of +11.26 (2). That value does not differ from those obtained from two samples ($\delta^{34}S$ = +10.96 ‰, sample LC308-13 and $\delta^{34}S$ = +11.54, sample LC308-15) collected in a nearby Late-Variscan lode (Federico lode, La Española shaft). Independently of the sources of sulphur involved in the mineralisation (see chapter 7), such consistency supports a Late-Hercynian origin for this occurrence which will not be given further consideration in this Chapter.

---

(2) sample duplicated, mean value.

Ironstones were found in the Urbana Limestone at La Despreciada quarry. A thin discontinuous bed of centimetric thickness consists of magnetite (dominant), pyrite, quartz (authigenic and detrital), siderite and minor berthieroid iron silicate (berthierite/chamosite, *sensu* Young, 1989). It is located a few cm. below a sedimentary reactivation suface (fig. 3.25, see 3.3. in this Chapter). Magnetite and pyrite are mostly euhedral, pyrite in crystals up to one cm. size. Siderite is present as matrix. Berthierod silicate appears in euhedral grains which can be deformed, surrounding the coarser grains of pyrite and magnetite. The presence of magnetite is limited to this bed but pyrite occurs (associated with accessory white mica) some cm. below, being relatively abundant in discontinuous lenses up to 3 cm. thick at 50 cm. below the 'magnetite bed'.

Two pyrite samples from the 'pyritic bed' and from the 'magnetitic bed' (LC73-2 and LC73-3, respectively) were analysed for sulphur isotopes, yielding $\delta^{34}S$ = +39.70 $^{o}/_{oo}$ and $\delta^{34}S$ = +45.40 $^{o}/_{oo}$, respectively. An other pyrite sample (LC90164-8) from a 'lumachelle' of the same formation but at diferent location (El Centenillo) gave a $\delta^{34}S$ value of +16.52 $^{o}/_{oo}$.

The origin of magnetite-rich ironstones remains controversial. Magnetite may be formed by metamorphic reactions such as breakdown of iron carbonate or primary iron silicate. Alternatively, it may precipitate at 'syngenetic-early diagenetic' conditions as shown by Garrels and Christ (1965). In most of the ironstones, magnetite is found in mineral equilibrium with siderite and/or iron silicate (e.g. berthierite) and a syngenetic-early diagenetic origin is commonly accepted if there are not unambiguous evidences to support the metamorphic origin (Brown, 1943; James, 1954; Harder, 1989 among others).

Similarly, pyrite, siderite and iron silicate can be stable at conditions encountered within the sediment (Curtis and Spears, 1968).

	LC73-3 'Magnetite Bed'	LC73-7 Karst Fe	LC73-8 Karst Fe-Mn
Ni	27	390	1015
Cu	17	55	41
Zn	27	3943	6372
Rb	3	11	6
Sr	176	35	356
Y	11	21	54
Zr	8	25	22
Nb	0	4	2
Ba	46	2166	11104
Pb	10	194	144
Th	7	5	4
U	1	2	1

Table 3.7. Trace element XRF analyses of iron ores in the Urbana Limestone Formation (in ppm). Note the high content in Zn and Ba in the samples from the karst-related deposit.

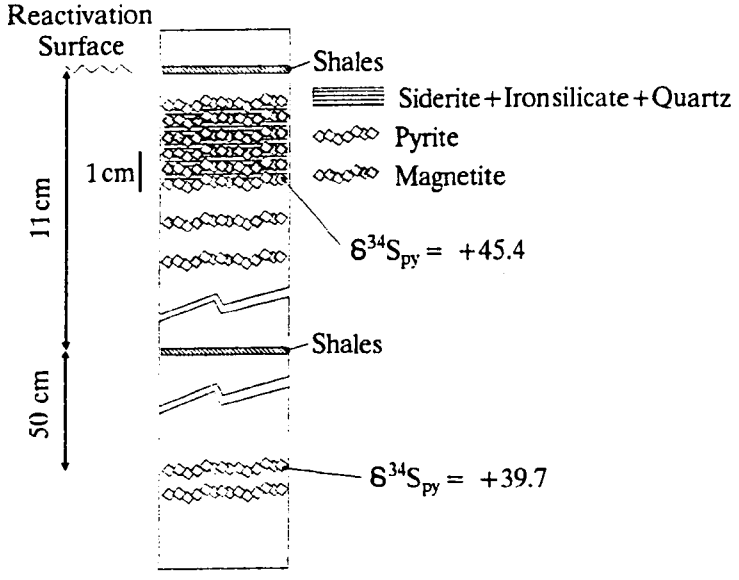

Fig.3.25. Skecth depicting the disposition and mineral associations of the magnetite and pyrite beds in the Urbana Limestone Fm.

Pyrite formation in sediments is usually early diagenetic, or a result of the reaction of H_2S generated by bacterial reduction of the sulphate in pore water with reactive iron from minerals present in the sediment (Berner, 1970). Iron minerals may be detrital (e.g. chlorite, iron-rich smectites, etc) or precipitated ferric oxihydroxides (e.g. $Fe(OH)_3 \cdot nH_2O$). In 'normal' marine sediments (those deposited in oxygenated bottom waters), the bacterial reduction of sulphate occurs in anoxic conditions, usually some cm. below the water-sediment interface, depending of the rate of oxygen-consuming microbial processes and the rate of oxygen transport due to molecular diffusion, physical stirring or bioturbational irrigation (Aller, 1980; Berner, 1980). Pyrite formation in this oxic zone is very limited.

Given the required anoxic conditions, the factors controlling the rate of sulphate reduction are the amount and reactivity of organic matter in the sediment and the dissolved sulphate concentration (Raiswell, 1982; Berner, 1984, Berner and Raiswell, 1983; Raiswell and Berner, 1986).

The bacteriogenic sulphide subsequently reacts with the iron present as Fe^{2+} species (formed in post-oxic reactions) to produce metastable iron monosulphides that transform to pyrite. In a closed system to SO_4^{2-} (which is the environment expected in the anoxic zone of 'normal' marine sediments), the remaining sulphate in pore water will be progressively depleted in ^{32}S (Goldhaber and Kaplan, 1980; Raiswell, 1982 among others). The availability of iron may determine if the system is open or closed to H_2S. When the supply of iron is limited, the system is open to H_2S as it remains in the system as aqueous specie. Alternatively, when an excess of reactive iron exists relative to the availability of aqueous sulphide (e.g. when the bacterial activity is limited by low amounts of readily metabolisable organic matter), the system is closed to H_2S: the aqueous sulphide is continuosly removed to form pyrite. In that case, the sequence of pyrite deposition reflects a trend towards heavier $\delta^{34}S$ values. Theoretically, if a Rayleigh distillation process is assumed, the $\delta^{34}S$ value of

sulphur incorporated in the latest formed pyrites may be higher than the original values of sulphate in sea water (fig. 3.26). In the reality, those values are unusual (Ohmoto and Rye, 1979) because low concentrations of SO_4^{2-} retard significatively the rate of reduction (Berner, 1984) and probably they are related to processes of thermal reduction of the remaining SO_4^{2-} during later stages of diagenesis (Bottrell, *pers. comm.*). In both cases (biogenic or thermal reduction), a previous ^{32}S depletion of SO_4^{2-} in pore water is required to explain the observed values. Note in fig. 3.26 that the $\delta^{34}S$ values from pyrites formed in open systems to H_2S are expected to be lower than those from closed systems and the $\delta^{34}S$ value of sea water. Therefore, pyrites with anomalous high $\delta^{34}S$ values above the $\delta^{34}S$ values of the coeval sea water (as the pyrites from the Urbana Fm.) formed in an anoxic environment, a system closed to SO_4^{-2} and H_2S, during the early diagenesis of a 'normal' marine sediment.

If the reactivation surface reflects a stage of winnowing or low rate of sediment deposition, then the occurrence of the heaviest isotopic values at top of the set is inconsistent with the variations of $\delta^{34}S$ values reported from modern sediments, where the lighter compositions are found close to the water-sediment interface (e.g. Vinogradov et al, 1962; Goldhaber and Kaplan, 1980). The stratigraphical 'inversion' of the $\delta^{34}S$ values in this section of the Urbana Limestone Fm. can be understood if the nature of these shallow-water sediments is considered. They deposited as sand-waves bodies developed in a tidal nearshore environment, where the rate of sedimentation is relatively high. Thus, an individual sand wave up to 15 m. thick may form in only one year (Allen, 1982). That rate is high enough to produce a rapid compaction and subsequent vertical-upwards movement of the pore water in a well-sorted and relatively homogeneous sediment. This process leads to the relocation of the 'heavy' pore water (generated in the anoxic zone during the early stage of low rate of sedimentation) at higher stratigraphic levels; the former oxic zone becomes rapidly an anoxic , sulphate depleted, iron-rich zone where most of the original organic matter has been already used in

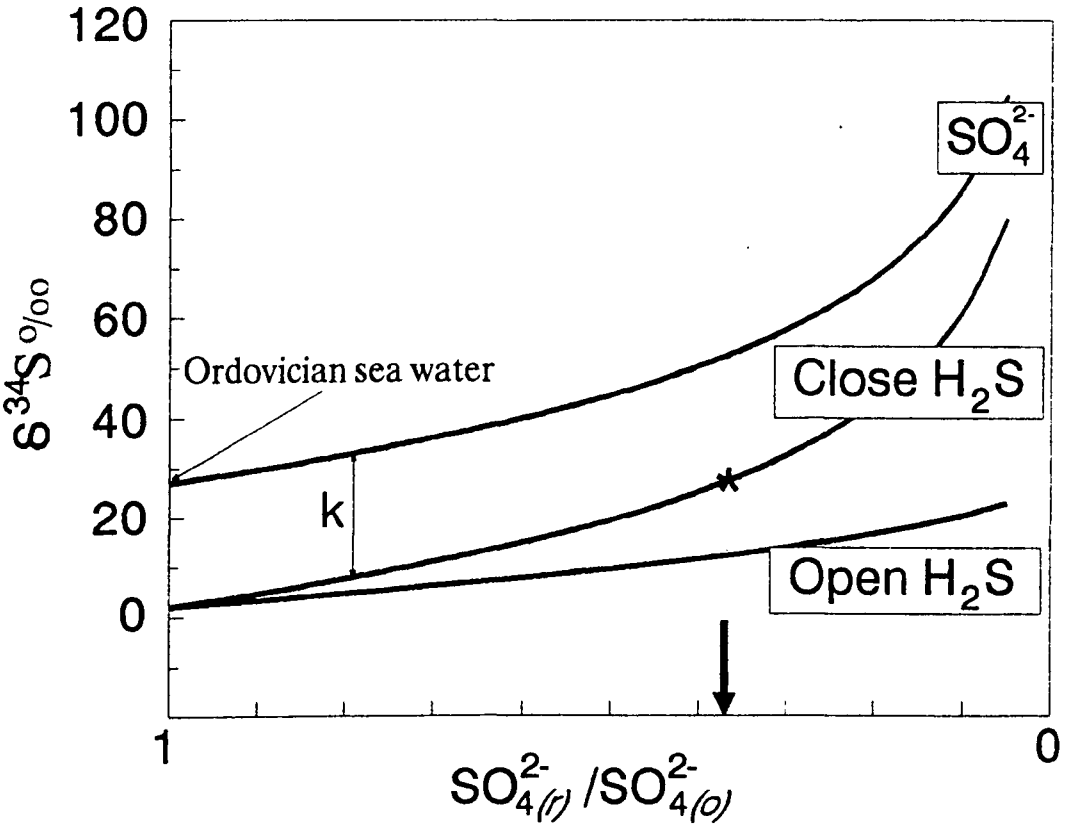

Fig.3.26. Variations of $\delta^{34}S$ values of sulphide produced and of residual sulphate in a system closed to $SO_4^{=}$. Close and open system to H_2S are *sensu* Ohmoto (1986). Curves calculated from the expressions proposed by Ohmoto and Rye (1979) assuming a Rayleigh distillation process. Kinetic factor: 1.025 (Schwarcz and Burnie, 1973). k: displacement due to the kinetic factor. Assumed starting composition of sulphate in Ordovician sea water: +27 $^{o}/_{oo}$ (Claypool et al., 1980). $SO_4^{2-}{}_{(r)}/SO_4^{2-}{}_{(o)}$ is the fraction of sulphate remaining in pore waters. Arrow indicates the fraction of sulphate from which the sulphide presents $\delta^{34}S$ values $\geq$ +27 $^{o}/_{oo}$.

oxic reactions. In that environment the formation of sulphide is limited due to the low concentrations of dissolved sulphate and low amount of reactive organic matter, and siderite precipitates (*cf.* Spears, 1989). The late formation of siderite is supported by textural evidence. However, this speculative model requires to be tested by further analytical work.

A supergenic iron-manganese karst-related body (up to 3 m. thick) exists at top of the Urbana formation. The ore basically consist of limonite (*s.l.*), 'wad' (material whose chief constituent is a hydrous manganese oxide of undeterminated identity), carbonates (calcite and dolomite) and clays. They appear as irregular masses or banded karstic fillings within a partially dolomitised limestone. Rubble breccias composed of fragments (of centimetric size) of limestone, dolostone, slate and intrakarstic material are found dispersed in calcareous bands alternating with iron- or iron-manganese-rich bands that can be massive, 'dusty' or tufaceous. Trace element analysis was carried out on two samples (LC73-7, 'iron-rich', and LC73-7-8, 'iron/manganese-rich'). Both samples show very high concentration of Zn and Ba (table 3.7). The content of Ni is elevated, specially in LC73-8. Cu and Pb concentrations are above the average in limestones (compare with tables 3.3 and 3.5). Rios (1977) reported Ag, Cu and Pb concentrations of 23.5, 2,950 ppm and 25,800 ppm, respectively. Advanced martitisation of magnetite with formation of limonite pseudomorphs indicate oxidation *in situ* of transported grains although most of the iron was likely precipitated from oxihydroxides in colloids or ionic species in bicarbonate solution. Colloids precipitate due to flocculation processes. Ionic species precipitate as a result of an increase in alkalinity of the solution (e.g. by mixing with meteoric water). Similar processes can be envisaged for the deposition of hydrous manganese oxides (Krauskopf, 1972).

The source of metals and how they were concentrated is puzzling. The Urbana Fm. itself may be a pausible source as there are locally metavolcanics and mineralisation (or relatively high

abundances of ore forming elements) from where the metals could be mobilizated by subaerial weathering and erosion. Most of the ore must be post-Hercynian in age as it is indicated by the presence of fragments of metapelites in the breccias but an early karstification/ reconcentration during the emersion in the late Ashgillian cannot be ruled out, given the cold climate at that time. In addition, several post-Hercynian stages of karstification/remobilization could take place. The multistage evolution could account for the high concentrations observed.

Chapter 4. Late Hercynian ore deposits in the Linares-La Carolina district.

4.1.Introduction.

Linares-La Carolina Pb-ore field was a word-class mining district during the 1875-1920 period, with an average lead production of 65,000 tn/yr. Silver was obtained as by-product (up to 500 g tn^{-1} Ag). The mining works (over 1,300 mine shafts and about 800 km of galleries) were concentrated on vein-type mineralisations which are extensively developed in Linares and La Carolina areas. Nowadays, the economic interest is reduced to one lode (El Cobre) but other minor mining works are being carried out on a stratabound mineralisation existing in the basal beds of the post-Hercynian succession (Las Torrecillas).

Minor Late-Hercynian Sb-(Zn), As-(Sn-W) and Cu-(Pb) vein-type deposits (not considered in this study) occur in the district.

This chapter examines briefly the regional geology as well as different aspects relating to ore geology: morphology and spatial distribution of the occurrences, and structures and textures of the ore deposits. Tectonic controls and timing of ore emplacement are treated with particular consideration.

Ore petrography, paragenesis and depositional sequences are mostly based on data from literature due to the lack of suitable mineral samples.

Finally, geochemical data on ore minerals (sphalerite, galena, pyrite) are presented.

4.2.Geographical setting.

The Linares-La Carolina district (Jaén province, Andalucía region) is located in the southeastern side of the Sierra Morena range. The study area extends over 1,500 km^2 (36x42 Km),

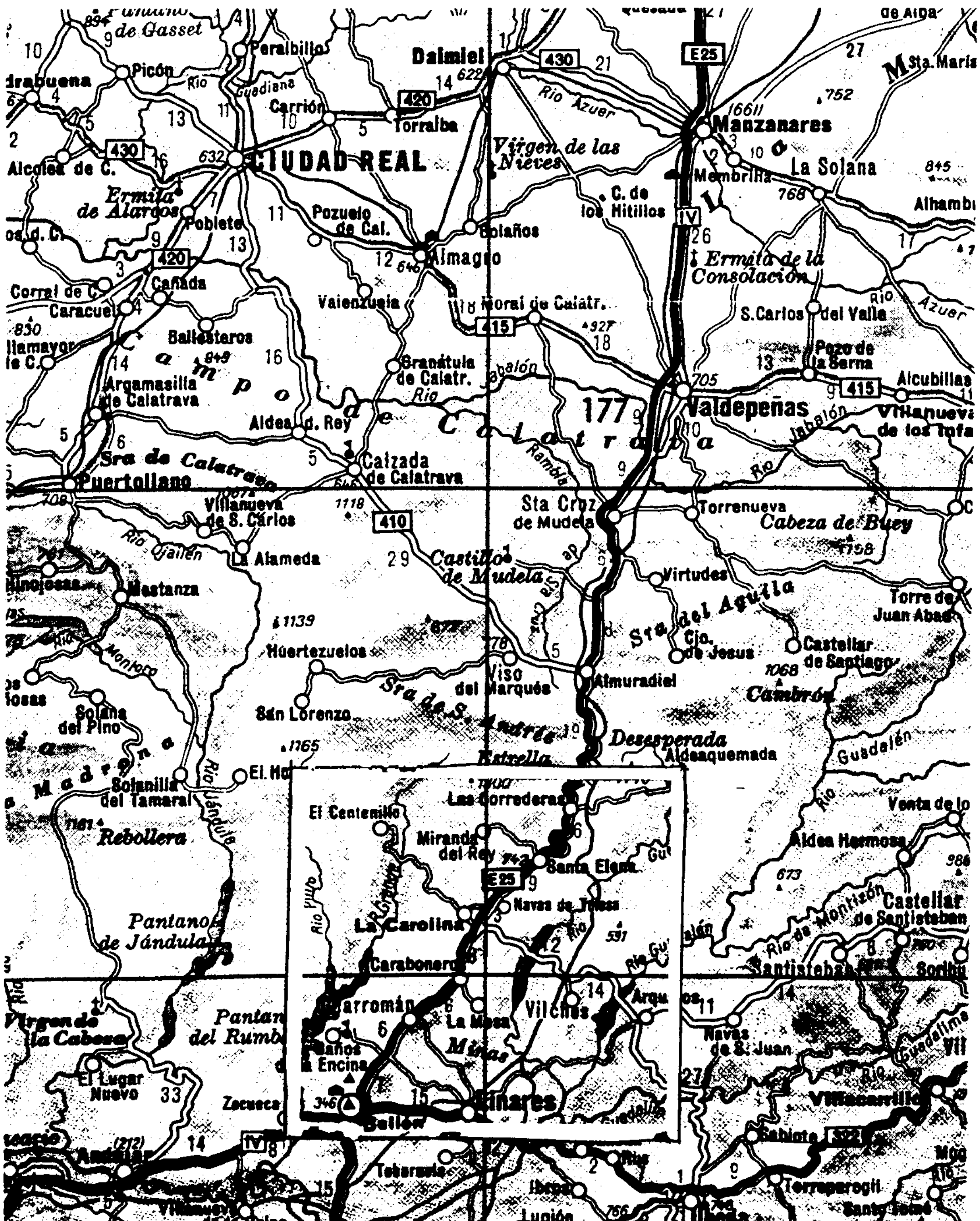

Fig.4.1. Geographic location of Linares-La Carolina Pb-ore field.

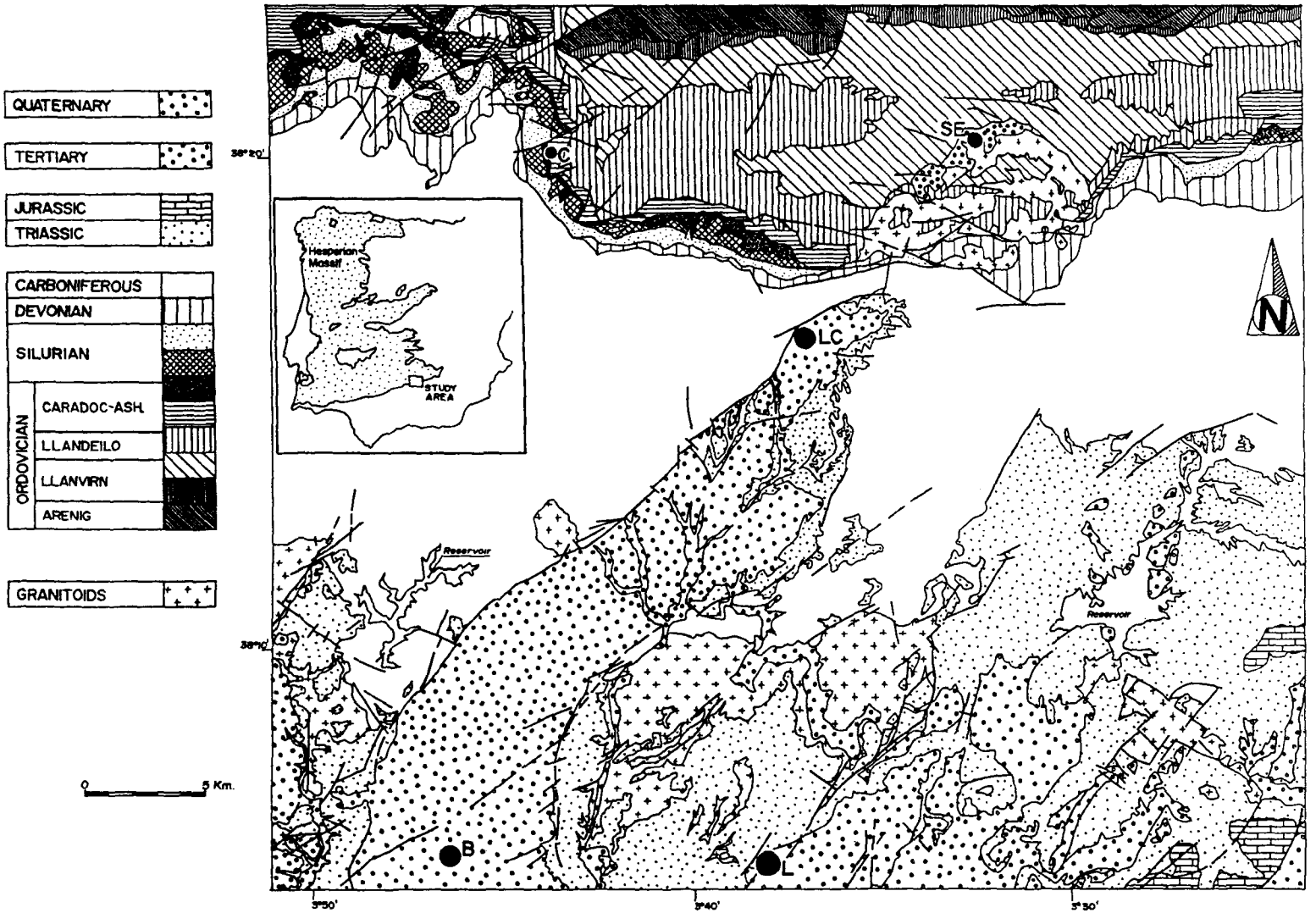

Fig.4.2. Geological sketch of Linares-La Carolina district (modificated from Enadimsa, 1981).

comprising the whole IGN(1) sheet num. 884 (La Carolina), most of the IGN sheet num. 906 (Linares) and part of the IGN sheets num. 862, 863, 885 and 906 (Santa Elena, Aldeaquemada, Santiesteban del Puerto and Ubeda, respectively). Important towns in the area are Linares, Bailén, and La Carolina. The district is drained by the Guarrizas and Guadalén rivers, tributaries of the Guadalquivir river (fig. 4.1).

4.3. Regional geology.

The study area lies at the southern edge of the Central Iberian zone of the Hesperian Massif (see chapter 2), where Mesozoic and Caenozoic sediments unconformably overlay the Palaeozoic basement (fig.4.2). The vein-type mineralisations are hosted by the Palaeozoic rocks consisting of metasediments and late-Hercynian granitoids. Minor stratabound occurrences are found in the lowermost portion of the (?)Permian-Triassic sedimentary succession.

4.3.1.Palaeozoic rocks.

The Palaeozoic metasedimentary succession has been widely studied by several authors (e.g. Henke, 1926; Tamain, 1972; Rios, 1977). It consists, from bottom to top, of:

-'Formation de Base'(Tamain, 1972): formation of variable thickness (up to 300 m.) consisting of shales, sandstones and conglomerates. Age: (?)Upper Tremadoc.

-'Armorican Quartzite' Fm.: formation of quartzites up to 600 m. of thickness. Age: (?)Upper Tremadoc-Arenig.

-Pochico Beds Fm.: ('Strates Pochico' of Tamain, 1972): 160 m. thick formation of alternating quartzites, sandstones, sandy shales and volcanic tuffs (rhyolitic?). Some quartzite and

---

(1)IGN: Instituto Geográfico Nacional, E:1/50,000

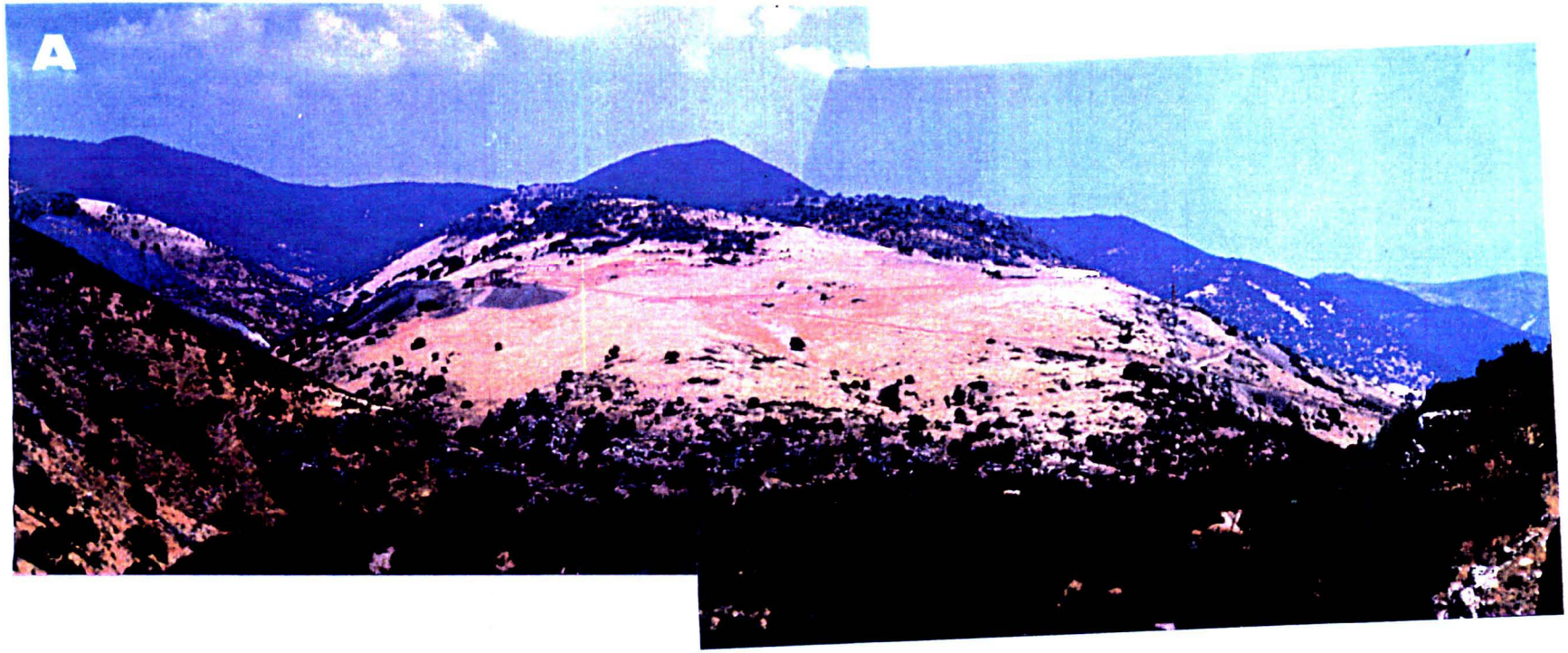

Plate 4.1. Los Curas-El soldado group at El Centenillo.

Plate 4.2. A) La Despreciada quarry. Location of the Fe-Mn karst is noted. B) Mine gallery at Castellar Quartzite Fm. C) Federico lode at Renegadero Valley.

Plate 4.3.A. The Araceli group.

sandstone beds are very rich in monazites and zircons. Age: Arenig.

-Las Correderas Shales Fm. ('Las Correderas Schiefer', Richter, 1967).: formation up to 400 m. in thickness made up of dark mudstones with fossiliferous nodules and intercalations of sandstones in the upper part. Interbedded basic volcanics occur in some outcrops of this formation found in adjacent areas.

-El Caño Quartzites Fm. (lower portion of 'El Caño Wechsellagerung' of Richter, 1967): formation up to 200 m. of thickness of alternating sandstones, quartzites and shales. Age: (?)Llanvirn-Llandeilo.

-Guindo Shales Fm. ('Guindo Schiefer', Henke, 1926): formation of 70-100 m. of thickness of mudstones and siltstones. Age: LLandeilo.

-Succession of quartzites, sandstones, slates and limestones up to 1500 m. of thickness whose formations and their geochemical and sedimentological features have been already covered in detail in chapter 3.

-'Shales with graptolites': formation up to 150 m. of thickness of shales with intercalated quartzites, sandstones and some volcanic layers. Age: Llandovery-Wenlock.

-Succession up to 450 m. of thickness of shales, quartzites and sandstones with glauconite and phosphate nodules. Age: Eifelian-Givetian.

-Succession of grey shales alternating with greywackes, conglomerates and sandstones and interbedded acid volcanic rocks. Thickness: up to 4000 m. Age: Visean.

During the Hercynian orogeny the Palaeozoic rocks were affected by low-grade regional metamorphism and two main folding phases (IGME, 1975; Charpentier, 1976; IGME, 1977; Rios, 1977). Thermal metamorphism (albite-epidote, hornblende and pyroxene

hornfels facies) is developed in aureoles up to 2 km. wide surrounding the granitoids, superimposed on the regional greenschist facies metamorphism (biotite-chlorite-white mica-albite) (Charpentier, 1976; IGME, 1977; Rios, 1977). The first Variscan folding phase gave rise to overturned south-verging folds with subhorizontal WNW-ESE-oriented axes, formation of penetrative schistosity and associated thrusting with hangingwall displacement to the south/southwest (Tamain, 1966; Charpentier, 1976, Rios, 1977). The thrusts appear to accommodate the folding rather the folds having initiated on thrust ramps. The second Variscan folding phase produced open folds of hecto-kilometric scale with subhorizontal E-W/SE-NW-oriented axes (IGME, 1977, Rios, 1977; ENADIMSA, 1981). A minor, late folding phase generated kink-bands.

As a prolongation of the Pedroches batholith, Late-Hercynian granitoids (adamellites, granodiorites, tonalites, diorites and quartzdiorites, Sánchez and Aparicio, 1969) are cropping out in the investigated area. The largest outcrops are the so-called Santa Elena and Linares massifs. The dominant rock-type of the Santa Elena massif, in the north of the district (fig.4.2), is a medium-grained, moderately peraluminous, adamellite-granodiorite (table 4.1., figs. 4.3 and 4.4) consisting of quartz (22-33 vol. %), plagioclase (22-45 vol. %, An_{48-32} but more calcic compositions may be present, fig. 4.5), K-feldspar (6-21 vol. %, Or_{95-89} Ab_{4-11}), and biotite (14-26 vol. %, Al_{VI}=0.30-0.41 atoms p.f.u., table 4.2). Muscovite occurs mostly as a secondary phase crystalising at the expense of biotite and feldspars. The southern edge of this massif displays a E-W-oriented zone up to 500 m. wide with brittle-ductile deformation, subparallel to the contact (by brittle fault) with the metamorphic rocks (plates 4.6.B and D). The cataclasis and mylonitisation, with well developed S-C planes, are related in the outermost zone to hydrothermal alteration with sericitic assemblage (white mica-quartz-pyrite-kaolinite). Textural evidence in the form of coexisting deformed and undeformed grains of secondary muscovite suggests that the rock-hydrothermal fluid interaction took place during and immediately after the deformation. The sericitic zone is separated from the

fresh (or less altered zone, as there is a pervasive incipient replacement of biotite by chlorite) undeformed rock by a narrow zone of foliated fabric with relatively well preserved biotite. There is no evident spatial relationship between the sericitic alteration and the lodes that are cutting the deformed rock. These veins are fillings of high angle transcurrent/normal faults defining a tectonic contact between the sericitic mylonite and the less altered foliated rock. Thus, the sericitic alteration may be only found in one wall of the vein. As the maximum relative displacement of the walls after the vein formation seems to be of metric or lesser order, the sericitic alteration appears to predate the main mineralising events (plate 4.6.B). Locally, the granitoid presents a muscovite facies (e.g. in La Nube lode environs) not related to mylonitisation. Further discussion concerning to this matter is presented in the next chapter.

The dominant rock-type of the Linares massif, located in the southern part of the district (fig.4.2), is a medium- to coarse-grained, moderately peraluminous, adamellite (table 4.1, figs. 4.3 and 4.4) consisting of quartz (25-30 vol. %), plagioclase (25-45 vol. %, An_{34} and albite-rich An_{12-6}), K-feldspar (10-30 vol. %, Or_{97-93} Ab_{3-6}, fig. 4.5) and biotite (4-11 vol %, Al_{VI}=0.21-0.18 atoms p.f.u., see table 4.2). Primary muscovite is rare. Andalusite and cordierite (up to 5 vol. %, IGME, 1975) occur in marginal zones close to the metamorphic rocks.

In addition to the petrographical and mineralogical differences , the two granitoids differ in both major and trace elements (table 4.1). The Linares adamellite is on average more siliceous, Sr and Zr depleted and with higher Rb/Sr ratios compared with the Santa Elena granodiorite-adamellite. The two granitoids show distinctive trends in the SiO_2 variation diagrams (fig. 4.6.a and 4.6.b); the Santa Elena granitoid displaying a wide scattered distribution whilst the Linares granitoid shows a more grouped distribution.

Single stage Pb-model ages calculated by Michard-Vitrac et al. (1981) for some granitoids of Sierra Morena are in a range of

	Santa Elena			Linares		
(n = 10)	Range	Mean	1σ	Range	Mean	1σ
SiO_2	61.77-65.16	63.86	0.81	66.94-69.00	68.15	0.70
TiO_2	0.84-0.88	0.87	0.03	0.47-0.57	0.53	0.03
Al_2O_3	16.36-17.46	16.89	0.29	15.63-16.02	15.90	0.26
Fe_2O_3*	5.23-6.37	5.53	0.31	3.37-4.11	3.78	0.19
MnO	0.07-0.09	0.08	0.00	0.05-0.06	0.06	0.00
MgO	1.59-2.01	1.72	0.12	1.01-1.17	1.08	0.05
CaO	3.04-3.91	3.57	0.27	2.34-2.66	2.52	0.12
Na_2O	2.74-3.12	2.92	0.12	3.16-3.49	3.27	0.09
K_2O	3.26-3.90	3.68	0.18	4.11-4.63	4.32	0.17
P_2O_5	0.23-0.40	0.27	0.04	0.20-0.22	0.21	0.01
Ni	11-14	12	0	4-7	6	1
Cu	8-16	11	2	5-9	7	1
Zn	66-82	70	4	54-62	58	2
Rb	152-135	143	5	163-180	173	5
Sr	227-253	235	7	154-202	170	14
Y	28-58	33	8	28-32	30	1
Zr	225-349	246	35	171-199	182	9
Nb	12-15	13	0	9-12	11	1
Ba	591-745	681	43	599-681	648	22
Pb	22-28	24	1	24-31	25	2
Th	12-20	17	2	18-22	21	1
U	3-5	3	0	4-6	5	0

Table 4.1. Average chemical composition of the Santa Elena and Linares granitoids from ten XRF analyses of unaltered samples of each massif.

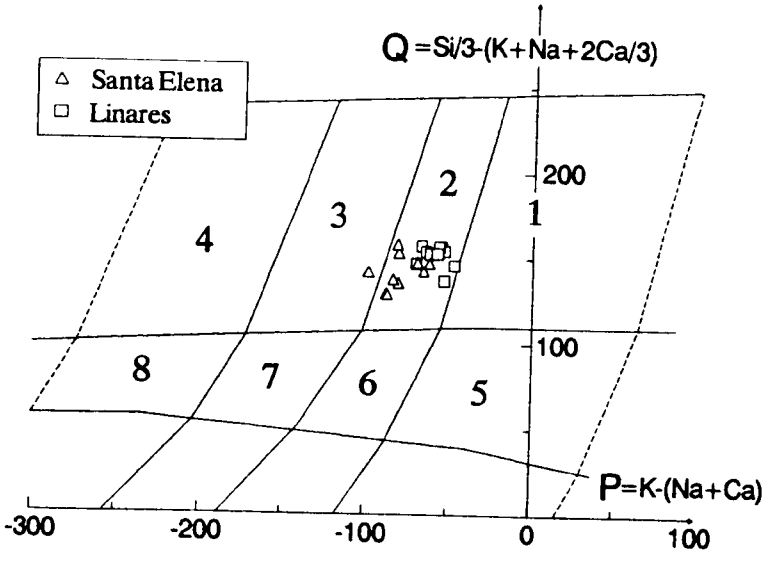

Fig.4.3. Debon-Le Fort nomenclature diagram (Debon and Le Fort, 1983) and classification of the Santa Elena and Linares granitoids. 1 Granite, 2 adamellite, 3 granodiorite, 4 tonalite, etc.

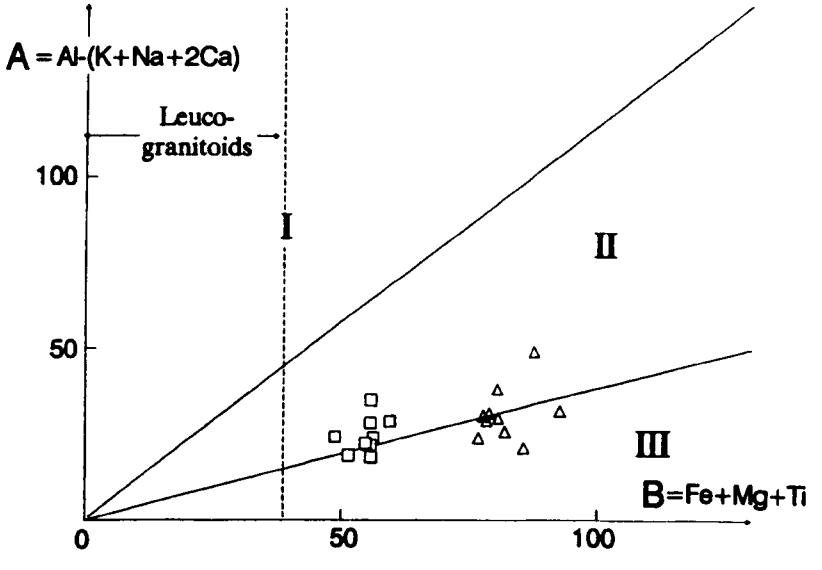

Fig.4.4. Debon-Le Fort 'characteristic minerals' diagram (Debon and Le Fort, 1983) and peraluminous character of the Santa Elena and Linares granitoids. I: Mu>Bi (by volume), II: Bi>Mus, III: Bi.

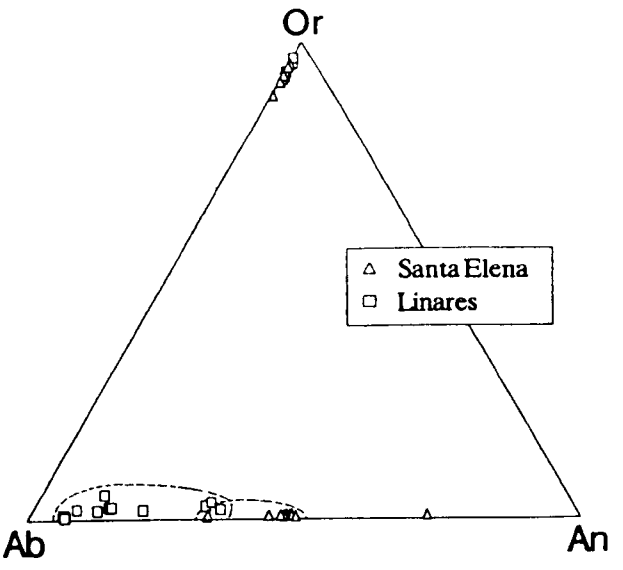

Fig. 4.5. Composition of feldspars in unaltered samples from the Santa Elena and Linares granitoids.

	Santa Elena		Linares	
SiO_2	34.66	34.72	34.93	34.35
TiO_2	3.31	2.97	3.90	3.43
Al_2O_3	18.03	19.15	16.36	16.61
FeO*	22.23	21.31	24.54	24.45
MnO	0.42	0.33	0.17	0.24
MgO	7.12	7.23	7.46	7.35
CaO	0.00	0.03	0.00	0.00
Na_2O	0.12	0.11	0.31	0.27
K_2O	9.45	9.41	9.32	9.46
Total	95.34	95.26	96.99	96.16
FeO* = total iron. Formulas based on 22 oxigens				
Si	2.6867	2.6570	2.6655	2.6500
ALIV	1.3134	1.3260	1.3345	1.3500
AlVI	0.3341	0.4130	0.1875	0.2120
Ti	0.1930	0.1720	0.2275	0.2025
Fe	1.4416	1.3725	1.5855	1.5965
Mn	0.0276	0.0220	0.0110	0.0160
Mg	0.8231	0.8309	0.8570	0.8540
ΣVI	2.8194	2.8103	2.8685	2.8810
Ca	0.0000	0.0028	0.0000	0.0000
Na	0.0192	0.0179	0.0485	0.0420
K	0.9351	0.9250	0.9065	0.9300
ΣXII	0.9543	0.9456	0.9550	0.9720

Table 4.2. Representative analyses and structural formulas of biotites from selected samples of the granitoids of Linares and Santa Elena.

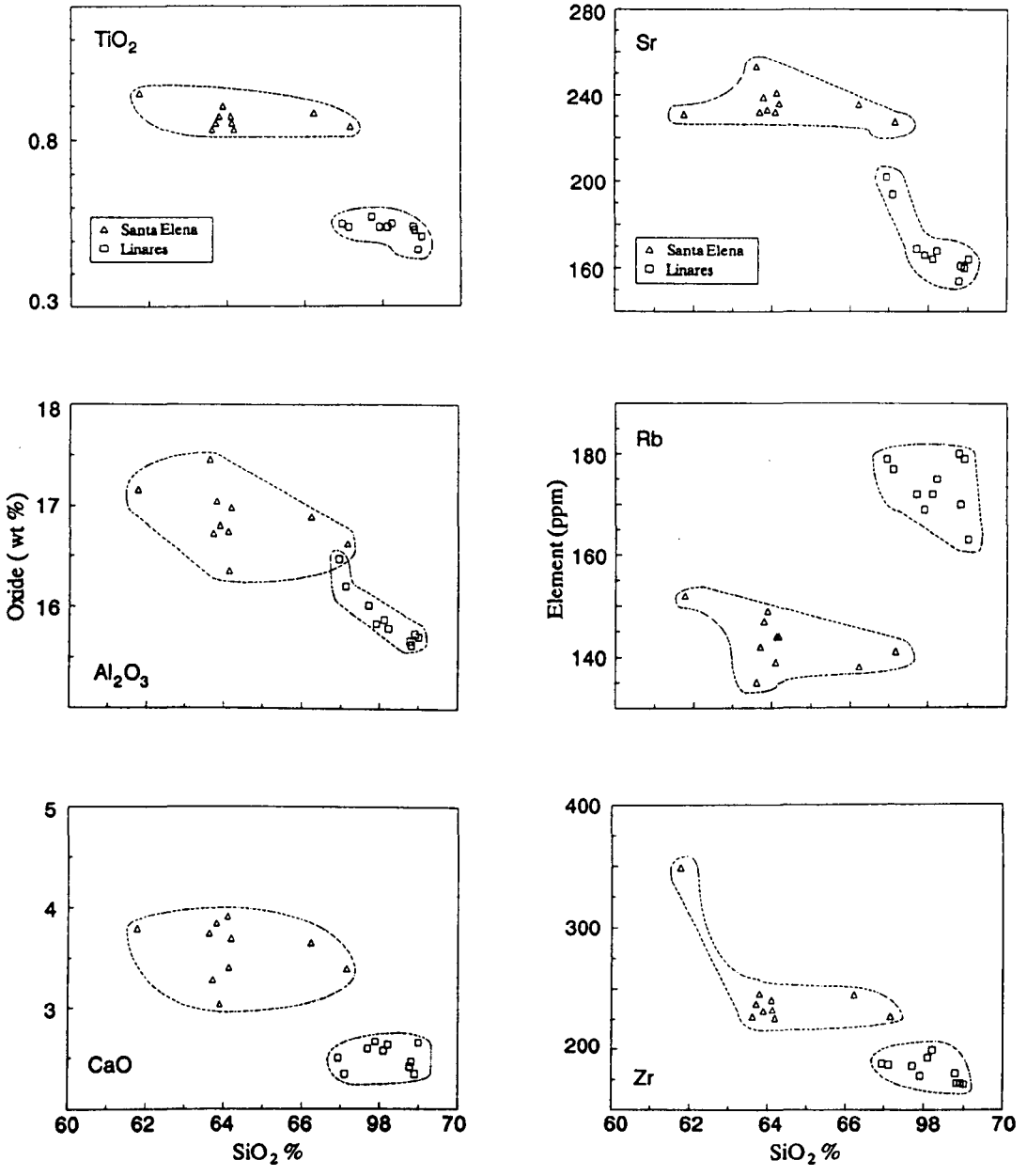

Fig.4.6. Some SiO_2 variation diagrams for the Santa Elena and Linares granitoids.

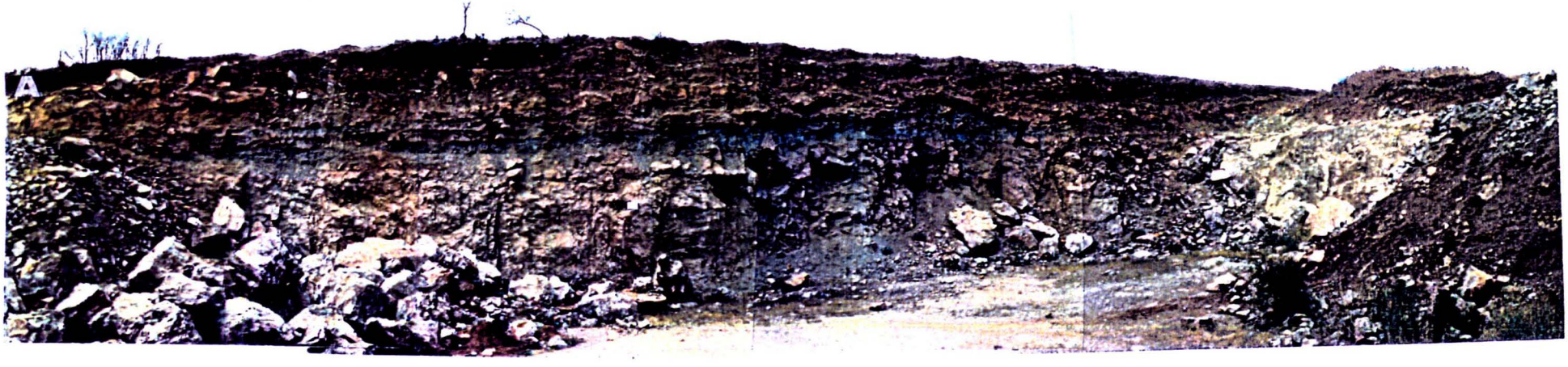

Plate 4.3.B. Las Torrecillas quarry. Location of erosional unconformity is pointed out by arrows.

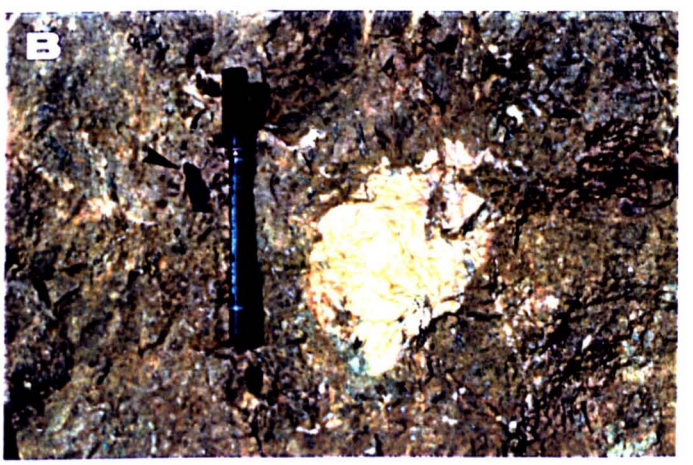

Plate 4.4. A) Galena in silicified breccias formed from a caliche. The arrow indicates a galena crystal. B) Section of a barite pipe in silicified breccias. A small fragment of dark jasperoid is indicated by the arrow.

Plate 4.5. The Las Torrecillas stratabound type mineralisation. A) Barite pipe-like bodies truncated by the erosional surface indicated in plate 4.3. (indicated by arrows). B) Vertical arrangement of the barite pipes (note the decimetric spacing). C) Vertical morphology of the pipes of barite and green jasperoid (indicated by arrows). D) Arrangement and morfology on a horizontal plane.

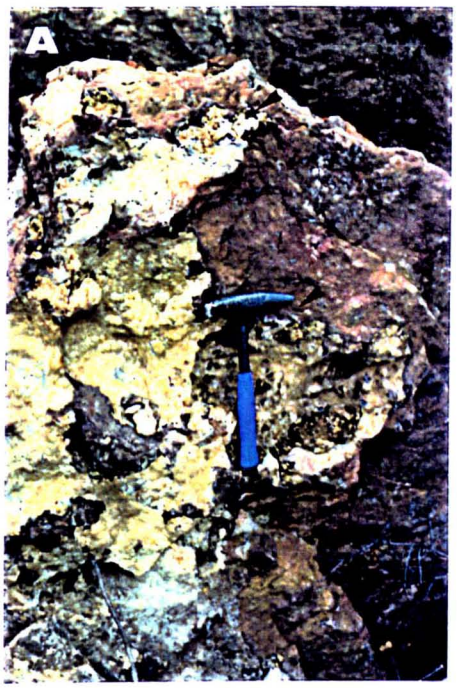
A


B


C

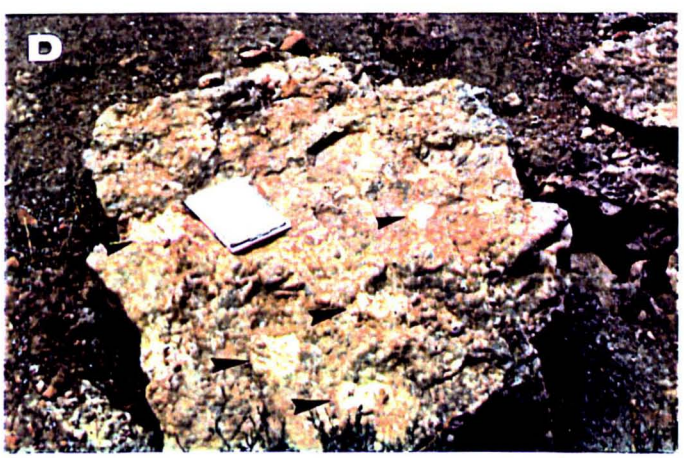
D

Plate 4.6. A) Vein in the mylonite of Santa Elena. On the left, a phyllic alteration develops, which does not occur in the vein-wall on the righ. B) Normal fault affecting metasediments (on the left) and the mylonite developed in the Santa Elena granodiorite-adamellite. C) Veinlet of chalcopyrite crosscutting the basal sandstones of the (?)Permian-Triassic succesion (Los Quinientos lode, Linares). D) Detail of the S-C fabric of the Santa Elena mylonite (note the low angle of the C planes).


A


B


C

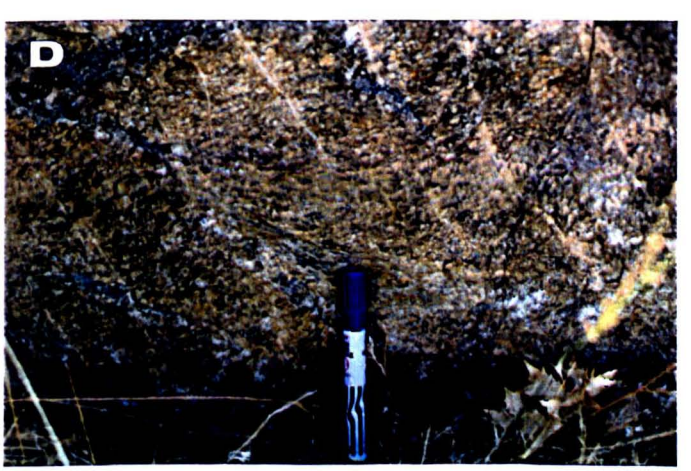
D

Plate 4.7. A), B), C) and D) BSE images of pisolitic dolostones associated with the stratabound deposit at Las Torrecillas. Textural evidence supports a hydrothermal origin for the late silicification of the voids.

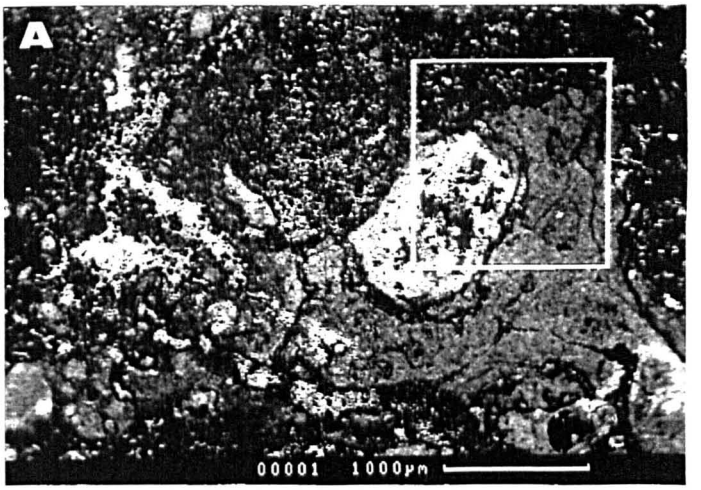
A
00001 1000µm

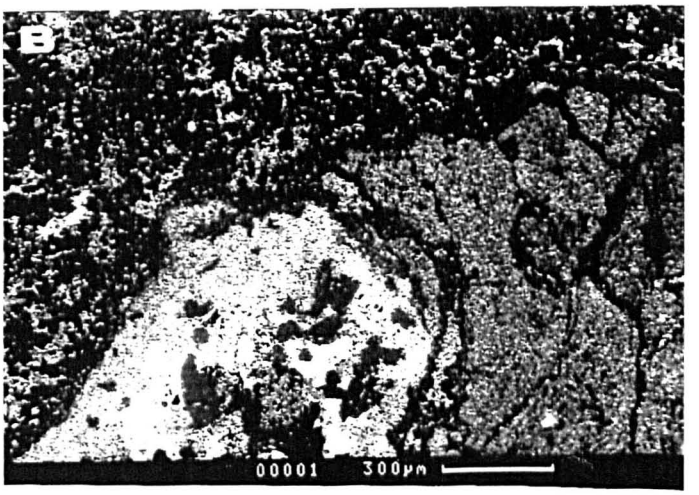
B
00001 300µm

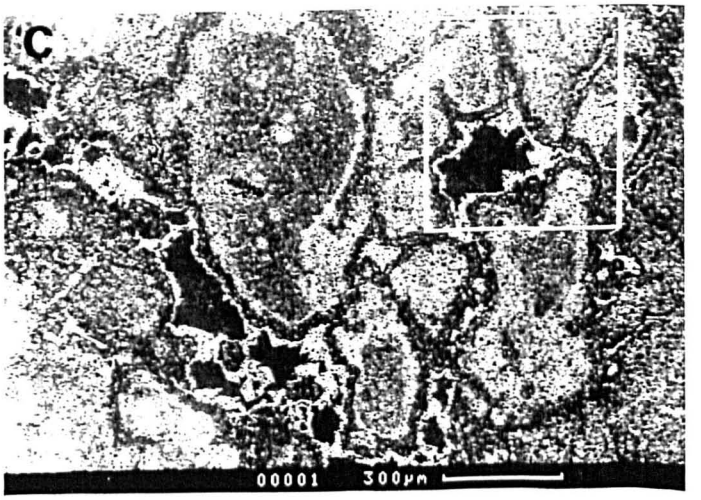
C
00001 300µm

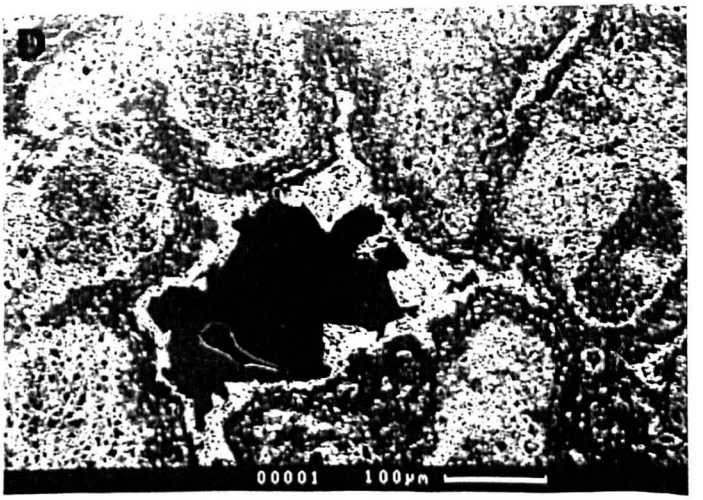
D
00001 100µm

338-297 Ma. The lead isotopic signature reflects an origin of the granitoids by remobilisation of a previously differentiated continental crust rather than a crust-mantle mixing during the Variscan orogeny (see chapter 7).

Late-Hercynian dykes, hosted by the metamorphic rocks and the granitoids, are consisting of porphyritic granitoids (granite-granodiorite), lamprophyres (minette-kersantite type), diabases and aplites (IGME, 1975; Charpentier, 1976; IGME, 1977; Rios, 1977). The dykes are variably altered by hydrothermal fluids.

4.3.2.(?)Permian-Triassic rocks.

The (?)Permian-Triassic succession ('Chiclana del Segura' formation, López Garrido, 1971) consists, from bottom to top, of:

-Basal portion of variable thickness (up to 20 m.) made up by caliches, dolostones, coarse conglomerates and sandstones whose cement is mainly silica with subordinate barite and iron oxides/hydroxides. Sedimentological interpretation of these deposits is not clear. Caliches, certain conglomerates and sandstones may be interpreted as having been formed in alluvial fan systems. Other conglomerates may be related to debris deposits. The discontinuous basal dolostones (up to 5 m. in thickness) are strongly silicified, showing Ba-(Pb-Zn-Cu-[Ag]) stratabound ores (pipes, veinlets, vugs, disseminations). The basal dolostones have been interpreted by Pineda et al., 1981 as caliches on the basis of textural criteria. The best exposure of this mineralisation is located in Las Torrecillas quarry, near to La Carolina town (plate 4.3.B). The thickness of the host beds is variable, from 5 to 1 m. They mostly consist of pisolitic dolostones, dolomitic breccias and conglomerates distributed irregularly in the rock . Thus, the three facies may be coexisting or only one may occur. Basal contact with the Palaeozoic rocks is gradual, showing the first 1.5 m. with silicified fragments of the metasediments and green-black jasperoid (plate 4.4.B) in a dolomitic 'matrix' composed of pisolites or rounded aggregates of

Subsector	Num.	Lode/Occurrence Name
Ia El Centenillo	1	Mirador
	2	Perdiz
	3	Pelaguindas
	4	Sur
	5	Crucero-Mirador
Ib La Carolina- Santa Elena	6	Crucero-Guindo
	7	Guindo
	8	Federico
	10	Sinapismo
	11	Melchor
	12	Rosa
	13	San José-El Piñón
	14	San Gabriel
	15	El Porvenir
	16	La Nube
Ic	17	Araceli Group
II Linares	18	La Lechuza
	19	Piedrahita
	20	Valdeinfierno
	21	Rosso Fault
	22	Matacabras
	23	El Cobre
	24	San Juan-Esmeralda
	25	El Correo
	26	El Principio El Fin
	27	Cañada Incosa-Los Quinientos
	28	Arrayanes

Stratabound-type	29	Navas de Tolosa
	30	Torrecillas
	31	Fernandina-Palazuelos

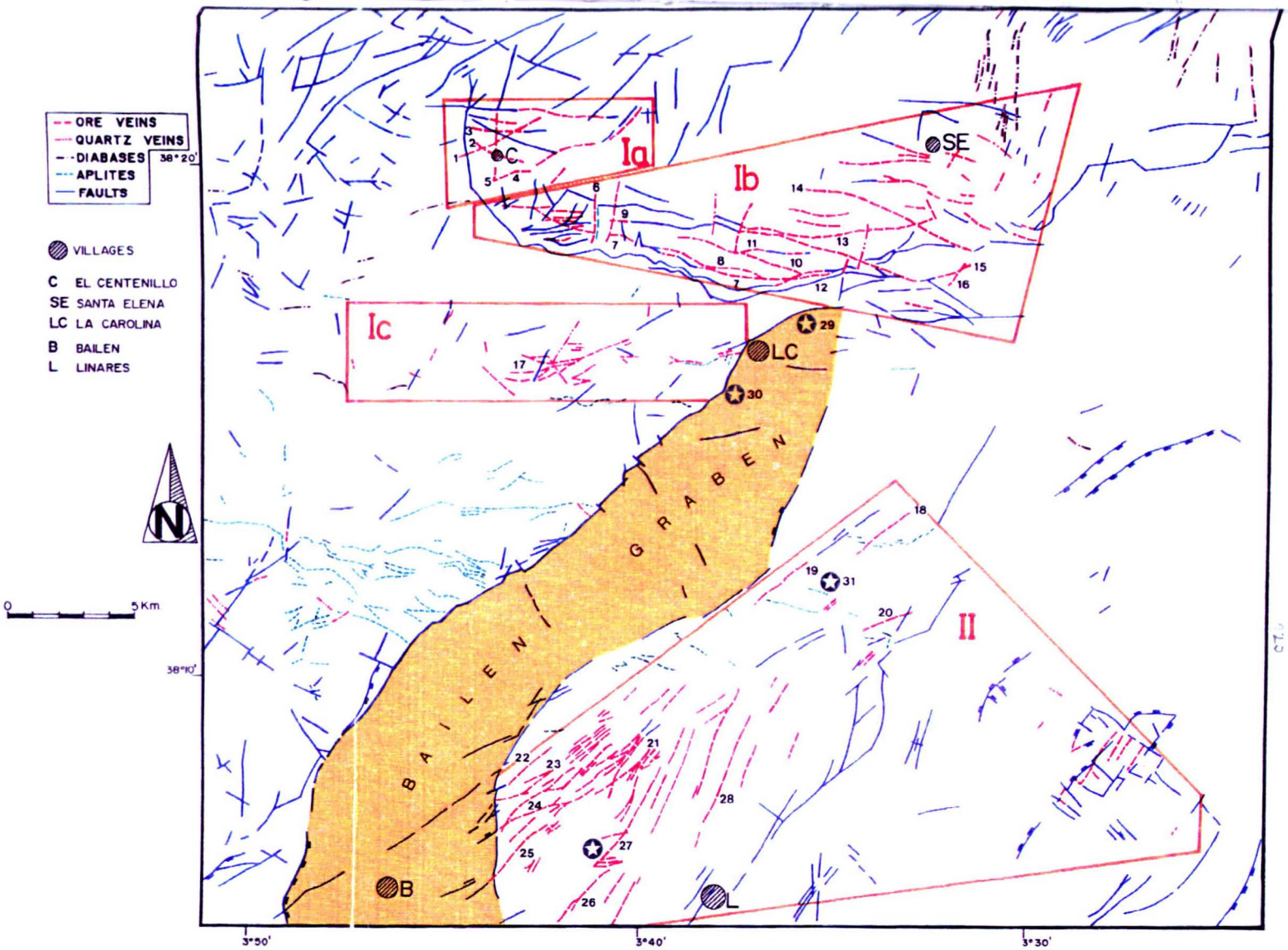

Fig. 4.7. Spatial distribution of veins, faults and dykes in Linares-La Carolina Pb-ore field (partly based on Enadimsa, 1981). Dykes referred as 'Aplites' consist of aplites (s.s.) and prphyritic granitoids. Stars indicate stratabound-type occurrences in the basal beds of the ?Permian-Triassic succession. Differentiated subsectors are explained in the text.

micrite/microesparite in a microesparitic matrix *(s.s)* (plates 4.7.A, B, C and D).

-Middle portion of 100-200 m. of thickness consisting of shales and argillites with intercalated thin beds of sandstones.

-Upper portion up to 50 m. of thickness with two sandstone sets separated by argillites, marls and dolomicrites.

The age estimated for the Chiclana del Segura formation from palynological data is Ladinian-Norian (Besems, 1981). An erosional surface was found during this study in the lowermost portion of the succession, between the dolomitic beds and the overlying shales/sandstones/conglomerates. Therefore, the age of the basal beds remains uncertain; they were deposited after the main Hercynian folding phases and probably before the Ladinian. Note that the dolomitc beds may be correlated with those found at the uppermost portion of the Autunian succession in others areas of the Hesperian massif (e.g. Celtiberian Range, see chapter 2)

4.4.Ore geology.

4.4.1.Ore morphology.

The vein-type mineralisations of Linares-La Carolina district are concentrated in two sectors: the El Centenillo-La Carolina-Santa Elena and the Linares sector. The El Centenillo-La Carolina-Santa Elena sector is a narrow band of about 4 km wide located in the northern area of the district, subparallel to the main Hercynian structures. The lodes are mostly hosted by Upper Ordovician-Lower Silurian metasediments and the Santa Elena granitoid. Dominant strikes are N110E and E-W with minor frequencies of veins striking N-S and N40-70E in El Centenillo area. In the Linares sector the veins are mainly trending N40-55E, most of them hosted by the Linares granitoid with a few occurrences hosted by the Lower Carboniferous rocks. The other minor area with mineralisation is that comprising the Araceli Group, a set of lodes hosted by the Lower Carboniferous succession

displaying a dominant E-W strike and some N60-75-oriented veins (figs. 4.2 and 4.7).

The lodes of the Linares-La Carolina ore-field are open-space filling bodies, usually of 1-2 m. of thickness but locally they may be up to 15 m. (e.g. El Mirador lode). Lengths are variable ranging from several meters to 10 km (e.g. El Guindo-Federico lode, table 4.4). Maximum depths reached by mining works were about 650 m. The ore bodies *(s.s.)* in the lodes are of centimetric order; exceptionally, they can extend up to 2 m. (e.g. El Mirador lode). Strike and dip can vary in each lode, which can deflect and be divided into several branches giving a characteristic anastomosing, branching morphology (the so-called 'arboles' of the local miners).

The vein textures found are:

a) Asymmetrical banding: the lode is made up by several bands of quartz, carbonates, barite and ore (galena, pyrite, sphalerite, etc.) of arbitrary thickness and irregular shape.

b) Breccias: renewed displacement of the vein-walls caused brecciation of earlier formed veins. Fragments of variable size of country rocks, ore and gangue were cemented by subsequent hydrothermal materials. According to Charpentier (1976), three main stages of brecciation can be distinguished (fig.4.8). The first stage was the faulting and opening episode related to the first hydrothermal deposit. The second stage is identified by vein and host rocks fragments cemented by ankerite and quartz. The third stage is recognized by a breccia cemented by calcite (with development of cockade textures and large number of vugs and voids) and minor quartz and barite.

c) Random texture: the ore is irregularly dispersed in the lode, yielding barren sectors and zones of mineralised pockets (the so-called 'bolsada' by the miners).

As noted above, the stratabound-type deposits occur locally in the basal rocks of the (?)Permian-Triassic succession (plates

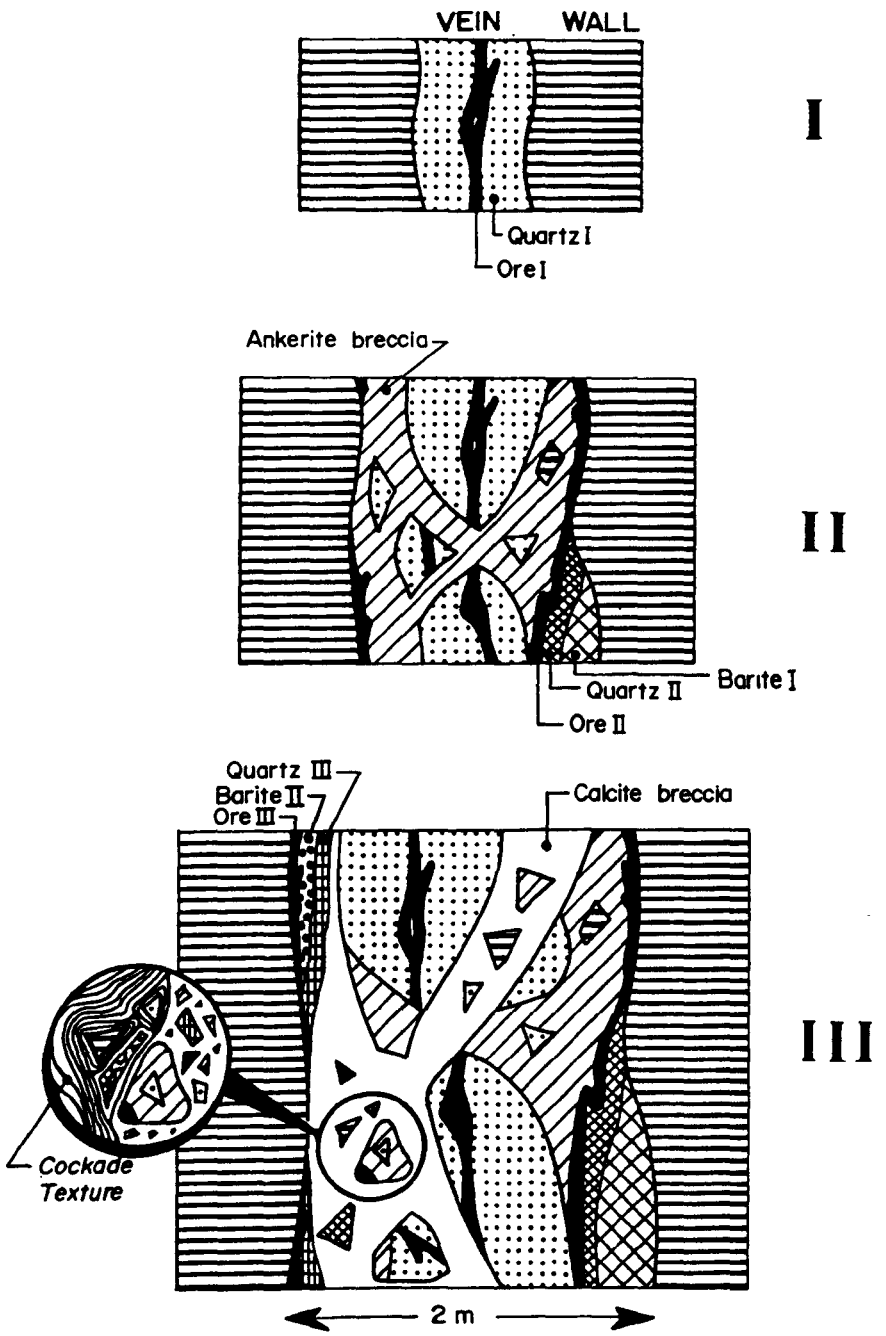

Fig. 4.8. Inter-brecciation stages: morphology and dominant mineral deposition in an idealised vein.

4.3.B and 4.5). Several outcrops have been documented: Las Torrecillas, Navas de Tolosa, Los Palazuelos-Fernandina, Baños de La Encina, etc. (Pineda et al., 1981, Font and Thibieroz, 1981). Nowadays, only Las Torrecillas is economically profitable, being worked for barite extraction (plate 4.3). The ore is hosted by strongly silicified pisolitic dolostones (plate 4.7), dolomitic breccias and conglomerates(plates 4.4.A and B). The mineralisation (galena, barite, quartz and subordinated chalcopyrite and sphalerite, with some smithsonite and supergenic alteration of galena to cerusite) appears as disseminations in the host rock and pipe-like bodies of barite and/or green jasperoid. The pipes, of circular section, do not always show vertical continuity and they may be interconnected by thin irregular veinlets. The average diameter of the pipes is 10 cm. with a maximum of 20 cm. Contact with the host rock may be gradual or sharp. Normally, the pipes are zoned with an outer envelope 5-10 cm. wide of green jasperoid and an inner core of barite and galena. The bodies may be regularly distributed in centimetric to decimetric spacing (plates 4.5.A, B, C and D).

The dolomitic beds and the mineralisation are truncated sharply by an erosional surface (plates 4.3.B and 4.5.A). Above this surface there is no mineralisation but barite may be locally present as cement in sandstones. Whole-rock geochemical data from the Las Torrecillas occurrence (table 4.3, fig 4.9) reflect a relative enrichment in base metals and barium upwards within the mineralised beds with some depletion in these in the upper centimeters next to the erosional surface. This may indicate some leaching related to weathering and formation of the erosional surface after ore emplacement. The relative enrichment in Ni against losses in Ba, Pb, Cu and Sr may indicate weathering processes developed in tropical climates (*c.f.* Lelong et al, 1976).

The stratabound deposits have been interpreted by Pineda et al. (1981) as having been formed by remobilisation from the lodes as they are spatially close to N60-70E faults. This interpretation

Sample	LC288-4	LC288-5	LC288-6	LC288-7	LC288-8	LC298-1
Rock	Dolostone	Dolostone	Dolostone	Dolostone	Dolostone	Sandstone
SiO_2	15.09	26.86	10.65	5.75	5.12	88.52
TiO_2	0.19	0.10	0.03	0.08	0.08	0.11
Al_2O_3	3.84	1.70	0.43	1.16	1.80	4.66
Fe_2O_3*	0.66	0.40	0.34	1.04	1.97	1.20
MnO	0.11	0.18	0.32	0.34	0.43	0.07
MgO	16.21	14.67	18.43	17.03	10.94	0.12
CaO	23.88	21.46	27.04	28.03	37.39	0.11
Na_2O	0.02	0.02	0.06	0.04	0.03	0.21
K_2O	0.95	0.43	0.15	0.30	0.71	2.96
P_2O_5	0.05	0.04	0.04	0.05	0.04	0.09
L.o.I.	37.55	33.50	41.53	45.17	41.86	1.25
Total	98.56	99.35	99.03	98.99	100.37	99.30
MgO/CaO	0.678	0.683	0.681	0.607	0.292	1.09
Ni	21	17	11	38	67	21
Cu	7	7	8	59	37	23
Zn	38	45	30	63	67	20
Rb	45	20	5	15	18	87
Sr	111	222	324	618	99	195
Y	8	5	2	7	11	6
Zr	30	14	5	10	20	33
Nb	3	2	1	0	1	2
Ba	420	4456	5544	12435	479	6399
Pb	51	109	533	1577	424	87
Th	6	4	0	0	1	4
U	2	2	1	0	2	3

Table 4.3. Chemical (XRF) analyses of Las Torrecillas beds. Major element oxides are in wt%. Fe_2O_3* is total iron. L.o.I. is loss on ignition. Trace elements are in ppm.

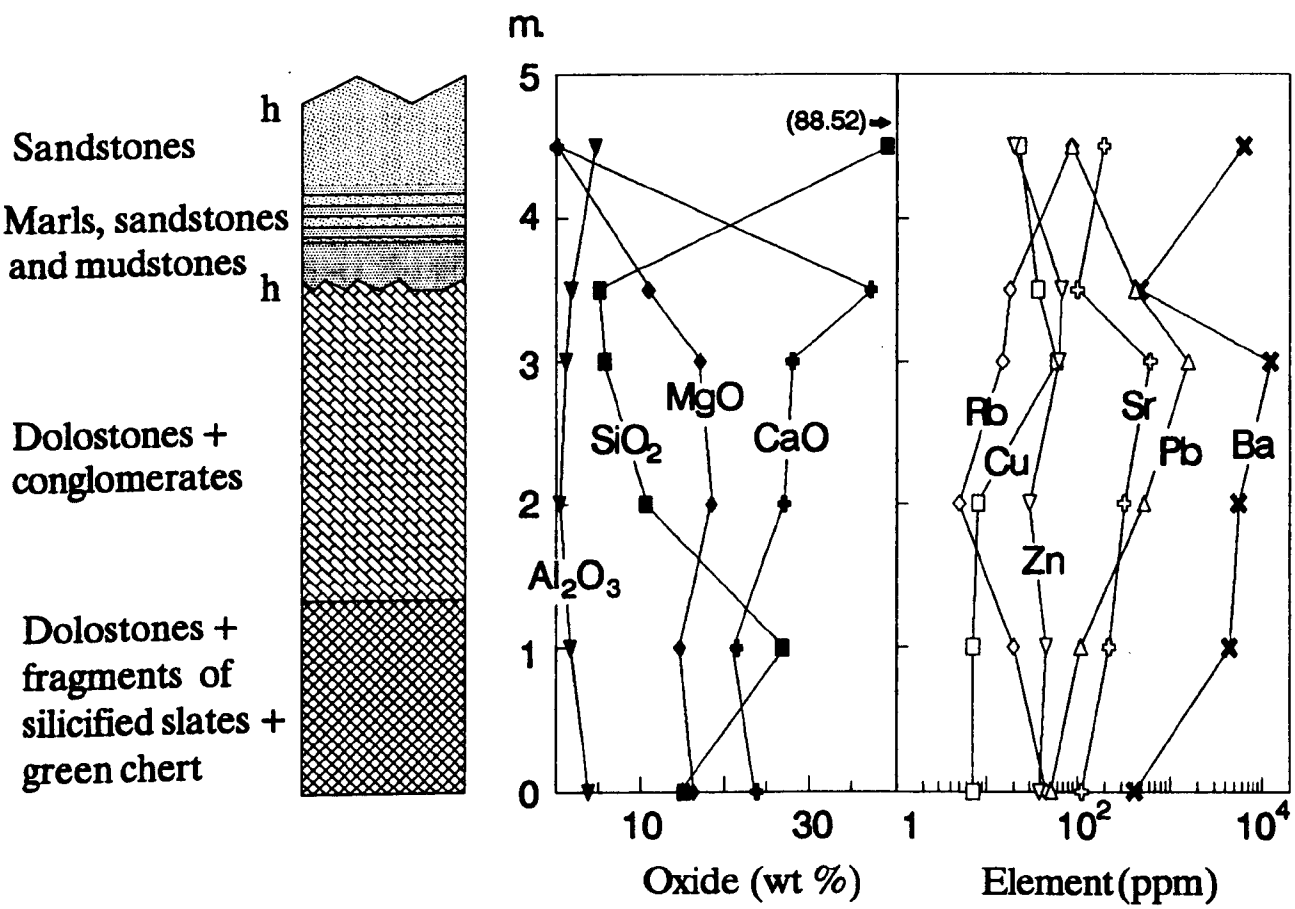

Fig. 4.9. Lithological sequence and vertical geochemical variation in the ?Permian-Triassic host rocks of the Las Torrecillas stratabound-type ore.

is speculative as there is no reported geochemical or fluid inclusions data to support it. An alternative interpretation (this study) is to consider these stratabound deposits as representative of the shallowest levels of the vein-type ore.

4.4.2.Spatial distribution, structural controls.

4.4.2.1.Vein pattern. Faulting.

It is assumed that the veins in both sectors, Linares and El Centenillo-La Carolina-Santa Elena, were formed during the same event(s) of mineralisation (Tamain, 1968; Azcárate and Vergara, 1971; Charpentier, 1976; Rios, 1977; IGME, 1977; among others) as no significant differences have been found in mineral assemblages, radiogenic isotopes and ore and vein textures. On the basis of vein distribution pattern, four areas or subsectors may be distinguished in the district (figs. 4.7 and 4.10):

-El Centenillo-La Carolina-Santa Elena sector (I):

*El Centenillo subsector (Ia): It comprises veins of variable strike, being oriented N5E, N40-70E or N85-100E. Lengths are also variable up to 3.3 km.

*La Carolina-Santa Elena subsector (Ib): It comprises veins with dominant strikes from N80E to N115E (plate 4.6.B) with minor occurrences striking N25E to N45E and N180E to N20E. The longest veins of the district are found in this subsector (e.g. El Guindo-Federico lode , up to 10 km. long) but most of the veins are 0.5 to 2 km. long.

*Araceli subsector (Ic): It comprises veins mostly striking N65E to N90E. They are normally 0.25 to 4 km. long.

-Linares sector (II): It comprises veins whose dominant strikes are ranging from N25E to N55E and some N60-80E-oriented veins. Most of the veins exhibit lengths of 0.50-1.25 km. but longer veins (up to 5.75 km. long) also occur.

Strike (degrees)	Dip (degrees)	Pre-vein displacements	Post-vein displacements	Lode-type	Surveyed length	Average thickness
N180-5E	70-90W	Strike-slip? /Dip-slip	Strike-slip /Dip-slip	Crucero Guindo	3,500 m.	2-3 m.
N40-55E	75-90 to NW or SE	?	Sinistral /Dip-slip	Sur Centenillo	1,800 m.	n.d.
N60-75E	70-90 to NNW or SSE	Dextral /Dip-slip	Sinistral /Dip-slip	Mirador El Centenillo	3,300 m.	7-10 m.
				El Cobre Linares	1,300 m.	2 m.
N80-100E	45-90 to N or S	Sinistral /Dip-slip	Strike-slip /Dip-slip	Pelaguindas El Centenillo	2,000 m.	1.7 m.
				Guindo-Federico	10,000 m.	0.8-2 m.
N105-115E	75-90 to N or S	Sinistral /Dip-slip	Dextral /Dip-slip	Ojo Vecino S. Elena	700 m.	very variable
				Sinapismo S. Elena	6,000 m.	n.d.

Table 4.4. Major sets of faults and main related lodes of Linares-La Carolina district (partly based on Charpentier, 1976; Rios, 1977 and ENADIMSA, 1981).(n.d.: no data available).

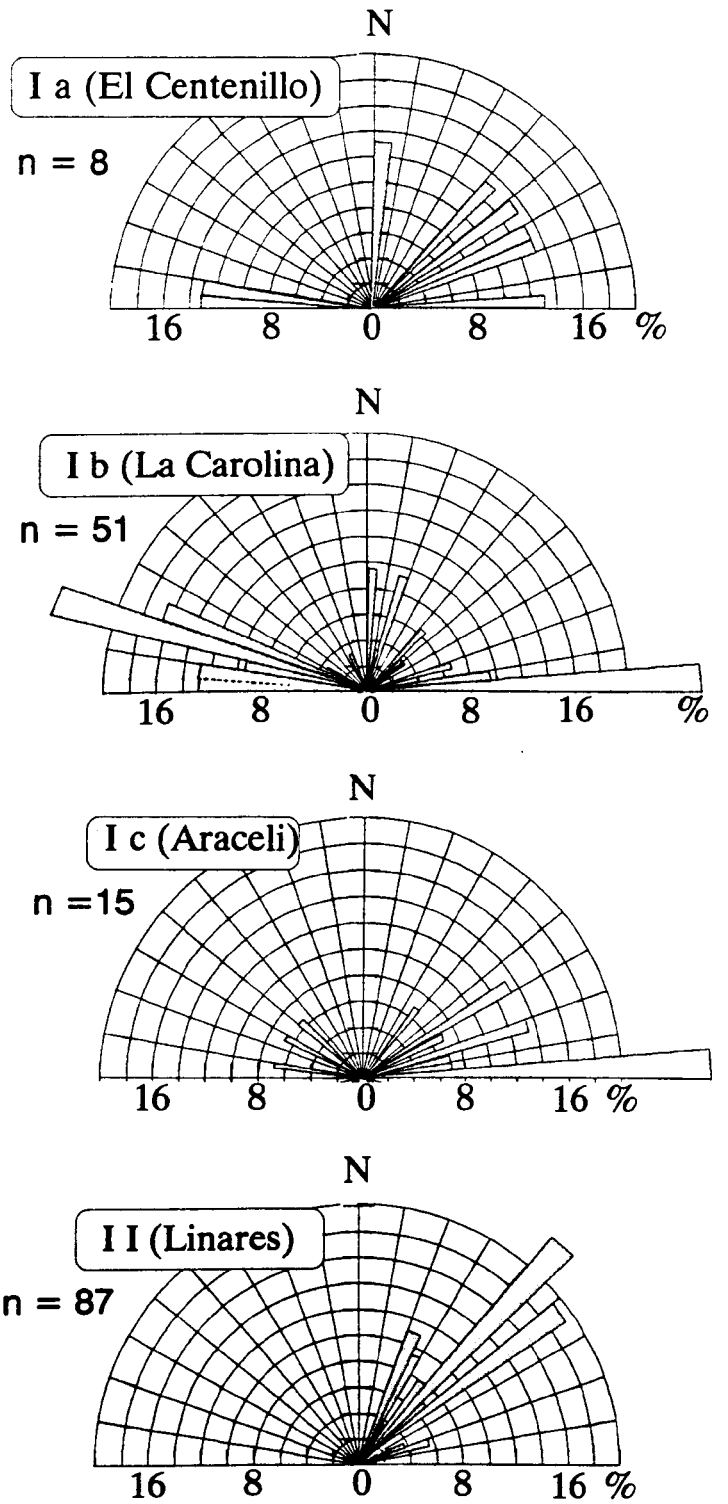

Fig. 4.10. Vein orientation distributions of the subsectors delineated in fig. 4.7.

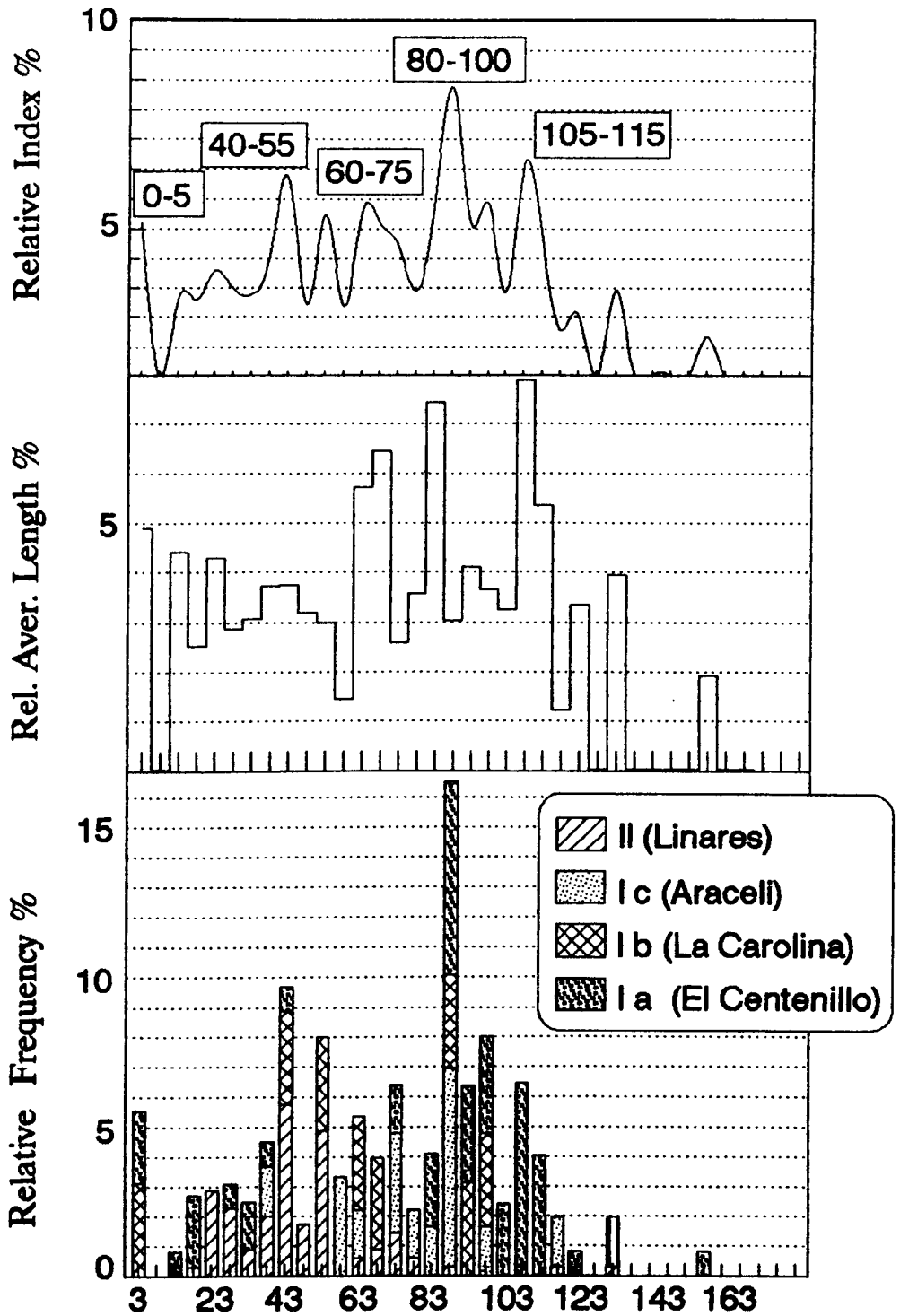

Fig. 4.11. Statistical discrimination of the dominant sets of lodes in Linares-La Carolina on the basis of orientation, length and relative index (relative index % = [rel. freq. % + rel. aver. length %] / 2).

Basic statistical analysis of strike and length data (based on detailed E:1/25,000 cartography from ENADIMSA, 1981) allows the differentiation of five major sets of premineralisation faults related to veins (table 4.4, fig. 4.11):

-N180-5E faults: They occur in the El Centenillo and La Carolina-Santa Elena subsectors, dipping 70 to 90 degrees to west. This set is considered as having been formed during the early stages of late-Hercynian faulting (Charpentier, 1976; Rios, 1977). Recent vertical displacements in large fractures belonging to this group have resulted en post-mineralisation deformation stages, some of them related to the post-Miocene evolution of the Bailen graben (fig.4.7) There is evidence of pre-mineralisation dip-slip movements and post-mineralisation strike- and dip-slip movements. Important veins related to this set are Crucero-Mirador and Crucero-Guindo.

-N40-55E faults: This group is present in all sectors, being dominant in the Linares sector. The faults have dips close to 90 degrees. There are no data available about relative displacements prior to mineralisation. Evidence exists of strike-slip (sinistral) and dip-slip post-ore reactivation. Important veins belonging to this system are Cañada Incosa-Los Quinientos, Arrayanes.

-N60-75E faults: As the system above, this group is present in all sectors, being extensively developed in the Linares sector. The faults typically dip 75 to 90 degrees either to NNW or to SSE. Evidence indicates dextral strike-slip and dip-slip displacements prior to the mineralisation, related to the early formation of the Bailén graben (fig. 4.7). Charpentier (1976) and Rios (1977) have considered these faults as the latest formed before the mineralisation. Some of the economically most important veins in the district are related to this group: Mirador, El Cobre, Matacabras, San Juan-Esmeralda.

-N80-100E faults: This set is well developed in the La Carolina-Santa Elena subsector. The faults dip from 45 to 90

degrees either to north or to south. Some faults belonging to this system are associated with the brittle-ductile deformation manifested in the southern edge of the Santa Elena granitoid (plates 4.5.B and C). Vein and dyke cross-cutting relationships indicate important dip-slip pre-ore relative displacements (Rios, 1977) although their formation could be intimately linked to the formation of the N180-5 system. Sinistral strike-slip displacements apparently took place after the formation of the N40-55 system (*c.f.* Charpentier, 1976). Important veins included in this group are Pelaguindas, Guindo-Federico, Rosa, Araceli.

-N105-115E: This group comprises the largest faults in the district. They are well developed in the La Carolina-Santa Elena subsector, with dips of 70 to 90 degrees either to north or to south. The faults of this group typically deflect into the N80-110E faults (e.g. El Guindo-Federico). There is evidence of sinistral strike-slip pre-mineralisation relative displacements (Rios, 1977). Significant dip-slip movements occurred during post-mineralisation reactivations. Charpentier (1976) has interpreted this system as having been formed during the late pre-ore stages of faulting before the formation of the system N60-75E. Veins belonging to this set are: Sinapismo, Ojo Vecino, San Gabriel.

Despite the large number of veins and late-Hercynian faults in the district, only Rios (1977, 1978) has presented fault-slip data relative to the pre- and syn-mineralisation faulting stages (figs.4.12.a, .b and .c) from the El Centenillo-La Carolina-Santa Elena sector.

The graphical projection (upper hemisphere) of 122 poles to faults is consistent with the five major sets statistically determined for the whole district (fig.4.12.a). It does not imply spatial homogeneity. Predominance of different systems in each sector indicates a certain spatial heterogeneity. Thus, the best developed systems in La Carolina-Santa Elena subsector are lacking in the Linares sector. The graphical projection (upper hemisphere) of 122 poles to 'movement planes' (a 'movement plane' contains the slip vector and the normal vector to the fault plane) displays a

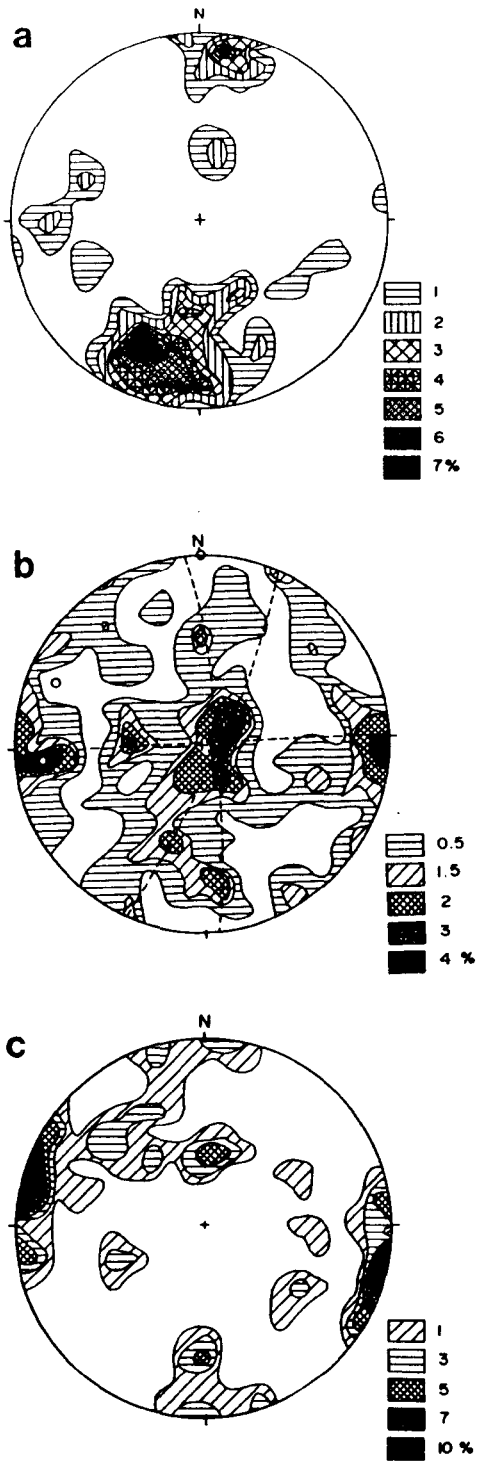

Fig. 4.12. A) Stereographical projection (upper hemisphere) of 122 poles to faults/lodes (Rios, 1977). B) Stereographical projection of 122 poles to 'movement planes' and extension axes have been deduced by Rios (1977) following the method proposed by Arthaud (1969). C) Stereographical projection of 49 poles to tension cracks (Rios, 1977).

multi-modal pattern of extension axes (extension and shortening axes lie in the 'movement plane')(fig. 4.12.b). The axes have been deduced after the method of Arthaud (1969) by Rios (1977). They are interpreted as extension axes given the sense-of-slip, with the exception of the 'vertical' axis which is a shortening axis (none of the analysed faults is reverse). This multi-modal pattern of extension axes represents kinematically heterogeneous faulting, which can be produced by several mechanisms (Marret and Allmendinger, 1990): triaxial deformation, anisotropy reactivation and/or multiple deformations.

Triaxial deformation produces three or four sets of faults arranged with orthorhombic symmetry and an equal number of distinct slip directions, also having orthorhombic symmetry (Reches, 1983). The study area is dominated by five sets of faults. Since the 'movement planes' are constructed from fault planes and slip directions, they and their poles must conserve the orthorhombic symmetry. The poles to 'movement planes' of faults and veins from El Centenillo-La Carolina-Santa Elena sector have very poor orthorhombic symmetry. The triaxial deformation apparently does not explain the kinematic heterogeneity in the faults of the district.

Stages of regional deformation may reactivate local, pre-existing anisotropies in the basement that are arbitrarily oriented for accommodating the overall deformation, thus producing kinematic heterogeneous faulting. In the study area some of the spatial and kinematic heterogeneity could be produced by pre-existing basement anisotropies. Charpentier (1976) and Rios (1977) have suggested the existence of two major tectonic anisotropies, one trending E-W and related to the El Centenillo-La Carolina-Santa Elena 'band', the other one trending NE-SW and associated with the Bailén graben. This point can not be tested, but it must be noted that in that 'band' most of the veins are subparallel to the main Hercynian folding axes trend, contrasting with the Linares sector (and the Pedroches batholith), where granitoids mostly host N40-75E-oriented veins.

A special kind of anisotropy reactivation results in multi-stage faulting, when the early faults are reactivated, generating a new set of striae. Thus, a single set of faults may have variable slip directions. The fault-slip kinematics of one deformation might be either incompatible or compatible with the kinematics of other deformation. Evidence for multiple deformation is provided by systematic cross-cutting relations and mutually exclusive chronologic constrains on fault sets.

The fault sets of the district show at least two sets of pre-mineralisation fault striae indicating both dip- and strike-slip movements. Furthermore, as indicated by Charpentier (1976) and Rios (1977), the fault sets are not coeval. It appears that the chronologically earliest faults (N180-5E and N80-100E), with strike-slip and dip-slip displacements respectively, were reactivated as strike-slip faults during the formation of N105-115E, N40-55E, and finally, N60-75E sets. Thus, the oldest faults, mainly occurring in the El Centenillo-La Carolina-Santa Elena 'band', could be generated by a basement anisotropy favorably oriented for accommodating the deformation during early stages of faulting.

Therefore, the multi-modal pattern of extension axis of vein-related faults at Linares-La Carolina is better explained by anisotropy reactivation in multi-stage faulting rather than by other heterogeneous faulting mechanisms.

4.4.2.2.Stages of fault evolution.

Vein pattern and deformational history of the related faults can be explained by a late-Hercynian evolution model involving three pre-ore deformation stages (Lillo, 1990):

-Early extensional stage (fig.4.13.a). During this stage, faults of the N180-5E and N80-100E systems were formed in the northern part of the district as result of a N-S-oriented extension. As suggested by Doblas (1991) for Central Iberia (see chapter 2), the extension could be produced by gravitational

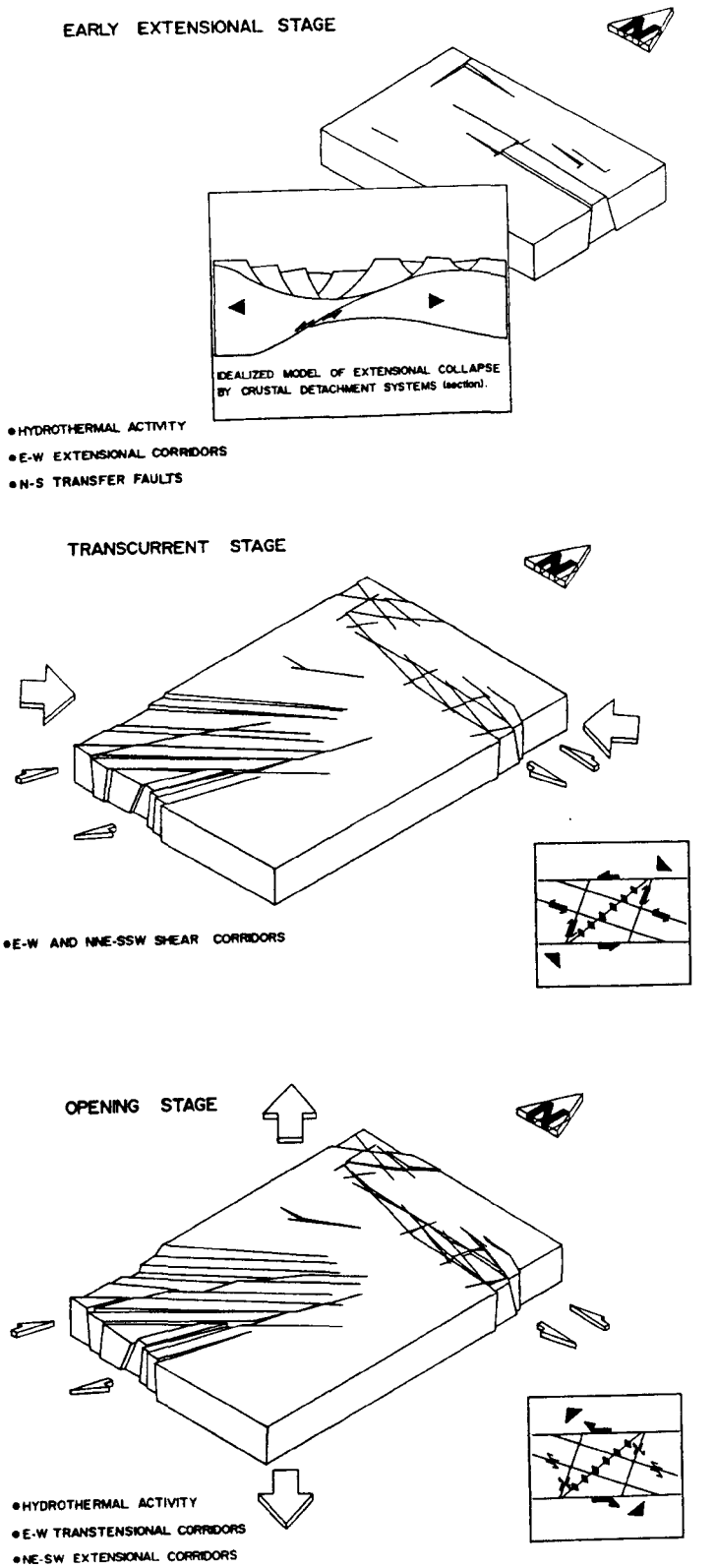

Fig. 4.13. Late-Hercynian evolution model of faulting (pre-ore stages) proposed for the Linares-La Carolina district (Lillo, 1990). Explanation in the text.

collapse through lithosphere scale, low-angle detachment faulting of the overthickened crust, when the overall gravitational potential became dominant over the residual Hercynian compressional stresses. This extensional event has been interpreted by Doblas et al., (1988), Concha et al., (1992) and Lillo et al., (1992) as being partially responsible for the observed patterns of (silver)-base metal veins in the Spanish Central System. As result of this tectonic denudation, a E-W-oriented extensional 'corridor' was created in Linares-La Carolina district, defined by N80-100E-oriented listric dip-slip faults and N180-5E (transfer?) faults. At relatively shallow levels, the transition from brittle to ductile deformation was attained, presumably because fluid flow was significant, being capable of inducing ductility in quartz and hydrothermal metasomatism. The mylonite/cataclasite of Santa Elena displays C-type shear planes of low-angle dip, typical of simple shear detachment faulting.

-Transcurrent stage (fig.4.13.b). When the gravitational potential had been released, the residual compressional Hercynian stresses became dominant again. The structural pattern of major strike-slip faults and thrust in the Ibero-Armorican Arc has been compared by Matte (1986) with the West-Himalayas rigid-plastic indentation model of Tapponier et al., (1982). The direction of rigid motion inferred for the Ibero-Armorican Arc is approximately N100E in terms of the actual configuration of the massif. Molnar and Tapponier (1977) showed that a systematic variation of the orientation of strike-slip lines and rotation of local stress axes occur in a rigid-plastic indentation. Thus, a local ENE-WSW-oriented shortening axis in the study area is compatible with a overall N100E-oriented indentation. In this local transpressional regime, the faults previously formed were strike-slip reactivated and the N40-55E and N105-110E systems were formed with some new N80-110E-oriented faults. The N60-75E system, with dip-slip displacements, was formed after the transcurrent sets. The whole fault pattern and slip directions are consistent with a sinistral Riedel shear system with a ENE-WSW-directed shortening axis.

-Opening stage (fig.4.13.c). This stage represents the emplacement of the base metal veins as consequence of the change from a compressional to an extensional cycle in Iberia. Most of the extension appears having been resolved by strike-slip and dip-slip reactivation of the already existing faults. The most favorably oriented fractures for accommodating the deformation were the N60-75 and the N40-55 sets, leading to the development of extensional grabens (Bailén graben). Poles to tension cracks from El Centenillo-La Carolina-Santa Elena sector indicate a dominant subhorizontal extension axis striking N110-120E (fig.4.12.c).

4.4.2.3.Regional setting and timing of faulting.

It is widely accepted that the change of tectonic cycle in Iberia took place during the early Upper Permian as Saxonian and Buntsandstein facies were deposited in extensional basins (Alvaro et al., 1979; Gisbert, 1983; Virgili et al., 1983; Sopeña et al., 1988, among others; see chapter 2). The transpressional local regime developed in the late stages of the Hercynian compressional cycle, during the late Westphalian-Lower Permian span (fig. 4.14). The age of the early extensional stage is uncertain. In the internal areas of the Hesperian Massif, the first extensional movements are dated Stephanian B-C (Julivert at al., 1971). As the dip-slip faults created in this stage were strike-slip reactivated during the transpressional regime, the early extensional stage took place before the Upper Permian and likely after the Stephanian B-C (note that if this deformation stage was caused by the gravitational instability of the orogenic building, it does not imply a change in the tectonic cycle).

Since the opening stage started in the Upper Permian and the veins do not cut sediments which are Ladinian in age, then the age of the mineralisation may be constrained to the Upper Permian-Anisian span.

The age thus inferred is partially consistent with K-Ar ages obtained from clay-size concentrates by Halliday and Mitchell (1984). The K-Ar ages are in the range of 204-285 Ma for samples

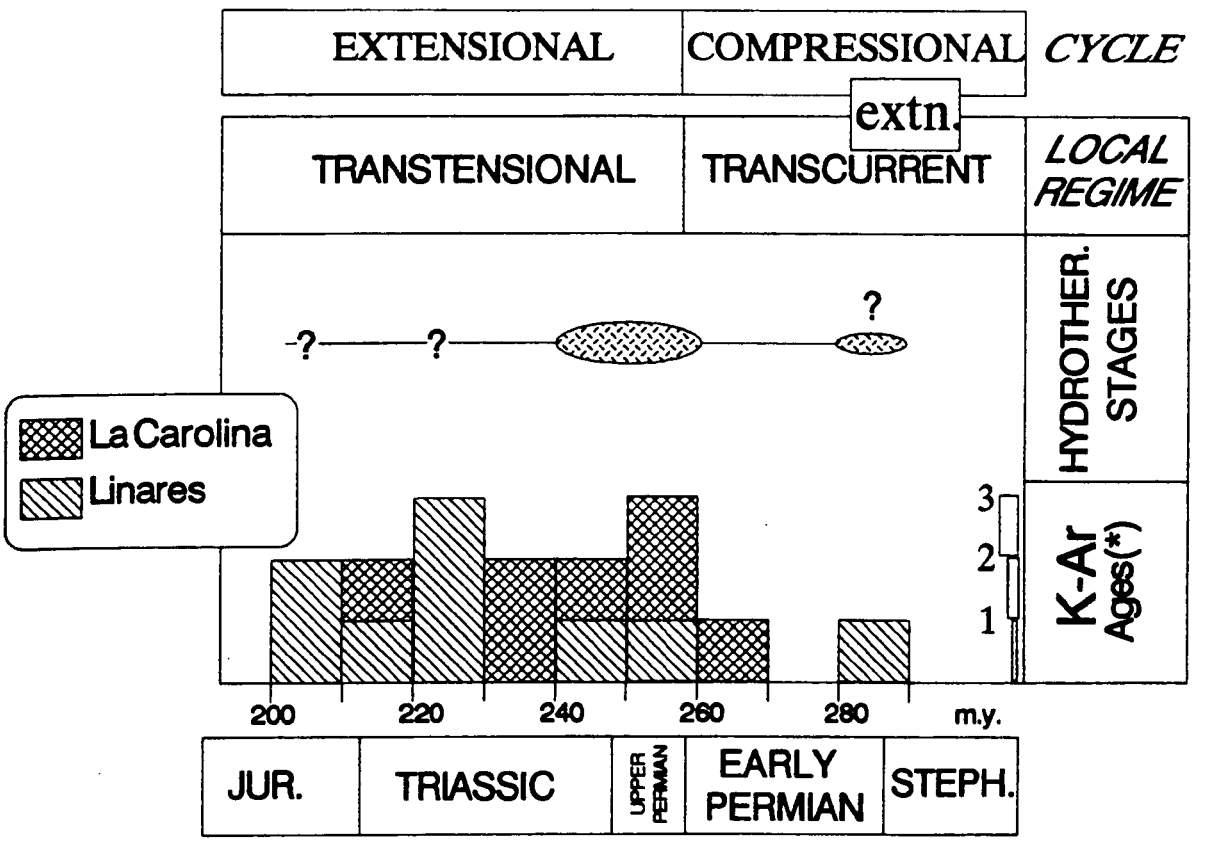

Fig. 4.14. Comparative diagram of timing of the (Ba)-(base metals-[Ag]) hydrothermal mineralisations in Linares-La Carolina district. Ages of both hydrothermal (major) stages are determined from local and regional structural, stratigraphical and sedimentological data (see text). K-Ar ages are from Halliday and Mitchell (1984).

from the Linares-la Carolina district, and in the range of 285-119 Ma with a mode of 230-210 Ma for samples from several mineralisations (including Linares-La Carolina) in the Pedroches batholith. These results are interpreted by Halliday and Mitchell (1984) as representative of a major hydrothermal event that caused partial isotopic 'resetting' of late-Hercynian ages.

4.4.3.Ore petrography, mineral assemblages and paragenetic sequence.

4.4.3.1.Ore petrography.

A total of 40 ore, gangue and supergene mineral species have been reported the (Ba)-(Base metals-[Ag]) hydrothermal mineralisations of Linares-La Carolina district (table 4.5).

The dominant ore minerals are galena, sphalerite, iron sulphides (pyrrhotite, pyrite, marcasite) and chalcopyrite. Relative abundances of these minerals vary from vein to vein and from sector to sector. Sphalerite is generally more abundant in veins located in the La Carolina-Santa Elena sector. Other subordinate ore species, some of them appearing as merely curiosities, are simple silver sulphides and sulphosalts (argentite, dyscrasite, freibergite, pyrargyrite, polybasite, boulangerite), copper sulphides and oxides (bornite, cubanite, covellite, chalcocite, digenite, cuprite, tenorite), native copper, arsenides (niccolite, löllingite, arsenopyrite), bismuth sulphides (bismuthinite, emplectite, cosalite) and Ni-Co minerals (linnaeite, ullmanite). Gangue minerals are ankerite, quartz, amorphous silica, barite, calcite and minor amounts of kaolinite. Barite may be important in volume, specially at the upper levels of the lodes. Fluorite is very rare, having been reported only as a curiosity. No adularia has been reported in the literature.

Other minor Late-Hercynian vein-deposits of different paragenesis (not considered in this study) occur in the district.

-Sb-(Zn): Stibnite, berthierite, pyrite, arsenopyrite, sphalerite. Occurrences: San Agustin, El Contadero, Maria Luisa,

Pb-Ag and Zn minerals:	
Galena	(Pb,Ag,Sb)S
Boulangerite	$Pb_5Sb_4S_{11}$
Polybasite	$Ag_{16}Sb_2S_{11}$
Pyrargyrite	Ag_3SbS_3
Freibergite	$(Ag,Cu)_{10}(Fe,Zn)_2Sb_4S_{13}$
Dyscrasite	Ag_3Sb
Argentite	Ag_2S
Cerussite	$PbCO_3$
Cu sulphides ans oxides:	
Bornite	Fe_2CuS_3
Cubanite	$FeCu_5S_4$
Chalcopyrite	$FeCuS_2$
Covellite	CuS
Chalcocite-Digenite	Cu_2S
Tetraedrite	CuSSb
Cuprite	CuO_2
Tenorite	CuO
Azurite	$Cu_3(OH)_2(CO_3)_2$
Malachite	$Cu_2(OH)_2CO_3$
Ni-Co minerals:	
Niccolite	NiAs
Bravoite	$NiFeS_2$
Ullmanite	SbNiS
Linnaeite	$(CoNiFeCu)_3S_4$
Löllingite	$(CoNiFe)As_2$
Fe minerals:	
Pyrite	FeS_2
Marcasite	FeS_2
Pyrrhotite	FeS_{1+x}
Arsenopyrite	FeSAs
Lepidocrocite	γFe O OH
Goethite	α.FeO.OH
Bi minerals:	
Native Bismuth	Bi
Bismuthinite	Bi_2S_3
Emplectite	$(BiCu)S_2$
Cosalite	$(Bi_2Pb_2)S_5$
Gangue Minerals:	
Ankerite	$Ca(Mg,Fe,Mn)(CO_3)_2$
Quartz	SiO_2
Amorphous silica	SiO_2
Calcite	$CaCO_3$
Aragonite	$CaCO_3$
Barite	$BaSO_4$
Fluorite	CaF_2

Table 4.5. Mineral species in the (Ba)-(base metals-[Ag]) mineralisations of Linares-La Carolina (reported by Enadimsa ,1971, and Charpentier, 1976).

Casa del Barranquillo (Tamain, 1968; Azcarate and Vergara, 1971; Gumiel, 1983; Gumiel and Arribas, 1987).

-As-(Sn-W): Arsenopyrite, cassiterite, wolframite. Occurrences: Fuente-Romualdo, Candalo (Bienvenida mine) (Tamain, 1968; Azcarate and Vergara, 1971).

-Cu-(Pb): Copper-iron sulphides and oxides dominant with minor galena. Gangue: quartz, calcite, barite. Several minor occurrences are located at the western border of the study area. (Tamain, 1968; Azcarate and Vergara, 1971).

Ore and gangue minerals in the (Ba)-(Base metals-[Ag]) hydrothermal mineralisations appears in mono- or poly-mineral veins, pods, pockets, breccias and pipes.

Galena is the most dominant ore phase by far. It is present in two habits (Charpentier, 1976): fine-grained galena and coarse-grained galena. The coarse-grained galena is commonly cube-octahedral and octahedral. Cubic habit is rare. Two generations have been distinguished: the first one is variably deformed, with small inclusions of silver minerals. The second generation is represented by subautomorphic grains with inclusions of chalcopyrite and pyrite. The galena grains are replaced in the rims by cerussite.

Sphalerite may appear with no intergrowths (1^{st} generation) or with intergrown chalcopyrite, pyrrhotite (replaced by pyrite) or rare Ni-Co phases (e.g. ullmanite), being considered of 2^{nd} generation. (*c.f.* Enadimsa, 1971; Charpentier, 1976; Rios, 1977).

Pyrite is ubiquitous, either primary with cubic habit or as marcasite pseudomorphs. It is abundant when associated with chalcopyrite.

Chalcopyrite may show frequent intergrowths of sphalerite. Cu minerals (covellite, chalcocite, bornite) appear in the grain edges of chalcopyrite grains. Chalcopyrite may be present as minor inclusions in galenas.

The dominant gangue minerals are ankerite and quartz. **Ankerite** presents several modes of occurrence. There is a white ankerite of medium-coarse rhombohedral grains found in veins or as hydrothermal breccias cemented by fine-grained grey ankerite. The other mode of occurrence of ankerite is as thin crusts surrounding sulphides.

'Milky' **quartz** is eminently associated with galena and sphalerite (early stage). 'Glassy' quartz showing 'comb' textures is mostly associated with pyrite, marcasite and chalcopyrite (late stage).

Calcite may be important in volume in veins located at the Linares sector, being scarce at the Santa Elena-La Carolina sector. It occurs in 'cockade', 'crust' and 'comb' textures cementing hydrothermal breccias including host rocks, sulphides, ankerite and barite or alternatively in decimetric banded structures.

Barite is common, but its abundance is variable. Some veins (e.g. Alto de Borras lode, Santa Elena-La Carolina sector) are found consisting almost exclusively of barite.

Charpentier (1976) reported the occurrence of minor amounts of kaolinite filling voids in 'milky' quartz in the Crucero-Guindo lode. During this study, this mode of occurence was observed on samples of 'milky' quartz with ankerite and galena from La Nube and Ojo Vecino lodes.

4.4.3.2.Paragenetic assemblages and deposition stages.

Paragenetic assemblages and mineral deposition stages are shown in fig.4.15. 28 Ore samples selected from 13 sites were surveyed by conventional optical microscopy (COM), by backscattered electron microscopy (BSE) and by energy dispersive X-ray microanalysis (EDX) to search for mineral species other than sphalerite, galena, pyrite, chalcopyrite and niccolite. No silver phases were detected. Only boulangerite ($Pb_5Sb_4S_{11}$) was found in a sample (LC308-13) from the Federico lode (La Española shaft). The

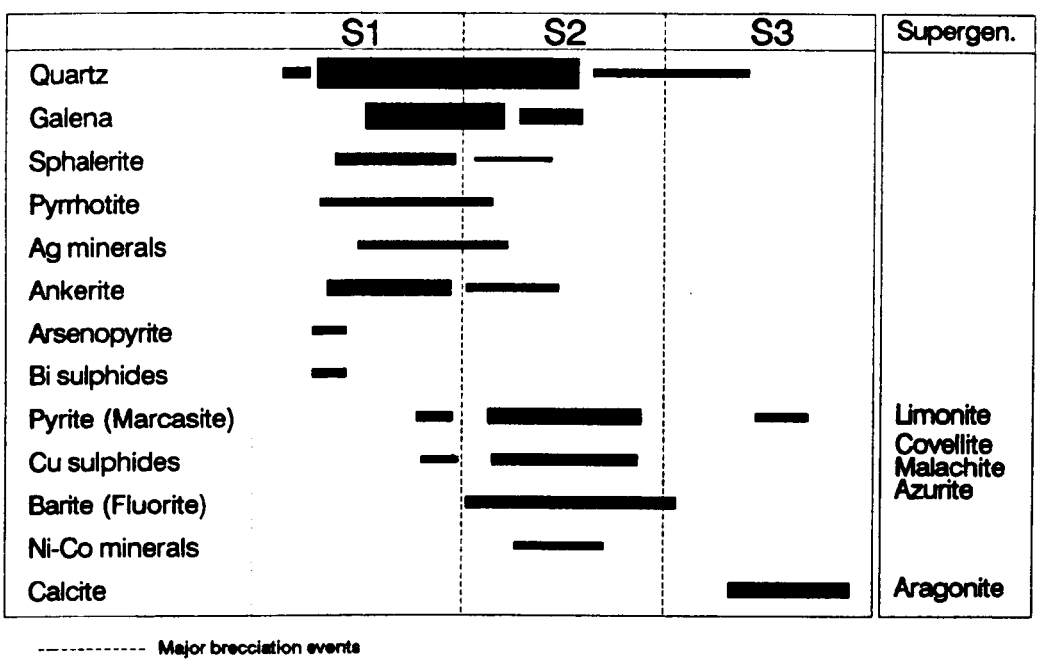

Fig. 4.15. Paragenetic assemblages and mineral deposition stages of the (Ba)-(base metals-[Ag]) hydrothermal mineralisations in Linares-La Carolina district (partly based on Enadimsa, 1971; and Charpentier, 1976).

scarcity of mineral species found in the samples collected during the present study precluded a correct definition of mineral assemblages and stages. Therefore, this sequence is mainly based on data from Enadimsa (1971) and Charpentier (1976). The depositional sequence is formed of three mineral stages separated by two major brecciation events.

There are some discrepancies between the depositional stage model proposed for the entire district in the present work and those depositional stages presented by Enadimsa (1971) and Charpentier (1976). The Enadimsa's stages, also defined for the whole Pb-ore field, consider that most of the barite was precipitated during the late stage of the ore emplacement. This observation is based on the assumption that barite precipitation took place during the post-Triassic times as some occurrences are found in the basal beds of the post-Hercynian cover. As discussed in the above paragraphs in this chapter, all hydrothermal mineralisations (veins and stratabound) are clearly pre-Ladinian in age, even if some hydrothermal activity took place in the district at *ca.* 220 Ma. Moreover, barite in the veins frequently occurs intergrown with 'glassy' quartz or as fragments in hydrothermal breccias (also including fragments of sulphides) cemented by calcite. Therefore, most of the barite had to be formed during the ore stage considered in the present work as the second (S2).

Charpentier (1976) established five stages of mineral deposition in the El Crucero-Guindo lode on the basis of brecciation episodes. Those stages and mineral assemblages reflect local variations from those defined for the whole district. Thus, the first and second stages of Charpentier may be grouped into one stage with an intra-stage brecciation event. Formation of sphalerite in the Crucero lode seems to be restricted to the first stage. Alternatively, chalcopyrite with sphalerite in exsolution are replacing rims of galena, suggesting precipitation of sphalerite during the second stage of ore emplacement, after a deposition of galena (1st generation?, Enadimsa, 1971).

4.4.4. Mineral chemistry.

112 Electron microprobe analyses (EMP) were carried out on 20 selected samples for trace elements in sphalerites (S, Zn, Mn, Fe, Ni, Cu, see table 4.9), galenas (S, Pb, Fe, Cu, Zn, Sb, Ag, see table 4.7) and pyrites (S, Fe, Co, Ni, Cu, Zn, As, Sb, Ag, see table 4.8.a).

Galena

Fe, Cu, and Zn are in insignificant amounts or below detection limits in galenas. Silver occurs as solid solution in galena with small amounts of antimony (tables 4.6.a and .b, table 4.7). Silver and antimony contents are variable between grains in the same sample as well as within the same galena grain. Appreciable amounts of Sb (about 1 wt %) were only found in a sample (LC9031-12) from El Guindo lode. This sample yielded the highest concentration of silver (up to 0.9 wt %) found during the present study. Bismuth quantities are very low. The differences of Ag content of galenas among different sectors and/or mode of occurrences lie in the range found in each single sample (tables 4.6.a-b, and table 4.7). Therefore, there is no evidence of selective Ag "enrichment" in relation to location or ore-type.

Ag is quite insoluble in PbS at geologically significant temperatures when Sb or Bi is absent (Amcoff, 1976). Complete solid solution between PbS and $AgSbS_2$ exists above 590 °C. Below 390 °C, the cubic solid solution splits into a Pb and an Ag-rich member. On the Pb-rich part, the solubility of $AgSbS_2$ in PbS is about 4 mole % at 300 °C and 2 mole % at 250 °C (Amcoff, 1976). Therefore, PbS accepts 1.4 wt % Ag and 1.6 wt % Sb at 300 °C, and 0.7 wt % Ag and 0.8 wt % Sb at 250 °C. Sb found in the samples was either higher or lower than Ag content. Even if the low contents of both elements in some samples could be explained by galena precipitation below 300 °C, the variability found within a single sample and the erratic Ag/Sb ratios requires another mechanisms, like insufficient availability of Ag and Sb at the time of galena formation. Support to this interpretation is given by the trace

a)

Sample	C14/20	C14/20*	C26/90	C34/37	C1/4
Lode	Crucero Guindo				
Pb	82.40	75.40	80.20	69.60	80.00
Cu	0.003	0.003	0.003	0.003	0.002
Zn	0.140	0.160	0.110	0.160	0.160
Bi	0.001	0.001	0.001	0.001	0.001
As	0.19	0.27	0.26	0.28	0.34
Sb	0.34	0.18	0.42	0.25	0.38
Ag	304	432	612	484	572

b)

Sample	E179/2	E179/3	E179/5	E179/17	E179/26
Lode	El Cobre			Matacabras	Ojo Vecino
Pb	n.a.	n.a.	n.a.	n.a	n.a.
Cu	0.000	0.000	0.001	0.001	0.025
Zn	<0.002	<0.002	0.010	0.006	>0.050
Bi	0.004	0.001	0.001	0.000	0.000
As	n.a.	n.a.	n.a.	n.a	n.a.
Sb	n.a.	n.a.	n.a.	n.a	n.a.
Ag	390	230	440	700	250

Tables 4.6.a and b. Chemical analyses of galenas from some lodes in Linares-La Carolina district. Table a) are data from Charpentier (1976). Table b) are data from Enadimsa (1971). All elements in wt% except Ag which is in ppm (n.a.: not analysed).

	LC33-5 (Las Torrecillas)				
S	13.748	13.572	(c) 13.546	(r) 13.429	13.466
Pb	85.293	85.374	85.935	86.759	85.683
Fe	0.000	0.000	0.000	0.000	0.000
Cu	0.035	0.000	0.000	0.000	0.026
Zn	0.000	0.015	0.012	0.015	0.110
Sb	0.246	0.000	0.115	0.048	0.000
Ag	0.561	0.047	0.000	0.000	0.009
Total	99.883	99.008	99.609	100.251	99.294

	LC318-3 (San Juan-Esmeralda)				
S	13.646	13.602	13.661	13.494	13.523
Pb	86.600	85.800	86.301	86.739	86.491
Fe	0.000	0.000	0.000	0.008	0.057
Cu	0.010	0.000	0.000	0.016	0.041
Zn	0.015	0.061	0.000	0.081	0.000
Sb	0.179	0.128	0.097	0.000	0.000
Ag	0.119	0.347	0.025	0.200	0.040
Total	99.570	99.939	100.083	100.539	100.51

	LC139-6 (Guindo)				
S	13.418	13.466	13.500	13.541	13.697
Pb	85.350	85.753	85.517	86.469	86.717
Fe	0.179	0.090	0.070	0.024	0.000
Cu	0.006	0.029	0.000	0.000	0.000
Zn	0.000	0.039	0.000	0.033	0.000
Sb	0.088	0.169	0.021	0.130	0.067
Ag	0.300	0.038	0.000	0.329	0.202
Total	99.342	99.583	99.103	100.526	100.684

Table 4.7. Electron microprobe chemical analysis of galenas in selected samples from some hydrothermal occurrences of Linares-La Carolina district. All elements in wt%. c) and r) are relative to analyses of the same grain, in core and rim zones, respectively.

a)

Sample	LC139-6		LC318-3		LC33-5
Lode	Guindo		San Juan-Esmeralda		Las Torrecillas
S	53.409	53.266	53.217	53.461	52.705
Fe	47.150	46.281	46.932	47.149	37.974
Co	0.000	0.005	0.000	0.000	5.263
Ni	0.000	0.000	0.066	0.000	3.048
Cu	0.027	0.000	0.000	0.148	0.000
Zn	0.117	0.091	0.000	0.000	0.009
As	0.000	0.572	0.000	0.000	0.074
Sb	0.037	0.028	0.040	0.011	0.034
Ag	0.117	0.059	0.000	0.000	0.132
Total	100.857	100.303	100.255	100.769	99.238

b)

Sample	E138	E179/4	E179/8
Lode	Guindo	El Cobre	
S	n.a.	n.a.	n.a.
Fe	n.a.	n.a.	n.a.
Co	0.023	0.000	0.960
Ni	0.030	0.000	0.140
Cu	0.048	0.035	0.850
Zn	>0.050	0.001	0.001
As	n.a.	n.a.	n.a.
Sb	n.a.	n.a.	n.a.
Ag	116	9	310

Tables 4.8.a and b. Chemical analyses of pyrites in selected samples from some hydrothermal mineralisations of Linares-La Carolina district. Table a) shows electron microprobe analyses. All elements in wt%. Table b) are data from Enadimsa (1971). All elements are in wt% except Ag which is in ppm (n.a.: not analysed)

	LC308-13 (Federico)		
n=12	Range	Mean	1σ
S	33.317-32.853	33.082	0.178
Mn	0.046-0.000	0.015	0.019
Fe	6.122-5.104	5.756	0.254
Ni	0.069-0.000	0.027	0.028
Cu	0.014-0.000	0.000	0.017
Zn	61.760-60.511	60.025	0.384
χ_{Zn}	0.912-0.895	0.901	0.004

	LC90174-1 (El Guindo)		
n=10	Range	Mean	1σ
S	33.397-32.838	33.109	0.168
Mn	0.052-0.018	0.026	0.020
Fe	11.639-4.541	6.676	2.320
Ni	0.066-0.000	0.028	0.029
Cu	0.062-0.000	0.018	0.022
Zn	61.743-54.146	59.827	2.511
χ_{Zn}	0.921-0.799	0.885	0.040

	LC90164-10 (Pelaguindas)		
n=8	Range	Mean	1σ
S	33.087-32.723	32.883	0.116
Mn	0.039-0.000	0.012	0.014
Fe	3.502-0.536	1.787	1.078
Ni	0.049-0.000	0.022	0.016
Cu	0.306-0.025	0.168	0.096
Zn	66.087-62.461	64.405	1.271
χ_{Zn}	0.991-0.938	0.969	0.019

Table 4.9. Composition of sphalerites in selected samples from Federico, Guindo and Pelaguindas lodes. Elements in wt%. χ_{Zn} is atomic fraction of Zn (Zn/Fe+Zn).(Samples analysed by electron microprobe, EMP).

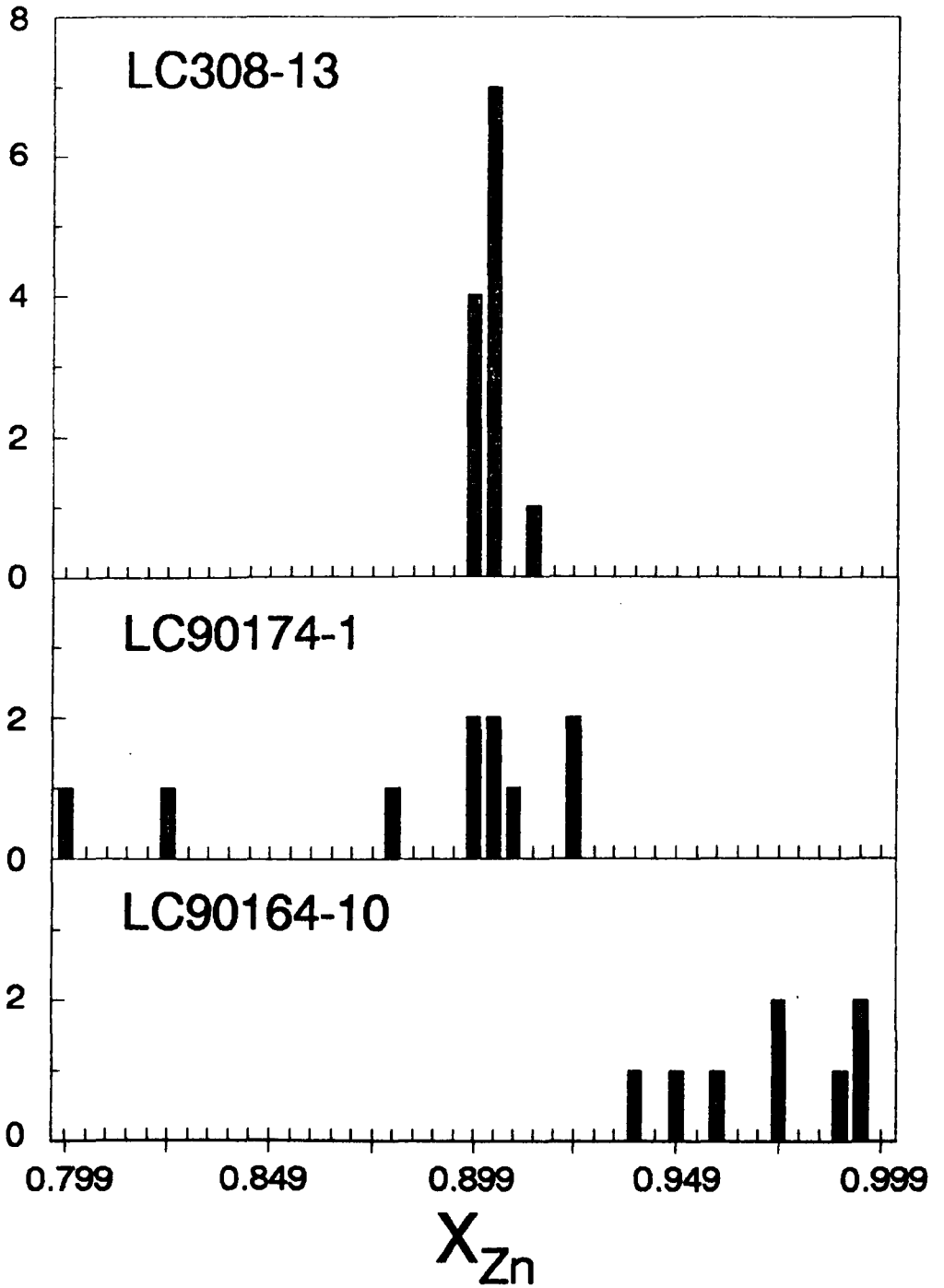

Fig. 4.16. Variation of the atomic fraction of Zn in selected samples of sphalerite.

occurrence of Ag, Sb and Bi mineral phases in the ores (*c.f.* Pearson et al., 1988).

Sphalerite

Mn and Ni concentration in sphalerites in three samples (LC308-13, LC90174-1 and LC90164-10 from Federico, El Guindo and Pelaguindas lodes, respectively) are very low. Sphalerites in sample LC90174-1 yielded the highest Fe content against sphalerites from sample LC90164-10, with the lowest Fe content. Atomic fraction of Zn yielded a range from 0.799 to 0.991 (table 4.9, fig.4.16), the largest range being found in sample LC90174-1 (0.921-0.799).

Pyrite

Cu, Zn, As and Sb amounts in pyrite are insignificant (table 4.8.a). A sample (LC33-5) from the Las Torrecillas stratabound ore yielded 5.26 wt % of Co and 3.04 wt % of Ni, although concentrations of these trace elements in pyrites from vein-type mineralisations are below 1 wt % (tables 4.8.a and .b)

Chapter 5. Hydrothermal alteration studies.

5.1.Introduction.

Metasomatic reactions between hydrothermal fluids and wall rocks are important not only because their potential effects on fluid chemistry and element transport but also because of the information that preserved alteration envelopes provide on the temperature and composition of the hydrothermal fluid involved in the ore mineralisation.

The purpose of this chapter is to evaluate the effects of fluid-rock chemical reactions on wall-rock lithology in order to get further constraints on the physico-chemical conditions of the ore deposition.

5.2.Sampling.

15 Samples of altered wall-rocks (granodiorite-adamellites of the Santa Elena and Linares massifs) were collected in situ from several outcrops (Ojo Vecino and La Nube lodes, and the Santa Elena mylonite) and from a mine gallery (level 11 of the South branch vein at El Cobre lode, at 400 m depth).

20 unaltered/less altered samples of those host rocks were collected from "fresh" outcrops at nearby places of the respective locations of the altered samples.

Two different approaches of sample collection were considered: a) at El Cobre lode, the sampling was carried out every meter on a profile of 9 m, nearly normal to the vein; b) at the Santa Elena massif, the sampling was done on selected outcrops, representative of different alterations.

5.3. Petrography of altered granitoids.

5.3.1. Primary mineralogy.

As partly described in Chapter 4, the adamellite-granodionite of Santa Elena consists of quartz (22-33 vol.%), plagioclase (22-45 vol.%, A_{n48-32} but more calcic compositions may be found, fig. 4.5), K-feldspar (6-21 vol.%, Or_{95-89} Ab_{4-11}) and biotite (14-26 vol. %, Al_{VI}= 0.30-0.41 atoms p.f.u., table 4.2).

The adamellite of Linares is a medium to coarse-grained rock consisting of quartz (25-30 vol %), plagioclase (25-45 vol %, An_{34} and albite-rich An_{12-6}), K-feldspar (10-30 vol %, Or_{97-93} Ab_{3-7}, fig. 4.5) and biotite (4-11 vol %, Al_{VI}= 0.21-0.18 atoms p.f.v., table 4.2). Pseudoprimary muscovite is very rare. Andalusite and cordierite (up to 5 vol%) have been reported (IGME, 1975) in marginal zones close to the metamorphic rocks although these minerals were observed in none of the studied samples.

Both lithologies (granodorite-adamellite of Santa Elena and adamellite of Linares) shows a texture anhedral to subhedral granular, with phenocrysts of K-feldspars with Carlsbad twins and microperthitic intergrowths. The plagioclase appears as zoned crystals with euhedral to subhedral habit, showing polysynthetic twinning. The quartz grains occur with anhedral to subhedral habit.

The accessory minerals include apatite, zircon, ilmenite and fluorite.

5.3.2.Wall-rock alteration halos.

5.3.2.1.General characteristics. Mineral assemblages.

Well developed alteration halos in initially homogeneous country rocks such as the Santa Elena and the Linares granitoids display textural and compositional zoning typically subparallel to the vein fractures. The halos of the major veins are commonly of decametric order, but incipient pervasive propylitic alteration

TABLE 5.1

m.	0.5	1	3	4	5	7	9
Chlorite	X	XXX	XX	XXX	◆	XX	X
White mica	XX	XXX	XXX	XXX	XXX	XX	X
Kaolinite	X	◆	XX	XXX	XX	-	◆
K-Spar	XX	XX	XX	XX	XX	X	◆
Albite	X	XX	X	XX	X	X	◆
Quartz	XX	◆	-	-	-	-	-
Calcite	-	◆	-	-	-	-	-
Pyrite	◆	◆	-	-	-	-	-
Biotite	A	VA	VA	VA	CD	A	LA
K-feldspar	A	A	A	A	A	LA	LA
Plagioclase	A	A	VA	VA	VA	LA	LA

TABLE 5.2

FACIES	AM	C	B	A
Epidote	-	-	◆	-
chlorite	-	-	◆	XX
white mica	XXX	XXX	XXX	◆
Kaolinite	X	XXX	XXX	X
K-Spar	X	XX	X	◆
Albite	X	◆	-	◆
Quartz	XX	-		-
Calcite	-	-	-	◆
Pyrite	X	X	-	-
Biotite	A	CD	VA	LA
K-Spar	A	VA	VA	A
Plag	A	VA	VA	A

Secondary minerals	
XXX:	very abundant
XX :	abundant
X :	scarce
◆ :	traces
- :	absent
Primary minerals	
LA :	little altered
A :	altered
VA :	very altered
CD :	completely destroyed

Tables 5.1 and 5.2. Alteration assemblages in the Linares and Santa Elena granitoids. A.M. corresponds to altered mylonite, C represents strong phyllic-argillic alteration, B is relative to phyllic-argillic alteration and, A is representative of weak propylitic alteration.

may be found farther from the veins. The halos are symmetrical but local variations occur in each side of the vein because the halos are strongly controlled by fluid flow along fissures at proximal zones.

The haloes display the "normal" sequence of alteration assemblages observed commonly in Cordilleran veins and some porphyry base-metal deposits (e.g. Meyer and Hemley, 1967; Guilbert and Park, 1986 and references therein).

As there is no available data about vertical zonation of the alteration envelopes, the sequence of assemblages encountered with increasing distance away from the vein is assumed to be approximately the same as the vertical sequence of assemblages in proximal zones along the veins. Thus, the zones pinch out or "telescope" in depth, decreasing the volume of the most proximal assemblages (e.g. the phyllic assemblage). At El Cobre lode, the surveyed profile displays argillic-propylitic to propylitic assemblages,the phyllic and argillic (s.s) assemblages being absent (table 5.1). The argillic-propylitic assemblage (sericite ± chlorite ± kaolinite ± calcite ± pyrite ± quartz) develops on the first 5-6 meter from the vein. The alkali metasomatism assemblage (K-feldspar ± albite ± muscovite) overprints that argillic-propylitic assemblage. A weak propylitic assemblage (chlorite ± sericite with traces of kaolinite) appears further than 5-6 meter from the veins. Alkali metasomatism is practically absent from that distance.

A sample (LC59-1, A.M.) of hydrothermally altered mylonite at Santa Elena exhibits an argillic assemblage (sericite ± quartz ± kaolinite) overprinting an older phyllic alteration (coarse white mica + quartz + pyrite). Potassic alteration in the form of recrystallised K-feldspar (plus minor coarse white mica) seems to postdate the argillic alteration. As noted in chapter 4, petrographical and field data indicate that the "old" phyllic alteration represents an episode of hydrothermal activity likely related to the early late-Hercynian extensional faulting in the district, prior to the main ore emplacement.

Two samples (LC159-6, C and LC159-5, B) from the granitic wall-rocks at La Nube lode exhibit the argillic-phyllic assemblage (kaolinite + sericite + pyrite, with all primary biotite altered to white mica in sample LC159-6, overprinted by a potassic assemblage (coarse white mica + K-feldspar). Traces of epidote occur in sample LC159-5 (Table 5.2).

A sample (LC159-3, A.) from the environs of the Ojo Vecino lode (near to the altered mylonite) displays a weak propylitic alteration (chlorite + sericite and kaolinite in traces, primary biotite being metestable). There is no evidence of a later potassic alteration.

5.3.3.Secondary minerals.

5.3.3.1.Texture and phase relations.

There are several modes of occurrence of the secundary minerals in the alteration envelopes in granitic wall-rocks at Linares-La Carolina:

-Filling textures:

a) Microveins: they are relatively frequent in proximal zones. They show commonly monomineral fillings: quartz, calcite, feldspar. Quartz is commonly the early fissure filling. Feldspars, either Na-rich albite or K-rich feldspar, appear as the late filling of fissures cross-cutting altered primary feldspar phenocrysts (Plates 5.2.A, B, C)

b) Vugs: they appear commonly as cavities formed on feldspar phenocrysts (mainly plagioclase) filled with white mica and kaolinite, which may be intergrown. Other spaces not directly formed by dissolution of feldspar show fillings consisting of white mica, chlorite and kaolinite (Plates 5.4.C, 5.1.A and C)

Plate 5.1. BSE images of altered samples from the El Cobre wall-rocks. A) New K-spar(II) and albite(II) replacing an old albite(I) in sample LC129-13 (0.5 m from the vein); B) chlorite zoning in sample LC129-20 (7 m from the vein); C) intergrowths of chlorite, white mica ("illite") and clays in voids and microfractures, sample LC129-17 (4 m from the vein); D) intergrowths of chlorite and white mica, sample LC129-17 (4 m from the vein).

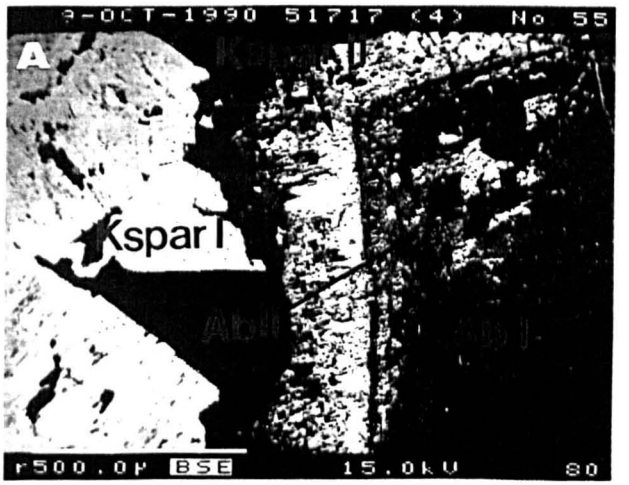
9-OCT-1990 51717 (4) No 55
A
Kspar I
r500.0P BSE 15.0kV 80

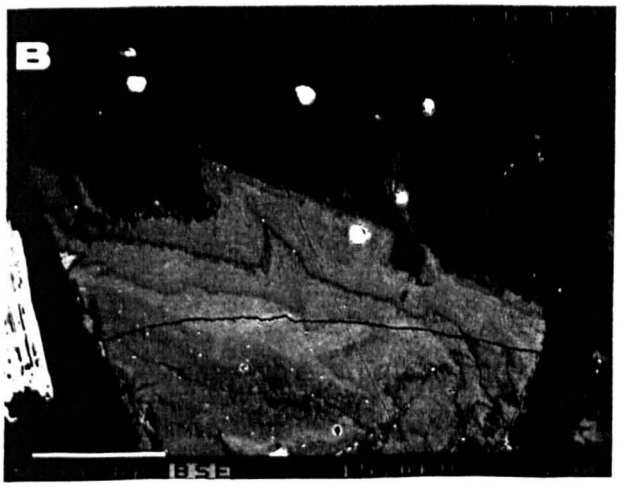
B

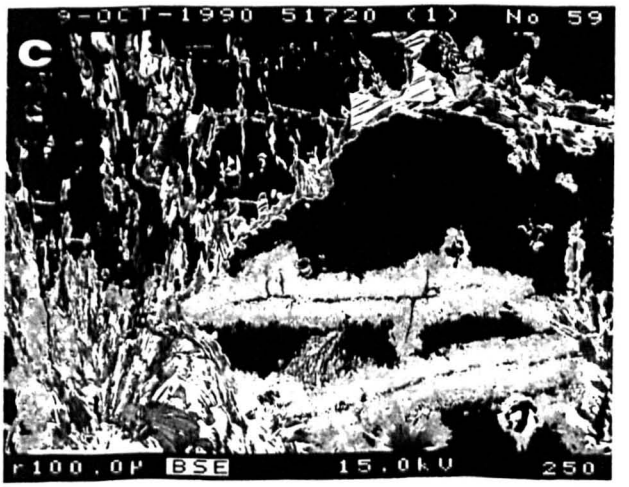
9-OCT-1990 51720 (1) No 59
C
r100.0P BSE 15.0kV 250

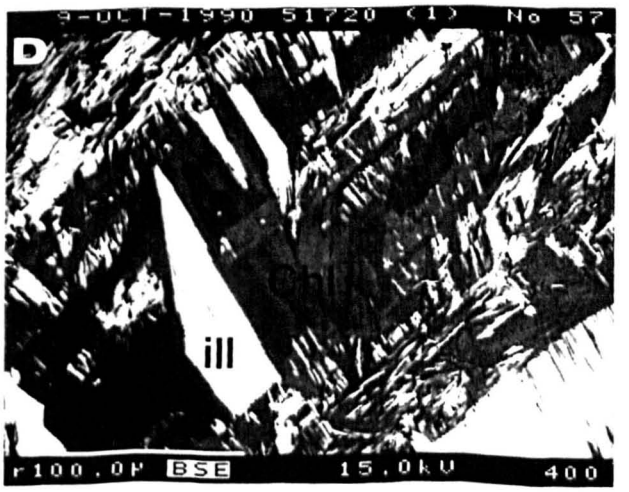
9-OCT-1990 51720 (1) No 57
D
ill
r100.0P BSE 15.0kV 400

Plate 5.2. BSE images of the sample LC159-6 from the alteration halo (facies C in the text) of La Nube lode (Santa Elena granodiorite-adamellite). A) New K-spar(II) and clays replacing old albite; B) new K-spar(II) filling voids and microfissures in old albite(I); C) detail of K-spar(II) microveins in albite(I).

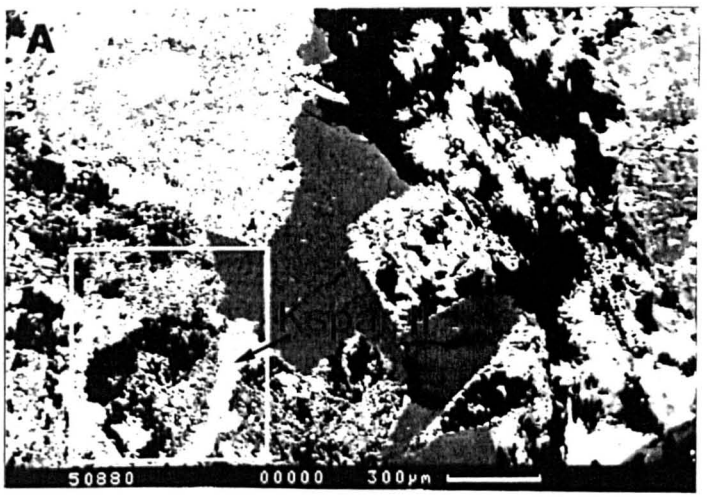
A
50880 00000 300µm

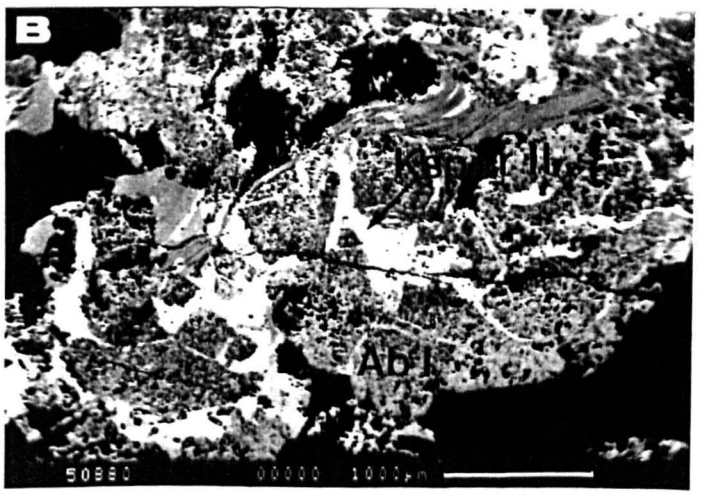
B
Ab I
50880 00000 1000µm

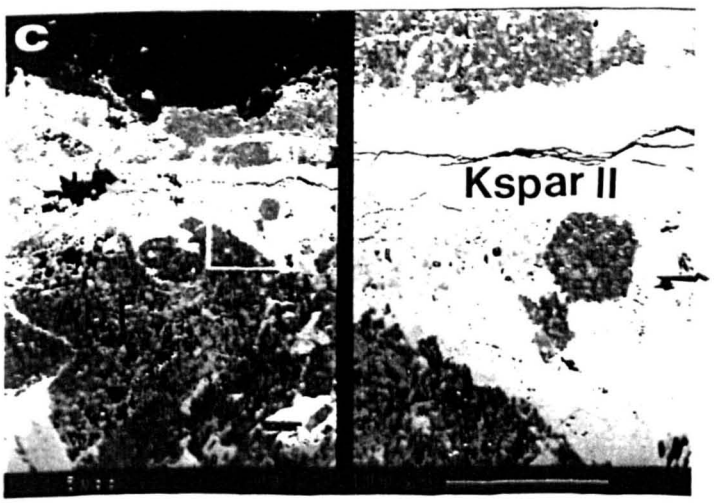
C
Kspar II

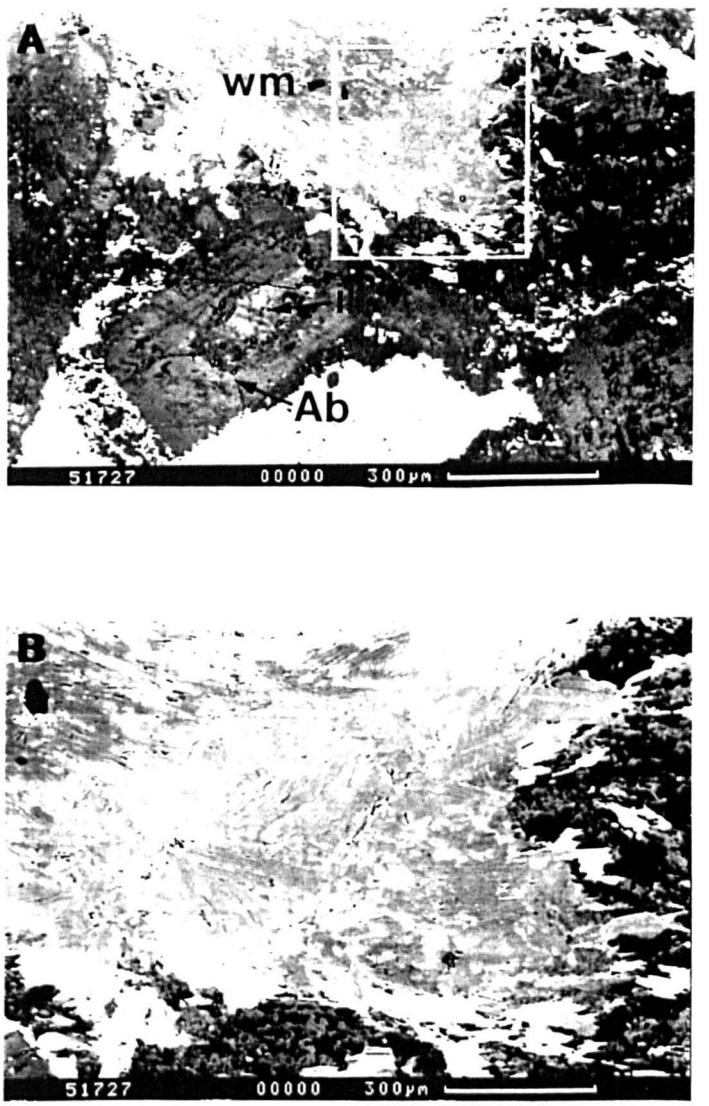

Plate 5.3. BSE images of the sample LC59-3 from the alteration halo (facies A in the text) of Ojo Vecino lode (Santa Elena granodiorite-adamellite). A) and B) white mica replacing albite.

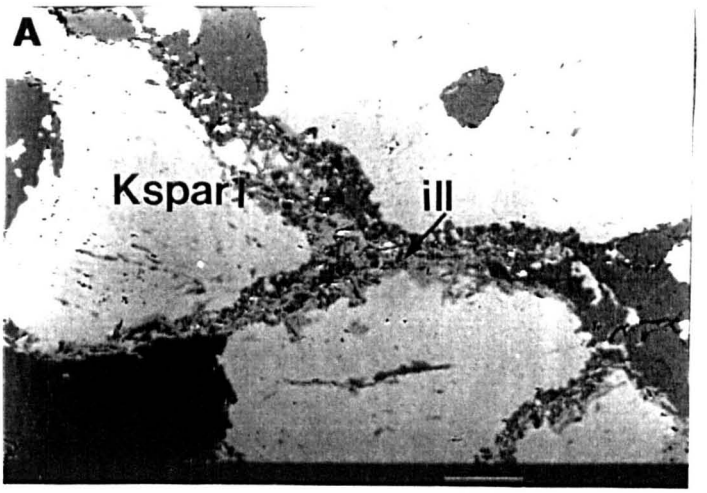

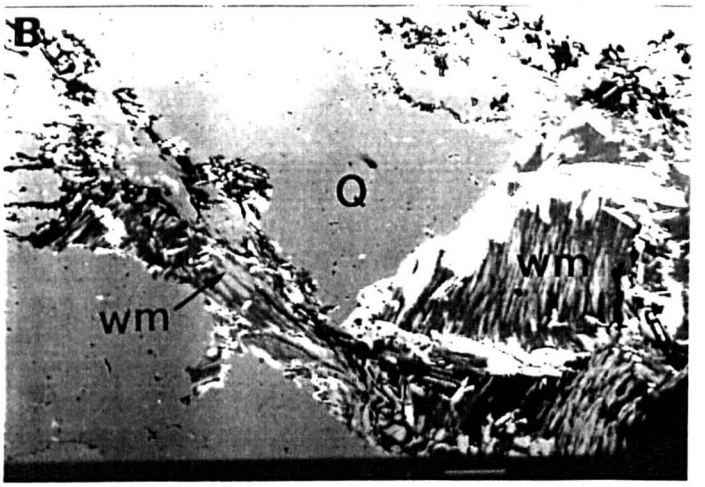

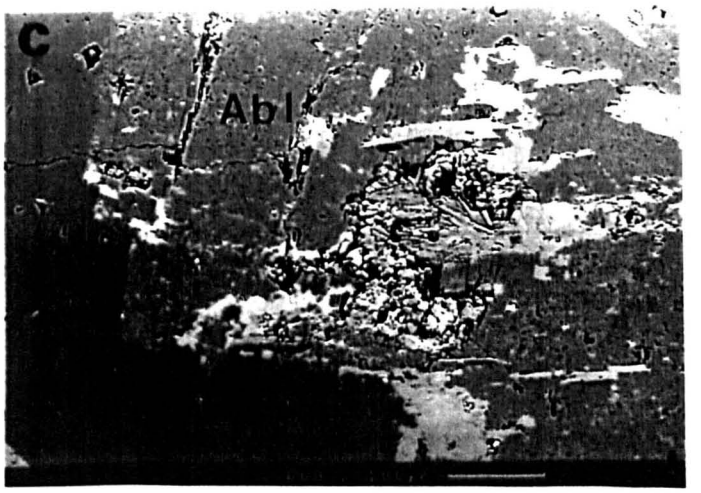

Plate 5.4. BSE images of the sample LC59-1 from the altered mylonite (Santa Elena granodiorite-adamellite). A) Late illite in rims of K-spar grains; B) lepidoblastic texture of white mica coexisting with undeformed grains of that mineral; C) kaolinite filling a void in albite.

-Replacement Textures:

c) Core replacement: they occur in feldspars (mainly in plagioclases) where illite is replacing the host mineral (Plate 5.3.A)

d) Rim replacement: Biotite rims are commonly replaced by chlorite and/or sericite/coarse white mica. Replacement of primary plagioclases by Na-rich albite or K-rich feldspar are ubiquitious. Less frequently, primary K-feldspars exhibit rim replacement by K-rich secundary feldspar. Primary plagioclases may be also replaced by white mica (Plates 5.3.A, Plate 5.1.A)

f) Isomorphic replacement: this is the extreme case when the primary mineral is altered completely to a single grain of a secundary mineral which retain the original grain shape. The mineralogies involved in this replacement are those observed in rim replacements (Plates 5.1.A)

-Overgrowths: Rim overgrowths of feldspars and quartz are ubiquitious, specially at proximal zones. Feldspar overgrowths are commonly associated with rim replacements of similar mineralogy, but coronas of secondary albite on K-feldspar or *viceversa* occur frequently (Plate 5.1.A).

-Intergrowth: They occur between secondary Na-rich albite and K-rich feldspar, both replacing primary feldspar. Intergrowths of white mica and chlorite appear when both minerals are replacing primary biotite. Intergrowths of sericite and kaolinite are common as filling of cavities in plagioclases.

The textural relations between different secondary phases are summarised in Fig.5.10.

5.3.3.2.Mineral chemistry.

-Chlorite.

Chlorite occurs as an alteration product commonly formed at the expense of primary biotite. Occasionally, chlorite is

	LC129-13	LC129-13	LC129-14	LC129-14	LC129-17	LC129-17	LC129-18	LC129-18	LC129-20	LC129-20	LC129-22	LC129-22
mts.	0.5	0.5	1	1	4	4	5	5	7	7	9	9
SiIV	2.662	2.674	2.667	2.664	2.659	2.630	2.647	2.595	2.728	2.770	2.732	2.729
AlIV	1.338	1.326	1.333	1.336	1.341	1.370	1.353	1.405	1.272	1.230	1.268	1.271
AlVI	1.514	1.557	1.495	1.460	1.490	1.477	1.548	1.472	1.329	1.240	1.321	1.358
Ti	0.004	0.0000	0.012	0.016	0.007	0.005	0.007	0.006	0.005	0.009	0.003	0.000
Fe	3.426	3.367	3.373	3.416	3.461	3.464	3.568	3.623	3.439	3.498	3.360	3.406
Mn	0.036	0.042	0.078	0.033	0.070	0.071	0.123	0.207	0.059	0.066	0.049	0.061
Mg	0.925	0.911	0.949	0.994	0.885	0.921	0.644	0.645	1.127	1.164	1.225	1.127
ΣVI	5.905	5.878	5.907	5.919	5.914	5.939	5.890	5.954	5.959	5.976	5.958	5.953
Vac	0.095	0.122	0.093	0.081	0.086	0.061	0.110	0.046	0.041	0.024	0.042	0.047
Ca	0.002	0.003	0.000	0.000	0.004	0.002	0.002	0.003	0.004	0.004	0.003	0.002
Na	0.000	0.004	0.000	0.000	0.000	0.000	0.006	0.004	0.002	0.012	0.011	0.002
K	0.002	0.002	0.000	0.005	0.001	0.001	0.001	0.002	0.005	0.001	0.007	0.001
ΣXII	0.004	0.009	0.000	0.005	0.005	0.003	0.009	0.009	0.011	0.017	0.021	0.005
Temp.II	368.7	365.1	367.4	368.2	369.7	379.1	373.6	390.4	347.8	334.3	346.2	347.4
Temp.I	301.5	299.1	300.6	301.2	302.2	308.3	304.7	315.8	287.7	278.8	286.7	287.5

Structural formulae calculated on the basis of 14 oxygens .

Geothermometer (^{o}C)

-Temp.I : Cathelineau and Nieva (1985)

-Temp. II: Cathelineau (1988)

Table 5.3. Compositional data of selected chlorites from El Cobre wall-rocks

A)	Si	AlVI	Ti	Fe	Mn	Mg
Si	1.000					
AlVI	-0.515	1.000				
Ti	-0.017	-0.096	1.000			
Fe	-0.533	-0.073	-0.069	1.000		
Mn	-0.424	0.156	-0.203	0.528	1.000	
Mg	0.702	-0.631	0.085	-0.692	-0.660	1.000

B)	Si	AlVI	Fe	Mg	Na	K	ΣXII
Si	1.000						
AlVI	-0.087	1.000					
Fe	-0.293	-0.842	1.000				
Mg	0.237	-0.971	0.824	1.000			
Na	-0.369	-0.575	0.783	0.508	1.000		
K	-0.452	0.578	-0.491	-0.650	-0.585	1.000	
XII	-0.861	0.209	0.066	-0.356	0.133	0.725	1.000

C)	Si	AlVI	Fe	Mg	Na	K	ΣXII
Si	1.000						
AlVI	-0.209	1.000					
Fe	-0.118	-0.912	1.000				
Mg	0.148	-0.881	0.726	1.000			
Na	-0.668	0.640	-0.427	-0.573	1.000		
K	0.053	-0.140	0.051	0.272	-0.124	1.000	
XII	-0.370	0.204	-0.149	-0.050	0.466	0.815	1.000

Table 5.4. Correlation of major chemical variables of chlorites (A), illites (B) and muscovite (C) from El Cobre wall-rocks.

D)	Si	AlVI	Fe	Mg	Na	K	ΣXII
Si	1.000						
AlVI	-0.711	1.000					
Fe	0.708	-0.930	1.000				
Mg	-0.759	-0.648	0.493	1.000			
Na	-0.463	0.247	-0.223	-0.502	1.000		
K	0.104	-0.657	0.475	0.185	-0.112	1.000	
XII	-0.033	-0.579	0.405	0.039	0.180	0.958	1.000

E)	Si	AlVI	Fe	Mg	Na	K	ΣXII
Si	1.000						
AlVI	0.249	1.000					
Fe	-0.510	-0.618	1.000				
Mg	0.243	-0.650	-0.181	1.000			
Na	-0.877	-0.518	0.509	0.090	1.000		
K	0.148	0.165	0.155	-0.228	-0.442	1.000	
XII	-0.621	-0.246	0.566	-0.168	0.414	0.632	1.000

F)	LC159-5	LC59-1(a)	LC59-1(b)	LC59-1(c)	LC59-1(d)	LC59-1(f)	LC59-1(g)
Muscovite	0.7131	0.7826	0.7859	0.7357	0.7298	0.7154	0.7269
Paragonite	0.0481	0.0497	0.0294	0.0521	0.0703	0.0646	0.0918
Ca-paragonite	0.0000	0.0066	0.0000	0.0000	0.0000	0.0000	0.0000
Fe-celadonite	0.0860	0.0783	0.1008	0.0835	0.1077	0.0933	0.1083
Mg-celadonite	0.0874	0.0479	0.0401	0.0485	0.0528	0.0497	0.0557
Pyrophyllite	0.0654	0.0349	0.0438	0.0802	0.0394	0.0770	0.0173
Temp. °C	290.9	303.2	299.6	285.0	301.4	286.3	210.2

Table 5.4.(cont.) Correlation of major chemical variables of illites (D) and muscovites (E) in altered samples from the granodiorite-adamellite of Santa Elena. The calculated molar fraction of end-members of illites is shown in F). Temperatures based on the calibration of Cathelineau (1988).

occupying cavities, intergrown with white mica. Chlorite is relatively abundant in all samples, except in a sample from 5 m, where it is only in traces.

The compositional data for chlorite are summarised in table 5.3 and displayed in Figs. 5.1.a and b. Only analyses with the sum of the interlayer cations (σXII) less than 0.1 have been considered because higher σXII values are likely caused by a contamination with white mica, feldspar or biotite (e.g.Lonker et al, 1990). All iron is considered to be divalent as a large number of chlorite analyses published in the literature show that the content of trivalent iron is generally less than 5 % of the total iron (e.g. Foster, 1962).

Table 5.4.a. presents the correlation matrix calculated for the complete set of analyses. The strongest correlations are between Si and Mg (0.702), Fe and Mg (-0.692), Mn and Mg (0.660), and octahedral Alv_1 and Mg (-0.631), which represents the exchange $FeMg_{-1}$ and the Tschermaks' susbtitution $Al^{IV}\ Al^{VI}\ Si^{IV}_{-1}\ Mg^{VI}_{-1}$. The positive correlation of Si and Mg and the negative correlation of Fe and Mg implies a positive correlation of the $Al^{IV}\ Al^{VI}\ Si^{IV}_{-1}\ Mg^{VI}_{-1}$ with $FeMg_{-1}$.

Silica increases toward the fresh rock, but the lowest values are found at 3-5 m (fig.5.1.a.). The silica in chlorites is independent of the original composition of the parent biotites (fig.5.3.b.).

The highest Mn-content is found at 5 m, which correlates positively with the Fe/(Fe/Mg) ratio.

The octahedral vacancy (Vac^{VI}) is almost constant in the profile, with a slight increase at the vicinity of the vein (fig.5.1.a.). Similarly, octahedral Al increases toward the vein.

At the first five meters some correlation seems to exist between grain abundance and the mineral chemistry (e.g. silica correlates negatively with chlorite abundance).

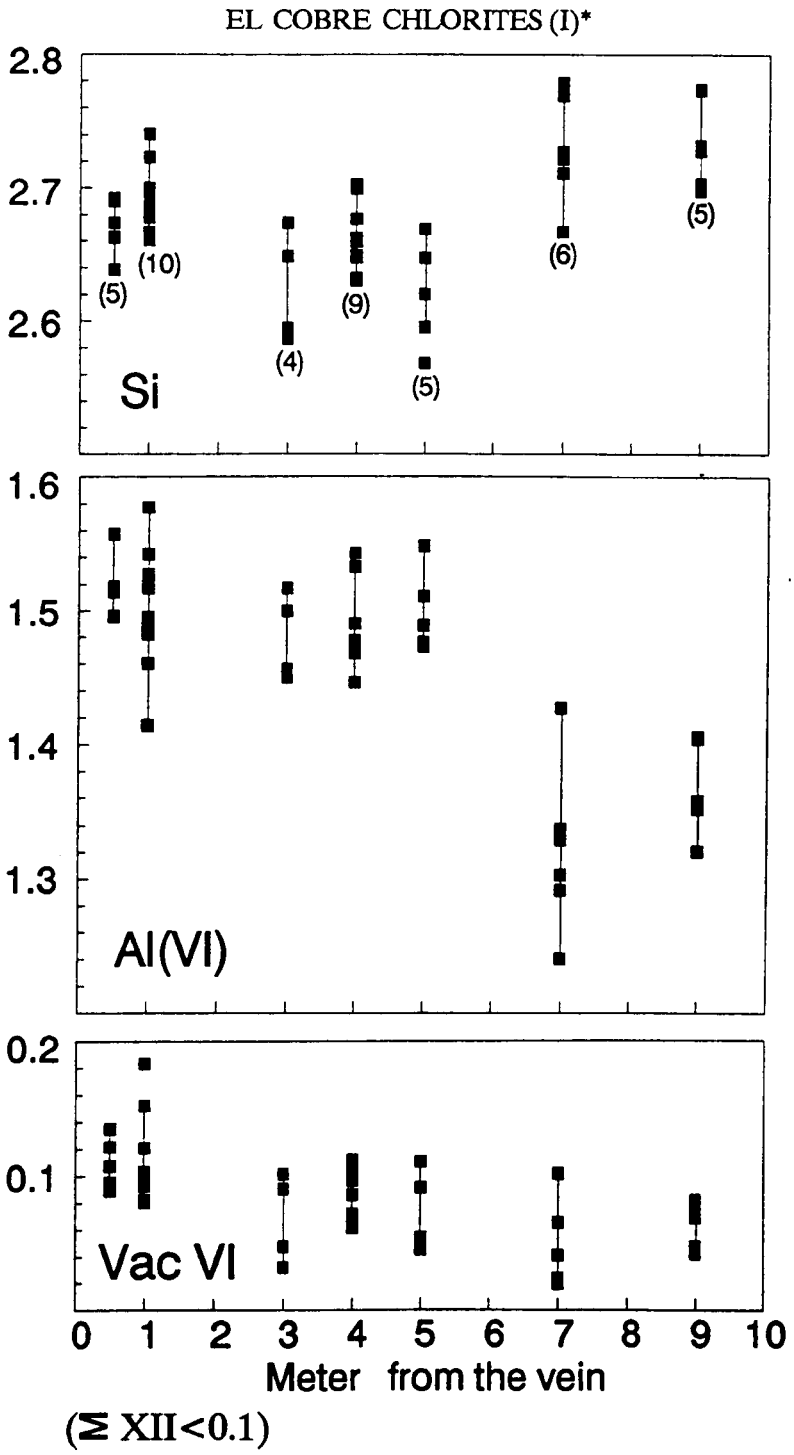

Fig. 5.1.a. Spatial variation of structural components of chlorites from El Cobre (number in brackets is number of analyses).

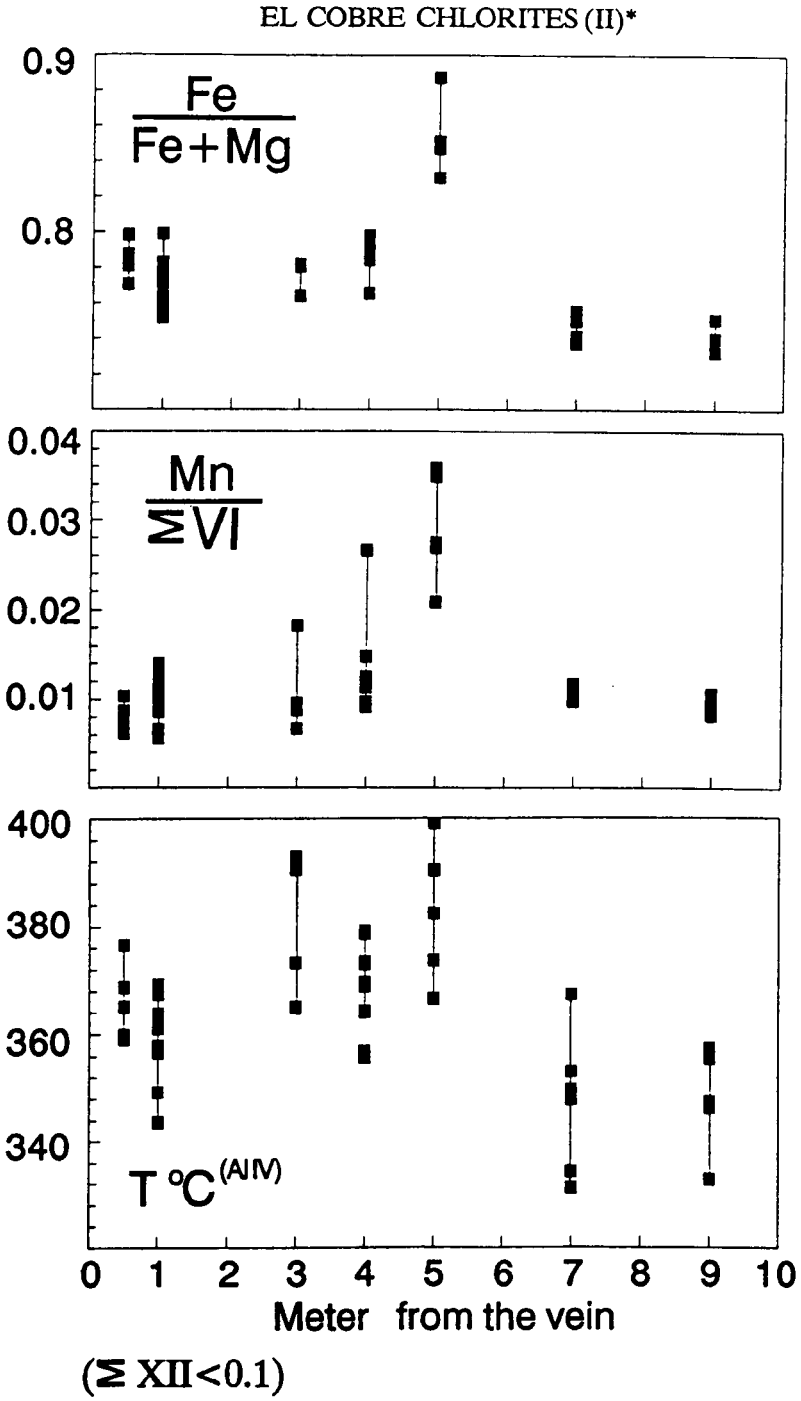

Fig. 5.1.b. Spatial variation of structural components of chlorites from El Cobre (number in brackets is number of analyses). Temperatures are based on the calibration proposed by Cathelineau (1988).

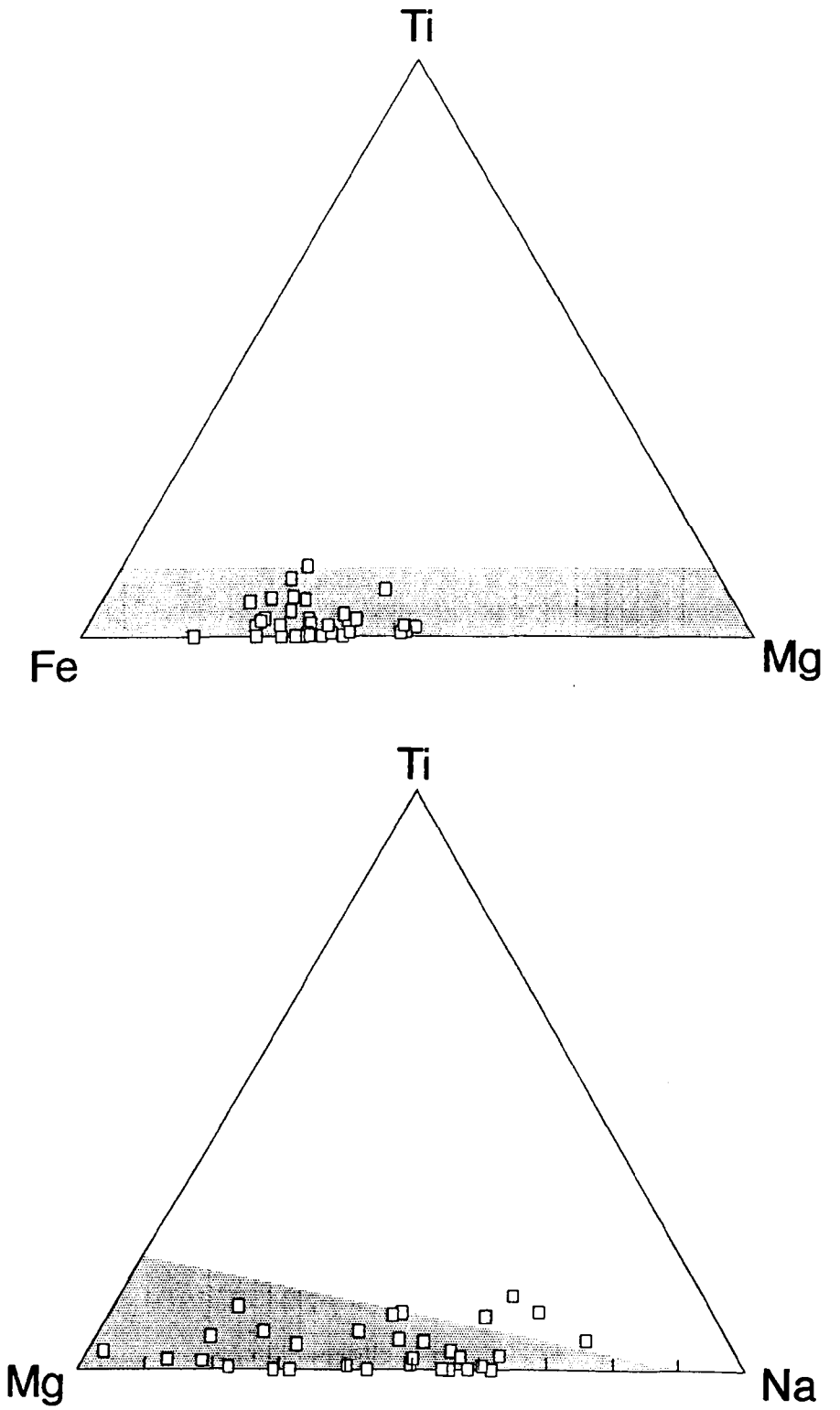

Fig. 5.2.a. Compositional discrimination of primary and secondary muscovites (dotted area) from El Cobre wall-rocks (after Miller et al., 1981 and Simon, 1990).

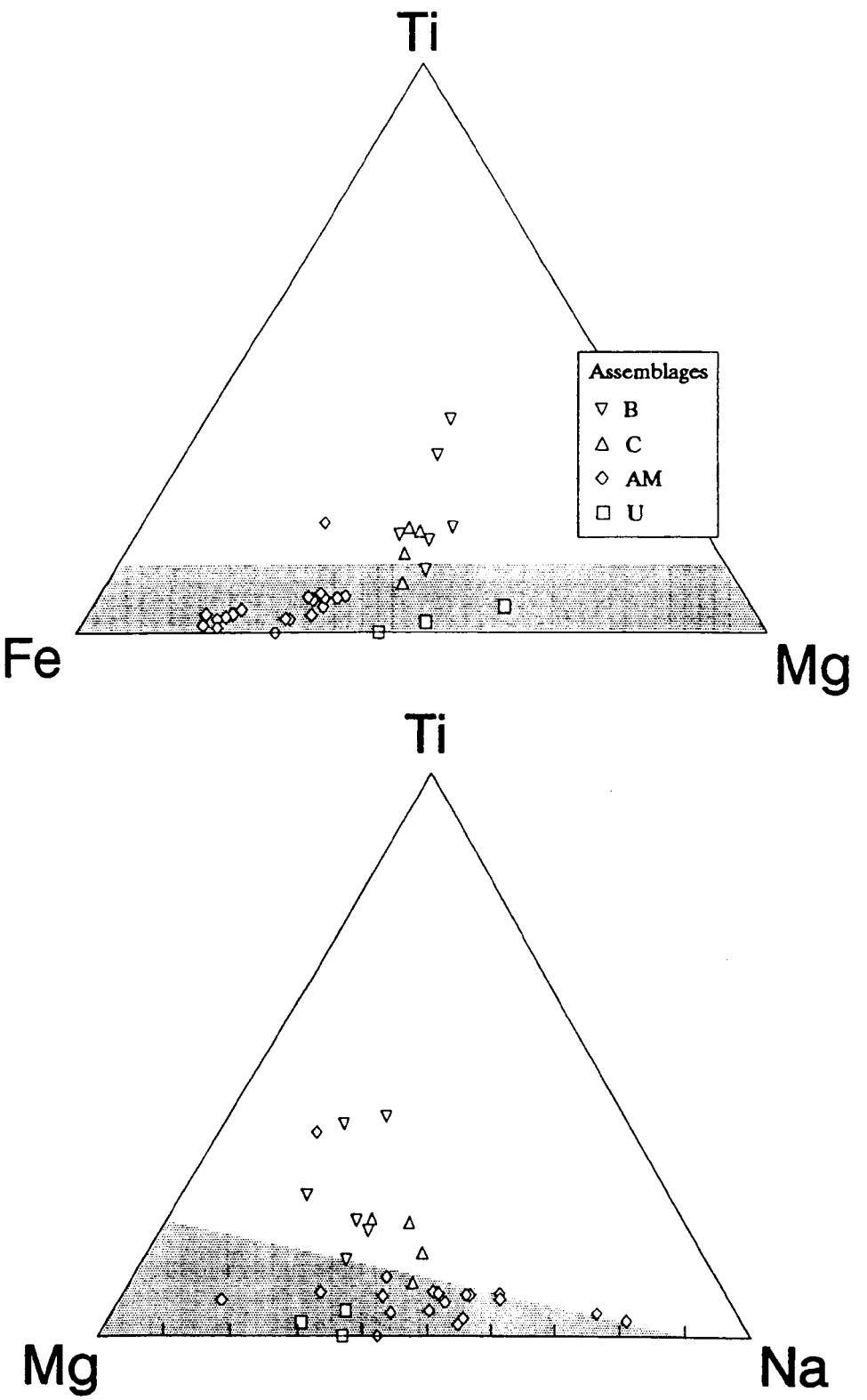

Fig. 5.2.b. Compositional discrimination of primary and secondary muscovites (dotted area) in altered samples from Santa Elena (after Miller et al., 1981 and Simon, 1990). A.M. corresponds to the altered mylonite, C represents strong phyllic-argillic alteration, B is relative to phyllic-argillic alteration, and U indicates unaltered or less altered samples.

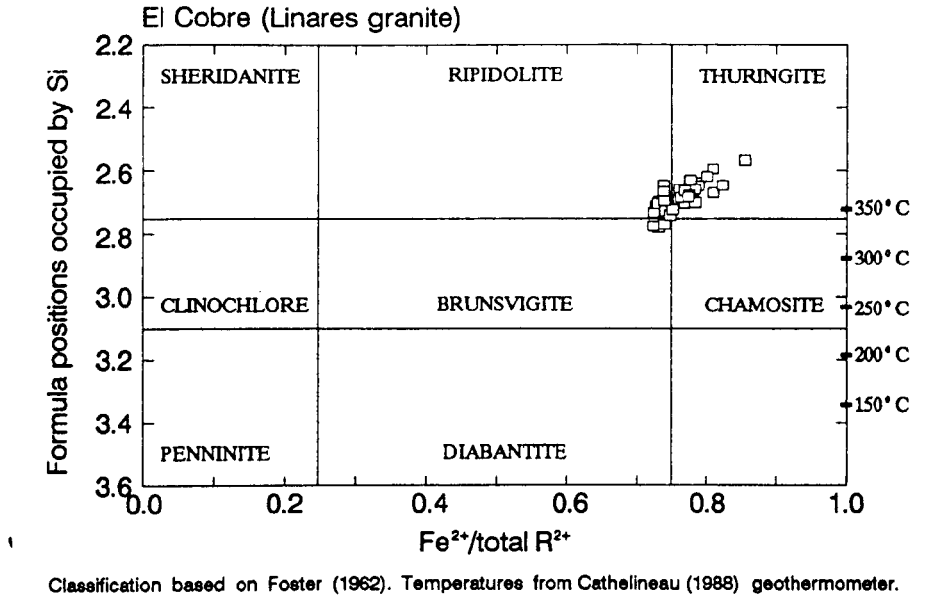

Fig. 5.3.a. Classification of chlorites from El Cobre wall-rocks based on Foster (1962).

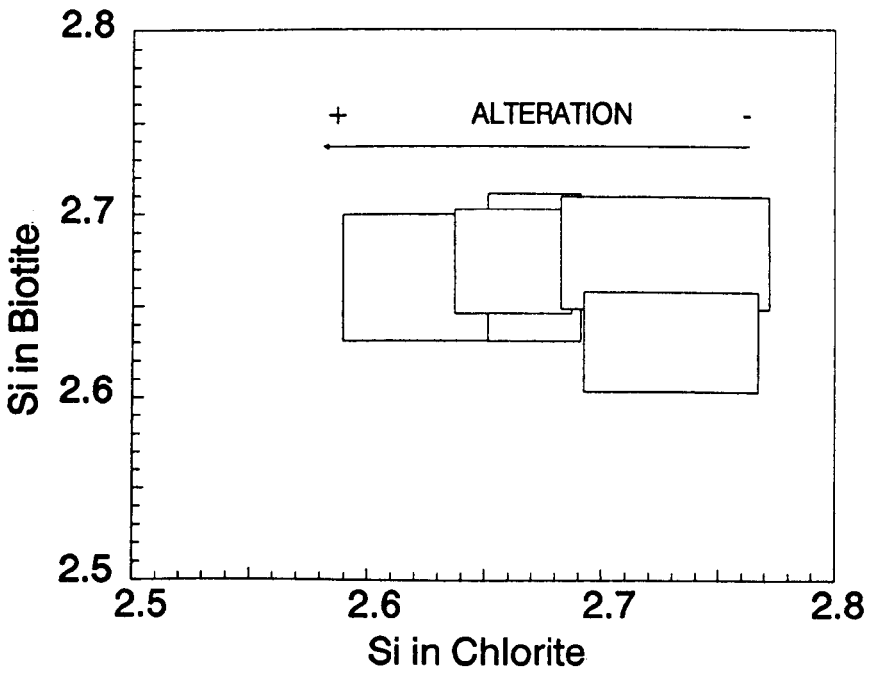

Fig. 5.3.b. Variation of Si-content of chlorite versus Si-content of primary biotite. Areas indicate the compositional range of different samples.

-White mica.

Secondary white mica grains were selected for EMP analysis on a textural basis. The composition of white mica from El Cobre alteration halo is consistent with its secondary origin, following the criteria suggested by Miller et al. (1981) and Simon (1990) (Fig.5.2.a. and b). Most analysed white mica grains from the La Nube yielded high Ti versus Mg, Fe and Na which could indicate a primary origin. There is textural evidence of the secondary origin of these grains, as they formed at the expense of biotite, and less frequently, of feldspars. Since a primary origin is rejected, the Ti-rich compositions are probably indicative of a contamination problem with the parent biotite. To avoid errors induced in the interpretation of the data, these analyses were not considered and they do not receive further consideration.

There are two modes of occurrence of secondary mica (Fig.5.4.a and b):

a) coarse "phengitic" muscovite, commonly filling vugs, intergrown with chlorite or replacing biotite and feldspar.

b) fine grained "illite", (texturally "sericite") frequently replacing feldspars or occupying dissolution carities, associated with kaolinite. "Illite" occurs less frequently replacing biotite.

Only analyses with σVI between 1.98 and 2.02 and $K \leq 1$ have been considered as true "illites" (Tables 5.5. and 5.6).

Table 5.4.b. shows the correlation matrix calculated for the complete set of illites from El Cobre wall-rocks (Table 5.5). The strongest correlations are between Si and Vac^{XII} (0.861), Al^{VI} and Mg (-0.971), Al^{VI} and Fe (-0.842), Fe and Mg (0.824), Fe and Na (0.783) and K and Vac^{XII} (-0.725).

There is no clear relationship between Si content and Fe/(Fe + Mg). Al^{VI} and Fe/(Fe + Mg) increase toward the vein. This positive correlation indicates that the Al^{VI} $(Mg + Fe)^{VI}_{-1}$ substitution is largely controlled by Mg (Fig.5.5.a. and b).

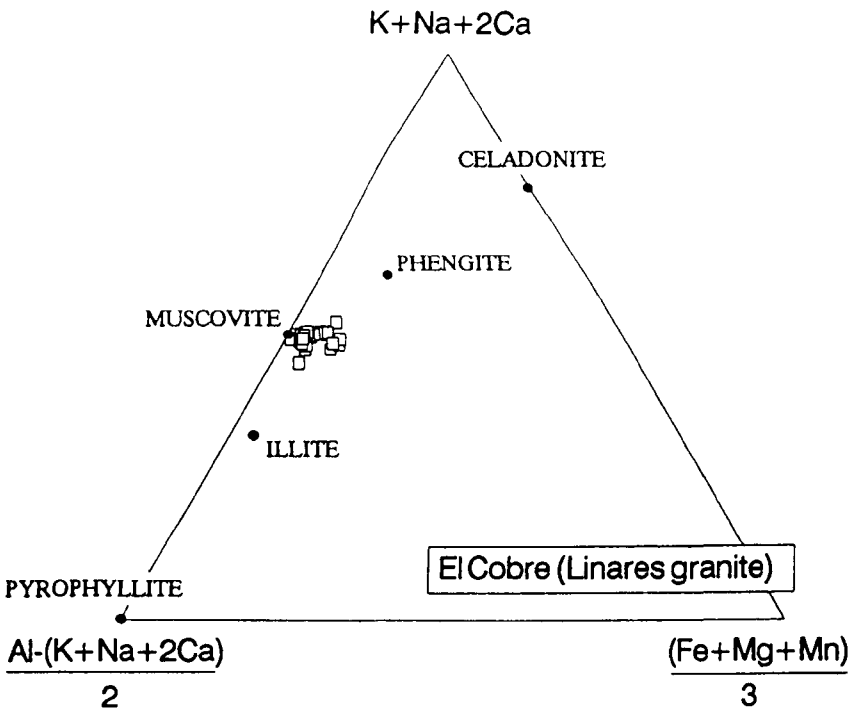

Fig. 5.4.a. Chemical composition of white micas in samples from El Cobre.

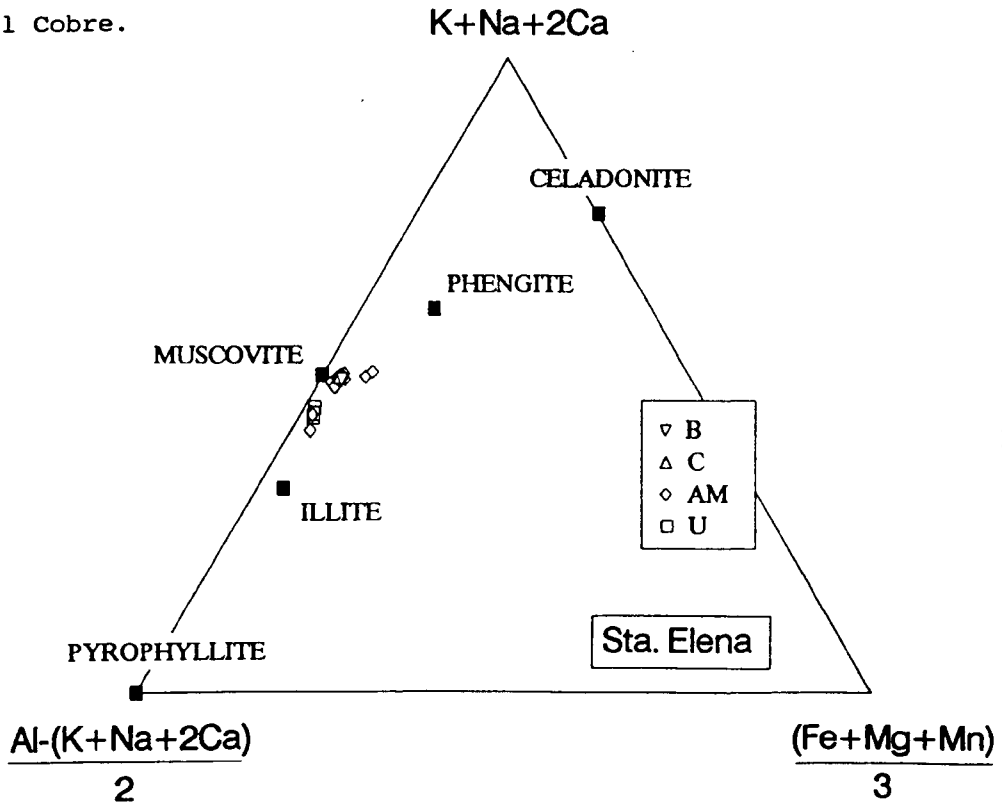

Fig.5.4.b. Chemical composition of white micas in samples from Santa Elena. A.M. corresponds to the altered mylonite, C represents strong phyllic-argillic alteration, B is relative to phyllic-argillic alteration, and U indicates unaltered or less altered samples.

	LC129-13	LC129-14	LC129-14	LC129-17	LC129-18	LC129-20	LC129-22
mts.	0.5	1	1	4	5	7	9
SiIV	3.051	3.090	3.059	3.057	3.024	3.065	3.129
AlIV	0.949	0.910	0.941	0.943	0.976	0.935	0.871
AlVI	1.920	1.960	1.909	1.873	1.902	1.830	1.851
Ti	0.006	0.001	0.003	0.000	0.016	0.014	0.001
Fe	0.052	0.026	0.074	0.090	0.077	0.088	0.072
Mn	0.000	0.001	0.000	0.000	0.000	0.000	0.003
Mg	0.023	0.013	0.038	0.058	0.035	0.072	0.068
ΣVI	2.001	2.001	2.024	2.021	2.030	2.004	1.995
Ca	0.000	0.001	0.000	0.000	0.000	0.000	0.003
Na	0.078	0.005	0.066	0.081	0.072	0.064	0.068
K	0.891	0.936	0.908	0.855	0.906	0.901	0.832
ΣXII	0.969	0.942	0.974	0.936	0.978	0.965	0.903
VacXII	0.031	0.058	0.026	0.064	0.021	0.035	0.097

Structural formulae calculated on the basis of 11 oxygens.

Table 5.5. Compositional data of illites from El Cobre wall-rocks

	ILLITE			MUSCOVITE			
	LC159-5	LC59-1	LC59-1	LC159-6	LC159-5	LC59-1	LC9098-5
Facies	B	A	A	C	B	A	A.M.
SiIV	3.076	3.061	3.040	3.089	3.092	3.056	3.059
AlIV	0.924	0.939	0.960	0.911	0.908	0.944	0.941
AlVI	1.825	1.873	1.855	1.872	1.826	1.884	1.854
Ti	0.021	0.008	0.009	0.014	0.064	0.006	0.006
Fe	0.086	0.084	0.093	0.076	0.067	0.083	0.158
Mn	0.000	0.004	0.005	0.000	0.001	0.010	0.000
Mg	0.088	0.048	0.050	0.067	0.076	0.044	0.041
ΣVI	2.020	2.017	2.012	2.029	2.034	2.027	2.059
Ca	0.000	0.000	0.002	0.000	0.000	0.000	0.000
Na	0.048	0.052	0.065	0.061	0.031	0.029	0.046
K	0.887	0.868	0.858	0.889	0.766	0.927	0.911
ΣXII	0.935	0.920	0.925	0.950	0.797	0.956	0.957
VacXII	0.065	0.080	0.075	0.050	0.203	0.044	0.043

Structural formulae calculated on the basis of 11 oxygens.

Table 5.6. Compositional data of selected illites and muscovites in altered samples from the granodiorite-adamellite of Santa Elena. A.M. corresponds to altered mylonite, C represents strong phyllic-argillic alteration, B is relative to phyllic-argillic alteration, and A is representative of weak propylitic alteration.

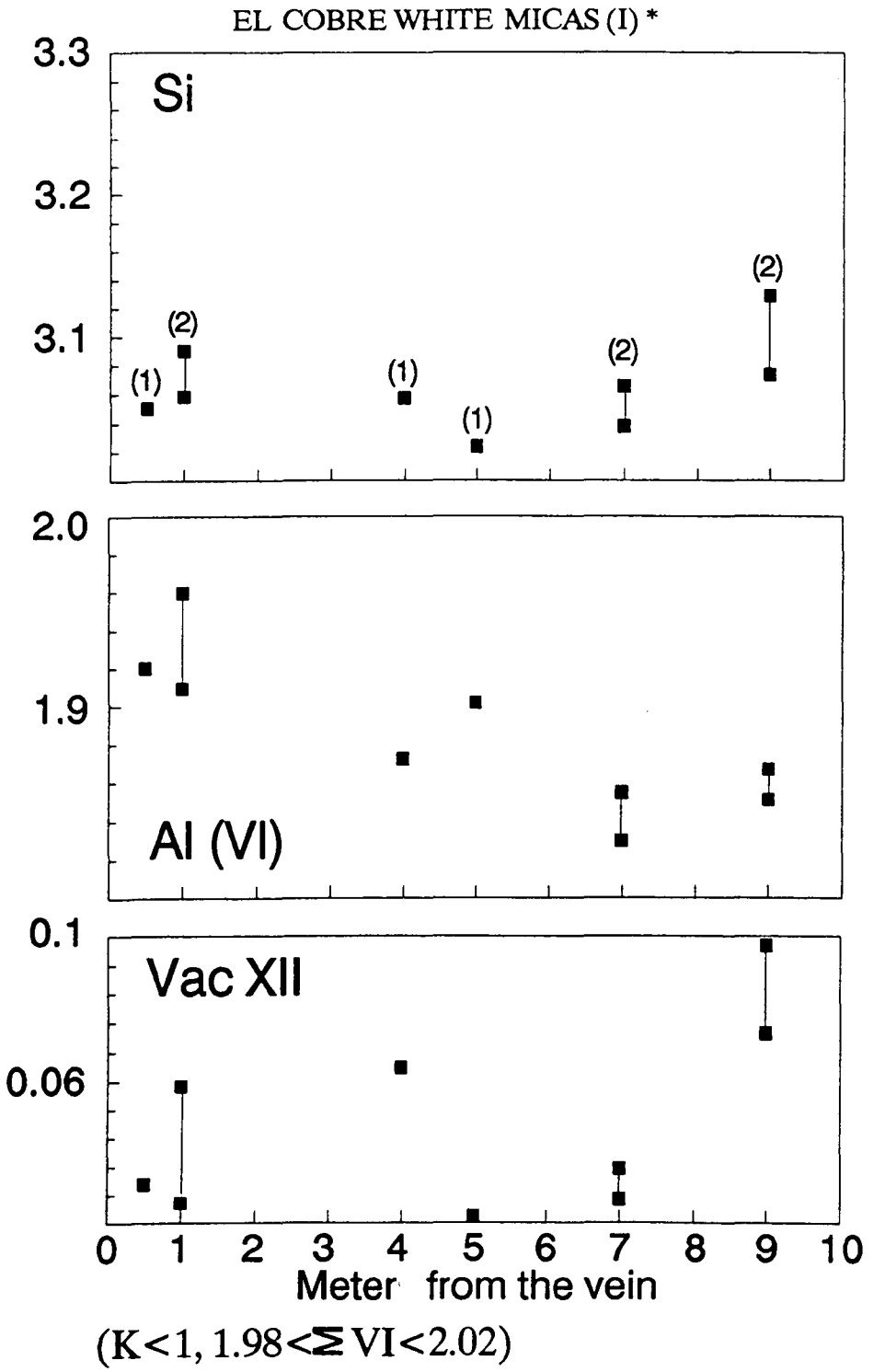

Fig. 5.5.a. Spatial variation of structural components of white micas ("illite") in samples from El Cobre (number in brackets is number of analyses).

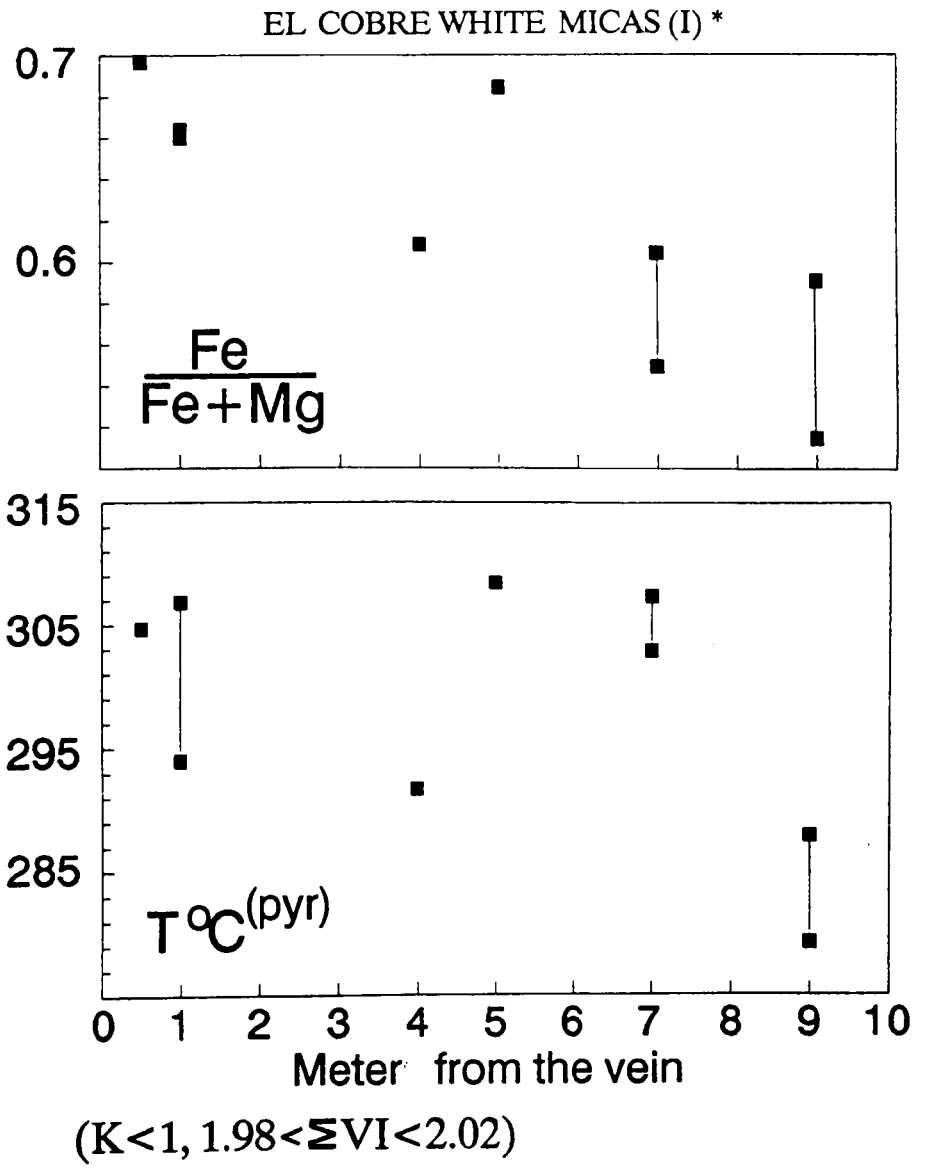

Fig. 5.5.b. Spatial variation of structural components of white micas ("illite") in samples from El Cobre.

Table 5.4.c. displays the correlation matrix calculated for the complete set of muscovites from El Cobre (Table 5.7.). The strongest correlations are between Al^{VI} and Fe (-0.912), Al^{VI} and Mg (-0.881), Fe and Mg (0.726), K and Vac^{XII} (-0.815) indicating similar exchanges than those for illites. However, Fe / (Fe + Mg) is negatively correlated with Al^{VI} (which increase toward the vein) suggesting that the Al^{VI} $(Mg + Fe)^{VI}_{-1}$ sustitution is mainly controlled by variations in Fe (Fig.5.6.b.).

As for chlorites, the highest Fe / (Fe + Mg) ratios are found in sample from 5 meter (Fig.5.6.b.).

Table 5.4.d. displays the correlation matrix calculated for the complete set of analysed illites from the Santa Elena altered rocks. Data are summarised in Table 5.6.

The strongest correlations are between Si and Na (-0.877), Al^{VI} and Mg (-0.650), Al^{VI} and Fe (0.618), Se and Vac ^{XII} (0.621) and K^{XII} and Vac^{XII} (-0.631). Fe and Mg are poorly correlated. These correlations may represents the exchanges K^{XII} Al^{IV} $(Vac + Na)^{XII}_{-1}$ Si^{IV}_{-1} and Al^{VI} $(Mg + Fe)^{VI}_{-1}$ Si^{IV}_{-1}. Despite the small number of analyses, Fe / $(Fe + Mg)^{-1}$ and Al^{VI} correlated positively, which indicates that the Al^{VI} $(Fe + Mg)^{VI}_{-1}$ substitution is largely controlled by Mg, as observed on samples from El Cobre (Fig.5.7.a. and b).

Table 5.4.c. displays the correlation matrix calculated for the complete set of analysed secondary muscovites from the Santa Elena altered rocks. The strongest correlations are between Al_{VI} and Fe (-0.930), K^{XII} and Vac^{XII} (-0.957), Si^{IV} and Al^{IV} and Mg^{VI} (0.758), Si^{IV} and Fe^{VI} (0.707) and Si^{IV} and Al^{VI} (-0.711). These correlations may represent the exchanges K^{XII} Al^{IV} $(Vac)^{XII}_{-1}$ Si^{IV}_{-1} and Al^{VI} Al^{IV} $(Mg + Fe)^{VI}$ Si^{IV}_{-1}. There appears to be no relationship between Al^{VI} and Fe/(Fe+Mg) (Fig.5.7.a. and b).

Muscovites from the altered mylonite of Santa Elena present the highest Si-content and Fe/Fe+Mg.

	LC129-14	LC129-17	LC129-18	LC129-20	LC129-22
mts.	1	4	5	7	9
SiIV	3.150	3.077	3.024	3.136	3.090
AlIV	0.850	0.923	0.976	0.864	0.910
AlVI	1.751	1.808	1.840	1.720	1.812
Ti	0.014	0.000	0.000	0.003	0.007
Fe	0.208	0.161	0.194	0.195	0.162
Mn	0.002	0.005	0.000	0.000	0.000
Mg	0.091	0.080	0.039	0.131	0.059
ΣVI	2.066	2.054	2.073	2.049	2.040
Ca	0.002	0.005	0.000	0.000	0.000
Na	0.024	0.061	0.064	0.019	0.042
K	0.914	0.898	0.922	0.920	0.838
ΣXII	0.940	0.964	0.986	0.940	0.880
VacXII	0.060	0.036	0.014	0.060	0.120

Structural formulae calculated on the basis of 11 oxygens.

Table 5.7. Compositional data of selected muscovites from El Cobre wall-rocks

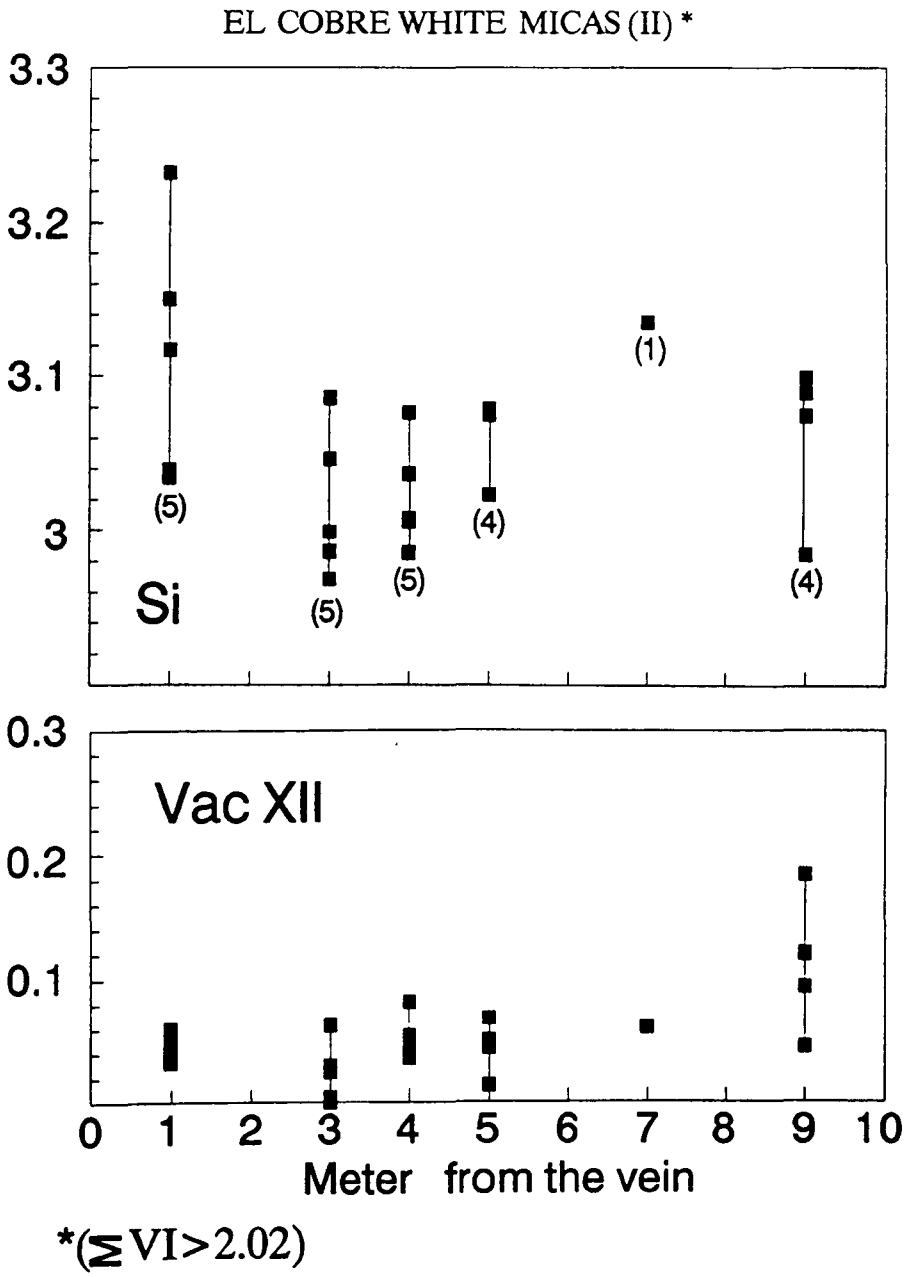

Fig. 5.6.a. Spatial variation of structural components of white micas ("muscovite") in samples from El Cobre (number in brackets is number of analyses).

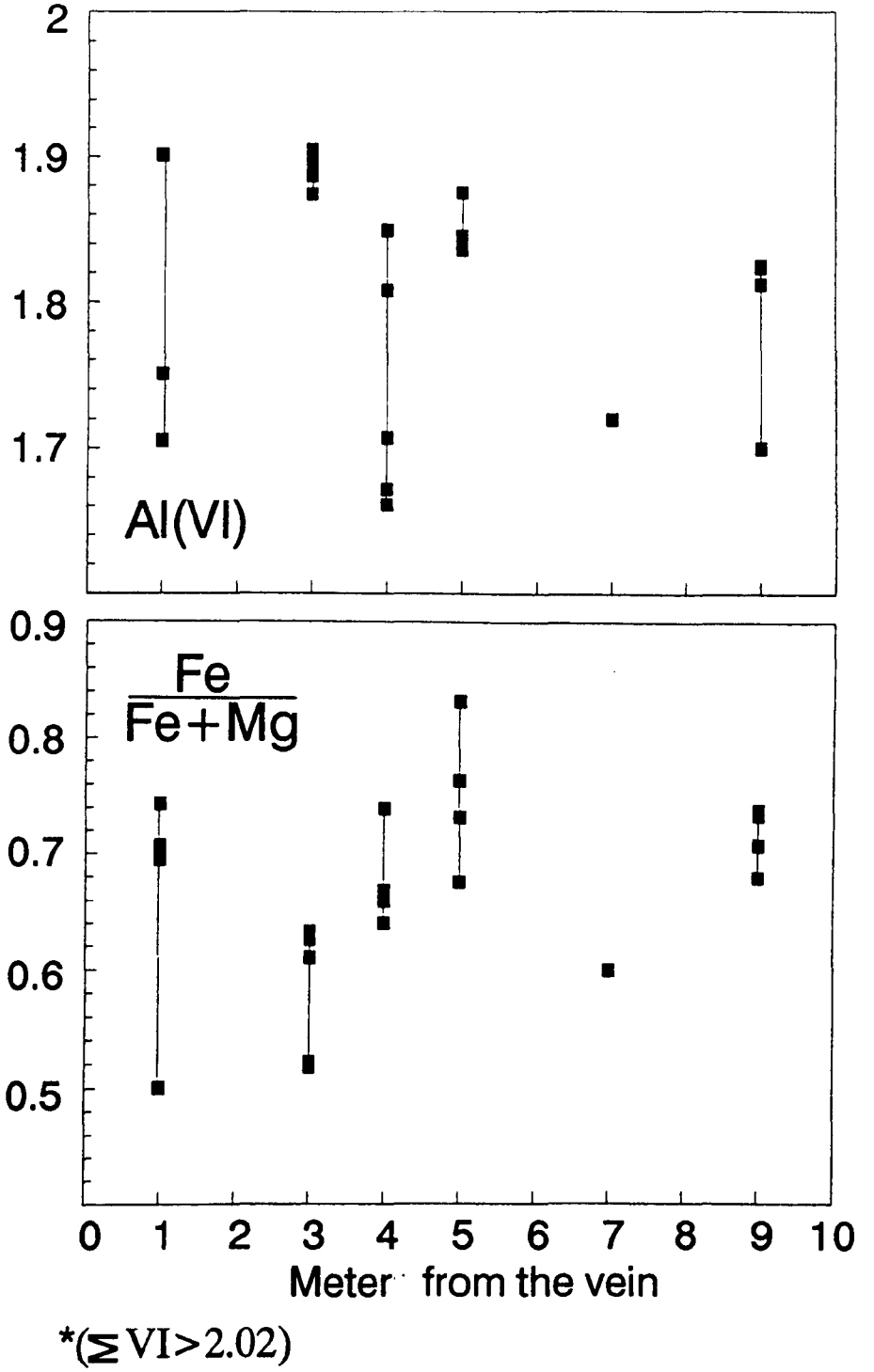

Fig. 5.6.b. Spatial variation of structural components of white micas ("muscovite") in samples from El Cobre.

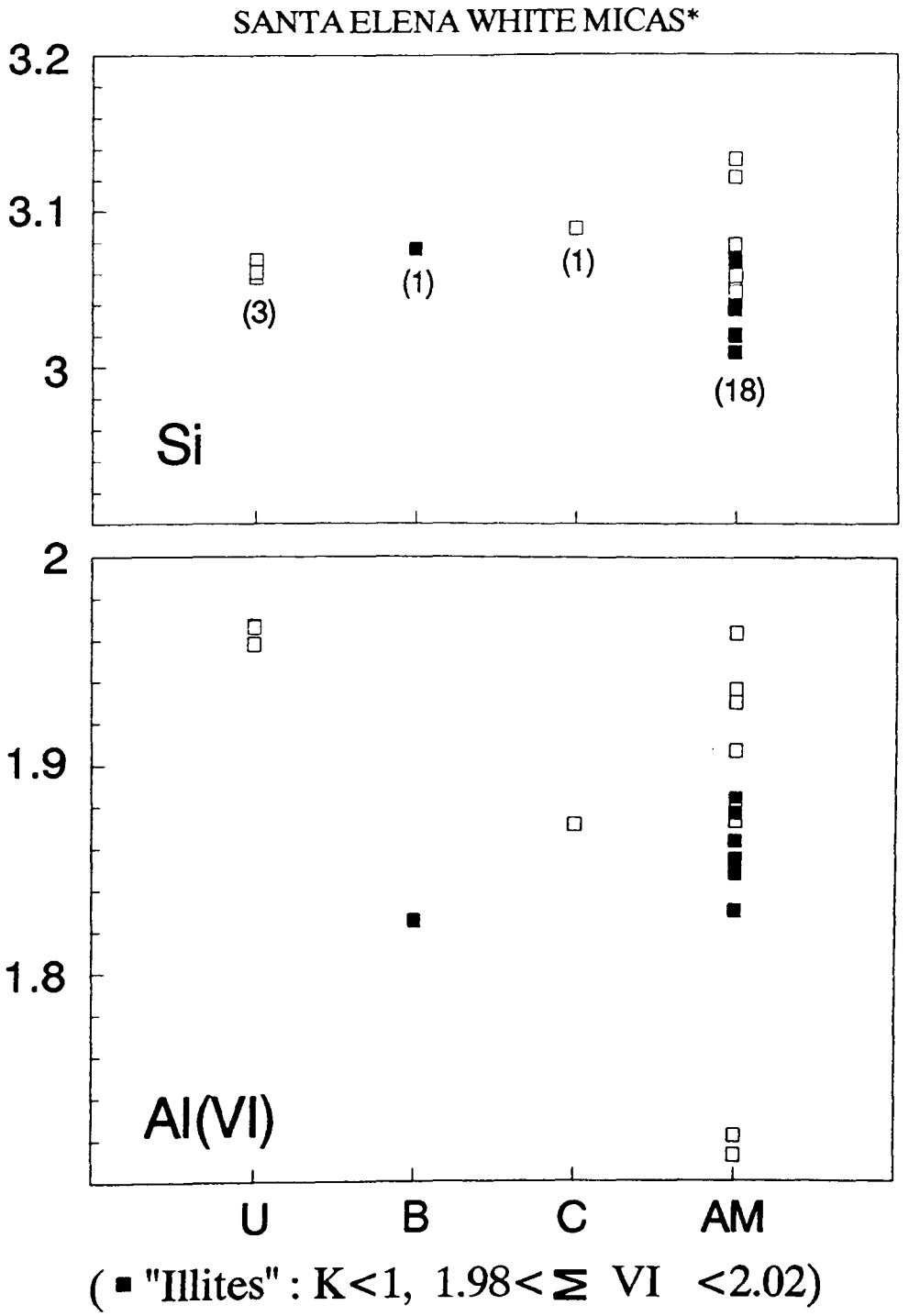

Fig. 5.7.a. Spatial variation of structural components of white micas ("muscovite" and "illite") in samples from Santa Elena (number in brackets is number of analyses). A.M. corresponds to the altered mylonite, C represents strong phyllic-argillic alteration, B is relative to phyllic-argillic alteration, and U indicates unaltered or less altered samples.

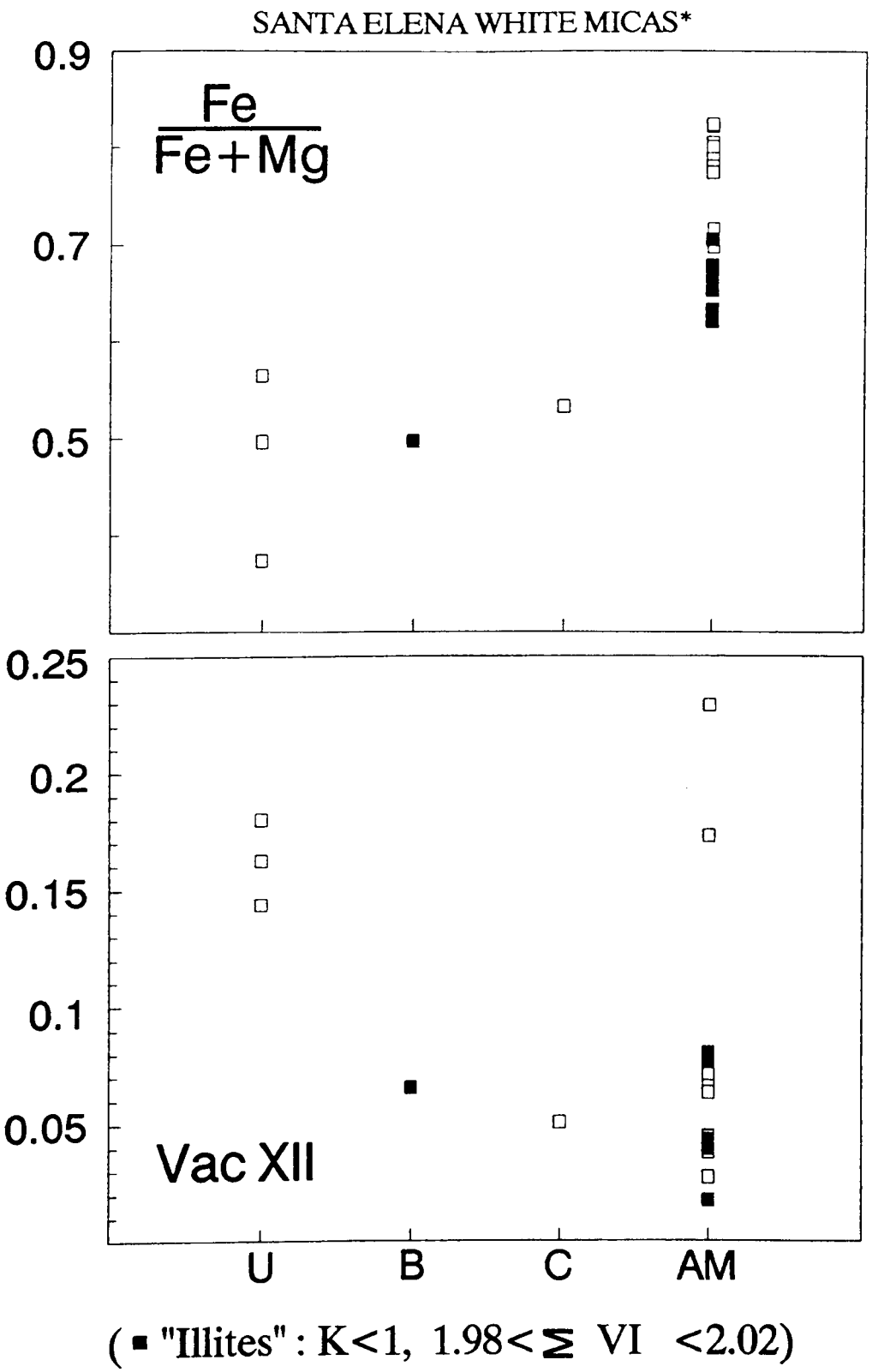

Fig. 5.7.b. Spatial variation of structural components of white micas ("muscovite" and "illite") in samples from Santa Elena. A.M. corresponds to the altered mylonite, C represents strong phyllic-argillic alteration, B is relative to phyllic-argillic alteration, and U indicates unaltered or less altered samples.

-Albite and K-feldspar.

Albite and K-feldspar occur mostly as replacement of primary plagioclase and overgrowths on primary K-feldspar and plagioclase, in common association with coarse white mica. K-feldspar also appears as microfracture fillings. Secondary K-feldspar grains are clear whereas secondary albite appears as "pitted" crystals.

The composition of secondary albite and K-feldspar ranges with no gaps from the primary compositions to pure compositions (X_i=0.999) (Fig.5.8.a., b; 5.9.a.,b).

The orthoclase (Or) content of coexisting albite and K-feldspar follow the prolongation of the feldspar solvus at low temperatures (Mc Dowell and Mc Curry, 1978).

5.3.4.Mineral Equilibrium.

Textural and chemical evidence can be used to establish if stable or metastable equilibrium has been attained between mineral phases. (e.g.Lonker et al., 1990, Hedenquist and Browne, 1989, etc.).

5.3.4.1.Textural Equilibrium.

Textural relations are summarised in fig.5.10. Textural equilibria between two secondary mineral phases have been assumed when:

a) Both phases present the same mode of occurrence (e.g.filling cavities) and they show mutual intergrowths (e.g. chlorite and white mica) (Plate 5.1.D.).

b) Both phases present the same mode of occurrence, discrete grains of both minerals are in contact and none shows crystallisation at the expense of the other one (e.g. Albite and K-feldspar) (Plate 5.1.A.).

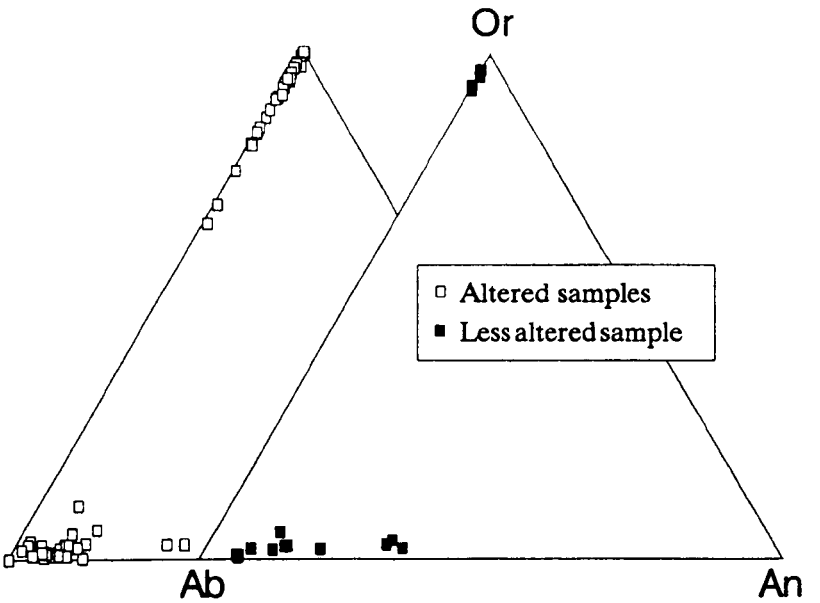

Fig. 5.8.a. Composition of feldspars in altered and unaltered samples from El Cobre.

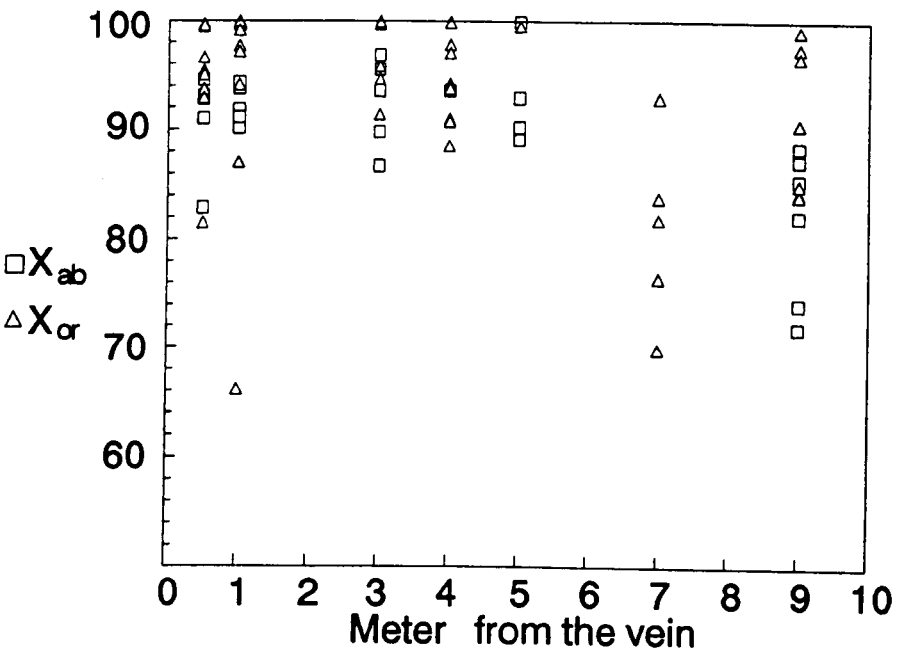

Fig. 5.8.b. Spatial variation of feldspars in altered samples from El Cobre.

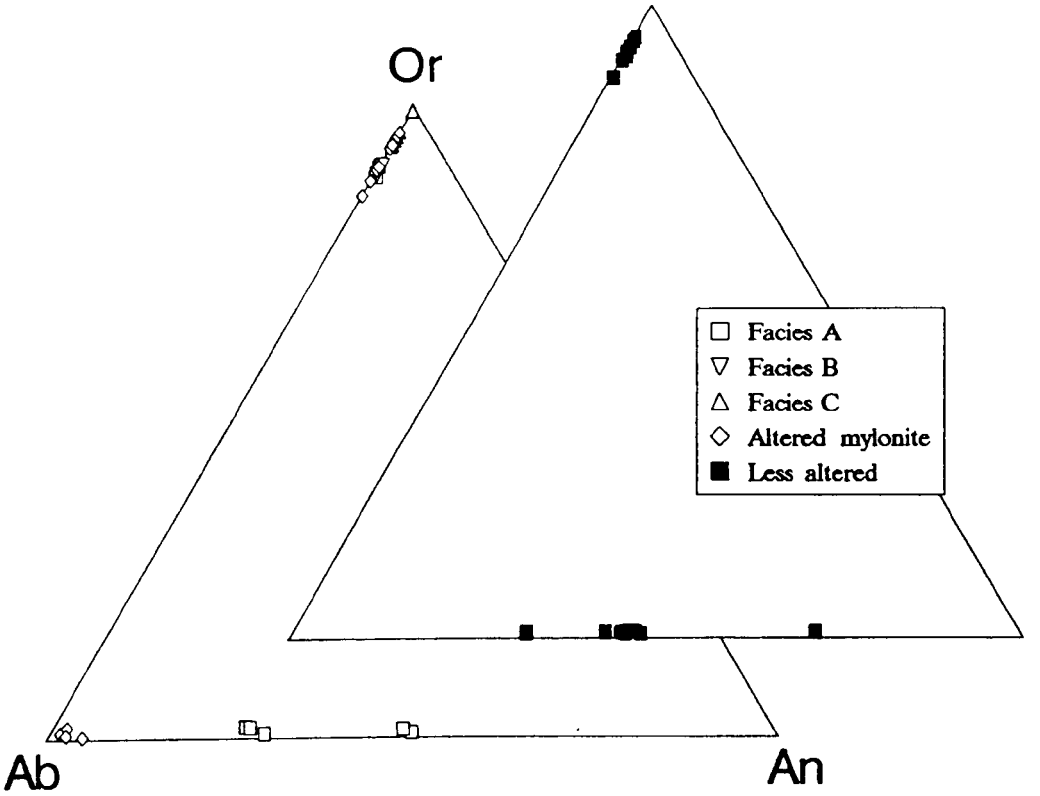

Fig. 5.9.a. Composition of feldspars in altered and unaltered samples from Santa Elena. C represents strong phyllic-argillic alteration, B is relative to phyllic-argillic alteration, and A is representative of weak propylitic alteration.

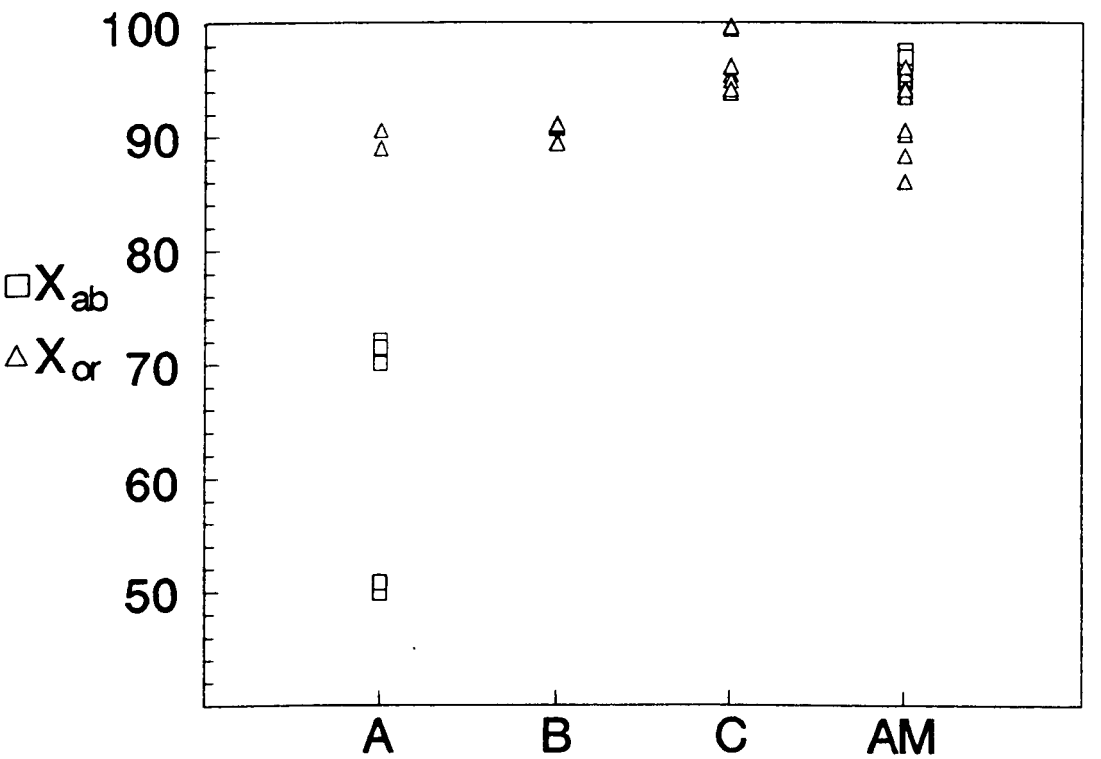

Fig. 5.9.b. Compositional variations of feldspars in altered samples from Santa Elena. A, B and C as in fig. 5.9.a. A.M. represents the altered mylonite.

Two equilibrium or near-equilibrium assemblages may be established:

a) Assemblage A: chlorite + sericite ("illite") + coarse white mica ("muscovite"?) + kaolinite.

b) Assemblage B: K-feldspar + albite + coarse white mica ("muscovite").

The assemblage B clearly postdates the assemblage A, but in sample LC59-1 (altered mylonite), coarse white mica is observed in textural disequilibrium with both assemblages.

5.3.4.2.Chemical Equilibrium.

Despite the compositional homogeneity it is difficult to assess in secondary phyllosilicates due to fine-scale intergrowths on the scale of an electron microprobe beam, the analysed chlorite, illite and muscovite seem compositionally homogeneous on the scale of a thin section, provided that the data are selected on the basis of the compositional restrictions noted above to avoid contamination from fine-grained mixtures.

Systematic element partitioning can be used to demonstrate chemical equilibrium of mineral pairs from analytical data. Fig. 5.11. shows the variation of K_DMg-Fe on the scale of a thin section at different distances from the El Cobre vein, where K_DMg-Fe (Chl-Ill) = Mg/Fe(Chl)/Mg/Fe (Ill).

The Fe-Mg distribution between chlorite and illite exhibits a fairly constant trend, suggesting that this mineral pair is in partition equilibrium in the alteration halo. The K_DMg-Fe(Chl-Mus) exhibits an irregular distribution, indicating that muscovite and illite are not in partition equilibrium, as expected since they are not in textural equilibrium.

Theoretically, the orthoclase content of coexisting (in equilibrium) albite and K-feldspar plotted onto the solvus curve for the system $NaAlSi_3O_8$-$KAlS_3O_8$ must indicate the same

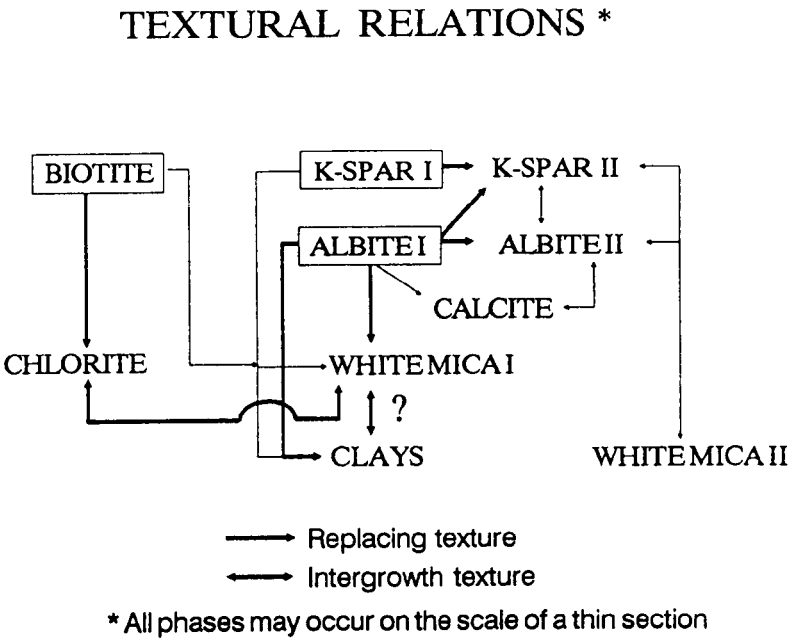

Fig. 5.10. Textural relations between primary and secondary minerals in the altered granitoids.

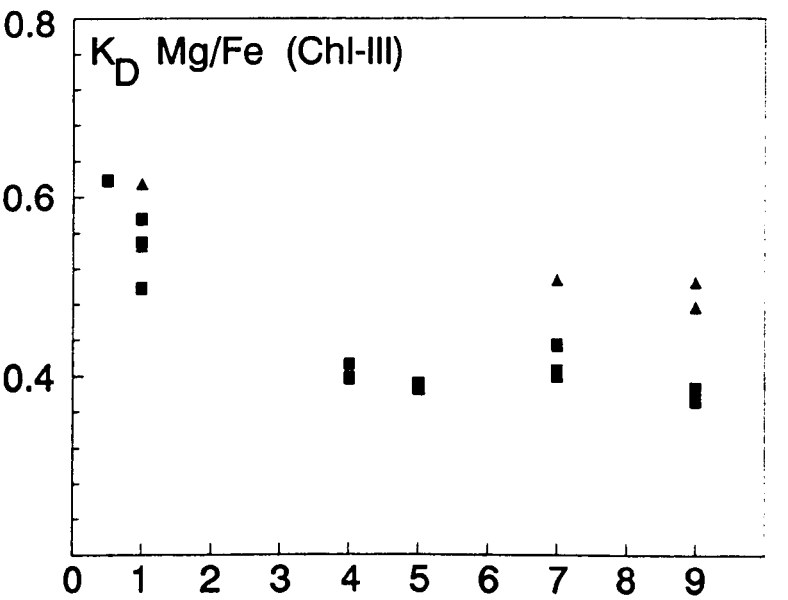

Fig. 5.11. Spatial variation of Mg/Fe partitioning in the pair chlorite-illite.

temperature of formation. Unfortunately, the branch for low Or-content is so steep at temperatures below 500°C that a given Xor (albite) may correspond to a wide range of temperatures (Figs. 5.12.a. and b).

5.3.5.Geothermometry.

5.3.5.1.Geothermometers based on micas.

Several geothermometers based on chlorites have been formulated (Walshe and Solomon, 1981; Walshe, 1986; Cathelineau and Nieva, 1985; Cathelineau, 1988). Walshe and Solomon (1981) developed a theoretical model based on several assumptions: the chlorite is a solid-solution of seven end-members. $\sigma V1 \times 6$ reflects the presence of Fe^{3+} whereas $\sigma V1 \leq 6$ indicates the $(R^{2+})_{+3}(Al_{-2} + Vac_{-1})^{VI}$ substitution.

Walshe (1986) established a revised model for the chlorite geothermometer based on that of Walshe and Solomon (1981). The model assumed that the ferric iron content, the water content and the vacancy of chlorites coexisting with quartz and an aqueous phase are buffered. Problems regarding the use of this geothermometer have been noted by Walshe (1986) (e.g. that exact solutions for proposed equation for iron-rich chlorites can not be obtained).

Cathelineau and Nieva (1985) and Cathelineau (1988) calibrated empirically the tetraedral Al content and the octahedral occupancy of hydrothermal chlorites with temperature but the strongest correlation is given by Al^{IV} which increases very regularly with temperature. The good regression coefficient ($r = 0.97$) argues in favour of its use as geothermometer.

Temperatures (table 5.3, fig. 5.1.b) have been calculated from Al^{IV} by using the following expressions:

$Al^{IV} = 4.71*10^{-3}T°C-8.26*10^{-2}$ (Cathelineau & Nieva, 1988)

$Al^{IV} = 3.105*10^{-3}T°C+0.19$ (Cathelineau, 1988)

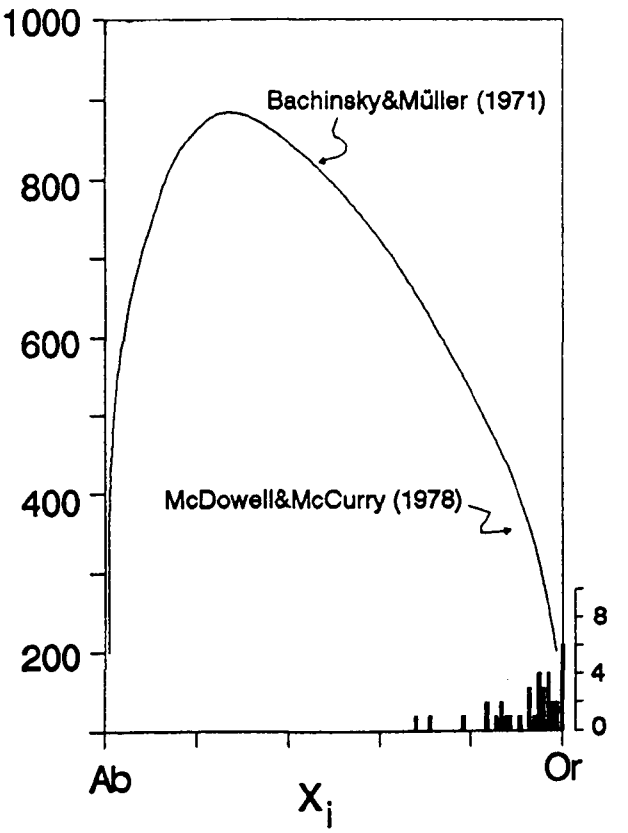

Fig. 5.12.a. Feldspar solvus and composition of feldspars in altered samples from El Cobre. Solvus curve is based on Bachinsky and Muller (1971) and McDowell and McCurry (1978).

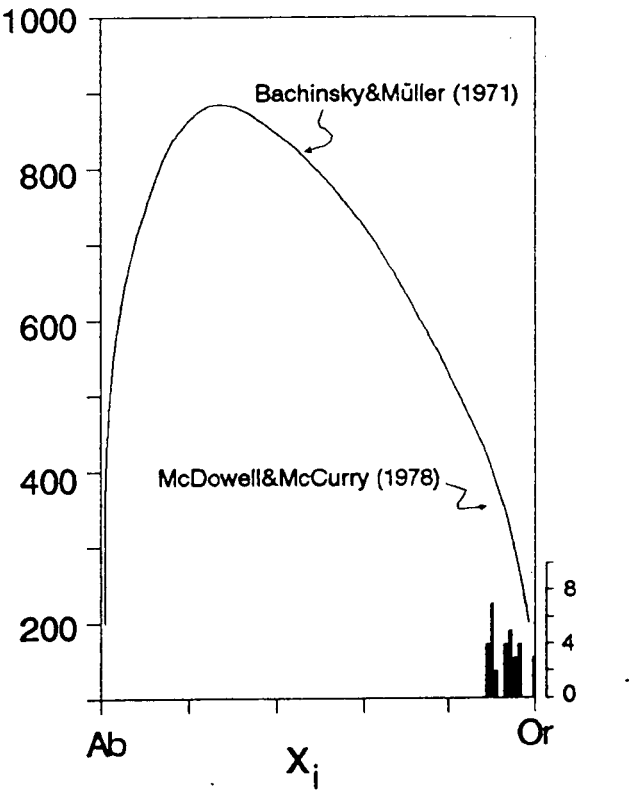

Fig. 5.12.b. Feldspar solvus and composition of feldspars in altered samples from Santa Elena. Solvus curve is based on Bachinsky and Muller (1971) and McDowell and McCurry (1978).

Hillier and Velde (1991) presented another linear expression estimated from diagenetic chlorites: Al^{IV}= $4.007*10^{-3}T°C+1.303546$, pointing out that the use of the chlorite geothermometer must be used with caution because the composition of chlorites is also dependent on bulk composition and kinetic factors.

The temperature estimated from the calibration proposed by Cathelineau and Nieva (1985) have been adopted as more probable temperatures, as the revised geothermometer of Cathelineau (1988) seems to give temperatures too high for high Al^{IV} contents. Moreover, the temperatures obtained in this study from the calibration of Cathelineau and Nieva (1985), ranging from 276.7° to 321.5°C (mean= 298.2°C, 1σ=9.96) are more consistent with the geothermometric estimations from illite.

Cathelineau (1988) established a illite geothermometer based on inter-site cation substitution and end-member molar fraction. Illite is considered a solid-solution of six theoretical end-member: muscovite, paragonite, Ca-paragonite, Fe-celadonite, Mg-celadonite and pyrophyllite.

The molar fraction of each member is calculated from the matrix,

$$(V) = M(X) = \begin{bmatrix} F(V_1) & F(V_2) \ldots, & F(V_n) \\ \alpha_{1,1} & \alpha_{1,2} \cdots, & \alpha_{1,n} \\ \ldots & & \ldots \\ \ldots & & \ldots \\ \alpha_{p,1} & \alpha_{p,2} \cdots, & \alpha_{p,n} \end{bmatrix} \cdot \begin{bmatrix} X1 \\ X2 \\ \cdot\cdot \\ \cdot\cdot \\ Xn \end{bmatrix}$$

of the relationships between the stoichiometric coefficients (α_i) of a chemical element in the structural formula, the molar fraction (X_i) of the different end-members, and the substitution vectors (FV_i) represented by the matrix of their coeficients ($\alpha_{p,n}$). The X_i are the unknowns and are calculated by solving this system of p equations with n unknows:

$$\begin{bmatrix} K \\ Na \\ Ca \\ Si \\ Al_{IV} \\ Al_{VI} \\ Fe \\ Mg \end{bmatrix} = \begin{bmatrix} F(V_m) & F(V_{pa}) & F(V_{cp}) & F(V_{fc}) & F(V_{mg}) & F(V_{py}) \\ 1 & -1 & -1 & 0 & 0 & -1 \\ 0 & 1 & 0 & 0 & 0 & 0 \\ 0 & 0 & 0.5 & 0 & 0 & 0 \\ 3 & 0 & 0 & 1 & 1 & 1 \\ 1 & 0 & 0 & -1 & -1 & -1 \\ 2 & 0 & 0 & -1 & -1 & -1 \\ 0 & 0 & 0 & 1 & 0 & 0 \\ 0 & 0 & 0 & 0 & 1 & 0 \end{bmatrix} \cdot \begin{bmatrix} X_m \\ X_{pa} \\ X_{cp} \\ X_{fc} \\ X_{mg} \\ X_{py} \end{bmatrix}$$

where $F(V_m)$, $F(V_{cp})$, $F(V_{fc})$, $F(V_{mg})$ and $F(V_{py})$ and X_m, X_{pa}, X_{fc}, X_{mg}, and X_{py} represented the sustitution vectors and the molar fractions for muscovite, paragonite, Ca-paragonite, Fe-celadonite, Mg-celadonite and pyrophyllite.

The best estimation is obtained from the pyrophyllite molar fraction which shows the strongest correlation with temperature (r= 0.82).

Estimated illite end-member molar fractions are presented in table 5.4.f. Spatial variation of the estimated temperature is shown in fig.5.5.b.

The estimated temperatures vary from 285° to 310.2°C (mean = 296.6°C, 1σ = 8.7).

5.3.5.2.Geothermometers based on feldspar.

Application of feldspar geothermometers, either based on semi-empirical approaches (e.g.Seck, 1971; Brown and Parsons, 1981) or thermodynamic mixing properties on feldspars (e.g.Stormer, 1975, Green and Usdansky, 1986) give unreliable results.

The experimental approach is limited because feldspar experiments to date have not been reversed and the total equilibrium have not been attained. The thermodynamically calibrated feldspar thermometers rely strongly on the state of order of the feldspar lattice and the mixing parameters, both factors being poorly known.

5.3.6.Whole rock geochemistry: Mass transfers.

Data on whole-rock geochemistry of hydrothermally altered rocks are presented in tables 5.8 and 5.9. Sample preparation and analytical techniques are described in Appendix I.

Calculation of the changes in chemical composition accompanying the hydrothermal alteration of host rocks requires that: a) the range of possible fresh-rock compositions (protoliths) is known, b) the altered sample analyses must be corrected for diluting effects of mineralisation or for the concentrating effects of net mass leaching.

In this study, the range of potential protoliths is well constrained from ten analyses of unaltered/less altered samples from the Linares and the Santa Elena granitoids.

The basic argument for calculations of metasomatic gains and losses is that some components are likely to have been immobile in the alteration processes (Gresens, 1967). If these elements can be identified, they can be used to correct the altered sample analyses for dilution or concentration effects. Commonly, the normalisation factor is the ratio of equivalent masses estimated from immobile element ratios before and after alteration (Grant, 1986).

Immobile elements are recognised by constant concentration ratios thoughout an alteration sequence or profile, despite the fact that the elements occur in different minerals (Gresens, 1967)

	LC129-13	LC129-14	LC129-15	LC129-16	LC129-17	LC129-18	LC129-19	LC129-20	LC129-21	LC129-22	LC129-23
mts.	0.50	1.00	2.00	3.00	4.00	5.00	6.00	7.00	8.00	9.00	10.00
SiO_2	76.03	73.19	73.71	75.44	76.66	76.07	76.75	72.73	71.08	71.43	71.50
TiO_2	0.18	0.14	0.23	0.11	0.12	0.05	0.09	0.24	0.26	0.27	0.25
Al_2O_3	12.94	13.53	14.40	13.57	12.73	13.52	12.87	15.09	14.63	14.93	14.99
Fe2O3*	1.71	1.25	1.43	1.04	1.46	0.80	1.20	2.47	2.41	2.51	2.35
MnO	0.03	0.05	0.02	0.03	0.04	0.03	0.03	0.05	0.04	0.05	0.04
MgO	0.32	0.26	0.26	0.23	0.22	0.13	0.21	0.56	0.48	0.59	0.61
CaO	0.33	1.19	0.25	0.55	0.56	0.44	0.41	1.47	1.45	1.27	1.26
Na_2O	1.98	1.76	1.56	1.92	2.64	3.07	2.80	3.15	3.06	2.83	3.12
K_2O	5.67	6.59	6.51	6.68	5.17	5.39	5.57	4.91	5.14	5.11	5.13
P_2O_5	0.12	0.12	0.16	0.13	0.15	0.18	0.12	0.14	0.15	0.17	0.16
L.o.I.	1.09	2.50	2.04	2.20	1.10	1.37	1.09	1.09	0.89	1.50	1.29
Total	100.41	100.59	100.56	101.90	100.84	101.05	101.15	101.52	99.59	100.66	100.69
Ni	3.00	2.00	3.00	3.00	2.00	1.00	2.00	4.00	2.00	2.00	4.00
Cu	1.00	3.00	2.00	2.00	2.00	6.00	3.00	5.00	4.00	3.00	4.00
Zn	28.00	21.00	20.00	17.00	30.00	17.00	19.00	52.00	52.00	48.00	55.00
Rb	218.00	212.00	197.00	226.00	238.00	271.00	230.00	200.00	188.00	199.00	195.00
Sr	20.00	31.00	32.00	28.00	23.00	18.00	21.00	95.00	89.00	83.00	88.00
Y	26.00	19.00	31.00	22.00	19.00	12.00	23.00	30.00	30.00	27.00	25.00
Zr	78.00	60.00	107.00	54.00	49.00	32.00	48.00	135.00	114.00	132.00	116.00
Nb	9.00	6.00	8.00	5.00	7.00	7.00	7.00	9.00	9.00	10.00	9.00
Ba	131.00	224.00	292.00	224.00	109.00	106.00	91.00	455.00	459.00	516.00	459.00
Pb	39.00	26.00	22.00	27.00	25.00	45.00	29.00	32.00	39.00	30.00	33.00
Th	11.00	10.00	12.00	10.00	10.00	7.00	10.00	16.00	14.00	15.00	15.00
U	8.00	8.00	5.00	7.00	8.00	10.00	9.00	8.00	6.00	7.00	8.00

Table 5.8. Whole-rock compositional data of altered samples from the El Cobre wall-rocks.

	LC59-3	LC159-5	LC159-6	LC9098-4
Facies	A	B	C	AM
SiO_2	62.87	66.24	68.78	76.04
TiO_2	0.91	0.64	0.85	0.03
Al_2O_3	17.19	18.12	18.53	15.74
Fe2O3	5.61	3.12	0.45	0.68
MnO	0.07	0.03	0.00	0.02
MgO	1.62	0.80	0.16	0.027
CaO	3.21	0.30	0.24	0.28
Na_2O	2.68	0.26	1.01	0.31
K_2O	4.34	6.87	6.85	6.38
P_2O_5	0.26	0.24	0.13	0.17
LoI	1.38	3.38	3.08	1.90
Total	100.14	100.00	100.07	101.82
Co	32.00	26.00	11.00	16.00
Ni	13.00	8.00	3.00	2.00
Cu	10.00	6.00	5.00	33.00
Zn	72.00	104.00	99.00	19.00
Rb	160.00	272.00	207.00	257.00
Sr	263.00	49.00	124.00	13.00
Y	31.00	28.00	47.00	12.00
Zr	243.00	202.00	245.00	28.00
Nb	14.00	19.00	23.00	8.00
Ba	805.00	834.00	456.00	159.00
Pb	29.00	296.00	744.00	15.00
Th	17.00	15.00	17.00	8.00
U	6.00	5.00	6.00	7.00

Table 5.9. Whole-rock compositional data of altered samples from the Santa Elena granodiorite-adamellite. A.M. corresponds to the altered mylonite, C represents strong phyllic-argillic alteration, B is relative to phyllic-argillic alteration and, A is representative of weak propylitic alteration.

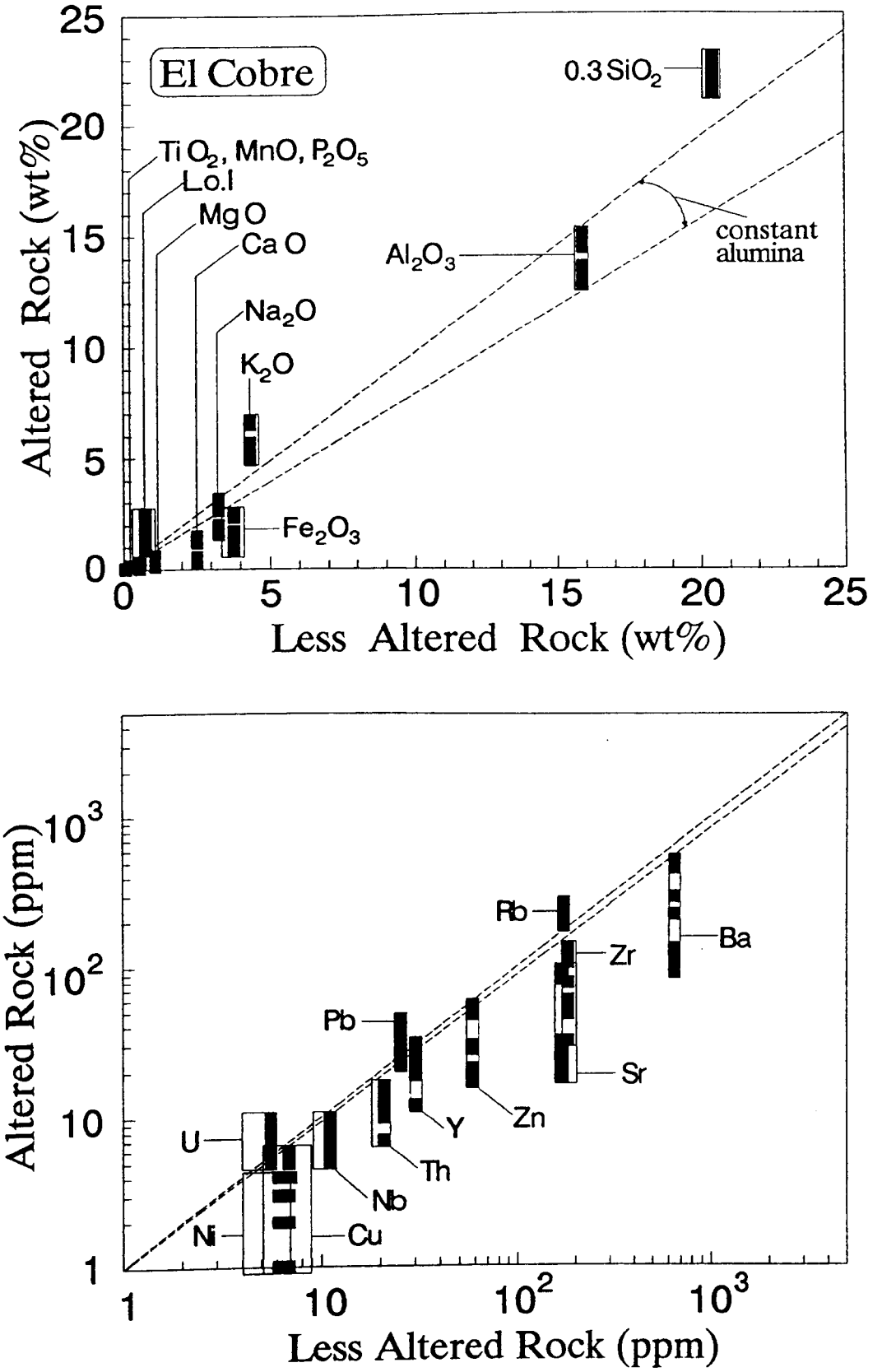

Fig. 5.13. Mass transfers in El Cobre wall-rocks. Isocon line for alumina is drawn for reference (based on Grant, 1986). Areas represent the compositional range for the analysed samples (altered and unaltered).

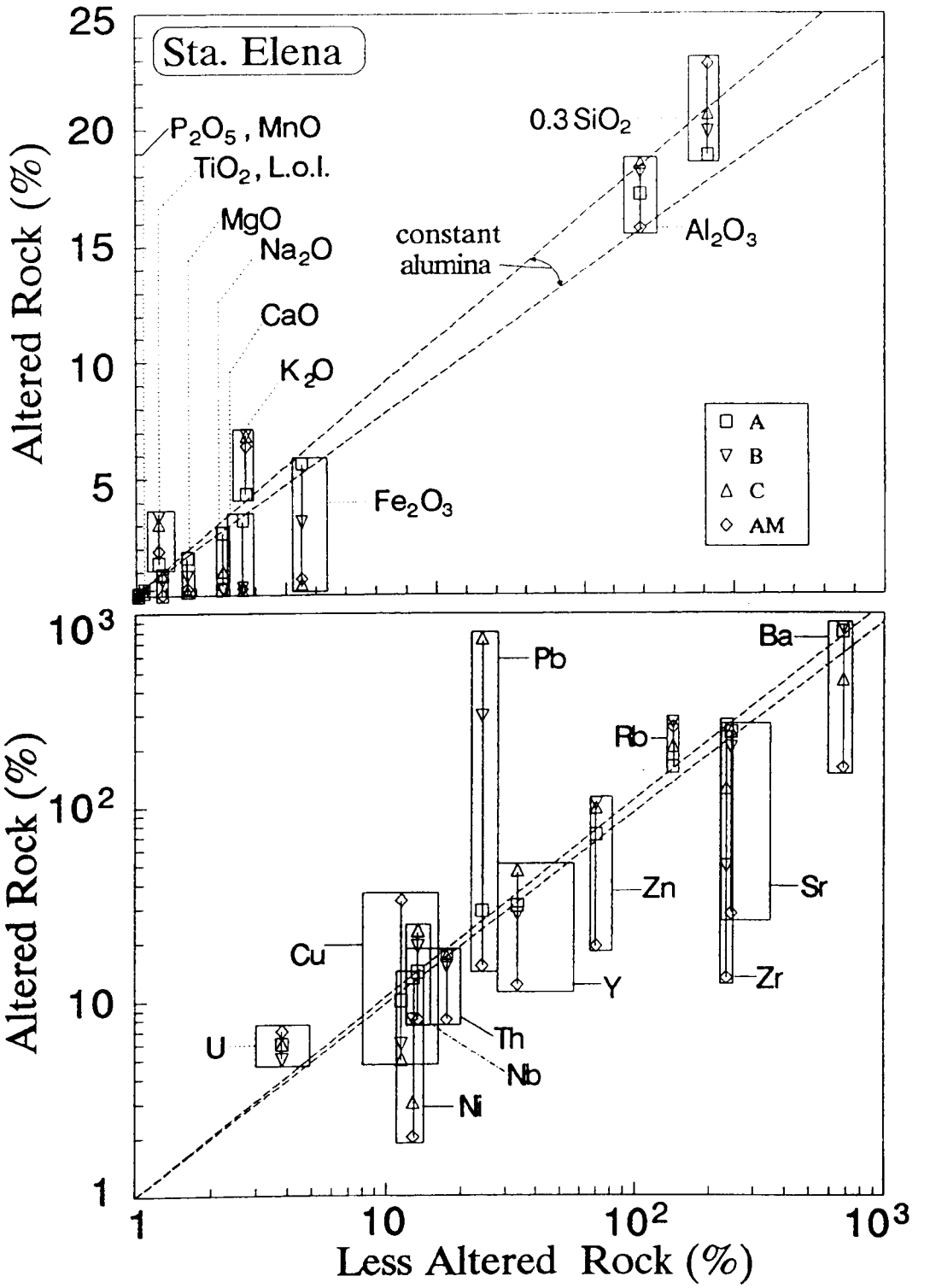

Fig. 5.14. Mass transfers in the granodiorite-adamellite of Santa Elena. Isocon line for alumina is drawn for reference (based on Grant, 1986). Areas represent the compositional range for the analysed samples (altered and unaltered). A.M. corresponds to the altered mylonite, C represents strong phyllic-argillic alteration, B is relative to phyllic-argillic alteration, and A is representative of weak propylitic alteration.

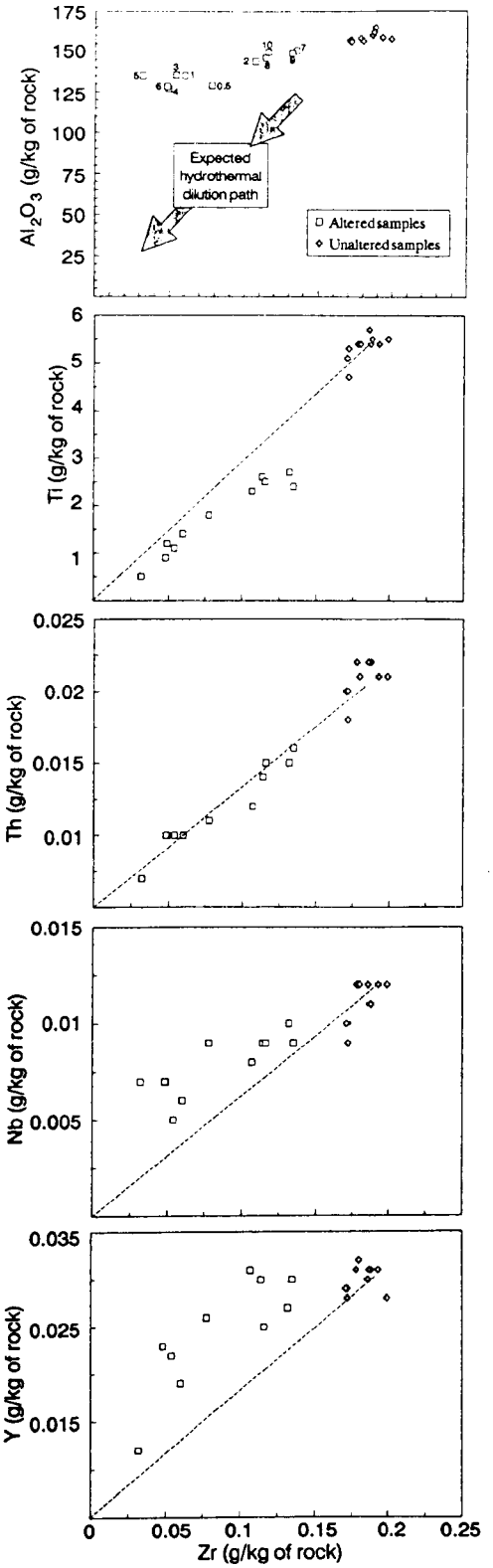

Fig. 5.15. Test for immobile elements in altered samples from El Cobre. Lines represent the expected path caused by hydrothermal dilution. Number in points indicates distance (m) from the vein.

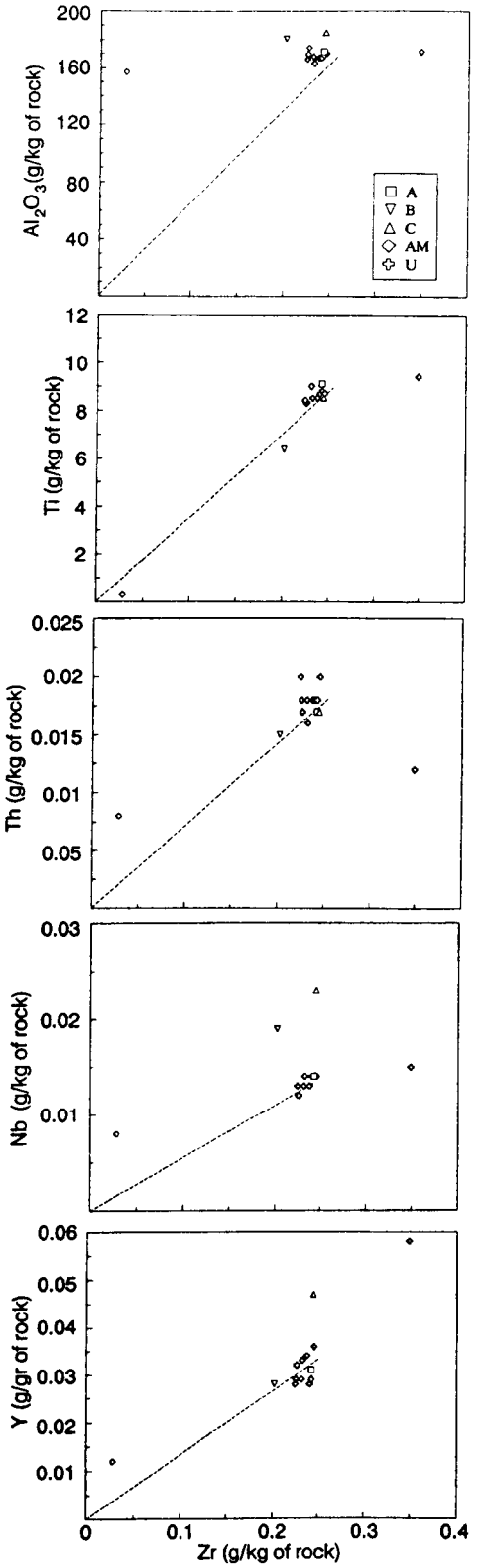

Fig. 5.16. Test for immobile elements in altered samples from Santa Elena. Lines represent the expected path caused by hydrothermal dilution.

	LC129-13	LC129-14	LC129-15	LC129-16	LC129-17	LC129-18	LC129-19	LC129-20	LC129-21	LC129-22	LC129-23
mts.	0.50	1.00	2.00	3.00	4.00	5.00	6.00	7.00	8.00	9.00	10.00
SiO_2	109.84	154.59	57.64	186.95	217.53	3.65.92	223.82	29.74	45.70	30.66	44.40
TiO_2	-0.11	-0.10	-0.14	-0.16	-0.08	-0.24	-0.19	-0.21	-0.11	-0.16	-0.14
Al_2O_3	14.39	25.28	8.67	29.99	31.54	61.25	33.06	4.51	7.53	4.75	7.70
Fe2O3*	0.22	0.02	-1.34	-0.26	1.66	0.79	0.79	-0.44	0.08	-0.31	-0.08
MnO	0.01	0.09	-0.03	0.04	0.09	0.11	0.05	0.01	0.00	0.01	0.00
MgO	-0.33	-0.29	-0.64	-0.30	-0.26	-0.34	-0.28	-0.32	-0.31	-0.26	-0.12
CaO	-1.75	1.10	-2.09	-0.66	-0.43	-0.01	-0.96	-0.53	-0.20	-0.76	-0.54
Na_2O	1.37	2.09	-0.61	3.22	6.57	14.25	7.38	0.99	1.63	0.64	1.64
K_2O	8.95	15.74	6.79	18.27	14.95	26.44	16.87	2.32	3.91	2.75	3.76
P_2O_5	0.07	0.16	0.06	0.23	0.35	0.82	0.25	-0.02	0.03	0.03	0.04
LoI	1.82	6.88	2.75	6.71	3.37	7.09	3.42	0.74	0.70	1.35	1.30
Normal. Factor	1.23	1.18	1.10	1.17	1.25	1.18	1.24	1.05	1.09	1.06	1.06
Co	40.23	30.87	12.66	71.44	59.44	89.83	76.52	2.46	10.04	1.82	14.08
Ni	0.92	-0.01	-0.98	4.04	1.35	-0.39	1.51	-0.69	-2.90	-3.33	0.20
Cu	-4.56	2.23	-3.49.00	-0.14	0.55	27.34	4.51	-0.14	-0.49	-2.75	-0.60
Zn	7.25	5.61	-24.17	-0.81	53.50	38.71	13.98	12.03	24.99	8.10	28.28
Rb	336.74	471.59	162.59	590.61	713.31	1372.79	701.36	96.62	127.53	101.68	133.36
Sr	-123.38	-75.86	-115.59	-75.52	-84.49	-67.49	-90.31	-41.70	-27.64	-55.38	-31.68
Y	30.87	27.82	22.90	44.39	40.80	38.48	57.50	10.58	18.05	7.35	9.35
Zr	0.00	0.00	0.00	0.00	0.00	0.00	0.00	0.00	0.00	0.00	0.00
Nb	9.97	7.16	2.55	5.81	14.99	28.84	15.53	1.07	3.32	2.73	3.07
Ba	-341.23	33.81	-149.59	109.55	-241.71	43.04	-301.72	-32.47	87.31	65.90	74.63
Pb	66.00	53.83	12.24	66.00	67.86	231.48	85.02	17.98	37.17	16.20	26.65
Th	4.85	9.53	-0.42	12.91	16.37	19.04	17.14	0.74	1.52	-0.15	2.71
U	13.13	18.75	2.93	18.07	24.21	51.46	28.64	5.22	4.01	4.08	6.99

Table 5.10. Gain and losses normalised to Zr of altered samples from El Cobre wall rocks.

	LC59-3	LC159-5	LC159-6	LC9098-4
Facies	A	B	C	AM
SiO_2	-0.21	16.81	5.20	604.21
TiO_2	0.05	-0.09	-0.02	-0.61
Al_2O_3	0.51	5.18	1.72	121.40
Fe2O3	0.15	-1.73	-5.08	0.44
MnO	-0.01	-0.04	-0.08	0.10
MgO	-0.08	-0.75	-1.56	0.65
CaO	-0.32	-3.20	-3.33	-1.11
Na_2O	-0.21	-2.60	-1.91	-0.20
K_2O	0.71	4.69	3.20	52.37
P_2O_5	-0.01	0.02	-0.14	1.22
LoI	0.64	3.36	2.33	15.93
Normal. Factor	1.01	1.22	1.00	8.79
Co	-1.30	-2.04	-22.66	106.87
Ni	0.36	-3.06	-9.79	4.77
Cu	-1.38	-4.19	-6.48	278.43
Zn	2.39	56.15	28.90	96.43
Rb	18.88	188.15	64.74	2114.83
Sr	30.75	-175.83	-110.99	-121.29
Y	-2.22	0.50	13.59	71.83
Zr	0.00	0.00	0.00	0.00
Nb	0.77	9.74	9.69	56.89
Ba	133.84	334.56	-223.24	715.83
Pb	5.06	336.18	722.74	107.49
Th	-0.29	0.77	-0.43	52.79
U	2.27	2.29	2.22	57.70

Table 5.11. Gains and losses normalised to Zr of altered samples from the Santa Elena granodiorite-adamellite. A.M. corresponds to altered mylonite, C represents strong phyllic-argillic alteration, B is relative to phyllic-argillic alteration and, A is representative of weak propylitic alteration.

In figs. 5.13 and 5.14. the compositions of altered samples have been plotted versus the compositions of unaltered/less altered samples. The isocon line or line of isoconcentration (Grant, 1986) of Al has been drawn. Th, Y, Zr, and Nb (usually considered as immobile, eg. McLean and Kranidiotis, 1987) show displacements from that isocon reflecting that Al is not truly immobile whereas Th, Y, Zr and Nb are relatively well correlated.

The observed poor correlation between Al and these elements (c.f.Mclean and Kranidiotis, 1987; McLean, 1990) can not be explained by original magmatic fractionation as unaltered samples (collected from different locations) display grouped distributions (Figs.5.15. and 5.16). Al may be mobile to some degree (Anderson and Burnham, 1983; Kerrick, 1990; Philippot and Selverstone, 1991). Addition of Al to alteration envelopes in granites has been reported in the literature (e.g. Böhlke, 1989).

In this study, Zr was selected as the normalising component for mass transfer calculations. Thus, gains and losses are calculated by the expression (Gresens, 1967; Grant, 1986),

$$\text{Gain/Loss} = \text{Mean } Co_{zr} / C^{A}_{zr} * Ci^{A} \_ Ci^{D}$$

Where C^{o}_{zr} and C^{A}_{zr} are concentrations of Zr in the protolith and the altered sample respectively; Ci^{o} and Ci^{A} are the concentration of the oxide or element i in the protolith and the altered sample respectively. The mass transfer is given in grams per 100 grams of protolith (oxides) or miligrams per kilogram of protolith (trace elements).

Gains and losses normalised to Zr are listed on tables 5.10. and 5.11. and plotted in figs. 5.17.a.,b.and 5.19.a.,b. For comparison, gains and losses normalised to Al are presented in figs.5.18.a.,b and 5.20.a.,b.

The use of Zr or Al as normalising component may change significatively the results on Na , Ba and Zn transfers, but the normalisation to Zr seems to fit better the petrographical and mineral chemistry variations. Thus, in the El Cobre alteration

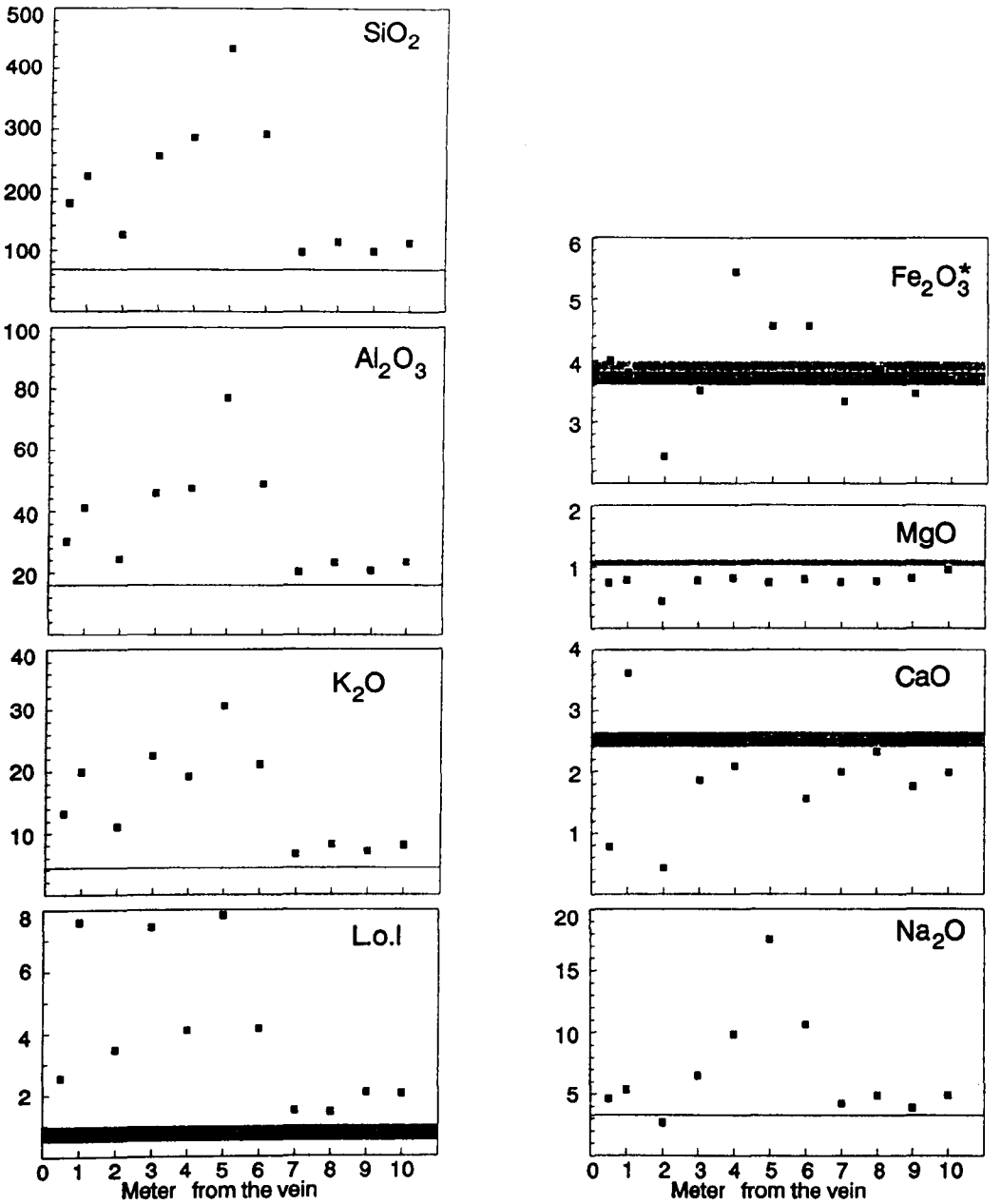

Fig. 5.17.a. Spatial variation of mass transfers in El Cobre wall-rocks. Original concentration has been normalised to constant Zr. Dotted areas represent the compositional range of ten unaltered samples.

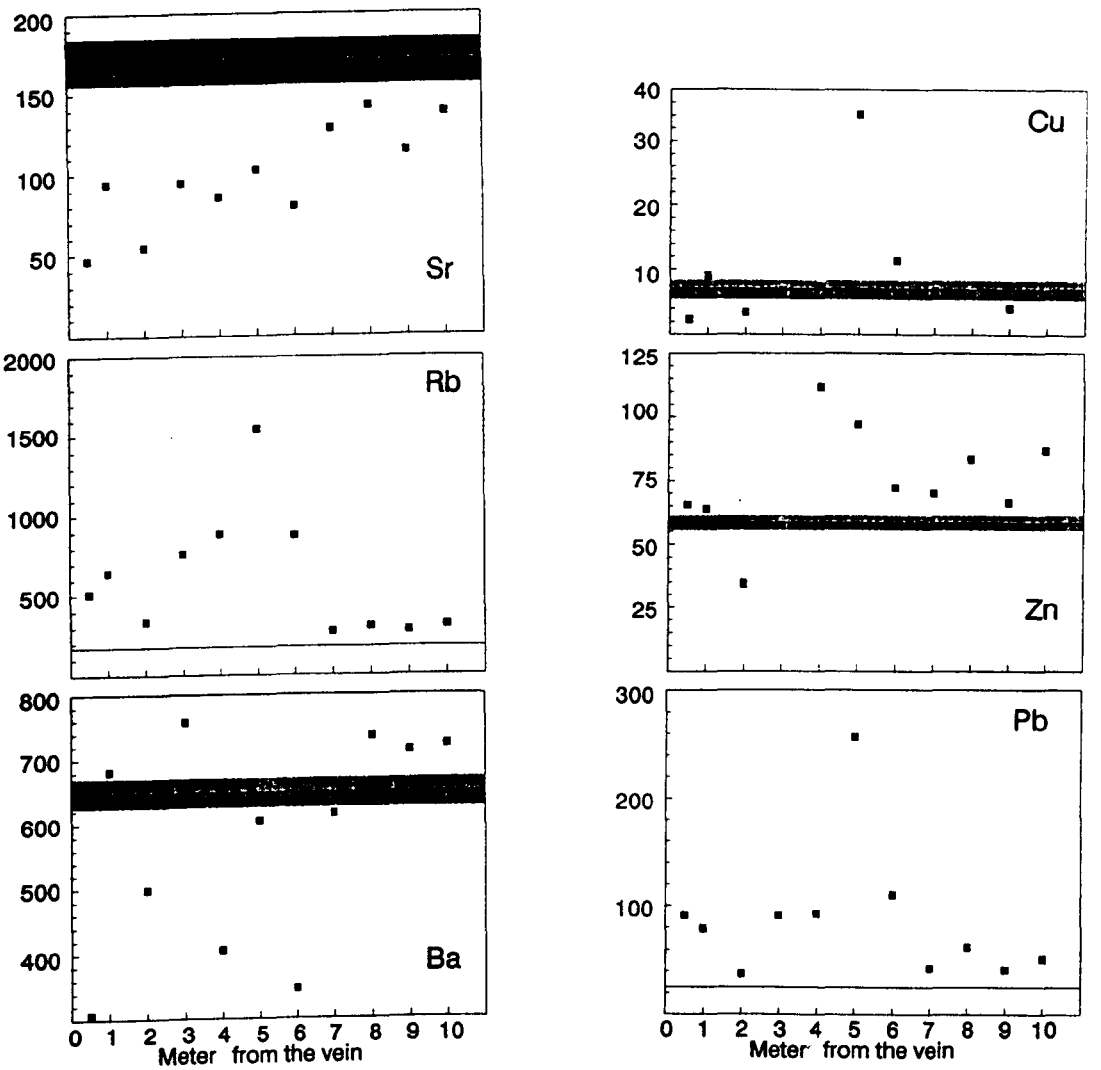

Fig. 5.17.b. Spatial variation of mass transfers in El Cobre wall-rocks. Original concentration has been normalised to constant Zr. Dotted areas represent the compositional range of ten unaltered samples.

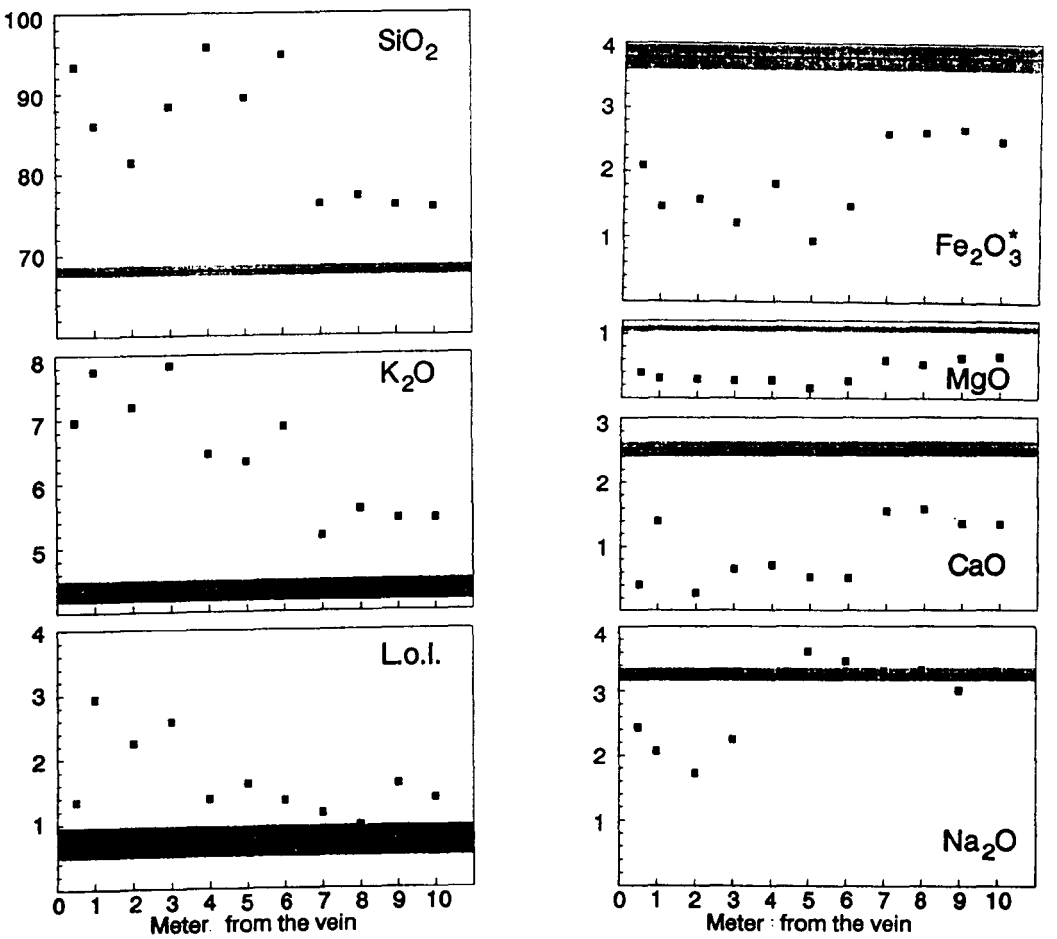

Fig. 5.18.a. Spatial variation of mass transfers in El Cobre wall-rocks. Original concentration has been normalised to constant Al. Dotted areas represent the compositional range of ten unaltered samples.

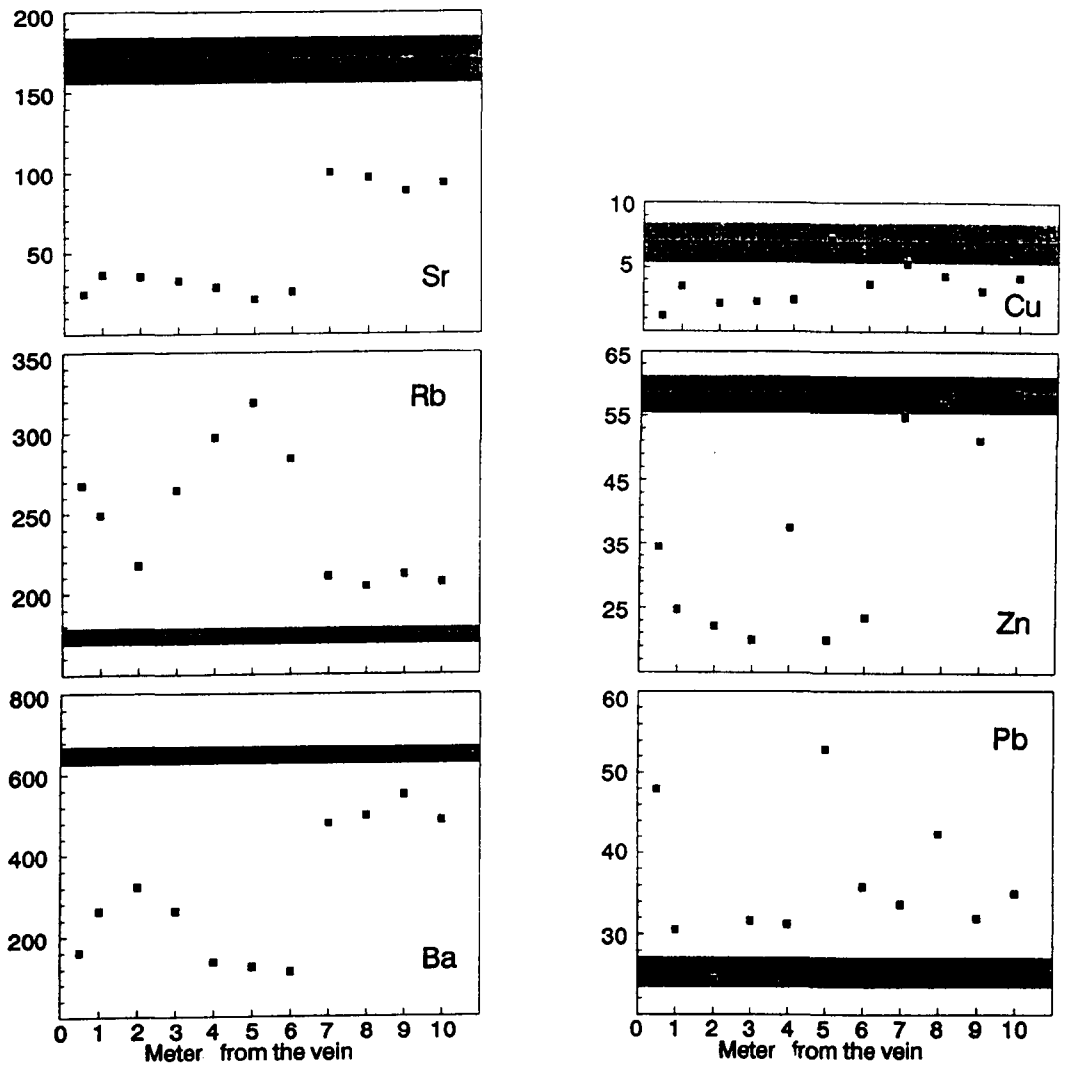

Fig. 5.18.b. Spatial variation of mass transfers in El Cobre wall-rocks. Original concentration has been normalised to constant Al. Dotted areas represent the compositional range of ten unaltered samples.

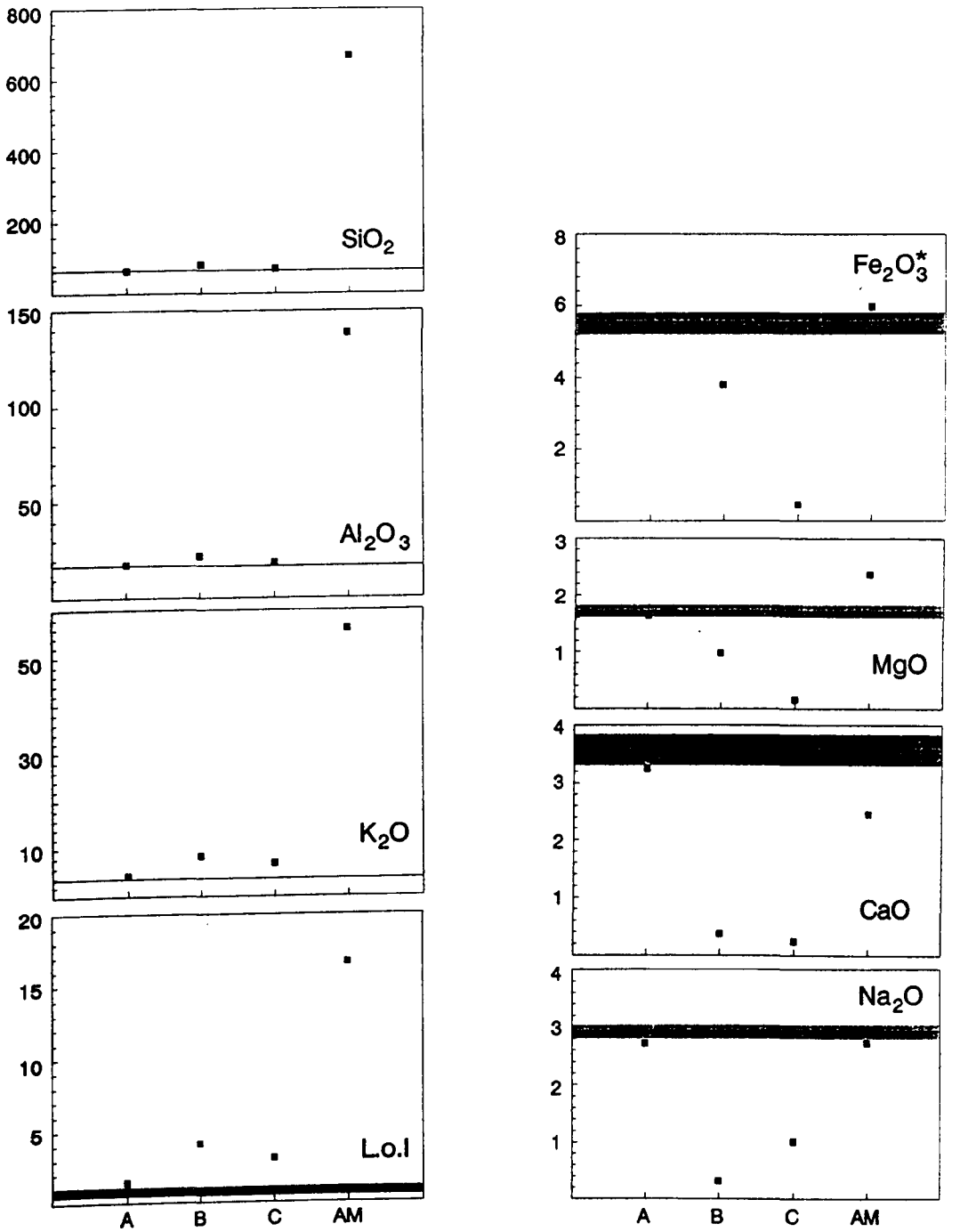

Fig. 5.19.a. Spatial variation of mass transfers in the altered granodiorite-adamellite of Santa Elena. Original concentration has been normalised to constant Zr. Dotted areas represent the compositional range of ten unaltered samples.

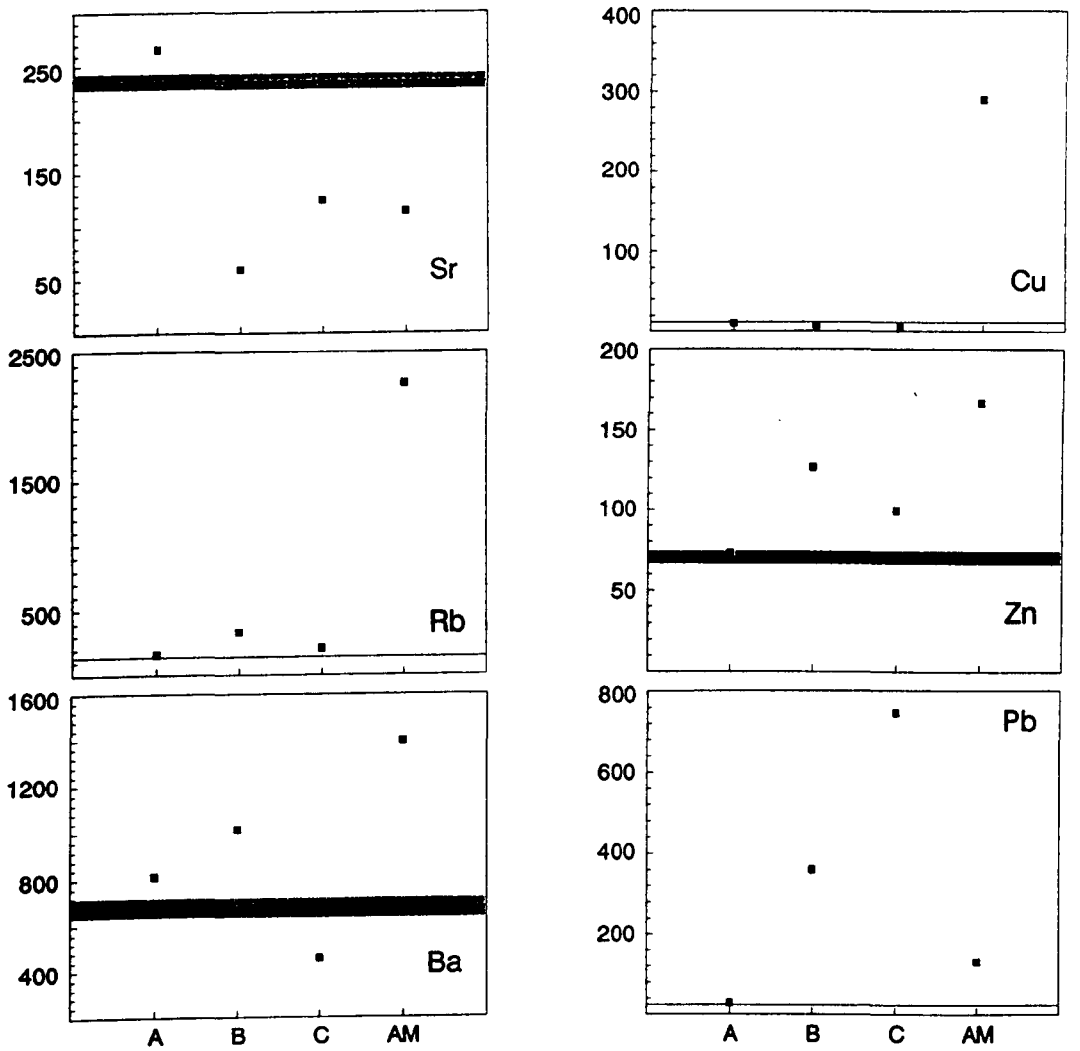

Fig. 5.19.b. Spatial variation of mass transfers in the altered granodiorite-adamellite of Santa Elena. Original concentration has been normalised to constant Zr. Dotted areas represent the compositional range of ten unaltered samples.

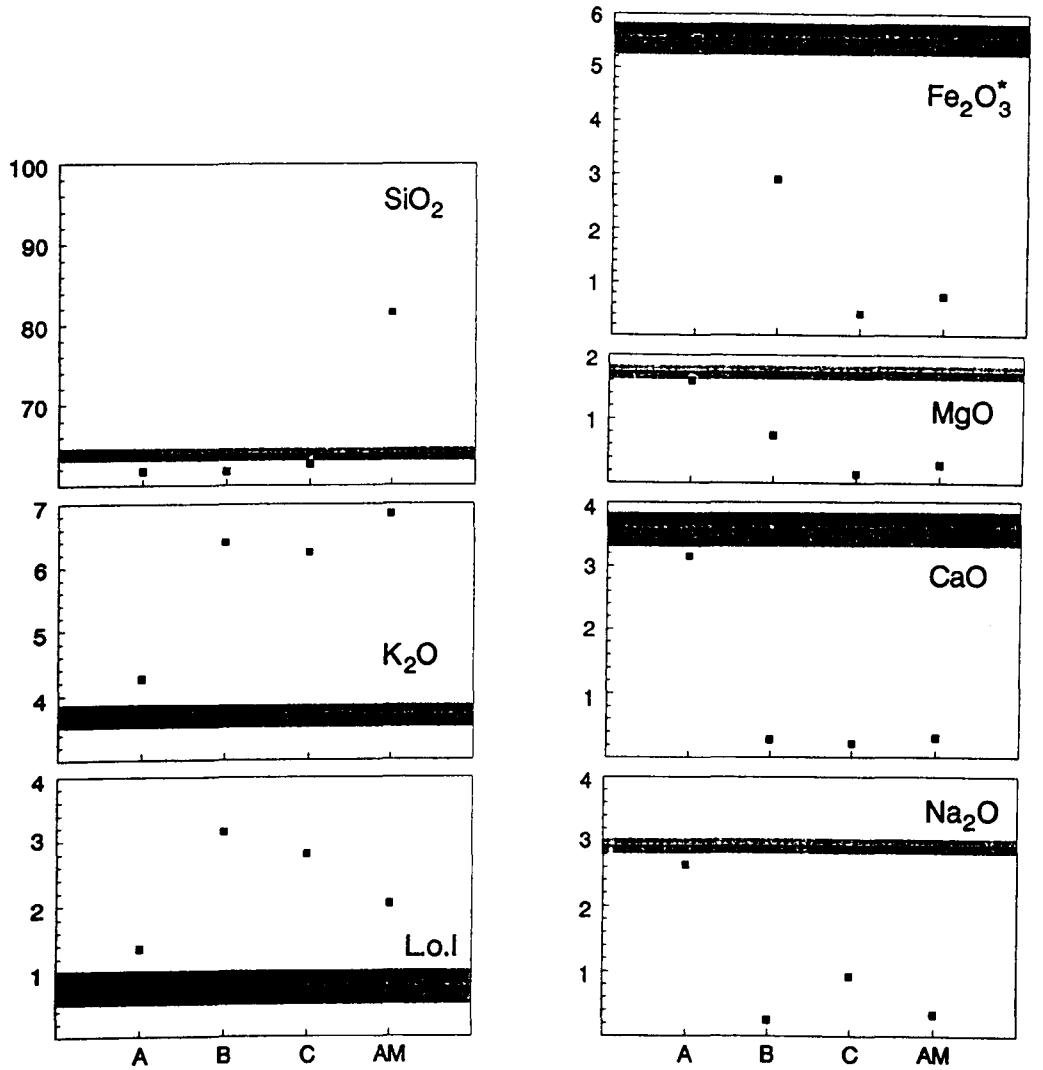

Fig. 5.20.a. Spatial variation of mass transfers in the altered granodiorite-adamellite of Santa Elena. Original concentration has been normalised to constant Al. Dotted areas represent the compositional range of ten unaltered samples.

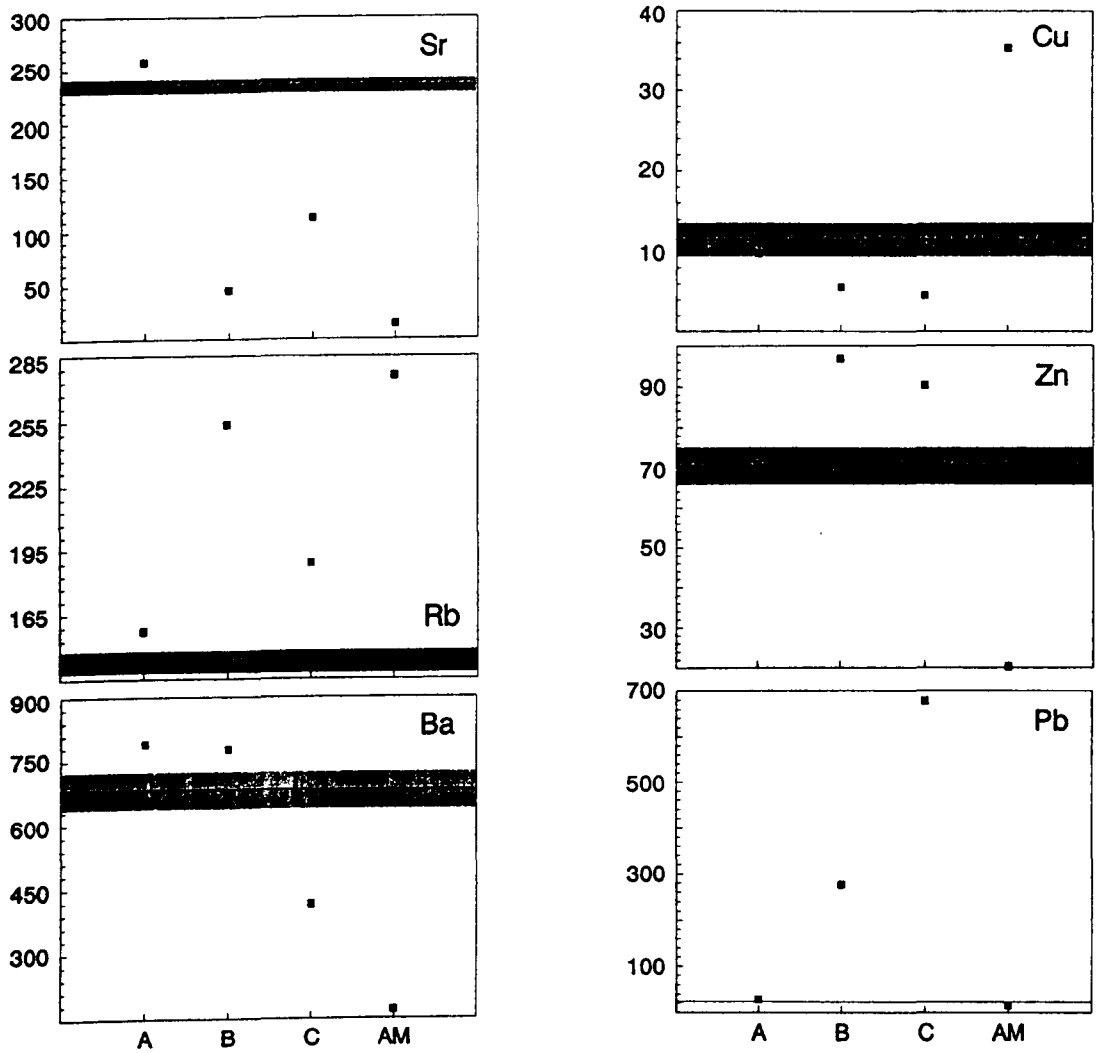

Fig. 5.20.b. Spatial variation of mass transfers in the altered granodiorite-adamellite of Santa Elena. Original concentration has been normalised to constant Al. Dotted areas represent the compositional range of ten unaltered samples.

halo, Si, Al, K, Na, Rb and Pb increase from the vein in the first five meter of the profile, to fall abruptly on the 7th m. to values close to those of the unaltered samples. Ba shows a scattered distribution. Ca and Sr show a regular depletion toward the vein.

Introduction of significant amounts of Si, Al, K, Ba and Cu occur in the altered mylonite (LC9098-4, AM in fig.5.19.a. and b), which is not associated with increase in Pb, likely because the gains in this sample are not associated with the main event of Pb-Zn mineralisation.

5.3.7.Summary.

The granitoids at Linares-La Carolina exhibit hydrothermal alteration envelopes with textural and compositional zoning subparallel to the veins.

The haloes display argillic-propylitic assemblages at depth but at shallow levels argillic-phyllic assemblages occur. Those alterations are variably overprinted by alkali metasomatism which led to the coeval precipitation of albite and K-feldspar.

Evidence of an early argillic alteration has been found in the mylonite of Santa Elena.

The alteration better developed (i.e. argillic-propylitic to propylitic) is characterised by formation of chlorite and white mica, together with minor amounts of kaolinite at the expense of the alteration of biotite and feldspars.

Textural equilibrium between white mica (illite) and chlorite is supported by Mg/Fe partitioning in equilibrium. Precipitation of secondary feldspars in textural equilibrium postdate the argillic-propylitic alteration.

The mineral chemistry of chlorites and white micas show variations between different alteration zones and within the same

zone. Thus, there is a strong correlation between the ratio Fe/(Fe + Mg) and the abundance of chlorite and specially illite.

Temperatures estimated from illite and chlorite geothermometers yielded temperatures of 276.7-321.5°C and 285-310.2°C respectively, which are consistent with temperatures obtained from immiscibility in inclusion fluids (see chapter 6).

The monitoring of immobile element variations in altered samples showed that Al mass transfer may be important. If the gains and losses are estimated from the normalisation of data to Zr constant, the variations are fairly consistent with the variations observed in mineral chemistry and mineralogy, showing that there is a significant introduction of Si, Al, K, Na, Rb and Pb whereas significant remobilisation of Ca and Sr occur.

Chapter 6. Fluid inclusions studies.

6.1.Introduction.

In this chapter, microthermometric data from fluid inclusions in quartz and barite samples from some hydrothermal occurrences of the Linares-La Carolina district are presented and interpreted. In addition to the assessment of the minimum temperature and pressure of mineral deposition, the microthermometry is used here to identify different compositional types of inclusions. The consideration of both interpretations (physical conditions and chemical composition) will be used in the last sections of this chapter to sketch a preliminary account of the evolution of fluids involved in the mineralisation.

6.2.Sampling.

25 Samples of ankerite, quartz and barite were collected at 12 ore occurrences from outcrops, mine galleries and, when in situ collection was not possible, from mine dumps. Special emphasis was put on collecting samples including ore minerals to constrain the paragenetic stage of the sample. After repeated surveys by conventional optical microscopy (COM), 14 samples were rejected because the inclusions were too small or/and too scarce to obtain reliable results.

Sample preparation and analytical procedures are those described elsewhere as standard (e.g. Roedder, 1984; Shepherd et al., 1985).

6.3.Microthermometry. Presentation of data.

6.3.1.Microthermometric data used in this study.

Microthermometric data are obtained by lowering or raising the temperature of the specimen and observing phase changes within individual fluid inclusions. The temperature at which these phase changes occur and their nature are then recorded. Thus, the determination of the composition of inclusion fluids is mostly

based on the temperatures of solid to liquid phase changes: first melting of ice (Te), final melting of ice (Tmi), melting of CO_2 (Tm_{CO2}), melting of sylvite (Tms), melting of halite (Tmh), melting of clathrate (Tmhy). The determination of minimum temperatures and pressures of formation is mainly based on liquid to vapour, vapour to liquid or $liquid_{(H2O)}$ to $liquid_{(CO2)}$ phase changes: homogenization to vapour (Th_V) or homogenization to liquid (Th_L).

In some cases, homogenization temperature may be used in compositional determinations: the homogenization of CO_2 (Th_{CO2}) phases defines uniquely the density (or molar volume) of the CO_2 fluid and combined with an estimate of the proportion of CO_2 and H_2O in the inclusion, permits the calculation of the bulk density and mole fraction of each phase. Most of the inclusions observed in this study homogenized into the liquid phase, showing that the density is greater than the critical density (0.468 g/cc).

In concentrated saline inclusions, solid phases (e.g. halite) can melt at higher temperature than Th_L. In that case, the minimum temperature of entrapment is Tmh. No Tmh higher than Th_L was observed in this study.

6.3.2.Presentation of microthermometric data.

Each sample analyzed is presented individually as multiple types of inclusions were present in each sample. In each case the data is presented in two figures. The first figure presents Tmi (including Tmhy, Tms, Tmh), Te and Th in three histograms (from which the most frequent values and groupings may be assessed). The second figure presents three plots, Th versus Tmi (which enables the distinction of homogenization ranges of different salinity groups), Te versus Tmi (from which information of the relationship between eutectic melting and overall salinity and hence composition of dissolved salt species may be deduced), and Th versus Te (from which the distinction of homogenization ranges of each compositional group may be gleaned).

The same types of figures are also presented including the totality of the data (figs.6.1). To ease the interpretation of the scatter plots, inclusions from barite and quartz as well as the different compositional types of inclusions have been differentiated in the graphs.

6.4.The microthermometric data: Compositional types of inclusions.

Several compositional types of inclusions have been identified in the studied samples (table 6.1.a., figs. 6.1.a-b). Type I inclusions are aqueous saline inclusions, either simple saline ($NaCl-H_2O$, Type Ia), bisaline ($NaCl-KCl-H_2O$, type Ib) or complex saline ($NaCl-KCl-CaCl_2-H_2O$, type Ic). Type II inclusions are aqueous-carbonic saline inclusions ($NaCl-CO_2-H_2O$).

6.4.1.Type Ia inclusions.

Microthermometric and compositional data for type Ia inclusions are summarised in table 6.1.a.

These are liquid rich aqueous inclusions which contain dissolved salts (assumed to be dominantly NaCl) from freezing point depression and first melting temperature, but no other gas phases. No petrographical evidence was found which could indicate a certain primary origin for inclusions of this type (e.g. growth zones defined by fluid inclusions, see Roedder, 1984). They commonly occur along healed cracks. Although few cases appeared as undoubtedly pseudosecondary, most of them may be either secondary or pseudosecondary.

This type of inclusion usually shows two phases, H_2O liquid and H_2O vapour at room temperature, the vapour phase occupies less than 40% of the apparent total volume of the inclusion. The average size of the inclusions varies from 5 to 50 μm.

The final melting of ice occurred at (Tm_i) -5.3° to -0.2° reflecting total salinity of 8.23 to 0.33 wt % equivalent NaCl. Apparent first melting was observed at temperatures (T_e) between

TYPE	L/V %	Te (°C)	Tmi (°C)	Tmh (°C)	Tms (°C)	Th (°C)
Ia	25 · 95 (most > 50 %)	-18.3 • -0.8 (m = -6.2)	-5.3 • -0.2 (m = -2.2)	____	____	87.4 • 392 (m = 291.2)
Ib	50 • 95	-30.8 • -22.3 (m = -27.4)	-19.9 • -0.7 (m = -7.7)	____	____	168 • 325 (m = 239.5)
Ic	10 • 95 (most > 50 %)	-68 •-37.3 (m = -51.2)	-33.2 • -3.1 (m = -20.4)	-1.5 • 10.3 (213.6)	-9.9 • 5.2	76 • 327 (m = 146.8)
	Vol.ume Frac. CO_2 %	$TmCO_2$ (°C)	Tmi (°C)	Tmhy (°C)	$TpCO_2$ ($TpCO_{2v}$) (°C)	$ThCO_2$ (Th_L) (°C)
II	85 • 50 (15 • 5)	-56.8 •-57.6	-5.8 • -3.0	4.6 • 9.1	22.2 • 26.0 (26.0 • 26.8)	293.4 • 373.0 (240.6 • 245.4)

Table 6.1.a. Summary of microthermometric data and types of inclusions in quartz and barite samples.

type	Te (°C)	Tmi (°C)	Th (°C)	wt % NaCl (°C)	density (g/cc)	Molar volume (cc/mole)
ss	-2.0	-1.3	240.0	2.14	0.83	22.02
s	-3.1	-0.8	318.0	1.32	0.67	27.21
ss	-3.5	-0.2	87.4	0.33	0.97	19.61
ss	-4.2	-2.5	370.0	4.07	0.59	31.32
s	-2.1	-1.0	357.1	1.65	0.57	31.74
s	-7.0	-2.4	316.0	3.92	0.72	25.81
s	-5.9	-2.1	383.0	3.44	0.54	34.11
ss	-5.5	-2.5	382.0	4.07	0.56	33.17
s	-8.4	-4.2	359.0	6.67	0.67	28.07
s	-10.1	-2.7	172.1	4.39	0.93	19.30

Table 6.1.b. Representative data from inclusions in the H_2O-NaCl system.

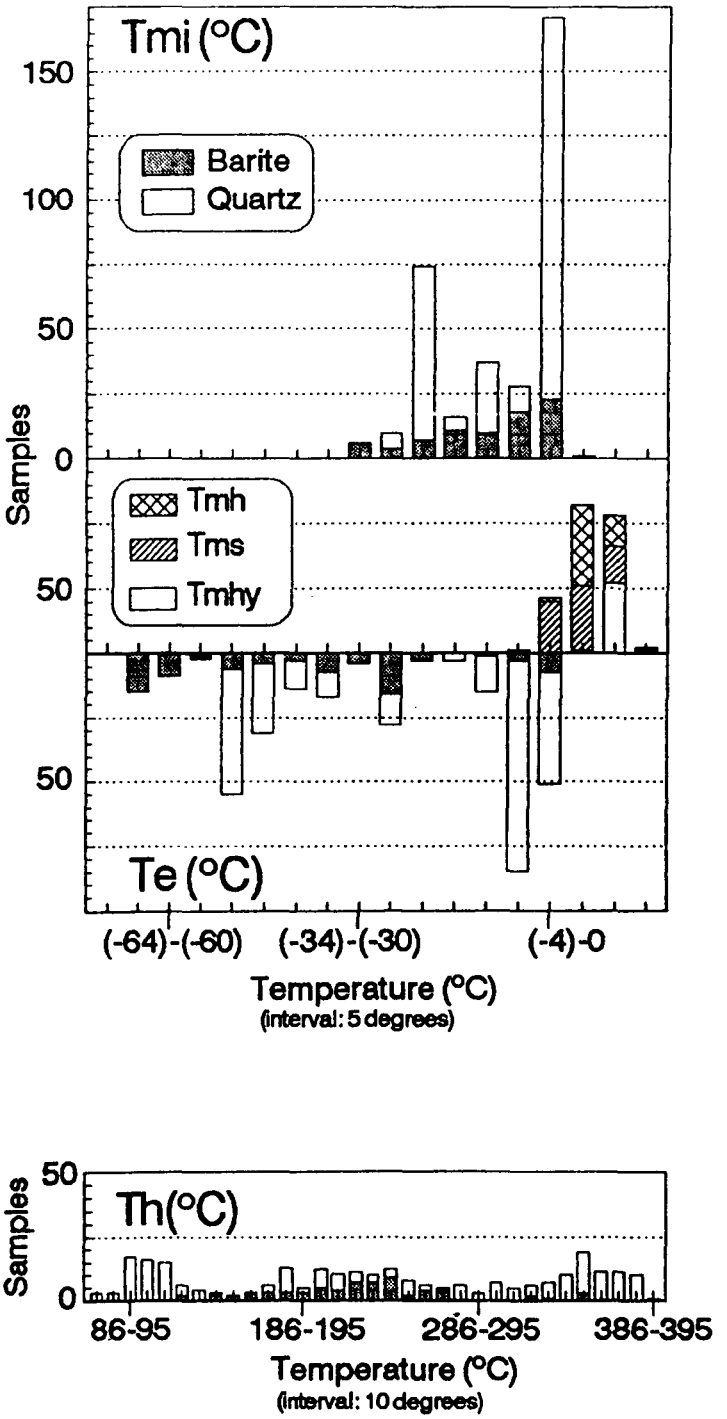

Fig. 6.1.a. Microthermometric data of the whole set of studied samples.

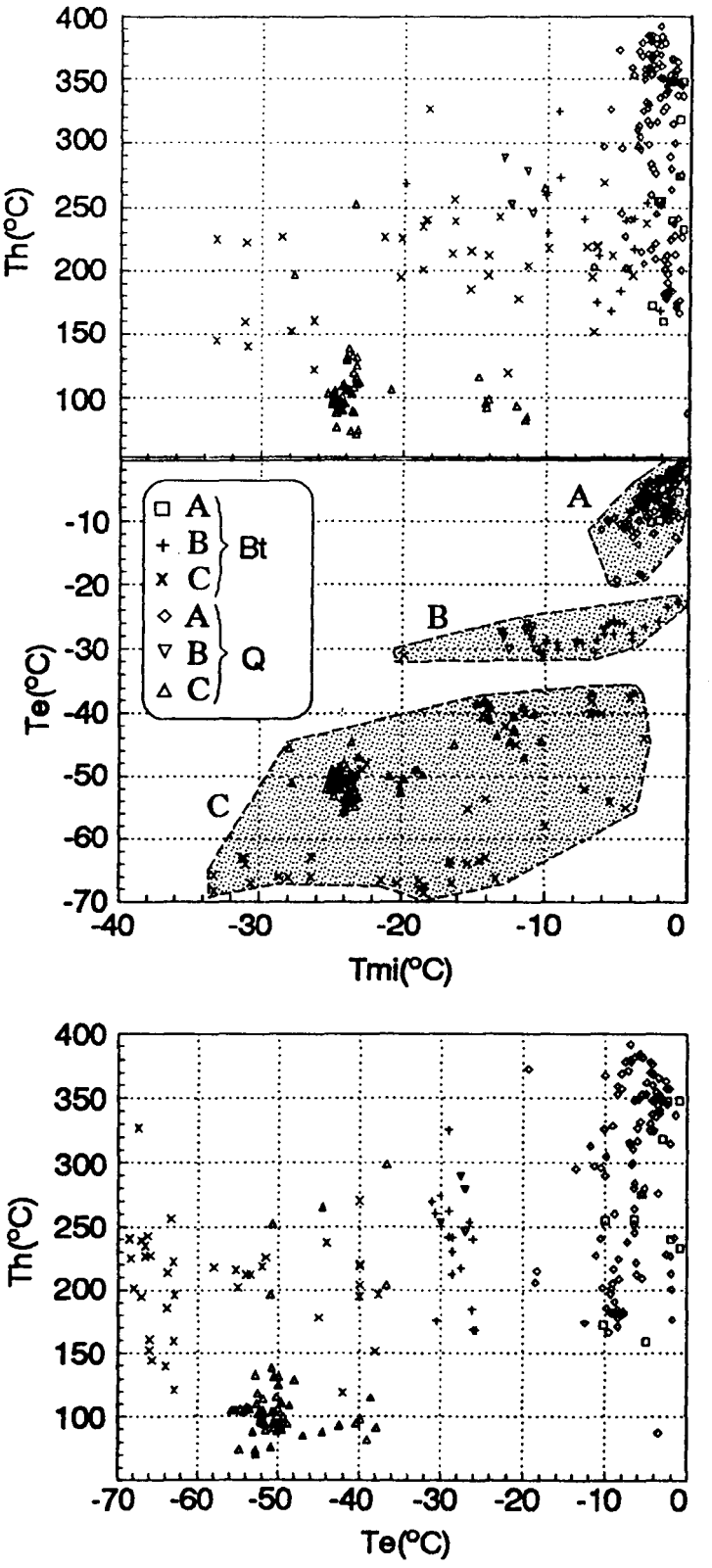

Fig. 6.1.b. Microthermometric data of the whole set of studied samples. A refers to populations of type Ia and II, B to type Ib, and C to type Ic.

-18.3° to -0.8°C (fig. 6.1.a-b). These temperatures, too high if compared to the eutectic temperature in the NaCl-H_2O system (Te= -28.8°C, Potter et al, 1978), are probably due to the difficulty of observation of the first melting of ice in low-salinity and/or irregular small inclusions where the formation of a single clear ice crystal precludes the recognition of the ice rim when it is close to the inclusion walls. No CO_2 or formation of solid phases or clathrates was observed.

Temperature of homogenization to the liquid phase (Th_2) lies between 87.4° and 392°C.

Inclusions of this type were observed in quartz and barite samples (LC9098-6, LC159-8, LC59-5, LC90174-3a, LC90148-2, LC288-1, LC79-1 and LC129-9, figs. 6.2.a-b, 6.3.a-b, 6.4.a-b, 6.5.a-b, 6.5.a-b, 6.6.a-b, 6.7.a-b, 6.8.a-b, 6.9.a-b) from ore occurrences located in both the Linares and El Centenillo-La Carolina-Santa Elena sectors. Samples from the latter showed almost exclusively inclusions of type Ia.

6.4.2.Type Ib inclusions.

Microthermometric data for type Ib inclusions are summarised in table 6.2.a.

Inclusions of this type are liquid-rich aqueous saline inclusions, which normally appear along healed cracks, most of the inclusions being unequivocally secondary following the criteria suggested by Roedder (1984). The average size of the inclusions typically varies from 25 to 50 μm.

This type of inclusions commonly shows two phases, H_2O liquid and H_2O vapour at room temperature. As in type Ia inclusions, the vapour phase usually occupies less than 40 % of the total apparent volume of the inclusion.

Apparent first melting was observed at temperatures (Te) between -30.8° and -22.3°C. These temperatures are puzzling to

type	Te	Tmi	Th	wt % NaCl*
s	-30.3	-6.6	175.4	9.973
s	-28.8	-7.4	241.7	10.98
s	-26.3	-3.1	253.5	5.01
s	-25.8	-5.6	168.3	8.65
ss	-28.8	-9.2	325.0	13.08
ss	-29.8	-9.1	274.0	12.97
s	-30.8	-19.9	269.0	22.87
s	-29.8	-12.5	253.0	16.43
s	-26.8	-11.0	246.0	14.98
s	-27.3	-13.0	289.0	16.89

(*)Total salinity as wt % equivalent NaCl (see text).

Table 6.2.a. Representative data from inclusions in the H_2O-NaCl-KCl system.

type	Te	Tmi	Th	wt % NaCl	wt % KCl	wt % $CaCl_2$	density (g/cc)	Molar vol. (cc/mole)
ss	-49.7	-20.9	106.0	14.02	4.81	8.66	1.66	39.21
ss	-50.6	-27.7	197.0	10.33	5.02	13.45	1.11	40.57
ss	-49.7	-23.3	125.0	14.87	4.45	8.48	1.15	39.61
ss	-50.3	-23.4	253.0	14.87	4.45	8.48	1.06	43.09
s	-50.1	-24.0	131.1	14.40	3.88	9.42	1.15	39.75
ss	-51.2	-24.3	94.7	14.85	3.30	9.35	1.18	38.81
ss	-50.4	-24.7	76.6	13.94	3.86	9.80	1.19	38.29
ss	-51.4	-24.8	105.1	13.94	3.86	9.80	1.17	39.03
ss	-50.0	-24.1	95.1	14.32	3.89	9.59	1.18	38.66
ss	-50.4	-23.8	138.5	14.71	3.57	9.21	1.14	40.09

Table 6.2.b. Representative data from inclusions in the H_2O-NaCl-KCl-$CaCl_2$ system.

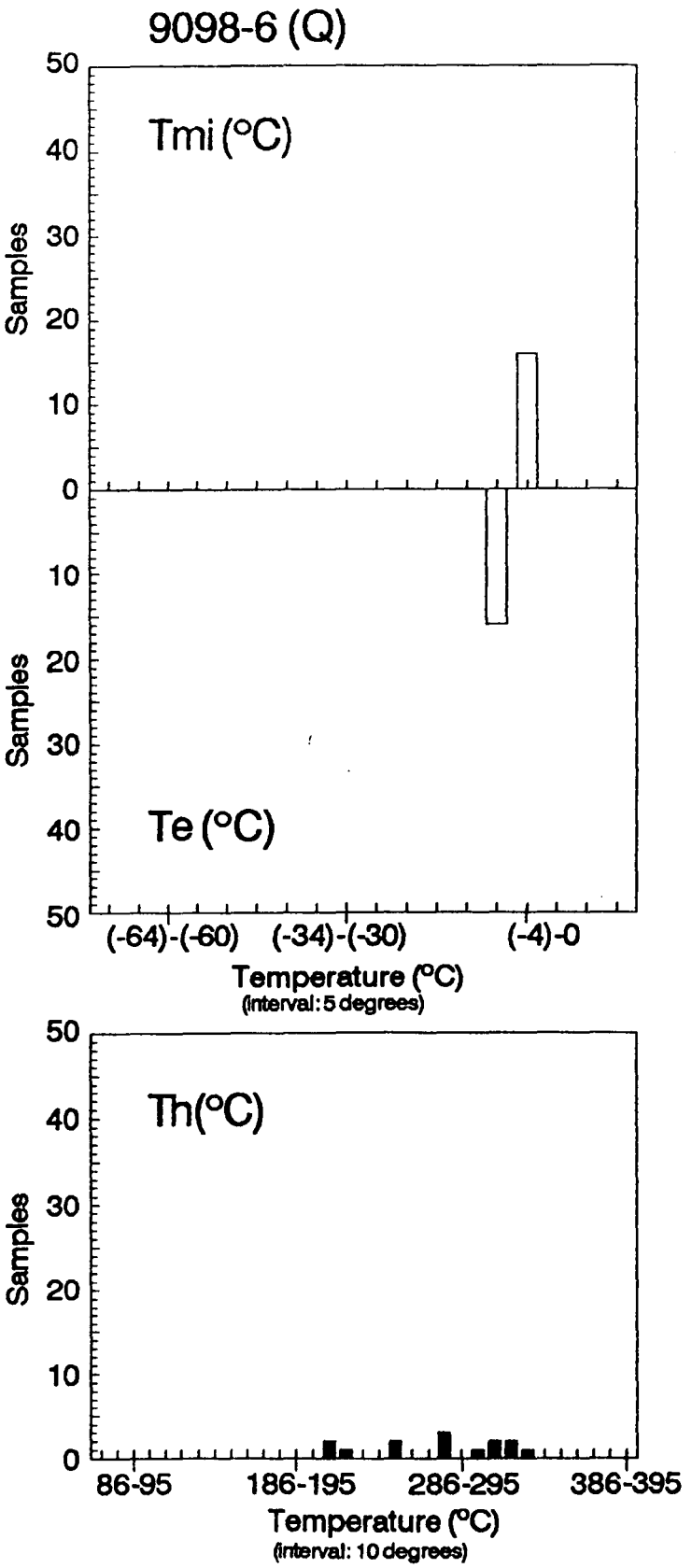

Fig. 6.2.a. Microthermometric data of inclusions in sample LC9098-6 (quartz).

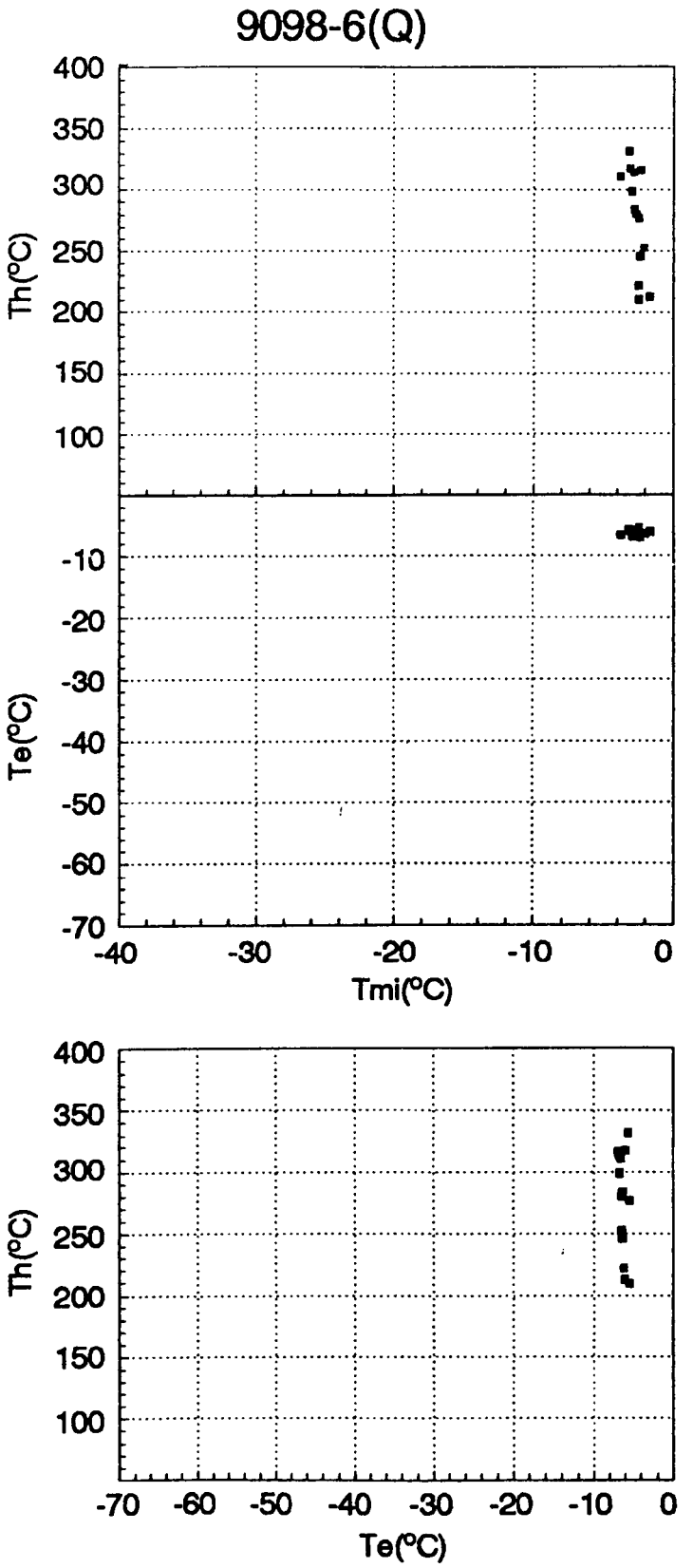

Fig. 6.2.b. Microthermometric data of inclusions in sample LC9098-6 (quartz).

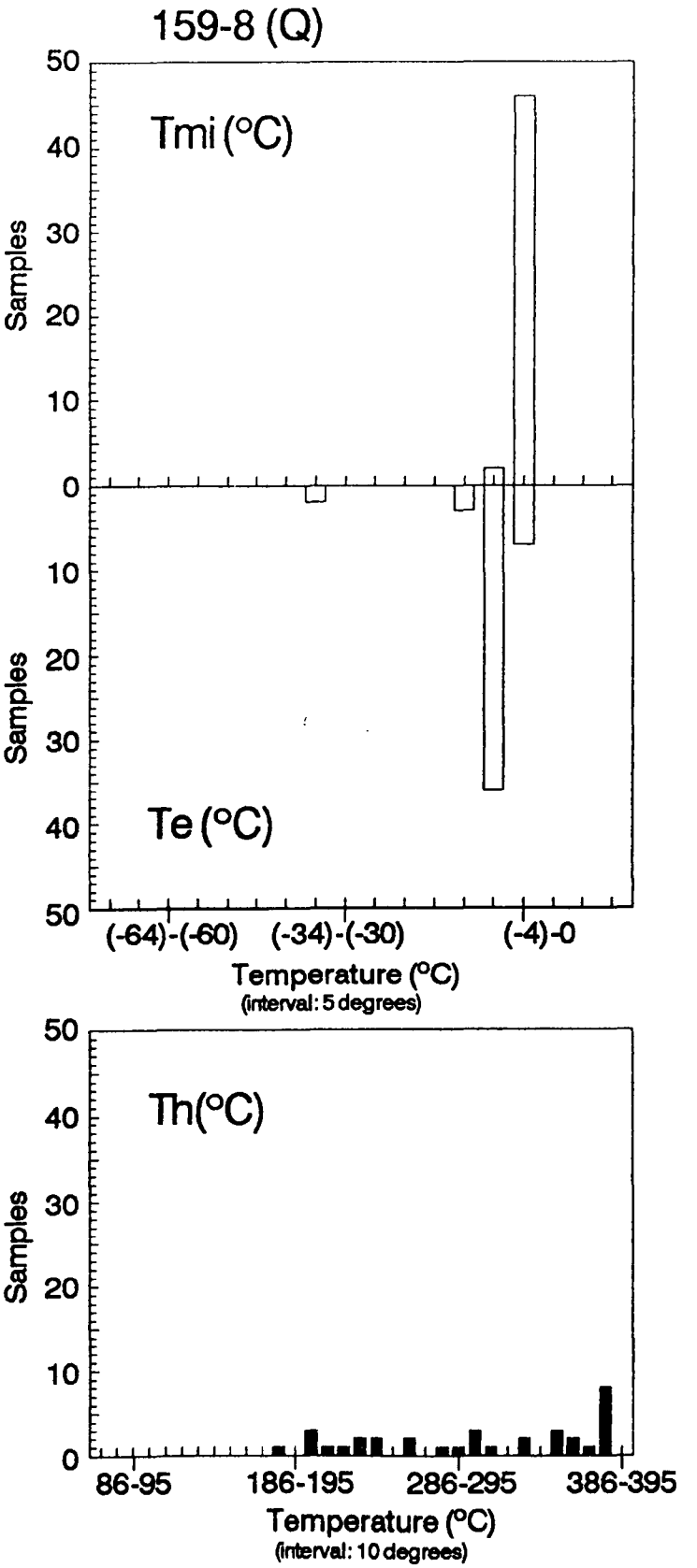

Fig. 6.3.a. Microthermometric data of inclusions in sample LC159-8 (quartz).

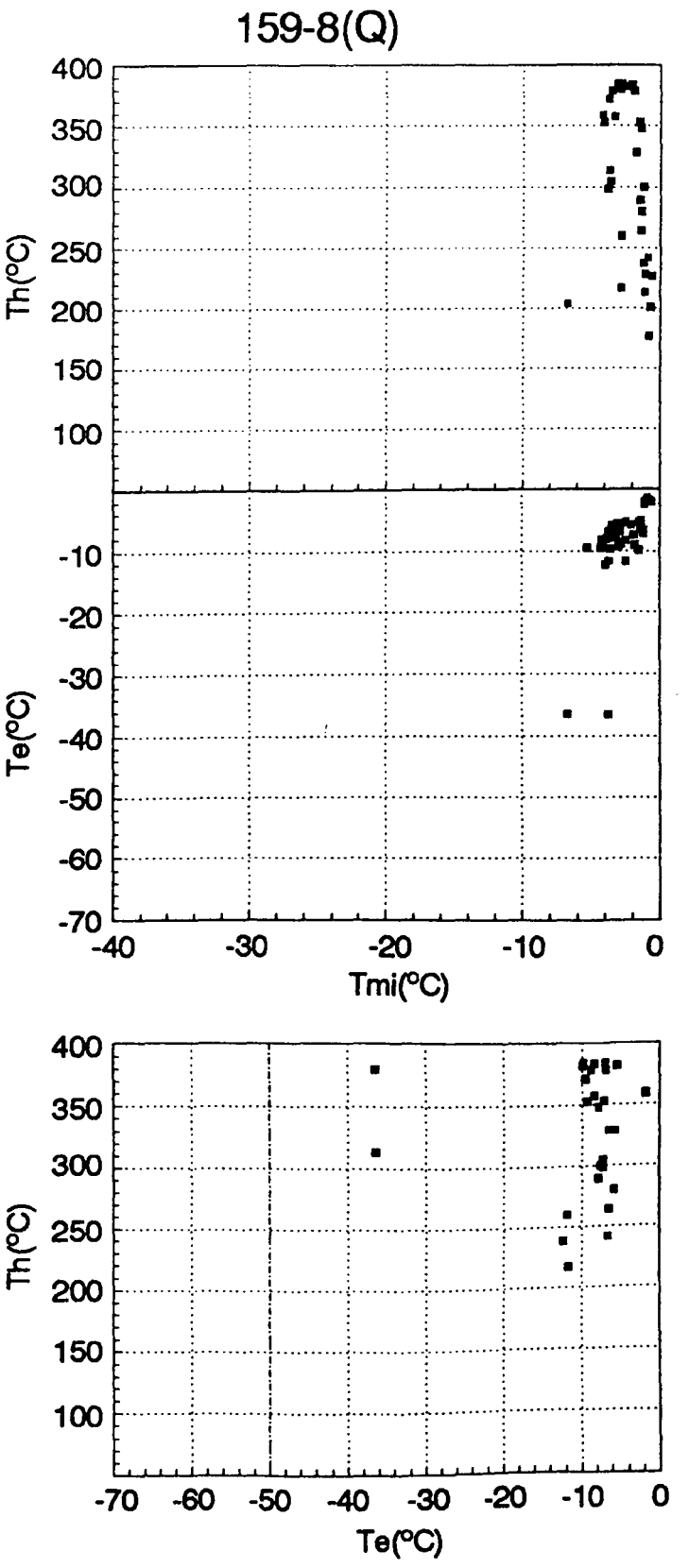

Fig. 6.3.b. Microthermometric data of inclusions in sample LC159-8 (quartz).

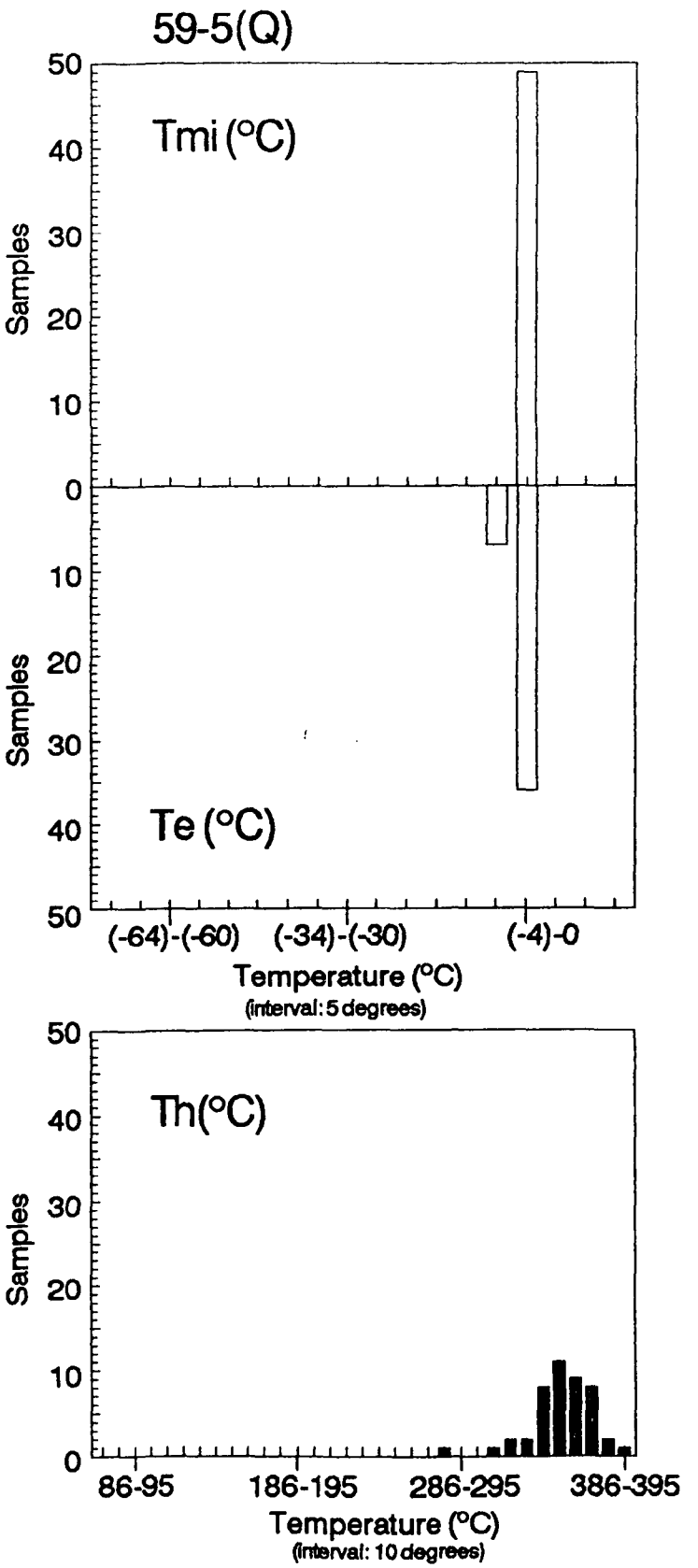

Fig. 6.4.a. Microthermometric data of inclusions in sample LC59-5 (quartz).

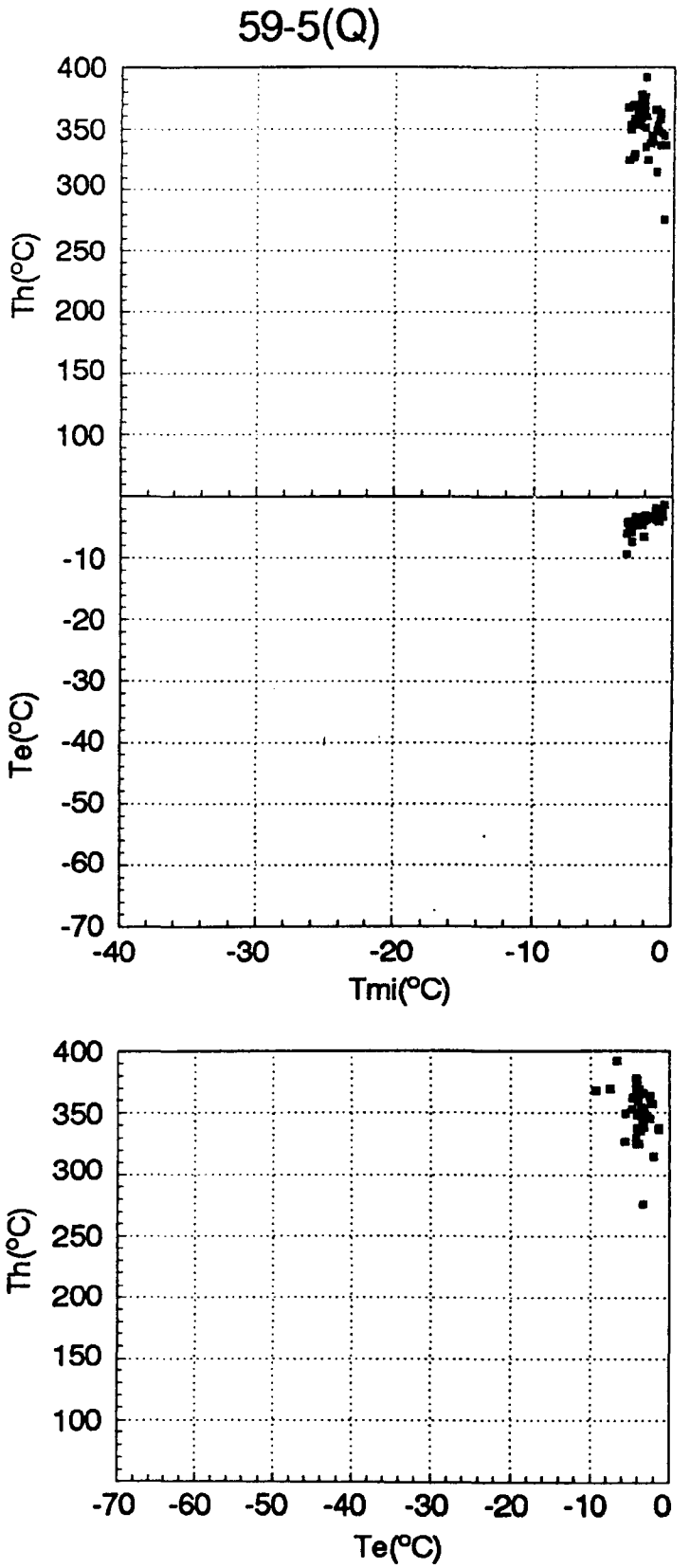

Fig. 6.4.b. Microthermometric data of inclusions in sample LC59-5 (quartz).

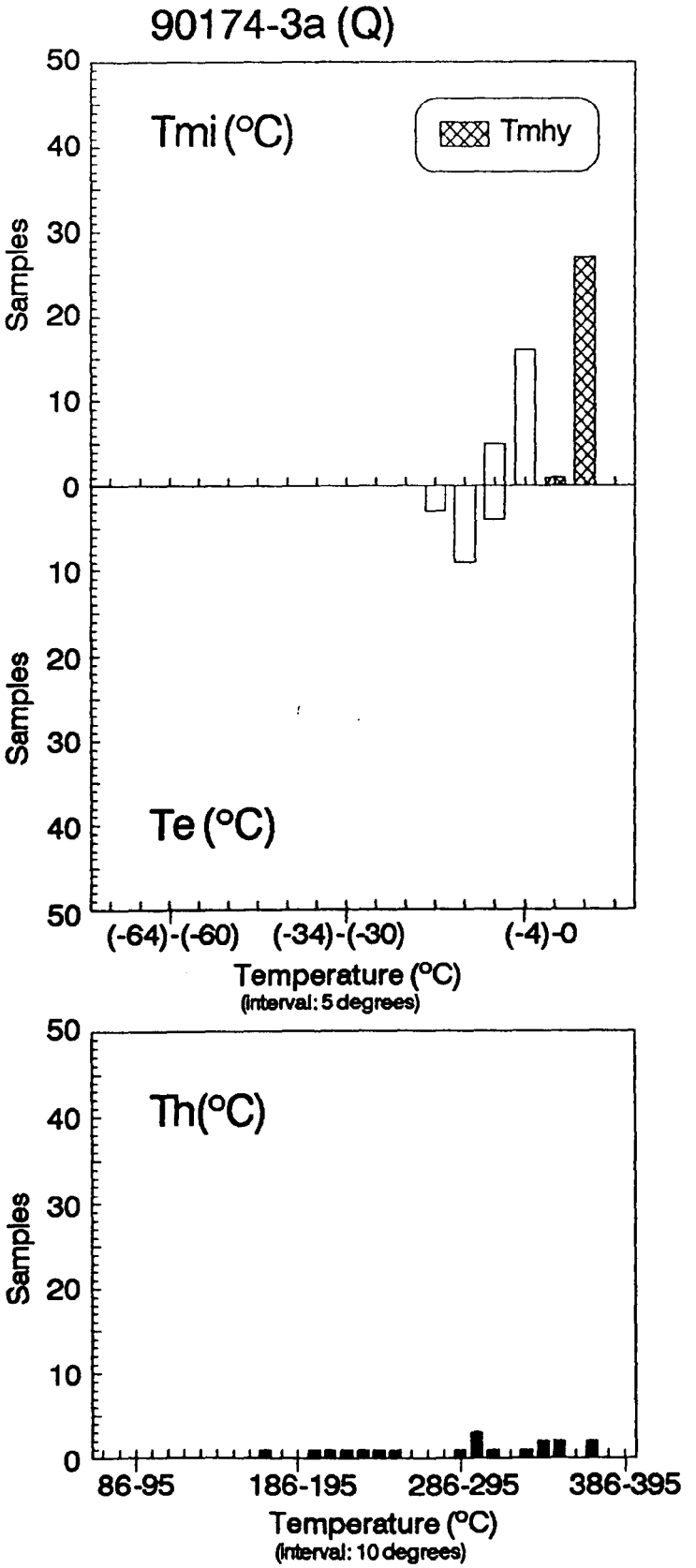

Fig. 6.5.a. Microthermometric data of inclusions in sample LC90174-3a (quartz).

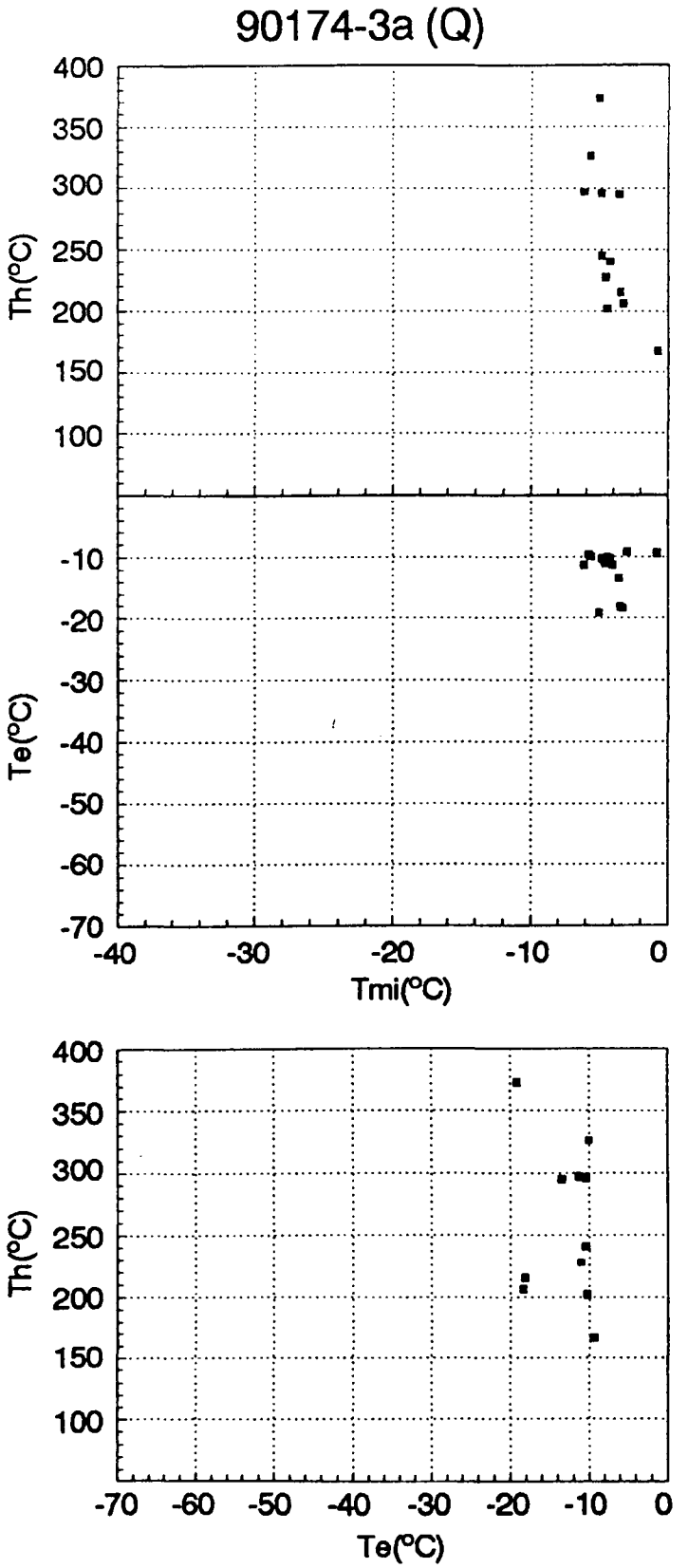

Fig. 6.5.b. Microthermometric data of inclusions in sample LC90174-3a (quartz).

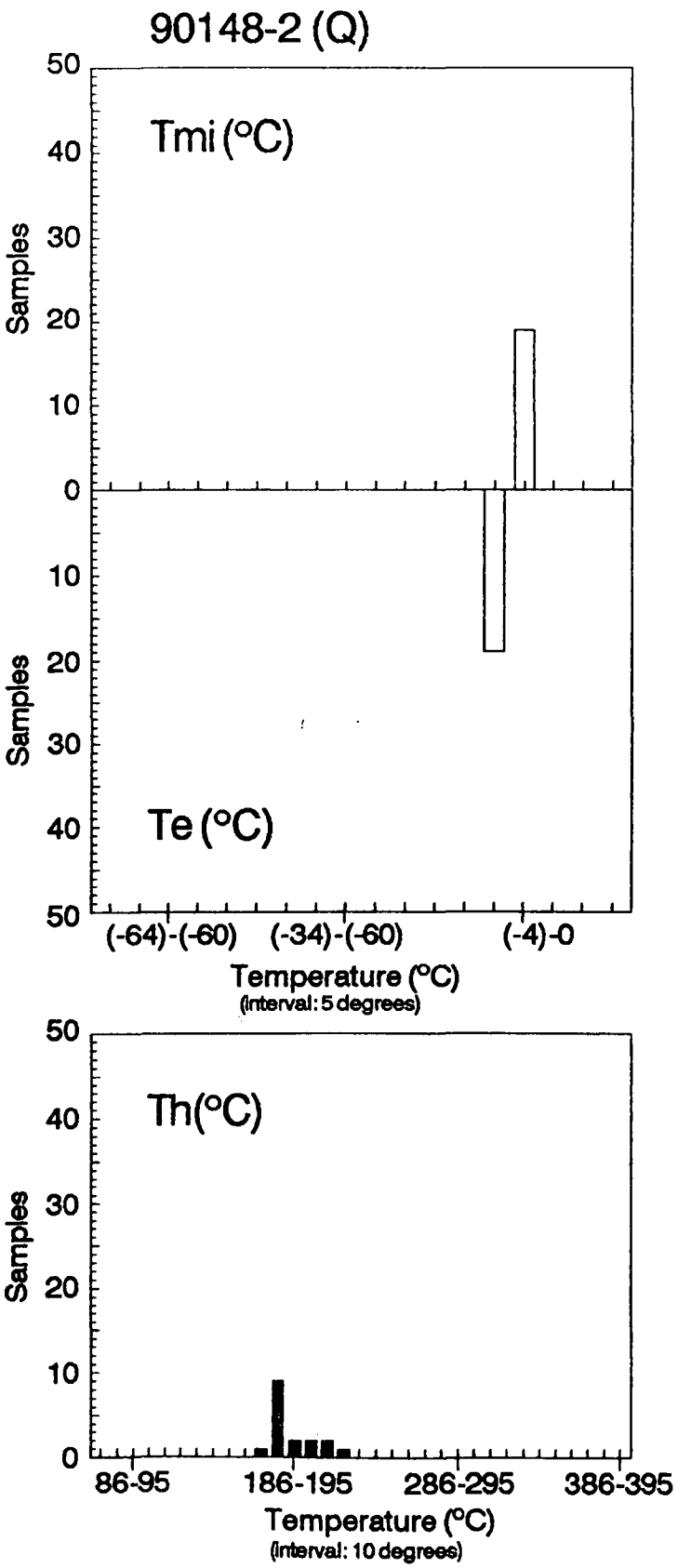

Fig. 6.6.a. Microthermometric data of inclusions in sample LC90148-2 (quartz).

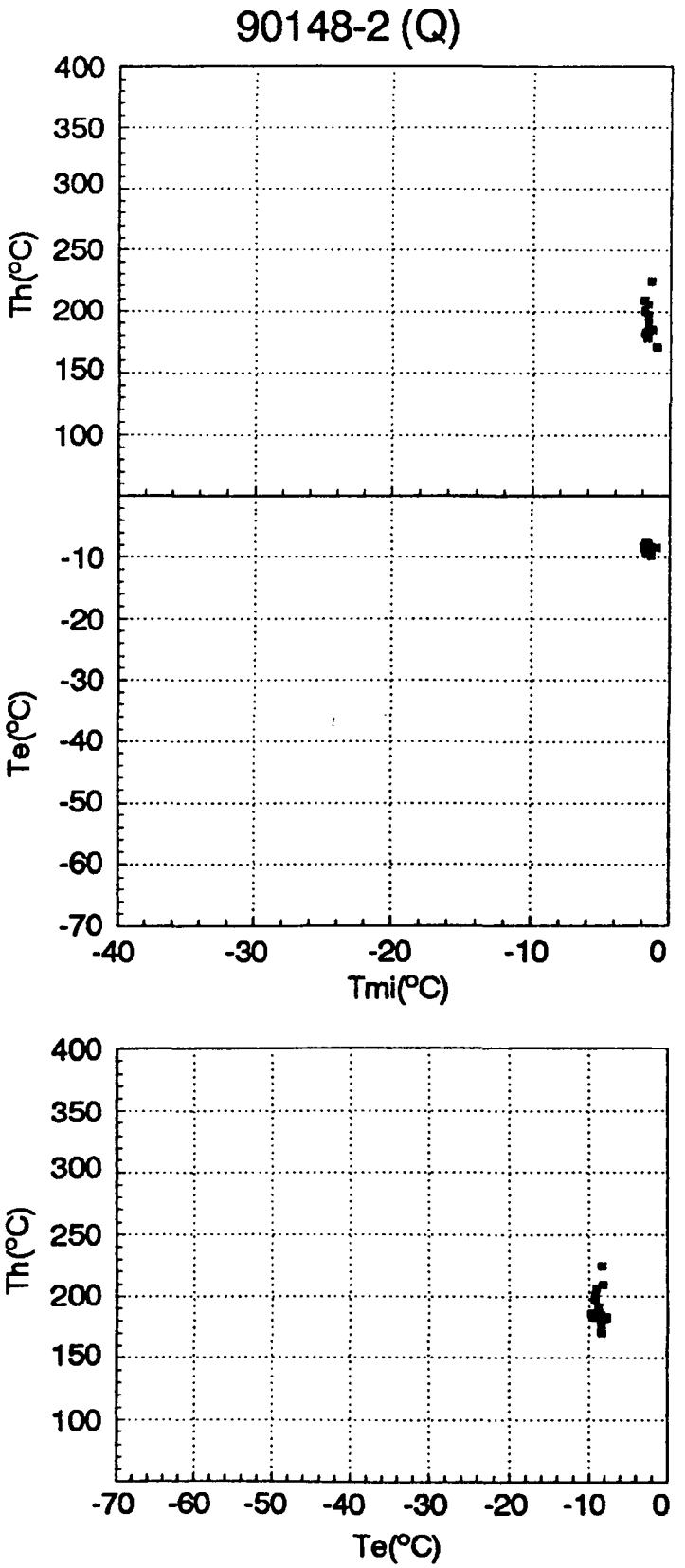

Fig. 6.6.b. Microthermometric data of inclusions in sample LC90148-2 (quartz).

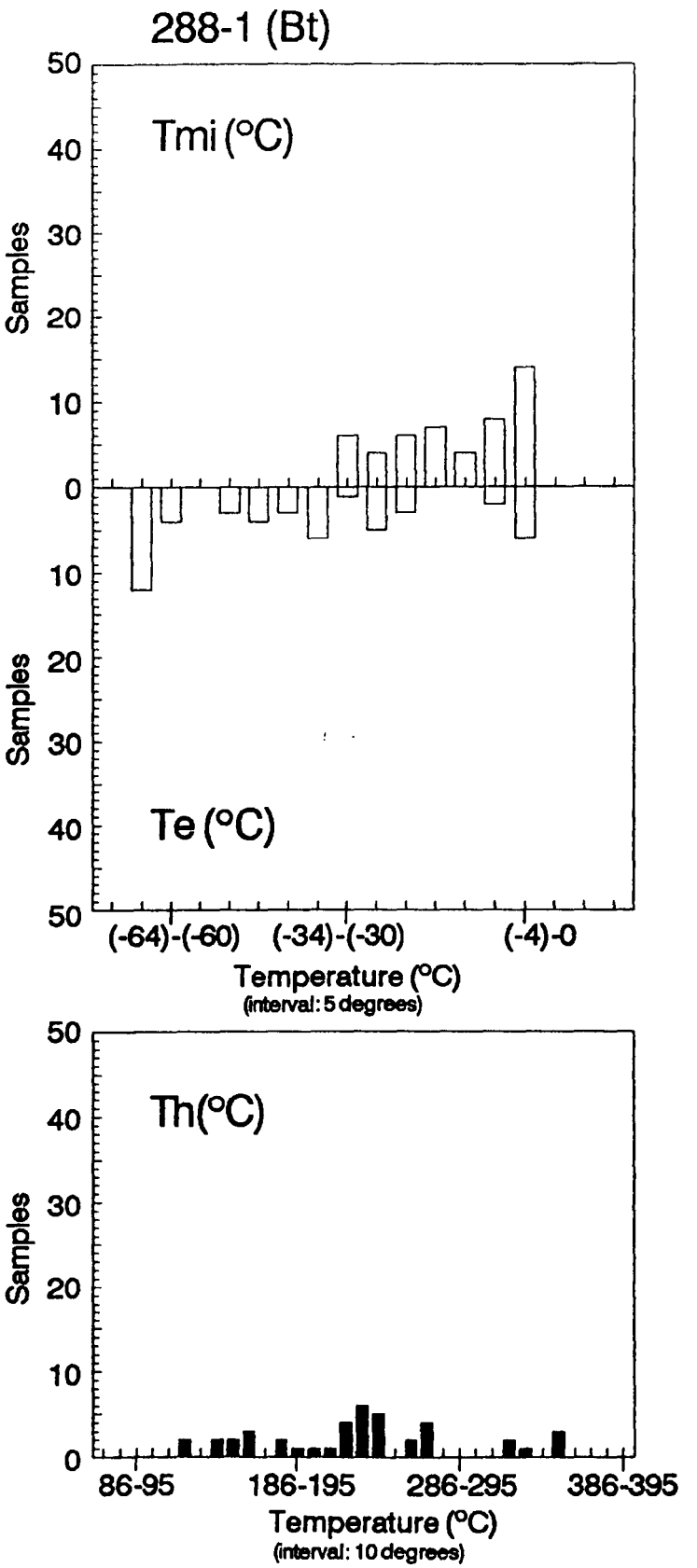

Fig. 6.7.a. Microthermometric data of inclusions in sample LC288-1 (barite).

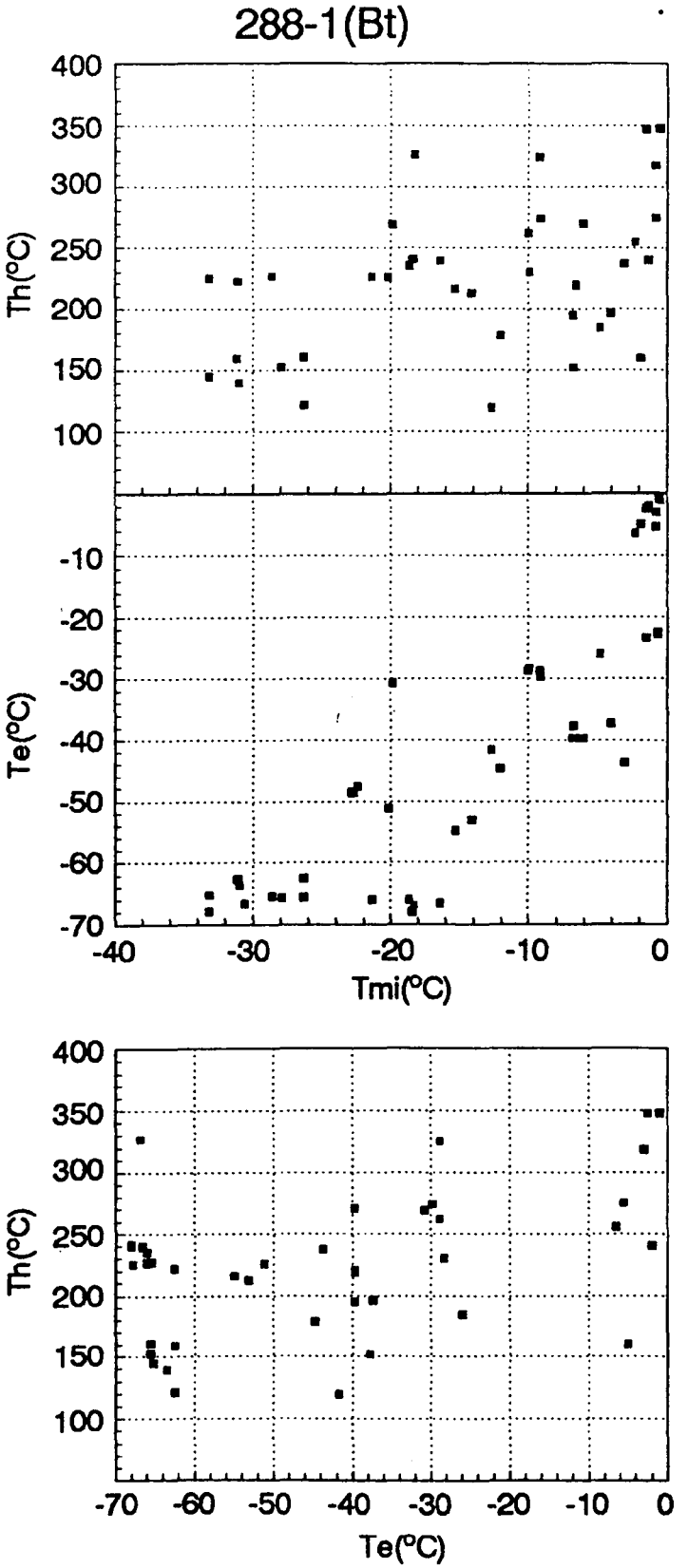

Fig. 6.7.b. Microthermometric data of inclusions in sample LC288-1 (barite).

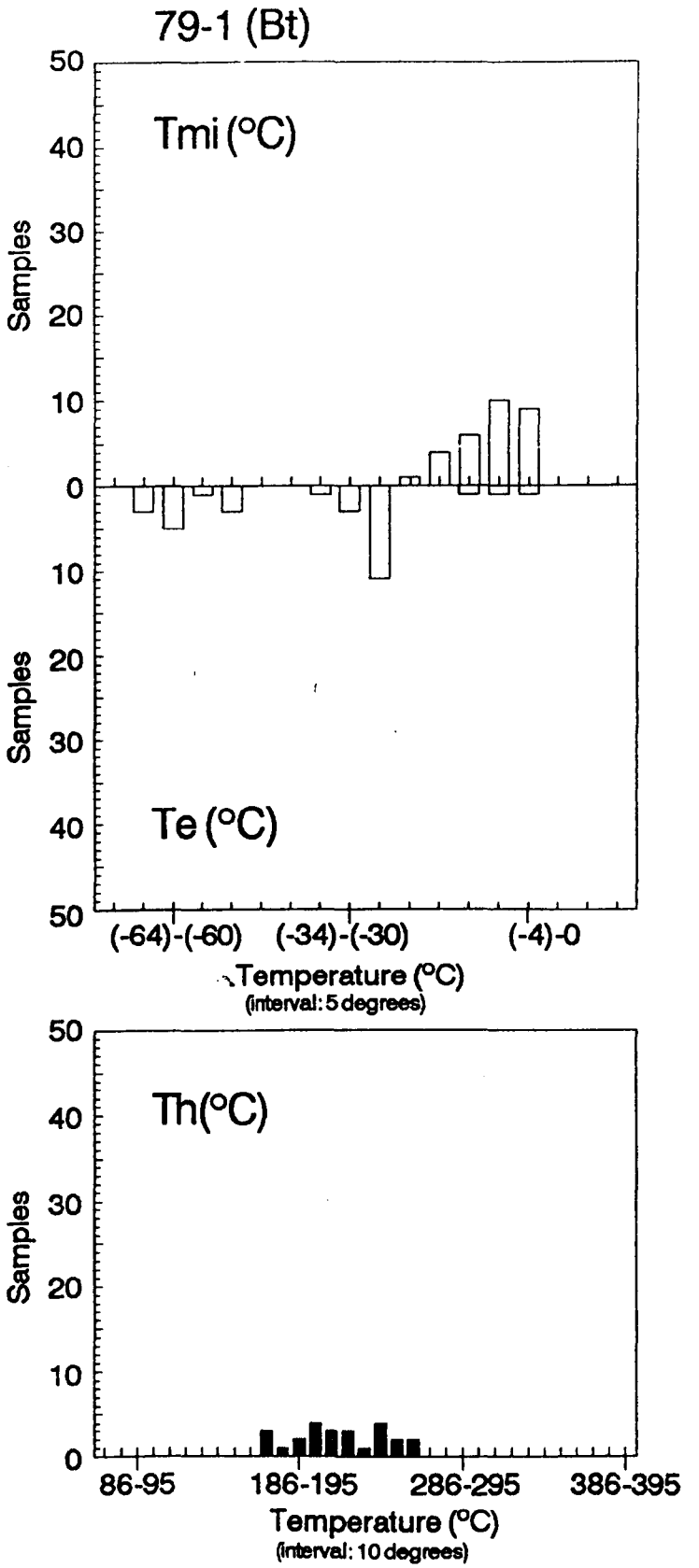

Fig. 6.8.a. Microthermometric data of inclusions in sample LC79-1 (barite).

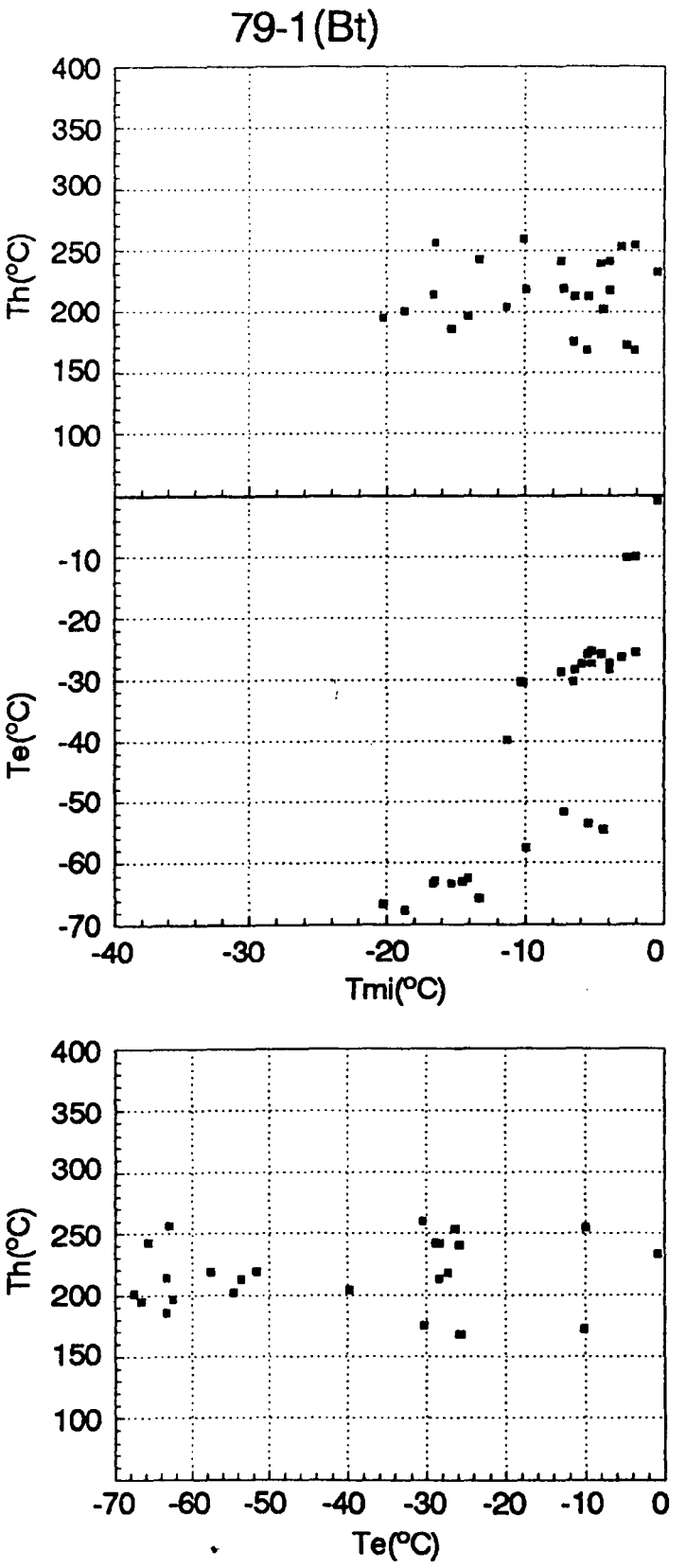

Fig. 6.8.b. Microthermometric data of inclusions in sample LC79-1 (barite).

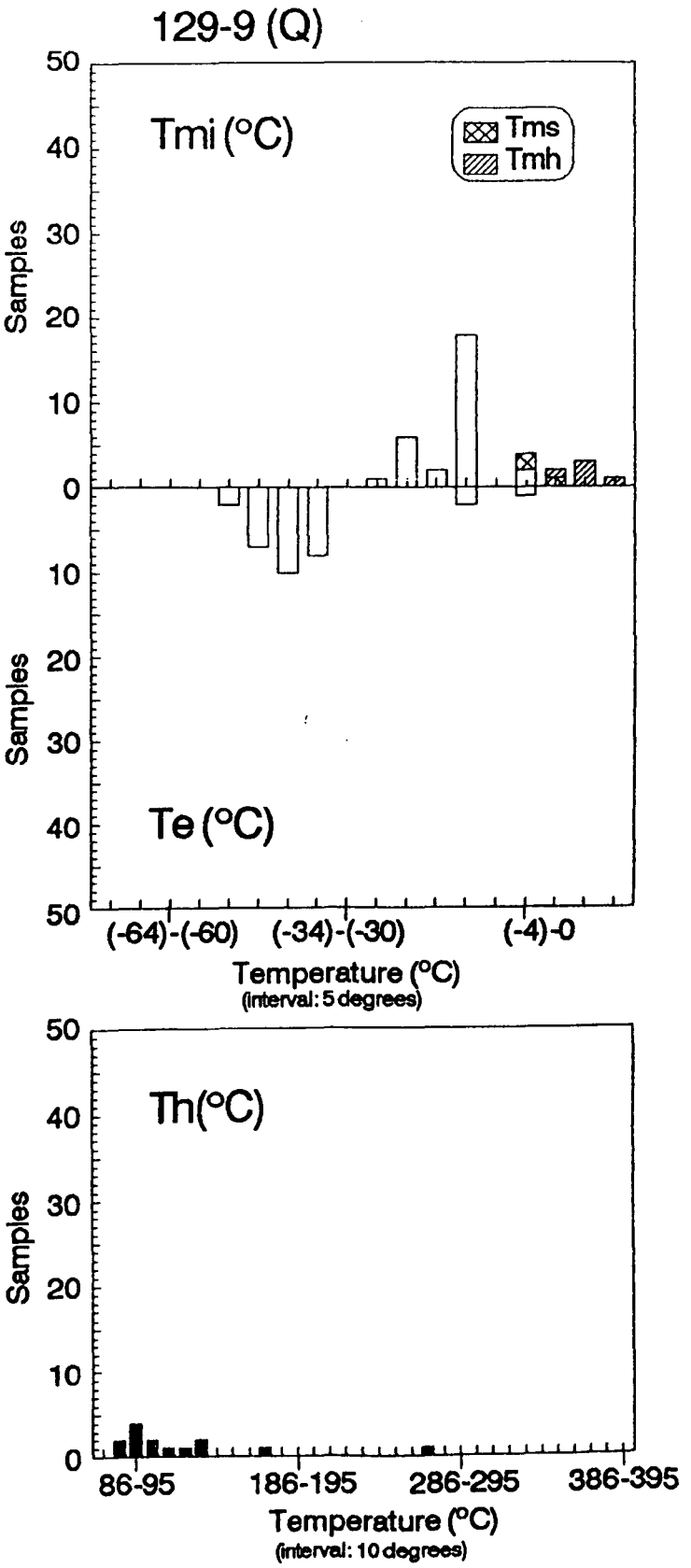

Fig. 6.9.a. Microthermometric data of inclusions in sample LC129-9 (quartz).

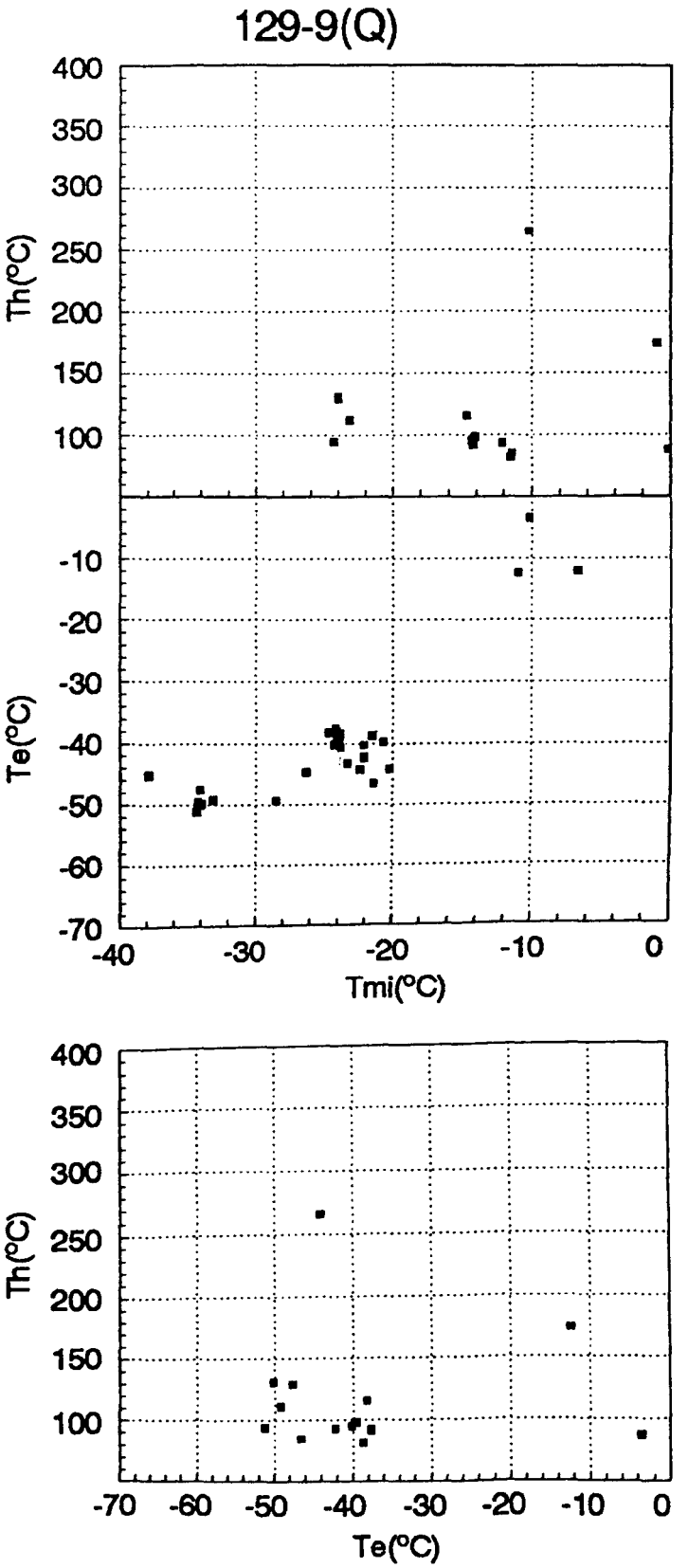

Fig. 6.9.b. Microthermometric data of inclusions in sample LC129-9 (quartz).

interpret in terms of solute compositions as no solid phases or hydrates except ice were observed during the cooling-heating runs.

Accurate determination of first melting temperatures is a difficult task due to the very small volumes of melt generated at the eutectic , particularly in low salinity fluids, or in brines with more than one dissolved salt, if the overall composition is not close to the eutectic minimum (Crawford, 1981). With only one exception (Te= -38.8), the recorded Te lies in the range of temperatures between the metastable eutectic temperature and the eutectic temperature in the systems H2O-NaCl and H_2O-KCl (-28° to 21.2°C, and -28° to -22.9°C, respectively, Davis at al, 1990). Metastable eutectics typically occur when heating frozen inclusions with very concentrated solutions, but also they may occur in solutions of moderate salinity (e.g. 5.2 wt % NaCl equivalent; Roedder, 1984).They are observed when inclusions are frozen quickly and the metastable assemblage ice plus halite (plus sylvite, if enough KCl is presented) forms instead of ice plus hydrohalite due to kinetic effects. On heating, in solutions with salinities lower than the eutectic concentration (27.60 wt % equivalent NaCl(1) in the NaCl-KCl-H_2O system, 23.20 wt % equivalent NaCl in the NaCl-H_2O system, after Hall et al, 1988), ice reacts with metastable halite to form hydrohalite at temperatures between the metastable eutectic and the eutectic points (Davis et al, 1990) but at those concentrations, all hydrohalite melts at the eutectic point. The observed final melting of ice on type Ib inclusions occurred at temperatures (Tmi) between -13° and -0.7°C (only one inclusion yielded Te= -19.9, i.e. 22.28 wt % equivalent NaCl) indicating total salinity of 16.88 tp 1.15 wt % equivalent NaCl(1). Despite the inaccuracy in recording the true first melting temperature, the observed Te in type Ib inclusions is always below the eutectic for NaCl-H_2O solutions and above the metastable eutectic, which indicates the

---

(1) total salinity is expressed here as wt % equivalent NaCl. As noted by Crawford (1981), this approach results in an error in estimating fluid salinities of up to 5 wt %. For the components found in type Ib inclusions, the resulting error will be an underestimation of the total salinity up to 1 %.

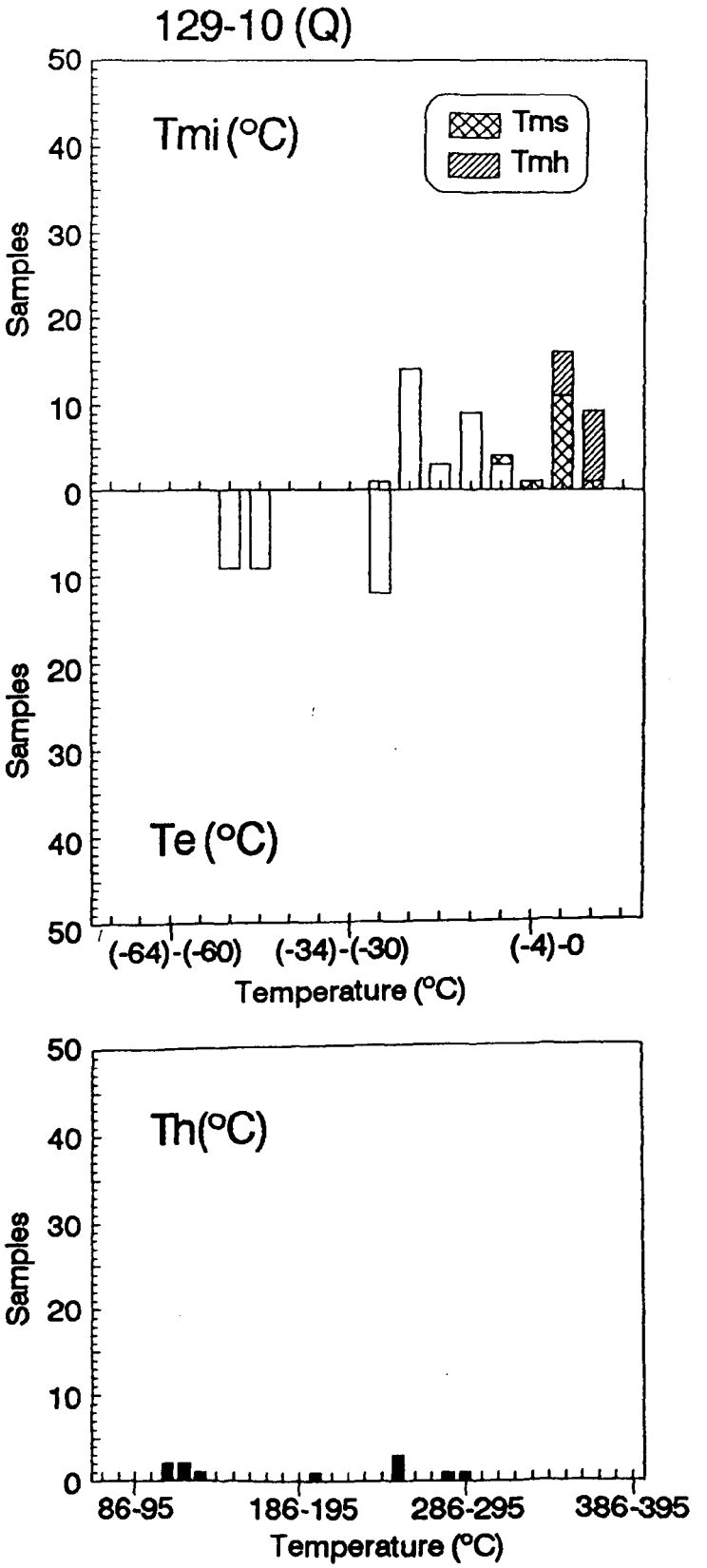

Fig. 6.10.a. Microthermometric data of inclusions in sample LC129-10 (quartz).

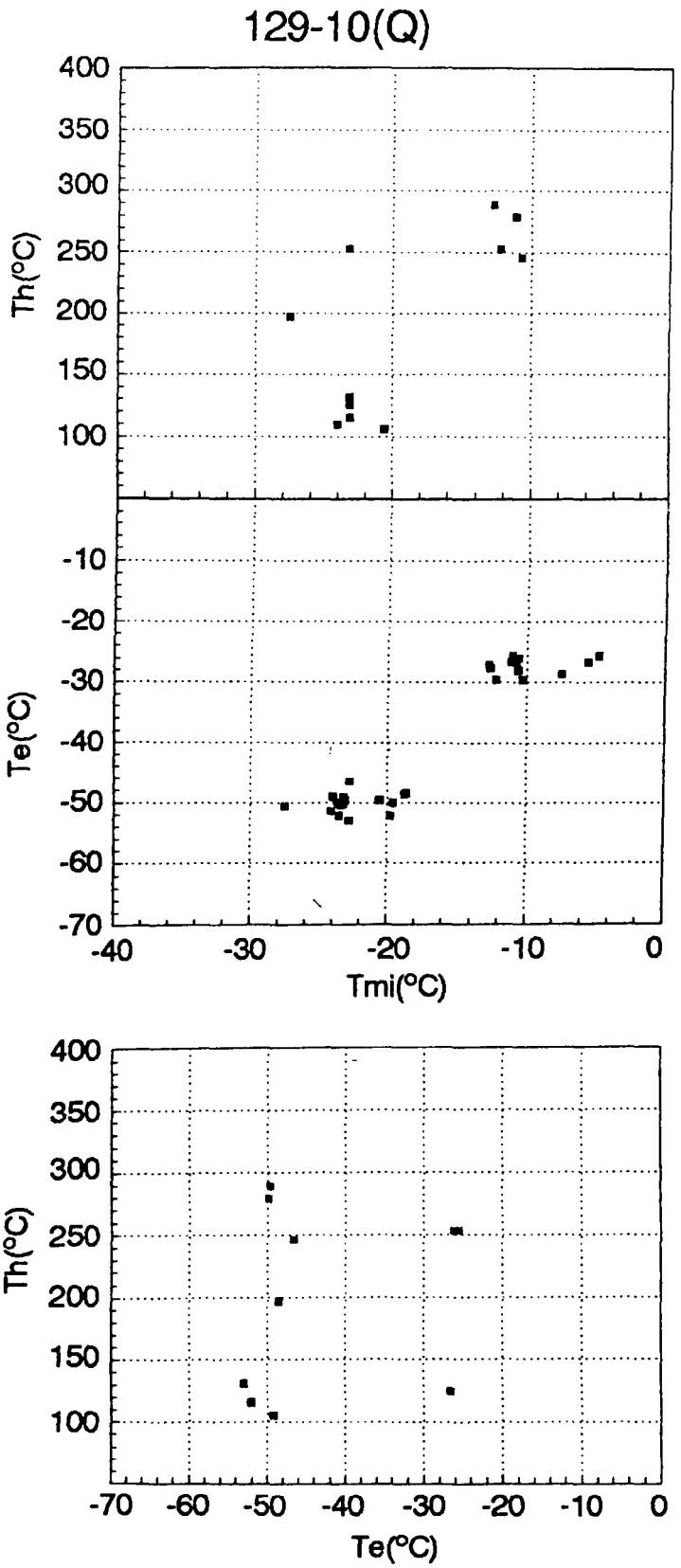

Fig. 6.10.b. Microthermometric data of inclusions in sample LC129-10 (quartz).

presence of additional components in the solution, likely KCl. As no hydrates, halite or sylvite were detected at temperatures above the eutectic temperature, the NaCl/(NaCl + KCl) ratio in the solutions must be close to the eutectic ratio (NaCl/(NaCl + KCl)= 0.78, Hall et al, 1988).

Melting behaviour of the type Ib inclusions has been assumed as being within the system NaCl-KCl-H_2O. To check this, qualitative X-ray dispersive energy (EDX) microanalysis following the technique described in appendix I and suggested by Ayora and Fontarnau (1990) were undertaken on some samples, but the results were rejected due to the noise induced by the host mineral as the size of the inclusions was too small.

Temperature of homogenization to the liquid phase (Th_2) lies in the range of 168-325°C.

Inclusions of type Ib were observed in samples of barite and quartz (LC288-1, LC79-1 and LC129-10, figs. 6.7.a-b, 6.8.a-b, 6.10.a-b), all from the Linares sector.

6.4.3.Type Ic inclusions.

Microthermometric and compositional data for type Ic inclusions are summarised in table 6.2.b.

Type Ic inclusions are liquid-rich aqueous saline inclusions. They are not primary inclusions as they occur along healed cracks but there is no petrographical evidence which may indicate unequivocally either secondary or pseudosecondary origin. The sizes of most of the inclusions vary from 20 to 50 μm, exceptionally they may reach 264 μm.

Inclusions of this type typically show two phases, H_2O liquid and H_2O vapour at room temperature. As in inclusions of type Ia and Ib, the vapour phase usually occupies less than 40% of the total apparent volume of the inclusion.

Temperature of homogenization to the liquid phase (Th_2) lies in the range 76° to 327°C. Apparent first melting was observed at temperatures (Te) between -68 and -37.3°C. These low Te reflect participation of solutes other than exclusively KCl and NaCl (e.g. $CaCl_2$, $MgCl_2$; but $MgCl_2$ is not relevant in neutral chloride waters, e.g. Giggenbach, 1988). Several systems may be found in natural inclusion fluids which show eutectic and metastable eutectic temperatures within the observed Te range.

In the system $NaCl-CaCl_2-H_2O$ a metastable eutectic is estimated at ~-70°C for the solids halite, ice and $CaCl_2-4H_2O$ (in practice, the metastable eutectic is partially controlled by the $CaCl_2$ concentration, Te being as low as -90°C for high concentrations; Davis et al, 1990). The stable eutectic involving the solids hydrohalite, ice and antarcticite ($CaCl_2.6H_2O$) occurs at -52°C.

A large number of type Ic inclusions show two optically distinct, very fine-grained solid phases at temperatures above the temperature of final melting of ice (Tm_i between -332° and -3.1°C). A yellowish, fine-grained solid phase melts at temperatures (Tms) ranging from -9.9° to 5.2°C. The other solid phase, greenish and coarser, melts at temperatures (Tmh) ranging from -1.5° to 10.3°C. One inclusion shows a cubic halite crystal at room temperature (Tmh = 213.6°C).

The melting temperatures above 0.1°C of these solid phases precludes their interpretation as hydrohalite or other KCl, $CaCl_2$ or $MgCl_2$ hydrate (e.g. Luzhnaya and Vereshtchetina, 1946; Linke, 1965; Davis et al, 1990). There is no evidence based on phase behaviour at low temperatures to support the presence of clathrates; moreover, the observed crystals show distinct optical features unlike those of clathrates.

Given the moderate to high salinity of the solutions in type Ic inclusions, the most probable solid phases are halite and sylvite. It is not possible to distinguish which solid corresponds to which salt as they are very fine-grained. However, the slope of

the halite-sylvite boundary curve (fig. 6.18) at the recorded temperatures of melting (close to the peritectic point) indicates that the last solid phase to melt is halite, after the melting of sylvite. The occurrence of halite and sylvite is supported by the observed Tmi close to the eutectic in the system H_2O-NaCl-KCl (Te=-22.9°C) in these inclusions. In those inclusions with no occurrence of solid phases after the last melting of ice, Tmi are significatively higher than -22.9°C.

Therefore, it seems clear that $CaCl_2$ and KCl are present in the type Ic inclusion solutions. Taking into account the data available from the literature about eutectics and metastable eutectics (above considered), the presence of $CaCl_2$ or/and other solutes is required to explain the observed low Te. As a) most of these temperatures are close to -52°C, b) $CaCl_2$ is dominant over $MgCl_2$ or other solutes with very low eutectic (e.g. LiCl) in most thermal solutions (e.g. Henley at al., (1984); Giggenbach, 1988), and c) this set of inclusions is ascribed to the late stage of mineralisation (S3) which is characterised by precipitation of large amounts of calcite, then type Ic inclusions may be compositionally interpreted in the H_2O-NaCl-KCl-$CaCl_2$ system although the participation of minor amounts of $MgCl_2$ or other components can not be ruled out.

To test the overall composition thus inferred, EDX microanalysis were performed on frozen inclusions in three samples, following the procedure described by Ayora and Fontarnau (1990). Again, the lack of inclusions with suitable sizes precluded the production of reliable results in two of the analysed samples due to excessive excitation of the host mineral by the electron beam. Microanalysis on sample LC129-10 yielded acceptable results for the qualitative determination of fluid compositions, Cl, Na, Ca and K being identified (fig. 6.17).

The salinity of type Ic inclusions may be expressed as wt % equivalent NaCl (i.e. the equivalent amount of NaCl necessary to depress the freezing point to the recorded Tmi temperatures) or alternatively, melting temperatures of solid phases may be used in

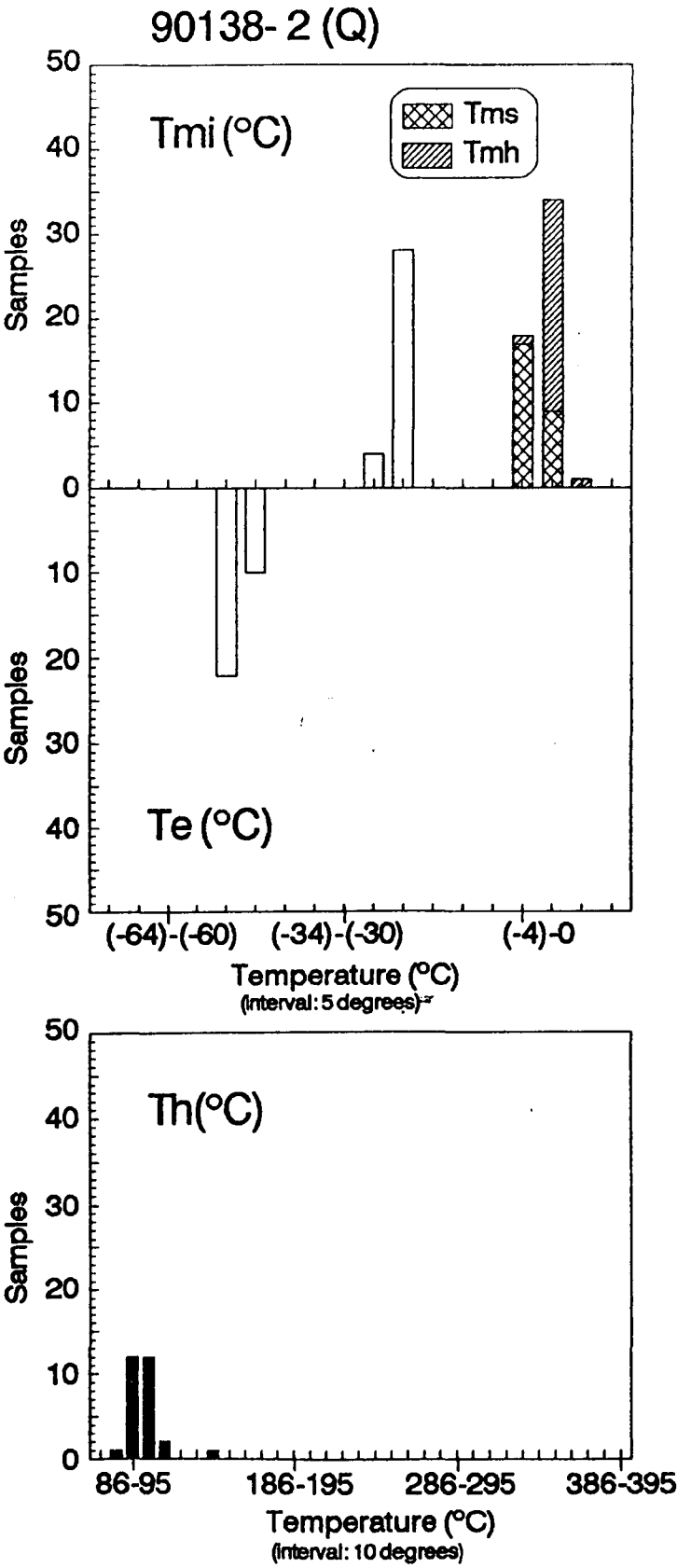

Fig. 6.11.a. Microthermometric data of inclusions in sample LC90138-2 (quartz).

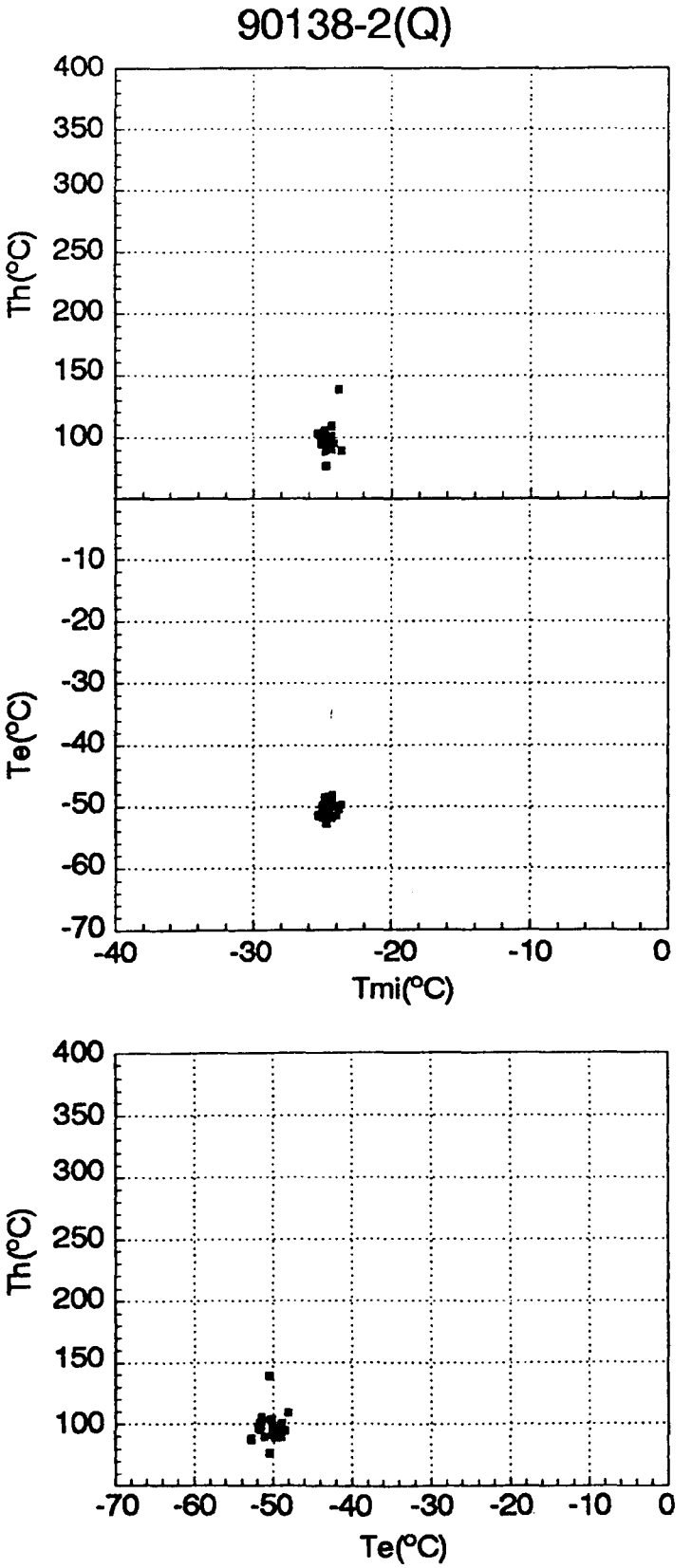

Fig. 6.11.b. Microthermometric data of inclusions in sample LC90138-2 (quartz).

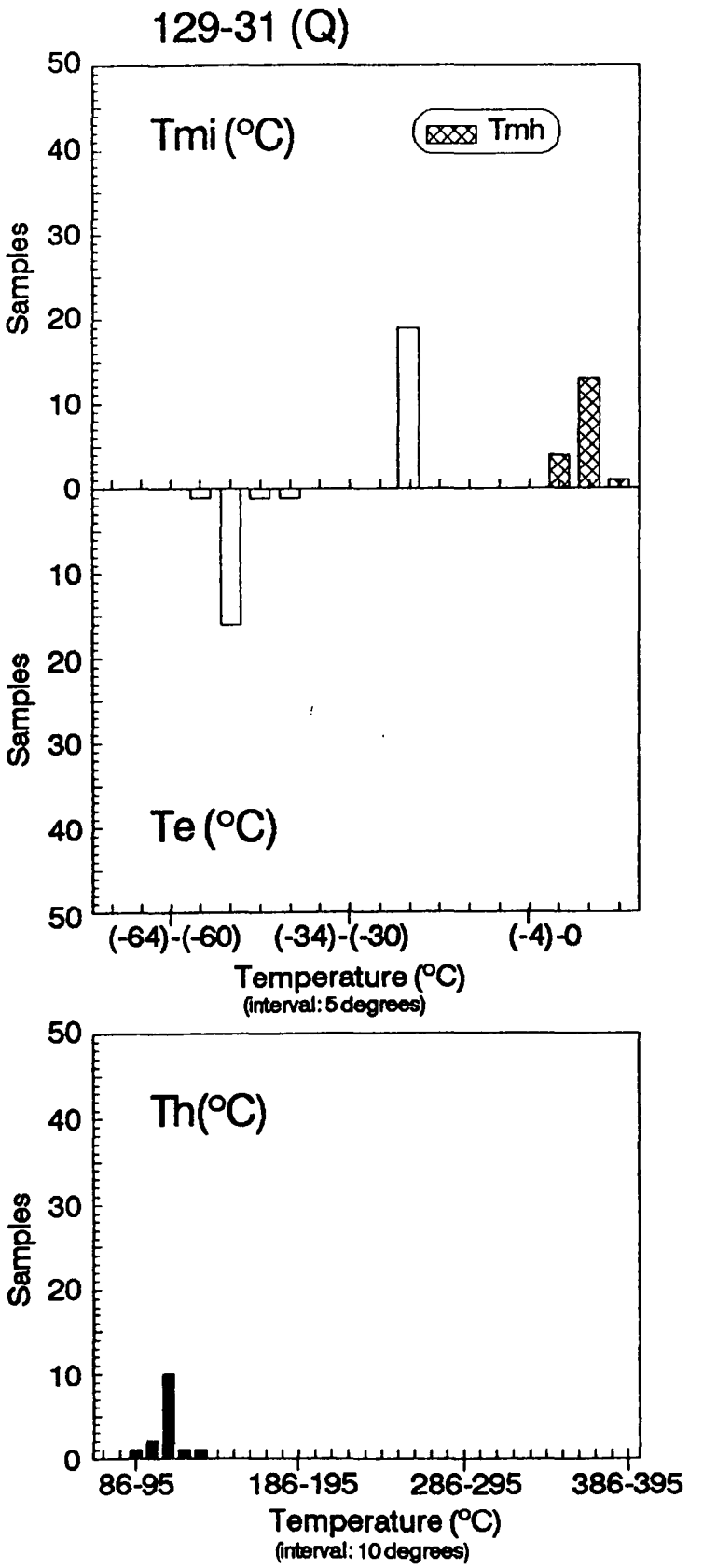

Fig. 6.12.a. Microthermometric data of inclusions in sample LC129-31 (quartz).

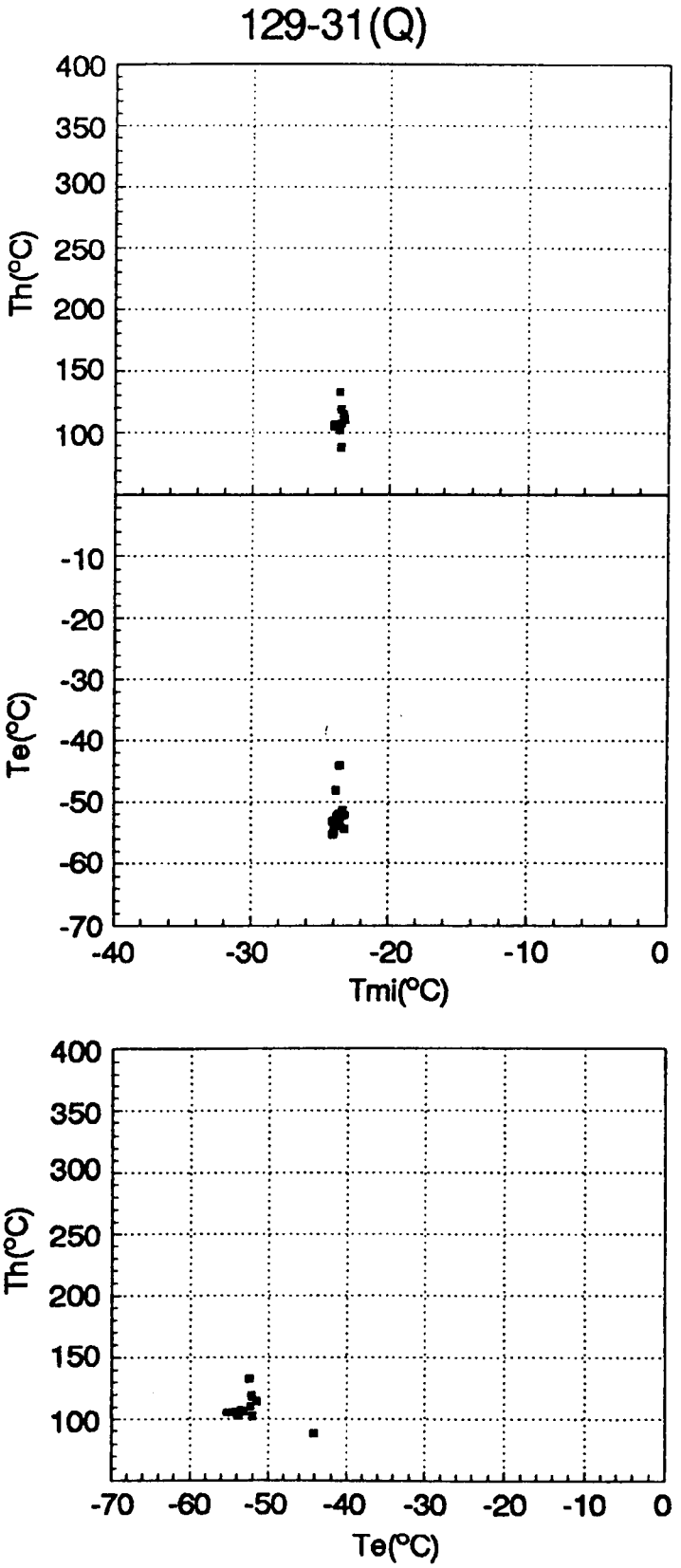

Fig. 6.12.b. Microthermometric data of inclusions in sample LC129-31 (quartz).

the determination of salt ratios (NaCl/total salt, KCl/total salt, and $CaCl_2$/total salt, where total salt = NaCl+KCl+$CaCl_2$) from temperature contours and phase relations in the H_2O- rich parts of the quaternary system H_2O-NaCl-KCl-$CaCl_2$ (Konnerup-Madsen, 1979, based on data from Linke, 1965) (fig.6.16). Determination of the compositional points in the interior of the tetrahedron is cumbersome and time-consuming, as an iterative process is required. The alternative procedure is to use the tetrahedron sides to calculate the salt ratios as in a two-salt system, projecting later the binary salt ratios on the base of the tetrahedron to determine the tertiary salt ratios. The overall salinity (wt % total salt) may be approached by calculating the arithmetic mean of the salinities calculated in each H_2O-salt side of the tetrahedron. This approach results in certain error as salinity is extrapolated without any consideration to phase boundaries and isotherms in the interior of the tetrahedron but the validity of this procedure is demonstrated by the fact that the calculated salinities lie between the overall salinity at the eutectic point in the H_2O-NaCl-KCl system (27.6 wt %, a minimum total salinity) and the approximate salinity estimated from melting temperatures of halite (maximum salinity). The error implicit in the total salinities determined using the procedure described here will always be smaller than the error produced if total salinity is calculated as wt % equivalent NaCl.

Inclusions of type Ic were observed in samples of barite and quartz (LC288-1, LC79-1, LC129-10, LC90138-2 and LC129-31, figs 6.7.a-b, 6.10.a-b, 6.11.a-b, 6.12.a-b) all from the Linares sector.

6.4.4. Type II inclusions.

Microthermometric and compositional data on type II inclusions are presented in tables 6.3.a-b.

Inclusions of this type commonly appear in healed cracks either as secondary or pseudosecondary inclusions.

Inclus. num..	type	$TmCO_2$ (^oC)	Tmi (^oC)	Tmhy (^oC)	$TpCO_2$ (^oC)	Th (^oC)	Vol.Frac. CO2 %
1	s?	-57.3		8.7	22.7	353.0	80
2	s?	-57		8.8	25.9	343.4	75
3	s?	-57.5	-5.1	8.3	23.9	373.0	80
4	s?	-57.3	-5.7	8.6	24.1	326.0	80
5	s?	-57.1	-4.9	8.9	25.2	296.1	50
6	s?	-57.4		8.5	24.1	373.0	80
7	s?	-57	-4.3	8.5	26 (v)	240.6	5
8	s?	-57.4		9.0	26.0	310.9	50
9	s?	-57.3	-3.6	8.8	25.8	295.2	50
10	s?	-57.4	-6.2	8.8	23.9	297	50

Table 6.3.a. Representative microthermometric data from inclusions in the H_2O-NaCl-CO_2 system.

Inclus. num.	XH_2O	XCH_4	XCO_2	XNaCl	wt % eq. NaCl	ρCO_2 (g/cc)	VH_2O (cc/mole)	VH_2O (cc/mole)
1	0.444	0.035	0.551	0.003	2.61	0.796	18.35	59.21
2	0.532	0.015	0.464	0.004	2.42	0.774	18.34	63.11
3	0.449	0.043	0.546	0.004	3.38	0.784	18.38	60.49
4	0.450	0.035	0.545	0.004	2.80	0.781	18.36	60.72
5	0.767	0.009	0.226	0.005	2.22	0.856	18.34	62.10
6	0.450	0.040	0.545	0.004	3.00	0.781	18.37	60.72
7	.985	------	0.005	0.009	3.00	0.971	18.38	172.10
8	.771	0.017	0.223	0.005	2.02	0.848	18.33	63.26
9	.769	0.015	0.224	0.006	2.42	0.852	18.35	62.96
10	.762	0.017	0.231	0.006	2.42	0.866	18.34	60.49

Table 6.3.b. Representative compositional data from inclusions in the H_2O-NaCl-CO_2 system.

These inclusions show three phases, H_2O liquid, CO_2 liquid and CO_2 vapour at room temperature. The observed relative volume of the single CO_2 phase at 40°C usually varies from 85 to 50 % of the inclusion volume (only five cases of carbonaceous-poor inclusions were observed).

Visual volumetric estimations may constitute a serious source of error in the calculation of bulk compositions. Several techniques have been proposed for the determination of phase volumes of inclusions in the system CO_2-H_2O-NaCl using microthermometric measurements (e.g. Parry, 1986; Schwartz, 1989). Parry's procedure is an iterative technique which is cumbersome to use. The graphical procedure presented by Schwartz (1989) is straightforward but limited to salinities from 0 to 6 wt % equivalent NaCl, moreover, volumetric determination for certain densities and temperatures is not always possible in the Schwartz's diagram. The relative volume values considered in this work are from visual estimations. As noted below, the VCO_2 and XCO_2 values show some consistency when P-T-XCO_2 space is considered.

The recorded temperature of CO_2 melting ($TmCO_2$) varies from -56.8° to -57.6°C reflecting minor amounts of other gases (although it may be assumed that the depression of $TmCO_2$ is produced by the presence of CH_4 as this compound is usually dominant over N_2, H_2S, etc in natural inclusion fluids).

Carbonaceous phases homogenize in the liquid phase at temperatures (Tp_{CO2}) between 22.2° and 26.0°C. A few vapour-rich inclusions homogenize in the vapour phase at temperatures (Tp_{CO2v}) between 26° and 26.8°C.

First melting of ice in the aqueous portion of these inclusions occurs at Te between -19.3° and -9.3°C, showing that the water is mainly an NaCl solution. Temperatures of final melting of ice (Tmi) vary from -5.8° to -3.0°C. Clathrate final melting was observed at temperatures (Tmhy) ranging from 4.6° to 9.1°C.

Type II inclusions have low to moderate salinities ranging from 1.32 to 9.69 wt % equivalent NaCl, the majority from 2 to 5 % wt as calculated from Tmhy (Bozzo et al, 1973).

The procedure suggested by Swanenberg (1979) has been used in order to determine the bulk composition of the carbonaceous member in the inclusion. This procedure requires both the final melting temperature of CO_2 (Tm_{CO2}) and the filling degree (volumetric ratio liquid /liquid + gas) at that Tm_{CO2}. Calculated CH_4 molar fractions in the carbonaceous phase range from 0.005 to 0.06, indicating that it is nearly pure CO_2. Similar results may be obtained using Tm_{CO2} and Th_{CO2} according to Shepherd et al (1985).

In most of the type II inclusions (CO_2-rich) the aqueous phase homogenized into the carbonaceous liquid phase at temperatures (Th_{CO2L}) between 293.4° and 373°C. In two cases (CO_2-poor inclusions) carbonaceous vapour phase homogenized into aqueous liquid phase at Th_L= 240.6° and 245.4°C.

Inclusions of type II were only observed in the sample LC901741-3a (El Guindo Lode, at the El Centenillo-La Carolina-Santa Elena sector), co-existing with apparently coeval type Ia inclusions (figs.6.5.a-b).

6.5.Temperature and pressure of trapping.

6.5.1.Homogenization involving aqueous phases.

Four modes of homogenization involving aqueous phases were observed in this study:

1.Homogenization of aqueous vapour to co-existing aqueous liquid ($L_{H2O} + V_{H2O} = L_{H2O}$).

2.Homogenization of aqueous liquid to co-existing vapour ($L_{H2O} + V_{H2O} = V_{H2O}$).

3.Homogenization of carbonaceous liquid to co-existing aqueous liquid ($L_{H2O} + L_{CO2} = L_{H2O}$).

4.Homogenization of aqueous liquid to co-existing carbonaceous liquid ($L_{H2O} + L_{CO2} = L_{CO2}$).

The complete range of homogenization temperatures in the whole set of inclusions is highly scattered between 76° to 392°C (fig. 6.1.b). Although each type of inclusion shows wide ranges of Th, type Ia commonly homogenize at higher temperatures than types Ib and Ic. Type Ic inclusions in quartz homogenize at the lowest temperatures recorded during the present study.

Type Ia inclusions homogenize in a wide range but inclusions in samples from El Centenillo-La Carolina-Santa Elena sector commonly homogenize at higher temperatures than those in samples from Linares.

Type II inclusions homogenize at Th_{CO2L} between 293.4° and 373°C. These high temperatures only were observed as Th_L in type Ic inclusions.

Homogenization measurements on inclusions in barite were carried out with great caution to avoid stretching leakage and runs were repeated to ensure reproducibility. Th of inclusions suspected of being leaked or stretched were rejected. Despite the careful collection of data, the homogenization temperature may be overestimated. However, Th of type Ia and Ib inclusions in barite are consistent with those for inclusions in quartz (fig. 6.1.b).

6.5.2.Fluid Isochores.

Interpretation of fluid inclusion trapping conditions is based on the assumption that the inclusions act as isochoric systems since volume and hence densities of fluids have remained constant since trapping, unless there is evidence that necking, stretching or leaking have taken place. If the above assumption is fulfilled, then a line of constant density or molar volume (isochore) may be drawn in P-T space on the basis of P-V-T properties of the fluids. Different procedures can be used to draw isochores for specific types of inclusions on the basis of the available data.

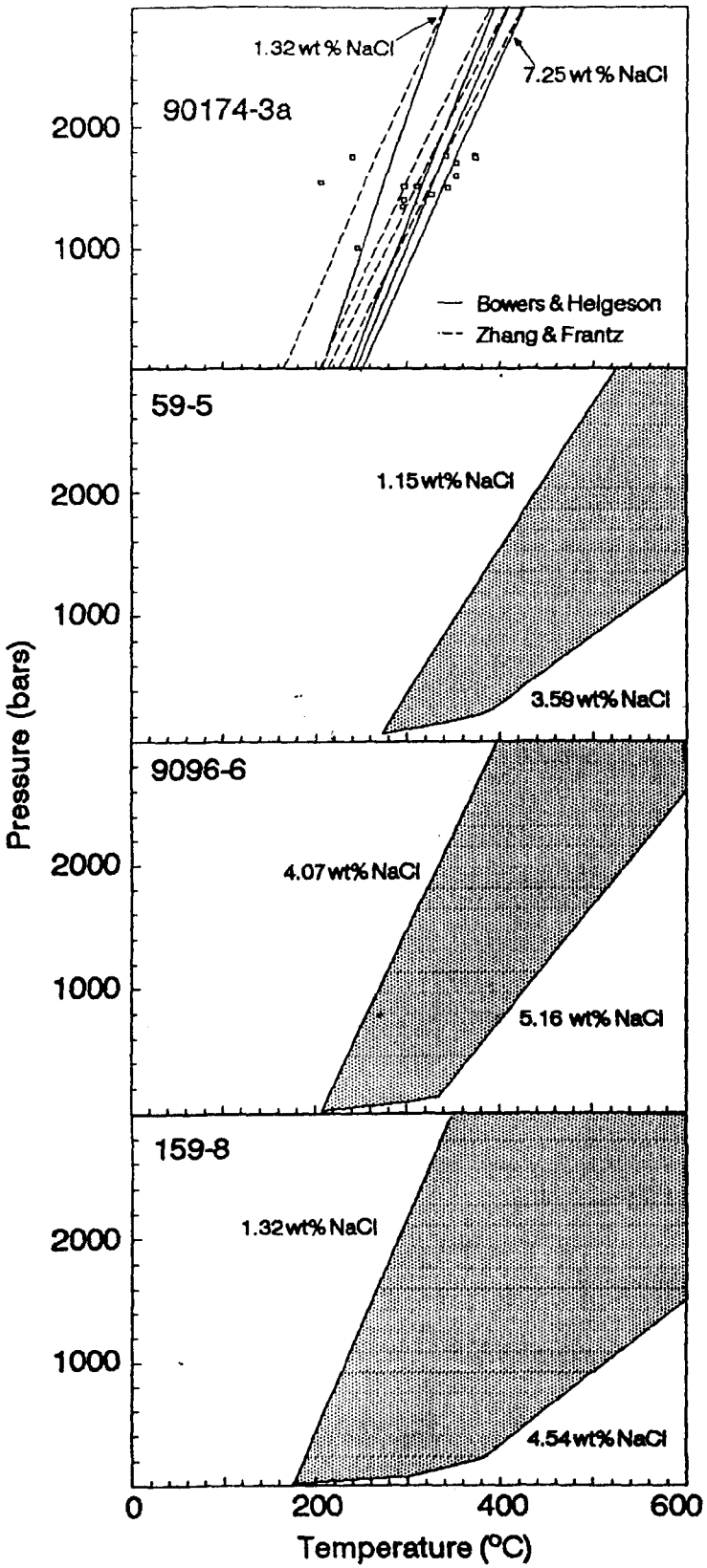

Fig. 6.13.a. P-T space from isochores of inclusions in the $NaCl-H_2O$ system (Zhang & Frantz, 1987). Graph of sample LC90174-3a shows the points of Th projected onto the respective isochores (Bowers & Helgenson, 1983) for type II inclusions.

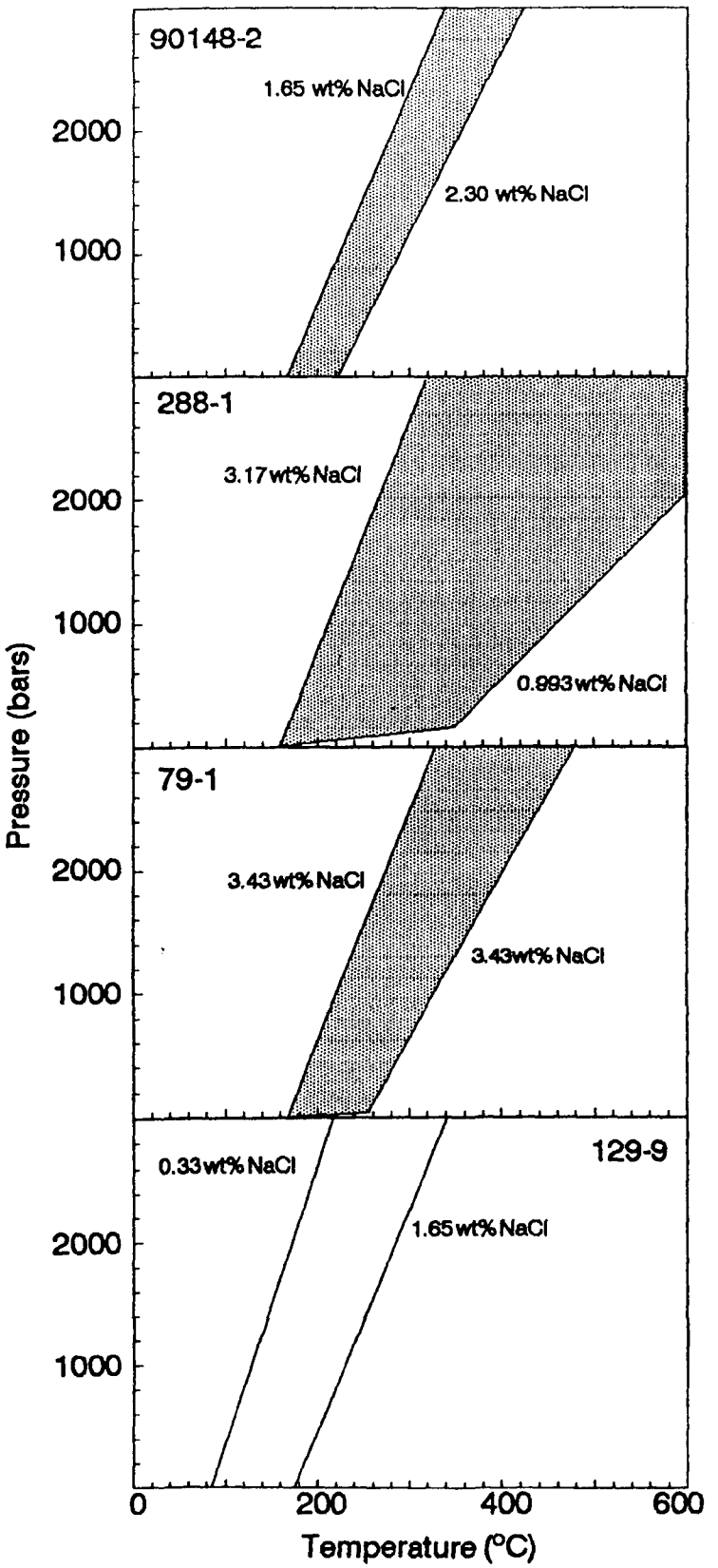

Fig. 6.13.b. P-T space from isochores of inclusions in the $NaCl-H_2O$ system (Zhang & Frantz, 1987).

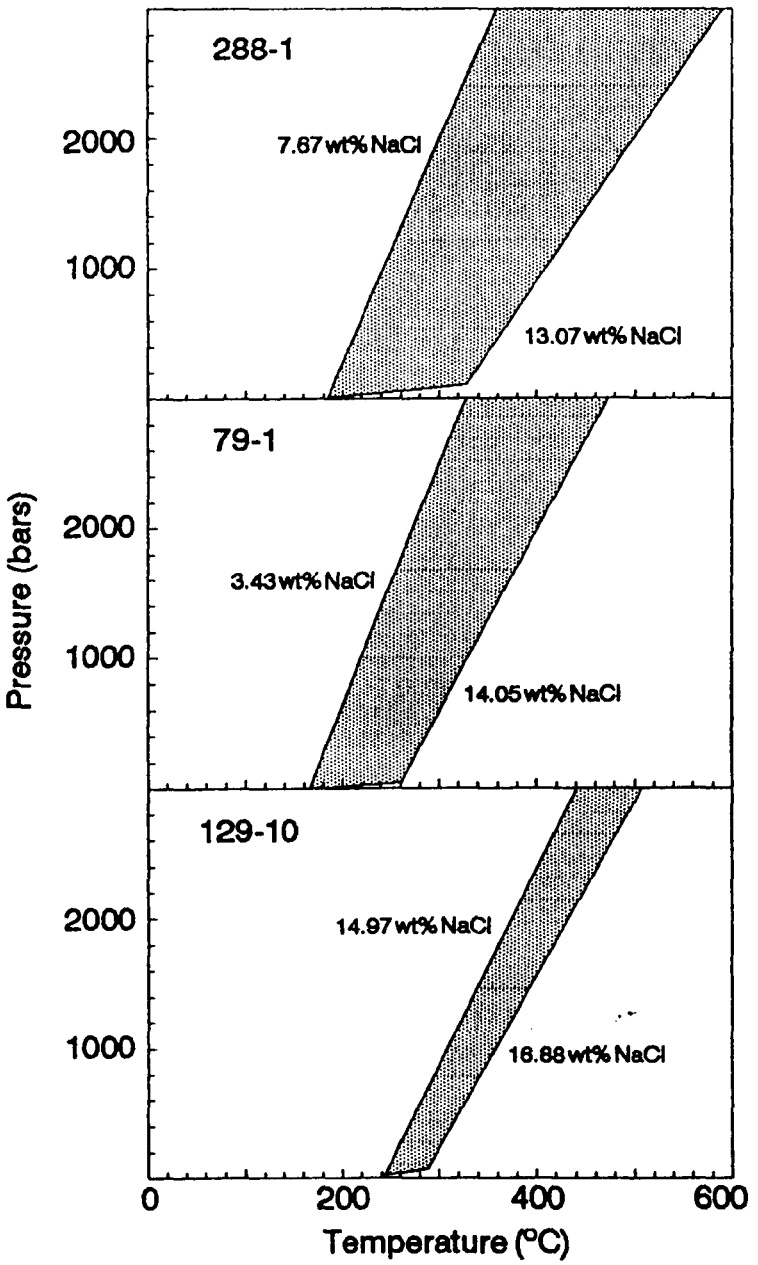

Fig. 6.14. P-T space from isochores of inclusions in the NaCl-KCl-H_2O system (Zhang & Frantz, 1987).

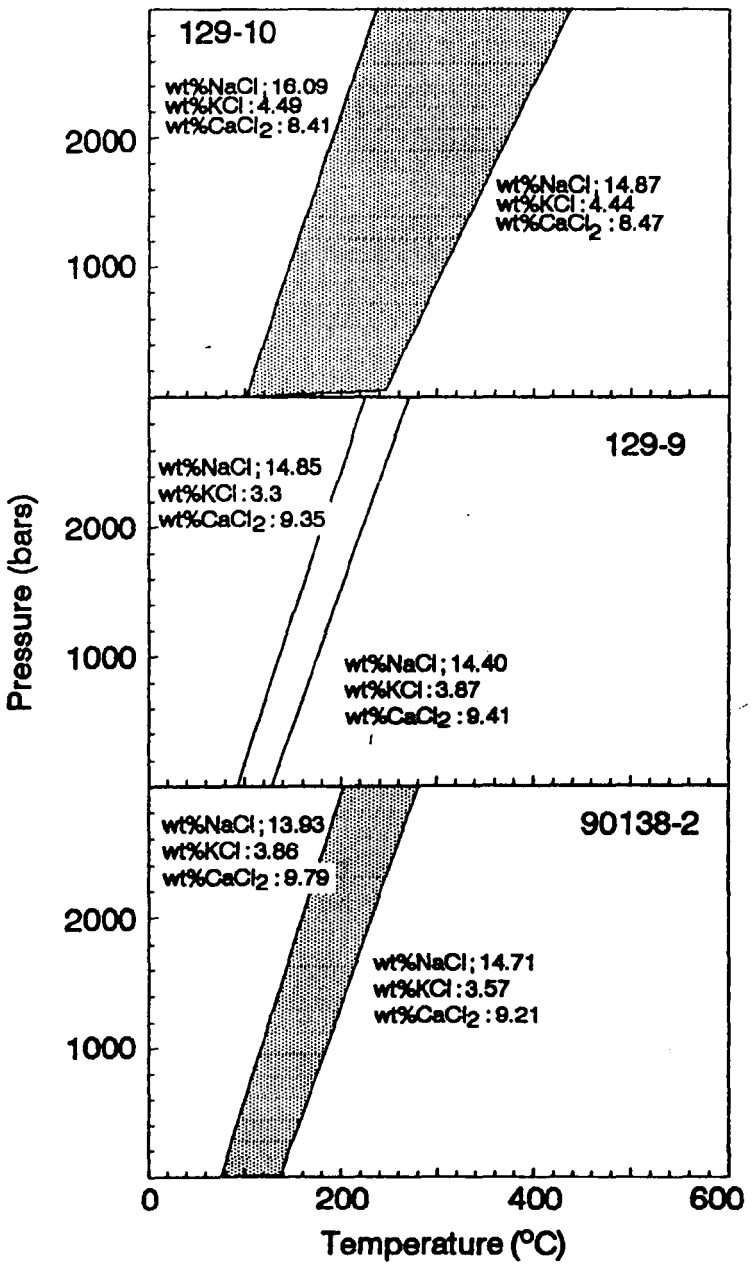

Fig. 6.15. P-T space from isochores of inclusions in the $NaCl-KCl-CaCl_2-H_2O$ system (Zhang & Frantz, 1987).

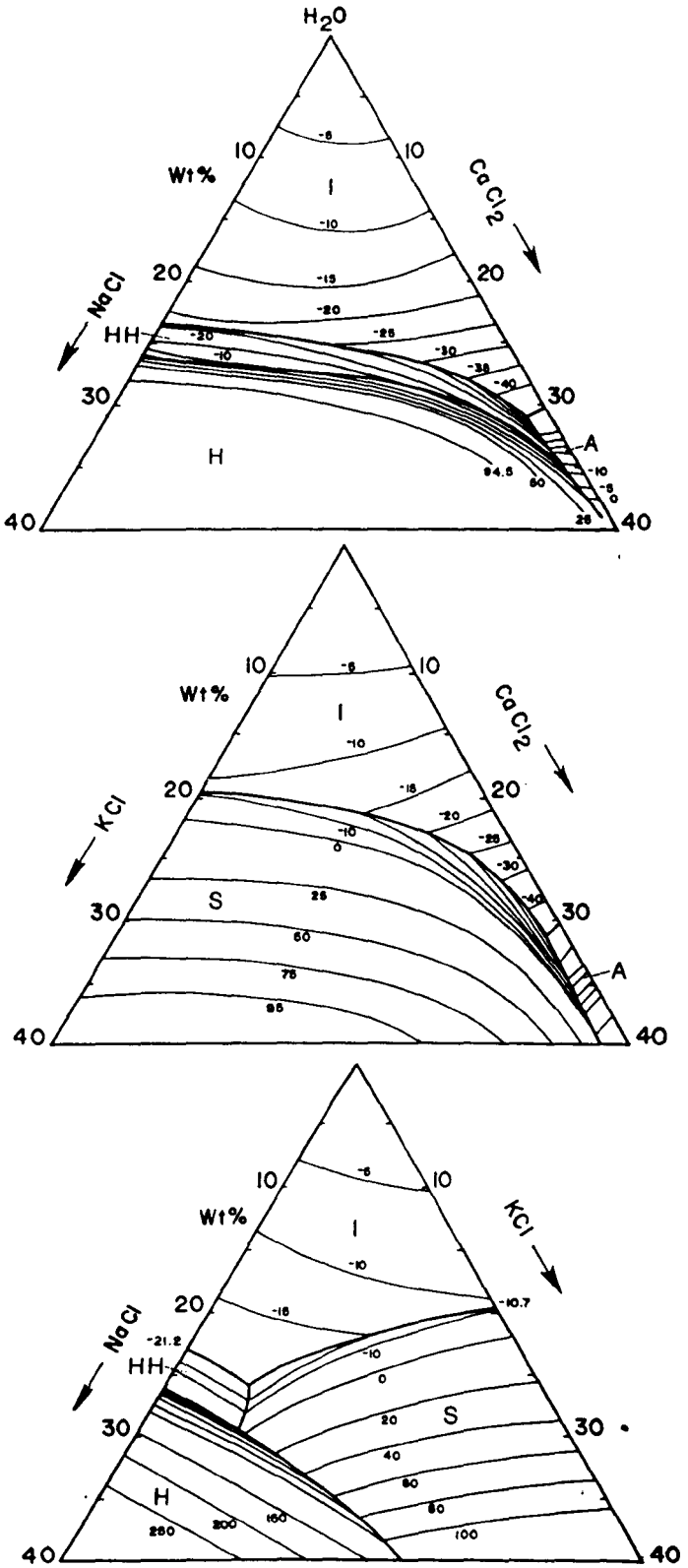

Fig. 6.16. Temperature contours and phase relations in the H_2O-rich part of the H_2O-NaCl-KCl-$CaCl_2$ tetrahedron (Konnerup-Madsen, 1979; based on data from Linke, 1965).

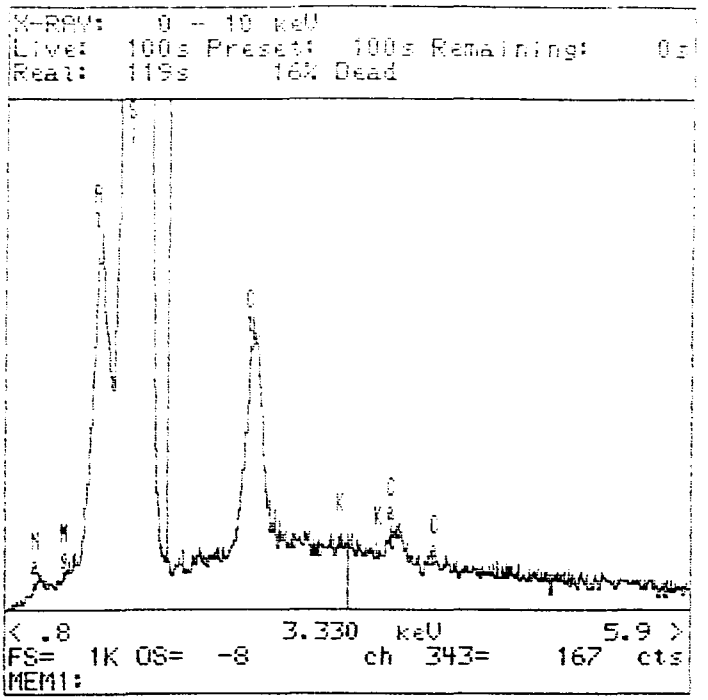

Fig. 6.17. EDX microanalysis of a frozen inclusion (sample LC129-10).

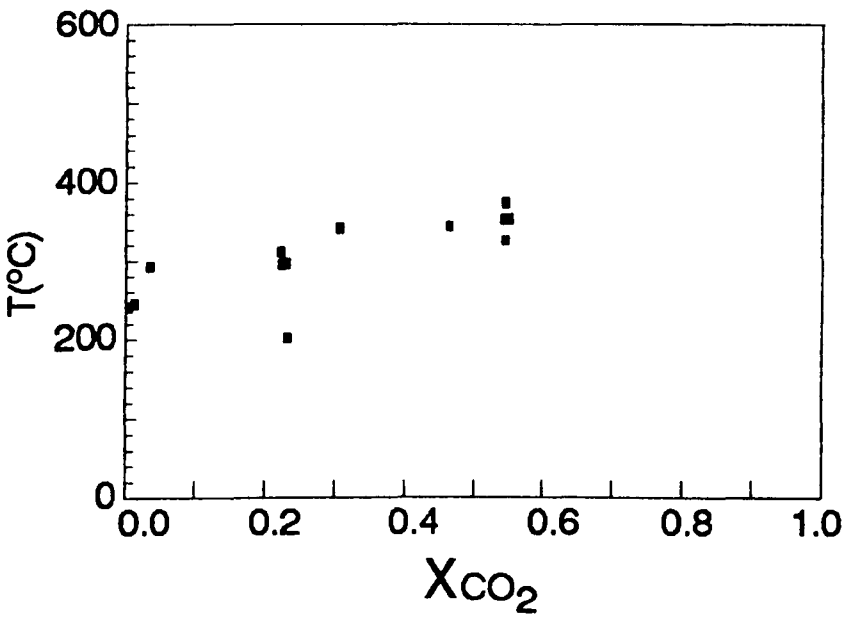

Fig. 6.18. Variation of Tn versus XCO_2 in type Ia and type II inclusions (sample LC90174-3a).

For aqueous inclusions of types Ia and Ib, the data from Zhang and Frantz (1987) was used for drawing the isochore and the determination of the bulk density (figs. 6.13.a-b, 6.14.a-b.) In H_2O-CO_2-NaCl (type II) inclusions the isochores were calculated after Bowers and Helgeson (1983) (fig. 6.13.a). Both calculations were done using the computer program Flincor (Brown, 1989). In type Ib (H_2O-NaCl-KCl) inclusions the calculation was as for the H_2O-NaCl system as isochores for the H_2O-NaCl and H_2O-KCl systems are almost identical (Zhang and Frantz, 1987). In type II inclusions, the amounts of CH_4 are so small that the resulting error is negligible (there is no substantial variation of the CO_2 densities).

Isochores for type Ic (H_2O-NaCl-KCl-CaCl) were calculated directly on a computer spreadsheet following the procedure suggested by Zhang and Frantz (1987) for solutions containing the three solutes (fig. 6.15).

6.5.3.Timing of trapping.

None of the studied samples showed clear evidence of inclusions of primary origin. All samples from the El Centenillo-La Carolina-Santa Elena sector exhibit almost exclusively type Ia inclusions. Alternatively, most of the samples from the Linares sector exhibit at least two types of inclusions, commonly type Ib and Ic.

Only type Ia inclusions occur in 'milky' quartz veinlets in mylonites (LC9096-6), and in 'milky' quartz with galena (LC159-8 and LC90148-2). Type Ia and type II inclusions appear in 'milky' quartz with sphalerite (LC90174-3a). Samples of barite (LC288-1 and LC79-1) and 'glassy' quartz (LC129-9 and LC129-10) show all aqueous saline types (Ia, Ib and Ic). Only type Ic inclusions were found in large monocrystals of 'glassy' quartz associated with pockets of pyrite and chalcopyrite (LC90138-2 and LC129-31).

Since i) the different types of inclusions seem to be restricted to different generations of host quartz related to the

ore and ii) the types of inclusions in barite samples include only those types found in the late generation of ('glassy') quartz, a pseudosecondary origin may be assumed for most of the studied inclusions. In this case, the trapped inclusion fluids reflect the conditions during crystal growth and the different generations of inclusions and their microthermometric and compositional data may be ascribed to stages of ore deposition (see chapter 4 for paragenetic assemblages relative to these stages). Types Ia and II inclusions ('milky' quartz) were trapped during the S1 to early S2 stages. Type Ib inclusions were trapped during the S2 stage ('milky' quartz plus barite). Trapping of type Ic inclusions ('glassy' quartz) took place during the late S2 to early S3 stage.

6.5.4.Temperature and pressure of trapping.

The homogenization temperature indicates the point at which the inclusion fluid as a whole leaves the liquid-vapour phase boundary and moves into a single phase field. The formation conditions of the inclusion must lie along an isochore from this point relative to Th (the minimum temperature of trapping) in P-T space, if it is assumed that the inclusion fluid was trapped as a single (homogeneous) supercritical phase.

Normally, to determine the true temperature of trapping (Tt), hence the pressure of trapping (Pt), another independent geobarometer or geothermometer is required. Alternatively Tt determinations may be based on simultaneous trapping of two immiscible fluids if present. In that case, both P and T can be determined from the Th values of the two inclusions (Roedder, 1984). A singular case of immiscibility occurs in boiling fluids, when a boiling liquid and its co-existing vapour phase are trapped separately. Such pairs are readily identified because Th must be identical. The homogenization temperature projected onto the boiling curve of that fluid indicates the (vapour) pressure. The main difference between immiscibility and boiling is that in boiling, vapour and liquid phase are compositionally the same fluid while in immiscibility the phases are compositionally distinct.

In the studied inclusions, no unequivocal evidence of boiling was found.

The mutual solubility of CO_2 and H_2O varies greatly with temperature and fluid composition. In a pure CO_2-H_2O system the field for co-existing two phases has been known to extend to 260°C at 0.64 Kb and 7 mole CO_2 (Burrus, 1981). Even at this CO_2-poor fluid, the immiscibility field is quite significant for a geological process to occur. The addition of NaCl or other components of higher critical point should increase this field to higher temperature and pressure (Gehrig et al, 1979; Bowers and Helgeson, 1983)

In most of type II (carbonaceous-rich) inclusions, the aqueous phase homogenized into the liquid carbonaceous phase at Th_{CO2} temperatures ranging from 193.4° to 373.0°C. In only three inclusions out of 28, did the liquid carbonaceous phase homogenize into the aqueous liquid phase, giving Th_L temperatures from 201.9° to 245.4°C. Type II inclusions co-exist with type Ia (liquid-rich H_2O-NaCl inclusions). The amount of CO_2 in these aqueous inclusions is constrained to $XCO_2 \leq 0.05$ (Burrus, 1981), as no clathrate or 'liquid' CO_2 were detected. In fact, the high Tmi temperatures preclude XCO_2 larger than 0.05 (*c.f.* Hedenquist and Henley, 1985). Th_L temperatures of these type Ia inclusions vary from 166.8° to 227.6°C.

Fig 6.18 shows the variation of Th versus XCO_2 of type II inclusions (those homogenizing to liquid CO_2) in sample LC90174-3a. Type Ia inclusions are also included for $XCO_2 = 0$. The highest Th temperatures correspond to those inclusions with highest XCO_2 while the lowest T_h temperatures are found in type Ia inclusions. Moreover, the overall distribution of the points is fairly consistent with the shape of the CO_2-H_2O-NaCl solvus curve at its H2O-rich side at pressures above 500 bars, considering that there are some variation due to differences in salinity (*c.f.* Bowers and Helgeson, 1983). Therefore it is reasonable to assume the simultaneous entrapment of type II and type Ia inclusions in a regime of fluid unmixing (CO_2 loss) when the system was on or

close to the solvus curve. The main objection to this interpretation is that the apparent Th vs. XCO_2 relations are not a conclusive proof for the coevality of type II and type Ia inclusions.

The isochores relative to type Ia inclusions and Th projected onto the respective isochores for type II inclusions in sample LC90974-3a are displayed in fig. 6.13.a. Most of the projected Th/Ph points relative to carbonaceous inclusions are close or within the P-T space defined by the H_2O-NaCl isochores, as expected if the conditions of both type of inclusions are close to the solvus. In this particular case Ph may be considered as pressure of trapping (Pt), as Th/Ph on are close or on the H_2O-NaCl isochores (i.e. the intersection of both isochores is close to Th/Ph points). The Pt thus determined ranges from 1,075 to 1,765 bars.

If the P-T space defined by H_2O-NaCl isochores relative to samples LC59-5, LC9096-6 and LC159-8 is considered (fig. 6.13.a), the Pt range determined from immiscibility in inclusions from the sample LC90174-3a is too high to fit on the overall range of isochores at reasonable Tt temperatures for this type of ore deposits (Tt < 400°C, e.g. Guilbert and Park 1986, and references therein). Considering that the lodes (and the pipes and veinlets found in the Permian-Triassic basal beds) are open-space filling bodies related to extensional/transtensional faults (see chapter 4), the vein system is assumed to be open to the surface at the time of the ore emplacement (i.e. the dominant pressure was hydrostatic). Obviously, is not possible to explain the Pt calculated above in terms of hydrostatic pressure.

The minimum depth required for fluids (5 wt% equivalent NaCl) to be below the boiling point at 370 °C (calculated by extrapolation of the boiling point curves of Haas, 1971) is around 2,800 m (3,210 m for pure H_2O). The maximum depth calculated from the thickness of the pre-Ladinian succession above the Late-Hercynian unconformity (≈2,900 m in the Iberian peninsula; Virgili et al., 1983; Sopeña et al., 1988) plus the actual maximum depth

of occurrence of the ore from that unconformity (≈600 m, Enadimsa, 1971) is around 3,500 m (i.e. the minimum hydrostatic pressure above vapor pressure > 310 bars). Given the high Th temperatures found in the NaCl-H_2O inclusions, a maximum Pt pressure of 400 bars may be reasonably assumed, otherwise Tt values are too high.

This pressure of trapping evaluated for type Ia inclusions has been assumed also for type Ib and Ic inclusions since no large variations of pressure are likely to occur along S1 to S3 stages.

To explain the high Pt values based on CO_2-H_2O immiscibility, two reasons may be considered: a) that type Ia and type II are not truly coeval inclusions, giving erroneous Pt, b) that the calculated Pt is a true Pt, which reflects local overpressure conditions likely due to the closure of the vein system from the surface by mechanisms like vein constriction by plastic deformation (Roedder and Bodnar, 1980) (sample LC90174-3a was collected in El Guindo lode, at Renegadero valley, where the vein is associated to a large ductile-brittle fault N115/85-70S oriented). Alternatively, overpressure may be reached by seismic pumping (e.g. Sibson et al., 1988).

The wide range of Th temperatures prevents the use of independent geothermometers (illite, chlorite, etc, see chapter 5) to evaluate Pt. No pressure corrections have been introduced and Th is taken as Tt.

6.5.5. Summary

Fluid inclusion data from some lodes of Linares-La Carolina ore field indicate that there were at least three events of fluid entrapment related to the vein formation. Most of the inclusions are pseudosecundaries. Four types of inclusion fluids were observed which are assumed to represent three stages of the entrapment.

Types Ia and II represent the first stage of entrapment, at hydrostatic pressures (310-400 bars) and Tt ranging from 87.4° to 392 °C, of moderate to low saline aqueous and saline CO_2-aqueous

solutions thought to be partly immiscible during the entrapment. Minor amounts ($XCH_4 \leq 0.06$) were detected in the type II inclusions. Pt determined from intersecting isochores (1,075 to 1,765 bars) may reflect local overpressures. This generation of inclusions is considered as representative of the late S1 stage and early S2 stage.

The second stage of entrapment (related to the main ore deposition stage S2) is characterised by type Ib ($NaCl-KCl-H_2O$) moderately saline inclusions homogenizing in the range of 168° to 325°C. The NaCl/(NaCl+KCl) ratios are close to the eutectic proportion. No volatile constituents occur in this type of inclusions.

The third stage of entrapment is ascribed to the late S2 and early S3. It is characterised by type Ic ($H_2O-NaCl-KCl-CaCl_2$) high to moderately saline inclusions, homogenizing at Th ranging from 76° to 327°C, with $XNaCl:XKCl:XCaCl_2 \approx 0.048:0.009:0.016$.

Therefore, temperature and compositional variations are observed from S1 (low to moderate salinity, locally? carbonaceous, hot fluids) to S3 (high to moderately polysaline, cooler fluids.

Chapter 7.Isotope geochemistry: Lead and sulphur.

7.1.Introduction.

This chapter presents radioisotope and stable isotopes data from Linares-La Carolina Pb-ore field. Lead data are discussed and some conclusions about the source rocks and their isotopic compositions are assessed. Systematics of sulphur isotope data enables the estimation of the isotopic variations and similarities among veins, sectors and ore-types together with the source/s of sulphur involved in the mineralisations.

7.2. Lead isotope geochemistry.

7.2.1.Sampling.

Ore-lead isotopic study of vein-type mineralisation in Linares-La Carolina district was carried out on unpublished data of analyses performed by Enadimsa (1971). Most of the samples of galena were collected in situ (e.g. El Cobre). Only one sample (E179/18) is from a Pb-Zn occurrence (La Caprichosa mine) located in a sector adjacent to the study area. Locations are shown in fig. 7.1 and listed in table 7.1. Analytical procedure is described in Appendix I.

7.2.2.Isotope geochemistry in ore deposits.

Radioisotope studies are based on the fact that the decay of any radioactive parent element decay goes an at a constant rate and is basically unaffected by the temperatures, pressures or chemical combinations (the percent differences between isotope masses is so small that fractionation effects may be disregarded). The number of nuclei of a radioactive element N remaining from an original number N_o at time t is given by the equation $N = N_o e^{-\lambda t}$, where λ is the constant decay. Lead isotope geochemistry involves four Pb isotopes: ^{206}Pb, ^{207}Pb, ^{208}Pb (daughter products of ^{206}U, ^{207}U and ^{232}Th decay, respectively) and the non-radiogenic ^{204}Pb. Thus, the relative abundances of radiogenic lead isotopes are

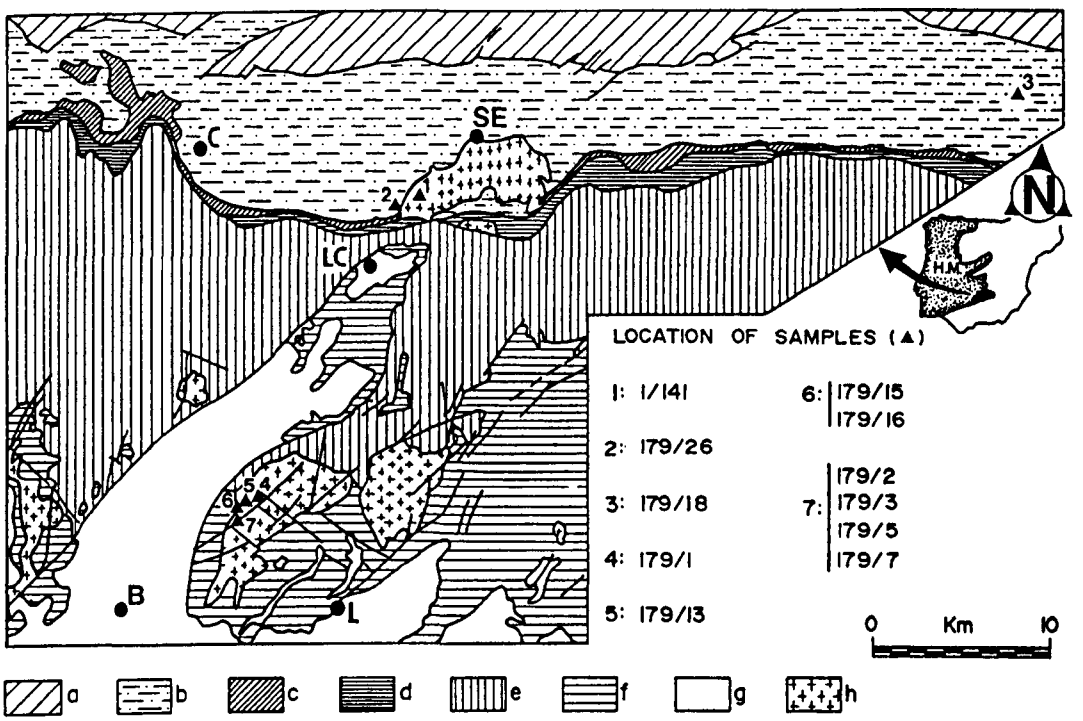

Fig. 7.1. Location of samples analised for Pb isotopes. a: Tremadoc-Arenig, b: Upper Arenig-Asghill, c: Silurian, d: Devonian, e: Carboniferous, f: Triassic, g: Neogene, h: Late-Hercynian granitoids. C: El Centenillo, SE: Santa Elena, LC: La Carolina, L: Linares, B: Bailén.

Sample	Location	$\frac{^{206}Pb}{^{204}Pb}$ $2\sigma = \pm 0.38$	$\frac{^{207}Pb}{^{204}Pb}$ $2\sigma = \pm 0.38$	$\frac{^{208}Pb}{^{204}Pb}$ $2\sigma = \pm 0.37$
E141	El Piñón[a]	18.225	15.765	38.678
E179/1	La Cruz[b]	18.372	15.801	38.992
E179/2	El Cobre 1[b]	18.694	16.080	38.788
E179/3	El Cobre 1[b]	18.580	15.948	39.273
E179/5	El Cobre 2[b]	18.504	15.897	39.062
E179/7	El Cobre 2[b]	18.285	15.765	38.834
E179/13	Num. 5-6[b]	18.768	16.035	39.231
E179/15	Igualdad[b]	18.503	15.869	39.417
E179/16	Igualdad[b]	18.545	15.925	39.199
E179/17	Matacabras[b]	18.525	15.829	39.035
E179/18	Caprichosa[c]	19.282	16.585	40.967
E179/26	Ojo Vecino[a]	18.556	16.041	39.318

Source of Data: Enadimsa,1971

(a) Sta. Elena sector (host rocks: mainly granitoids)

(b) Linares sector (host rocks: mainly granitoids)

(c) S. Morena sector (host rocks: Paleozoic metasediments)

Table 7.1. Lead isotopic composition of galenas from Linares-La Carolina lodes.

presented as $^{206}Pb/^{204}Pb$, $^{207}Pb/^{204}Pb$, $^{208}Pb/^{204}Pb$ ratios. Original U-Th-Pb ratios may be fixed in a closed system since the formation of the Earth (single-stage model) or alternatively, they may be have been modified in large cycles (two-stage, three-stage model, etc). Lead isotope ratios may plot on growth curves from where model-lead ages (i.e. when lead is removed from a single-stage, two-stage, etc. source and deposited in a phase, like galena, with U/Pb infinitesimal) are obtained (e.g. Faure, 1977). Therefore, model-lead ages in galenas are constrained by the isotopic composition of the source at the time of mineralisation but they do not indicate the true age of the ore emplacement if the ratios do not plot on the appropriate growth curve. Thus, lead isotope geochemistry is used to infer the source of lead rather the age of ore deposition.

7.2.3.Presentation of data.

The $^{206}Pb/^{204}Pb$, $^{207}Pb/^{204}Pb$, $^{208}Pb/^{204}Pb$ ratios in table 7.1. are plotted in the conventional $^{207}Pb/^{204}Pb$ versus $^{206}Pb/^{204}Pb$ (α/β, uranogenic) and $^{208}Pb/^{204}Pb$ versus $^{206}Pb/^{204}Pb$ (α/γ, thorogenic) model ages diagrams (fig. 7.2.a and fig. 7.2.b, respectively) relative to the two stage-model proposed by Stacey and Kramers (1975). The reported data are considered to be accurate at the 95% confidence level to within the errors limits listed in table 7.1.

7.2.4.Model ages.

The Pb isotopic compositions of galena samples from the hydrothermal occurrences do not point out significant differences between the El Centenillo-La Carolina-Sta. Elena and the Linares sectors (the sample E179/18 yielded anomalous isotopic ratios that will be considered later, table 7.1). These undiscriminating compositions indicate that the Pb was ultimately derived from the same source or sources with similar U/Pb and Th/Pb ratios in both sectors.

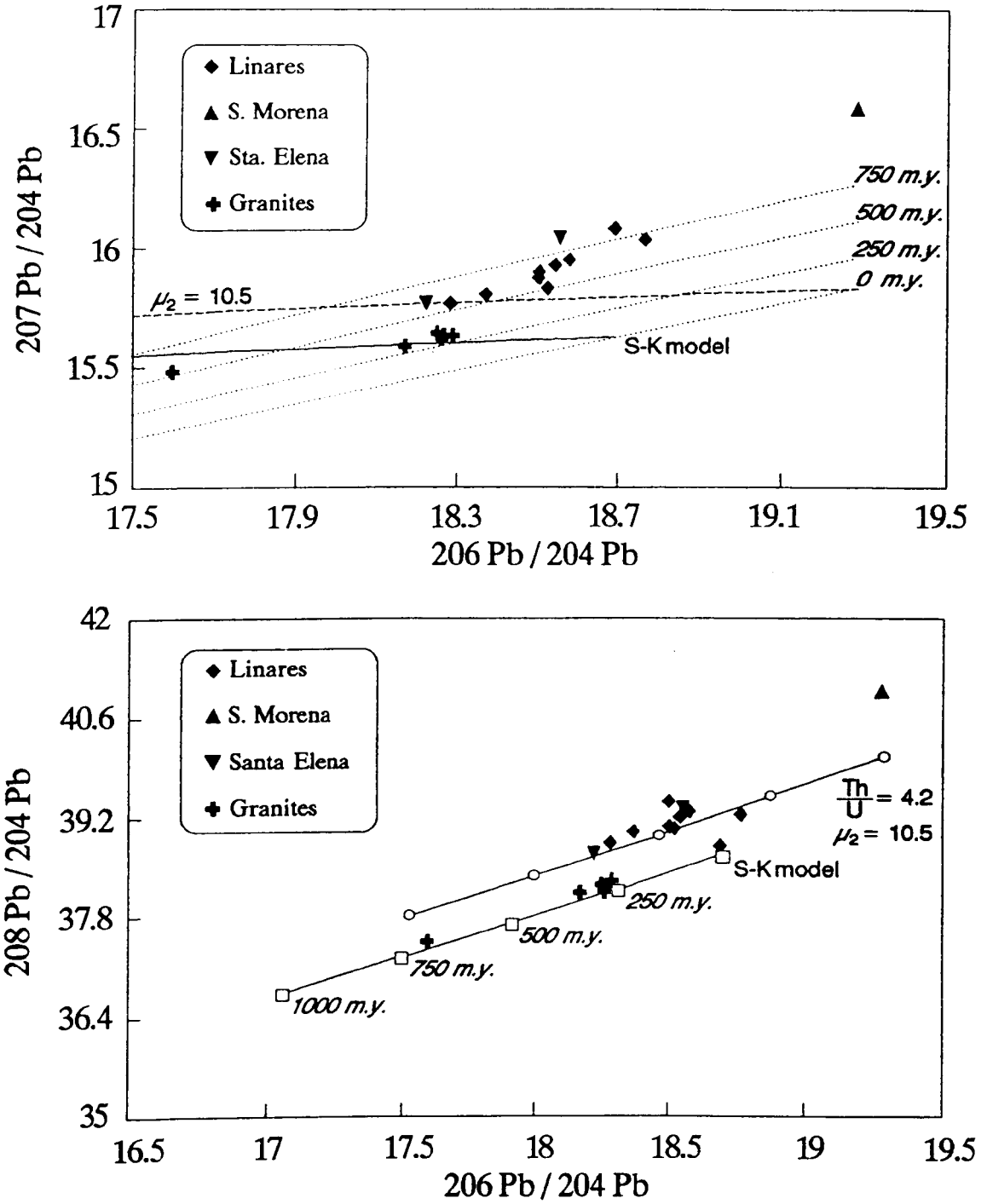

Fig. 7.2. a) $^{207}Pb/^{204}Pb$ versus $^{206}Pb/^{204}Pb$ and b) $^{208}Pb/^{204}Pb$ versus $^{206}Pb/^{204}Pb$ diagrams of Linares-La Carolina galenas (data from Enadimsa, 1971). Crosses are Hercynian K-feldspars from Michard-Vitrac et al.,(1981). The lower curves are the Stacey-Kramers growth curve (Stacey and Kramers, 1975). The upper curves are ajusted to μ_2 = 10.5 and K = 4.2.

In the $^{207}Pb/^{204}Pb$ versus $^{206}Pb/^{204}Pb$ diagram (Fig. 7.2.a), all samples plot above the evolution curve after Stacey and Kramers, (1975). They are indicating $^{238}U/^{204}Pb$, $\mu_2 \geq 10.5$, yielding Upper Proterozoic $^{207}Pb/^{206}Pb$ model ages, which are too old to reflect the time of formation of the veins that is Upper Permian-Anisian (see chapter 4 for a more complete discussion about the age of the veins).

The Pb isotopic composition of feldspars from some granites of Sierra Morena (data from Michard-Vitrac et al, 1981) lie very close to the Stacey-Kramers' curves, pointing out model ages consistent with the geological late-Variscan age assumed for these rocks and isotopic ratios, (excluding one of them, a pre-Variscan granitoid), with no large variations.

7.2.5.Source of lead.

No enrichment or anomalous U and Th values are observed in the Late Variscan granitoids of Sierra Morena. This fact may indicate that the radiogenic enrichment in galenas from the veins is caused by the incorporation of lead derived from other sources not related to the Late Variscan magmatism.

If a lead provenance from the Palaeozoic basement is assumed, the discrepancy between the α/β model ages (Fig. 7.2.a) and the geological age argues for source rocks that were at one stage depleted in U, after most of the ^{235}U had already decayed to ^{207}Pb. This depletion in ^{238}U may be consistent with the high $^{208}Pb/^{204}Pb$ values showed in the $^{208}Pb/^{204}Pb$ versus $^{206}Pb/^{204}Pb$ diagram (Fig. 7.2.b) which indicates a higher average ratio **K** ($^{232}Th/^{238}U$) than that assumed in the Stacey-Kramers' model (second stage: **K** = 3.78). High **K** ratios may indicate some U-loss relative to Th in rocks subjected to granulites facies or higher grade of metamorphism (Wedepohl et al, 1978; Doe and Zartman, 1979). In shallow levels of the crust, weathering-erosion-deposition processes may also account for U-depletion (Koeppel and Schroll, 1983; Samama, 1986).

Lead derived from U-depleted crustal rocks by remobilisation processes is normally expected to plot near or below the evolution curve in the $^{207}Pb/^{204}Pb$ versus $^{206}Pb/^{204}Pb$ diagram and near or above the evolution curve in the $^{208}Pb/^{204}Pb$ versus $^{206}Pb/^{204}Pb$ diagram (Doe and Zartman, 1979). Nevertheless, if the U depletion after most of the ^{235}U had decayed to ^{207}Pb took place in U-rich rocks, the ratio $^{207}Pb/^{204}Pb$ may still be high and the data points may plot above the growth curve for average crustal leads, as suggested in the α/β diagram, where the lead isotopic compositions in galenas plot near/above the growth curve ($^{238}U/^{204}Pb$) μ_2 = 10.5, but the growth of ^{206}Pb with respect to ^{207}Pb was retarded by ^{238}U depletion and consequently the uranogenic model ages are too high. Therefore, in this case, a provenance from originally U-rich rocks with ^{238}U depletion after most of the ^{235}U decayed to ^{207}Pb is required to explain: a) the older uranogenic model ages relative to the geological ages accepted for the host rocks, and b) the high $^{238}U/^{204}Pb$ ratio above the growth curve μ_2. If the abundance of ^{238}U relative to ^{204}Pb, even after the depletion, is still higher than that assumed as crustal average and the ratios $^{232}Th/^{238}U$ are above the thorogenic growth curves in the Zartman & Doe's model, then necessarily the abundance of ^{232}Th relative to ^{204}Pb must be higher than that expected in the average crust.

The mechanisms that generated these 'atypical' high radiogenic abundances relative to non-radiogenic lead reflect the complex evolution undergone by the upper crustal rocks. Metamorphism and deformation are related to processes of preferential remobilisation in the whole rock (e.g., loss of Th<Pb<U in rocks subjected to granulite or higher rank of metamorphism, after Wedepohl et al., 1978) and redistribution of Th-U-Pb in the minerals (e.g. Pb is preferentially leached from zircons and reconcentrated in K-feldspars). Relative looses/gains of Pb and U occur in the material derived from the metamorphic rocks by subsequent erosion, weathering and sedimentation (e.g Doe and Delevaux, 1972, have suggested increases in the $^{207}Pb/^{204}Pb$ ratio as result of epigenetic processes). Furthermore, mechanical

concentration of specific minerals may give sedimentary rocks with 'atypical' ratios $^{232}Th/^{204}Pb$ and $^{238}U/^{204}Pb$.

In fact, sample E179/18 (La Caprichosa mine) which was not considered above, yielded very high isotopic ratios. The most probable explanation for this radiogenic Pb is an origin derived from the Lower Ordovician host rocks where beds of metasediments and quartzites very rich in zircon and monazite exist (whole-rock average U_3O_8 concentration of 0.069 %; Arribas, 1962). This sample represents the extreme case in which the incorporation of radiogenic lead from the pre-Hercynian basement is of paramount importance.

Despite most of the radiogenic lead found in samples of galena from the Linares-La Carolina Pb-ore fields seems derived from the metasedimentary country rocks, the observed trend and the wide range of the isotopic ratios in galenas do not contradict a mixing of lead from both different sources: by lateral secretion from the metamorphic basement and minor proportions of Late Hercynian granite-related Pb.

7.2.6.Regional setting.

If we assume that the granitoids are mostly derived from a U-Pb-zoned continental crust (Michard-Vitrac et al, 1981), the ore-lead isotope pattern from the veins indicates a source from the upper levels of this crust which were already U-Th-enriched relative to the radiogenic composition of the intermediate or lower crust.

The above assertion does not necessarily imply 'enrichment' (or Pb-depletion) during the primitive differentiation. As it was noted before, complex changes in the compositional parameters are likely to occur during the Pb-evolution of the crust (e.g. Pb-loss events during the Proterozoic), moreover, if this evolution can follow different paths in the upper and lower continental crust (Doe and Zartman, 1979) multi-stage models are required to

interpret the crustal Pb evolution because there may have been more than one episodic Pb-loss/U-Th-enrichment.

Anomalous Pb isotopic evolution of the crustal reservoir has been suggested from lead isotopic data about base-metals ores in Sardinia where Ludwig et al, (1989) point out some participation of lead from "a crustal source which has been undepleted for most of its existence since the early Archean". However, the lead isotopic pattern in Linares-la Carolina vary from their assumptions on the existence of an undepleted Western Mediterranean crustal-Pb province as the data point out a lead source involving U-Th-enriched (relative to non-radiogenic lead) upper crustal rocks where some ^{235}U-depletion could occur but the concentration in U and Th was high enough to keep the ratios above those considered as average in orogenic settings. It is probably indicating local variations in the upper levels of the crust and the model of an undepleted Western Mediterranean crustal province as source of lead in late-Variscan base-metals deposits may not be pertinent to this sector.

7.3.Sulphur isotope geochemistry.

7.3.1.Sampling.

92 analyses of sulphur isotopes have been carried out on 72 samples of barite and sulphides collected from 18 hydrothermal occurrences and 3 different country rock formations. Collection of samples for sulphur isotope determinations was planned to cover a large number of deposits rather than exhaustive sampling of few of them, given the scope of this thesis. Samples were collected from outcrops, mine galleries or, in few cases from mine dumps. Five samples of metasediments containing biogenic pyrite were collected from Upper Ordovician formations. Locations of samples are listed in tables 7.2, 7.3, 7.4.a-b. Details about sample preparation and analytical procedures are explained in the Appendix I. When it was

			$\delta^{34}S$ °/oo			
Sample	Lode	Locality	Barite	Galena	Sphal.	Marcas.
LC90164-2	Pelaguindas	El Centenillo				+3.9
LC90164-3				+1.0		
LC90164-4				+3.9		
				+3.9		
LC90164-9				+2.1		
LC90164-10						
LC90164-12			+6.2			
LC90164-13			+10.0			
LC90164-20			+9.2	+5.1		
LC143-3	Sur	El Centenillo	+9.4			
LC309-1	Crucero	El Centenillo		-3.3		
LC93-3	Guindo/ Crucero	Los Guindos			+11.1	
					+11.4	
LC139-15						+10.8
LC139-16				+3.6		
LC139-22			+10.2			
LC139-23			+14.1			
LC9031-6			+9.1			
			+7.7			
LC9031-12				+3.2		
LC308-9	Federico (La Española)	Los Guindos	+9.6			
LC308-10			+10.5			
LC308-13					+10.9	
LC308-15					+11.5	
LC49-5	Sinapismo	Sta. Elena		+3.3		
LC49-6				-1.6		
				-1.1		
LC49-7				+1.8		
LC90174-4a	Sinapismo	Los Guindos	+9.6			
LC90174-4c			+9.3			
LC139-2	Araceli	La Carolina		-1.1		
				-1.0		
LC139-3				-1.6		
LC139-10			+9.3			

Table 7.2. Sulphur isotope data from lodes located in the El Centenillo, Los Guindos, Santa Elena and La Carolina (exclusively hosted by Paleozoic metasediments).

			$\delta^{34}S$ °/oo				
Sample	Lode	Locality	Barite	Galena	Sphal.	Fe_2S	Chpyr.
LC59-6	Ojo Vecino	Sta. Elena		+2.5			
LC59-7				-4.8			
LC59-10				+0.2		+1.8[m]	
LC159-9	La Nube	Sta Elena	+12.9				
LC159-11						-29.0[m]	
LC159-12			+9.1	-6.4	-4.1		
				-6.3			
LC159-13			+7.9	-6.5			
				-6.9			
LC318-10	Palazuelos	Linares	+9.3				
LC33-2	El Cobre (Level 11)	Linares		-1.9			
LC33-4				-1.9			
				-1.8			
LC129-11				-1.9			
LC129-12				-2.1			
LC129-27							-0.1
LC129-25						-1.9[p]	
						-1.4[p]	
LC318-1	San Juan/ Esmeralda	Linares	+8.8				
LC318-2			+8.7				
LC318-3				-3.6			
				-3.5			
LC318-4				-1.6			
LC318-6			+7.1				
LC318-7				-1.9		+6.7[p]	
LC129-5	Cañada Incosa	Linares		-2.2			
LC129-7			+7.4				
LC129-8			+8.7				

(p): Pyrite

(m): marcasite

Table 7.3. Sulphur isotope data from lodes located in Santa Elena and Linares hosted by granitoids and in less extension by Paleozoic metasediments.

a)

Sample	Ore	Locality	$\delta^{34}S$ °/oo Barite	Galena
LC288-1	Torrecillas	La Carolina	+8.9	
LC288-2			+9.2	
			+9.3	
LC288-3			+9.4	
LC298-2			+7.9	-1.6
LC298-3a			+8.2	-2.9
LC298-3c				-2.8
LC298-5			+9.2	
LC298-6			+8.7	
LC298-7			+8.5	
LC79-1	Fernandina (Palazuelos)	Linares	+7.0	
LC79-2			+7.1	
LC79-3			+7.2	
LC129-1	Cañada Incosa	Linares		-3.1
				-3.0
LC129-4				-2.5

b)

Sample	Formation	Locality	$\delta^{34}S$ °/oo Pyrite
LC9098-5	Mylonite (Granodiorite)	Sta. Elena	+2.9
LC73-2	Urbana	Stn. Elena (La Despreciada)	+39.7
LC73-3			+45.4
LC90164-8		El Centenillo	+16.5
LC163-1	Chavera	El Centenillo	-13.6
LC90164-6	Mixed Beds	El Centenillo	+8.3
			+8.1

Tables 7.4. a) Sulphur isotope data from stratabound hydrothermal ores in the basal Permian?-Triassic beds. b) Sulphur isotope data from a hydrothermal pyrite (LC9098-5) and biogenic pyrites in metasediments

possible, analyses were performed on several minerals coexisting in the same sample.

7.3.2.Sulphur isotope geochemistry: sources and processes.

Sulphur isotope studies are generally based on the variation of the two most abundant sulphur isotopes in the nature: ^{32}S and ^{34}S.

Thus, the sulphur isotopic composition of a compound is commonly expressed as the $\delta^{34}S$ value given by the expression,

$$\delta^{34}S = \left[\frac{(^{34}S/^{32}S)_{sample}}{(^{34}S/^{32}S)_{CDT}} - 1 \right] \cdot 1000$$

where the $(^{34}S/^{32}S)_{CDT}$ ratio is that in the troilite phase of the Cañon Diablo Meteorite.

The partitioning of isotopes (i.e. isotope fractionation) between two substances with different isotope ratios is usually produced by:

a) isotope exchange reactions:

$$A^{34}S + B^{32}S \longleftrightarrow A^{32}S + B^{34}S$$

where A and B are compounds having sulphur as a common constituent. When isotopic equilibrium is attained between the compounds A and B, the isotopic fractionation factor (α) is related to the equilibrium constant, K_e (Ohmoto and Rye, 1979),

$$\alpha_{(A,B)} = \frac{(^{34}S/^{32}S)_B}{(^{34}S/^{32}S)_A} = K_e$$

The fractionation factor, hence the equilibrium constant are a function of the temperature while the effect of pressure is

negligible at the pressure conditions commonly related to ore depositional environments. There are several calibration equations available for the calculation of temperatures from $\delta^{34}S$ data (e.g. Sakai, 1968; Sakai and Dickson, 1978, Grootenboer and Schwarcz, 1969; Kajiwara and Krouse, 1971; Czamanske and Rye, 1974; Ohmoto and Rye, 1979, Ohmoto and Lasaga, 1982). The following equations are adopted in this study,

Pair sphalerite-galena:

$1000 \ln \alpha = 0.8 \cdot 10^6 T^{-2}$ (Kajiwara and Krouse, 1971)

Pair barite-sphalerite:

$1000 \ln \alpha = 6.44 \cdot 10^6 T^{-2}$ (Sakai and Dickson, 1978)

Combining both equations,

Pair barite-galena:

$1000 \ln \alpha = 7.24 \cdot 10^6 T^{-2}$

b) kinetics effects:

During nonequilibrium chemical reactions, the fractionation of sulphur isotopes is controlled by chemical reaction rates (which are mass dependent) where one isotopic species (the lighter isotope) reacts more rapidly than another. Consequently, the product tends to have a lower $^{34}S/^{32}S$ ratio than that of the reactant. Ohmoto and Rye (1979) have noted that kinetic isotopic effects during oxidation of H_2S may be responsible for the important variation of $\delta^{34}S$ values observed on hypogene sulphate minerals.

c) other physico-chemical factors: Ohmoto (1972) showed that $m_{\Sigma S}$, fO_2, fS_2 and pH control the isotopic composition of hydrothermal minerals which may exhibit isotopic compositions

markedly different from those of the ore-forming fluids from they formed.

7.3.3.Presentation of data.

Data are expressed as $\delta^{34}S$ values relative to the CDT (Cañon Diablo Troilite) standard (tables 7.2., 7.3. and 7.4.a-b). Analytical uncertainty is ± 0.2 °/oo. Fig. 7.3 shows the distribution of $\delta^{34}S$ values in barite and sulphides collected from different sectors. $\delta^{34}S$ values in samples collected from the basal Permian?-Triassic beds and Ordovician metasediments are indicated. Fig. 7.4 display the isotopic composition of mineral pairs and the equilibrium isotherms calculated from the fractionation factors suggested by Kajiwara and Krouse (1971) and Sakai and Dickson (1978).

7.3.4.Sulphur isotopes in metasediments.

$\delta^{34}S$ determinations were performed on five samples of biogenic pyrite from Upper Ordovician formations. Two pyrite samples (LC73-3 and LC73-2) from the 'iron beds' of the Urbana Limestone Fm. at La Despreciada quarry yielded $\delta^{34}S$ = +45.4 °/oo and $\delta^{34}S$ = +39.7. Another pyrite sample (LC 90164-8) from a lumachelle in the same formation but at different location (El Centenillo) gave a $\delta^{34}S$ value of 16.5 °/oo. One pyrite sample from the Mixed Beds (Bancos Mixtos) Fm. at El Centenillo yielded to +8.2 °/oo. One sample from Chavera Shales Fm. showed $\delta^{34}S$ = -13.3 °/oo (table 7.4b).

The mechanisms required for the production of the observed $\delta^{34}S$ values have been already discussed in chapter 3 (sections 3.4.2 and 3.5). Assuming that late diagenetic processes and regional metamorphism did not sustantially change the $\delta^{34}S$ values of the analysed pyrites, the large positive variations found in the Mixed Beds Fm and the Urbana Limestone Fm. are interpreted as due to the formation of pyrite in an environment closed to $SO_4^=$ with high rates of sedimentation. The very 'heavy' $\delta^{34}S$ values of pyrites from the Urbana Limestone may only be explained by pyrite

deposition in an environment closed to H_2S with excess of reactive iron relative to the availability of aqueous sulphide (see fig. 3.26, chapter 3). Alternatively, the light isotopic composition of pyrites in the Chavera Shales Fm. reflects deposition in an open system to SO_4= developed in a euxinic basin with slow rate of sedimentation (Ohmoto and Rye, 1979).

7.3.5.Sulphur isotopes in hydrothermal ores.

Barite exhibits a range of $\delta^{34}S$ from +14.1 to +6.2 °/oo (mean = +8.9 °/oo, 1σ = 1.5). Galenas yield a range from +5.1 to -6.9 °/oo. Sphalerite displays a range from +11.5 to -4.1 °/oo. The largest $\delta^{34}S$ variations in galenas are found in Ojo Vecino (+2.5 to -4.8 °/oo , n = 3), Pelaguindas (+5.1 to +1.0 °/oo, n = 4) and Sinapismo (+3.3 to -1.1 °/oo, n = 4). The smallest $\delta^{34}S$ variations in galenas are found in El Cobre (-1.8 to -2.1 °/oo, n = 4). The isotopically heaviest sulphides are found in Pelaguindas, Crucero Guindo, Sinapismo and Federico. The lightest sulphides are found in La Nube, El Cobre and San Juan (fig. 7.5). Sulphides from Las Torrecillas yielded $\delta^{34}S$ values very similar to those given by samples from El Cobre (tables 7.2, 7.3, 7.4.a-b, fig. 7.3).

7.3.5.1.Isotopic equilibrium and sources of sulphur.

Only sulphide-sulphide (galena-sphalerite) and sulphide-sulphate (galena-barite and sphalerite-barite) pairs from La Nube lode are near to isotopic equilibrium (fig. 7.4). None of the samples from the other hydrothermal occurrences yielded reasonable equilibrium temperatures of the mineral phases which are assumed as co-precipitated during the main depositional stage (S2) (only in Pelaguindas lode the pair galena-sphalerite could be in near equilibrium). Several mechanisms can be envisaged to explain the apparent disequilibrium (Ohmoto and Rye, 1979; Ohmoto, 1986):

-Sulphide-sulphide disequilibrium:

a) kinetic effects in a closed system to H_2S. If the $m_{H2S}/m_{\Sigma metals} << 1$, most of reduced sulphur is removed during precipitation and $\delta^{34}S$ of the remaining H_2S becomes progressively

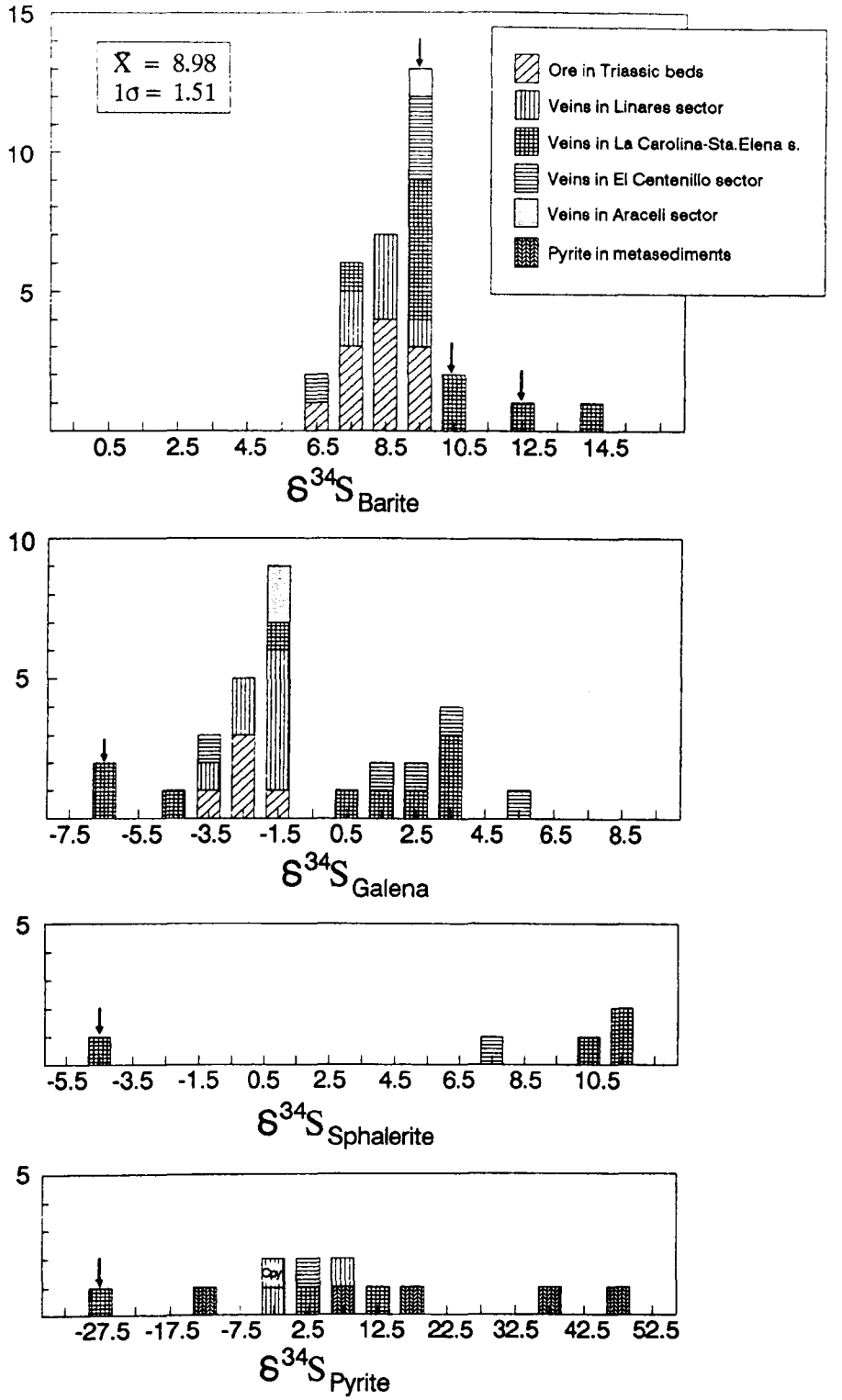

Fig. 7.3. Histograms of $\delta^{34}S$ values of barites and sulphides from hydrothermal ores and biogenic pyrites in Linares-La Carolina. Samples from several veins have been ascribed to different sectors on the basis of host rocks. Also the samples from metasediments and ores in Permian?-Triassic beds are indicated. Arrows denote samples from La Nube lode.

"heavier", which causes isotopic disequilibrium among sulphides precipitated sequentially (i.e. galena and sphalerite).

b) introduction of H_2S from an external source during the mineral formation (open system). Reduced sulphur may be acquired at the depositional site during the sulphide precipitation, causing disequilibrium and large variations of $\delta^{34}S$ values in mineral phases precipitated from a fluid with m_{H2S} exceeding largely $m_{\Sigma metals}$.

Sulphides from occurrences located in El Centenillo-Santa Elena area exhibit isotopic disequilibrium (fig. 7.4), the heaviest $\delta^{34}S$ values and the largest variations (fig. 7.3), suggesting incorporation of external reduced sulphur (likely derived from hydration of pyrite in the metasediments, given the large $\delta^{34}S$ variations of biogenic pyrites) to 'magmatic'? H_2S at the depositional site. As sulphides from the Linares-La Carolina area (including the Araceli group, La Nube and Las Torrecillas) do not display large variations, being isotopically lighter (fig. 7.3), then the observed disequilibrium could be due to kinetic effects in a system relatively closed to H_2S at the time of ore deposition. At $m_{H2S}/m_{\Sigma metals} << 1$, $\delta^{34}S_{H2S}$ may be approximated to the $\delta^{34}S_{galena}$ values (Ohmoto, 1986) that reflect a 'magmatic' signature. In fact, the very low $\delta^{34}S$ value (-29.0 °/oo) found in marcasite (LC59-10) from La Nube, can only be explained if most of the H_2S is 'magmatic'-derived (Ohmoto and Rye, 1979).

Note that $\delta^{34}S$ values in the mineralisations hosted by Permian?-Triassic sediments are not very different from those in El Cobre or San Juan-Esmeralda.

2-Sulphide-sulphate disequilibrium: Isotopic disequilibrium among coprecipitated barites and sulphides in ore deposits at T > 200°C is caused by the incorporation of $SO_4^=$ at the depositional site. Mechanisms of sulphate acquisition at depositional site include:

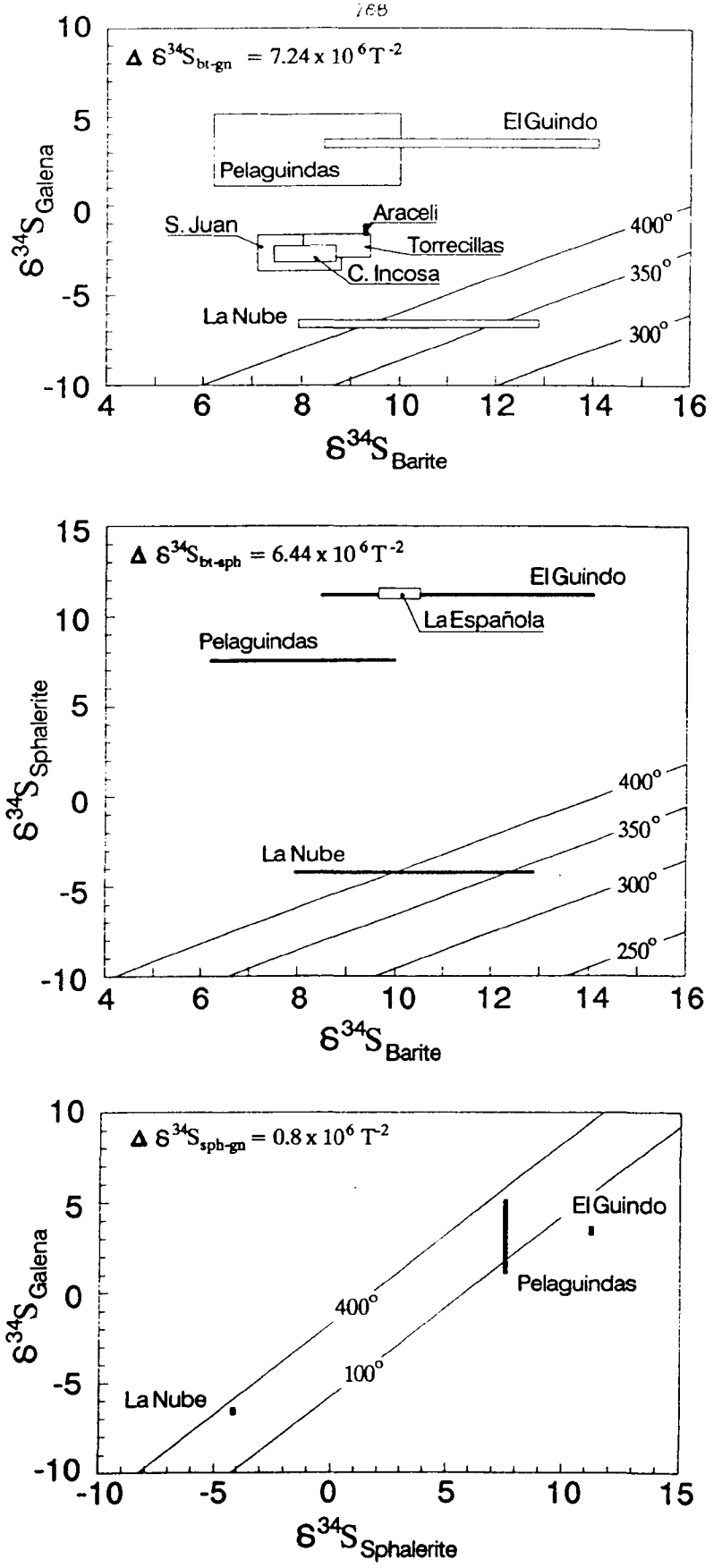

Fig. 7.4. Isotopic equilibrium/disequilibrium in sulphide-sulphide and sulphide-sulphate pairs. Fractionation factors have been obtained from Kajiwara and Krouse, 1971 and Sakai and Dickson, 1978.

a) mixing of sulphate-bearing fluid (e.g. basinal waters). In this case, $\delta^{34}S$ values would be between the $\delta^{34}S$ of the original $SO_4^=$ in the fluid and the $\delta^{34}S$ of the incorporated $SO_4^=$. Thus, in a mixing of "magmatic" fluid with $\delta^{34}S_{SO4^=}$ typically around +25 °/oo and Permian-Triassic basinal waters with $\delta^{34}S_{SO4^=} \approx$ +13-+15 °/oo (Claypool et al., 1980), the precipitated sulphate (if no fractionation to aqueous H_2S takes place) would have $\delta^{34}S$ values ranging from +13 to +25 °/oo as expressed by the following mass balance equation (Ohmoto, 1986):

$$\delta^{34}S_{\Sigma SO4^=} = \delta^{34}S_{SO4^=,\text{'magmatic'}} \, X_{SO4^=,\text{'magmatic'}} + \delta^{34}S_{SO4^=,\text{'sedim'}} \, X_{SO4^=,\text{'sedim'}}$$

where X_i is the molar fraction ($X_{SO4^=,\text{'magmatic'}} + X_{SO4^=,\text{'sedim'}} = 1$).

If the system is dominated by 'sedimentary' sulphate, the $\delta^{34}S_{barite}$ would be within a narrow range close to +13-+15 °/oo . If fractionation to H_2S occurs at low temperatures (which is improbable to occur because a large time of residence is required), $\delta^{34}S_{SO4^=}$ could be even larger than +25 °/oo. As most of observed $\delta^{34}S_{barite}$ values are within the range +7.4 to +10.4 °/oo, it seems unlikely that incorporation of $SO_4^=$ derived from Permian-Triassic basinal brines took place.

b) generation of $SO_4^=$ from hydration of pyrite in host rocks. Given the possible origin of some H_2S derived from the hydration of pyrite, it could be reasonable to consider the participation of $SO_4^=$ derived from the hydration of pyrite but it seems improbable because the $\delta^{34}S$ range in barites is too narrow to reflect any signature of an original biogenic sulphur with very large $\delta^{34}S$ ranges.

c) generation of $SO_4^=$ from oxidation of H_2S by shallow ground waters. Oxidation of 'magmatic' H_2S by ground waters at shallow levels may create enough $SO_4^=$ with $\delta^{34}S$ values essentially identical to those of H_2S. Subsequent mixing of the $SO_4^=$ thus formed with 'old magmatic' equilibrated $SO_4^=$ ($\delta^{34}S_{SO4^=} \approx$ +25 °/oo)

caused $\delta^{34}S$ values between the $\delta^{34}S_{H2S}$ and $\delta^{34}S_{'old'SO4=}$ values. The observed $\delta^{34}S_{barite}$ values are within that range. At La Nube site, the temperature could be high enough to allow the attainment of isotopic re-equilibrium among the aqueous species immediately prior to the mineral deposition.

If most of the observed sulphide-sulphide disequilibrium at Linares-La Carolina area is interpreted as due to kinetic effects in a system closed to H_2S where $m_{H2S}/m_{\Sigma metals} << 1$, them the oxidation of the aqueous sulphide must take place prior to the sulphide deposition; otherwise all sulphide would be incorporated in the sulphides.

7.3.5.2.$\delta^{34}S$ values of iron sulphides.

$\delta^{34}S_{S2Fe}$ values from veins are erratic, partly due to the processes inherent to the formation of pyrite (e.g. Ohmoto and Rye, 1979; Ohmoto, 1986), partly due to the consideration of samples precipitated in different stages and partly due to post-depositional changes (e.g. replacement of pyrite by marcasite).

Mechanisms of formation of pyrite and chalcopyrite under normal hydrothermal conditions involve redox reactions that require both H_2S and $SO_4=$. Pyrite and chalcopyrite formed in such disequilibrium systems may inherit the $\delta^{34}S$ values of H_2S and $SO_4=$ as follows (Ohmoto and Rye, 1979):

$$\delta^{34}S_{pyrite} = 7/8\ \delta^{34}S_{H2S} + 1/8\ \delta^{34}S_{SO4} =$$

$$\delta^{34}S_{chalcopyrite} = 15/16\ \delta^{34}S_{H2S} + 1/16\ \delta^{34}S_{SO4} =$$

these equations were resolved for the $\delta^{34}S$ values of coeval minerals found in samples LC129-27 and LC129-25, yielding unrealistic $\delta^{34}S_{H2S}$ and $\delta^{34}S_{SO4=}$ values. This is due to variations likely in relation to a sequential precipitation of the mineral phases or other unknown mechanisms involved in the precipitation.

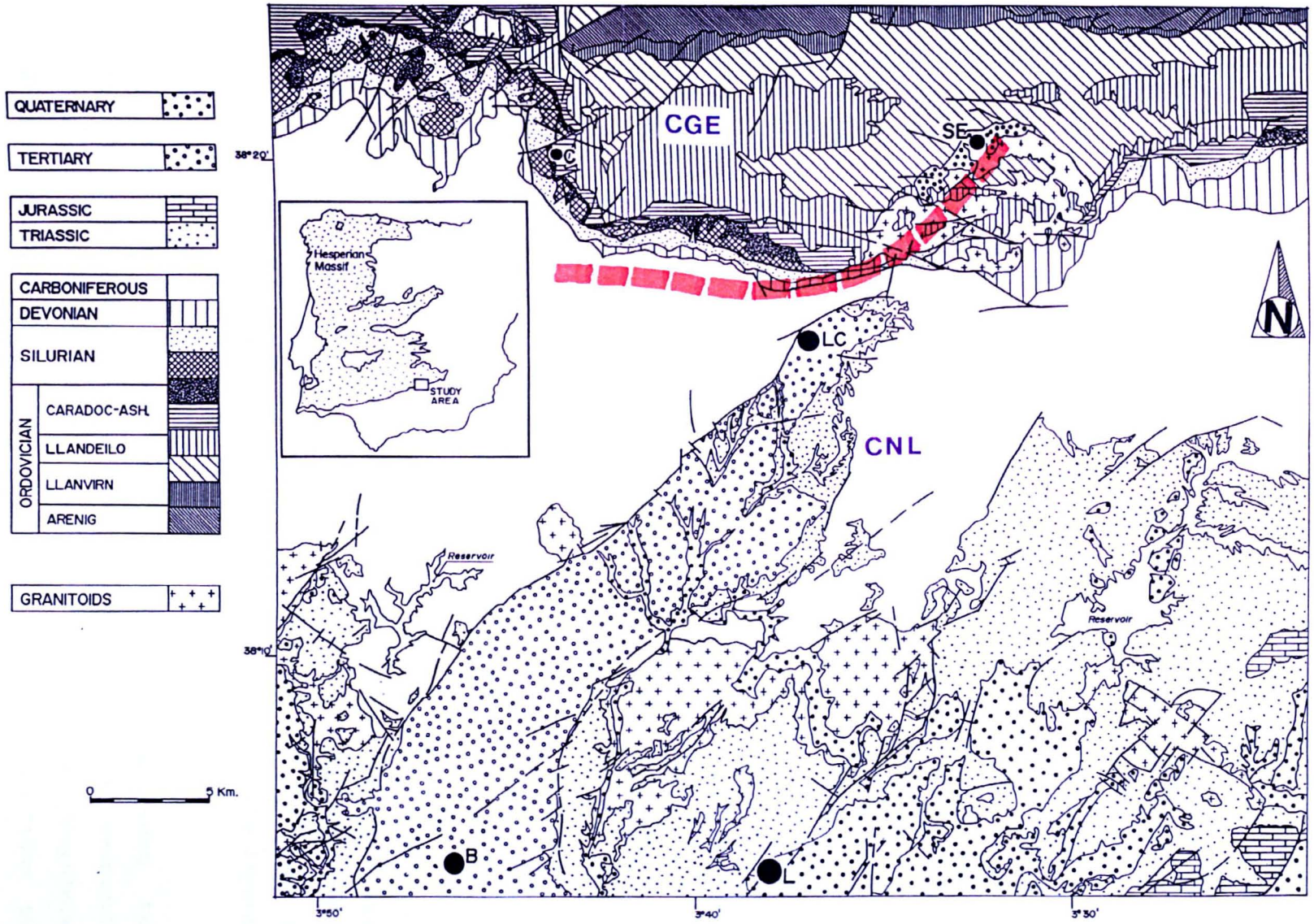

Fig 7.5. Sectors differenciated on sulphur isotopes basis. CGE: El Centenillo-Los Guindos-Santa Elena, CNL: La Carolina-La Nube-Linares. Geological base modificated from Enadimsa, 1981.

7.4.Summary.

7.4.1.Lead isotope geochemistry.

The high μ_2 and K values ($^{238}U/^{204}Pb \geq 10.5$ and $^{232}Th/^{238}U \geq 4.2$, respectively) above those considered by Stacey and Kramers (1975) or Cumming and Richards (1975), and the uranogenic and thorogenic model ages pattern of lead data from Linares-La Carolina indicate apparent U-Th-enriched (relative to common lead) upper crustal rocks (likely Palaeozoic metasediments) as a source for the lead in the veins formed during the Permian-Triassic mineralisation event. Even if some ^{238}U-depletion relative to ^{235}U occurred, that loss took place in already U-'enriched' rocks, probably as a consequence of preceding Pb-loss stages developed in a complex crustal evolution. Some participation of varying amounts of Late Hercynian granitoid-derived lead can not be ruled out, although the isotopic compositions of feldspars from these granitoids (Michard-Vitrac et al, 1981) lie very close to the Stacey-Kramers' curves, pointing out model ages consistent with the geological age assumed for these rocks.

7.4.2.Sulphur isotope geochemistry.

On the basis of sulphur isotopes geochemistry, two major areas may be differentiated in the district: El Centenillo-Los Guindos-Santa Elena (CGE) and La Carolina-La Nube-Linares (CNL). The CGE area exhibits wide ranges and 'heavy' values of $\delta^{34}S_{sulphides}$. The CNL area displays narrower ranges and lighter $\delta^{34}S_{sulphides}$ values than those in the CGE area.

There are no substantial $\delta^{34}S$ disparities among the hydrothermal occurrences in the basal beds of the Permian?-Triassic succession and the veins in the CNL area. Therefore, sulphur source/s and processes involved in both ore-types are assumed to be the same.

Sulphur isotopic systematics indicates that:

-Mixing of 'magmatic' waters with isotopically equilibrated aqueous sulphur species and shallower waters with H_2S likely derived from the hydration of biogenic pyrite in the metasediments took place in the CGE area.

-Waters carrying 'magmatic' sulphur in a system relatively closed to H_2S ($m_{H2S}/m_{\Sigma metals} << 1$) were dominant in the CNL area.

-Most of the SO_4= in both areas seems to be derived from the oxidation of H_2S by 'meteoric' shallow ground waters. A source of SO_4= from basinal Permian?-Triassic waters is ruled out.

Recent geochemical studies on Late to post-Hercynian Ba-(F)-(base metal) deposits in other areas of the Hesperian massif indicate that there are contrasted sources of sulphur involved in the mineralisation. Regarding to Late Triassic mineralisation hosted by Palaeozoic metasediments, Late-Hercynian granitoids and Triassic red beds, Canals et at. (1992) point out that SO_4= in barite ($\delta^{34}S_{barite}$ = +14.0 to +17.9 ‰) from the Atrevida vein (Catalonian Coastal Ranges) was derived from Triassic marine/sedimentary sulphate. Alternatively, $\delta^{34}S$ values in sulphides (which did not approach isotopic equilibrium with barite) are interpreted as representative of two sources of sulphur: H_2S derived from in situ bacteriogenic reduction of that sulphate and H_2S of deep origin.

As briefly described in chapter 2, data on sulphur isotopes from the Hiendelaencina silver-Ba-base metal veins (Spanish Central System) suggest two sources of sulphur for these Permian-Triassic mineralisations exclusively hosted by metamorphic rocks: 'magmatic' and 'metasediment'-derived sulphur. Barite and sulphide are in isotopic non-equilibrium. Most of the SO_4= incorporated in the barite ($\delta^{34}S_{barite}$ ranging from +26.14 to +6.14 ‰) was produced from the oxidation of the mixed $H_2S_{'magmatic'}$ and $H_2S_{'metasedimentary'}$ by meteoric waters (Concha et al., 1992a and b).

Lillo et al. (1992) interpreted the sulphur isotope data from other 'late Hercynian' Ba-(F)-(base metal) vein deposits hosted by Late Hercynian granitoids in the Spanish Central System as representative of sulphur derived from a 'magmatic' source. Isotopic geothermometry reflects deposition of barites ($\delta^{34}S_{barite}$ ranging from +12.27 to +16.59 °/oo) in isotopic equilibrium with galena and sphalerite ($\delta^{34}S_{sulphides}$ = -4.42 to +0.46 °/oo).

Palero et al., (1992) have presented an extensive study about the base metal deposits in the Alcudia Valley region, at the southern border of the Centroiberian zone of the Hesperian massif. This district represents the western prolongation of the Linares-La Carolina Pb-ore field, displaying several generations/types of base metal veins. The set of lodes denominated 'type IV' by Palero et al., (1992) may be analogous to the lodes studied in the present thesis. Those 'type IV' lodes are hosted by Palaeozoic metasedimens. $\delta^{34}S$ values in galenas are ranging -8.6 to -2.7 °/oo. $\delta^{34}S$ values found in sphalerites vary from -5.9 to -8.6 °/oo, reflecting deposition in isotopic non-equilibrium relative to galena. The sulphur isotope data are interpreted as the result of variable mixing of 'magmatic'-derived sulphur and biogenic sulphur derived from the host metasediments.

The interpretation proposed in this study is consistent with those for the base-metal deposits in the Spanish Central System and the Alcudia valley since some participitation of sulphur derived from a 'magmatic' source is considered. In addition, there is a variable participation of sulphur derived from the metasediments.

Chapter 8. Conclusions.

An investigation of the previously reported syn-diagenetic stratabound/stratiform Pb-Zn-(Ba) ore occurrences in the Upper Ordovician-Lower Silurian was among the initial aims of this thesis. During this study, no other ore occurrences than iron beds (Ashgill) and a supergenic iron-manganese karts-related deposit of uncertain (late-Hercynian?) age were found in the area. Moreover, some occurrences alluded in the literature (see chapter 3 for references) are clearly related to the Late-Hercynian vein-type mineralisation (e.g. veinlets in the Castellar Quartzite Fm. at the Renegadero valley. Despite the scarcity of mineral deposits (at least in the studied area) related to the Upper Ordovician-Lower Silurian sediments, these rocks may not be rejected as potential source for the metals in the Late-Hercynian lodes. Upper Ordovician-Lower Silurian sandstones show Ni, Zn and Pb content above the average values for sandstones. Pb, Ba and Zn enrichment is also observed in the Ashgillian limestones. In fact, on the basis of lead isotope geochemistry, most of the radiogenic lead involved in the Late-Hercynian veins seems to be derived from Ordovician U-"enriched" country rocks. The origin of those high concentrations of metals remains unknown.

The sedimentological study indicated that the Upper Ordovician-Lower Silurian metasediments represent several episodes of progradation of nearshore/inner shelf storm-influenced marine deposits over outer shelf muds. These episodes are grouped into two stratigraphical sequences that reflect sea-level rise-fall cycles which were caused by a combination of eustatic processes and regional processes like intraplate extensional tectonics. The geochemical composition of the metasediments suggested a sedimentary basin developed in a passive margin with very little participation of volcanogenic or igneous material, which is consistent with the biogenic/sedimentary source of sulphur incorporated in the metasediments as pyrite. Thus, most sediments were derived from older sedimentary rocks, although there is a petrochemical trend indicating maturity towards the top of the

sedimentary succession (where in apparent paradox the highest content of Pb, Zn and Ba are found).

Regarding the late-Hercynian ores, there is no evidence to support an origin for the Ba-(Pb-Zn) stratabound mineralisation hosted by Permian?-Triassic sediments different to that for the late-Hercynian lodes, since the isotopic, geochemical and fluid inclusions data are similar to those from the vein-type deposits. Moreover, both (lodes and stratabound deposits) seem the different expression of the same processes. The stratabound mineralisation at the basal beds of the post-Hercynian cover are truncated sharply by an erosional unconformity showing that the hydrothermal mineralisations must be pre-Ladinian in age. The stratigraphical discontinuity is also indicated by whole-rock geochemistry, with 'normal' metal content being observed in the overlaying beds. Furthermore, the structural pattern of the lodes is consistent with the age constrains thus estimated as the vein emplacement took place during an opening stage starting in the Upper Permian, subsequent to a transcurrent stage associated with the residual compressional Hercynian stresses.

Three ore deposition stages have been recognised, separated by major brecciation events. The first stage is characterised by the deposition of pyrrhotite, Ag sulphosalts, and minor amounts of arsenopyrite and Bi sulphides together with significantly amounts of galena and sphalerite.

The second stage is characterised by deposition of pyrite, Cu sulphides , barite and Ni-Co minerals. The main deposition of galena and sphalerite took place at the end of the first stage and the beginning of the second stage.

The third stage is characterised by minor deposition of pyrite and large amounts of calcite, specially at the Linares sector.

There is no selective Ag "enrichment" in relation to location or mode of occurrence.

An early phyllic alteration (coarse white mica + quartz + pyrite) no associated with the ore emplacement could occur during an extensional episode taking place before the end of the compressional Hercynian cycle. If our interpretation is correct, the fluids involved in this hydrothermal event were low saline aqueous fluids, with minimum temperatures of entrapment between 331.70 and 209.70°C.

The hydrothermal alteration related to the late-Hercynian veins is characterised by argillic-phyllic, argillic-propylitic and propylitic assemblages variably overprinted by late alkali metasomatism, with formation of albite and K-feldspar in textural equilibrium. The alteration more frequent (i.e. more important in volume) is defined by argillic-propylitic to propylitic assemblages, with formation of chlorite and white mica, at the expenses of biotite and feldspars, respectively. The ubiquitous occurrence of small amounts of kaolinite may be related to an early acidic alteration (advanced argillic alteration) whose alteration envelopes (at shallower levels) would have been eroded.

Mineral chemistry of chlorite and white micas from the alteration haloes show variations between different alteration zones and within the same alteration zone. There is a strong relation between some chemical variables and the mineralogy of the altered rock (e.g. silica in chlorite correlates negatively, and the Fe/(Fe+Mg) ratio in chlorite and white micas correlates positively, with the abundance of grains of chlorite) which identifies discrete zones relatively far away from the vein (in the scale of the alteration envelope) which are probably in relation to a larger water/rock interaction. Textural and chemical equilibrium between 'illite' and chlorite distinguishes the probable main stage of hydrothermal alteration: a transition from early strong acidic conditions, with leaching of feldspars and precipitation of kaolinite, likely as a consequence of the oxidation of reduced, deep waters (which could be responsible for the first ore stage characterised by the formation of pyrrhotite); to more alkaline conditions, represented by the formation of

orthoclase and albite, and related to the last ore deposition. Therefore, the geothermometry based on chlorite and illite compositions, which indicates temperatures of 276.7-321.5°C and 285-310.2°C respectively, may be used to constrain the T conditions of the main ore deposition stage.

The largest variations in mass transfer of different elements occur where the largest variations are observed in mineral chemistry. The monitoring of immobile element variations showed that there is a significant introduction of Si, Al, K, Na, Rb and Pb whereas remobilisation of Ca and Sr occur. Gains in Al may be up to 61.25 gr (in El Cobre lode) per 100 gr of unaltered Linares adamellite and up to 121.40 gr per 100 gr of unaltered Santa Elena granodiorite-adamellite (in the altered mylonite).

Four types of inclusion fluids have been observed which are assumed to represent three events of fluid entrapment related to vein formation.

The first stage of entrapment which is considered representative of the (late) first ore stage-(early) main ore stage, took place at hydrostatic pressures (310-400 bars, although overpressures above 1Kb occur locally) and Tt ranging from 87.4 to 392°C, involving moderate to low saline aqueous and saline CO_2-aqueous solutions thought to be partly immiscible during the entrapment.

The second stage of entrapment (related to the main ore deposition stage) is characterised by moderately saline NaCl-KCl-H_2O inclusions with minimum temperatures of trapping in the range of 168° to 325°C. The NaCl/(NaCl+KCl) ratios are close to the eutectic proportion (NaCl/(NaCl+KCl) = 0.78, after Hall et al., 1988)

The third stage of entrapment may represent the (late) main ore deposition stage and the (early) third ore deposition stage. It is characterised by high to moderately H_2O-NaCl-KCl-$CaCl_2$

saline fluids in inclusions homogenizing at Th ranging from 76° to 327°C.

Sulphur isotope distribution is not homogeneous throughout the whole district. Differences appear between those deposits located at the El Centenillo-Los Guindos-Santa Elena and those located at the La Carolina-La Nube-Linares. Dominant process at El Centenillo-Los Guindos-Santa Elena is mixing of deep waters carrying magmatic sulphur and shallower waters with sulphur derived from the metasediments. Biogenic pyrite shows a wide range of $\check{S}^{34}S$ values with very "heavy" compositions found in those sediments deposited in nearshore (high energy) environments.

Most of the aqueous sulphate incorporated into the mineralisation in both areas could be derived from the oxidation of H_2S by meteoric shallow ground waters.

In conclusion, the vein-type mineralisation in the Linares-La Carolina Pb-ore field was produced by hydrothermal fluids that evolved from low to moderately saline, (locally?) carbonaceous, hot fluids with 'magmatic'/metasedimentary H_2S as dominant sulphur specie, to high to moderately polysaline cooler fluids, with a higher $SO_4=/H_2S$ ratio as a result of mixing of the reduced and hot deep waters with shallower and cold waters. The high-moderate polysaline fluids must not be interpreted as due to the participation of basinal brines of marine origin because the sedimentary environments during the time of vein emplacement (Permian-Anisian) were exclusively continental (alluvial fan deposits, low-sinuosity fluvial systems). A more plausible origin of the polysaline fluids is related to the incorporation into the hydrothermal system of brines derived from local shallow playa-lakes developing under arid climate during the Autunian (the main host rock of the late-Hercynian stratabound deposits -e.g. Las Torrecillas- is a pisolitic dolostone that was deposited in that environment).

References

ÅBERG, G., AGUIRRE, L., LEVI, B. and NYSTRÖM, S.O. 1984. Spreading-subsidence and generation of ensialic marginal basins: an example from the early Cretaceous of Central Chile. In: Kokelnar, B.P. and Howells, M.F. (eds.). Marginal Basin Geology: Volcanic and Associated Sedimentary and Tectonic Processes in Modern and Ancient Marginal Basins. *Geol. Soc. Spec. Publ.*, **16**, 185-93.

AGUE, J.J. 1991. Evidence for major mass transfer and volume strain during regional metamorphism of pelites. *Geology*, **19**, 855-858.

AIGNER, T. and REINECK, H.E. 1982. Proximality trends in modern storm sands from the Heligoland Bight (North Sea) and their implication for basin analysis. *Senkenbergiana Maritima*, **14**, 183-185.

ALLEN, J.R.L. 1980. Sand waves: a model of origin and internal structure. *Sedimentary Geology*, **26**, 281-328.

ALLEN, J.R.L. 1982. Sedimentary structures: their character and physical basis. Elsevier, Amsterdam, 663 p.

ALLER, R.C. 1980. Quantifying solute distributions in the bioturbated zone of marine sediments by defining an average microenvironment. *Geochimica Cosmochimica Acta*, **44**, 1955-1965.

ALVARO, M.; CAPOTE, M. and VEGAS, R. 1979. Un modelo de evolucion geotectonica para La Cadena Celtiberica. *Acta Geologica Hispanica*, **14**, 172-177.

AMCOFF, O. 1976. The solubility of silver and antimony in galena. *Neves Jahrb. Mineralogie Abh.V6*, 297-261.

ANCOCHEA, E., ARENAS, R., BRÄNDLE, J.L., PEINADO, M., SAGREDO, J. 1988. Caracterización de las rocas metavolcánicas Silúricas del Noroeste del Macizo Ibérico. *Geociências*, **3**, 23-34.

ANDERSON, G.M.; BURNHAM, C.W. 1983. Feldspar solubility and the transport aluminium under metamorphic conditions. *American Journal of Science*, **283-A**,283-297.

ARENAS, R. 1991. Opposite P, T, t paths of Hercynian metamorphism between the upper units of Cabo Ortegal Complex and their

substratum (nothwest of the Iberian Massif). *Tectonophysics,* **191**, 347-364.

ARRIBAS, A. 1962. Mineralogia y metalogenia de los yacimientos españoles de uranio: Santa Elena (Jaen). *Bol. Real Soc. Esp. Hist. Nat. (G),* **60**, 243-251.

ARTHAUD, F. 1969. Methode de determination graphique des directions de raccourcissement, d'allongement et intermediare d'una population de failles. *Bull.Soc.Geol.France, XI,* 729-737.

ARTHAUD, F. and MATTE, Ph. 1975. Les décrochements tardihercyniens du sud-ouest de l'Europe. Géometrie et essai de reconstruction des conditions de déformation. *Tectonophysics,* **25**, 131-171.

AYORA, C. and FONTARNAU, R. (1990). X-ray microanalysis of frozen fluid inclusions. *Chemical Geology,* **89**, 135-148.

AZCARATE, J.E. AND VERGARA, A. 1977. Rasgos metalogenicos y metalotecticos del extremo de Sierra Morena. Metodologia y tecnicas para su investigacion. *I Congreso Hispano-Luso Americano de Geologia Economica. Madrid,* 1, seccion 4, 33-49.

BACHINSKI, S.W. and MULLER. 1971. Experimental determination of the microcline-low albite solvus. *Journal of petrology,* **12**, 329-356.

BARD, JP.; BURG, JP.; MATTE, Ph. and RIBEIRO, A. 1980. La chaîne hercynienne d'Europe occidentale en termes de tectonique des plaques. *Mem. Bur. Rech. Geol. Min.* , **108**, 233-246.

BEA, F.; CARNICERO, A.; GONZALO, J.C.; LOPEZ PLAZA, M. and RODRIGUEZ ALONSO, M.D. (Eds). Geología de los granitoides y rocas asociadas del Macizo Hespérico. Rueda. Madrid. 542 p.

BELLON, H., BLACHERE, H.; CROUSILLES, M.; SIMON, D. and TAMAIN, G. 1979. Radiochronologie, évolution tectono-magmatique et implications métalogeniques dans les Cadomo-variscides du Sud-Est hespérique. *Bull. Soc. Géol. France (7),* **21**, 113-120.

BERNER, R.A. 1970. Sedimentary pyrite formation. *American Journal Science,* **268**, 1-23.

BERNER, R.A. 1980. Early Diagenesis: A theoretical Approach. *Princeton University Press,* 241p.

BERNER, R.A. 1984. Sedimentary pyrite formation: An update. *Geochimica et Gosmochimica Acta,* **48,** 605-615.

BERNER, R.A. AND RAISWELL, R.1983. Burial of organic carbon and pyrite sulphur in sediments over phanerozoic time: A new theory. *Geochimica and Gosmochimica Acta,* **87,** 855-862.

BESSEMS, R.E. 1981. Aspects of Middel and Late Triassic palynology. 1. Palynostratigraphical data from the Chiclana de Segura Formation of the Linares-Alcaraz region. (southeastern Spain) and correlation with palynological assemblages from the Iberian Peninsula. *Rev.Paleobot.Palynol.,* **32,** 309-400.

BHATIA, M.R. 1983. Plate tectonics and geochemical compositions of sandstones. *Journal of Geology,* **91,** 611-627.

BHATIA, M.R. 1985. Composition and classification of Paleozoic Flysch mudrocks of eastern Australia: implications in provenance and tectonic setting interpretation. *Sedimentary Geology,* **41,** 249-268.

BLATT, H.; MIDDLETON, G. AND MURRAY, R. 1980. Origin of sedimentary rocks. Prentice-Hall, New Jersey.

BOERSMA, J.R. and TERWINDT, J.H.J. 1981. Neap-spring tide sequences of intertidal shoal deposits in a mesotidal estuary. *Sedimentology,* **35,** 449-464.

BOHLKE, J.K. 1989. Comparision of metasomatic reactoins between a common CO_2-rich vein and diverse wall rocks: intensive variables, mass transfers and Au mineralisation at Alleghany, California. *Economic Geology,* **84,** 291-327.

BOWERS, T.S. and HELGENSON, H.C. 1983. Calcualtion of the thermodynamic and geochemical consequences of nonideal mixing in the system H_2O-CO_2-NaCl on phase relations in geologic systems: Equation of state for H_2O-CO_2-NaCl fluids at high pressures and temperatures. *Geochimica et Cosmochimica Acta,* **47,** 1247-1275.

BRENCHLEY, P.J. and NEWALL, G. 1982. Storm-imfluenced inner-shelf sand lobes in the Caradoc (Ordovician) of Shropshire, England. *Journal of Sedimentary Petrology,* **52,** 783-815.

BRENCHLEY, P.J. AND STORCH, P. 1989. Environmental changes in the Hirnantian (Upper ordovician) of the Prague Basin, Czechoslovakia. *Geological Journal*, **24**, 165-181.

BRENCHLEY, P.J.; ROMANO, M. and GUTIERREZ-MARCO, JC. 1986. Proximal and distal ummocky cross-stratified facies on a wide Ordovician shelf in Iberia. In: Knight, R.J. & McLean, S.R. (eds.). Shelf Sands and Sandstones. *Can. Soc. Petrol. Geol. Mem.*, 11, 241-55.

BROUTIN, J. 1983. El Pérmico del borde suroeste de la Meseta. In: Martinez, C. (Ed). Carbonífero y Pèrmico de España. Inst. Geol. y Min. España Madrid. 440-450.

BROWN, J.S. 1943. Supergene magnetite. *Economic Geology*, 38, 137-148.

BROWN, P.E. 1989. FLINCOR: A microcomputer program for the reduction and investigation of fluid-inclusion data. *American Mineralogist*, **74**, 1390-1393.

BROWN, W.L. and PARSONS, L. 1981. Towards a more practical two-feldspar geothermometer. *Contributions to Minerology and Petrology*, **76**, 369-377.

BURRUSS, R.C. 1981. Analysis of phase equilibria in C-O-H-S fluid inclusions. In: Hollister, L.S. and Crawford, M.L. (eds.). Short course in fluid inclusions to petrology. Mineralogical Association of Canada, Calgary, 39-74.

CALSTEREN, P.W.C. Van; BOELRIJK, N.A.I.M.; HEBEDA,E.H.; PRIEM, H.N.A.; TEX, E.Den; VERDURMEN, E.A.Th. and VERSCHURE, R.H. 1979. Isotopic dating of older elements (including the Cabo Ortegal mafic-ultramafic complex) in the Hercynian orogen of NW Spain: manifestations of a presumed early Paleozoic mantle plume. *Chemical Geology*, **24**, 35-36.

CALVO, F.A. and GUILEMANY, J.M. 1975. Structure and origin of the mercury ore from Almadén, Spain. *Inst. Min. Metall. Trans. (B)*, **84**, B146-B149.

CANALS, A.; CARDELLACH, E.; RYE, D.M. and AYORA, C. 1992. Origin of the Atrevida Vein (Catalonian Coastal Ranges, Spain): Mineralogic, Fluid Inclusion, and Stable Isotope Study. *Economic Geology*, **87**, 142-153.

CAPOTE, R. 1983a. Los tiempos precámbricos: discusión e interpretaciones de conjunto. In: Libro Jubilar J.M Rios. Geología de España. Vol. I. Inst. Geol. y Min. España Madrid. 113-116.

CAPOTE, R. 1983b. La estructura de la extensión SE de la Zona Centroibérica en el Sistema Central. In: Libro Jubilar J.M. Rios. Geología de España. Vol. I. Inst. Geol. y Min. España. Madrid. 656p. 467-476.

CAPOTE, R. 1983c. La fracturación subsecuente a la Orogenia Hercínica. In: Libro Jubilar J.M. Rios. Geología de España. Vol. II. Inst. Geol. y Min. España. Madrid. 17-25.

CATHELINEAU, M. 1988. Cation site occupancy in chlorites and illites as a function of temperature. *Clay mineralogy*, **23**, 471-485.

CATHELINEAU, M. and NIEVA, D. 1985. A chlorite solid solution geothermometer. The Los Azufres (Mexico) geothermal system. *Contributions to mineralogy and petrology*, **91**, 235-244.

CHACON, J.; OLIVEIRA, V.; RIBEIRO,A. and OLIVEIRA, JT. 1983. La estructura de la Zona de Ossa-Morena. In: Libro Jubilar J.M. Rios. Geología de España. Vol. I. Inst. Geol. y Min. España. Madrid. 490-504.

CHARPENTIER, J.L. 1976. Géologie et métallogénie de la Sierra Carolina (Jaén, Espagne). Thése 3^{e} cycle. Centre d'Orsay. Univer. Paris-Sud. 156 pp.

CHRISTIE-BLICK, N.; GROTZINGER, J.P. and VON DER BORCH, C.C. 1988. Sequence stratigraphy in Proterozoic successions. *Geology*, **16**, 100-104

COLEMAN, M.L. 1980. Corrections for mass analysis of sulphur dioxide. IGS *Isotope Geology Unit stable Isotope Report*, **45**.

CONCHA, A.; LUNAR, R.; SIERRA, J.; LILLO, J. and OYARZUN, R. (1991). Estudio de inclusiones fluidas de las mineralizaciones epitermales de Ag-barita-metales de base de Hiendelaencina y de barita de Atienza (Sistema Central Español). *Estudios Geológicos*, **47**, 137-147.

CONCHA, A.; OYARZUN, R.; LUNAR, R.; SIERRA, J.; DOBLAS, M. and LILLO, J. (1992). The Hiendelaencina epithermal Silver-base

metal district, Central Spain: Tectonic and mineralizing processes. *Mineralium Deposita*, **27**, 83-89.

CONDIE, K.C. and MARTELL, C. 1983. Early proterozoic metasediments form north-central Colorado: Metamorphism, provenance and tectonic setting. *Geol.Soc.America Bull.*, **94**, 1215-1224.

CORRETGE, L.G. 1983. Las rocas graníticas y granitoides del Macizo Ibérico. In: Libro Jubilar J.M. Rios. Geología de España. Vol. I. Inst. Geol. y Min. España. Madrid. 569-592.

CRAWFORD, M.C. 1981. Phase equilibria in aqueous fluid inclusions. In: Hollister, L.S. and Crawford, M.L. (eds.) Short Course in fluids inclusions: Applications to petrology. *Mineral Assoc. Canada*, **6**, 75-100.

CROOK, K.A.W. 1974. Lithogenesis and geotectonics: the significance of compositional variation in flysch arenites (greywackes). In: Dott, R.H. and Shaver, R.H. (eds.). Modern and ancient geosynclinal sedimentation. *Soc. Econ. Paleon. Mineral. Spec. Publ.*, 19, 304-310.

CUMMING, G.L. and RICHARDS, J.R. 1975. Ore lead isotope ratios in a continuosly changing Earth. *Earth and Planetary Science Letters*, **28**, 155-171.

CURTIS , C.D. and SPEARS, D.A. 1968. The formation of sedimentary iron minerals. *Econ. Geology*, 63, 257-270.

CZAMANSKE, G.K. and RYE, R.O. 1974. Experimentally determined sulfur isotope fractionations between sphalerite and galena in the temperature range 600° to 275°C. *Economic Geology*, **69**, 17-25.

DAVIS, D.W.; LOWENSTEIN, T.K. ; SPENCER, R.J. 1990. Melting behaviour of fluid inclusions in laboratory-grown halite crystals in the systems NaCl-KCl-H_2O, Na-$MgCl_2$-H_2O and NaCl-$CaCl_2$-H_2O. *Geochimica et Cosmochimica*, Acta **54**, 591-601.

DEMAREST, J.M. and KRAFT, J.C. 1987. Stratigraphic record of Quaternary sea levels: implications for more ancient strata. In: Nummedal, D.; Pilkey, O.H. and Howard, J.D. (eds.). Sea-level fluctuation and coastal evolution. *Soc. Econ. Paleon. Mineral. Spec. Publ.*, **41**, 223-239 .

DEVON, F. and LE FORT, P. 1983. Chemical-mineralogical classification of plutonic rocks and associations. Examples from Southerm Asia belts. *Earth Sciences*, **73**, 135-149.

DEWEY, J.G. and BURKE, K.C.A. 1973. Tibetan, Variscan and Precambrian basement reactivation: products of continental collision. *Journal of Geology*, **81**, 683-692.

DOBLAS, M. 1991. Late Hercynian extensional and transcurrent tectonics in Central Iberia. *Tectonophysics*, **191**, 325-334.

DOBLAS, M. and OYARZUN, R. 1990. Caledonian and Late Caledonian Europe: A working hypothesis involving two contrasted compressional/extensional scenarios. *Estudios Geológicos*, **46**, 217-222.

DOBLAS, M.; OYARZUN, R.; LUNAR, R.; MAYOR, N. and MARTINEZ, J. 1988. Detachment faulting and late Paleozoic epithermal Ag-base metal mineralization in the Spanish Central system. *Geology*, **16**. 800-803.

DOE, B.R. and DELEVAUX, M.H. 1972. Source of lead in Southeast Missouri Galena Ores. *Economic Geology*, **67**, 409-425.

DOE, B.R. and ZARTMAN, R.E. 1979. Plumbotectonics, the Phanerozoic. In: Barnes, H.L. (ed.). Geochemistry of Hydrothermal Ore Deposits, 2nd edition. J. Wiley and Sons. New York. 22-70.

DREVER, J.I. 1982. The geochemistry of natural waters. Prentice-Hall. New Jersey, 388 p.

DUKE. W.L.; ARNOTT, R.W.C. AND CHEEL, R.J. 1991. Shelf sandstones and hummocky cross-stratification: New insights on a stormy debate. *Geology*, **19**, 625-628.

DUPONT, R.; LINARES, E. and PONS,J. 1981. Premiéres datations radiométriques par la méthode potassium-argon des granitoides de la Sierra Morena Occidentale (Provincie de Badajoz; Espagne): Consequences géologiques et metallogéniques. *Boletín Geológico y Minero*, **92**, 370-374.

EICHMANN, R.; SAUPE, F and SCHIDLOWSKI, M. 1977. Carbon and oxygen isotope studies in rocks of the vicinity of the Almaden mercury deposit (Province of Ciudad Real, Spain). In: Klemm, D.D. and Schneider, H.J. (Eds). Time- and strata-bound ore deposits. Berhn. Springer-Verlag. 396-405.

ENADIMSA. 1981. Exploration geologico-minera del area de Linare-La Carolina-Santa Elena (Jaen). Unpublished Report, I.G.M.E.

EUGSTER, M.P. and GUNTER, W.D. 1981. The compositions of supercritical metamorfic solutions. *Bulletin Mineralogy*, 104, 817-826.

FAIRCHILD, I.; HENDRY, G.; QUEST, M. and TUCKER, M. 1988. Chemical analysis of sedimentary rocks. In: Tucker, M. (ed.). Techniques in sedimentology. Blackwell, Oxford. 274-354.

FAURE, G. 1977. Principles of Isotope Geology. John Wiley & Sons, New York.

FLOYD, P.A. and LEVERIDGE, B.E. 1987. Tectonic environment of the Devonian Gramsctho basin, south Corwall: framework mode and geochemical evidence from turbiditic sandstones. *Journal Geol. Soc.*, 144, 531.

FLOYD, P.A.; SHAIL, R.; LEVERIDGE, B.E. AND FRANKE, W. 1991. Geochemistry and provenance of Rhenohercynian synorogenic sandstones: implications for tectonic environment discrimination. In: Morton, A.C.; Todd, S.P. and Haughton, P.D.W. (eds.). Developments in Sedimentary Provenance Studies. *Geol. Soc. Spec. Publ.*, 57, 173-188.

FULTHORPE, C.S. 1991. Geological controls on seismic sequence resolution. *Geology*, 19, 61-65.

GARRELS. R.M. and CHRIST, C.L. 1965. Solutions, minerals and equilibria. Harper and Row, New York.

GEHRIG, M.; LENZ, H. and FRANCK, K.U. 1979. Thermodynamic properties of water-carbon dioxide-sodium chloride mixtures at high temperatures and pressures. In: timmerhaus K.D. and Barber (eds.). High pressure science and technology.I, properties and material synthesis. Ponum, New York, 539-542.

GIGGENBACH, W.F. 1988. Geothermal solute equilibria. Derivation of Na-K-Mg-Ca geoindicators. *Geochimica et Cosmochimica Acta*, 52, 2749-2765.

GIL IBARGUCHI, J.I. and ORTEGA GIRONES, E. 1985. Petrology, structure and geotectonics implications of glaucophane-bearing eclogites and related rocks from the Malpica-Tuy

(MT) Unit, Galicia, Notrhwest Spain. *Chemical Geology*, **50**, 145-162.

GILLOU, J. 1969. Contribution à l'étude des minéralisations ordoviciennes en antimoine de la Sierra de Caurel (Provinces de Lugo et d'Orense, Espagne). *Sciences de la Terre Univ. Nancy*, **14**, 5-26.

GILLOU, J. 1971. Quelques régularités dans la distribution de minéralisations sulfurées (en particulier en antimoine) dans les niveaux carbonates du Paléozoique inférieur du géosynclinal Asturien. *Ann. Soc. Géol. Belgique*, **94**, 21-37.

GISBERT, J. 1983. Las Molasas tardihercinicas del Pirineo. In: Libro Jubilar, J.M. Rios. Geologia de España. 160-184.

GOLDHABER, H.B. and KAPLAN, I.R. 1980. Machanism of sulphur incorporation and isotope fractionation during early diagenesis in sediments of Gulf of California. *Marine Chemistry*, **9**, 95-143.

GRANT, J.A. 1986. The isocon diagram-A simple solution to Gresens' equation for metasomatic alteration. *Economic Geology*, **81**, 1976-1982.

GREEN, N.L. and USDANSKY, S.I. 1986. Tertiary-feldspar mixing relations and thermobarometry. *American Mineralogist*, **71**, 1100-1108.

GRESENS, R.L. 1967. Composition-volume relationships of metasomatism. *Chemical Geology*, **2**, 47-65.

GROOTENBOER, J. and SCHWARCZ, H.P. 1969. Experimentally determined sulfur isotope fractionations between sulfide minerals. *Earth and Planetary Science Letters*, **7**, 162-166.

GUILBERT, J.M. and PARK, C.F.Jr.1985. The geology of the ore deposits. W.H. Freeman.

GUMIEL, P. & ARRIBAS, A. 1987. Antimony deposits in the Inerian Peninsula. *Economic Geology*, **82**, 1453-1463.

GUMIEL, P. 1982. Metalogenia de los yacimientos de antimonio de la Península Ibérica. Ph.D. thesis, Univ. Salamanca, 324p.

GUTIERREZ-MARCO, J.C. AND PINEDA, A. 1988. Datos biostratigráficos sobre los materiales Silúricos del subsuelo de El Centenillo (Jaén). Congreso Geológico de España. Vol. 1, 91-94.

GUTIERREZ-MARCO, J.C.; RABANO, I. and ROBARDET, M. 1984. Estudio bioestratigráfico del Ordovícico en el sinclinal del Valle (Provincia de Sevilla, SO. de España). *Memórias e Notícias*, **97**, 11-37.

HAFENRICHTER, M. 1979. The lower and upper boundary of the Ordovician system of some selected regions (Celtiberia, eastern Sierra Morena) in Spain. Part II: The Ordovician-Silurian boundary in Spain. *N. Jb. Geol. Paläontol. Abh.*, **160**, 138-148.

HALAS, S.; SHAKUR, A. and KROUSE, H.R. 1982. A modified method of SO_2 extraction from sulphates for isotopic analysis using $NaPO_3$. *Isotopenpraxis*, **18**, 433-435.

HALL, D.L.; STERNER, S.M. and BODNAR, R.J. 1988. Freezing point depression of NaCl-KCl-H_2O solutions. *Economic Geology*, **83**, 197-202.

HALLIDAY, A.N. and MITCHELL, J.G. 1984. K-Ar ages of clay-size concentrates from the mineralisation of the Pedroches Batholith, Spain, and evidence for Mesozoic hydrothermal activity associated with the break up of Pangea. *Earth and Planetary Science Letters*, **68**, 229-239.

HAMMAN, W.; ROBARDET, M. and ROMANO, M. 1982. The Ordovician System in Southwestern Europe (France, Spain and Portugal). Correlation Chart and Explanatory Notes. *Int. Union Geol. Sci. Publ.*, **11**, p. 1-47.

HAQ, B.V.; HARDENBOL, J. and VAIL, P.R. 1987. Chronology of fluctuating sea levels since the Triassic. *Science*, **235**, 1156-1167.

HARMS, J.C.; SOUTHARD, J.B. and WALKER, R.G. 1982. Structures and sequences in clastic rocks. *Soc. Econ. Paleon. Mineral. Short Course*, **9**, 251 p.

HARMS, J.C.; SOUTHARD, J.B.; SPEARING, D.R. and WALKER, R.G. 1985. Depositional environments as interpreted from primary sedimentary structures. *Soc. Econ. Paleon. Mineral. Short Course*, **2**, 161 p.

HARRIS, C.W. and ERIKSSON, K.A. 1990. Allogenic controls on the evolution of storm to tidal shelf sequences in the Early

Proterozoic Uncompahgre Group, Southwest Colorado, U.S.A. *Sedimentology*, 37, 189-213.

HASS, J.S. 1971. The effect of salinity on the maximum thermal gradient of a hydrothermal system at hydrostatic pressure. *Economic Geology*, 66, 940-946.

HEDENQUIST, J.W. and BROWNE, P.R.L. 1989. The evolution of the Wasotapu geothermal system, New Zealand, based on the chemical and isotopic composition of its fluids, minerals and rocks. *Geochimica et Cosmochimica Acta*, 53, 2235-2257.

HEDENQUIST, J.W. and HENLEY, R.W. 1985. The importance of CO_2 on freezing point measurements of fluids inclusions: evidence from active geothermal systems and implications for epithermal ore deposition. *Economic Geology*, 80, 1379-1406.

HEMLEY, R.W.; TRUESDELL, A.M.; BARTON, P.B. and WHITNEY, J.A. 1984. Fluid-mineral equilibria in hydrothermal systems. Reviews in Economic Geology, 1, 267p.

HENKE, W. 1926 Beitrag zur Geologie der Sierra Morena nördlich von La Carolina (Jaén). *Abh. Senckenberg. Naturf. Gesells*, 39, 183-204.

HERNANDO, S. 1977. Pérmico y Triásico de la región de Ayllón-Atienza (Provincias de Segovia, Soria y Guadalajara). *Seminarios de Estratigrafía, Mon.*, 2, 408pp.

HERRANZ, P. 1984. Las discontinuidades estratigráficas principales en el sector central del NE de "Ossa-Morena": Rango y significado tectosedimentario. *Memórias e Notícias*, 97, 51-80.

HILLIER, S. and VELDE, B. 1991. Octahedral occupancy and the chemical composition of diagenetic (low-temperature) chlorites. *Clay Minerals*, 26, 149-168.

IBARROLA, E.; VILLASECA, C.; VIALETTE, Y.; FUSTER, J.M.; NAVIDAD, M.; PEINADO, M. and CASQUET, C. 1988. Dating of Hercynian granites in the Sierra de Guadarrama (Spanish Central System). In: Bea, F.; Carnicero, A.; Gonzalo, J.C.; Lopez Plaza, M. and Rodriguez Alonso, M.D. (Eds). Geología de los granitoides y rocas asociadas del Hespérico. Rueda Ed. Madrid. 377-383.

IGLESIAS, M.; RIBEIRO, M.L. and RIBEIRO, A. 1983. El N.O. de la Zona Centroibérica con metamorfismo de alto grado: la interpretación aloctonista de la estructura del Noroeste peninsular. In: Libro Jubilar J.M. Rios. Geología de España. Vol. I. Inst. Geol. y Min. de España. 459-467.

IGME. 1977. Hoja 905 Linares. Mapa Geologico de España, E.1:50,000. In: IGME de España, 33p.

JACKSON, M.J.; SIMPSON, E.L. AND ERIKSSON, K.A. 1990. Facies and sequence stratigraphic analysis in an intracratonic, thermal-relaxation basin: the Early Proterozoic, Lower Quilalar Formation and Ballara Quartzite, Mount Isa Inlier, Australia. *Sedimentology*, **37**, 1053-1078.

JACQUIN, J.P.; PINEDA, A. 1980. Sobre la metalogenia del subdistrito de la Carolina (Sierra Morena Oriental, España). Una nueva interpretación posible. Reflexiones sobre su investigación. *Studia Geologica Salmanticensa*, **16**, 59-70.

JOHNSON, H.D. and BALDWIN, C.T. 1986. Shallow siliciclastic seas. In: Reading, H.G. (ed.). Sedimentary environments and facies. Blackwell. Oxford. 229-282.

JULIVERT, M. 1983a. Generalidades. División en zonas del Macizo Ibérico. In: Libro Jubilar J.M. Rios. Geología de España. Vol. I. Inst. Geol. y Min. España Madrid. 67-71.

JULIVERT, M. 1983b. La estructura de la Zona Cantábrica. In: Libro Jubilar J.M. Rios. Geología de España. Vol. I. Inst. Geol. y Min. España Madrid. 339-381.

JULIVERT, M. 1983c. La estructura de la Zona Asturoccidental-Leonesa. In: Libro Jubilar J.M. Rios. Geología de España. Vol.I. Inst. Geol. y Min. España Madrid. 381-408.

JULIVERT, M. 1983d. La evolución sedimentaria durante el Paleozoico y el registro de la deformación en la columna estratigráfica Paleozoica. In: Libro Jubilar J.M. Rios. Geología de España. Vol.I. Inst. Geol. y Min. España Madrid. 593-601.

JULIVERT, M. and TRUYOLS, J. 1972. La coupe du Cabo Peñas, une coupe de référence pour l'Ordovicien du Nord-Ouest de l'Espagne. *C.R. Somm. Soc. Géol. France*, **6**, 241-243.

JULIVERT, M. and TRUYOLS, J. 1983. El Ordovícico en el Macizo Ibérico. In: Libro Jubilar J.M. Rios. Geología de España. Vol.I. Inst. Geol. y Min. España Madrid. 192-238.

JULIVERT, M.; FONTBOTE, J.M.; RIBEIRO, A. and NABAIS CONDE, L.E. 1972a. Mapa Tectónico de la Península Ibérica y Baleares E. 1:1.000.000, Memoria Explicativa: 1-113. Inst. Geol. y Min. España.

JULIVERT, M.; MARCOS, A. and TRUYOLS, J. 1972b. L'évolution paléogéographique du NW de l'Espagne pendant L'Ordovicien-Silurien. *Bull. Soc. Géol. Mineral. Bretagne,* **4**, 1-7.

JULIVERT, M.; TRUYOLS, J. and VERGES, J. 1983. El Devónico en el Macizo Ibérico. In: Libro Jubilar J.M. Rios. Geología de España. Vol.I. Inst. Geol. y Min. España Madrid. 265-310.

KAJIWARA, Y. and KROUSE, H.R. 1971. Sulphur isotope partitioning in metallic sulphide systems. *Canadian Journal of Earth Sciences,* **8**, 1397-1408.

KERRICK, D.M. 1990. Aluminium metasomatism. In: Ribbe, P.H. ed The Al_2SiO_5 polymorphs. *Reviews in Mineralogy,* **22**, 3311-3352.

KLEIN, G. de V. 1970. Depositional and dispersal dynamics of intertidal sand bars. *Journal of Sedimentary Petrology,* **40**, 1095-1127.

KOEPPEL, V. and SCHROLL, E. 1983. Lead isotopes of Palaeozoic strata-bound to stratiform galena-bearing sulphide deposits of the Eastern Alps (Austria); implications for their geotectonic setting. *Schweiz. Min. Petr. Mitt.*, **63**, 347-360.

KONNERUP-MADSEN, J. 1979. Fluid inclusions in quartz from deep-seated granitic intrusions, South Norway. *Lithos* 12, 13-23.

KRAUSKOPF, K.B. 1982. Introduction to Geochemistry (2nd edition). McGraw-Hill, 617p.

KUIJPER, R.P. and ARPS, C.E.S. 1983. El N.O. de la zona Centroibérica con metamorfismo de alto grado: Un modelo de evolución basado en el desarrollo de una "mantle plume". In: Libro Jubilar J.M. Rios. Geología de España. Vol.I. Inst. Geol. y Min. España Madrid. 455-458.

KUIJPER, R.P; PRIEM, H.N.A and TEX, E. DEN. 1982. Late Archean-Early Proterozoic source areas of zircons in rocks from the

Paleozoic orogen of Western Galicia. *Precambrian Research*, **19**, 1-29.

KUMAR, N. and SANDERS, J.E. 1976. Characteristics of shoreface storm deposits: modern and ancient examples. *Journal of Sedimentary Petrology*, **46**, 145-162.

LEFORT, J.P. and VOO, R. Van Der. 1981. A kinematic model for the collision and complete suturing between Gondwanaland and Laurasia in the Carboniferous. *Journal of Geology*, **89**, 537-550.

LEFORT, LP. and RIBEIRO, A. 1980. La faille Porto-Badajoz-Cordue a-t-elle controlé l'evolution de l'ocean paléozoïque Sud-armoricain?. *Bull. Soc. Géol. France* (7^e), **22**, 455-462.

LELONG, F.; TARDY, Y; GRANDIN, J; TRESCASES, J.J. and BBOULANGE. 1976. Pedogenesis, chemical weathering, and processes of formation of some supergene ore deposit. In: Wolf K.M. ed Handbook of Stratabound and Stratiform Deposits, 6, 93-173.

LILLO, J. 1990. Tectonic controls in Linares-La Carolina Pb-ore field: inheritance from a collisional regime. Mineral deposits study group. Annual Meeting, Dublin, p-20.

LILLO, J.; OYARZUN, R.; LUNAR, R.; DOBLAS, M.; GONZALEZ, A. and MAYOR, N. (1992). Geologic and metallogenic aspects concerning the Late Variscan Ba-(F)-(base metal) Vein deposits of the Spanish Central System. *Inst. Min. Metall. Trans.*, 101, b24-B32

LINKE, W.F. 1965. Solubillities of inorganic and metal-organic compounds. Van Nostan, Princeton, 1407p.

LOCUTURA, J. and TORNOS, F. 1985. Consideraciones sobre la metalogenia del sector medio del Sistema Central Español. *Rev. Real Acad. Ciencias Fis. Exac. Nat.*, **59**, 589-623.

LOCUTURA, J. and TORNOS, F. 1987. Aspectos genéticos de las mineralizaciones de F(Ba-Pb) del área de Colmenar de Arroyo (Sistema Central Español). *Boletín Geológico y Minero*, **98**, 680-694.

LONKER, S.W.; GERALD J.D.F.; HEDENQUIST, J.W. and WALSHE, J.L. 1990. Mineral fluid interactions in the broadlands-chaaki geothermal system, New Zealand. *American Journal of Science*, **290**, 995-1068.

LOPEZ GARRIDO, A.C. 1971. Geologia de la zona prebetica al NE de la provincia de Jaen. Tesis Universidad de Granada, 317p.

LORENZ, V. and NICHOLLS, I.A. 1976. The Permo-Carboniferous Basin and range of Europe. Am application of plate tectonics. In: Falke, H. (ed.). The Continental Permian in Central, West and South Europe. Reidel. Dordrecht.313-342.

LOTZE, F. 1945. Zur Gliederung der Varisziden der Iberischen Meseta. *Geotekt. Forsch*, 6, 78-92.

LUDWIG, K.R.; VOLLMER, R.; TURI, B., SIMMONS, K.R. and PERNA, G. 1989. Isotopic constrains on the genesis of base-metal ores in southern and central Sardinia. *European Journal of Mineralogy*, **1**, 657-666.

LUZHNAYA, N.P. and VERESHTCHETINA, I.P. 1946. Sodium, calcium, magnesium chlorides in aqueous solutions at -57 to +25° (polythermic solubility). *Zhurnl. Prike. Knimii*, **19**, 723-733.

MACAYA, J.; GONZALEZ-LODEIRO, F.; MARTINEZ-CATALAN, J.R. and ALVAREZ, F. 1991. Continuous deformation, ductile thrusting and backfolding of cover and basament in the Sierra de Guadarrama, Hercynian orogen of central Spain. *Tectonophysics*, **191**, 291-309.

MACLEAN, W.H. 1990. Mass change calculations in altered rock series. *Mineralium Deposita*, **25**, 44-49.

MACLEAN, W.H. and KRANIDIOTIS, P. 1987. Immobile elements as monitors of mass transfer in hydrothermal alteration: Phelps Dodge Massive Sulfide Deposit, Matagami, Quebec. *Economic Geology*, **82**, 951-962.

MARRET, R. and ALLMENDINGER, R.W. 1990. Kinematic analysis of fault-slip data. *Journal of Structural Geology*, **12**, 973-986.

MARTINEZ FRIAS, J. 1987. Mineralogía y metalogenia de las mineralizaciones de plata del sector oriental del Sistema Central. Ph.D. Thesis. Univ. Complutense Madrid. 379p.

MARTINEZ FRIAS, J.; OYARZUN, R.; MAYOR, N.; LUNAR, R. and VINDEL, E. 1988. Mineralizaciones de la Sierra de Guadarrama. Aplicación del modelo epitermal. *Bol. Soc. Española Mineral.*, **11**, 27-34.

MARTINEZ GARCIA, E. 1983a. El Pérmico de la Cordillera Cantábrica. In: Martinez, C. (Ed) Carbonífero y Pérmico de España. Inst. Geol. y Min. España Madrid. 389-402.

MARTINEZ GARCIA, E. 1983b. Permian Mineralizations in the Cantabrian Mountains (North-West Spain). In: Schneider, H.J. (Ed). Mineral Deposits of the Alps and of the Alpine Epoca in Europe. Springer-Verlag, Berlin-Heidelberg. 259-274.

MARTINEZ, F.J. and GIL IBARGUCHI, I. 1983. El metamorfismo en el Macizo Ibérico. In: Libro Jubilar J.M. Rios. Geologia de España. Vol. I. Inst. Geol. y Min. España Madrid.

MATTE, Ph. 1964. Sur le volcanisme silurien du synclinal de Truchas (N.O de l'Espagne). *C.R. Somm. Soc. Géol. France*, **1964 (2)**, 57-58.

MATTE, Ph. 1986. La Chaîne varisque parmi les chaînes paléozoiques péri atlantiques, modelé d'évolution et position des grands blocs continentaux au Permo-Carbonifére. *Bull. (8^e) Soc. Géol. France*, 2, 9-24.

MAYNARD, J.B.; VALLONI, R. and YU, H. 1982. Composition of modern deep sea sands from arc-related basins. In: Leggett, J.K. (ed.). Trench-Forearc Geology. *Geol. Soc. Spec. Publ.*, **10**, 551-561.

MAYOR, N.; LUNAR, R. and OYARZUN, R. 1988. Mineralizaciones filonianas de barite-fluorite-cuarzo-(metales de base-Ag) del sector centro-occidental del Sistema Central Español. *Bol. Soc. Española Mineral.*, 11, 137-9.

McCACE, P.J. and JONES, C.M. 1977. The formation of reactivation surfaces within superimposed deltas and bedforms. *Journal of Sedimentary Petrology*, **47**, 707-715.

McDOWELL, S.D. and McCURRY, M. 1978. Mineralogical variations in borehole #1, Salton Sea geothermal area, preliminary report. Univ.California, Riverside report VCR/IGPP-78/11.

MEER MOHR Van Der, C.G.; KUIJPER, R.P.; CALSTEREN, P.W.C. Van and TEX, E. Den. 1981. The Hesperian Massif: from Iapetus aulacogen to ensialic orogen. A model for its development. *Geologische Rundschau*, 70, 459-472.

MEGARD, F. and PHILIP, H. 1976. Plio-Quaternary tectonomagmatic zonation and plate tectonics in the Central Andes. *Earth Planetary Science Letters*, **33**, 231-238.

MEYER, C. and HEMLEY, J.J.. 1967. Wall rock alteration. In: Barnes H.L. (eds.). Geochemistry of hydrothermal ore deposits New York, Holt, Rinehart and Winston, 166-235.

MIDDLETON, G.V. 1967. Experiments on density and turbidity currents. III. Deposition of sediment. *Canadian Journal of Earth Sciences*, **22**, 108-125.

MILLER, C.F.; STODDARD, E.F.; BRADFISH, L.S.; and DOLLASE, W.A. 1981. Composition of plutonic muscovite: genetic implications. *Canadian Mineralogist*, **22**, 25-34.

MITCHELL, W.J. 1974. An outline of the stratigraphy and palaeontology of the Ordovician rocks of Central Portugal. *Geological Magazine*, **111**, 385-396.

MOLNAR, P. and TAPPONNIER, P. 1977. Relation of the tectonics of eastern China to the India-Eurasia collision: Application of Slip-line field theory to large-scale continental tectonics. *Geology*, **5**, 212-216.

MOREL, P. and IRVING, E. 1978. Tentative paleocontinental maps for the early Phaneozoic and Proterozoic. *Journal of Geology*, **86**, 535-561.

MUÑOZ, M.; ANCOCHEA, E.; SAGREDO, J.; PEÑA, J.A.; HERNAN, F.; BRANDLE, J.L. and MARFIL, R. 1985. Vulcanismo Permo-Carbonífero de la Cordillera Ibérica. In: C.R. del X Congreso Intal. de Estratigrafía y Geología del Carbonífero. Vol.3. Inst. Geol. y Min. España Madrid. 27-52.

NAVIDAD, M. 1983. El vulcanismo permocarbonífero de la Península Ibérica. In: Martinez, C. (Ed). Carbonífero y Pèrmico de España. Inst. Geol. y Min. España Madrid. 472-482.

NUMMEDAL, D. and SWIFT, D.J.P. 1987. Transgressive stratigraphy at sequence-bounding unconformities: some principles derived from Holocene and Cretaceous examples. In: Nummedal, D.; Pilkey, O.H. and Howard, J.D. (eds.). Sea-level fluctuation and coastal evolution. *Soc. Econ. Paleon. Mineral. Spec. Publ.*, **41**, 241-259.

NøTTVEDT, A. and KREISA, R.D. 1987. Model for combined flow origin of hummocky cross-stratification. *Geology*, **15**, 357-361.

OHMOTO, H. 1972. Systematics of sulfur and carbon isotopes in hydrothermal ore deposits. *Economic Geology*, **67**, 557-578.

OHMOTO, H. 1986. Stable isotope geochemistry of ore deposits. In Valley, J.H.; Taylor, H.P.; O'neil, J.R.(ed.), "Stable isotopes in high temperature geological processes". Reviews in Mineralogy., v.16.

OHMOTO, H. and LASAGA, A.C. 1982. Kinetics of reactions between aqueous sulfates and sulfides in hydrothermal systems. *Geochimica et Cosmochimica Acta*, **46**, 1727-1745.

OHMOTO, H. and RYE, R.O. 1979. Isotopes of sulfur and carbon. In: Barnes, H.L. (ed.). Geochemistry of Hydrothermal Ore Deposits, 2nd edition. J. Wiley and Sons. New York. 509-567

ORTEGA, L.; VINDEL, E. and LUNAR, R. 1988. Estudio de los filones de baritina intragraníticos del Sector Cenicientos-Cadalso de los Vidrios (Sistema Central). *Bol. Soc. Española Mineral.*, **11**, 89-99.

PALERO, F. and MARTIN-IZARD, A. 1988. Las mineralizaciones estratoides de Zn-Pb en la Caliza Urbana del paraje de Peña del Aguila, Calzada de Calatrava (Ciudad Real). *Bol. Soc. Española Mineral.*, **11**, 179-189.

PALERO, F.; BOTH ROSS A.; MANGAS VIÑUELA, J.; MARTIN-IZARD, A. and REGUILLON BRAGADO, R. 1992. Metalogenesis de los yacimientos de Pb-Zn de la region del Valle de Alcudia (Sierra Morena Occidental). In: Fernandez Frias, J. and Garcia Guinea, J. Los Recursos Minerales de España, 1027-1067.

PARIS, F. AND ROBARDET, M. 1990. Early Palaeozoic palaeobiogeography of the Variscan Regions. *Tectonophysics*, **177**, 193-213

PARRY, W.T. 1986. Estimation of XCO_2, P and fluid inclusion volume from fluid inclusion temperature measurements in the system $NaCl-CO_2-H_2O$. *Economic Geology*, **81**, 1009-1013.

PEARCE, J.A.; HARRIS, N.B.W. and TINDLE, A.G. 1984. Trace element discrimination for the tectonic interpretation of granitic rocks. *Journal of Petrology*, **25**, 956-983.

PEARSON, D.G. 1989. The petrogenesis of pyroxenites containing octahedral graphite and associated mafic and ultramafic rocks of the Beni Boussera Peridotite massif, N. Morocco. Ph. Thesis, University of Leeds, 413 pp.

PEARSON, M.K.; CLARK, K.F. and PORTER, E.W. 1988. Mineralogy, fluid characteristics and silver distribution at Real de los Angeles, Zacatecas, Mexico. *Economic Geology*, **83**, 1737-1759.

PEUCAT,J.J.; BERNAND-GRIFFITHS, J.; GIL IBARGUCHI, J.I.; DALLMEYER, R.D., MENOT, R.P.; CONICHET, J.; IGLESIAS PONCE DE LEON, M. 1990. Geochemical and geochronological cross section of the deep Variscan crust: The Cabo Ortegal high-pressure nappe (northwestern Spain). *Tectonophysics*, **177**, 263-292.

PHILIPPOT, P. and SELVERSTONE, J. 1991. Trace-element-rich brines in eclogitic veins: Implications for fluid composition and transport during subduction. *Contributions to Mineralogy and Petrology*, **106**, 417-430.

PINEDA, A. 1987. La Caliza Urbana (Ordovícico Superior) y sus tramos volcanoclásticos en el subsuelo del norte de El Centenillo (Jaén). *Boletín Geológico y Minero*, **98**, 780-793.

PINTO, M.S. 1984. Granitóides Caledónicos e hercínicos na zona de Ossa-Morena (Portugal). Nota sobre aspectos geocronológicos. *Memórias e Notícias*, **97**, 81-94.

PINTO, M.S. and ANDRADE, A.S. 1987. Geocronologia dos granitódes da zona de Ossa-Morena (Maciço Hespérico) no contexto do arco Ibero-Armonicano. *Geociências*, **2**, 95-103.

PORTERO, J.M. and DABRIO, C. 1988. Evolución tectosedimentaria del Ordovícico y Silúrico de los Montes de Toledo meridionales y Campo de Calatrava. In: Congreso Geológico de España. Vol. I, 161-164.

POSAMENTIER, H.W. and VAIL, P.R. 1988. Eustatic controls on clastic deposition II-Sequence and systems tract models models. In: Wilgus, C.K.; Hastings, B.S.; Kendall, C.G.St.C.; Posamentier, H.W.; Ross, C.A. and Van Wagoner, J.C. (eds.). Sea-level changes: An integrated approach. *Soc. Econ. Paleon. Mineral. Spec. Publ.*, **42**, 125-154.

POSAMENTIER, H.W.; JERVEY, M.T. and VAIL, P.R. 1988. Eustatic controls on clastic deposition I-Conceptual framework. In: Wilgus, C.K.; Hastings, B.S.; Kendall, C.G.St.C.; Posamentier, H.W.; Ross, C.A. and Van Wagoner, J.C. (eds.). Sea-level changes: An integrated approach. *Soc. Econ. Paleon. Mineral. Spec. Publ.*, **42**, 109-124.

PRIEM, H.N.A.; BOELRIJK, N.A.I.M.; VERSHURE, R.H.; HEBEDA, E.H. and VERDURMEN, E.A. T.h. 1970. Dating events of and plutonism through the Paleozoic of the Western Iberian Peninsula. *Eclogae Geologicae Helvetia*, **63**, 255-274.

QUESADA, C. AND RIBEIRO, A. 1989. Paleozoic terrane map of the Iberian Peninsula. In: Keppie, J.D. and Dallmeyer, R.D. (Compilers). Tectonic Map of Pre-Mesozoic Terranes in Circum-Atlantic Phanerozoic Orogens. IGCP Project 233: Terranes in Circum-Atlantic Paleozoic Orogens.

RAISWELL, R. 1982. Pyrite texture, isotopic composition, and the availability of iron. *Amer.Journal Science*, **282**, 1244-1263.

RAISWELL, R. and BERNER, R.A. 1986. Pyrite and organic matter in phanerozoic normal marine shales. *Geochimica et Cosmochimica Acta*, **50**, 1967-1976.

RAMOS, A. 1979. Estratigrafía del Pérmico y Triásico al Oeste de Molina de Aragón (Provincia de Guadalajara). *Seminarios Estratigrafía, Mon.*, **6**, 313pp.

RECHES, Z. 1983. Faulting of rocks in three-dimensional strain fields II. Theoretical analysis. *Tectonophysics*, **95**, 133-156.

RIBEIRO, M.L. 1987. Petrogenesis of early peralkaline rhyolites from the Macedo de Cavaleiros region (NE Portugal). *Geologische Rundschau*, **76**, 147-168.

RICHTER, P. 1967. Stratigraphie und tektonik in der Sierra de san Andrés (östliche Sierra Morena, Spanien). *Münst. Forsch. Geol. Paläont.*, **3**, 1-144.

RIDING, R. 1974. Model of the Hercynian foldbelt. *Earth and Planetary Science Letters*, **24**, 125-135.

RIOS, S. 1977. Estudio geológico del metalotecto plumbífero del Ordoviciense (La Carolina-Santa Elena, Sierra Morena Oriental). Ph.D.thesis. Univ. Politécnica. Madrid. 271 p.

RIOS, S. 1984. Aspectos geologicos del metalotecto plumbifero de La Carolina-Santa Elena, Sierra Morena Oriental (Jaen, España). *Boletín Geológico y Min*ero, **88**, 99-108.

RIOS, S.; CLAVERIAS, P. 1979. Nota acerca de la existencia de indicios estratoligados de Zn-Pb en el Ordoviciense Superior del extremo SE de la Meseta Hercínica Española. *Boletín Geológico y Minero*, **90**, 1-5.

ROBARDET, M. 1976. L'Orginalité du segment hercynien sud-ibérique au Paléozoique inférieur Ordovicien, Silurien et Dévonien dans le Nord de la Province de Séville (Espagne). *C.R. Acad. Sci. Paris (Ser.D.)*, **283**, 999-1002.

ROBINSON, B.W. and KUSAKABE, M. 1975. Quantitative preparation of sulphur dioxide for $^{34}S/^{32}S$ analysis from sulphides by combustion with cuprous oxide. *Analytical Chemistry*, **47**, 1179-1181.

ROEDDER, E. 1984. Fluid Inclusions. *Reviews in mineralogy*, **12**. Mineralogical Society of America, 644pp.

ROEDDER, E. and BODNAR, R.J. 1980. Geological pressure determination from fluid inclusions studies. Ann. Rev. *Earth Planetary Sciences*, **8**, 263-301.

ROSER, B.P. and kORSH, R.J. 1986. Determination of tectonic setting of sandstone-mudstone suites using SiO_2 content and K_2O/Na_2O ratio. *Journal of Geology*, **94**, 635-650.

SAKAI, H. 1968. Isotopic properties of sulfur compounds in hydrothermal processes. *Geochem. Jour.*, **2**, 29-49.

SAKAI, H. and DICKSON, R. 1978. Experimental determination of the rate equilibrium fractionation factors of sulphur isotope exchange between sulphate and sulphide in slightly acid solution at 300°C and 1000 Bars. *Earth Planetary Science Letters*, **39**, 151-161.

SAMAMA, J.C. 1986. Orefields and continental weathering. Van Nostrand reinhold Company. New York. 326 p.

SANCHEZ, V.; APARICIO, A. 1969. Estudio petrologico de los afloramientos graniticos de Sta. Elena y Linares. *Boletín Geológico y Minero*, **80**, 344-351.

SAUPE, F. 1971. la série Ordovicienne et Silurienne d'Almadén (province de Ciudad Real, Espagne). Point des connaissances actuelles. *Mem. Bur. Rech. Geol. Min.* , **73**, 355-365.

SAUPE, F. 1990. Geology of the Almadén Mercury Deposit, Province of Ciudad Real, Spain. *Economic Geology*, **85**, 482-510.

SAWYER, E.W. 1986. The influence of source rock type, chemical weathering and sorting on the geochemistry of clastic sediments from the Quetico Metasedimentary Belt, Superior Province, Canada. *Chemical Geology*, **55**, 7-95.

SCHWARTZ, M.O. 1989. Determining phase volumes of mixed CO_2-H_2O inclusions using microthermometric measurements. *Mineralium deposits*, **24**, 43-47.

SCOTESE, C.; BAMBACH, P.K.; BARTON, C.; VOO Van Der, R. and ZIEGLER, A. 1979. Paleozoic Base Maps. *Journal of Geology*, **87**, 217-277.

SECK. 1971. Der einflub des drucks aut die Zusammensetzung koexistierender alkalifeldspate und plagioklase im system $NaAlSi_3O_8$-H_2O. *Contributions to mineralogy and petrology*, **31**, 67-86.

SHAW, D.M. 1956. Geochemistry of pelitic rocks. Part III: major elements and general geochemistry. *Geological Society of America Bull.*, **67**, 919-934.

SHAW, D.M. 1968. A review of K-Rb fractionation trends by covariance analysis. *Geochimica et Cosmochimica Acta*, **32**, 573-602.

SHEPHERD, T.J.; RANKIN, A.H. and ALDERTON, D.H.M. 1985. A practical guide to fluid inclusion studies. Glasgow, Blackie and son, 239p.

SIBSON, R.H.; ROBERT, F. and POULSEN, K.H. 1988. High-angle reverse faults, fluid-pressure cyclyng, and mesothermal gold-quartz deposits. *Geology*, **16**, 551-555.

SIERRA, J.; VINDEL, E.; LUNAR, R.; LOPEZ, J.A. and MARTINEZ FRIAS, J. 1988. Estudio de inclusiones fluidas en la mineralizacion de plata de la Bodera (Sistema Central Español). *Bol. Soc. Española Mineral.*, **11**, 61-66.

SIEVER, R. 1979. Plate-tectonic controls on diagenesis. *Journal of Geology*, **87**, 127-155.

SIMON, K. 1990. Hydrothermal alteration of Variscan granites, southern Schwarzwald, Federal Republic of Germany. *Contributions to Mineralogy and Petrology,* **105**, 177-196.

SIMPSON, E.L. and ERIKSSON, K.A. 1990. Early Cambrian progradational and transgressive sedimentation patterns in Virginia: an example of the early history of a passive margin. *Journal of Sedimentary Petrology,* **60**, 84-100.

SMITH, A.G. 1981. Phanerozoic Equal-Area Maps. *Geologische Rundschau,* **70**, 91-127.

SOPEÑA, A. 1979. Estratigrafía del Pérmico y Triásico del NW de la Provincia de Guadalajara. *Seminarios de Estratigrafía, Mon.*, **5**, 329pp.

SOPEÑA, A.; LOPEZ, J.; ARCHE, A.; PEREZ-ARLUCEA, M.; RAMOS, A.; VIRGILI, C. and HERNANDO, S. 1988. Permian and Triassic rift basins of the Iberia Peninsula. In: Manspeizer, W (ed.). Triassic-Jurassic rifting. Continental Breakup and the Origin of the Atlantic Ocean and Passive Margins. *Developments in Geotectonics*, **22** (B), 757-786.

SPEARS, D.A. 1989. Aspects of iron incorporation into sediments with special reference to the Yorkshire Ironstones. In: Young T.P. and Taylor, W.E.G. eds. Phamerozoic Ironstones. *Geological Society Special Publi.*, **46**, 19-30.

SPEARS, D.A. and AMIN, M.A. 1981. A mineralogical and geochemical study of turbidite snandstones and interbedded shales, Mam Tor, Derbyshire, U.K. *Clay Minerals,* **16**, 333-345.

STACEY, J.S. and KRAMERS, J.D. 1975. Approximation of terrestrial lead isotope evolution by a two-stage model. *Earth and Planetary Science Letters,* **26**, 207-221.

STORMER, J.C. Jr. 1975. A practical two-feldspar geothermometer. *American mineralogist,* **60**, 667-674.

SWANENBERG, H.E.C. 1979. Phase equilibria in Carbonic systems, and their application to freezing studies of fluid inclusions. *Contributions to Mineralogy and Petrology,* **68**, 303-306.

SWIFT, D.J.P.; FIGUEIREDO, A.G.; FREELAND, G.L. AND OERTEL, G.F. 1983. Hummocky cross-stratification and megaripples: a geological double standard?. *Journal of Sedimentary Petrology,* **53**, 1295-1317.

TAMAIN, G. 1966. Les ecailles du Centenillo (Jean, Espagne). Contribution a l'etude structurale du rebord meridional de la Meseta Iberique. C.R. *Acad.Sci.Paris (ser.D)*, **263**, 1355-1358.

TAMAIN, G. 1967. El Centenillo, Zone de référence pour L'etude de l'Ordovicien de la Sierra Morena orientale (Espagne). *C. R. Acad. Sci. Paris (ser. D)*, **265**, 389-392.

TAMAIN, G. 1972. Recherches géologiques et minières en Sierra Morena Orientale (Espagne). Thèse. Univ. Paris-Sud (Centre d'Orsay), 3 Vols., 870 pp.

TAPPONIER, P.; PELTZER, G.; LE DAIN, A.Y.; ARMIJO, R. and GOBBOLD, P. 1982. Propaling extension tectonics in Asia: new insights from sample experiments with plasticine. *Geology*, **110**, 611-616.

TAYLOR, S.R. AND McLENNAN, S.M. 1985. The continental crust: its composition and evolution. Blackwell, Oxford. 312 pp.

TORNOS, F.; CASQUET, C.; LOCUTURA, J. and COLLADO, R. 1991. Fluid inclusion and geochemical evidence for fluid mixing in the genesis of Ba-F (Pb-Zn) lodes of the Spanish Central System. *Mineralogical Magazine*, **55**, 225-234.

TUREKIAN, K.K. AND WEDEPOHL, K.H. 1961. Distribution of the elements in some major units of the Earth's crust. *Geol. Soc. America Bull.*, **72**, 172-192.

VAIL, P.R. 1987. Seismec stratigraphy interpretation using sequence stratigraphy. Part 1: Seismic stratigraphy interpretation procedure. In: Bally, A.W. (ed.). Atlas of seismic stratigraphy. *Amer. Assoc. Petr. Geol. Studies in Geology*, **27**, v.1, 1-10.

VAIL, P.R.; HARDENBOL, J. and TODD, R.G.. 1984. Jurassic unconformities, chronostratigraphy, and sea-level changes from seismic stratigraphy and biostatigraphy. In: Schlee, J.S. (ed.). Interregional unconformities and hydrocarbon accumulation. *Amer. Assoc. Petr. Geol. Mem.*, **36**, 129-144.

VAIL, P.R.; MITCHUM, R.M.; TODD, R.G.; WIDMIER, J.M.; THOMPSON, S.; SANGREE, J.R.; BUBB, J.N. AND HATFIELD, W.G. 1977. Seismic stratigraphy and global changes in sea level. In: Payton, C.E. (ed.). Seismic stratigraphy -applications to

hydrocarbon exploration. *Amer. Assoc. Petr. Geol. Mem.*, **26**, 49-205.

VAN WAGONER, J.C.; POASAMENTIER, H.W.; MITCHUM, R.M.Jr.; VAIL, P.R.; SARG, J.F.; LOUTIT, T.S. AND HARDENBOL, J. 1988. An overview of the fundamentals of sequence stratigraphy and key definitions. In: Wilgus, C.K.; Hastings, B.S.; Kendall, C.G.St.C.; Posamentier, H.W.; Ross, C.A. and Van Wagoner, J.C. (eds.). Sea-level changes: An integrated approach. *Soc. Econ. Paleon. Mineral. Spec. Publ.*, **42**, 39-45

VIELZEUF, D. and PIN, Ch. 1989. Geodynamic implications of Hercynian granulitic rocks. In: Daly, J.S., Cliff, R.A. and Yardley, B.W.D. (eds). Evolution of Metamorphic Belts. *Geol. Soc. Spec. Publ.*, **43**, 343-348.

VINDEL, E. 1980. Estudio mineralógico y metalogénico de las mineralizaciones de la Sierra de Guadarrama. Ph.D. Thesis. Univ. Complutense Madrid. 249 pp.

VINOGRADOV, A.P.; GRINENKO, V.A. and USTINOV, V.I. 1962. Isotopic composition of sulphur compounds in the Black Sea. *Geokhimiya*, **10**, 973-997.

VIRGILI, C.; SOPEÑA, A.; RAMOS, A.; ARCHE, A. and HERNANDO, S. 1983. El relleno posthercínico y el comienzo de la sedimentación Mesozoica. In: Libro Jubilar J.M. Rios. Geología de España. Vol. II. Inst. Geol. y Min. España. Madrid. 25-36.

VOO Van Der, R. 1982. Pre-Mesozoic paleomagnetism and plate tectonics. *Ann. Review Earth Planetary Sciences*, **10**, 191-220.

WALKER, R.G.; DUKE, W.L. and LECKIE, D.A. 1983. Hummocky stratification: significance of its variable bedding sequences: discussion. *Geol. Soc. America Bull.*, **94**, 1245-1251.

WALSHE, J.L. 1986. A six-component chlorite solid solution model and the conditions of chlorite formation in hydrothermal and geothermal systems. *Economic Geology*, **81**, 681-703.

WALSHE, J.L. and SOLOMON, M. 1981. An investigation into the environment of formation of the volcanic-hosted Mt Lyell copper deposits, using geology, mineralogy, stable

isotopes, and a six-component chlorite solid solution model. *Economic Geology*, **76**, 246-284.

WEBER, R. 1984. Variscan events: early Palaeozoic continental rift metamorphism and Late Palaeozoic crustal shortening. In: Hutton, D.H.W. and Sanderson D.J. (eds.) Variscan tectonics of the North Atlantic Region. *Geol. Soc. Spec. Publ.*, **14**, 3-22.

WEDEPOHL, K.H.; DELEVAUX, M.H. and DOE, B.R. 1978. The potential source of lead in the Permian Kupferschiefer bed of Europe and some selected Palaeozoic mineral deposits in the Federal Republic of Germany. *Contributions to Mineralogy and Petrology*, **65**, 273-278.

WERNICKE, B. 1985. Uniform sense simple shear of the continental lithosphere. *Canadian Journal of Earth Sciences*, **22**, 108-125.

WOOD, B.J. and WALTHER, J.V. 1986. Fluid flow during metamorphism and its implications for fluid-rock ratios. In: Walther, J.V. and Wood, B.J. eds. Fluid-rock interactions during metamorphism. New York, Springer-Verlag, 89-108.

WRONKIEWICZ, D.J. and CONDIE, K.C. 1987. Geochemistry of Archaean shales from the Witwatersrand Supergroup, South africa: source-area weathering and provenance. *Geochimica et Cosmochimica Acta*, **51**, 2401-2416.

YARDLEY, B.W.D. 1977. Relations between the chemical and modal compositions of metapelites from Connemara, Ireland. *Lithos*, **10**, 235-242.

YARDLEY, B.W.D. 1986. Fluid migration and veining in the Connemara schist, Ireland. In: Walther, J.V.; and Wood, B.J. eds. Fluid-rock interactions during metamorphism: New York, Springer-Verlag, 109-131.

YARDLEY, B.W.D. 1989. An introduction to metamorphic petrology. Longman, Essex. 248 pp.

YOUNG, T.P. 1989. Phamerozoic ironstones: an introduction and review. In: Young, T.P. and Taylor, W.E.G. eds. Phanerozoic ironstones. *Geological Society Special Publication*, **46**, IX-XXV.

YUDOVICH, Y.E.; KETRIS, M.P.; MERTS, A.V. and BELYAEV, A.A. 1985. Petrochemical identification of volcanic products in the Pay Khoy black shales. *Geochemistry International*, **21**, 71-84

ZHANG, YI-GANG and FRANTZ, J.D. 1987. Determination of the homogenization temperatures and densities of supercritical fluids in the system NaCl-KCl-$CaCl_2$-H_2O using synthetic fluids inclusions. *Chemical geology*, **64**, 335-350.

ZITZMANN, A. and NEUMANN-REDLIN, C.H.R. 1976. The Iron Ore Deposits of Spain. In: Zitzmann, A. (ed.). The Iron Ore Deposits of Europe and Adjacent Areas. Vol.1. 1977. 269-278.

ZONENSHAIN, L.P.; KUZMIN, M.I. and KONONOV, M.V. 1985. Absolute reconstruction of the Paleozoic oceans. *Earth and Planetary Science Letters*, **74**, 103-116.

Appendix I. Sample preparation. Operating conditions.

I.1. X-Ray fluorescence (XRF) analysis.

I.1.1.Sample preparation.

Samples of 1-5 Kg weight were initially washed with hot water and detergent, and dried. The clean samples were broken down into regular cubes of 4 cm. side using a hydraulic splitter. Weathered portions were removed at this stage. The cubes were crushing by hand in a steel mortar until the fragments reached a size of 3 mm. Grinding into fine powder was done by a tungsten carbide Tema mill at high speed during 50-60 seconds. Equipment was scrupulously washed with hot water and detergent and dried to use for each sample. Levels of potential contamination derived from the equipment used throughout this procedure are shown in table I.1. Powders were placed in clean plastic bags. Representative portions were transferred into small glass bottles which were kept in a drying oven at temperature of 105°-110°C for at least four hours.

XRF analyses were conducted on fused discs (major elements) and pressed pellets (trace elements) from the powders obtained with the above procedure.

Preparation of fused discs began with ignition of 1 g. of dried sample in a furnace for one hour at a temperature of 1000°C. After ignition the samples were reweighted and the loss in weight was assumed to be equivalent to the loss on ignition (L.o.I). 0.4 g. of sample powder was mixed thoroughly with 4 g. of Johnson Mattey Spectroflux 110 and the mixture was fused in a Pt-Au crucible in a furnace for 30 minutes at 1000°C. The mixture was reweighted and spectroflux was newly added to reach the original weight of the mixture (4.4 g.). The crucible was then placed on a gas burner until a homogeneous melt was got. The melt was poured into a hot copper ring of about 4 cm. diameter on a hot plate to form the glass disc, which was transferred to a sealed plastic bag to avoid atmospheric moisture attack.

Pressed pellets were made by mixing of 15 g. of finely pulverized samples with approximately 1.5 g. of polyvinil glue. Powder and glue were thoroughly mixed in clean, throw-away containers. The mixture was pressed at a minimum pressure of 10 tons in a cylinder die. Each pellet thus made was dried in a oven at a temperature of 105°-110°C for at least one hour before to be placed in a sealed plastic bag.

I.1.2. Operating conditions, limits of detection.

The analyses were performed at the University of Leeds using a Phillips PW 1400 X-Ray spectrometer at the operating conditions shown in table I.2.

For element oxides in excess of 5% the reproducibility is generally better than 1% of the quoted value, elements present at levels of between 0.5 and 5 % are reproducible to within 1 to 2 % of the quoted value. Elements that constitute between 0.1 and 0.5 % of the rock are reproducible to within 5 % whereas <0.1 % of an element can only be reproduced at the 20 % level (Pearson, 1989). For trace elements, values below 10 ppm are generally outside the detection limits of the machine.

I.2. Electron microprobe (EMP) analysis.

I.2.1. Sample preparation.

Polished thin sections were made of 30 microns thickness, without glass covers. These thin sections were studied by conventional optical microscopy (COM) to selected suitable areas or mineral grains prior to SEM and EMP work.

I.2.2. Operating conditions.

A CAMECA SX-50 instrument (University of Leeds) fitted with a LINK 10/55S energy dispersive system, was used for the EMP work. Operating conditions are given in table I.3.

I.3. Scanning electron microscopy (SEM).

Test of the contamination introduced during the crushing of an industrial silica sand in three separate Tema® swing mill barrels (ten 50 g samples in each). Milling time 1 min at high speed for W carbide and steel, 3 min for agate. Analysis by XRF of duplicate 15 g powder pellets. Oxides as percentages, elements as ppm. The low value for Ni crushed in carbide is caused by a W background interference. The difference in mean Zr values for carbide and agate can be explained by sampling errors

	W carbide			Agate			Steel		
	Range	$\bar{x}$	s	Range	$\bar{x}$	s	Range	$\bar{x}$	s
Fe_2O_3*	0.259–0.284	0.267	0.01	0.233–0.994	0.268	0.02	0.290–0.344	0.311	0.02
MnO	0.002–0.004	0.003	0.001	0.002–0.003	0.003	0.001	0.003–0.006	0.005	0.001
CaO	0.156–0.209	0.193	0.03	0.161–0.206	0.195	0.02	0.176–0.202	0.189	0.01
K_2O	0.107–0.137	0.125	0.01	0.107–0.159	0.133	0.02	0.119–0.146	0.133	0.02
Ni	1–2	1.5	0.6	4–7	4.8	1.3	4375–7163	5588	1194
Cr	14–23	18	3.8	8–24	15	6.3	629–962	775	143
Zr	48–107	70	25.6	50–137	88	33.6	84–126	102	18
Sr	12–13	12.6	0.6	11–13	12.0	0.7	11–14	12	1.3
Pb	2–4	3.0	0.7	48–134	90	37	2–4	2.8	0.8
W	751–1855	1430	457	<2	—	—	<2	—	—

Table I.1. Levels of potential contamination in crushing of samples (Fairchild et al., 1988)..

Element	Line	Collimator	Detector	Crystal	2-theta	Offsets +	Offsets -	Time (Secs)	KV	Ma
Na	Ka	Coarse	Flow	PX 1	28.58	1.2	1.2	160	40	60
Mg	Ka	Coarse	Flow	PX 1	23.67	1.6	1.6	80	40	60
Al	Ka	Coarse	Flow	PET	144.90	2.0	---	40	60	60
Si	Ka	Coarse	Flow	InSb	144.56	2.2	---	20	40	60
P	Ka	Coarse	Flow	Ge	141.03	2.0	---	20	40	60
K	Ka	Fine	Flow	LiF 200	136.69	5.0	---	20	40	60
Ca	Ka	Fine	Flow	LiF 200	113.09	---	---	20	40	60
Ti	Ka	Fine	Flow	LiF 200	86.14	3.0	---	20	40	60
Mn	Ka	Fine	Flow	LiF 200	62.97	1.6	---	20	40	60
Fe	Ka	Fine	Flow	LiF 200	57.52	---	1.5	16	40	60
Co	Ka	Fine	Flow	Lif 220	77.89	0.5	---	80	80	30
Ni	Ka	Fine	Flow	LiF 200	48.67	1.0	---	80	80	30
Cu	Ka	Fine	Flow	LiF 200	45.03	0.6	1.0	80	80	30
Zn	Ka	Fine	Scint	LiF 200	41.76	1.0	---	80	80	30
Rb	Ka	Fine	Scint	LiF 200	26.62	0.5	0.8	80	80	30
Sr	Ka	Fine	Scint	LiF 200	25.15	0.6	0.6	80	80	30
Y	Ka	Fine	Scint	LiF 200	23.80	0.8	0.8	80	80	30
Zr	Ka	Fine	Scint	LiF 200	22.55	0.4	0.8	80	80	30
Nb	Ka	Fine	Scint	LiF 220	30.39	0.6	0.6	80	80	30
Ba	Ka	Fine	Scint	LiF 220	15.54	0.5	0.3	80	80	30
Th	La	Fine	Scint	Lif 220	39.23	0.9	0.5	00	80	30
U	La	Fine	Scint	Lif 200	26.11	1.0	0.4	400	80	30
Pb	Lb	Fine	Scint	LiF 200	28.26	0.5	1.0	80	80	30

Table I.2. Operating conditions for X-ray fluorescence analysis.

1.	Silicates & opaque oxides, excluding feldspars etc. Beam energy 15 KV; Beam current; 15 nanoamps; Count times; Na, Mg, Al, Si, K, Ca, Ti- all 15 secs on peak 10 on background. Cr, Mn, Fe, Ni - 30 secs on peak, 10 secs background.
2.	Feldspars, micas, & chlorites. Beam energy 15 KV; Beam current; 10 nanoamps; Count times for all elements - 10 secs on peak, 10 secs background. Where necessary, beam broadened to 2 - 5 μ to prevent excessive element loss.
3.	Raw counts were corrected for inter-element effects using CAMECA PaP proprietary software.
4.	Standards used; Na - albite; Mg - spinel; Al - kyanite; Si - diopside; K - orthoclase; Ca - wollastonite; Ti - sphene; Cr - chromite; Mn - rhodonite; Fe - haematite; Ni nickel oxide; F - cryolite; Cl - KCl.
5.	Sulphides; 20 KV at 20 nanoamps all elements 10 secs. Standards used; pure elements, except S + Zn sulphide.

Table I.3. Instrumental conditions of the CAMECA SX 50 electron microprobe.

I.3.1. Sample preparation.

SEM work at Leeds was carried out on thin sections prepared as for EMP. SEM/EDX study on frozen inclusions was done at the University of Barcelona (Spain) following the procedure suggested by Ayora and Fontarnau (1990).

I.3.2. Operating conditions.

A Cambridge instrument was used with a 7 Na beam current and 20 KV accelerating voltage. Images were produced in backscattered electron atomic number (Z) contrast mode (SEM/BSE/Z).

I.4. Fluid inclusions.

I.4.1. Sample preparation.

Sample preparation to double polished thin sections was the standard for fluid inclusions studies (e.g. Roedder, 1984; Shepherd et al., 1985).

I.4.2. Equipment.

The heating-freezing stage used for all fluid inclusion microthermometric work was a LINKAM THM 600 fitted to a LEITZ DIALUX microscope with X10 and X25 eyepieces and X32 magnification objective. At temperatures below 0°C, factor of correction was 0.933. No correction was done for temperatures above 0°C.

I.5. Sulphur isotopes.

I.5.1. Sample preparation.

I.5.1.1.Mineral separation.

Mineral separates from barite and coarse-grained sulphides were obtained by drilling from a cut section of the sample using a jeweller's drill with a tungsten carbide bit. Medium-grained sphalerite and pyrite were extracted by "soft" crushing using a steel mortar and removal of monomineral grains by careful hand picking under binocular microscope to avoid impurities.

Sulphur from samples containing only very fine-grained pyrite as mineral involving sulphur was extracted following the technique commonly adopted for pyrite sulphur determinations in sediments. Approximately 0.5 g. of sample powder (obtained by the described crushing procedure) and 10 ml. of ethanol are placed in the digestion flask (fig. I.1). 20 ml. of "working" copper solution (cupric acetate) is added to the collecting head and the apparatus is then placed on a hot plate. Flush of nitrogen creates a reducing environment inside the digestion flask. Addition of distilled water to the collecting head is made until only the top bulb of the spreader is exposed. 20 ml. of concentrated hydrochloric acid is injected via the addition tube, and the contents is allowed to simmer for 120 minutes. The reaction in the flask is as follows:

$$2CrCl_2 + 2FeS_2 + 4HCl \rightarrow 2CuCl_3 + 2CuCl_3 + 2H_2S + FeCl_2$$

The H_2S liberated was collected as copper sulphide, which is extracted as solid residue when the solution is filtered through a 12.5 cm. (Watman No. 42) filter paper. The solution collected in a 750 ml conical flask is titrated against EDTA (Ethylenediaminetetra acetic acid disodium salt) with glycine cresol red (0.5 % solution) as indicator, the pH being kept constant (5.5) by the addition of 75 ml. of a 1 M sodium acetate buffer solution. The EDTA solution (approximately 0.1 M) is standardised against a standard copper solution containing approximately 6 g. of Cu per liter (accurately known). The amount of copper removed is equivalent to the amount of reduced sulphur liberated from the sample, and therefore the percentage of sulphur can be calculated.

The recovery of pyrite sulphur by this technique may be up to 99±0.6 %.

I.5.1.2. Analytical procedure.

Sulphur isotope analyses were performed on sulphides using the method proposed by Robinson and Kusakabe (1975). The sulphide

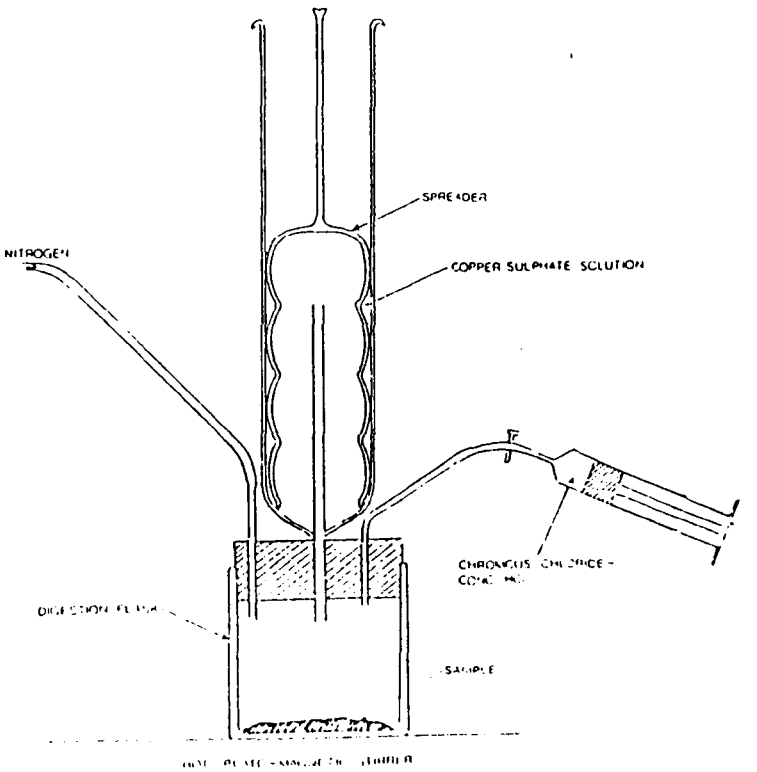

Fig. I.1. Sketch of the apparatus used to sulphur extraction using chromous chloride.

was intimately mixed with an excess of Cu_2O (usually 5-10 mg of sulphide with 200 mg of Cu_2O) and ground to a grain size of about 150 μ in a small agate mortar. Combustion of the sample took place in the furnace of a vacuum line at 1120 °C for 15 minutes, producing SO_2.

Analyses on barite were determined using a method modified from Halas et al. (1982). Sulphate (20 mg) was intimately mixed with 60-80 mg of trisodium trimetaphosphate (TMP). Combustion of the sample was at 950 °C during 25 minutes, yielding SO_2.

CO_2 produced with SO_2 was effectively extracted by distillation of CO_2 at -129.7 °C in a n-pentane trap. Sample yields were measured, being the reaction efficiency greater than 97 %.

The SO_2 samples were analysed using a VG SIRA 10 gas source mass spectrometer. The raw data were corrected for instrumental and isobaric effects using standard correction procedures (e.g. Coleman, 1980). A chalcopyrite standard (British geological Survey Cp-1) was used as internal standard for the analyses. As primary standards were used IAEA NZ-1 and IAEA OG-S-1. Analytical uncertainty is ±0.20 °/oo. All results are reported as $\delta^{34}S$ relative to Cañon Diablo Troilite (CDT) standard.

Appendix II. Data.

II.1. XRF analyses.

File: Sedall Disk: Metasediments provenance

LINARES-LA CAROLINA METASEDIMENT WHOLE-ROCK CHEMISTRY

Sample	149-1	59-12	9088-2	9088-3	9098-7	308-7	308-6	153-1	153-2	143-1	93-5	9031-13	9031-2	9078-1	9078-2	9078-3
Formation	El Cañ	El Cañ	El Cañ	El Cañ	Bot. Qz.	Mixed B.	Mixed B.	Mixed B.	Mixed B.	Mixed B.	Mixed B.	Mixed B.	Mixed B.	Cas.Qz.	Cas.Qz.	Cas.Qz.
Location	Palanco	Miranda	Grande	Grande	Curas	Cente	Cente	Cente	Cente	Cente	Guindo	Guindo	Guindo	Grande	Grande	Grande
SiO2	83.92	80.01	79.43	83.53	97.61	72.36	75.41	63.10	80.75	77.68	70.98	84.09	72.64	83.70	87.26	92.41
TiO2	.65	.46	.57	.65	.09	.91	1.16	.82	.43	.78	.87	.68	.75	.49	.51	.23
Al2O3	7.02	7.47	8.22	6.61	1.38	16.53	15.00	20.76	10.43	13.98	17.84	9.54	15.23	10.06	7.85	4.74
Fe2O3	2.99	2.44	3.05	3.79	.93	1.49	1.70	3.32	1.98	.91	1.14	.88	2.55	1.12	.39	.42
MnO	.11	.06	.05	.01	.03	.00	.00	.01	.01	.00	.01	.01	.01	.01	.01	.01
MgO	.90	.63	.64	.62	.09	.31	.28	1.01	.37	.36	.41	.26	.75	.13	.16	.07
CaO	1.00	2.92	1.54	.17	.06	.04	.04	.11	.14	.02	.06	.03	.20	.03	.02	.02
Na2O	1.11	1.61	1.73	.69	.07	.29	.25	.43	2.90	.20	.88	.10	.51	.13	.07	.08
K2O	1.46	2.10	2.61	1.06	.44	2.87	2.40	6.99	1.82	3.74	4.47	2.93	3.36	2.81	2.12	1.28
P2O5	.08	.05	.12	.11	.07	.11	.15	.08	.06	.04	.06	.04	.10	.13	.05	.05
L.o.I	1.20	3.21	1.97	1.78	.29	4.77	3.58	4.00	1.66	2.80	3.67	1.40	4.30	2.23	1.50	.77
Total	100.42	100.96	99.93	99.02	101.05	99.69	99.94	100.62	100.54	100.51	100.38	99.97	100.41	100.82	99.93	100.07
Co	35.00	22.00	31.00	30.00	33.00	13.00	10.00	16.00	16.00	12.00	10.00	16.00	19.00	18.00	15.00	30.00
Ni	13.00	9.00	5.00	21.00	3.00	16.00	5.00	17.00	5.00	4.00	10.00	2.00	12.00	4.00	5.00	2.00
Cu	26.00	5.00	6.00	7.00	.00	16.00	16.00	18.00	4.00	7.00	5.00	1.00	20.00	11.00	2.00	.00
Zn	42.00	27.00	25.00	100.00	53.00	68.00	61.00	29.00	21.00	13.00	88.00	16.00	177.00	41.00	21.00	24.00
Rb	49.00	63.00	67.00	38.00	16.00	116.00	87.00	231.00	60.00	99.00	116.00	92.00	121.00	75.00	55.00	31.00
Sr	108.00	161.00	128.00	30.00	7.00	77.00	40.00	72.00	97.00	35.00	42.00	13.00	40.00	30.00	19.00	12.00
Y	41.00	20.00	25.00	27.00	8.00	61.00	33.00	22.00	17.00	22.00	40.00	26.00	42.00	17.00	18.00	8.00
Zr	750.00	354.00	463.00	555.00	43.00	344.00	326.00	258.00	283.00	380.00	329.00	571.00	304.00	367.00	502.00	193.00
Nb	13.00	9.00	10.00	11.00	1.00	18.00	29.00	16.00	8.00	15.00	19.00	13.00	16.00	10.00	10.00	4.00
Ba	268.00	485.00	791.00	233.00	51.00	695.00	899.00	1,406.00	478.00	608.00	627.00	284.00	663.00	279.00	236.00	114.00
Pb	40.00	8.00	21.00	15.00	11.00	45.00	93.00	48.00	21.00	96.00	54.00	12.00	74.00	665.00	737.00	419.00
Th	19.00	12.00	18.00	18.00	5.00	16.00	14.00	15.00	10.00	13.00	15.00	14.00	15.00	5.00	5.00	3.00
U	4.00	3.00	4.00	4.00	2.00	5.00	5.00	3.00	3.00	4.00	7.00	5.00	5.00	2.00	2.00	1.00

File: Sedall Disk: Metasediments provenance

LINARES-LA CAROLINA METASEDIMENT WHOLE-ROCK C

Sample	59-13	90138-4	9098-8	90148-1	308-8	9031-4
Formation	Corred.	Botella	Cantera	Chavera	Chavera	Chavera
Location	Miranda	Curas	Curas	Grande	Cente	Guindo
SiO2	64.30	54.10	64.54	73.74	50.24	57.48
TiO2	.99	1.30	.90	.53	1.17	1.11
Al2O3	19.26	25.42	17.88	8.65	25.47	20.40
Fe2O3	5.22	5.83	4.93	9.13	8.39	7.14
MnO	.02	.03	.02	.14	.06	.05
MgO	1.41	1.33	1.23	1.72	2.58	1.88
CaO	.09	.23	.11	.04	.15	.21
Na2O	.87	.34	.75	.16	.49	.72
K2O	4.51	6.72	5.22	2.26	5.20	6.62
P2O5	.12	.13	.06	.08	.21	.12
L.o.I	3.51	4.72	3.29	3.29	5.51	3.60
Total	100.31	100.15	98.94	99.74	99.47	99.32
Co	19.00	20.00	26.00	42.00	28.00	27.00
Ni	15.00	48.00	32.00	44.00	58.00	30.00
Cu	18.00	10.00	17.00	18.00	38.00	22.00
Zn	86.00	66.00	50.00	4,301.00	235.00	574.00
Rb	161.00	216.00	209.00	114.00	233.00	232.00
Sr	38.00	65.00	45.00	10.00	139.00	25.00
Y	37.00	35.00	23.00	21.00	52.00	38.00
Zr	293.00	234.00	232.00	347.00	145.00	180.00
Nb	20.00	24.00	18.00	10.00	25.00	22.00
Ba	886.00	1,135.00	786.00	212.00	1,224.00	1,226.00
Pb	23.00	11.00	12.00	389.00	25.00	18.00
Th	16.00	22.00	18.00	7.00	28.00	21.00
U	6.00	4.00	4.00	2.00	7.00	5.00

File: Guarr Disk: XRF Jan '90

LINARES-LA CAROLINA METASEDIMENT WHOLE-ROCK GEOCHEMISTRY

Sample	73-1	73-2	73-3	73-4	73-5	73-7	73-8
Formation	Urbana	Urbana	Urbana	Urbana	Urbana	Urbana	Urbana
Location	Desprec.	Desprec.	Desprec.	Desprec.	Desprec.	Desprec.	Desprec.
SiO2	7.64	5.65	n.a.	7.85	1.87	n.a.	n.a.
TiO2	.04	.23	n.a.	.25	.10	n.a.	n.a.
Al2O3	.30	.88	n.a.	1.88	.53	n.a.	n.a.
Fe2O3	.25	1.01	n.a.	.95	.57	n.a.	n.a.
MnO	.09	.18	n.a.	.04	.04	n.a.	n.a.
MgO	.52	.51	n.a.	.69	.66	n.a.	n.a.
CaO	49.71	50.05	n.a.	47.79	53.03	n.a.	n.a.
Na2O	.02	.04	n.a.	.05	.03	n.a.	n.a.
K2O	.08	.26	n.a.	.52	.13	n.a.	n.a.
P2O5	.02	.03	n.a.	.05	.03	n.a.	n.a.
L.o.I	40.27	40.50	n.a.	39.06	42.37	n.a.	n.a.
Total	98.93	99.34	n.a.	99.15	99.38	n.a.	n.a.
Co	4.00	4.00	14.00	6.00	6.00	101.00	251.00
Ni	5.00	6.00	27.00	7.00	2.00	390.00	1015.00
Cu	6.00	11.00	17.00	5.00	6.00	55.00	41.00
Zn	12.00	18.00	27.00	12.00	362.00	3943.00	6372.00
Rb	1.00	8.00	3.00	16.00	3.00	11.00	6.00
Sr	216.00	253.00	176.00	198.00	183.00	35.00	356.00
Y	5.00	9.00	11.00	5.00	4.00	21.00	54.00
Zr	3.00	20.00	8.00	43.00	11.00	25.00	22.00
Nb	.00	2.00	.00	4.00	3.00	4.00	2.00
Ba	25.00	41.00	46.00	126.00	26.00	2166.00	11104.00
Pb	1.00	9.00	10.00	2.00	101.00	194.00	144.00
Th	7.00	6.00	7.00	7.00	7.00	5.00	4.00
U	1.00	2.00	1.00	1.00	.00	2.00	1.00

File: Lingran Disk: Linares XRF
LINARES ADAMELLITE WHOLE-ROCK GEOCHEMISTRY (UNALTERED)

Sample	90118-2 fresh	90138-3 fresh	91416-9 fresh	91416-10 fresh	91416-11 fresh	91416-12 fresh	91416-13 fresh	91416-14 fresh	91416-15 fresh	91416-16 fresh
SiO2	68.78	68.11	68.91	69.00	67.11	68.82	68.22	67.90	67.70	66.94
TiO2	.54	.54	.47	.51	.54	.53	.55	.54	.57	.55
Al2O3	15.67	15.88	15.74	15.71	16.21	15.63	15.79	15.84	16.02	16.48
Fe2O3	3.88	3.84	3.37	3.54	3.84	3.79	3.82	3.77	4.11	3.82
MnO	.06	.06	.05	.05	.06	.06	.06	.05	.06	.06
MgO	1.06	1.08	1.01	1.02	1.10	1.07	1.07	1.06	1.17	1.16
CaO	2.41	2.57	2.34	2.65	2.34	2.46	2.63	2.66	2.59	2.50
Na2O	3.24	3.49	3.29	3.32	3.17	3.24	3.27	3.21	3.16	3.32
K2O	4.35	4.16	4.45	4.11	4.56	4.33	4.15	4.21	4.27	4.63
P2O5	.21	.20	.20	.21	.22	.20	.22	.20	.22	.21
L.o.I	1.09	.49	.50	.89	.90	.70	.30	.87	.99	.59
Total	101.29	100.42	100.34	101.02	100.04	100.83	100.08	100.33	100.85	100.26
Co	31.00	34.00	31.00	28.00	30.00	24.00	28.00	34.00	32.00	28.00
Ni	7.00	7.00	7.00	6.00	7.00	6.00	6.00	5.00	6.00	4.00
Cu	7.00	7.00	5.00	5.00	8.00	5.00	8.00	6.00	9.00	9.00
Zn	54.00	59.00	54.00	55.00	62.00	59.00	60.00	59.00	62.00	59.00
Rb	180.00	172.00	179.00	163.00	177.00	170.00	175.00	169.00	172.00	179.00
Sr	154.00	164.00	160.00	164.00	194.00	161.00	168.00	166.00	169.00	202.00
Y	32.00	31.00	28.00	29.00	31.00	29.00	28.00	31.00	30.00	31.00
Zr	180.00	193.00	172.00	171.00	187.00	172.00	199.00	178.00	186.00	188.00
Nb	12.00	12.00	10.00	10.00	11.00	9.00	12.00	12.00	12.00	11.00
Ba	647.00	631.00	657.00	642.00	681.00	599.00	679.00	642.00	644.00	657.00
Pb	31.00	24.00	25.00	25.00	25.00	24.00	25.00	25.00	25.00	24.00
Th	21.00	21.00	20.00	20.00	22.00	18.00	21.00	22.00	22.00	22.00
U	6.00	6.00	5.00	4.00	7.00	6.00	6.00	5.00	5.00	6.00

iFile: Lingran Disk: Linares XRF
iLINARES ADAMELLITE WHOLE-ROCK GEOCHEMISTRY (ALTERED -EL COBRE)

Sample	129-13	129-14	129-15	129-16	129-17	129-18	129-19	129-20	129-21	129-22	129-23
	.50	1.00	2.00	3.00	4.00	5.00	6.00	7.00	8.00	9.00	10.00
SiO2	76.03	73.19	73.71	75.44	76.66	76.07	76.75	72.37	71.08	71.43	71.50
TiO2	.18	.14	.23	.11	.12	.05	.09	.24	.26	.27	.25
Al2O3	12.94	13.53	14.40	13.57	12.73	13.52	12.87	15.09	14.63	14.93	14.99
Fe2O3	1.71	1.25	1.43	1.04	1.46	.80	1.20	2.47	2.41	2.51	2.35
MnO	.03	.05	.02	.03	.04	.03	.03	.05	.04	.05	.04
MgO	.32	.26	.26	.23	.22	.13	.21	.56	.48	.59	.61
CaO	.33	1.19	.25	.55	.56	.44	.41	1.47	1.45	1.27	1.26
Na2O	1.98	1.76	1.56	1.92	2.64	3.07	2.80	3.15	3.06	2.83	3.12
K2O	5.67	6.59	6.51	6.68	5.17	5.39	5.57	4.91	5.14	5.11	5.13
P2O5	.12	.12	.16	.13	.15	.18	.12	.14	.15	.17	.16
L.o.I	1.09	2.50	2.04	2.20	1.10	1.37	1.09	1.09	.89	1.50	1.29
Total	100.41	100.59	100.56	101.90	100.84	101.05	101.15	101.52	99.59	100.66	100.69
Co	30.00	20.00	25.00	30.00	24.00	21.00	28.00	24.00	25.00	23.00	28.00
Ni	3.00	2.00	3.00	3.00	2.00	1.00	2.00	4.00	2.00	2.00	4.00
Cu	1.00	3.00	2.00	2.00	2.00	6.00	3.00	5.00	4.00	3.00	4.00
Zn	28.00	21.00	20.00	17.00	30.00	17.00	19.00	52.00	52.00	48.00	55.00
Rb	218.00	212.00	197.00	226.00	238.00	271.00	230.00	200.00	188.00	199.00	195.00
Sr	20.00	31.00	32.00	28.00	23.00	18.00	21.00	95.00	89.00	83.00	88.00
Y	26.00	19.00	31.00	22.00	19.00	12.00	23.00	30.00	30.00	27.00	25.00
Zr	78.00	60.00	107.00	54.00	49.00	32.00	48.00	135.00	114.00	132.00	116.00
Nb	9.00	6.00	8.00	5.00	7.00	7.00	7.00	9.00	9.00	10.00	9.00
Ba	131.00	224.00	292.00	224.00	109.00	106.00	91.00	455.00	459.00	516.00	459.00
Pb	39.00	26.00	22.00	27.00	25.00	45.00	29.00	32.00	39.00	30.00	33.00
Th	11.00	10.00	12.00	10.00	10.00	7.00	10.00	16.00	14.00	15.00	15.00
U	8.00	8.00	5.00	7.00	8.00	10.00	9.00	8.00	6.00	7.00	8.00

File: Sangran Disk: Linares XRF

SANTA ELENA ADAMELLITE WHOLE-ROCK GEOCHEMISTRY (UNALTERED)

Sample	9098-2	9098-3	91416-1	91416-2	91416-3	91416-4	91416-5	91416-6	91416-7	91416-8
	Fresh	Fresh	Fresh	Fresh	Fresh	Fresh	Fresh	Fresh	Fresh	Fresh
SiO2	63.62	63.71	64.10	64.23	61.77	64.13	64.19	63.89	65.16	63.80
TiO2	.83	.85	.87	.88	.94	.85	.83	.90	.84	.87
Al2O3	17.46	16.73	16.75	16.90	17.16	16.36	16.99	16.81	16.64	17.05
Fe2O3	5.34	5.49	5.45	5.48	6.37	5.36	5.23	5.67	5.28	5.60
MnO	.08	.08	.08	.08	.09	.08	.07	.08	.08	.08
MgO	1.70	1.79	1.60	1.70	2.01	1.65	1.65	1.78	1.69	1.59
CaO	3.74	3.28	3.91	3.65	3.79	3.40	3.69	3.04	3.39	3.84
Na2O	3.12	2.78	3.05	2.89	2.93	2.74	2.98	2.78	3.03	2.89
K2O	3.72	3.90	3.26	3.67	3.52	3.75	3.82	3.86	3.62	3.67
P2O5	.25	.25	.27	.26	.40	.25	.27	.26	.23	.29
L.o.I	.86	.89	.39	.39	.39	1.28	.89	.89	.78	.79
Total	100.71	99.76	99.74	100.13	99.37	99.85	100.62	100.33	100.74	100.48
Co	35.00	37.00	32.00	29.00	35.00	33.00	34.00	33.00	31.00	38.00
Ni	12.00	13.00	11.00	13.00	13.00	14.00	13.00	14.00	12.00	13.00
Cu	11.00	9.00	12.00	8.00	13.00	12.00	12.00	11.00	11.00	16.00
Zn	68.00	71.00	69.00	66.00	82.00	68.00	68.00	72.00	67.00	74.00
Rb	135.00	142.00	139.00	138.00	152.00	144.00	144.00	149.00	141.00	147.00
Sr	253.00	232.00	232.00	231.00	231.00	241.00	236.00	233.00	227.00	239.00
Y	32.00	34.00	28.00	29.00	58.00	33.00	29.00	29.00	28.00	36.00
Zr	227.00	238.00	241.00	243.00	349.00	233.00	226.00	232.00	225.00	246.00
Nb	12.00	13.00	14.00	14.00	15.00	14.00	12.00	13.00	13.00	14.00
Ba	711.00	686.00	632.00	697.00	591.00	678.00	701.00	720.00	650.00	745.00
Pb	25.00	25.00	23.00	25.00	22.00	24.00	28.00	22.00	26.00	23.00
Th	17.00	18.00	18.00	18.00	12.00	16.00	18.00	18.00	20.00	20.00
U	3.00	4.00	4.00	4.00	4.00	4.00	3.00	3.00	4.00	5.00

File: SanFile: Sangran Disk: Linares XRF

SANTA ELESANTA ELENA ADAMELLITE WHOLE-ROCK GEOCHEMISTRY (ALTERED)

Sample	59-3 Ojo Vecin.	159-5 Nube biot.	159-6 Nube mos.	9098-4 alter.Myl.
SiO2	62.87	66.24	68.78	76.04
TiO2	.91	.64	.85	.03
Al2O3	17.19	18.12	18.53	15.74
Fe2O3	5.61	3.12	.45	.68
MnO	.07	.03	.00	.02
MgO	1.62	.80	.16	.27
CaO	3.21	.30	.24	.28
Na2O	2.68	.26	1.01	.31
K2O	4.34	6.87	6.85	6.38
P2O5	.26	.24	.13	.17
L.o.I	1.38	3.38	3.08	1.90
Total	100.14	100.00	100.07	101.82
Co	32.00	26.00	11.00	16.00
Ni	13.00	8.00	3.00	2.00
Cu	10.00	6.00	5.00	33.00
Zn	72.00	104.00	99.00	19.00
Rb	160.00	272.00	207.00	257.00
Sr	263.00	49.00	124.00	13.00
Y	31.00	28.00	47.00	12.00
Zr	243.00	202.00	245.00	28.00
Nb	14.00	19.00	23.00	8.00
Ba	805.00	834.00	456.00	159.00
Pb	29.00	296.00	744.00	15.00
Th	17.00	15.00	17.00	8.00
U	6.00	5.00	6.00	7.00

II.2. Electron microprobe analyses.

File: Sphalin Disk: sulph/enadimsa
SPHALERITES LINARES-LA CAROLINA
MICROPROBE DATA

Sample	(analysis: 51926) LC308-13 La Española											
Point	1a	1b	1c	1d	2a	2b	2c	3a	3b	3c	4b	4c
S	32.697	33.317	33.056	33.053	33.264	32.853	33.057	33.079	33.167	32.937	33.217	33.289
Mn	.003	.000	.000	.000	.000	.043	.046	.012	.000	.043	.030	.000
Fe	5.969	5.745	5.104	5.885	6.122	5.643	5.873	5.637	5.510	5.759	5.953	5.870
Ni	.005	.053	.000	.069	.029	.069	.000	.056	.000	.000	.000	.045
Cu	.000	.014	.000	.000	.000	.061	.000	.000	.000	.000	.000	.000
Zn	60.962	61.409	61.760	61.548	60.934	60.832	61.263	60.965	60.529	60.587	60.998	60.511
TOTAL	99.636	100.539	99.920	100.555	100.349	99.501	100.239	99.749	99.206	99.326	100.198	99.715

Sample	(analysis: 52493) LC90174-1 cascada Renegadero									
Point	1a	1b	2a	2b	3a	3b	4a	4b	5a	5b
S	33.163	32.838	33.397	33.218	33.177	32.886	32.964	33.149	33.027	33.273
Mn	.000	.000	.018	.049	.012	.012	.021	.049	.043	.052
Fe	4.541	4.579	10.506	11.639	7.173	5.866	5.570	5.329	5.719	5.836
Ni	.066	.000	.000	.028	.057	.000	.061	.003	.000	.062
Cu	.000	.000	.000	.062	.018	.000	.018	.050	.000	.036
Zn	61.743	62.701	56.194	54.146	59.243	60.829	60.790	60.930	61.054	60.635
TOTAL	99.513	100.118	100.115	99.142	99.680	99.593	99.424	99.510	99.843	99.894

Sample	(analysis: 52503) LC90164-10 Pelaguindas							
Point	1a	1b	1c	2a	2b	3a	3b	4a
S	32.860	32.782	32.956	32.841	32.723	33.008	33.087	32.805
Mn	.000	.000	.021	.000	.027	.000	.039	.012
Fe	3.114	.536	3.502	.877	.580	2.583	1.488	1.618
Ni	.005	.020	.000	.031	.043	.013	.018	.049
Cu	.150	.025	.143	.238	.298	.086	.306	.096
Zn	62.849	66.087	62.461	65.115	65.890	63.411	64.644	64.784
TOTAL	98.978	99.450	99.083	99.102	99.561	99.101	99.582	99.364

File: Galen Disk: Sulph/enadimsa

GALENAS LINARES-LA CAROLINA

MICROPROBE DATA

Sample	LC90164-10 (Pelag) A:52503	LC33-5 (Torr) An:51922									
Point	2a	2a	2b	2c	2d	3a	3b(rim)	3d(core)	3c(rim)	3e(core)	5a
S	13.578	13.748	13.621	13.509	13.647	13.572	13.473	13.546	13.429	13.466	13.632
Pb	87.221	85.293	86.368	86.326	86.431	85.374	85.928	85.935	86.759	85.683	86.603
Fe	.005	.000	.000	.048	.000	.000	.043	.000	.000	.000	.056
Cu	.000	.035	.000	.000	.000	.000	.000	.000	.000	.026	.000
Zn	.038	.000	.079	.044	.024	.015	.000	.012	.015	.110	.028
Ag	.044	.246	.033	.000	.000	.000	.000	.115	.048	.000	.000
Sb	.045	.561	.086	.011	.000	.047	.000	.000	.000	.009	.072
Total	100.931	99.883	100.189	99.939	100.102	99.008	99.444	99.609	100.251	99.294	100.390

Sample	LC318-3 (Esmeralda) Analysis: 51729					LC139-16 (Guindo) Analysis: 51730					LC308-13 (EspaM.) An:51926
Point	1a	1b	2a	3a	3b	2a	3a	3b	4a	4b	B O U L A N G E R I T E
S	13.646	13.602	13.661	13.494	13.523	13.418	13.466	13.500	13.541	13.697	18.320
Pb	85.600	85.800	86.301	86.739	86.491	85.350	85.753	85.512	86.469	86.717	54.617
Fe	.000	.000	.000	.008	.057	.179	.090	.070	.024	.000	.000
Cu	.010	.000	.000	.016	.041	.006	.029	.000	.000	.000	.000
Zn	.015	.061	.000	.081	.000	.000	.039	.000	.033	.000	.025
Ag	.179	.128	.097	.000	.000	.088	.169	.021	.130	.067	.030
Sb	.119	.347	.025	.200	.040	.300	.038	.000	.329	.202	26.250
Total	99.570	99.939	100.083	100.539	100.151	99.342	99.583	99.103	100.526	100.684	99.242

File: Galen Disk: Sulph/enadimsa
GALENAS LINARES-LA CAROLINA
MICROPROBE DATA
Pb and S prefixed to 86.6 and 13.4 %, respectively

Sample	LC129-11 (El Cobre)			LC129-15 (Cañada Incosa)		LC314-4 (San Juan)			LC398-3c (Torrecillas)	
Point	1a	2a	3a	1a	1b	1a	2a	3a	1a	2b
As	.000	.000	.000	.000	.000	.000	.000	.000	.000	.000
Ag	.020	.037	.037	.006	.000	.035	.030	.000	.000	.000
Sb	.053	.051	.054	.000	.000	.033	.032	.016	.000	.001
Pb	86.600	86.600	86.600	86.600	86.600	86.600	86.600	86.600	86.600	86.600
S	13.400	13.400	13.400	13.400	13.400	13.400	13.400	13.400	13.400	13.400
Total	100.074	100.088	100.091	100.006	100.000	100.068	100.062	100.016	100.000	100.001

Sample	LC159-12 (La Nube)		LC9031-12 (El Guindo)		LC90164-4(Pelaguindas)			LC129-12 (El Cobre)		
Point	1b	2b	1a	2b	1a	1b	1c	1a	1b	1c
As	.000	.000	.001	.000	.000	.000	.000	.000	.000	.000
Ag	.000	.000	.612	.906	.000	.000	.012	.000	.019	.000
Sb	.000	.000	.974	1.020	.152	.161	.171	.044	.060	.075
Pb	86.600	86.600	86.600	86.600	86.600	86.600	86.600	86.600	86.600	86.600
S	13.400	13.400	13.400	13.400	13.400	13.400	13.400	13.400	13.400	13.400
Total	100.000	100.000	101.587	101.926	100.153	100.161	100.183	100.044	100.079	100.075

Sample	LC49-7 (Sinapismo)			LC139-3 (Araceli)			LC309-1 (El Centenillo)		
Point	1a	2a	3a	1a	1b	1c	1a	2a	3a
As	.000	.000	.000	.000	.000	.000	.000	.000	.000
Ag	.000	.007	.031	.019	.009	.004	.000	.000	.000
Sb	.002	.021	.052	.022	.026	.020	.008	.016	.026
Pb	86.600	86.600	86.600	86.600	86.600	86.600	86.600	86.600	86.600
S	13.400	13.400	13.400	13.400	13.400	13.400	13.400	13.400	13.400
Total	100.002	100.027	100.083	100.048	100.035	100.024	100.008	100.016	100.026

Sample	LC298-2 (Torrecillas)			LC90164-20 (Pelaguindas)			LC90204-1 (La Nube) An: 51928					
Point	1a	2a	3a	1a	2a	3a	1a	1b	1c	2a	2b	3a
As	.000	.000	.000	.000	.000	.000	.010	.006	.009	.000	.000	.009
Ag	.000	.000	.000	.000	.000	.000	.000	.004	.000	.000	.000	.000
Sb	.006	.012	.015	.011	.032	.002	.004	.002	.000	.000	.005	.000
Pb	86.600	86.600	86.600	86.600	86.600	86.600	86.600	86.600	86.600	86.600	86.600	86.600
S	13.400	13.400	13.400	13.400	13.400	13.400	13.400	13.400	13.400	13.400	13.400	13.400
Total	100.006	100.012	100.011	100.011	100.032	100.002	100.013	100.012	100.009	100.000	100.005	100.009

File: Pyrite Disk: sulph/enadimsa
PYRITES LINARES-LA CAROLINA
MICROPROBE DATA

Sample:	LC139-6 (El Guindo) Analysis:51730			LC218-3 (San Juan) An:51729		LC33-5 (Torrec.) An: 51922
Point:	1a	2a	Biogenic	3a	4a	1a
S	53.409	52.993	52.993	53.217	53.461	52.705
Fe	47.150	46.244	46.244	46.932	47.149	37.974
Co	.000	.043	.043	.000	.000	5.263
Ni	.000	.061	.061	.066	.000	3.048
Cu	.027	.045	.045	.000	.148	.000
Zn	.117	.056	.056	.000	.000	.009
As	.000	.000	.000	.000	.000	.074
Sb	.037	.071	.071	.040	.011	.034
Ag	.117	.066	.066	.000	.000	.132
Total	100.857	100.303	99.579	100.255	100.769	99.238

File: Feldco Disk: THESIS DATA
FELDSPARS EL COBRE-LINARES Date: 30/1/91
Microprobe Raw Data

Sample: LC129/13 (0.5m) Analysis:51717

Point:	1a	1b	1c	2a	3a	3b	3c	3d	3f	4a	4b	4c	4d	4f	5a	5b	6a	7a
SiO2	64.96	65.43	67.33	65.05	65.33	64.78	65.67	64.66	66.43	65.44	65.62	65.33	67.51	67.23	68.62	65.15	65.48	65.08
TiO2	.00	.05	.07	.00	.04	.01	.00	.00	.02	.02	.00	.00	.01	.05	.01	.00	.00	.00
Al2O2	19.06	18.84	20.80	18.47	19.17	18.47	18.79	18.20	21.25	18.36	18.22	18.39	20.53	21.08	19.83	18.92	18.32	18.70
Fe2O3	.00	.00	.14	.06	.00	.06	.00	.00	.16	.00	.00	.06	.10	.00	.11	.01	.02	.03
MgO	.00	.00	.01	.00	.00	.01	.00	.00	.04	.00	.01	.00	.00	.00	.00	.00	.00	.00
CaO	.02	.00	.43	.00	.00	.02	.00	.02	1.34	.05	.00	.00	.91	1.73	1.20	.08	.00	.02
MnO	.13	.00	.05	.00	.04	.11	.00	.00	.05	.03	.03	.02	.00	.00	.00	.05	.02	.01
Na2O	.73	.69	11.19	.37	.50	.54	.03	.05	9.27	.77	.03	.04	10.89	10.71	10.59	2.01	.05	.77
K2O	15.76	15.48	.63	15.87	15.62	15.86	16.49	16.49	1.79	15.70	16.51	16.85	.49	.16	.18	13.76	16.56	15.47
total	100.66	100.49	100.64	99.83	100.69	99.86	100.98	99.42	100.36	100.37	100.43	100.70	100.44	100.97	100.53	99.98	100.46	100.08
Ab	6.59	6.32	94.50	3.43	4.61	4.92	.28	.45	82.86	6.95	.30	.34	92.96	91.00	93.12	18.11	.43	7.01
Or	93.32	93.68	3.49	96.57	95.39	94.99	99.72	99.47	10.51	92.78	99.70	99.66	2.75	.87	1.07	81.49	99.57	92.90
An	.09	.00	2.02	.00	.00	.09	.00	.08	6.63	.27	.00	.00	4.29	8.14	5.81	.40	.00	.09

Sample: LC129/14 (1m) Analysis:52506

Point:	1a	1b	1c	1d	1e	2a	2b	3a	3b	3c	3d	5a	5b	5c	6a	6c	7a
SiO2	65.45	64.70	64.54	66.54	66.29	65.47	66.98	65.54	64.59	67.26	67.02	64.74	65.21	67.33	65.50	65.21	64.48
Al2O2	18.73	18.59	18.47	21.53	21.39	19.22	18.70	18.28	17.92	20.64	21.01	17.89	18.42	20.85	17.95	18.73	18.56
Fe2O3	.16	.11	.01	.05	.00	.00	.01	.04	.00	.06	.00	.00	.00	.01	.00	.07	.00
MgO	.02	.01	.00	.00	.01	.00	.00	.00	.00	.00	.00	.01	.01	.00	.00	.03	.00
CaO	.06	.13	.03	1.59	1.98	.10	.02	.05	.00	1.22	1.63	.03	.04	.91	.01	.10	.00
Na2O	.22	.58	1.42	10.92	10.70	3.72	.00	.00	.04	11.10	10.91	.00	.00	11.15	.00	.03	.32
K2O	16.21	15.68	16.64	.14	.11	11.19	14.94	17.07	16.55	.10	.25	16.82	16.39	.26	16.86	15.78	16.24
total	100.86	99.78	99.11	100.77	100.49	99.69	100.65	100.99	99.11	100.38	100.81	99.48	100.07	100.50	100.32	99.96	99.59
Ab	1.99	5.25	12.87	91.86	90.12	33.39	.00	.00	.40	93.75	91.10	.00	.00	94.33	.00	.33	2.87
Or	97.69	94.11	87.00	.77	.64	66.12	99.91	99.76	99.59	.53	1.36	99.87	99.80	1.43	99.97	99.13	97.13
An	.33	.63	.13	7.38	9.24	.49	.09	.24	.01	5.71	7.54	.13	.20	4.25	.03	.54	.00

Sample: LC129/16 (3m) Analysis:52507

Point:	1a	1b	1c	1d	2a	2b	3a	3b	3c	4a	4c	6a	6b
SiO2	64.64	64.78	63.96	66.05	63.90	67.59	64.68	66.96	65.04	65.44	68.50	65.05	64.37
Al2O2	18.45	18.37	21.95	21.24	18.37	20.15	18.29	20.37	18.25	18.18	19.72	18.34	18.64
Fe2O3	.00	.00	.58	.05	.06	.00	.00	.00	.03	.00	.05	.00	.09
MgO	.00	.00	.05	.00	.00	.00	.00	.00	.00	.00	.00	.00	.01
CaO	.16	.00	1.82	2.12	.01	.86	.04	1.13	.07	.05	.29	.01	.09
Na2O	.87	.02	10.11	10.58	.46	11.51	.00	11.03	.00	.00	11.46	.00	.54
K2O	15.95	17.03	.94	.13	16.71	.15	17.36	.25	17.20	16.98	.35	17.32	16.37
total	100.06	100.19	99.41	100.18	99.51	100.26	100.37	99.75	100.59	100.65	100.37	100.72	100.11
Ab	7.86	.17	86.69	89.77	4.17	95.46	.00	93.59	.00	.00	96.81	.00	4.95
Or	91.39	99.83	5.06	.71	95.77	.78	99.83	1.32	99.68	99.77	1.87	99.94	94.64
An	.75	.00	8.25	9.52	.07	3.77	.17	5.09	.32	.23	1.32	.06	.41

Sample:	LC129/17 (4m)				Analysis:51720				
Point:	1a	2a	3a	4a	5a	6a	7a	7b	8a
SiO2	64.80	64.83	64.92	65.12	64.96	65.35	64.47	64.44	65.02
TiO2	.00	.00	.00	.03	.05	.06	.01	.00	.07
Al2O2	18.93	18.71	18.58	18.77	18.64	18.57	18.20	18.65	18.74
Fe2O3	.08	.00	.09	.00	.00	.14	.32	.00	.00
MgO	.00	.00	.00	.00	.00	.00	.00	.00	.00
CaO	.00	.04	.00	.05	.00	.01	.00	.03	.01
MnO	.00	.09	.00	.04	.02	.08	.00	.05	.00
Na2O	1.27	.97	.64	1.02	.01	.24	.25	.32	.70
K2O	14.19	15.26	15.86	15.50	16.73	16.45	16.81	16.45	16.14
total	99.99	99.89	100.09	100.53	100.41	100.88	100.05	99.94	100.68
Ab	11.46	8.83	5.77	9.04	.12	2.17	2.18	2.84	6.18
Or	88.54	90.98	94.21	90.72	99.88	97.80	97.82	97.02	93.76
An	.00	.19	.02	.24	.00	.03	.00	.14	.06

LC129/18 (5m)	Analysis:52508				
3a	3b	3b	4a	4b	5a
64.55	66.45	65.01	65.40	67.98	6.33
18.47	21.26	21.63	21.72	19.90	21.39
.00	.00	.00	.00	.00	.04
.04	.01	.00	.00	.00	.00
.02	1.20	1.74	1.62	.00	1.73
n.a.	n.a.	n.a.	n.a.	n.a.	n.a.
.05	10.87	10.63	10.60	11.91	10.33
16.52	.25	.05	.38	.01	.47
99.65	100.03	99.54	99.72	99.81	100.28
.41	92.93	89.07	90.22	99.92	89.07
99.49	1.42	2.87	2.14	.05	2.67
.09	5.65	8.06	7.64	.02	8.26

Sample:	LC129/20 (7m)		Analisis:51719			
Point:	1a	1b	2a	2b	4a	5a
SiO2	63.32	64.02	64.15	64.58	64.03	64.02
TiO2	.02	.00	.02	.00	.00	.04
Al2O2	18.60	18.97	18.99	18.90	19.11	18.91
Fe2O3	.01	.05	.01	.00	.00	.06
MgO	.00	.02	.00	.01	.00	.02
CaO	.08	.04	.06	.02	.02	.02
MnO	.00	.09	.01	.00	.11	.04
Na2O	.78	2.70	3.46	1.79	2.06	.78
K2O	16.42	13.45	12.32	14.13	14.21	15.85
total	99.24	99.35	99.02	99.44	99.54	99.76
Ab	6.68	23.35	29.81	16.12	18.05	6.96
Or	92.93	76.48	69.89	83.77	81.83	92.92
An	.38	.17	.30	.11	.12	.12

Sample: LC129/22 (9M)	Analysis:51718													
Point:	1a	1b	1c	1d	2a	3a	3b	4a	4b	4c	5a	5b	5c	5d
SiO2	65.31	65.09	64.78	64.06	65.85	62.72	64.97	64.11	64.18	62.15	63.86	63.81	65.37	64.96
TiO2	.02	.00	.03	.00	.02	.03	.00	.00	.01	.05	.00	.01	.00	.02
Al3O2	21.01	21.30	18.19	18.21	21.42	23.20	18.35	18.39	18.51	23.68	18.01	18.70	21.68	21.38
Fe2O3	.01	.00	.00	.17	.00	.00	.00	.67	.02	.00	.52	.04	.03	.24
MgO	.01	.00	.11	.01	.00	.00	.00	.02	.00	.00	.00	.00	.00	.02
CaO	1.85	2.54	.01	.00	2.68	4.83	.00	.00	.00	5.27	.00	.00	2.44	2.24
MnO	.00	.06	.03	.00	.00	n.a.	n.a.	.00	.00	.14	.02	.10	.03	.00
Na2O	10.36	9.58	1.80	.29	10.40	8.65	.10	1.70	1.85	8.28	.38	1.09	10.00	10.21
K2O	.50	1.03	14.71	16.98	.04	.49	16.79	14.70	14.83	.50	16.71	15.87	.54	.41
total	99.08	99.61	99.56	99.72	100.42	99.92	100.21	99.59	99.40	100.06	99.51	99.64	100.09	99.51
Ab	88.43	82.15	15.69	2.50	87.32	74.29	.91	14.97	15.95	71.85	3.32	9.48	85.45	87.21
Or	2.83	5.80	84.27	97.50	.24	2.79	99.09	85.03	84.05	2.88	96.68	90.52	3.04	2.27
An	8.74	12.05	.04	.00	12.44	22.92	.00	.00	.00	25.27	.99	.00	11.51	10.52

Sample: LC90118/2(unalt.)	Analysis:53103																	
Point:	1a	1b	1c	1d	2a	2b	2c	2d	2f	3a	3b	3c	4a	4b	4c	4d	5a	5b
SiO2	65.04	63.24	64.95	66.56	64.71	64.11	60.39	64.13	59.14	64.15	66.61	59.85	64.20	64.07	65.11	64.01	66.72	66.17
Al3O2	18.70	23.38	22.02	21.18	18.52	18.24	24.68	23.37	25.67	18.55	20.62	24.82	17.93	21.90	21.68	18.26	20.86	20.81
Fe2O3	.00	.00	.00	.00	.15	.02	.07	.02	.12	.00	.02	.09	.14	.08	.00	.08	.00	.02
MgO	.02	.03	.02	.00	.00	.00	.00	.02	.01	.00	.00	.01	.02	.00	.01	.00	.00	.00
CaO	.00	4.46	3.06	1.76	.09	.11	6.62	2.48	7.46	.02	1.46	6.80	.00	3.20	2.62	.03	1.41	1.45
Na2O	.58	9.25	9.98	10.61	.72	.42	7.55	9.58	7.46	.33	11.09	7.43	.36	10.12	10.10	.65	11.41	10.97
K2O	16.31	.37	.47	.39	15.82	16.59	.50	.96	.40	16.28	.15	.66	16.67	.50	.34	15.99	.17	.09
total	100.65	100.73	100.49	100.51	100.00	99.49	99.82	100.57	100.25	99.34	99.94	99.66	99.32	99.86	99.87	99.03	100.57	99.50
Ab	5.37	78.08	83.90	89.97	6.66	3.87	66.39	83.30	63.97	3.12	92.74	64.89	3.27	83.43	86.29	6.05	93.05	93.02
Or	94.63	1.95	2.49	2.10	92.89	95.61	2.80	5.27	2.14	96.78	.78	3.66	96.71	2.59	1.85	93.81	.87	.48
An	.00	19.96	13.61	7.93	.45	.51	30.82	11.43	33.89	.10	6.47	31.45	.02	13.98	11.86	.14	6.08	6.50

File: Felen Disk: THESIS DATA
FELDSPARS SANTA ELENA Date: 30/1/91
Microprobe Raw Data

Sample:	LC59/3 (Ojo Vecino)							Analysis:51727							LC159/5 (La Nube biotitic)							Analysis:51723
Point:	3a	4a	5a	5b	5c	6a	7a								1a	2a	3a	3b	4a	7a	7b	
SiO2	60.73	64.01	61.67	61.35	55.60	55.73	64.02								64.87	64.46	64.87	64.53	64.67	64.32	64.37	
TiO2	.02	.03	.00	.00	.03	.00	.00								.00	.00	.00	.00	.07	.09	.00	
Al3O2	24.87	18.70	24.07	24.10	27.91	27.73	18.61								19.23	18.92	18.86	19.29	18.81	18.86	19.12	
Fe2O3	.16	.03	.00	.00	.08	.07	.00								.06	.16	.05	.00	.02	.04	.06	
MgO	.02	.01	.00	.00	.00	.01	.00								.00	.00	.01	.02	.00	.00	.00	
CaO	6.28	.00	5.51	5.75	10.44	10.28	.08								.07	.02	.03	.05	.08	.00	.08	
MnO	.07	.05	.01	.01	.00	.03	.05								.00	.09	.00	.04	.02	.06	.03	
Na2O	8.35	1.06	8.45	8.51	5.85	6.03	1.19								.99	1.02	1.00	1.14	1.14	1.04	.96	
K2O	.14	15.51	.34	.32	.15	.25	15.19								15.35	15.67	15.85	15.16	15.08	15.84	15.42	
total	100.64	99.42	100.04	100.04	100.06	100.13	99.14								100.58	100.34	100.67	100.22	99.88	100.25	100.04	
Ab	70.09	9.39	72.13	71.51	49.93	50.81	10.61								8.91	9.03	8.73	10.23	10.27	9.10	8.57	
Or	.76	90.61	1.88	1.79	.85	1.37	89.02								90.72	90.86	91.14	89.51	89.36	90.88	91.05	
An	29.16	.00	25.98	26.70	49.22	47.81	.37								.36	.11	.13	.25	.37	.02	.37	

Sample:	LC159/6 (La Nube mosc.)			Analysis:51724						
Point:	1a	2a	2b	3a	4a	4b	4c	5a	5b	5c
SiO2	64.89	64.50	64.86	65.07	64.18	65.14	64.53	65.39	64.64	66.41
TiO2	.00	.00	.00	.07	.01	.06	.02	.00	.01	.00
Al3O2	18.34	18.17	18.28	18.17	18.22	17.83	18.35	17.66	18.14	17.45
Fe2O3	.03	.11	.01	.11	.16	.04	.00	.00	.00	.13
MgO	.01	.01	.00	.00	.00	.00	.00	.01	.00	.00
CaO	.00	.00	.01	.00	.00	.00	.00	.00	.00	.00
Na2O	.42	.68	.50	.56	.65	.05	.66	.03	.41	.04
K2O	16.06	15.79	16.22	16.00	16.06	16.31	16.06	16.70	15.87	16.32
total	99.75	99.27	99.89	99.98	99.28	99.45	99.62	99.78	99.06	100.36
Ab	3.85	6.14	4.48	5.05	5.76	.50	5.84	.24	3.78	.35
Or	96.15	93.84	95.45	94.95	94.24	99.48	94.16	99.76	96.22	99.65
An	.00	.02	.07	.00	.00	.02	.00	.00	.00	.00

Sample:	LC9098/3 Sta.Elena.(unal.) Analysis:53104																	
Point:	1a	1b	1c	2a	2b	3a	3b	4a	4b	4c	4d	4f	5a	5b	5c	5d	6a	6b
SiO2	64.33	57.26	65.22	64.76	60.76	64.70	56.51	64.36	64.44	57.84	57.44	56.23	65.27	64.77	56.62	60.49	57.64	55.94
Al302	18.50	27.31	18.65	18.49	25.12	18.19	27.90	18.39	18.86	27.08	26.95	27.66	18.25	18.39	27.37	24.96	26.26	27.50
Fe203	.20	.07	.09	.00	.00	.04	.00	.00	.06	.00	.07	.03	.10	.00	.00	.00	.00	.08
MgO	.00	.00	.00	.01	.00	.00	.00	.00	.00	.00	.01	.00	.00	.00	.00	.00	.00	.01
CaO	.00	9.52	.02	.06	6.72	.00	9.98	.01	.04	9.16	9.70	9.90	.02	.00	10.10	6.87	8.72	10.15
Na20	.68	6.15	.89	.80	7.78	.75	6.32	.90	1.19	6.58	6.24	6.01	.49	.55	6.12	7.91	6.63	5.98
K20	15.82	.16	15.30	15.37	.12	15.50	.20	15.37	14.91	.16	.13	.17	15.78	15.57	.16	.17	.16	.12
total	99.52	100.47	100.18	99.49	100.51	99.19	100.90	99.03	99.50	100.82	100.53	100.00	99.90	99.30	100.38	100.41	99.41	99.77
Ab	6.10	53.44	8.12	7.31	67.22	6.87	52.81	8.17	10.78	56.00	53.38	51.84	4.50	5.12	51.83	66.92	57.37	51.28
Or	93.90	.91	91.76	92.40	.70	93.13	1.08	91.80	89.01	.92	.75	.96	95.41	94.88	.92	.97	.91	.66
An	.00	45.66	.12	.30	32.08	.00	46.11	.04	.21	43.08	45.87	47.20	.08	.00	47.26	32.10	41.72	48.06

Sample:	LC59/1 (mylonite) Analysis:51721							LC9098/5 (mylonite) Analysis:53106								
Point:	1a	2a	2b	3a	4a	5a	5b	1a	2a	2b	3a	4a	4b	5a	6a	7a
SiO2	64.38	64.81	64.71	64.37	64.56	64.41	67.36	64.84	65.08	68.23	64.84	64.74	67.80	65.20	65.16	68.33
TiO2	.00	.06	.07	.02	.03	.01	.00	n.a.	n.a.	n.a.	n.a.	n.a.	n.a.	n.a.	n.a.	n.a.
Al302	18.78	18.50	18.68	18.74	18.55	18.92	20.62	19.23	19.25	20.03	18.95	19.01	20.41	19.18	18.54	20.38
Fe203	.00	.02	.08	.04	.02	.00	.03	.00	.04	.05	.00	.04	.11	.00	.00	.01
MgO	.01	.01	.00	.00	.00	.00	.01	.00	.00	.00	.01	.00	.00	.00	.00	.00
CaO	.00	.01	.00	.00	.00	.00	1.02	.00	.01	.31	.00	.00	.41	.00	.00	.49
MnO	.05	.08	.00	.00	.00	.00	.00	n.a.	n.a.	n.a.	n.a.	n.a.	n.a.	n.a.	n.a.	n.a.
Na20	.71	.69	.55	1.32	.52	.73	11.28	1.08	1.56	11.39	.65	1.04	11.54	.42	.43	11.61
K20	16.09	16.45	16.28	15.16	16.87	15.99	.07	15.07	14.60	.17	15.79	15.27	.35	16.07	16.30	.13
total	100.01	100.62	100.37	99.65	100.55	100.05	100.39	100.23	100.53	100.18	100.24	100.10	100.62	100.87	100.44	100.95
Ab	6.25	5.97	4.87	11.68	4.45	6.46	94.88	9.86	13.93	97.59	5.85	9.39	96.21	3.85	3.88	97.02
Or	93.75	94.00	95.12	88.32	95.55	93.54	.37	90.14	86.02	.97	94.15	90.61	1.92	96.15	96.12	.71
An	.00	.03	.00	.00	.00	.00	4.75	.00	.05	1.45	.00	.00	1.87	.00	.00	2.28

File: Bioco Disk: El Cobre (Probe) II
BIOTITES EL COBRE-LINARES
MICROPROBE DATA (cations)

Sample:	LC129-13 (0.5 m) Analysis:51717				LC129-14 (1 m) Anal: 52506					LC129-16 (3 m) Analysis:52507									
	8a	6a	6b	6c	2a	2b	2c	2d	5a	1a	1b	1c	1d	3a	4a	4b	5a	5b	5c
Si	5.2188	5.3299	5.4375	5.3803	5.3977	5.4086	5.3583	5.3996	5.2979	5.2799	5.2419	5.2987	5.4023	5.3427	5.3293	5.3866	5.2032	5.4188	5.3972
Ti	.5199	.3791	.4319	.4317	.3956	.3683	.3524	.3599	.4290	.3958	.4999	.3937	.4020	.4335	.4034	.4055	.4005	.4265	.4406
Al	3.1944	3.4813	3.2084	3.2958	3.1315	3.4642	3.4616	3.4861	3.5944	3.5306	3.5872	3.4946	3.4075	3.5876	3.5481	3.5168	3.7532	3.4733	3.4245
Mg	1.0320	1.0428	1.0263	1.0125	1.0583	1.0957	1.1498	.9577	.9111	1.0151	.8940	1.0109	.9341	.9128	.9622	.8478	.6902	1.0177	1.0425
Ca	.0000	.0007	.0065	.0000	.0000	.0000	.0125	.0000	.0000	.0037	.0047	.0051	.0000	.0000	.0000	.0000	.0000	.0000	.0017
Mn	.0385	.0345	.0646	.0370	.0275	.0411	.0230	.0439	.0338	.0266	.0330	.0388	.0387	.0213	.0251	.0501	.0455	.0013	.0315
Fe	3.4339	3.3210	3.4059	3.4650	3.2350	3.2074	3.2419	3.2914	3.2688	3.3426	3.2433	3.3758	3.3362	3.1767	3.3035	3.2880	3.5244	3.1171	3.1657
Na	.0648	.0684	.0728	.0601	.0542	.0612	.0884	.0660	.0695	.0701	.0809	.0582	.0835	.0758	.0531	.0689	.0602	.0927	.0877
K	1.7521	1.8537	1.8176	1.7754	1.8367	1.7504	1.8295	1.8515	1.8123	1.8592	1.8401	1.8270	1.8586	1.8349	1.7905	1.8404	1.7450	1.8342	1.8050
SiIV	2.6094	2.6650	2.7188	2.6902	2.6989	2.7043	2.6792	2.6998	2.6490	2.6400	2.6210	2.6494	2.7012	2.6714	2.6647	2.6933	2.6016	2.7094	2.6986
AlIV	1.3906	1.3351	1.2813	1.3099	1.3012	1.2957	1.3209	1.3002	1.3511	1.3601	1.3791	1.3507	1.2989	1.3287	1.3354	1.3067	1.3984	1.2906	1.3014
AlVI	.2066	.4056	.3230	.3381	.2646	.4364	.4100	.4429	.4462	.4053	.4146	.3967	.4049	.4652	.4387	.4517	.4782	.4461	.4109
Ti	.2600	.1896	.2160	.2159	.1978	.1842	.1762	.1800	.2145	.1979	.2500	.1969	.2010	.2168	.2017	.2028	.2003	.2133	.2203
Fe	1.7170	1.6605	1.7030	1.7325	1.6175	1.6037	1.6210	1.6457	1.6344	1.6713	1.6217	1.6879	1.6681	1.5884	1.6518	1.6440	1.7622	1.5586	1.5829
Mn	.0193	.0173	.0323	.0185	.0138	.0206	.0115	.0220	.0169	.0133	.0165	.0194	.0194	.0107	.0126	.0251	.0228	.0007	.0158
Mg	.5160	.5214	.5132	.5063	.5292	.5479	.5749	.4789	.4556	.5076	.4470	.5055	.4671	.4564	.4811	.4239	.3451	.5089	.5213
ΣVI	2.7188	2.7943	2.7873	2.8112	2.6228	2.7927	2.7935	2.7693	2.7675	2.7953	2.7497	2.8063	2.7604	2.7373	2.7858	2.7474	2.8085	2.7274	2.7510
Ca	.0000	.0004	.0033	.0000	.0000	.0000	.0063	.0000	.0000	.0019	.0024	.0026	.0000	.0000	.0000	.0000	.0000	.0000	.0009
Na	.0324	.0342	.0364	.0301	.0271	.0306	.0442	.0330	.0348	.0351	.0405	.0291	.0418	.0379	.0266	.0345	.0301	.0464	.0439
K	.8761	.9269	.9088	.8877	.9184	.8752	.9148	.9258	.9062	.9296	.9201	.9135	.9293	.9175	.8953	.9202	.8725	.9171	.9025
ΣXII	.9085	.9614	.9485	.9178	.9455	.9058	.9652	.9588	.9409	.9665	.9629	.9452	.9711	.9554	.9218	.9547	.9026	.9635	.9472

File: Bioco Disk: El Cobre (Probe) II
BIOTITES EL COBRE-LINARES
MICROPROBE DATA (cations)

Sample:	LC129-17 (4 m) Analysis: 51720								LC129-20 (7m) Anal:51719			LC129-22 (9 m) An:71718	LC90118-2(unal.) Analysis: 53103		
	2a	2b	7a	7b	7c	1ba	1bb	1bc	1a	2a	5a	1a	1a	2a	5a
Si	5.3428	5.4040	5.4525	5.3048	5.2948	5.3871	5.2957	5.3029	5.2938	5.1837	5.3045	5.4002	5.3310	5.3000	5.4420
Ti	.4700	.4504	.4195	.3678	.3106	.4891	.4802	.3492	.5099	.4780	.4255	.4087	.4550	.4050	.4500
Al	3.5404	3.4886	3.4827	3.7182	3.7839	3.3005	3.3906	3.7875	3.2162	3.4220	3.3407	3.2130	3.0440	3.1240	2.9400
Mg	.7527	.8218	.8282	.7717	.7468	.8965	.9737	.7615	.9714	1.0171	1.0771	1.1735	1.7140	1.7080	1.6660
Ca	.0000	.0005	.0000	.0000	.0000	.0003	.0000	.0052	.0059	.0010	.0000	.0000	.0000	.0000	.0010
Mn	.0281	.0455	.0389	.0511	.0415	.0398	.0551	.0381	.0171	.0222	.0551	.0304	.0220	.0320	.0380
Fe	3.0822	3.2442	3.2144	3.2787	3.3582	3.4088	3.3991	3.2494	3.6012	3.1819	3.4466	3.3879	3.1710	3.1930	3.1510
Na	.0742	.0681	.0597	.0798	.0617	.0883	.0867	.0628	.0742	.1036	.0522	.0562	.0970	.0840	.1040
K	1.7448	1.8248	1.8413	1.8719	1.8720	1.8145	1.7824	1.8575	1.6430	1.8552	1.7230	1.6758	1.1813	1.8600	1.7950
SiIV	2.6714	2.7020	2.7263	2.6524	2.6474	2.6936	2.6479	2.6515	2.6469	2.5919	2.6523	2.7001	2.6655	2.6500	2.7210
AlIV	1.3286	1.2980	1.2738	1.3476	1.3526	1.3065	1.3522	1.3486	1.3531	1.4082	1.3478	1.2999	1.3345	1.3500	1.2790
AlVI	.4416	.4463	.4676	.5115	.5394	.3438	.3432	.5452	.2550	.3029	.3226	.3066	.1875	.2120	.1910
Ti	.2350	.2252	.2098	.1839	.1553	.2446	.2401	.1746	.2550	.2390	.2128	.2044	.2275	.2025	.2250
Fe	1.5411	1.6221	1.6072	1.6394	1.6791	1.7044	1.6996	1.6247	1.8006	1.5910	1.7233	1.6940	1.5855	1.5965	1.5755
Mn	.0141	.0228	.0195	.0256	.0208	.0199	.0276	.0191	.0086	.0111	.0276	.0152	.0110	.0160	.0190
Mg	.3764	.4109	.4141	.3859	.3734	.4483	.4869	.3808	.4857	.5086	.5386	.5868	.8570	.8540	.8330
ΣVI	2.6081	2.7273	2.7181	2.7462	2.7679	2.7609	2.7972	2.7443	2.8048	2.6525	2.8248	2.8069	2.8685	2.8810	2.8435
Ca	.0000	.0003	.0000	.0000	.0000	.0002	.0000	.0026	.0030	.0005	.0000	.0000	.0000	.0000	.0005
Na	.0371	.0341	.0299	.0399	.0309	.0442	.0434	.0314	.0371	.0518	.0261	.0281	.0485	.0420	.0520
K	.8724	.9124	.9207	.9360	.9360	.9073	.8912	.9288	.8215	.9276	.8615	.8379	.5907	.9300	.8975
ΣXII	.9095	.9467	.9505	.9759	.9669	.9516	.9346	.9628	.8616	.9799	.8876	.8660	.6392	.9720	.9500

File: Proclo2 Disk: El Cobre (probe) I
CLORITES EL COBRE-LINARES
MICROPROBE DATA (cations)

Sample:	LC129-13 (0.5 m) Analysis:51717					LC129-14 (1 m) Analysis:52506									
Point:	P-2	P-3	P-4	P-5	P-7	p1	p1b	p2a	p4a	p4b	p4c	p6a	p6b	p6c	p7a
Si	5.3248	5.3475	5.3795	5.2761	5.3843	5.3333	5.4806	5.4461	5.3215	5.3725	5.3922	5.3282	5.3552	5.4000	5.3665
Ti	.0085	.0000	.0056	.0290	.0397	.0231	.0157	.0266	.0000	.0007	.0000	.0316	.0417	.0000	.0085
Al	5.7029	5.7672	5.6111	5.7159	5.6525	5.6571	5.6743	5.6382	5.7291	5.6611	5.5890	5.5923	5.4734	5.6545	5.5973
Mg	1.8493	1.8227	1.9040	1.7549	1.9558	1.8976	2.0084	1.9958	1.9750	1.9380	2.1490	1.9888	1.9328	1.7175	1.8952
Ca	.0044	.0068	.0183	.0103	.0000	.0005	.0303	.0046	.0100	.0023	.0004	.0000	.0077	.0030	.0110
Mn	.0724	.0842	.0965	.1023	.1213	.1570	.1256	.1409	.1183	.1394	.1489	.0657	.0780	.1653	.1015
Fe	6.8515	6.7346	6.7878	6.9439	6.5765	6.7465	6.3282	6.4480	6.6601	6.6822	6.5248	6.8321	6.9549	6.8214	6.8366
Na	.0000	.0090	.0033	.0079	.0312	.0000	.0067	.0039	.0000	.0000	.0159	.0000	.0201	.0177	.0144
K	.0029	.0029	.0100	.0013	.0079	.0000	.0000	.0120	.0000	.0000	.0017	.0106	.0252	.0047	.0049
SiIV	2.6624	2.6738	2.6898	2.6381	2.6922	2.6667	2.7403	2.7231	2.6608	2.6863	2.6961	2.6641	2.6776	2.7000	2.6833
AlIV	1.3376	1.3263	1.3103	1.3620	1.3079	1.3334	1.2597	1.2770	1.3393	1.3138	1.3039	1.3359	1.3224	1.3000	1.3168
AlVI	1.5139	1.5574	1.4953	1.4960	1.5184	1.4952	1.5775	1.5422	1.5253	1.5168	1.4906	1.4603	1.4143	1.5273	1.4819
Ti	.0043	.0000	.0028	.0145	.0199	.0116	.0079	.0133	.0000	.0004	.0000	.0158	.0209	.0000	.0043
Fe	3.4258	3.3673	3.3939	3.4720	3.2883	3.3733	3.1641	3.2240	3.3301	3.3411	3.2624	3.4161	3.4775	3.4107	3.4183
Mn	.0362	.0421	.0483	.0512	.0607	.0785	.0628	.0705	.0592	.0697	.0745	.0329	.0390	.0827	.0508
Mg	.9247	.9114	.9520	.8775	.9779	.9488	1.0042	.9979	.9875	.9690	1.0745	.9944	.9664	.8588	.9476
ΣVI	5.9047	5.8781	5.8923	5.9111	5.8651	5.9073	5.8164	5.8478	5.9020	5.8970	5.9020	5.9194	5.9180	5.8794	5.9028
Vac	.0953	.1219	.1078	.0890	.1350	.0927	.1836	.1522	.0980	.1031	.0981	.0807	.0820	.1207	.0972
Ca	.0022	.0034	.0092	.0052	.0000	.0003	.0152	.0023	.0050	.0012	.0002	.0000	.0039	.0015	.0055
Na	.0000	.0045	.0017	.0040	.0156	.0000	.0034	.0020	.0000	.0000	.0080	.0000	.0101	.0089	.0072
K	.0015	.0015	.0050	.0007	.0040	.0000	.0000	.0060	.0000	.0000	.0009	.0053	.0126	.0024	.0025
ΣXII	.0037	.0094	.0158	.0098	.0196	.0003	.0185	.0103	.0050	.0012	.0090	.0053	.0265	.0127	.0152

File: Proclo2 Disk: El Cobre (probe) I
CLORITES EL COBRE-LINARES
MICROPROBE DATA (cations)

Sample:	LC129-16 (3 m)		Analysis: 52507		LC129-17 (4 m)	Analysis:51720								LC129-18 (5 m) Analysis:52508				
Point:	p1	p2	p3	p6	P-1	P-1b	P-1.2	P-4	P-5	P-5.2	P-5.3	P-6.1	P-6.2	p1a	p2a	p2b	p5a	p5b
Si	5.3480	5.1740	5.2970	5.1890	5.2985	5.3532	5.3989	5.2958	5.3245	5.2636	5.4060	5.3187	5.2602	5.3385	5.2944	5.1900	5.2400	5.1365
Ti	.0220	.0440	.0130	.0090	.0171	.0070	.0194	.0000	.0359	.0184	.0033	.0143	.0104	.0220	.0143	.0128	.0079	.0066
Al	5.6510	5.7380	5.7370	5.7100	5.6433	5.7116	5.4929	5.6390	5.6251	5.8220	5.5400	5.6610	5.6938	5.6383	5.8018	5.7543	5.7110	5.8846
Mg	1.9100	1.9430	2.0390	1.9200	1.7726	1.8063	1.8129	2.0193	1.8603	1.8303	1.8684	1.7710	1.8423	1.2485	1.2882	1.2900	1.4581	.9646
Ca	.0070	.0000	.0000	.0020	.0005	.0000	.0054	.0034	.0084	.0000	.0120	.0069	.0044	.0000	.0044	.0055	.0000	.0027
Mn	.0790	.1040	.1130	.2170	.1077	.1468	.1342	.3148	.1147	.1148	.1740	.1409	.1420	.4238	.2451	.4148	.3185	.3265
Fe	6.7870	6.9020	6.6200	6.8910	7.0174	6.7525	6.9693	6.6050	6.8461	6.7579	6.7998	6.9224	6.9288	7.1461	7.1353	7.2461	7.1558	7.5910
Na	.0000	.0000	.0000	.0150	.0000	.0045	.0011	.0124	.0034	.0001	.0112	.0001	.0001	.0000	.0123	.0079	.0107	.0043
K	.0000	.0190	.0030	.0050	.0114	.0088	.0038	.0025	.0205	.0000	.0233	.0025	.0008	.0061	.0014	.0051	.0000	.0000
SiIV	2.6740	2.5870	2.6485	2.5945	2.6493	2.6766	2.6995	2.6479	2.6623	2.6318	2.7030	2.6594	2.6301	2.6693	2.6472	2.5950	2.6200	2.5683
AlIV	1.3260	1.4130	1.3515	1.4055	1.3508	1.3234	1.3006	1.3521	1.3378	1.3682	1.2970	1.3407	1.3699	1.3308	1.3528	1.4050	1.3800	1.4318
AlVI	1.4995	1.4560	1.5170	1.4495	1.4709	1.5324	1.4459	1.4674	1.4748	1.5428	1.4730	1.4899	1.4770	1.4884	1.5481	1.4722	1.4755	1.5106
Ti	.0110	.0220	.0065	.0045	.0086	.0035	.0097	.0000	.0180	.0092	.0017	.0072	.0052	.0110	.0072	.0064	.0040	.0033
Fe	3.3935	3.4510	3.3100	3.4455	3.5087	3.3763	3.4847	3.3025	3.4231	3.3790	3.3999	3.4612	3.4644	3.5731	3.5677	3.6231	3.5779	3.7955
Mn	.0395	.0520	.0565	.1085	.0539	.0734	.0671	.1574	.0574	.0574	.0870	.0705	.0710	.2119	.1226	.2074	.1593	.1633
Mg	.9550	.9715	1.0195	.9600	.8863	.9032	.9065	1.0097	.9302	.9152	.9342	.8855	.9212	.6243	.6441	.6450	.7291	.4823
ΣVI	5.8985	5.9525	5.9095	5.9680	5.9283	5.8887	5.9138	5.9370	5.9033	5.9035	5.8958	5.9142	5.9388	5.9086	5.8896	5.9540	5.9457	5.9549
Vac	.1015	.0475	.0905	.0320	.0717	.1113	.0862	.0631	.0967	.0965	.1043	.0859	.0613	.0914	.1105	.0460	.0544	.0451
Ca	.0035	.0000	.0000	.0010	.0003	.0000	.0027	.0017	.0042	.0000	.0060	.0035	.0022	.0000	.0022	.0028	.0000	.0014
Na	.0000	.0000	.0000	.0075	.0000	.0023	.0006	.0062	.0017	.0001	.0056	.0001	.0001	.0000	.0062	.0040	.0054	.0022
K	.0000	.0095	.0015	.0025	.0057	.0044	.0019	.0013	.0103	.0000	.0117	.0013	.0004	.0031	.0007	.0026	.0000	.0000
ΣXII	.0035	.0095	.0015	.0110	.0060	.0067	.0052	.0092	.0162	.0001	.0233	.0048	.0027	.0031	.0091	.0093	.0054	.0035

File: Proclo2 Disk: El Cobre (probe) I
CLORITES EL COBRE-LINARES
MICROPROBE DATA (cations)

Sample:	LC129-20 (7 m) Analysis: 51719						LC129-22 (9 m) Analysis: 51718					LC90118-2(less al)Anal: 53103		
Point:	P-1	P-3	P-3.2	P-6	P-6.2	P-6.3	p1	p1b	p2a	p4a	p4b	p1a	p1b	p2a
Si	5.3340	5.4438	5.5579	5.5390	5.4551	5.4229	5.4647	5.3961	5.5475	5.4079	5.4572	5.3370	5.5530	5.4730
Ti	.0172	.0028	.0432	.0171	.0094	.0214	.0068	.0316	.0000	.0351	.0000	.0120	.0150	.0190
Al	5.5201	5.1626	5.1167	4.9408	5.2031	5.1605	5.1766	5.4135	5.1572	5.4043	5.2592	5.4550	4.9860	5.0500
Mg	2.2081	2.2479	2.3149	2.3274	2.2542	2.4266	2.4510	2.3176	2.4174	2.2990	2.2544	3.1790	3.3950	3.2860
Ca	.0015	.0000	.0073	.0077	.0083	.0102	.0062	.0042	.0080	.0065	.0038	.0120	.0180	.0110
Mn	.1397	.1169	.1240	.1317	.1188	.1173	.0980	.0988	.1126	.1258	.1229	.1030	.0630	.0930
Fe	6.6502	6.9808	6.6403	6.9969	6.8783	6.8126	6.7191	6.5949	6.6275	6.5641	6.8124	5.8230	5.8950	6.0360
Na	.0242	.0258	.0100	.0244	.0034	.0001	.0221	.0174	.0001	.0163	.0044	.0000	.0000	.0000
K	.0115	.0084	.0628	.0016	.0100	.0078	.0135	.0005	.0073	.0077	.0021	.0040	.0270	.0290
SiIV	2.6670	2.7219	2.7790	2.7695	2.7276	2.7115	2.7324	2.6981	2.7738	2.7040	2.7286	2.6685	2.7765	2.7365
AlIV	1.3330	1.2781	1.2211	1.2305	1.2725	1.2886	1.2677	1.3020	1.2263	1.2961	1.2714	1.3315	1.2235	1.2635
												2.7275	2.4930	2.5250
AlVI	1.4271	1.3032	1.3373	1.2399	1.3291	1.2917	1.3207	1.4048	1.3524	1.4061	1.3582	1.3960	1.2695	1.2615
Ti	.0086	.0014	.0216	.0086	.0047	.0107	.0034	.0158	.0000	.0176	.0000	.0060	.0075	.0095
Fe	3.3251	3.4904	3.3202	3.4985	3.4392	3.4063	3.3596	3.2975	3.3138	3.2821	3.4062	2.9115	2.9475	3.0180
Mn	.0699	.0585	.0620	.0659	.0594	.0587	.0490	.0494	.0563	.0629	.0615	.0515	.0315	.0465
Mg	1.1041	1.1240	1.1575	1.1637	1.1271	1.2133	1.2255	1.1588	1.2087	1.1495	1.1272	1.5895	1.6975	1.6430
ΣVI	5.9347	5.9774	5.8985	5.9765	5.9595	5.9807	5.9581	5.9263	5.9311	5.9181	5.9531	5.9545	5.9535	5.9785
Vac	.0654	.0226	.1015	.0236	.0406	.0194	.0419	.0738	.0689	.0819	.0470	.0455	.0465	.0215
Ca	.0008	.0000	.0037	.0039	.0042	.0051	.0031	.0021	.0040	.0033	.0019	.0060	.0090	.0055
Na	.0121	.0129	.0050	.0122	.0017	.0001	.0111	.0087	.0001	.0082	.0022	.0000	.0000	.0000
K	.0058	.0042	.0314	.0008	.0050	.0039	.0068	.0003	.0037	.0039	.0011	.0020	.0135	.0145
ΣXII	.0186	.0171	.0401	.0169	.0109	.0091	.0209	.0111	.0077	.0153	.0052	.0080	.0225	.0200

File: MICO2 Disk: Cobre (Probe II) Updating: 2/6/91

WHITE MICAS EL COBRE-LINARES

MICROPROBE DATA (cations)

	LC129-13	LC129-14 (1 m) Analysis:52206							LC129-16 (3 m) Analysis:52507					LC129-17 (4 m) Analysis:51720					
	p2a	p6a	p6b	p7a	p7b	p1a	p4a	p4b	p2a	p2b	p4	p5a	p5b	p1a	p1b	p4a	p4b	p6a	p8a
Si	6.1014	6.3005	6.1809	6.0681	6.2339	6.1173	6.0777	6.4632	5.9370	6.0930	6.1720	5.9730	5.9980	6.0168	6.0744	5.9719	6.1541	6.1141	6.0129
Ti	.0111	.0281	.0025	.0000	.0122	.0052	.0270	.0117	.0140	.0020	.0060	.0020	.0060	.0060	.0003	.0000	.0000	.0003	.0019
Al	5.7388	5.2007	5.7384	5.7338	5.2671	5.7014	5.7261	4.9469	5.8360	5.6950	5.5760	5.8370	5.8070	5.3970	5.6238	5.3721	5.4619	5.6306	5.3098
Mg	.0457	.1824	.0264	.0873	.1670	.0760	.0711	.3398	.1320	.1550	.1500	.1110	.1120	.3080	.1374	.2624	.1607	.1160	.3225
Ca	.0000	.0014	.0048	.0041	.0080	.0052	.0000	.0000	.0000	.0000	.0000	.0000	.0000	.0058	.0000	.0000	.0000	.0000	.0013
Mn	.0000	.0038	.0018	.0000	.0113	.0000	.0000	.0000	.0000	.0090	.0000	.0020	.0070	.0099	.0000	.0164	.0098	.0000	.0260
Fe	.1050	.4162	.0521	.2042	.4845	.1473	.1718	.3404	.2070	.1690	.1610	.1860	.1930	.6044	.2441	.7414	.3226	.1802	.6216
Na	.1566	.0476	.0093	.1094	.0364	.1315	.1738	.0080	.1420	.1040	.1510	.1700	.1510	.0673	.1647	.1075	.1224	.1627	.0922
K	1.7813	1.8285	1.8716	1.8253	1.8363	1.8171	1.7436	1.8913	1.8680	1.7610	1.7900	1.8200	1.7930	1.7594	1.7264	1.7773	1.7960	1.7099	1.7915
SiIV	3.0507	3.1503	3.0905	3.0341	3.1170	3.0587	3.0389	3.2316	2.9685	3.0465	3.0860	2.9865	2.9990	3.0084	3.0372	2.9860	3.0771	3.0571	3.0065
AlIV	.9493	.8498	.9096	.9660	.8831	.9414	.9612	.7684	1.0315	.9535	.9140	1.0135	1.0010	.9916	.9628	1.0141	.9230	.9430	.9936
AlVI	1.9201	1.7506	1.9597	1.9010	1.7505	1.9094	1.9019	1.7051	1.8865	1.8940	1.8740	1.9050	1.9025	1.7069	1.8491	1.6720	1.8080	1.8724	1.6614
Ti	.0056	.0141	.0013	.0000	.0061	.0026	.0135	.0059	.0070	.0010	.0030	.0010	.0030	.0030	.0002	.0000	.0000	.0002	.0010
Fe	.0525	.2081	.0261	.1021	.2423	.0737	.0859	.1702	.1035	.0845	.0805	.0930	.0965	.3022	.1221	.3707	.1613	.0901	.3108
Mn	.0000	.0019	.0009	.0000	.0057	.0000	.0000	.0000	.0000	.0045	.0000	.0010	.0035	.0050	.0000	.0082	.0049	.0000	.0130
Mg	.0229	.0912	.0132	.0437	.0835	.0380	.0356	.1699	.0660	.0775	.0750	.0555	.0560	.1540	.0687	.1312	.0804	.0580	.1613
ΣVI	2.0010	2.0659	2.0011	2.0467	2.0880	2.0236	2.0369	2.0510	2.0630	2.0615	2.0325	2.0555	2.0615	2.1711	2.0400	2.1821	2.0546	2.0206	2.1474
Ca	.0000	.0019	.0009	.0000	.0057	.0000	.0000	.0000	.0000	.0045	.0000	.0010	.0035	.0050	.0000	.0082	.0049	.0000	.0130
Na	.0783	.0238	.0047	.0547	.0182	.0658	.0869	.0040	.0710	.0520	.0755	.0850	.0755	.0337	.0824	.0538	.0612	.0814	.0461
K	.8907	.9143	.9358	.9127	.9182	.9086	.8718	.9457	.9340	.8805	.8950	.9100	.8965	.8797	.8632	.8887	.8980	.8550	.8958
ΣXII	.9690	.9400	.9414	.9674	.9420	.9743	.9587	.9497	1.0050	.9370	.9705	.9960	.9755	.9183	.9456	.9506	.9641	.9363	.9549
VacXI	.0311	.0601	.0587	.0327	.0580	.0257	.0413	.0504	-.0050	.0630	.0295	.0040	.0245	.0817	.0545	.0494	.0359	.0637	.0452

File: MICO2 Disk: El Cobre (probe) II
WHITE MICAS EL COBRE-LINARES
MICROPROBE DATA (cations)

	LC129-18 (5 m) Analysis:52508					LC129-20 (7 m) Anal:51719			LC129-22 (9 m) Analysis: 51718					
	p1a	p1b	p2a	p3a	p5a	p6a	p5a	p1a	p1a	p1b	p4a	p4b	p4c	p1a
Si	6.1513	6.0482	6.0474	6.1589	6.1589	6.2717	6.1305	6.0762	5.9715	6.2572	6.1809	6.1517	6.1469	6.2007
Ti	.0262	.0000	.0312	.0226	.0256	.0056	.0283	.0083	.0000	.0024	.0146	.0111	.0084	.0089
Al	5.5202	5.6314	5.7559	5.5902	5.5306	5.1686	5.5286	5.6330	5.4287	5.4444	5.4424	5.4941	5.5864	5.4481
Mg	.0976	.0787	.0710	.0859	.1216	.2613	.1444	.1071	.2838	.1361	.1179	.1050	.1092	.1318
Ca	.0013	.0032	.0058	.0002	.0000	.0000	.0000	.0016	.0000	.0000	.0062	.0000	.0040	.0000
Mn	.0035	.0000	.0000	.0000	.0000	.0000	.0000	.0047	.0096	.0058	.0000	.0059	.0000	.0176
Fe	.3144	.3881	.1538	.2333	.2528	.3907	.1757	.1636	.6006	.1442	.3244	.2960	.1574	.3183
Na	.1602	.1278	.1446	.1399	.1134	.0381	.1268	.1368	.1312	.1348	.0832	.0967	.1391	.0615
K	1.7358	1.8450	1.8119	1.7244	1.7983	1.8410	1.8023	1.8050	1.7688	1.6645	1.6767	1.7099	1.7147	1.5542
SiIV	3.0757	3.0241	3.0237	3.0795	3.0795	3.1359	3.0653	3.0381	2.9858	3.1286	3.0905	3.0759	3.0735	3.1004
AlIV	.9244	.9759	.9763	.9206	.9206	.8642	.9348	.9619	1.0143	.8714	.9096	.9242	.9266	.8997
AlVI	1.8358	1.8398	1.9017	1.8746	1.8448	1.7202	1.8296	1.8546	1.7001	1.8508	1.8117	1.8229	1.8667	1.8244
Ti	.0131	.0000	.0156	.0113	.0128	.0028	.0142	.0042	.0000	.0012	.0073	.0056	.0042	.0045
Fe	.1572	.1941	.0769	.1167	.1264	.1954	.0879	.0818	.3003	.0721	.1622	.1480	.0787	.1592
Mn	.0018	.0000	.0000	.0000	.0000	.0000	.0000	.0024	.0048	.0029	.0000	.0030	.0000	.0088
Mg	.0488	.0394	.0355	.0430	.0608	.1307	.0722	.0536	.1419	.0681	.0590	.0525	.0546	.0659
ΣVI	2.0566	2.0732	2.0297	2.0455	2.0447	2.0490	2.0038	1.9965	2.1471	1.9951	2.0401	2.0319	2.0042	2.0627
Ca	.0018	.0000	.0000	.0000	.0000	.0000	.0000	.0024	.0048	.0029	.0000	.0030	.0000	.0088
Na	.0801	.0639	.0723	.0700	.0567	.0191	.0634	.0684	.0656	.0674	.0416	.0484	.0696	.0308
K	.8679	.9225	.9060	.8622	.8992	.9205	.9012	.9025	.8844	.8323	.8384	.8550	.8574	.7771
ΣXII	.9498	.9864	.9783	.9322	.9559	.9396	.9646	.9733	.9548	.9026	.8800	.9063	.9269	.8167
VacXI	.0503	.0136	.0218	.0679	.0442	.0605	.0355	.0268	.0452	.0975	.1201	.0938	.0731	.1834

File: MICOEL2 Disk: Sta. Elena (Probe I) Date: 6 June'91
WHITE MICAS SANTA ELENA
MICROPROBE DATA (cations)

Sample	LC159-5 (La Nube biotitic)Analysis:51723						LC159-6 (La Nube mosc.)An:51724				LC9098-3 (less alt.) An:53104		
Point	1a	1b	4a	4b	6a	7a	1a	2a	3a	4a	6a	6b	6c
Si	6.1844	6.1665	6.1458	6.0473	6.1061	6.1516	6.1320	6.1272	6.1176	6.1775	6.1370	6.1141	6.1213
Ti	.1288	.0709	.0766	.0488	.1592	.0425	.0580	.0364	.0607	.0269	.0042	.0081	.0000
Al	5.4688	5.5061	5.4102	5.6542	5.4479	5.4986	5.5782	5.6631	5.5883	5.5662	5.7796	5.8195	5.8111
Mg	.1515	.1747	.1708	.1299	.1515	.1748	.1334	.1065	.1284	.1343	.1134	.1067	.0854
Ca	.0000	.0000	.0000	.0000	.0066	.0000	.0000	.0037	.0000	.0000	.0000	.0000	.0000
Mn	.0012	.0012	.0049	.0000	.0062	.0000	.0000	.0000	.0047	.0000	.0036	.0000	.0073
Fe	.1338	.1413	.2008	.1244	.1169	.1719	.1363	.1202	.1415	.1523	.1114	.0636	.1104
Na	.0623	.0988	.0569	.0818	.0980	.0962	.0853	.1024	.1110	.1215	.0488	.0621	.0500
K	1.5311	1.7034	1.8457	1.8610	1.7903	1.7730	1.7621	1.7694	1.8137	1.7773	1.5910	1.6502	1.6253
SiIV	3.0922	3.0833	3.0729	3.0237	3.0531	3.0758	3.0660	3.0636	3.0588	3.0888	3.0685	3.0571	3.0607
AlIV	.9078	.9168	.9271	.9764	.9470	.9242	.9340	.9364	.9412	.9113	.9315	.9430	.9394
AlVI	1.8266	1.8363	1.7780	1.8508	1.7770	1.8251	1.8551	1.8952	1.8530	1.8719	1.9583	1.9668	1.9662
Ti	.0644	.0355	.0383	.0244	.0796	.0213	.0290	.0182	.0304	.0135	.0021	.0041	.0000
Fe	.0669	.0707	.1004	.0622	.0585	.0860	.0682	.0601	.0708	.0762	.0557	.0318	.0552
Mn	.0006	.0006	.0025	.0000	.0031	.0000	.0000	.0000	.0024	.0000	.0018	.0000	.0037
Mg	.0758	.0874	.0854	.0650	.0758	.0874	.0667	.0533	.0642	.0672	.0567	.0534	.0427
ΣVI	2.0343	2.0304	2.0046	2.0023	1.9939	2.0197	2.0190	2.0267	2.0206	2.0286	2.0746	2.0560	2.0678
Ca	.0000	.0000	.0000	.0000	.0033	.0000	.0000	.0019	.0000	.0000	.0000	.0000	.0000
Na	.0312	.0494	.0285	.0409	.0490	.0481	.0427	.0512	.0555	.0608	.0244	.0311	.0250
K	.7656	.8517	.9229	.9305	.8952	.8865	.8811	.8847	.9069	.8887	.7955	.8251	.8127
ΣXII	.7967	.9011	.9513	.9714	.9475	.9346	.9237	.9378	.9624	.9494	.8199	.8562	.8377
VacXII	.2033	.0989	.0487	.0286	.0526	.0654	.0763	.0623	.0377	.0506	.1801	.1439	.1624

File: MICOEL2 Disk: Sta. Elena (Probe I) Date: 6 June'91
WHITE MICAS SANTA ELENA
MICROPROBE DATA (cations)

Sample	LC59-1 (Mylonite) Analysis: 51721											
Point	2a	2b	2bb	2c	4a	4b	5b	5bb	5c	5d	6a	6b
Si	6.0921	6.0735	6.1118	6.1474	6.1223	6.0393	6.1375	6.0809	6.1566	6.2663	6.1010	6.0176
Ti	.0068	.0169	.0120	.0000	.0166	.0194	.0093	.0181	.0040	.0161	.0220	.0241
Al	5.6645	5.6950	5.6567	5.5806	5.6243	5.6208	5.7370	5.6293	5.6006	5.1778	5.5954	5.6433
Mg	.0870	.0958	.0887	.0801	.0970	.1055	.0980	.0994	.0541	.1929	.1065	.1113
Ca	.0000	.0066	.0000	.0000	.0000	.0000	.0000	.0038	.0000	.0010	.0066	.0000
Mn	.0201	.0000	.0201	.0024	.0071	.0047	.0000	.0106	.0000	.0262	.0118	.0082
Fe	.2017	.1565	.1666	.2015	.1669	.2153	.1977	.1865	.2492	.4610	.2249	.2166
Na	.0687	.0994	.0658	.0587	.1042	.1406	.0990	.1291	.0680	.0382	.0801	.1835
K	1.8416	1.8175	1.8585	1.8536	1.7354	1.7806	1.4428	1.7167	1.7980	1.8188	1.8246	1.7818
SiIV	3.0461	3.0368	3.0559	3.0737	3.0612	3.0197	3.0688	3.0405	3.0783	3.1332	3.0505	3.0088
AlIV	.9540	.9633	.9441	.9263	.9389	.9804	.9313	.9596	.9217	.8669	.9495	.9912
AlVI	1.8783	1.8843	1.8843	1.8640	1.8733	1.8301	1.9373	1.8551	1.8786	1.7221	1.8482	1.8305
Ti	.0034	.0085	.0060	.0000	.0083	.0097	.0047	.0091	.0020	.0081	.0110	.0121
Fe	.1009	.0783	.0833	.1008	.0835	.1077	.0989	.0933	.1246	.2305	.1125	.1083
Mn	.0101	.0000	.0101	.0012	.0036	.0024	.0000	.0053	.0000	.0131	.0059	.0041
Mg	.0435	.0479	.0444	.0401	.0485	.0528	.0490	.0497	.0271	.0965	.0533	.0557
ΣVI	2.0361	2.0189	2.0280	2.0060	2.0171	2.0025	2.0898	2.0124	2.0323	2.0702	2.0308	2.0106
Ca	.0000	.0033	.0000	.0000	.0000	.0000	.0000	.0019	.0000	.0005	.0033	.0000
Na	.0344	.0497	.0329	.0294	.0521	.0703	.0495	.0646	.0340	.0191	.0401	.0918
K	.9208	.9088	.9293	.9268	.8677	.8903	.7214	.8584	.8990	.9094	.9123	.8909
ΣXII	.9552	.9618	.9622	.9562	.9198	.9606	.7709	.9248	.9330	.9290	.9557	.9827
VacXII	.0449	.0383	.0379	.0439	.0802	.0394	.2291	.0752	.0670	.0710	.0444	.0174

Sample	LC9098-5 (Mylonite) Analysis: 53106						
Point	1a	2a	3a	4a	4b	5a	6a
Si	6.1396	6.0399	6.1172	6.2426	6.1153	6.1872	6.0944
Ti	.0065	.0066	.0112	.0175	.0127	.1057	.0027
Al	5.7884	5.8220	5.5920	5.1827	5.6391	5.3493	5.7209
Mg	.0341	.0421	.0825	.1409	.0677	.1439	.0570
Ca	.0000	.0000	.0000	.0000	.0000	.0000	.0000
Mn	.0048	.0184	.0000	.0288	.0135	.0124	.0025
Fe	.1592	.1528	.3156	.5794	.2316	.3016	.2282
Na	.1181	.1913	.0922	.0667	.1113	.0428	.0691
K	1.5359	1.7300	1.8222	1.8467	1.8340	1.8215	1.8045
SiIV	3.0698	3.0200	3.0586	3.1213	3.0577	3.0936	3.0472
AlIV	.9302	.9801	.9414	.8787	.9424	.9064	.9528
AlVI	1.9640	1.9310	1.8546	1.7127	1.8772	1.7683	1.9077
Ti	.0033	.0033	.0056	.0088	.0064	.0529	.0014
Fe	.0796	.0764	.1578	.2897	.1158	.1508	.1141
Mn	.0024	.0092	.0000	.0144	.0068	.0062	.0013
Mg	.0171	.0211	.0413	.0705	.0339	.0720	.0285
ΣVI	2.0663	2.0409	2.0593	2.0960	2.0400	2.0501	2.0529
Ca	.0000	.0000	.0000	.0000	.0000	.0000	.0000
Na	.0591	.0957	.0461	.0334	.0557	.0214	.0346
K	.7680	.8650	.9111	.9234	.9170	.9108	.9023
ΣXII	.8270	.9607	.9572	.9567	.9727	.9322	.9368
VacXII	.1730	.0394	.0428	.0433	.0274	.0679	.0632

II.3. Fluid inclusions data.

FLUID INCLUSIONS: 52490 Q Renegadero (90174/3a)

Type	Dim(d)	Dim(p)	LH20	LC02	Vapour	Te(r)	Te(corr)	Tmi(r)	Tmi(corr)	Th	to	TeC02 (raw)	TeC02 (correc)	TmiC02	TmiC02(c)	Tmhydrat	ThC02	to
s	14.00	33.60	20.00	55.00	25.00			-3.50	-3.48			-97.90	-97.21	-57.40	-57.00	8.50	24.70	L
s	11.00	26.40	20.00	60.00	20.00			-3.40	-3.38			-98.40	-97.71	-57.40	-57.00	7.90	25.90	L
s	9.00	21.60	20.00	60.00	20.00			-3.40	-3.38			-99.50	-98.80	-57.30	-56.90	8.90	24.70	L
s?	9.00	21.60	40.00	40.00	20.00					341.40	LC02	-97.50	-96.82	-57.40	-57.00	7.80	24.90	L
s	10.00	24.00	20.00	65.00	15.00					353.00	LC02	-101.90	-101.19	-57.30	-56.90	8.70	24.40	L
s	15.00	36.00	90.00	.10	9.90	-18.30	-18.17	-3.50	-3.48	215.40	LH20							
s	6.00	14.40	5.00	75.00	10.00					353.00	LC02	-100.50	-99.80	-57.70	-57.30	8.70	22.70	L
s	15.00	36.00	85.00	.10	14.90	-18.50	-18.37	-3.30	-3.28	206.00	LH20							
s	30.00	72.00	20.00	50.00	25.00			-4.20	-4.17			-98.00	-97.31	-57.40	-57.00	8.00	26.00	L
s	15.00	36.00	15.00	40.00	45.00					293.40	LC02	-96.90	-96.22	-57.40	-57.00	8.20	26.20	V
s	15.00	36.00	15.00	45.00	40.00							-97.50	-96.82	-57.30	-56.90	8.80	26.00	L
s	15.00	36.00	15.00	50.00	35.00	-9.80	-9.73	-5.80	-5.76			-97.00	-96.32	-57.40	-57.00	8.90	25.60	L
s	12.00	28.80	25.00	40.00	35.00	-10.00	-9.93	-5.70	-5.66			-98.30	-97.61	-57.20	-56.80	9.10	26.00	L
s	10.00	24.00	25.00	50.00	25.00					343.40	LC02	-98.90	-98.21	-57.40	-57.00	8.80	25.90	L
s	7.00	16.80	20.00	60.00	20.00							-99.70	-99.00	-57.40	-57.00	4.60	25.50	L
s	10.00	24.00	15.00	40.00	45.00							-97.00	-96.32	-57.40	-57.00	9.10	25.80	L
s	7.00	16.80	15.00	45.00	40.00	-9.30	-9.23	-3.00	-2.98			-101.30	-100.59	-57.20	-56.80	8.80	25.60	L
s	21.00	50.40	90.00	.10	9.90	-11.50	-11.42	-4.10	-4.07									
s	12.00	28.80	20.00	50.00	30.00	-19.30	-19.16	-5.10	-5.06	373.00	LC02	-100.00	-99.30	-57.90	-57.50	8.30	23.90	L
s	7.00	16.80	20.00	45.00	35.00	-10.10	-10.03	-5.70	-5.66	326.00	LC02	-99.50	-98.80	-57.70	-57.30	8.60	24.10	
s	5.00	12.00	85.00		15.00	-11.10	-11.02	-4.60	-4.57	227.60	LH20							
s	5.00	12.00	50.00	40.00	10.00	-10.50	-10.43	-4.90	-4.87	296.10	LC02	-100.00	-99.30	-57.50	-57.10	8.90	25.20	L
s	8.00	19.20	45.00	35.00	20.00					373.00	LC02	-103.20	-102.48	-57.80	-57.40	8.50	24.10	L
s	7.00	16.80	75.00	1.00	24.00	-10.50	-10.43	-4.30	-4.27	240.60	LH20	-98.00	-97.31	-57.40	-57.00	8.50	26.00	V
s	12.00	28.80	50.00	40.00	10.00					310.90	LC02	-103.70	-102.97	-57.80	-57.40	9.00	26.00	L
s	8.00	19.20	50.00	40.00	10.00	-13.60	-13.50	-3.60	-3.57	295.20	LC02	-98.00	-97.31	-57.70	-57.30	8.80	25.80	L
s	4.00	9.60	70.00	1.00	29.00			-4.90	-4.87	245.40	LH20	-99.80	-99.10	-57.50	-57.10	8.90	26.80	V
s	12.00	28.80	50.00	40.00	10.00	-11.40	-11.32	-6.20	-6.16	297.00	LC02	-102.20	-101.48	-57.80	-57.40	8.80	23.90	L
s	7.00	16.80	10.00	50.00	40.00							-99.00	-98.31	-57.50	-57.10	8.40	23.60	L
s?	7.00	16.80	85.00		15.00	-9.50	-9.43	-.80	-.79	166.80	LH20							
s?	8.00	19.20	85.00	1.00	14.00	-10.30	-10.23	-4.50	-4.47	201.90	LH20					8.70	23.50	L
s	12.00	28.80	15.00	70.00	15.00							-99.00	-98.31	-58.00	-57.60	8.60	22.20	L
s	6.00	14.40	55.00	5.00	40.00	-10.90	-10.82	-4.70	-4.67					-57.40	-57.00	8.80	26.20	V

FLUID INCLUSIONS: 53664 Q Mylonite Sta. Elena (9098/6)

Type	Dim(d)	Dim(p)	L/V%	Te(raw)	Te(corr)	Tmi(raw)	Tmi(cor)	Th	Tmhydrat
s	8.0	19.2	90.0	-5.9	-5.9	-2.8	-2.8		
s	4.0	9.6	80.0	-6.0	-6.0	-3.1	-3.1	317.0	
s	2.0	4.8	65.0	-6.4	-6.4	-2.8	-2.8	284.0	
s	3.0	7.2	65.0	-6.6	-6.6	-3.8	-3.8	310.8	
s	5.0	12.0	75.0	-6.8	-6.8	-3.0	-3.0	298.8	
s	5.0	12.0	65.0	-5.7	-5.7	-3.2	-3.2	331.7	
s	4.0	9.6	85.0	-6.5	-6.5	-2.1	-2.1	252.2	
s	7.0	16.8	80.0	-6.9	-6.9	-2.9	-2.9	314.0	
s	5.0	12.0	85.0	-6.5	-6.5	-2.7	-2.7	280.0	
s	8.0	19.2	75.0	-5.5	-5.5	-2.5	-2.5	276.7	
s	4.0	9.6	80.0	-5.5	-5.5	-2.5	-2.5	209.7	
s	5.0	12.0	85.0	-6.1	-6.1	-1.7	-1.7	212.3	
s	3.0	7.2	60.0	-7.0	-7.0	-2.4	-2.4	316.0	
s	5.0	12.0	75.0	-6.2	-6.2	-2.5	-2.5	221.5	
s	4.0	9.6	60.0	-6.2	-6.2	-1.7	-1.7		
s	8.0	19.2	75.0	-6.4	-6.4	-2.4	-2.4	245.3	

FLUID INCLUSIONS: 52509 Q San Juan (90138/2) Monocrystal

Type	Dim(d)	Dim(p)	L/V%	Te(raw)	Te(cor)	Tmi(raw)	Tmi(cor)	Th	TmhyI	TmhyII
p?	10.0	24.0	90.0	-52.2	-51.8	-24.6	-24.4	96.6	2.3	6.9
p?	10.0	24.0	90.0	-51.8	-51.4	-25.0	-24.8	98.2	-2.5	4.0
p?	9.0	21.6	80.0	-51.8	-51.4	-25.5	-25.3	103.4	-.3	2.8
p?	10.0	24.0	90.0	-52.0	-51.6	-24.5	-24.3	100.2	.9	2.5
p?	10.0	24.0	75.0	-50.8	-50.4	-24.9	-24.7	76.6	-1.5	3.5
p?	8.0	19.2	70.0	-51.8	-51.4	-25.0	-24.8	105.1	-1.0	4.0
p?	10.0	24.0	80.0	-51.8	-51.4	-25.1	-24.9	101.0	-.6	3.4
p?	11.0	26.4	90.0	-53.1	-52.7	-24.9	-24.7	88.0	.5	3.4
s?	14.0	33.6	90.0	-51.5	-51.1	-24.9	-24.7	89.9	1.7	
s?	8.0	19.2	90.0	-50.5	-50.1	-25.1	-24.9	103.1	.3	
s?	16.0	38.4	90.0	-50.5	-50.1	-24.7	-24.5	91.0	-.8	3.9
s?	13.0	31.2	90.0	-50.5	-50.1	-24.8	-24.6	96.0		
s?	10.0	24.0	90.0	-49.5	-49.2	-24.5	-24.3	89.9		4.0
s?	7.0	16.8	90.0	-50.7	-50.3	-25.1	-24.9	103.1	-.8	
s?	15.0	36.0	90.0	-50.5	-50.1	-25.0	-24.8	95.8	.8	3.6
s?	6.0	14.4	90.0	-49.3	-49.0	-24.9	-24.7	100.0	-.3	1.5
s?	18.0	43.2	90.0	-48.9	-48.6	-25.0	-24.8	94.5	.4	3.7
s?	10.0	24.0	90.0	-50.1	-49.7	-25.1	-24.9	94.5	-.5	2.3
s?	8.0	19.2	90.0	-52.1	-51.7	-25.2	-25.0	96.0	-.1	3.2
s?	5.0	12.0	85.0	-50.5	-50.1	-25.2	-25.0	94.5	1.0	2.8
p?	20.0	48.0	95.0	-49.7	-49.4	-24.8	-24.6	89.9	.4	3.3
s?	17.0	40.8	87.0	-49.8	-49.5	-24.8	-24.6	93.6	-.3	3.0
s?	25.0	60.0	95.0	-52.0	-51.6	-25.2	-25.0	95.0	-.3	2.9
s?	17.0	40.8	87.0	-49.3	-49.0	-25.0	-24.8	94.9	-3.4	-1.5
p?	25.0	60.0	95.0	-50.1	-49.7	-23.8	-23.6	88.8	-1.2	.1
p?	15.0	36.0	90.0	-50.4	-50.0	-24.3	-24.1	95.1	-.6	1.6
p?	10.0	24.0	90.0	-50.8	-50.4	-24.0	-23.8	138.5	-4.9	4.0
p?	5.0	12.0	85.0	-48.5	-48.2	-24.5	-24.3	109.0		
s?	32.0	76.8	95.0	-51.9	-51.5	-24.2	-24.0			.5
s?	13.0	31.2	95.0	-51.7	-51.3	-24.8	-24.6		-3.2	2.6
s?	13.0	31.2	95.0	-50.5	-50.1	-24.7	-24.5			1.5
s?	16.0	38.4	95.0	-49.6	-49.3	-24.8	-24.6			2.6

FLUID INCLUSIONS: 53665 Q El Cobre (129/31)

Type	Dim(d)	Dim(y)	L/V%	Te(raw)	Te(cor)	Tmi(raw)	Tmi(cor)	Th	Tmhydrat
s?	20.0	48.0	95.0	-51.8	-51.4	-23.5	-23.3	114.2	6.3
p?	10.0	24.0	95.0	-44.5	-44.2	-23.7	-23.5	88.1	5.3
s	20.0	48.0	90.0	-48.6	-48.3	-24.0	-23.8		6.0
s	15.0	36.0	90.0	-54.3	-53.9	-23.8	-23.6	103.5	5.3
s	5.0	12.0	92.0	-54.1	-53.7	-24.0	-23.8	105.8	5.2
s	5.0	12.0	90.0	-53.6	-53.2	-24.2	-24.0	106.8	
s	7.0	16.8	90.0	-53.5	-53.1	-24.1	-23.9	105.9	4.8
s	7.0	16.8	92.0	-54.7	-54.3	-24.1	-23.9	106.0	4.5
s	6.0	14.4	92.0	-55.7	-55.3	-24.2	-24.0	105.6	5.8
s	5.0	12.0	90.0	-55.2	-54.8	-24.1	-23.9	105.6	4.7
s	12.0	28.8	95.0	-54.8	-54.4	-23.4	-23.2		6.3
s	30.0	72.0	95.0	-52.4	-52.0	-23.8	-23.6	102.3	7.4
s?	15.0	36.0	95.0	-54.1	-53.7	-23.9	-23.7	105.2	7.5
s?	5.0	12.0	90.0	-52.5	-52.1	-23.7	-23.5	118.5	6.1
s?	4.0	9.6	95.0	-52.7	-52.3	-23.5	-23.3		5.3
s?	10.0	24.0	92.0	-53.9	-53.5	-23.7	-23.5	107.4	8.7
s	12.0	28.8	92.0	-52.8	-52.4	-23.8	-23.6	133.1	10.1
s?	6.0	14.4	95.0	-52.7	-52.3	-23.9	-23.7		6.4
s	7.0	16.8	90.0	-52.6	-52.2	-23.4	-23.2	110.4	8.0

FLUID INCLUSIONS: 53424 Bt Fernandina (79/1)

Type	Dim(d)	Dim(p)	L/V%	Te(raw)	Te(cor)	Tmi(raw)	Tmi(cor)	Th
s	15.0	36.0	85.0	-25.7	-25.5	-2.1	-2.1	168.0
s	14.0	33.6	80.0	-25.5	-25.3	-5.3	-5.3	
s	10.0	24.0	90.0	-30.5	-30.3	-6.6	-6.6	175.4
s	6.0	14.4	85.0	-29.0	-28.8	-7.5	-7.4	241.7
s	11.0	26.4	85.0	-26.5	-26.3	-3.1	-3.1	253.5
s	6.0	14.4	85.0	-26.0	-25.8	-5.6	-5.6	168.3
s	4.0	9.6	75.0	-28.6	-28.4	-6.5	-6.5	212.5
s	12.0	28.8	85.0	-27.5	-27.3	-4.0	-4.0	217.6
s	22.0	52.8	85.0	-26.0	-25.8	-4.6	-4.6	239.7
s	15.0	36.0	75.0	-27.7	-27.5	-6.0	-6.0	
s	8.0	19.2	85.0	-27.6	-27.4	-5.3	-5.3	
s	20.0	48.0	85.0	-28.5	-28.3	-4.0	-4.0	241.5
s	12.0	28.8	65.0	-30.7	-30.5	-10.2	-10.1	260.0
s	10.0	24.0	50.0	-30.5	-30.3	-10.4	-10.3	
s?	10.0	24.0	80.0	-66.2	-65.7	-13.4	-13.3	243.0
s?	10.0	24.0	80.0	-63.5	-63.1	-14.6	-14.5	
s?	4.0	9.6	80.0	-63.8	-63.4	-15.4	-15.3	185.8
s	10.0	24.0	80.0	-52.0	-51.6	-7.3	-7.2	219.0
s	7.0	16.8	80.0	-67.0	-66.5	-20.4	-20.3	195.0
s	7.0	16.8	80.0	-68.0	-67.5	-18.8	-18.7	201.0
s?	9.0	21.6	80.0	-55.0	-54.6	-4.4	-4.4	202.0
s?	4.0	9.6	80.0	-58.0	-57.6	-10.0	-9.9	218.0
s	10.0	24.0	80.0	-54.0	-53.6	-5.5	-5.5	212.6
s	10.0	24.0	85.0	-10.2	-10.1	-2.7	-2.7	172.1
s	20.0	48.0	85.0	-10.0	-9.9	-2.1	-2.1	255.0
s?	4.0	9.6	85.0	-63.4	-63.0	-16.6	-16.5	256.0
s?	4.0	9.6	80.0	-.8	-.8	-.5	-.5	233.0
s?	3.0	7.2	85.0	-62.9	-62.5	-14.2	-14.1	196.4
s?	4.0	9.6	80.0	-40.0	-39.7	-11.4	-11.3	203.9
s?	4.0	9.6	80.0	-63.8	-63.4	-16.7	-16.6	214.1

FLUID INCLUSIONS: 53918 Q CaNada Incosa (129/9)

Type	Dim(d)	Dim(p)	L/V%	Te(raw)	Te(cor)	Tmi(raw)	Tmi(cor)	Th	Tmhydrat	Tmhydrat	Daughter
p?	15.0	36.0	85.0	-12.5	-12.4	-1.0	-1.0	174.0			
p?	9.0	21.6	95.0	-12.1	-12.0	3.3					
p?	12.0	28.8	95.0	-3.5	-3.5	-.2	-.2	87.4			
s	25.0	60.0	90.0	-50.5	-50.1	-24.2	-24.0	131.1	-1.1	10.3	
s	10.0	24.0	79.4	-48.0	-47.7	-24.2	-24.0	129.5		7.6	
s?	9.0	21.6	95.0	-38.5	-38.2	-14.8	-14.7	115.5			
s?	10.0	24.0	95.0	-39.0	-38.7	-11.6	-11.5	81.7			
s?	7.0	16.8	95.0	-40.0	-39.7	-10.8	-10.7				
s?	10.0	24.0	95.0	-40.5	-40.2	-12.2	-12.1				
p?	20.0	48.0	92.0	-39.8	-39.5	-14.2	-14.1	98.0			
p?	8.0	19.2	80.0	-37.9	-37.6	-14.3	-14.2	92.1			
p?	6.0	14.4	90.0	-40.4	-40.1	-14.4	-14.3	95.4			
p?	12.0	28.8	95.0	-38.8	-38.5	-13.9	-13.8				
s?	34.0	81.6	90.0	-39.1	-38.8	-13.9	-13.8				
p?	10.0	24.0	95.0	-38.3	-38.0	-14.2	-14.1				
p?	11.0	26.4	95.0	-40.3	-40.0	-14.0	-13.9				
p?	12.0	28.8	95.0	-40.9	-40.6	-13.9	-13.8				
s?	25.0	60.0	30.0	-49.7	-49.4	-18.6	-18.5				
p?	24.0	57.6	80.0	-50.3	-49.9	-24.1	-23.9			1.3	
p?	8.0	19.2	95.0	-49.6	-49.3	-23.3	-23.1	111.5			
p?	22.0	52.8	10.0	-45.5	-45.2	-28.1	-27.9		4.8		213.6
p	15.0	36.0	92.0	-51.6	-51.2	-24.5	-24.3	94.7	-2.9	5.4	
p	15.0	36.0	90.0	-50.0	-49.7	-24.4	-24.2			6.7	
p?	40.0	96.0	85.0	-43.5	-43.2	-13.4	-13.3				
p?	40.0	96.0	75.0	-45.0	-44.7	-16.4	-16.3				
p?	15.0	36.0	95.0	-44.5	-44.2	-10.3	-10.2	265.1			
p?	60.0	144.0	95.0	-42.5	-42.2	-12.2	-12.1	93.1			
p?	10.0	24.0	90.0	-46.9	-46.6	-11.5	-11.4	85.0			
s?	110.0	264.0	95.0	-42.8	-42.5	-12.2	-12.1				
s?	40.0	96.0	95.0	-44.5	-44.2	-12.5	-12.4				

FLUID INCLUSIONS: 51914 Q CaÑada Incosa (129/10)

Type	Dim(d)	Dim(p)	L/V%	Te(raw)	Te(cor)	Tmi(raw)	Tmi(cor)	Th	TmhyI	TmhyI(c)	TmhyII
s	22.0	52.8	70.0	-30.0	-29.8	-12.6	-12.5	253.0			
s	12.0	28.8	80.0	-27.0	-26.8	-11.1	-11.0	246.0			
s	15.0	36.0	90.0	-28.0	-27.8	-13.0	-12.9				
s	12.0	28.8	70.0	-28.5	-28.3	-11.0	-10.9				
s	12.0	28.8	80.0	-30.0	-29.8	-10.7	-10.6				
s	5.0	12.0	70.0	-26.0	-25.8	-11.4	-11.3				
s	15.0	36.0	90.0	-29.0	-28.8	-7.9	-7.8				
s	22.0	52.8	80.0	-27.5	-27.3	-13.1	-13.0	289.0			
s	9.0	21.6	75.0	-27.0	-26.8	-11.5	-11.4	279.0			
s	12.0	28.8	85.0	-26.5	-26.3	-11.0	-10.9				
s	12.0	28.8	85.0	-47.0	-46.7	-23.2	-23.0		4.5	4.5	7.5
s?	15.0	36.0	90.0	-50.0	-49.7	-21.0	-20.9	106.0	1.8	1.8	4.5
s?	13.0	31.2	60.0	-51.0	-50.6	-27.9	-27.7	197.0	5.0	5.0	8.0
s?	11.0	26.4	70.0	-50.9	-50.5	-23.8	-23.6		4.5	4.5	8.2
s?	12.0	28.8	80.0	-50.0	-49.7	-23.5	-23.3	125.0	4.8	4.8	7.8
s?	11.0	26.4	80.0	-50.7	-50.3	-23.6	-23.4	253.0	5.2	5.2	8.5
s?	60.0	144.0	95.0	-50.0	-49.7	-23.5	-23.3	131.5	3.8	3.8	4.2
s?	40.0	96.0	90.0	-50.2	-49.8	-23.5	-23.3	115.5	3.5	3.5	3.8
s?	7.0	16.8	95.0	-49.0	-48.7	-19.2	-19.1		.9	.9	
s?	17.0	40.8	95.0	-50.5	-50.1	-20.0	-19.9				2.5
s?	20.0	48.0	90.0	-49.6	-49.3	-23.6	-23.4		.2	.2	3.4
s?	4.0	9.6	90.0	-48.9	-48.6	-19.0	-18.9		.1	.1	
s?	4.0	9.6	90.0	-49.5	-49.2	-24.4	-24.2	110.0			
s	30.0	72.0	85.0	-27.0	-26.8	-6.0	-6.0				
s	40.0	96.0	85.0	-26.0	-25.8	-5.2	-5.2				
s?	10.0	24.0	65.0	-53.4	-53.0	-23.2	-23.0		-10.0	-9.9	10.0
s?	15.0	36.0	75.0	-52.5	-52.1	-20.2	-20.1				
s?	12.0	28.8	95.0	-51.8	-51.4	-24.5	-24.3		1.6	1.6	6.9
s?	25.0	60.0	95.0	-50.5	-50.1	-24.0	-23.8		-1.4	-1.4	5.7
s?	11.0	26.4	85.0	-52.5	-52.1	-23.9	-23.7				

FLUID INCLUSIONS: 53425 Bt Torrecillas (288/1)

Type	Dim(d)	Dim(p)	L/V%	Te(raw)	Te(cor)	Tmi(raw)	Tmi(cor)	Th
s	40.0	96.0	95.0	-23.5	-23.3	-1.5	-1.5	
s?	15.0	36.0	85.0	-23.0	-22.8	-.7	-.7	
s?	40.0	96.0	75.0	-22.5	-22.3	-.7	-.7	
p?	15.0	36.0	80.0	-2.5	-2.5	-1.5	-1.5	347.5
p?	10.0	24.0	75.0	-1.0	-1.0	-.6	-.6	348.0
p?	12.0	28.8	80.0	-1.0	-1.0	-.5	-.5	347.8
p?	9.0	21.6	75.0	-2.0	-2.0	-1.3	-1.3	240.0
p?	20.0	48.0	95.0	-26.1	-25.9	-4.9	-4.9	184.5
s	25.0	60.0	75.0	-3.0	-3.0	-.8	-.8	318.0
s	12.0	28.8	85.0	-5.5	-5.5	-.8	-.8	275.0
p?	6.0	14.4	80.0	-28.5	-28.3	-10.0	-9.9	230.0
p?	4.0	9.6	80.0	-29.0	-28.8	-10.1	-10.0	262.0
s	22.0	52.8	95.0	-63.0	-62.6	-31.3	-31.1	222.2
s	20.0	48.0	95.0	-62.9	-62.5	-26.5	-26.3	121.6
s	5.0	12.0	95.0	-64.0	-63.6	-31.2	-31.0	140.0
p?	10.0	24.0	90.0	-5.0	-5.0	-1.9	-1.9	159.9
p?	10.0	24.0	95.0	-37.6	-37.3	-4.1	-4.1	196.2
s	9.0	21.6	75.0	-40.0	-39.7	-6.1	-6.1	270.0
s	8.0	19.2	95.0	-67.0	-66.5	-30.8	-30.6	
s	9.0	21.6	80.0	-44.0	-43.7	-3.1	-3.1	237.0
s	10.0	24.0	95.0	-63.0	-62.6	-31.4	-31.2	159.8
s	10.0	24.0	75.0	-6.5	-6.5	-2.3	-2.3	255.1
s	5.0	12.0	80.0	-66.0	-65.5	-26.5	-26.3	160.7
s	8.0	19.2	80.0	-65.7	-65.2	-33.4	-33.2	144.7
s	8.0	19.2	80.0	-66.0	-65.5	-28.1	-27.9	152.5
p?	45.0	108.0	95.0	-38.0	-37.7	-6.8	-6.8	152.0
p?	40.0	96.0	95.0	-42.0	-41.7	-12.8	-12.7	119.0
s	17.0	40.8	75.0	-48.0	-47.7	-22.6	-22.4	
s	6.0	14.4	85.0	-49.0	-48.7	-22.9	-22.7	
s	7.0	16.8	85.0	-48.9	-48.6	-23.0	-22.8	
s	8.0	19.2	80.0	-49.0	-48.7	-23.0	-22.8	
s?	35.0	84.0	75.0	-29.0	-28.8	-9.3	-9.2	325.0
p?	6.0	14.4	75.0	-30.0	-29.8	-9.2	-9.1	274.0
s	5.0	12.0	80.0	-31.0	-30.8	-20.0	-19.9	269.0
p?	7.0	16.8	80.0	-40.0	-39.7	-6.6	-6.6	219.0
p?	5.0	12.0	95.0	-40.0	-39.7	-6.9	-6.9	195.0
p?	4.0	9.6	90.0	-40.0	-39.7	-6.6	-6.6	220.0
s	10.0	24.0	90.0	-65.9	-65.4	-28.8	-28.6	227.0
p?	10.0	24.0	92.0	-68.3	-67.8	-33.4	-33.2	225.5
p?	15.0	36.0	90.0	-45.0	-44.7	-12.1	-12.0	178.2
p?	4.0	9.6	80.0	-53.5	-53.1	-14.2	-14.1	212.5
s	9.0	21.6	75.0	-66.5	-66.0	-18.8	-18.7	235.0
s	10.0	24.0	85.0	-66.5	-66.0	-21.5	-21.3	226.7
s	15.0	36.0	85.0	-55.3	-54.9	-15.4	-15.3	215.8
s	7.0	16.8	75.0	-67.4	-66.9	-18.4	-18.3	327.0
p?	5.0	12.0	90.0	-51.5	-51.1	-20.3	-20.2	225.8
s	30.0	72.0	85.0	-67.0	-66.5	-16.5	-16.4	239.5
s	15.0	36.0	85.0	-68.5	-68.0	-18.5	-18.4	241.0
s	7.0	16.8	90.0	-68.5	-68.0	-18.6	-18.5	240.0

FLUID INCLUSIONS: 51919 Q Ojo Vecino (59/5)

Type	Dim(d)	Dim(p)	L/V%	Te(raw)	Te(cor)	Tmi(raw)	Tmi(cor)	Th
p?	10.4	25.0	75.0	-3.3	-3.1	-2.1	-2.1	
p?	3.8	9.0	60.0	-3.5	-3.3	-.7	-.7	276.0
p?	10.4	25.0	60.0	-3.8	-3.5	-2.2	-2.2	335.5
p?	7.5	18.0	30.0	-7.0	-6.5	-2.2	-2.2	392.0
p?	14.6	35.0	50.0	-4.5	-4.2	-2.5	-2.5	370.0
s	39.2	94.0	65.0	-2.2	-2.1	-1.0	-1.0	357.1
s	5.0	12.0	60.0	-4.3	-4.0	-1.1	-1.1	347.9
s	14.6	35.0	65.0	-2.5	-2.3	-1.0	-1.0	
s	12.5	30.0	75.0	-1.4	-1.3	-.6	-.6	337.1
p?	33.3	80.0	60.0	-5.0	-4.7	-2.8	-2.8	353.0
p?	4.2	10.0	50.0	-4.0	-3.7	-1.3	-1.3	348.5
p?	5.0	12.0	70.0	-3.7	-3.5	-2.8	-2.8	354.0
p?	10.0	24.0	55.0	-8.0	-7.5	-3.1	-3.1	369.3
p?	12.5	30.0	40.0	-4.2	-3.9	-2.2	-2.2	368.9
s	10.4	25.0	55.0	-3.4	-3.2	-1.8	-1.8	338.0
s	8.3	20.0	60.0	-3.6	-3.4	-1.7	-1.7	344.5
s	12.5	30.0	60.0	-3.5	-3.3	-1.7	-1.7	340.0
s	12.5	30.0	60.0	-3.4	-3.2	-1.6	-1.6	341.0
s	22.9	55.0	60.0	-3.5	-3.3	-1.4	-1.4	366.0
s?	6.3	15.0	55.0	-3.2	-3.0	-1.2	-1.2	349.0
s?	25.0	60.0	60.0	-3.4	-3.2	-1.2	-1.2	352.0
p?	20.0	48.0	50.0			-2.9	-2.9	358.0
p?	5.0	12.0	50.0			-2.7	-2.7	360.0
p?	15.0	36.0	65.0			-2.8	-2.8	366.0
p?	10.0	24.0	60.0			-3.0	-3.0	359.0
p?	6.0	14.4	60.0			-3.3	-3.3	353.0
p?	20.0	48.0	50.0			-2.5	-2.5	358.0
p?	10.0	24.0	65.0	-4.0	-3.7	-2.0	-2.0	325.0
p?	22.9	55.0	50.0	-3.5	-3.3	-1.3	-1.3	366.0
p?	16.7	40.0	60.0	-3.5	-3.3	-2.2	-2.2	351.0
p?	10.4	25.0	60.0	-4.9	-4.6	-2.3	-2.3	362.0
p?	12.5	30.0	60.0	-4.2	-3.9	-2.1	-2.1	360.0
p?	16.7	40.0	45.0	-10.0	-9.3	-3.5	-3.5	368.0
p?	16.7	40.0	55.0	-4.5	-4.2	-2.5	-2.5	378.0
p?	20.8	50.0	55.0	-4.3	-4.0	-2.2	-2.2	376.0
p?	10.0	24.0	75.0	-6.0	-5.6	-3.1	-3.1	327.0
p?	15.0	36.0	60.0	-6.3	-5.9	-3.1	-3.1	
s	12.0	28.8	85.0	-2.1	-2.0	-1.3	-1.3	315.0
p?	25.0	60.0	80.0	-6.5	-6.1	-3.5	-3.5	
s	18.0	43.2	60.0	-5.9	-5.5	-3.3	-3.3	349.5
s	7.0	16.8	70.0	-4.5	-4.2	-3.4	-3.4	325.0
s	7.0	16.8	80.0	-4.5	-4.2	-3.0	-3.0	330.0
p?	50.0	120.0	70.0	-2.5	-2.3	-1.1	-1.1	357.0
p?	15.0	36.0	60.0	-4.1	-3.8	-2.8	-2.8	368.5
p?	20.0	48.0	75.0	-4.3	-4.0	-1.0	-1.0	337.2
p?	30.0	72.0	70.0	-2.9	-2.7	-.9	-.9	347.0
s?	20.0	48.0	60.0	-2.6	-2.4	-1.0	-1.0	363.5
p?	25.0	60.0	75.0	-2.5	-2.3	-.7	-.7	345.0
p?	25.0	60.0	55.0	-3.5	-3.3	-2.0	-2.0	350.0

FLUID INCLUSIONS: 53663 Q Torrecillas (90148/2)

Type	Dim(d)	Dim(p)	L/V%	Te(raw)	Te(cor)	Tmi(raw)	Tmi(cor)	Th
s	4.0	9.6	75.0	-8.5	-8.4	-1.3	-1.3	184.1
s	7.0	16.8	75.0	-9.1	-9.0	-1.5	-1.5	
s	3.0	7.2	80.0	-7.8	-7.7	-1.8	-1.8	181.7
s	7.0	16.8	80.0	-8.4	-8.3	-1.4	-1.4	224.5
s	5.0	12.0	80.0	-8.5	-8.4	-1.6	-1.6	181.5
s	3.0	7.2	80.0	-9.3	-9.2	-1.8	-1.8	181.9
s	4.0	9.6	80.0	-9.8	-9.7	-1.4	-1.4	185.5
s	9.0	21.6	85.0	-9.1	-9.0	-1.7	-1.7	182.0
s	5.0	12.0	85.0	-7.8	-7.7	-1.7	-1.7	182.8
s	5.0	12.0	87.0	-7.9	-7.8	-1.6	-1.6	181.6
s	3.0	7.2	80.0	-8.5	-8.4	-1.7	-1.7	177.9
s	5.0	12.0	85.0	-9.3	-9.2	-1.6	-1.6	197.3
s	4.0	9.6	85.0	-8.3	-8.2	-1.9	-1.9	209.1
s	3.0	7.2	80.0	-9.0	-8.9	-1.7	-1.7	
s	8.0	19.2	90.0	-9.1	-9.0	-1.6	-1.6	205.3
s	4.0	9.6	85.0	-9.2	-9.1	-1.8	-1.8	200.8
s	4.0	9.6	85.0	-8.8	-8.7	-1.6	-1.6	190.8
s	3.0	7.2	80.0	-8.0	-7.9	-1.6	-1.6	180.4
s	5.0	12.0	85.0	-8.5	-8.4	-1.0	-1.0	170.9

FLUID INCLUSIONS: 51920 Q La Nube (159/8)

Type	Dim(d)	Dim(p)	L/V%	Te(raw)	Te(cor)	Tmi(raw)	Tmi(cor)	Th
s	20.0	48.0	80.0	-5.2	-5.2	-1.4	-1.4	280.0
s?	15.0	36.0	60.0	-6.0	-6.0	-3.5	-3.5	
s?	6.0	14.4	75.0	-1.5	-1.5	-.9	-.9	241.3
s?	8.0	19.2	60.0	-9.1	-9.0	-1.8	-1.8	328.5
s?	10.0	24.0	60.0	-9.1	-9.0	-1.8	-1.8	328.5
s?	10.0	24.0	55.0	-6.6	-6.6	-3.2	-3.2	
s	6.0	14.4	65.0	-6.5	-6.5	-1.4	-1.4	264.1
s	7.0	16.8	50.0	-5.9	-5.9	-2.1	-2.1	383.0
s?	7.0	16.8	25.0	-5.5	-5.5	-2.5	-2.5	382.0
s?	12.0	28.8	75.0	-6.7	-6.7	-1.2	-1.2	299.8
s	7.0	16.8	50.0	-5.8	-5.8	-3.1	-3.1	384.0
s	8.0	19.2	40.0	-6.5	-6.5	-2.9	-2.9	381.7
s	12.0	28.8	55.0	-5.7	-5.7	-2.8	-2.8	384.0
s?	14.0	33.6	65.0	-6.5	-6.5	-1.4	-1.4	348.3
s?	15.0	36.0	25.0	-8.5	-8.4	-2.5	-2.5	
s	7.0	16.8	55.0	-5.5	-5.5	-1.5	-1.5	352.7
s	12.0	28.8	50.0	-7.6	-7.5	-1.9	-1.9	378.2
s	10.0	24.0	50.0	-7.0	-7.0	-2.9	-2.9	379.5
s	13.0	31.2	85.0	-10.0	-9.9	-1.5	-1.5	289.4
s	17.0	40.8	85.0	-9.9	-9.8	-3.6	-3.6	304.8
s	10.0	24.0	80.0	-7.9	-7.8	-3.2	-3.2	
s	5.0	12.0	60.0	-7.0	-7.0	-3.5	-3.5	
s	7.0	16.8	45.0	-7.2	-7.1	-3.7	-3.7	371.6
s	9.0	21.6	50.0	-6.9	-6.9	-3.5	-3.5	378.5
p?	5.0	12.0	65.0	-36.7	-36.4	-3.8	-3.8	298.5
s?	7.0	16.8	60.0	-8.0	-7.9	-3.3	-3.3	357.3
p?	7.0	16.8	75.0	-7.3	-7.2	-1.2	-1.2	237.5
p?	5.0	12.0	60.0	-9.0	-8.9	-2.8	-2.8	216.5
s	6.0	14.4	55.0	-9.0	-8.9	-2.8	-2.8	
p?	4.0	9.6	55.0	-9.6	-9.5	-5.3	-5.3	
p?	4.0	9.6	60.0	-8.9	-8.8	-2.8	-2.8	260.0
s	4.0	9.6	75.0	-7.3	-7.2	-3.6	-3.6	
s?	7.0	16.8	55.0	-8.5	-8.4	-4.1	-4.1	353.0
s	7.0	16.8	90.0	-12.5	-12.4	-4.0	-4.0	
s	6.0	14.4	60.0	-11.8	-11.7	-3.7	-3.7	313.3
s	4.0	9.6	60.0	-8.5	-8.4	-4.2	-4.2	359.0
s?	6.0	14.4	55.0	-8.3	-8.2	-3.9	-3.9	
p?	5.0	12.0	55.0	-11.9	-11.8	-2.5	-2.5	
s	5.0	12.0	55.0	-9.8	-9.7	-4.3	-4.3	
s	5.0	12.0	70.0	-9.4	-9.3	-3.0	-3.0	
p?	6.0	14.4	55.0	-8.2	-8.1	-3.8	-3.8	
p?	7.0	16.8	80.0	-36.7	-36.4	-6.8	-6.8	203.7
s?	5.0	12.0	85.0	-1.8	-1.8	-.8	-.8	176.6
s?	7.0	16.8	80.0	-2.0	-2.0	-.6	-.6	226.5
s?	7.0	16.8	85.0	-1.9	-1.9	-.7	-.7	200.8
s?	7.0	16.8	80.0	-2.5	-2.5	-1.1	-1.1	228.2
s	9.0	21.6	80.0	-2.0	-2.0	-1.1	-1.1	213.0
s	9.0	21.6	80.0	-1.9	-1.9	-.7	-.7	200.5

II.4. Sulphur isotope analyses.

File: sulph Disk: sulph/enadimsa

LINARES-LA CAROLINA SULPHUR ISOTOPE DATA

SULPHATE

Mineral	Sample	Cent	Arac	Car-Sta	Lin	Trias	Replic
Barite	318-10				9.30		
	79-1					7.00	
	159-9			12.90			
	288-1					8.95	
	288-3					9.40	
	298-5					9.20	
	298-2					7.99	
	308-10			10.50			
	288-2					9.20	9.30
	129-7				7.42		
	318-1				8.80		
	139-23			14.10			
	143-3	9.43					
	139-22			10.22			
	129-8				8.70		
	308-9			9.64			
	159-12			9.14			
	159-13			7.97			
	79-3					7.20	
	79-2					7.13	
	298-6					8.70	
	298-7					8.50	
	9031-6			9.16			7.77
	318-6				7.10		
	90164-13	10.00					
	90164-20	9.20					
	90174-4a			9.60			
	90174-4c			9.30			
	90164-12	6.20					
	139-10		9.30				
	318-2				8.75		
	298-3a					8.20	

File: sulph Disk: sulph/enadimsa

LINARES-LA CAROLINA SULPHUR ISOTOPE DATA

SULPHIDES

Mineral	Sample	Cent	Arac	Car-Sta	Lin	Trias	Metased	Replic
Galena	33-4				-1.90			-1.86
Galena	33-2				-1.97			
Galena	49-5			3.38				
Galena	49-6			-1.68				-1.14
Galena	49-7			1.83				
Galena	59-6			2.53				
Galena	59-7			-4.81				
Galena	59-10			.22				
Galena	129-1					-3.19		-3.08
Galena	129-4				-2.53			
Galena	129-5				-2.25			
Galena	129-11				-1.98			
Galena	129-12				-2.17			
Galena	139-2		-1.14					-1.06
Galena	139-3		-1.68					
Galena	139-16			3.69				
Galena	159-12			-6.40				-6.38
Galena	159-13			-6.57				-6.98
Galena	298-3a					-2.90		
Galena	298-3c					-2.84		
Galena	298-2					-1.65		
Galena	309-1	-3.39						
Galena	318-3				-3.67			-3.56
Galena	318-4				-1.62			
Galena	318-7				-1.97			
Galena	9031-12			3.23				
Galena	90164-3	1.08						
Galena	90164-4	3.94						3.99
Galena	90164-9	2.19						
Galena	90164-20	5.16						
Sphalerite	93-3			11.43				11.10
Sphalerite	159-12			-4.16				
Sphalerite	308-13			10.96				
Sphalerite	308-15			11.54				
Sphalerite	90164-10	7.52						
Chalcopy.	129-27				-.19			
Marcasite	139-15			10.83				
Marcasite	159-11			-29.01				
Pyrite	163-1						-13.65	
Pyrite	318-7				6.76			
Pyrite	9098-5			2.98				
Marcasite	90164-2	3.97						
Pyrite	90164-6						8.32	8.11
Pyrite	90164-8						16.52	
Pyrite	73-2						39.70	
Pyrite	73-3						45.40	
Pyrite	129-25				-1.94			-1.44
Marcasite	59-10							